Lecture Notes in Networks and Systems 179

Devendra Kumar Sharma
Le Hoang Son
Rohit Sharma
Korhan Cengiz *Editors*

Micro-Electronics and Telecommunication Engineering

Proceedings of 4th ICMETE 2020

Springer

Lecture Notes in Networks and Systems

Volume 179

The series "Lecture Notes in Networks and Systems" publishes the latest developments in Networks and Systems—quickly, informally and with high quality. Original research reported in proceedings and post-proceedings represents the core of LNNS.

Volumes published in LNNS embrace all aspects and subfields of, as well as new challenges in, Networks and Systems.

The series contains proceedings and edited volumes in systems and networks, spanning the areas of Cyber-Physical Systems, Autonomous Systems, Sensor Networks, Control Systems, Energy Systems, Automotive Systems, Biological Systems, Vehicular Networking and Connected Vehicles, Aerospace Systems, Automation, Manufacturing, Smart Grids, Nonlinear Systems, Power Systems, Robotics, Social Systems, Economic Systems and other. Of particular value to both the contributors and the readership are the short publication timeframe and the world-wide distribution and exposure which enable both a wide and rapid dissemination of research output.

The series covers the theory, applications, and perspectives on the state of the art and future developments relevant to systems and networks, decision making, control, complex processes and related areas, as embedded in the fields of interdisciplinary and applied sciences, engineering, computer science, physics, economics, social, and life sciences, as well as the paradigms and methodologies behind them.

Indexed by SCOPUS, INSPEC, WTI Frankfurt eG, zbMATH, SCImago.

All books published in the series are submitted for consideration in Web of Science.

More information about this series at http://www.springer.com/series/15179

Devendra Kumar Sharma · Le Hoang Son ·
Rohit Sharma · Korhan Cengiz
Editors

Micro-Electronics and Telecommunication Engineering

Proceedings of 4th ICMETE 2020

Springer

Editors
Devendra Kumar Sharma
Department of Electronics and Communication Engineering
SRM Institute of Science and Technology
Ghaziabad, India

Rohit Sharma
Department of Electronics and Communication Engineering
SRM Institute of Science and Technology
Ghaziabad, India

Le Hoang Son
Institute of Information Technology
Vietnam National University
Cay Giay, Vietnam

Korhan Cengiz
Department of Electrical and Electronics Engineering
Trakya University
Edirne, Turkey

ISSN 2367-3370 ISSN 2367-3389 (electronic)
Lecture Notes in Networks and Systems
ISBN 978-981-33-4686-4 ISBN 978-981-33-4687-1 (eBook)
https://doi.org/10.1007/978-981-33-4687-1

This Springer imprint is published by the registered company Springer Nature Singapore Pte Ltd.
The registered company address is: 152 Beach Road, #21-01/04 Gateway East, Singapore 189721, Singapore

Preface

The book presents high-quality papers from the Fourth International Conference on Microelectronics and Telecommunication Engineering (ICMETE 2020). It discusses the latest technological trends and advances in major research areas such as microelectronics, wireless communications, optical communication, signal processing, image processing, big data, cloud computing, artificial intelligence, and sensor network applications. This book includes the contributions of national/international scientists, researchers, and engineers from both academia and the industry. The contents of this volume will be useful to researchers, professionals, and students alike.

Ghaziabad, India — Devendra Kumar Sharma
Cay Giay, Vietnam — Le Hoang Son
Ghaziabad, India — Rohit Sharma
Edirne, Turkey — Korhan Cengiz

Contents

Editors and Contributors

About the Editors

Dr. Devendra Kumar Sharma received his B.E. degree in Electronics Engineering from M.N.R. Engineering College, Allahabad, M.E. degree from University of Roorkee, and Ph.D. degree from NIT Kurukshetra, India in 1989, 1992 and 2016 respectively. He served PSUs in different positions for more than 8 years in QA & Testing/R & D departments. In addition, he is having a long experience of 20 years in academics and research. His research interests include VLSI interconnects, Digital design, Testing and Signal processing. He is currently a Professor & Dean of SRM Institute of Science and Technology, Delhi-NCR Campus, Ghaziabad, India. He holds a Ph.D. degree in Electronics & Communication Engineering (VLSI Design) from National Institute of Technology, Kurukshetra, India. Dr. Sharma has authored many papers in SCOPUS/SCI index journals and International Conferences. His research interests are in VLSI interconnects, Electronic Circuits, Digital Design, Testing and Signal Processing. He has been the Editor to International Conferences on Microelectronics and Telecommunication. He is member of Professional Societies like IEEE, LISTE, LIETE, VSI and is a reviewer of many International Journals/Conferences. He has served as General Chair and Convener for many conferences. Dr. Sharma has participated in many International and National conferences as Session Chair and member in Steering, Advisory and Program Committees.

Dr. Le Hoang Son obtained the Ph.D. degree in Mathematics–Informatics at VNU University of Science, Vietnam National University (VNU), in 2013. He has been promoted to Associate Professor in Information Technology since 2017. Dr. Son worked as Senior Researcher and Vice Director at the Center for High Performance Computing, VNU University of Science, Vietnam National University during 2007–2018. From August 2018, he is Head of the Department of Multimedia and Virtual Reality, VNU Information Technology Institute, VNU. His major fields include artificial intelligence, data mining, soft computing, fuzzy computing, fuzzy recommender systems, and geographic information system. He is a member of

International Association of Computer Science and Information Technology (IACSIT), Vietnam Society for Applications of Mathematics (Vietnam), and Key Laboratory of Geotechnical Engineering and Artificial Intelligence in the University of Transport Technology (Vietnam). Dr. Son serves as Editorial Board of Applied Soft Computing (ASOC, in SCIE), International Journal of Ambient Computing and Intelligence (IJACI, in SCOPUS), and Vietnam Journal of Computer Science and Cybernetics (JCC). He is Associate Editor of Journal of Intelligent & Fuzzy Systems (JIFS, in SCIE), IEEE Access (in SCIE), Neutrosophic Sets and Systems (NSS), Vietnam Research and Development on Information and Communication Technology (RD-ICT), VNU Journal of Science: Computer Science and Communication Engineering (JCSCE), and Frontiers in Artificial Intelligence. Dr. Son served as a reviewer for various international journals and conferences. He gave a number of invited talks at many conferences since 2015. Up to now, he has 131 publications in prestigious journals and conferences including 74 ISI papers (SCI: 18, SCIE: 50, ESCI: 6) and 01 SCOPUS paper and undertaken more than 20 major joint international and national research projects. He has published 6 books and book chapters. So far, he has awarded "2014 VNU Research Award for Young Scientists," "2015 VNU Annual Research Award," "2015 Vietnamese Mathematical Award," and "2017 Vietnamese Mathematical Award."

Dr. Rohit Sharma is working as Assistant Professor of Electronics and Communication Engineering, SRM University, Delhi NCR Campus Ghaziabad, India. He has completed his Ph.D. in Electronics and Communication Engineering (Title—Evolution in RFID Security to building it in the Global Environment) from Teerthanker Mahaveer University, Moradabad, India, M.Tech. (Communication Engineering) from Shobhit University, India, and B.Tech. (Electronics and Communication Engineering) from Uttar Pradesh Technical University, Lucknow, India. He joined SRM University in 2011. He has a teaching experience of over 7 years at SRM University and Dewan V S group of Institution, India. Dr. Sharma is an active member of ISTE, IEEE, ICS, IAENG, and IACSIT. He is an editorial board member and a reviewer of more than 8 international journal and conferences. He has published about 38 research papers in international/national journals and about 09 research papers in international/national conferences. Dr. Sharma has been Editor of the 2nd International Conference on Microelectronics and Telecommunication. Dr. Sharma has served as a Technical Committee member in "CSMA2017, Wuhan, Hubei, China," "EEWC 2017, Tianjin, China," IWMSE2017 "Guangzhou, Guangdong, China," "ICG2016, Guangzhou, Guangdong, China," and "ICCEIS2016 Dalian Liaoning Province, China." Dr. Sharma is a reviewer of many international journals/conferences. Dr. Sharma has served as Technical Chair of the 2nd International Conference on Microelectronics and Telecommunication (ICMETE-2018) held in India. Dr. Sharma has participated in many international and national conferences as Session Chair and a member in Steering, Advisory or International Program Committees.

Dr. Korhan Cengiz received his B.S. degree in Electronics and Communication Engineering in 2008 from Kocaeli University, Turkey. He received his Ph.D. degree in Electronics Engineering in 2016 from Kadir Has University, Turkey. Dr. Cengiz has more than 30 articles related to wireless sensor networks and wireless communications. Dr. Cengiz serves as a TPC member for more than 20 conferences. He is Editor-in-Chief of 2 journals and Editor of several journals. His honors include Tubitak Priority Areas Ph.D. scholarship and two best paper awards in conferences ICAT 2016 and ICAT 2018.

Contributors

Lakshay Aggarwal Department of Computer Science and Engineering, Bharati Vidyapeeth's College of Engineering, New Delhi, India

Ridhi Aggarwal ABES Engineering College, Ghaziabad, Uttar Pradesh, India

Kiran Ahuja DAV Institute of Engineering Technology, Jalandhar, Punjab, India

B. Ajith Kumar Easwari Engineering College, Chennai, Tamil Nadu, India

A. Aline Gratia Velammal Institute of Technology, Chennai, Tamil Nadu, India

Kumari Alka Sagar Institute of Science & Technology, Bhopal, India

C. H. Amulya Nissy Department of Electronics and Communication Engineering, Velammal Institute of Technology, Chennai, India

P. Anantha Prabha Department of Computer Science & Engineering, Sri Krishna College of Technology, Coimbatore, Tamil Nadu, India

Anuranjana Amity School of Engineering and Technology, Amity University Uttar Pradesh, Noida, India

Simrann Arora Department of Computer Science and Engineering, Bharati Vidyapeeth's College of Engineering, New Delhi, India

G. Babu Department of Electronics and Communication Engineering, Velammal Institute of Technology, Panjetty, Tamil Nadu, India

Indu Bala Lovely Professional University, Phagwara, Punjab, India

S. Balaji Panimalar Engineering College, Chennai, Tamil Nadu, India

Basha Electronics and Communication Engineering, Hindustan Institute of Technology and Science, Chennai, TN, India

S. Baskaran ECE Department, SKP Engineering College, Tiruvannamalai, Tamil Nadu, India

Pradeep Bedi Graphic Era Hill University, Dehradun, India

V. S. Kanchana Bhaaskaran School of Electronics Engineering, Vellore Institute of Technology, Chennai, India

V. R. Bharath Raj Easwari Engineering College, Chennai, Tamil Nadu, India

Anurag Bhatnagar School of Computing and Information Technology, Manipal University Jaipur, Jaipur, Rajasthan, India

Nikhar Bhatnagar Department of Computer Science and Engineering, Swami Keshvanand Institute of Technology Jaipur, Jaipur, India

Akshada Bhosale Department of Electronics and Telecommunication, Pimpri Chinchwad College of Engineering, SPPU, Pune, India

Shilpi Birla Manipal University, Jaipur, India

S. Bragadesh Bharatwaj Easwari Engineering College, Chennai, Tamil Nadu, India

Vaibhav Chaudhari School of Electronics Engineering, Vellore Institute of Technology, Chennai, India

Nilkanth Chopade Department of Electronics and Telecommunication, Pimpri Chinchwad College of Engineering, SPPU, Pune, India

Naina Dahiya Amity School of Engineering and Technology, Amity University Uttar Pradesh, Noida, India

M. Deva Priya Department of Computer Science and Engineering, Sri Krishna College of Technology, Coimbatore, Tamil Nadu, India

Bali Devi Department of Computer Science & Engineering, Manipal University Jaipur, Jaipur, Rajasthan, India;
School of Computing and Information Technology, Manipal University Jaipur, Jaipur, Rajasthan, India

T. Divyani Department of Electronics and Communication Engineering, Velammal Institute of Technology, Panjetty, Tamil Nadu, India

Dhirendra Kumar Diwedi RKG Group of Institutions, Ghaziabad, India

Aakash Gadge School of Electronics Engineering, Vellore Institute of Technology, Chennai, India

T. R. Ganesh Babu Department of Electronics and Communication Engineering, Muthayammal Engineering College, Rasipuram, Tamil Nadu, India

Soham Gautam ABES Engineering College, Ghaziabad, Uttar Pradesh, India

K. Gopalakrishnan Indian Technology Congress Association and Convener, Consortium of 75 Students' Satellites: Mission 2020, Bengaluru, India

Priyanshi Goyal Department of Electronic Science, University of Delhi South Campus, New Delhi, India

S. B. Goyal City University, Petaling Jaya, Malaysia

K. Gunasekaran Department of Electronics and Communication Engineering, GRT Institute of Engineering and Technology, Tiruttani, Tamil Nadu, India; Electronics and Communication Engineering, GRT Institute of Engineering and Technology, Tiruttani, Tamil Nadu, India

P. Gunavathi Department of Electronics and Communication Engineering, Velammal Institute of Technology, Panchetti, India

Akash Gupta Department of Computer Science and Engineering, Bharati Vidyapeeth's College of Engineering, New Delhi, India

Rajeev Kumar Gupta Sagar Institute of Science & Technology, Bhopal, India

Sindhu Hak Gupta Department of Electronics and Communication Engineering, ASET, Amity University, Noida, India

Harsh Harsola Department of Computer Science & Engineering, Manipal University Jaipur, Jaipur, Rajasthan, India

L. K. Hema Aarupadai Veedu Institute of Technology, Salem, Tamil Nadu, India

Suraiya Jabin Department of Computer Science, Jamia Millia Islamia, New Delhi, India

Kunal Jain Department of Computer Science and Engineering, Bharati Vidyapeeth's College of Engineering, New Delhi, India

Rachna Jain Department of Computer Science and Engineering, Bharati Vidyapeeth's College of Engineering, New Delhi, India

Nidhi Jakhmola Lagozon Technologies Private Limited, Noida, India

Lazar Jeftić Committee for Space Programme Development (CSPD), Novi Sad, Serbia

J. Jerin Godbell Department of Electronics and Communication Engineering, Velammal Institute of Technology, Chennai, India

R. Jeyaprakashini Department of Electronics and Communication Engineering, Velammal Institute of Technology, Panchetti, India

J. Jijin Godwin Velammal Institute of Technology, Chennai, Tamil Nadu, India

G. O. Jijina Department of Electronics and Communication Engineering, Aarupadai Veedu Institute of Technology, Chennai, Tamil Nadu, India

Sujata Joshi Nitte Meenakshi Institute of Technology, Bangalore, India

R. Jothi Chitra Department of Electronics and Communication Engineering, Velammal Institute of Technology, Chennai, India

K. Kajendran Panimalar Engineering College, Chennai, Tamil Nadu, India

R. Kanmani Department of Information Technology, Sri Krishna College of Technology, Coimbatore, Tamil Nadu, India

K. Karthik Department of ECE, St. Martin's Engineering College, Secunderabad, India

P. Karthika Department of Computer Application, Kalasalingam Univerity, Viruthunagar, Tamilnadu, India

R. Karthikeyan Aarupadai Veedu Institute of Technology, Salem, Tamil Nadu, India

Neha Katiyar Madan Mohan Malviya University of Technology, Gorakhpur, India

Harsupreet Kaur Department of Electronic Science, University of Delhi South Campus, New Delhi, India

Sanmukh Kaur Amity School of Engineering and Technology, Amity University Uttar Pradesh, Noida, India

Prachi Kaushik Department of Computer Science, Jamia Millia Islamia, New Delhi, India

K. Keerthanaa Velammal Institute of Technology, Chennai, Tamil Nadu, India

Chandra KiranKumar Electronics and Communication Engineering, Hindustan Institute of Technology and Science, Chennai, TN, India

B. Kiruthika Velammal Institute of Technology, Chennai, Tamil Nadu, India

T. Kumanan Faculty of Engineering and Technology, Meenakshi Academy of Higher Education and Research, Chennai, India

Brijesh Kumar Manav Rachna International Institute of Research and Studies, Faridabad, India

S. Sravan Kumar Amritha Sai Institute of Science and Technology, Kodad, India; ASS&T, Kodad, India

Sheo Kumar CSE, CMREC, Hyderabad, India

Sumit Kumar Electronics and Telecommunication Department, Symbiosis Institute of Technology, Symbiosis International (Deemed University), Pune, India

Rajmohan Madasamy Hindustan Institute of Technology & Science, Chennai, Tamilnadu, India

A. Christy Jeba Malar Department of Information Technology, Sri Krishna College of Technology, Coimbatore, Tamilnadu, India

Rajeshwari R. Malekar Electronics and Telecommunication Department, Symbiosis Institute of Technology, Symbiosis International (Deemed University), Pune, India

Deepak Mangal GLA University, Mathura, UP, India

Pritish Manjarwar Lagozon Technologies Private Limited, Noida, India

B. Meenakshi Electronics and Electrical Engineering, Sairam Engineering College, Chennai, TN, India

Suman Mishra Department of ECE, CMR Engineering College, Hyderabad, India

S. Mohan Kumar Department of Computer Science and Engineering, Faculty of Engineering, Meenakshi Academy of Higher Education and Research, Chennai, India

R. Mohana Priya Department of Electronics and Communication Engineering, Aarupadai Veedu Institute of Technology, Chennai, Tamil Nadu, India

N. Mohankumar EECE Department, Gitam School of Technology, Bengaluru, India

S. Mohankumar New Horizon College of Engineering(NHCE), Bangalore, India

T. H. Monikca Department of Electronics and Communication Engineering, Velammal Institute of Technology, Chennai, India

M. Monisha Department of Electronics and Communication Engineering, Velammal Institute of Technology, Panjetty, Tamil Nadu, India

G. Moorthy Department of Mechanical Engineering, Velammal Institute of Technology, Panchetti, India

A. Mugilan Department of IT, VIT, Vellore, India

M. Mukesh Khanna Department of Electronics and Communication Engineering, Velammal Institute of Technology, Chennai, India

L. V. Muralikrishna Reddy Committee for Space Programme Development (CSPD), Novi Sad, Serbia

D. Muthukumaran Department of ECE, SCSVMV, Kanchipuram, Tamil Nadu, India;
Department of ECE, SCSVMV, Kanchipuram, Tamilnadu, India

V. Nagaraju Department of Electronics and Communication Engineering, Rajalakshmi Institute of Technology, Chennai, India

Mydhili K. Nair M.S. Ramaiah Institute of Technology, Bangalore, India

V. Auxilia Osvin Nancy S. A. Engineering College, Chennai, Tamil Nadu, India

Lakshay Narang Department of Computer Science and Engineering, Manipal University Jaipur, Jaipur, Rajasthan, India

Anand Nayyar Graduate School, Faculty of Information Technology, Duy Tan University, Da Nang, Vietnam

Kriti Nigam Department of Computer Science and Engineering, Manipal University Jaipur, Jaipur, Rajasthan, India

Nirav Nikhil Lagozon Technologies Private Limited, Noida, India

R. Nivetha Department of Electronics and Communication Engineering, Velammal Institute of Technology, Chennai, India

M. Pandimadevi Sethu Institute of Technology, Virudhunagar, Tamil Nadu, India

D. Pavithra Department of Electronics and Communication Engineering, Velammal Institute of Technology, Panjetty, Tamil Nadu, India

S. Sam Peter Department of Computer Science and Engineering, Sri Krishna College of Technology, Coimbatore, Tamilnadu, India

S. Poongodi Department of ECE, CMR Engineering College, Hyderabad, India

R. Poornachandran ECE Department, SKP Engineering College, Tiruvannamalai, Tamil Nadu, India

K. Venkata Ratna Prabha Department of ECE, SRMIST, Chennai, Tamil Nadu, India

S. Prabhu Department of Electronics and Communication Engineering, Mahendra Institute of Technology, Namakkal, India

A. Praveen Kumar Department of Electronics and Communication Engineering, Velammal Institute of Technology, Chennai, India

M. Deva Priya Department of Computer Science and Engineering, Sri Krishna College of Technology, Coimbatore, Tamilnadu, India

N. Pugazhendi Panimalar Engineering College, Chennai, Tamil Nadu, India

Dušan Radosavljević Committee for Space Programme Development (CSPD), Novi Sad, Serbia

Ganesh Rahate Department of Electronics and Telecommunication, Pimpri Chinchwad College of Engineering, SPPU, Pune, India

M. Rakesh Department of Electronics and Communication Engineering, Velammal Institute of Technology, Chennai, India

G. P. Ramesh Department of ECE, St. Peters Institute of Higher Education and Research, Chennai, India

P. Ramesh Department of Conservative Dentistry and Endodontics, Drs Sudha and Nageswara Rao Siddhartha Institute of Dental Sciences, Chinoutpalli, Andhra Pradesh, India

B. Ramesh Naik CSE Department, GITAM School of Technology, Bengaluru, India

Gundala Srinivasa Rao CMR College of Engineering & Technology, Hyderabad, India

Surbhi Rathore School of Electronics Engineering, Vellore Institute of Technology, Chennai, India

Hema Raut Electronics and Telecommunication Department, Symbiosis Institute of Technology, Symbiosis International (Deemed University), Pune, India

Viraja Ravi Department of Computer Science and Engineering, Sri Krishna College of Technology, Coimbatore, Tamilnadu, India

Werner Retschitzegger Johannes Kepler University Linz, Computer Science Building, Linz, Austria

Ujwal Sachdeva Department of Computer Science & Engineering, Manipal University Jaipur, Jaipur, Rajasthan, India

P. Sailaja Department of Information Technology, Velammal Institute of Technology, Chennai, India

S. Sampath Raju CMR College of Engineering & Technology, Hyderabad, India

M. Sandhya Department of Electronics and Communication Engineering, Velammal Institute of Technology, Chennai, India

R. Sankar Raj Department of Electrical Engineering, Velammal Institute of Technology, Panchetti, India

B. V. Santhosh Krishna New Horizon College of Engineering, Bangalore, Karnataka, India

R. Saravana Kumar ECE Department, Bannari Amman Institute of Technology, Sathyamangalam, Tamil Nadu, India

N. Sathish Panimalar Engineering College, Chennai, Tamil Nadu, India

P. J. Sathish Kumar Panimalar Engineering College, Chennai, Tamil Nadu, India

J. Sengathir Department of Information Technology, CVR College of Engineering, Mangalpally, Vastunagar, Hyderabad, Telangana, India

R. Senthamizh Selvi Easwari Engineering College, Chennai, Tamil Nadu, India

Venkatesh Gauri Shankar Department of Information Technology, Manipal University Jaipur, Jaipur, Rajasthan, India;
School of Computing and Information Technology, Manipal University Jaipur, Jaipur, Rajasthan, India

G. Shanmugaraj Department of Electronics and Communication Engineering, Velammal Institute of Technology, Chennai, India;
Department of Electronics and Communication Engineering, Velammal Institute of Technology, Panchetti, India

Akhilesh Kumar Sharma School of Computing and IT, Manipal University Jaipur, Jaipur, Rajasthan, India

Deepika Sharma Manipal University, Jaipur, India

Dilip Kumar Sharma GLA University, Mathura, UP, India

Monika Sharma Galgotias University, Greater Noida, India

Rohit Sharma SRM Institute of Science and Technology, Ghaziabad, India

Himanshu Shekhar Hindustan Institute of Technology & Science, Chennai, Tamilnadu, India

Laxmikant Shevada Electronics and Telecommunication Department, Symbiosis Institute of Technology, Symbiosis International (Deemed University), Pune, India

Tatiana R. Shmeleva A.S.Popov Odessa National Academy of Telecommunications, Odessa, Ukraine

Asmita Singh Department of Electronics and Communication Engineering, ASET, Amity University, Noida, India

Hare Ram Singh JJTU, Raj, India

P. Solainayagi Department of Computer Science and Engineering, Madha Engineering College, Kundrathur, Chennai, India

B. Sridevi Department of Electronics and Communication Engineering, Velammal Institute of Technology, Panjetty, Tamil Nadu, India

S. SriSahithya Department of Electronics and Communication Engineering, Velammal Institute of Technology, Chennai, India

Devesh Kumar Srivastava School of Computing and IT, Manipal University Jaipur, Jaipur, Rajasthan, India

Jyoti Srivastava Madan Mohan Malviya University of Technology, Gorakhpur, India

Sumit Srivastava Department of Information Technology, Manipal University Jaipur, Jaipur, Rajasthan, India

Venkata Subhash Electronics and Communication Engineering, Hindustan Institute of Technology and Science, Chennai, TN, India

K. Subhashini Department of ECE, SRMIST, Chennai, Tamil Nadu, India

S. Sudha Easwari Engineering College, Chennai, Tamil Nadu, India

R. Suganya Department of Information Technology, Sri Krishna College of Technology, Coimbatore, Tamil Nadu, India

R. Suguna Devi Department of Electrical and Electronics Engineering, Mohamed Sathak A. J. College of Engineering, Chennai, Tamil Nadu, India

Pallikonda Sarah Suhasini Department of ECE, Velagapudi Ramakrishna Siddhartha Engineering College, Vijayawada, Andhra Pradesh, India

Ajay Suri ABES Engineering College, Ghaziabad, Uttar Pradesh, India

J. Swetha Department of Electronics and Communication Engineering, Velammal Institute of Technology, Panchetti, India

R. Tamilselvi Sethu Institute of Technology, Virudhunagar, Tamil Nadu, India

B. R. Tapas Bapu Department of Electronics and Communication Engineering, S. A. Engineering College, Chennai, India

Abhishek Tyagi Department of Electronics and Communication Engineering, ASET, Amity University, Noida, India

K. Umapathy Department of ECE, SCSVMV, Kanchipuram, Tamil Nadu, India

D. Vaishali Department of ECE, SRMIST, Chennai, Tamil Nadu, India

R. Vallikannu Electronics and Communication Engineering, Hindustan Institute of Technology and Science, Chennai, TN, India

V. Vanitha Aarupadai Veedu Institute of Technology, Salem, Tamil Nadu, India

Manisha Vashisht Manav Rachna International Institute of Research and Studies, Faridabad, India

Vipul Vashisht Lagozon Technologies Private Limited, Noida, India

Rasika Verma SRM Institute of Science and Technology, Ghaziabad, India

K. Vidhya Department of Electronics and Communication Engineering, Saveetha School of Engineering, SIMATS, Chennai, Tamil Nadu, India

S. A. Vighneshbalaji Department of Computer Science & Engineering, Sri Krishna College of Technology, Coimbatore, Tamil Nadu, India

Sathish Voggu Sri Sai Educational Society Group of Institutions, Ramapuram, India;
Sri Sai Educational Society's Group of Institutions, Ramapuram, India

Dileep Kumar Yadav Galgotias University, Greater Noida, India

S. K. Yadav JJTU, Raj, India

Vamsidhar Yendapalli CSE Department, GITAM School of Technology, Bengaluru, India

S. A. Yuvaraj Department of ECE, GRT Institute of Engineering and Technology, Tiruttani, Tamil Nadu, India;
GRT Institute of Engineering and Technology, Tiruttani, Tamilnadu, India

Dmitry A. Zaitsev Odessa State Environmental University, Odessa, Ukraine

A Review on MIMO Dielectric Resonator Antenna for 5G Application

Rajeshwari R. Malekar, Hema Raut, Laxmikant Shevada, and Sumit Kumar

Abstract Multiple input multiple output (MIMO) is the next-generation technology for the 5G mobile terminals. MIMO uses multiple antennas and integrates multiple antennas within constrained space which is a crucial issue. This requires high isolation between antennas. MIMO technology will increase system capacity, link reliability, and the data rate required for 5G communication. This paper presents a recent MIMO dielectric resonator antenna (DRA) proposed by authors for future 5G applications. It also compares various techniques used to improve isolation between antennas and gain for MIMO DRA while maintaining a compact size. In this paper, we have compared different 5G antennas available in the literature based on parameters like isolation, gain, radiation efficiency, and envelope correlation coefficient (ECC).

Keywords MIMO · Dielectric resonator antennas · Millimeter wave · Mutual coupling · 5G communication

1 Introduction

Mobile communication technology has developed rapidly since the last few decades. Previous generation mobile phones are targeted for one type of device and one type of user (for 2G mobile phones and 3G/4G smartphones). Consumer demands are

R. R. Malekar · H. Raut · L. Shevada · S. Kumar (✉)
Electronics and Telecommunication Department, Symbiosis Institute of Technology, Symbiosis International (Deemed University), Pune, India
e-mail: er.sumitkumar21@gmail.com

R. R. Malekar
e-mail: rajeshwari.malekar@gmail.com

H. Raut
e-mail: hdraut2083@gmail.com

L. Shevada
e-mail: lp.aish@gmail.com

D. K. Sharma et al. (eds.), *Micro-Electronics and Telecommunication Engineering*,
Lecture Notes in Networks and Systems 179,
https://doi.org/10.1007/978-981-33-4687-1_1

increasing day by day because of advancing technologies like 4 K or 8 K video streaming, multiple devices, the virtual reality which required large information exchange. Now due to the Internet of things, networks are in such a way that all systems are connected. It means people and various objects are very much connected to every object and different data. The same device may host or relay different applications maybe ranging from voice services to IoT services. It means the new network must be much more flexible, faster, and cheaper [1].

The following are the five technologies that could give new directions in component design and architectural changes required by 5G technology for lower latencies and higher data rates [2]: massive MIMO, device-centric architectures, native support for machine-to-machine communication, millimeter wave (mm-wave), and smarter devices. To enhance system performance, the massive MIMO is the optimistic technology for 5G communication. It is also called full-dimension (FD) MIMO for 5G communication [3].

Out of these five technologies, MIMO will be playing a considerable role in future 5G communication devices. MIMO can improve the link reliability, capacity, data rate, through multiple transmission between the transmitter and receiver. Multiple antennas should be installed in the transmitter and receiver for the MIMO system [4].

Long, McAllister, and Shen [5] in the 1980s examined the characteristics of dielectric resonator antennas for different shapes of the form such as cylindrical, hemispherical, and rectangular. Dielectric resonator antennas are efficient radiators, versatile, and having design flexibility. Dielectric resonators are considered to be a good alternative for the antenna with low gains like dipoles, monopole, and microstrip patches as suggested in [5]. A Dielectric resonator antenna (DRA) can be used as a resonator as well as an antenna. Bandwidth (BW) of the DRA is inversely proportional to the dielectric constant ε_r. The dielectric resonator antenna can be made more compact by using a material having a high dielectric constant ε_r. A dielectric resonator constructively uses its radiating structure, due to which ohmic loss is reduced. Even in a millimeter-wave frequency band, a DRA can achieve high radiation efficiency. In the literature review, it is found that a various MIMO employs DRA to improve isolation, gain, and various parameters.

In Sect. 2, a dielectric resonator antenna is discussed. In Sect. 3, we discussed a literature review of recent work on MIMO dielectric resonator antenna design. In Sect. 4, a comparative study of MIMO DRAs is presented according to various parameters like isolation, gain, frequency range, efficiency. Lastly, the survey is concluded in Sect. 5 followed by references.

2 Dielectric Resonator Antennas

In late 1960, dielectric resonators (DRs) had been utilized in microwave circuit applications as high-Q-factor elements. Instead of wave guide-cavity resonators, DRs are used because it is more compact and more compliant to printed-circuit

integration. For compactness, the material used was having a relatively high dielectric constant ($\varepsilon_r \geq 35$). For Dielectric resonator antenna having a characteristic that its (D) maximum dimension was linked to (λ_0) the free-space wavelength (resonant). The relation between D and (λ_0) is given by $D\ \alpha\ \lambda_0\ \varepsilon_r - 0.5$. Here, the dielectric constant is (ε_r) for the dielectric resonator antenna. As the radiation efficiency was not affected by (ε_r), a broad range of values was used ($2 < \varepsilon_r < 140$). The size of the dielectric resonator antenna is made compact by using a material having a high value of ε_r. So that, it is feasible for low frequencies as well [5].

Various applications of dielectric resonator antennas are IMT-2000, mobile handsets for PCS, mobile base-station antennas, wireless LANs, radars, USB applications, RFID, all-dielectric wireless receivers, spatial power combining, and direction-finding.

Dielectric resonator antennas are normally preferred because it is compact and has low profile, high radiation efficiency, wide bandwidth, and high Q. It is especially used in applications where the requirement is a small size, ease of coupling for planar transmission lines, and temperature-stable resonant at microwave frequency. Due to this advantage, this can also be used at mm-wave integrated circuits.

Different types of antennas like the antipodal Vivaldi antenna is also used in 5G applications [21, 22]. In this paper, MIMO DRA is studied for improving isolation for 5G applications.

Low-Profile Dielectric Resonator Antennas. The compact dielectric resonator antenna can be constructed where a low antenna profile is required. This antenna can be designed using high ε_r by keeping antenna dimensions small. Different shapes of low-profile DRA are shown in Fig. 1 [5].

Compact DRA. A combination of high dielectric substrates and metal loading a compact antenna designs can be made. This results in a reduction of bandwidth and can be used in narrowband applications. Figure 2 [5] shows the compact DRA with metal loading.

In MIMO, high isolation between antenna elements is needed. Various technologies are suggested to improve the isolation of MIMO dielectric resonator antennas (DRAs). These techniques are used to resist the current displacement between antenna elements. The following are the different techniques used for enhancing isolation of MIMO DRAs: parasitic structures including metallic entities

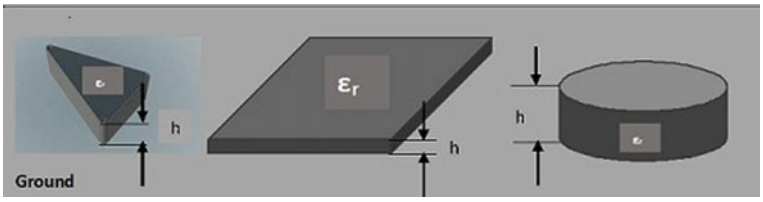

Fig. 1 Low-profile DRA

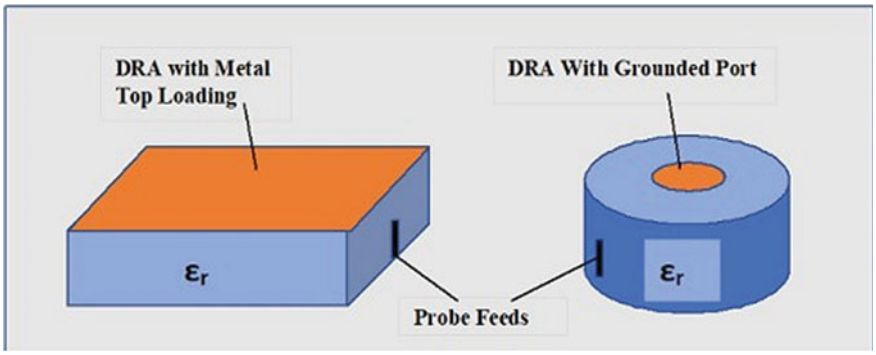

Fig. 2 Compact DRA with metal loading

[11], frequency selective surfaces (FSSs) [12], hybrid feeding mechanism generating orthogonal modes [13–16], metasurface shields [17]. Different challenges of DRA-based MIMO are addressed and investigated above 3.5 GHz bands in [18–20].

3 Recent Work on MIMO Dielectric Resonator Antenna

When we are using a multiple input multiple output (MIMO) technique, one important aspect that needs to be considered is the isolation between two antennas. The paper [6] has discussed the method where two rectangular dielectric resonators were kept on a Rogers 5880 substrate. This was excited by a rectangular microstrip-fed slot which was kept under dielectric resonators. On the upper surface of two DRs, a metal strip was printed. This construction was used for isolation purposes. Because of that metal strip, the strongest part of the coupling field will move away from adjacent lots of dielectric resonator antennas.

An important requirement of the 5G antenna is that its size must be compact and efficient. For short-range and high-speed data links, it must fit on the edge of handheld devices. In paper [7], a millimeter-wave dielectric resonator MIMO antenna system is presented with two linear arrays. Single multiple input multiple output antenna contains four cylindrical dielectric resonator antennas (cDRAs) which are operating at 30 GHz frequency and with 1 GHz bandwidth. Each cylindrical dielectric resonator antenna has a diameter of 3.2 mm and height 3.1 mm. The proposed system consists of two- and four-element linear cylindrical DRA arrays (total of eight elements). The Center-to-center spacing between two adjacent cDRAs was 6 mm. Four-element arrays are proposed with a beam pattern that was tilted by 450. A good correlation coefficient was achieved by a well-designed feed network. This enables acceptable phase and magnitude excitation for separate cylindrical DRAs for radiation.

The paper [8] has studied enhanced diversity compact single-fed wideband circularly polarized MIMO DRA for 5G application. Two diagonal edges of the dielectric

resonator were truncated at 450 so as to achieve a greater axial ratio which was greater than 0.65 GHz. A Cross-ring slot was used to excite DRA to produce circularly polarized fields. The adhesive material was used to attach DR to the PCB. This additional layer of adhesive material affects the radiation characteristics like the quality of polarization and antenna impedance. Instead of adhesive material, short triangular stands were used. These are attached at the border of the dielectric resonator to grip it in place.

In [9], the isolation of mm-wave MIMO DRA was improved by attaching simple metallic vias. It was observed that by inserting the vias vertically within the dielectric resonator antenna at a suitable place and without an increase in height of the antenna mutual coupling was significantly decreased. Decoupling metallic vias affect the field distribution and reduce the coupled field. Thus, isolation between MIMO DRA can be enhanced. Even though vias were inserted inside the dielectric resonator antenna without additional footprint, the complete antenna design becomes compact and simple. The decoupling method was used in the H-plane and E-plane coupled_2 MIMO antennas.

For square DRAs, aperture coupling (*L* monopole) feeding technique is used [10]. This technique is used to achieve multi-band frequencies. The coupling energy of the DRAs is controlled by the aperture couple. The desired band of frequencies can be adjusted without disturbing fundamental mode. The desired frequency band is achieved by adopting L monopole aperture coupled feeding. A triple-band dual-polarized MIMO SDRA for 4G and 5G was suggested and studied. This proposed method can be used for LTE bands: 1.63–1.84 GHz (9/24), 2.43–2.71 GHz (38/41), and 3.27–3.75 GHz (48/52) (Table 1).

Table 1 MIMO DRAs for 5G

S. No	DRA shape	Dimensions (mm^3)	Substrate	Feed type	ECC	References
1	Rectangular	20 × 20 × 0.254	Rogers 5880	Microstrip	0.013	[6]
2	Cylindrical	10 × 45 × 3.1	HiK500	Microstrip	0.002	[7]
3	Circular polarized CP-DRA	46 × 46 × 1.6	FR-4 epoxy	Microstrip	0.02	[8]
4	Rectangular	4.4 × 4.5 × 1.27	Rogers 6010	Microstrip	0.002	[9]
5	Square	44 × 44 × 20	FR4	Microstrip	0.02	[10]

4 Comparative Study of MIMO DRAs

The result of the simulation shows impedance bandwidth obtained from the proposed antenna [6] is (S11 $\leq$ $-$ 10 dB) for the frequency range of 27.25–28.59 GHz. So, this will cover the 28 GHz band. We know the Federal Communications Commission has allotted 27.5 to 28.35 GHz band for 5G application. Because of a metal strip, the isolation is improved to 24 dB. Results are simulated using HFSS software. The envelope correlation coefficient for suggested MIMO DRA was <0.013 in the 28 GHz frequency band. ECC is another critical figure in the MIMO system, and this contributes to an improved diversity gain and channel capacity. For the proposed system, diversity gain measured is > 9:9 dB. HFSS software was used for simulation purposes.

The MIMO cylindrical dielectric resonator antennas proposed in [7] provide minimum field correlation which is less than 0.002 throughout the band. In this paper, peak gain achieved is more than 7 and with better radiation efficiency. Simulated and measured results show that mutual coupling was less than -25 dB. The efficiency of simulated results was 95% and with a feed system, it reduced to 80% for DRA array. Results are simulated using HFSS software.

In [8], an antenna gain achieved for DRA is about 4.83 dB and impedance bandwidth around 0.8 GHz. The electromagnetic band-gap structure is used to construct a circular polarized DRA array. The proposed MIMO array achieves isolation better than 26 dB while keeping a compact size. Axial ratio BW is about 18.7% and impedance of 25.9% for the system proposed. The diversity gain of the antenna proposed is above 9.8 dB, and the ECC is <0:02. Results are simulated using HFSS software.

In [9], simulated results of the proposed MIMO antenna show that the antenna provides a gain of 6.4 dBi. It is also observed that the increase in vias did not enhance isolation significantly. At 26 GHz, the isolation of the H-plane is increased starting at 15.2–34.2 dB for the MIMO DRA array. For the E-plane array, the isolation is increased starting at 13.1–43 dB. It is observed that the envelope correlation coefficient (ECC) value for the suggested MIMO antenna system is below 0.002. For 1 $\times$ 2 MIMO DRA arrays, the coupling for H-plane and an E-plane was decreased to 19.8 dB and 22.7 dB, respectively. This also leads to high isolation of over 30 dB by the proposed decoupling method. So, this proposed system has a compact size, simple structure, and high isolation level.

In [10], impedance bandwidth is suggested for the MIMO antenna system, at 1.7 GHz about 12%, at 2.6 GHz about 10.89%, and at 3.6 GHz about 13.68%. The expected frequency band is achieved by adopting L monopole aperture coupled feeding. An antenna gain measured is 5.5 dBi at 1.7 GHz, 5.9 dBi at 2.6 GHz, and 6.9 dBi at 3.6 GHz. The value of ECC is 0.0070 at 1.7 GHz, 0.0072 at 2.6 GHz, and 0.0038 at 3.6 GHz. For the proposed system, ECC is <0:02, and diversity gain is about 10 dB. It also maintains compact size, polarization diversity, and good impedance bandwidth. Results are simulated using HFSS software (Table 2).

Table 2 Comparative study of MIMO DRAs

S. No	DRA shape	Isolation (dB)	Gain (dBi)	Frequency (GHz)	Efficiency	References
1	Rectangular	24	9.9	27.528.35	Not given	[6]
2	Cylindrical	25	7	30	High	[7]
3	Circular polarized (CP-DRA)	26	9.8	3.33.8	Not given	[8]
4	Rectangular	30	6.4	26	Not given	[9]
5	Square	20	5.5	1.7	Not given	[10]
			5.9	2.6		
			6.9	3.6		

5 Conclusion

The main concern for 5G antennas is to improve gain, bandwidth, isolation, and high radiation efficiency. This paper elaborates methods by using various shapes of dielectric resonator antennas. They are compared for MIMO DRA in the 5G application. The main requirement of the MIMO technique is high isolation between antenna elements. After comparing different methods, it is observed that high isolation is achieved from 20 to 30 dB while maintaining a compact size. For triple-band frequencies, isolation achieved is 20 dB. The gain is also maintained from a minimum of 5.5 dB to a maximum of up to 9.9 dB. In this paper, the millimeter-wave band is also considered.

References

1. Chandramouli D, Chandrashekar S, Maeder A, Niemela T, Theimer T, Thiebaut L (2019) Next generation network architecture. Wiley, London
2. Boccardi F, Heath RW, Lozano A, Marzetta TL, Popovski P (2014) Five disruptive technology directions for 5G. IEEE CommunMaga 52(2). doi:https://doi.org/10.1109/MCOM.2014.6736746
3. Vikstedt DJ (2017) Test challenges of smart antenna systems. In: 2017 IEEE international symposium on electromagnetic compatibility signal/power integrity (EM- CSI). doi:https://doi.org/10.1109/ISEMC.2017.8078068
4. Vook FW, Ghosh A, Thomas TA (2017) Massive MIMO communications. In: Book chapter towards 5G: applications, requirements and candidate technologies, 1st edn. Wiley, London. doi:https://doi.org/10.1002/9781118979846.ch15
5. Petosa A, Ittipiboon A (2010) Dielectric resonator antennas: a historical review and the current state of the art. IEEE Antennas Propag Maga 52(5):91–116. https://doi.org/10.1109/MAP.2010.5687510
6. Zhang Y, Deng JY, Li MJ, Sun D, Guo LX (2019) A MIMO dielectric resonator antenna with improved isolation for 5G mm-wave applications. IEEE Antennas Wirel Ess Propag Lett 18(4):747–751. https://doi.org/10.1109/LAWP.2019.2901961

7. Sharawi MS, Podilchak SK, Hussain MT, Antar YM (2017) Dielectric resonator based MIMO antenna system enabling millimetre-wave mobile devices. IET Microwaves Antennas Propag 11(2):287–293. https://doi.org/10.1049/iet-map.2016.0457
8. Chen HN, Song JM, Park JD (2019) A compact circularly polarized MIMO dielectric resonator antenna over electromagnetic band-Gap surface for 5G applications. IEEE Access 7:140889–140898. https://doi.org/10.1109/ACCESS.2019.2943880
9. Pan YM, Qin X, Sun YX, Zheng SY (2019) A simple decoupling method for 5G millimeter-wave MIMO dielectric resonator antennas. IEEE Trans Antennas Propag 67(4). doi:https://doi.org/10.1109/TAP.2019.2891456
10. Anuar SU, Jamaluddin MH, Din J, Kamardin K, Dahri MH, IdrisIH. Triple band MIMO dielectric resonator antenna for LTE applications. Int J Electron Commun 153172. doi: https://doi.org/10.1016/j.aeue.2020. (© 2020 Published by Elsevier GmbH)
11. Sharawi MS, Podilchak SK, Khan MU, Antar YM (2017) Dual-frequency DRA-based MIMO antenna system for wireless access points. IET Microwaves Antennas Propag 11(8):1174–1182. https://doi.org/10.1049/iet-map.2016.0671
12. Karimian R, Kesavan A, Nedil M, Denidni TA (2017) Low-mutual-coupling 60-GHz MIMO antenna system with frequency selective surface wall. IEEE Antennas Wirel Propag Lett 16:373–376. https://doi.org/10.1109/LAWP.2016.2578179
13. Yan J, Bernhard JT (2012) Design of a MIMO dielectric resonator antenna for LTE femtocell base stations. IEEE Trans Antennas Propag 60(2):438–444. https://doi.org/10.1109/TAP.2011.2174021
14. Zou L, Abbott D, Fumeaux C (2012) Omnidirectional cylindrical dielectric resonator antenna with dual polarization. IEEE Trans Antennas Propag 60(2):438–444. https://doi.org/10.1109/LAWP.2012.2199277
15. He Y, Liu T, Du X, Wu W (2016) The design of a tripolarization rectangle dielectric resonator antenna. In: 2016 10th European conference on antennas and propagation (EuCAP), 2016, pp 1–3. doi:https://doi.org/10.1109/EuCAP.2016.7481834
16. Ahmad Abdalrazik, Anwer S. Abd El-Hameed, Adel B. Abdel-Rahman: A Three-Port MIMO Dielectric Resonator Antenna Using Decoupled Modes. In: IEEE Antennas and Wireless Propagation Letters, vol. 16, pp. 3104–3107, 2017. doi:https://doi.org/10.1109/LAWP.2017.2763426
17. Dadgarpour A, Zarghooni B, Virdee BS, Denidni TA, Kishk AA (2017) Mutual coupling reduction in dielectric resonator antennas using metasurface shield for 60-GHz MIMO systems. IEEE Antennas Wirel Propag Lett 16:477–480. https://doi.org/10.1109/LAWP.2016.2585127
18. Huitema L, Koubeissi M, Mouhamadou M, Arnaud E, Decroze C, Monediere T (2011) Compact and multiband dielectric resonator antenna with pattern diversity for multistandard mobile handheld devices. IEEE Trans Antennas Propag 59(11):4201–4208. https://doi.org/10.1109/TAP.2011.2164183
19. Tian R, Plicanic V, Lau BK, Ying Z (2010) A compact six-port dielectric resonator antenna array: MIMO channel measurements and performance analysis. IEEE Trans Antennas Propag 58(4):1369–1379. https://doi.org/10.1109/TAP.2010.2041174
20. Yan JB, Bernhard JT (2013) Implementation of a frequency-agile MIMO dielectric resonator antenna. IEEE Trans Antennas Propag 61(7):3434–3441. https://doi.org/10.1109/TAP.2013.2255092
21. Dixit AS, Kumar S (2020) The enhanced gain and cost-e_ective antipodal Vivaldi antenna for 5G communication applications. Microw Opt Technol Lett 62:2365–2374. https://doi.org/10.1002/mop.32335
22. Dixit AS, Kumar S (2020) A survey of performance enhancement techniques of antipodal Vivaldi antenna. IEEE Access 8:45774–45796. https://doi.org/10.1109/ACCESS.2020.2977167

Comparative Study of CMOS and FinFET-Based SRAM Cell Using SVL Technique

Deepika Sharma and Shilpi Birla

Abstract The data stability issues in SRAM cells become more prominent with the decreasing of feature sizes in CMOS technology. The focus of memory manufacturers always remains on reducing power consumption and stability improvements of the SRAM cells. In this work, the critical parameters of FinFET and CMOS transistors based on SRAM cells are compared. This paper focuses on the simulation of 10T SRAM cell topologies design using sleep transistor, drowsy cache, and self-controllable voltage technique (SVL) techniques and their comparison. Among all these techniques, SVL shows the best results by consuming 4768 nw power for FinFET technology and 15.8383 n W power for CMOS technology. Evaluated results show 40%, 26%, and 10% improvement in HSNM, RSNM, and WSNM, respectively, and 80.93% reduction in leakage power. FinFET design SRAM cells result in higher RSNM, HSNM, and WSNM. For simulation, the HSPICE tool is used at 32 nm PTM CMOS and FinFET transistor with a supply voltage of 900 mV and 25 °C temperature.

Keywords SVL · SNM · Power · 10T SRAM · FinFET

1 Introduction

In today's worlds, the key design challenges are proper optimization of power for battery-operated devices and portable electronic gadgets. For circuit manufacturers, there are two conflict requirements. The first requirement for portability is keeping power at minimum, and the second requirement is high functionality and speed. Nowadays, most of the chips and microprocessors use SRAMs and it covers a large amount of space and power of chips [1]. Therefore for low power design, it is necessary to reduce the power of the SRAM cells [2]. Among various methods proposed by the researchers for low power voltage scaling are mostly used. From the relation of power and supply voltage, it is known that power can vary with supply. In voltage

D. Sharma (✉) · S. Birla
Manipal University, Jaipur, India
e-mail: deepikajhalani92@gmail.com

D. K. Sharma et al. (eds.), *Micro-Electronics and Telecommunication Engineering*,
Lecture Notes in Networks and Systems 179,
https://doi.org/10.1007/978-981-33-4687-1_2

scaling method, power is reduced by scaling of voltage [3–5]. The supply can also be applied below the threshold voltage [6].

In conventional 6T SRAM cells due to aggressive scaling of features size, several issues like stability and performance occurred. Therefore, to eliminate the problems occur in 6T SRAM cells transistors increased and new cells formed. To reduce the power in standby region, several techniques such as MTCMOS and VTCMOS have been proposed [7–10]. These techniques decrease leakage power but there are various drawbacks with the use of these techniques such as large area and power penalty. The purpose of this study is to design an improved novel 10T SRAM cell in 32 nm CMOS and FinFET technology which can perform read/write operations. Figure 1 represents the flowchart of proposed work having the main focus of research work in designing low power and improved stability SRAM cell.

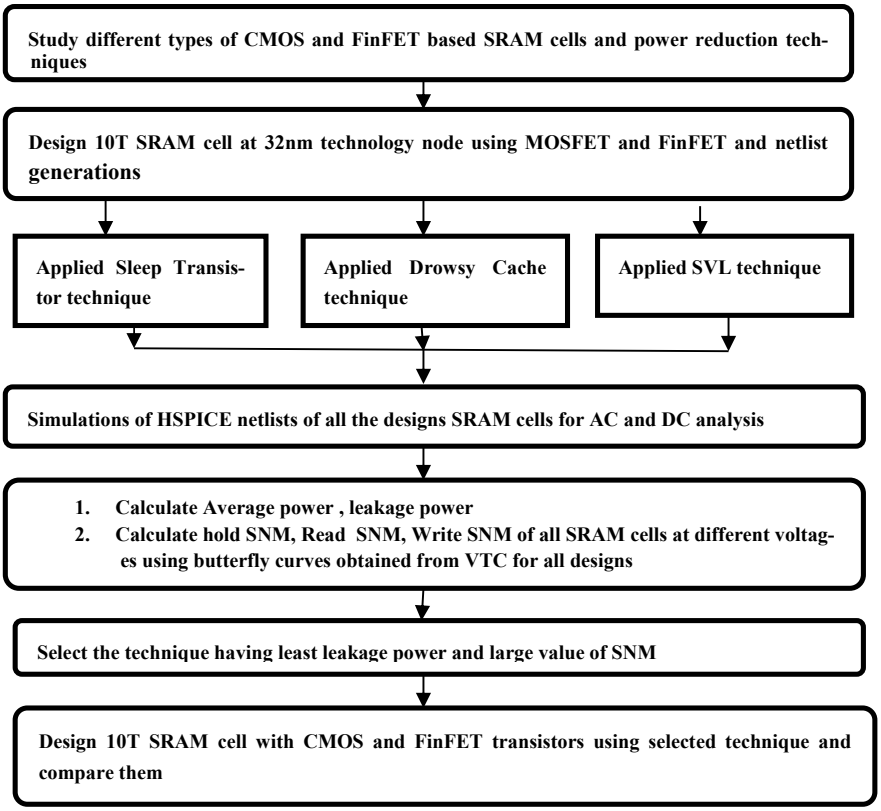

Fig. 1 Flowcharts of proposed work

2 Basics SRAM Models

This section includes the design of basic SRAM models such as conventional and sleep transistor-based 10T SRAM cell using CMOS and FinFET technology are discussed.

2.1 Conventional 10T SRAM Model

Read operation. Before initiating this operation, bitlines (BL and BLB) and wordline (WL) are maintained at VDD. Write-wordline (WWL) is pulled down to the ground to turn off the read path through the M6 and M5 transistors [11–13]. Storage nodes are disconnecting from bit lines with the turn off of M5 and M6 transistor to prevent bit line interference. During this operation, the M8 and M7 transistors behave like as read buffers. For example, if Q stored data 1, then the read operation is performed such that the M9 and M10 transistors are ON and the M5 and M6 transistors OFF. As the Q stored 1, the M8 transistor will be ON for a correct read operation and BL will be discharged through the M10-M8 transistor.

Write operation. During this operation, both wordlines (WL and WWL) are charged with VDD. In order to maintain good writeability, WWL keeps higher than VDD. For the transfer of data from bitlines to nodes, two access transistors are connected on both sides which should be ON [14]. Before writing 1 at node Q, BL is kept to VDD and BLB kept at 0 V. During write "0", the bitline is maintained at ground and bitlinebar is kept at VDD. Figures 2 and 3 represent the existing cells.

3 Research Method

3.1 Sleep Transistor Technique

In this technique, a NMOS and PMOS switch are connected between upper and lower parts of the SRAM cell. A PMOS switch is connected between supply and cell, whereas the NMOS switch is connected between cell and GND [16–20]. During read and write operations, both switches are forced to be ON by using signals (S and SD), and in hold operations, they are forced to be OFF. Because of the path between VDD and GND during active mode, there is no change in operations. During sleep mode, there is no connection of power supply and cell creating virtual VDD and GND path. The signal S and SD are set to 1 V and 0 V for active mode and vice versa for hold mode. The reduction in output voltage is reduced from VDD to (VDD-Vth) in hold; operations cause a further reduction in leakage currents and power.

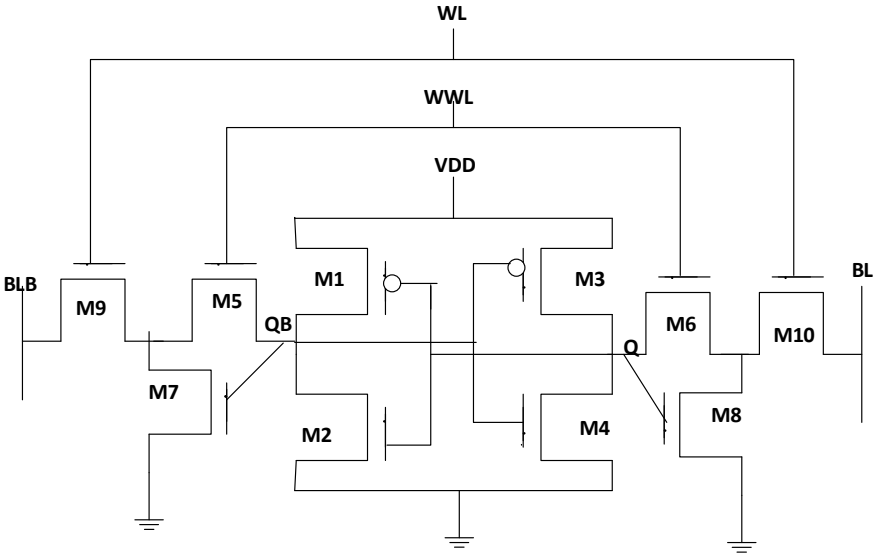

Fig. 2 CMOS-based cell [15]

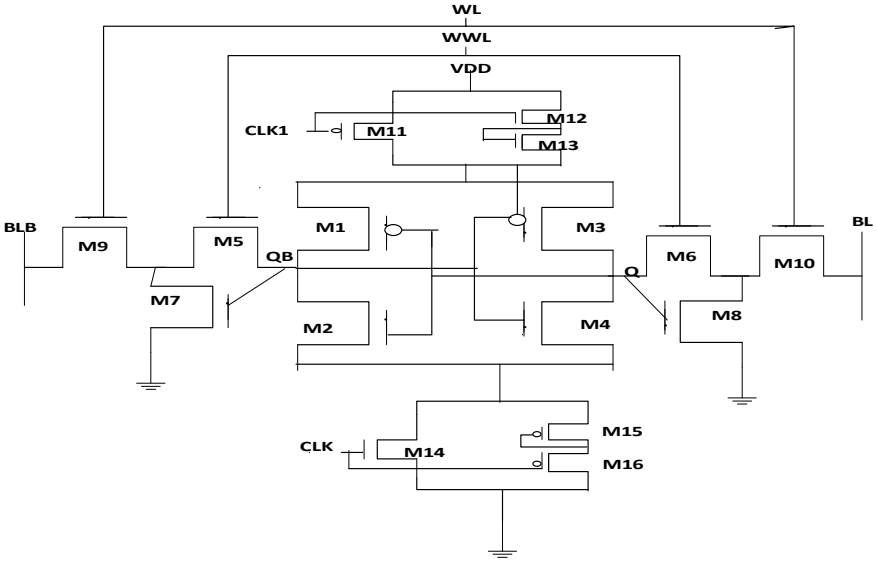

Fig. 3 10T CMOS-based SRAM cell using SVL technique

3.2 Drowsy Cache Technique

In this method, two types of supply voltages are used in active and sleep modes. In sleep mode, half of the supply voltage (VDD/2) is used, whereas in active mode high supply voltage (VDD) is preferred. In sleep mode, reduction in the supply causes reduction in leakage and thus provides an improvement in performance and reduction in static power dissipation [20]. In the active mode of operation, M11 transistor provides the supply as VDD while in hold mode M12 transistor maintained it at VDD/2.

3.3 Self-controllable Voltage Technique

Among all the low power techniques SVL provides the least power. Power is calculated by combining the upper and lower parts of the circuit. An upper circuit known as USVL (upper SVL) consists of series connection of two (NMOS) transistors M12 and M13 in parallel with one (PMOS) M11. The same connection is formed for lower circuit known as LSVL (lower SVL) by making some small changes replacing of NMOS transistor with PMOS and vice-versa. Both the upper and lower parts are connected with supply and ground. USVL and LSVL combine reduced leakage in the cell [21]. As seen in Figs. 4 and 5, the clock signal clk is kept high, whereas the clk1 is kept low in active mode and vice-versa in hold mode. The function of the USVL circuit is to keep the supply lower than the actual supply. The purpose of the LSVL circuit is to increases the GND value from the original value [14, 22, 23]. This results in a reduction in the value of overall voltage and leakage power.

4 Results and Analysis

The existing and proposed bit cells have been simulated for a supply voltage from 200 to 900 mv.

4.1 Hold SNM

It can be seen from the graph that the HSNM of CMOS and FinFET design cell is 220 mV and 320 mV, respectively, @ VDD = 900 mV. So we can conclude that proposed FinFET design cell offers improvements in HSNM in comparison with CMOS.

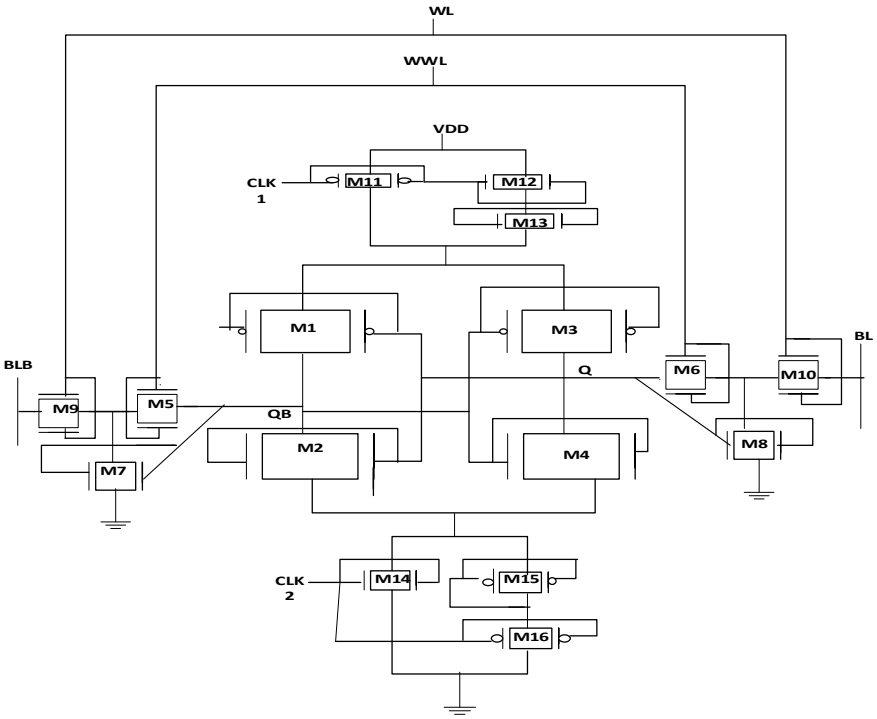

Fig. 4 10T FinFET-based SRAM cell using SVL Technique

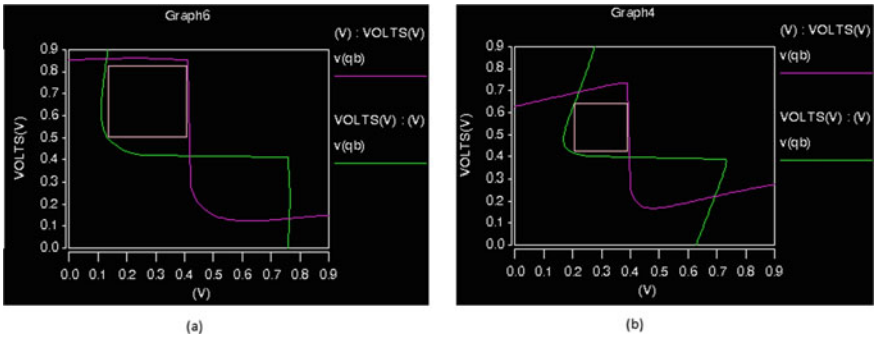

Fig. 5 Hold SNM of cell **a** FinFET **b** CMOS

4.2 Read SNM

It is more prone to disturbance in the cell. Figure 6 shows that RSNM of CMOS and FinFET design cell is 360 mV and 380 mV, respectively, @ VDD = 900 mV.

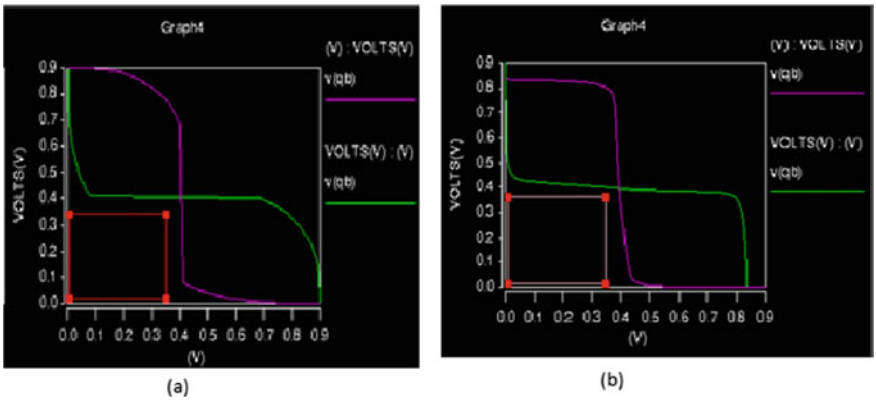

Fig. 6 Read SNM of cell **a** FinFET **b** CMOS

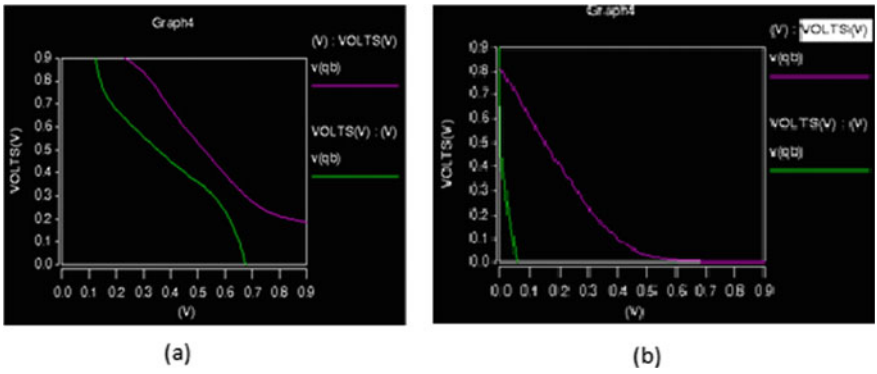

Fig. 7 Write SNM of cell **a** CMOS **b** FinFET

4.3 Write SNM

It is the capability to write "0" when node storing "1" and to write "1" when node storing "0" in the cell. The butterfly curve for both CMOS and FinFET at VDD = 900 mV. There is an improvement in SNM for FinFET design cell (Fig. 7).

4.4 Static Power Dissipation

The existing and proposed bit cells have been simulated for a supply voltage of 200–900mv. Table 1 shows that proposed cell having less power consumption from existing ones.

Table 1 Static power analysis

Parameter	Existing techniques				Proposed techniques	
Supply voltage (mv)	CMOS SRAM	FinFET SRAM	CMOS SRAM using sleep transistor technique	FinFET SRAM using sleep transistor technique	CMOS SRAM using SVL technique	FinFET SRAM using SVL technique
900	34.4585 uW	16.5592 nW	16.4836 nW	7.7448 nW	15.8383 nW	1.4768 nW
800	21.9411 uW	12.2207 nW	12.2446 nW	3.7563 nW	11.5626 nW	840.7311 pW
700	12.8689 uW	8.7420 nW	1.7544 nW	1.8101 nW	8.1805 nW	480.3579 pW
600	5.9319 uW	6.0069 nW	1.2596 nW	857.3134 pW	5.5596 nW	272.9018 pW
500	1.7240 uW	3.9100 nW	859.9792 pW	395.2036 pW	3.5803 nW	151.8647 pW
400	264.3335 nW	2.3565 nW	546.7171 pW	175.3316 pW	2.1354 nW	81.2259 pW
300	24.3040 nW	1.2612 nW	311.5105 pW	72.9579 pW	1.1520 nW	40.5329 pW
200	1.5361 nW	548.2671 pW	146.8124 pW	26.9760 pW	534.1768 pW	17.7137 pW

5 Conclusion

The paper postulates a new 10T-SRAM cell with betterment in read–write margins and less power consumption. Results signify that the SVL technique provides efficient stability for both devices. FinFET design SRAM cell is more stable than CMOS. The SVL technique reduces static power dissipation by 80.93% as compared to the sleep transistor technique. As the transistors become more in the cell, area and delay increase significantly with less static power. In future by using this SVL circuit, many SRAM cells can be designed which can work on reduced power and find usage in ultra-low power applications.

References

1. Vittoz E, Fellrath J (1977) CMOS analog integrated circuits based on weak inversion operation. IEEE J Solid-State Circ 12(3):224–231
2. Chandrakasan AP, Sheng S, Brodersen RW (1992) Low-power CMOS digital design. IEEE J Solid-State Circ 27(4):473–484
3. Mutoh S, Douseki T, Matsuya Y, Aoki T, Shigematsu S, Yamada J(1995) 1-V power supply high-speed digital circuit technology with multi-threshold-voltage CMOS. IEEE J Solid-State Circ 847–854
4. Verma N, Chandrakasan AP (2007) A 65 nm 8T Sub-Vt SRAM employing sense-amplifier redundancy. In: Proceedings of IEEE ISSCC digest of technical papers, pp 328–606
5. Kim TH, Liu J, Keane J, Kim CH (2007) A high-density subthreshold SRAM with data-independent bitline leakage and virtual-ground replica scheme. In: Proceedings of IEEE ISSCC digest of technical papers, pp 330–606
6. Bhavnagarwala AJ, Kosonocky S, Radens C, Chan Y, Stawiasz K, Srinivasan U, Kowalczyk SP, Ziegler MM (2008) A sub-600 mV, fluctuation tolerant 65-nm CMOS SRAM array with dynamic cell biasing. IEEE J Solid-State Circ 43(4):946–955
7. Carlson AE (2008) Device and circuit techniques for reducing variation in nanoscale SRAM. Ph.D. dissertation, University California Berkeley, Berkeley, CA
8. Vaddi R, Dasgupta S, Agarwal RP (2010) Device and circuit co-design robustness studies in the subthreshold logic for ultralow-power applications for 32 nm CMOS. IEEE Trans. Electron Devices 57(3):654–664
9. Islam A, Hasan M (2012) Leakage characterization of 10T SRAM cell. IEEE Trans Electron Devices 59(3):631–638
10. Priya MG, Baskaran K, Krishnaveni D (2012) Leakage power reduction techniques in deep submicron technologies for VLSI applications 1163–1170
11. Sathishkumar A, Saravanan S (2014) Analysis and design of low power high speed dynamic latch comparator using CMOS. Int J Sci Eng Res 5(5):173–177
12. Pal S, Bhattacharya A, Islam A (2014) Comparative study of CMOS- and FinFET-based10T SRAM cell in subthreshold regime. In: IEEE international conference on advanced communication control and computing technologies (ICACCCT)
13. Gupta V, Khandelwal S, Raj B, Gupta RD (2015) Leakage current reduction in FinFET based 6T SRAM cell for minimizing power dissipation in nanoscale memories. In: 2015 IEEE Nirma University international conference on engineering
14. Sneha G, Krishna BH, Kumar CA (2017) Design of 7T FinFET based SRAM cell design for nanometer regime. In: International conference on inventive systems and control
15. Hosseini-Salekdeh SR (2016) A comparative analysis of 6T and 10T SRAM cells for sub-threshold operation in 65nm CMOS technology. M.Sc thesis, Waterloo, Ontario, Canada

16. Venugopal K, Babu PS (2015) Low power SRAM cell of leakage current and leakage power reduction. Int J Sci Eng Technol Res (IJSETR) 4(8)
17. VR Member, Saravanakumar M (2016) Design and analysis of SRAM cells for power reduction using low power techniques. In: IEEE region 10 conference (TENCON), proceedings of the international conference
18. Ruhil S, Shukla NK (2017) Leakage current optimization in 9T SRAM bit-cell with sleep transistor at 45nm CMOS technology. In: International conference on computing and communication technologies for smart nation (IC3TSN)
19. Mishra JK, Srivastava H (2018) A 40nm low power high stable SRAM cell using separate read port and sleep transistor methodology. In: IEEE international symposium on smart electronic systems
20. Madhumalini M, Iyshvarya R (2019) Design of low power SRAM cell using 10transistors. J VLSI Design Sign Process 37–44
21. Maute JM, Puebla VK, Nericua RT, Gerasta OJ, Hora JA (2018) Design implementation of 10T static random access memory cell using stacked transistors for power dissipation reduction. IEEE
22. Badran MS, Issa HH, Eisa SM, Ragai HF (2018) Low power 7 nm FinFET based 6T-SRAM design. J Adv Res Appl Mech
23. Jaiswal K, Saxena S (2017) A review on FinFET based SRAM design for low power applications. Int J Technol Res Manage

Capacity Evaluation and Analysis of Long Range for IoT

Asmita Singh, Abhishek Tyagi, and Sindhu Hak Gupta

Abstract Internet of Things(IoT) thought is growing in the past few years, and the range of IoT devices is increasing apace. With the advancement of wireless networks, the evolution of cutting-edge data analytics and the decline in the outlay of connected devices, there is a rise in cloud platform adoption, and the market is anticipated to evolve at a positive pace. LoRaWAN is the progressive evolved technology that is anticipated as it holds up a large sector of the billions of approximated IoT. This paper focuses on the network QoS by analyzing the signal quality and channel capacity on the different configuration settings of LoRa. The simulated result demonstrates the utmost combination to achieve maximum channel capacity, SNR, and minimum bit error rate irrespective of the spreading factor, code rate, and bandwidth. Result demonstrates that there are approx. 27.21% more nodes can be active at SF-7 concerning SF-12 and concludes that capacity deteriorates as the SF increases which further concludes that link quality is 27.1% averagely superior in SF-7 region that the SF-12.

Keywords Code rate · Internet of Things(IoT) · LoRaWAN · Channel capacity · Spreading factor

1 Introduction

Internet of Things is an emerging technology, and it does not require building a brand-new infrastructure. It primarily uses the basic structure consisting of sensor networks,

A. Singh (✉) · A. Tyagi · S. H. Gupta
Department of Electronics and Communication Engineering, ASET, Amity University, Uttar Pradesh, Noida 201313, India
e-mail: asmita.singh1630@gmail.com

A. Tyagi
e-mail: tyagiabhishek043@gmail.com

S. H. Gupta
e-mail: shak@amity.edu

D. K. Sharma et al. (eds.), *Micro-Electronics and Telecommunication Engineering*,
Lecture Notes in Networks and Systems 179,
https://doi.org/10.1007/978-981-33-4687-1_3

communication technologies, cloud computing, big data analytics, and embedded system [1]. The pace of IoT integrates with nearly all industries and conforms to user needs and the evolving new technology IoT among the eminent base or pillar, because of the existence of millions and millions of users or end devices which are increasing and increasing rapidly. One of the major constraints of IoT is its energy of sensor nodes. Servers are also overloaded as billions and billions of devices are connected to it which leads to casting effect on the link or network capacity, and thus we need to optimize accordingly [2]. Capacity evaluation is very important for the proper functioning of IoT [3].

There were enormous technologies with its all merits and drawbacks as one is not capable of fitting in every circumstance and scenario. Each shows their superiority compared to others with different aspects, and according to the requirement, it will be best for the environment. Presently, WiFi is one of the appealed technologies for communicating long distance, whereas Bluetooth and ZigBee are some of the techs for shorter distance and preferred in IoTs. These technologies also are battery consuming and thus then LoRa introduced which have the features of low cost, smart city, industries, and secure bidirectional [4].

As our classic well-established cellular network (2G, 3G, 4G) is built for high data throughput but optimization of energy is challenging, thus small data for transmission is not a good option and LoRa in this empower these technologies by consuming less power.

Similarly, WiFi (wireless fidelity) is restricted to a small area for communication and also considers to be less secure when large data are flooded, and it cannot be distinguished and received by the wrong receiver. LoRa is a technology that maintains quality of service (QoS) and considered to be safe due to its double AES encryption [5]. LoRa also works on chirp spread spectrum (CSS) defiant toward multipath fading.

Also, ZigBee communicates over a small distance and works on high-level communication protocol works on mesh networks, and transmitting to a distant node is done by multiple hops which are power-consuming [6]. LoRa on the other hand works on a star topology and thus no hop is likely to be needed and thus takes less power.

Previous technologies like the Internet and mobile communication had heavy traffic in its network, and now IoT is also playing a major role. Thus, IoT assigns to the worldwide network (WWW) of the linked nodes merely located, which is dependent on the common protocols related to the communication.

LoRaWAN technology due to its characteristic of energy constraints and high data throughput is trending in research studies which includes performance and characteristic analysis with simulation tools and mathematical approach [7]. The author focuses on the packet loss ratio, coverage range, and the impact of the communication link of various modulation parameters [8]. The work done on capacity analysis of LoRaWAN is based on the payload size of applications and the rate of message generation from end devices [9]. The author also focuses that the capacity will decrease when to end devices are farther and SF will increase.

Also, there is a paper which broadly focuses on how RSSI impacts the capacity of LoRaWAN based on non-destructive awareness [10]. Existing work is communicated to analyze the capacity but channel capacity was not the prime objective.

This paper focuses on the capacity evaluation, i.e., amount of traffic the network can employ at a particular time, modifying different combinations of LoRa, theoretically the maximum capacity is gained by synchronization, and number of end devices which will be supported by 6 SF of networks in cell area maintaining the quality of coverage needed [11]. Maximum capacity leads to the addition of nodes, and maximum SNR represents better signal quality and low noise.

Further sections will include highlights of LoRaWAN and their frequency range and range suitable for Indian scenario and the impact of spreading factor and code rate on capacity and how these factors are related to each other.

2 LoRa (Long Range)

LoRaWAN is standardized by the Lora alliance and is a MAC protocol designed to operate wirelessly, i.e., IoT devices.

For the rural area, it ranges between 35 and 45 km, whereas in urban areas it ranges up to 5 km [2]. Low-power wide area (LPWA) provides a balance between battery-efficient communication and long distance at the cost of throughput. LoRa is one of the most popular technologies among the other technologies as it works on an unlicensed spectrum which makes it cost effective, and long battery lifespan is an additive advantage to be an optimum choice for day-to-day applications.

LoRa technique is patent by Semtech Corporation and is a type of modulation technology that helps in transferring the information over the large area having a small value of the transfer rate [12]. For efficiency improvement and capacity increment, it introduces six orthogonal spreading factors: SF 7, SF 8, SF 9, SF 10, SF 11, and SF 12 which results in different data rates. LoRa networks are extremely flexible as they are capable of tuning their transmission parameters of devices. It provides an optimum global configuration that provides proper utilization of channel bandwidth, and thus maximum throughput is achieved. LoRa is considered to be best for IoT applications as its data rates range up to 50 kbps and lifetime is approximately 10 years.

3 System Model (LoRaWAN)

This section focuses on the capacity evaluation of LoRa. LoRaWAN is open standard MAC protocol allows SF from 7 to 12 with code rate 4/5 to 4/8. Because of its low receiver sensitivity, it communicates to the long range. Therefore, multiple end devices can communicate with a long-distance deployed gateway.

For the current scenario, it is assumed that the bandwidth is represented by ‘BW’, the spreading factor is represented as ‘SF’, and the code rate of the system is ‘CR’.

The signal-to-noise ratio (SNR) of the link is dependent on the spreading factor, code rate, and bandwidth. Link quality gets better as the SNR improves.

$$\text{SNR} = \frac{E_\text{b}}{N_0} * sf * \frac{\text{BW}}{2^{sf}} * \frac{4}{4+\text{CR}} \tag{1}$$

The second parameter of the LoRa is the bit error rate (BER) which helps in getting the better performance of the LoRa:

$$\text{BER} = \left(\frac{1}{\frac{E_\text{b}}{N_0} * sf * \frac{\text{BW}}{2^{sf}} * \frac{4}{4+\text{CR}}} \right)^{\text{K}} \tag{2}$$

Network capacity refers to when maximum messages can transmit from nodes to Lora gateway. Signals in LoRa networks are orthogonal to each other when the spreading factor varies 7–12, which results in a change in data rates and thus gateway is capable of receiving respective data rates on the same channel.

$$C = \text{BW} * \log_2 \left(1 + \left(\frac{E_\text{b}}{N_0} * sf * \frac{\text{BW}}{2^{sf}} * \frac{4}{4+\text{CR}} \right) \right) \tag{3}$$

Above Equation depicts that capacity of the channel is dependent on the bandwidth of spectrum, spreading factor, and noise figure. Out of these parameters, the noise figure is a constrained parameter. Bandwidth is fixed for every technology, i.e., 125 kHz. The spread factor is a free parameter that ranges between 4 and 256 (downlink) and range extends to 512 for uplink. According to the LoRaWAN specifications, spreading factor is restricted to six exclusive spreading factors states that up to six nodes can transmit in the same channel simultaneously. For this scenario, SF ranges from 7 to 12. The code rate is also a free parameter and can be in various ranges depending on the addition of forward error correction (FEC) in data transmission. In this scenario, 4-bit data encoding with 5–8-bit redundancies is implemented.

Further in the upcoming section, capacity is evaluated with the help of a simulative tool with the corresponding parameters.

4 Simulated Results

The simulation is achieved with the aid of MATLAB. Theoretically perfect synchronization and node scheduling lead to maximum capacity. The accumulated capacity of the LoRaWAN end device(Gateway) is calculated as the number of end devices by all SF while maintaining the quality of service requirement.

Channel capacity is one of the important factors as the capacity increases, and the network can be more scalable, where more devices can be active and applications can run. There is the inverse relationship between the capacity of the network and the spreading factor, i.e., capacity of the network decreases as the spreading factor

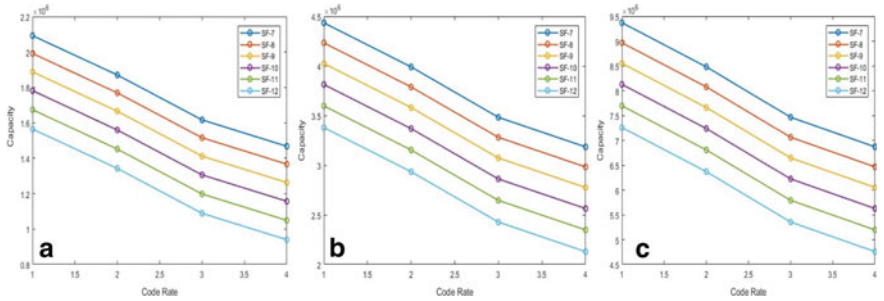

Fig. 1 Capacity vs code rate at **a** BW = 125 kHz **b** BW = 250 kHz **c** BW = 500 kHz

increases. The redundancies in the packet were added to enable error-free transmission, whereas after analyzing the result the channel capacity deteriorates as the redundancies were increased.

Figure 1 represents the effect of coding rate and spreading factor on the capacity of the channel. The maximum channel capacity at the code rate 4/5 got a drastic drop between 4/7 and 4/6. Spreading factor 7 upholds the maximum capacity in comparison to SF = 12.

Table 1 depicts the capacity achieved at the respective configuration for bandwidth 125 kHz, 250 kHz, and 500 kHz. There is approximately 27.21% degradation in channel capacity which is found as the spreading factor increases irrespective of bandwidth for code rate-4/5.

With the help of Fig. 2, there is the comparison between the link quality which is measured in terms of signal-to-noise ratio at the different values of spreading factors (SF) 7, 8, 9, 10, 11, and 12 with respect to CR. Spreading factor 7 shows the better resultant output as the transmission time is less in comparison with other SF.

Table 2 depicts that at SF = 7, which represents the nearer the end device from the gateway, the better the communication established. The maximum value is determined at the 4/5 code rate, when encoding data are 4 and the redundant bit is 5, increasing bit leads to degraded signal. Average 27.12% of the link quality fades as the signal is reaching toward SF-12.

Table 1 Maximum capacity achieved at CR-4/5

Spreading Factor	Capacity (bits/sec/kHz)		
	BW-125 kHz	BW-250 kHz	BW-500 kHz
7	**2.09×10^6**	**4.43×10^6**	**9.36×10^6**
8	1.99×10^6	4.23×10^6	8.96×10^6
9	1.88×10^6	4.02×10^6	8.55×10^6
10	1.78×10^6	3.81×10^6	8.12×10^6
11	1.67×10^6	3.59×10^6	7.69×10^6
12	1.56×10^6	3.37×10^6	7.25×10^6

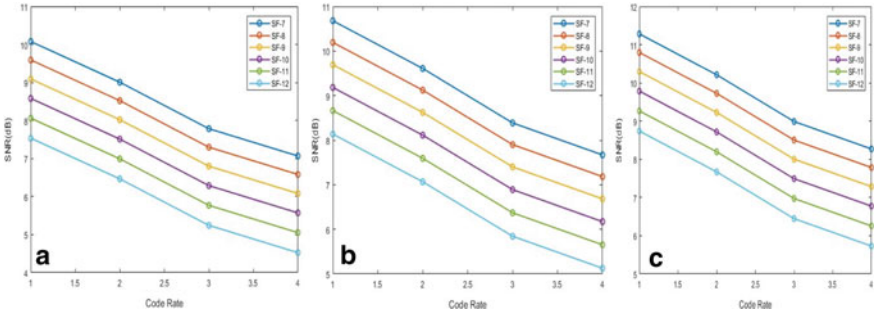

Fig. 2 SNR versus code rate at **a** BW = 125 kHz **b** BW = 250 kHz **c** BW = 500 kHz

Table 2 Maximum SNR achieved at CR-4/5

Spreading Factor	SNR (dB)		
	BW-125 kHz	BW-250 kHz	BW-500 kHz
7	**10.07**	**10.67**	**11.28**
8	9.59	10.19	10.79
9	9.09	9.69	10.29
10	8.58	9.18	9.78
11	8.06	8.66	9.26
12	7.53	8.13	8.73

The capacity of the channel will increase as SNR increases. Spreading factor 7 has the maximum SNR compared to SF = 12. As SNR represents the signal-to-noise ratio and as much the SNR is high, the channel has the least noise and maximum signal. The bit error rate is dependent on SNR, and as SNR of a signal increases then the BER decreases which leads to the better efficiency of the channel.

In Fig. 3, there is a comparison between the different values of BER, $\frac{E_b}{N_0}$ at the different values of spreading factor (SF) 7, 8, 9, 10, 11, and 12. With the help of this, we find out that at the SF = 7, the LoRa modulation works better than others. Minimum BER achieved is at bandwidth 500 kHz and CR-4/5 at which signal has the highest SNR showed in Table 3.

5 Conclusion

To get the best solution of parameters with SF = 7 to SF = 12 with code rate 4/5, 4/6, 4/7, 4/8 at bandwidth 125 kHz, SF = 7 and SF = 8 represent the best output as it reaches the maximum capacity level, whereas the code rate 4/5 outshined compared to the 4/8 code rate. As discussed in LoRaWAN finding, spreading factor which works better as to control SF so that communication occurs at different levels by

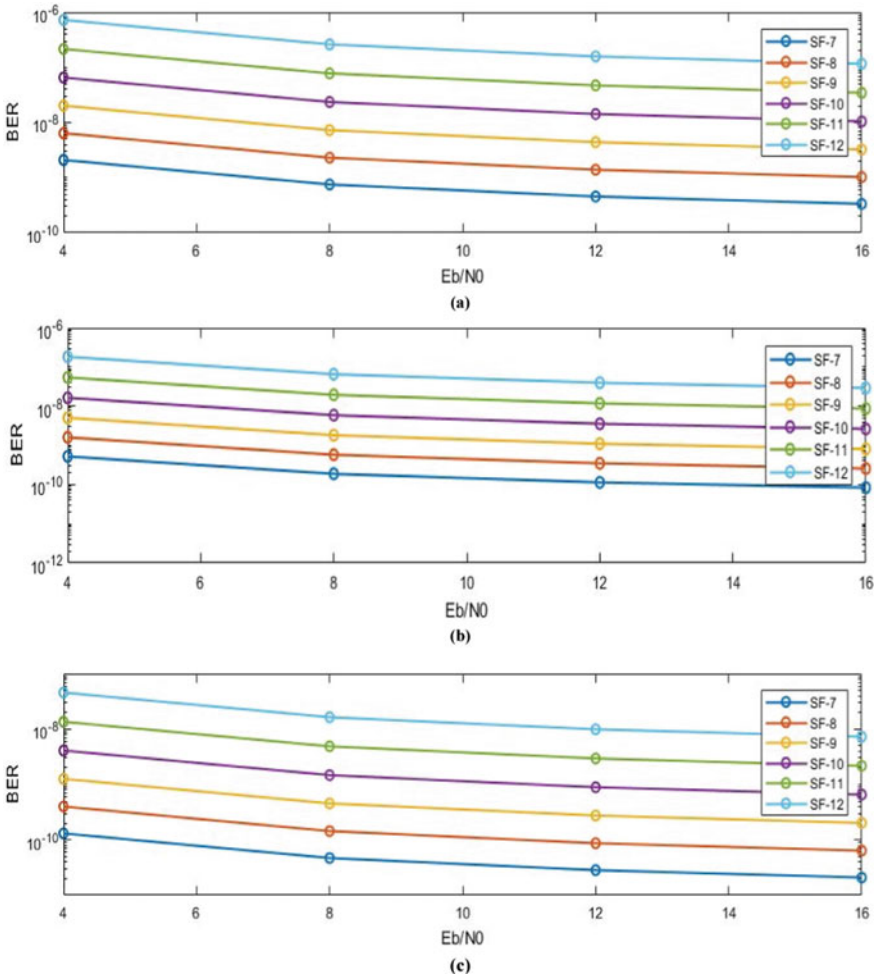

Fig. 3 BER versus Eb/No at **a** BW = 125 kHz **b** BW = 250 kHz **c** BW = 500 kHz

Table 3 Minimum bit error rate achieved at BW-500 kHz

Spreading factor	Bit error rate		
	BW-125 kHz	BW-250 kHz	BW-500 kHz
7	0.0334×10^{-8}	0.0053×10^{-8}	0.0209×10^{-9}
8	0.1024×10^{-8}	0.0016×10^{-7}	0.0640×10^{-9}
9	0.0324×10^{-7}	0.0052×10^{-7}	0.0202×10^{-8}
10	0.1049×10^{-7}	0.0017×10^{-6}	0.0655×10^{-8}
11	0.0347×10^{-6}	0.0055×10^{-6}	0.0217×10^{-7}
12	0.1165×10^{-6}	0.0019×10^{-5}	0.0728×10^{-7}

setting virtual channels and simultaneously message can be received and maintains the quality of service. The simulated result ensures that the signal quality deteriorates by approximately 27.1% as SF increases for CR-4/5 irrespective of bandwidth. The maximum number of end devices that are connected wirelessly to a particular BS or gateway collision must be avoided to drop in the number of packets. As by increasing the traffic or end devices in the network in future, it will increase the collision rate and decrease in throughput so for the increasing traffic it requires greater capacity and thus higher value of spreading factor allows longer-range transmission but smaller spreading factor more device to transmit, and in this paper, we are customizing each spreading factor with respect to code rate to maximize the network. Average 27.21% more nodes can be deployed irrespective of bandwidth in SF-7 than SF-12.

Future scope lies by optimizing the channel capacity to deploy more number of nodes and subscribers be added in the network, improving link quality by improvising SNR and reducing BER.

References

1. Polak L, Milos J (2020) Performance analysis of LoRa in the 2.4 GHz ISM band: coexistence issues with Wi-Fi. Telecommunication Systems, 1–11
2. Nurgaliyev M, Saymbetov A, Yashchyshyn Y, Kuttybay N, Tukymbekov D (2020) Prediction of energy consumption for LoRa based wireless sensors network. Wirel Netw 1–14
3. Bhatter S, Verma A, Sinha S (2020) Application of IoT in predictive maintenance using long-range communication (LoRa). Innovation in electrical power engineering, communication, and computing technology. Springer, Singapore, pp 147–155
4. Židek K, Piteľ J, Lazorík P (2020) IoT system with switchable GSM, LoRaWAN, and sigfox communication technology for reliable data collection to open-source or industrial cloud platforms. New approaches in management of smart manufacturing systems. Springer, Cham, pp 311–333
5. Singh D, Aliu OG, Kretschmer M (2018) LoRa WanEvaluation for IoT communications. In: 2018 international conference on advances in computing, communications and informatics (ICACCI). IEEE, pp 163–171
6. Gambiroža JČ, Mastelić T, Šolić P, Čagalj M (2019) Capacity in LoRaWAN networks: challenges and opportunities. In: 2019 4th international conference on smart and sustainable technologies (SpliTech). IEEE, pp 1–6
7. Ali IT, Sari RF (2018) Research opportunities of LoRaWAN for internet of things implementation. In: 2018 2nd international conference on applied electromagnetic technology (AEMT). IEEE, pp 61–66
8. Ikpehai A, Adebisi B, Rabie KM, Anoh K, Ande RE, Hammoudeh M, Gacanin H, Mbanaso UM (2018) Low-power wide area network technologies for internet-of-things: a comparative review. IEEE IoT J 6(2):2225–2240
9. Infso D (2008) Networked enterprise and RFID INFSO G. 2 micro and nanosystems, in co-operation with the working group RFID of the ETP EPOSS, Internet of Things in 2020, roadmap for the future. Information Society and Media, technical report
10. Magrin D, Capuzzo M, Zanella A (2019) A thorough study of LoRaWAN performance under different parameter settings. IEEE IoT J
11. Gupta V, Devar SK, Kumar NH, Bagadi KP (2017) Modelling of IoT traffic and its impact on LoRaWAN. In: GLOBECOM 2017–2017 IEEE global communications conference. IEEE, pp 1–6

12. Fernandes R, Oliveira R, Luís M, Sargento S (2019) On the real capacity of LoRa networks: the impact of non-destructive communications. IEEE Commun Lett 23(12):2437–2441
13. Oukessou Y, Baslam M, Oukessou M (2018) LPWAN IEEE 802.11 ah and LoRaWAN capacity simulation analysis comparison using NS-3. In: 2018 4th international conference on optimization and applications (ICOA). IEEE, pp 1–4
14. Devalal S, Karthikeyan A (2018) LoRa technology-an overview. In: 2018 2nd international conference on electronics, communication and aerospace technology (ICECA). IEEE, pp 284–290
15. Dalela PK, Sachdev S, Tyagi V (2019) LoRaWAN network capacity for practical network planning in India. In: 2019 URSI Asia-Pacific radio science conference (AP-RASC). IEEE, pp 1–4
16. El-Aasser M, Elshabrawy T, Ashour M (2018) Joint spreading factor and coding rate assignment in Lorawan networks. In: 2018 IEEE global conference on Internet of Things (GCIoT). IEEE, pp 1–7
17. NASSCOM (2017) IoT: Landscape and Nasscom Initiatives

VLSI Implementation of PN Sequence Generator Using Two Different Multiplication Algorithms

Vaibhav Chaudhari, Surbhi Rathore, Aakash Gadge, and V. S. Kanchana Bhaaskaran

Abstract Wireless communication system plays an essential role in data transmission system. In wireless systems like satellite network, mobile communication, or any data transmitted network, a specified band is allotted. Such network has its own specified allotted spectrum for secure communication. Safe data transmission and reception are important and difficult tasks. Such data transmission needs some secure techniques to transmit data securely, and one such technique is hiding the transmission data or hiding the message signals. To provide security to message signal, random noise is added through pseudo-noise (PN) sequence generator. When PN sequence is added to a message signal, it resembles like a noise making it hard to decode and increases the signal bandwidth to utilize the whole spectrum. In this paper, the approach to generate PN sequence using Vedic multiplier has been proposed. In a Vedic multiplier, multiplication is done by using Urdhva Tiryagbhyam sutra, and basic multiplication method is used to design conventional multiplier. The PN sequence generator is implemented using Verilog HDL. The comparative analysis of Vedic multiplier over the conventional multiplier is implemented using Altera FPGA. Vedic multiplication gives an effective result when compared to conventional multipliers.

Keywords Vedic mathematics · Urdhva tiryagbhyam sutra · Add and shift multiplier · PN sequence

1 Introduction

A good communication network reduces the risk of the theft of data from hazardous spyware. Data security is of paramount importance in military-based application, spread-spectrum communications, and cryptography where the data redundancy can lead to the nation's financial loss and security. One of the techniques used to secure communication is by increasing the signal bandwidth through the spread spectrum.

V. Chaudhari · S. Rathore · A. Gadge · V. S. K. Bhaaskaran (✉)
School of Electronics Engineering, Vellore Institute of Technology, Chennai, India
e-mail: vskanchana@gmail.com

D. K. Sharma et al. (eds.), *Micro-Electronics and Telecommunication Engineering*,
Lecture Notes in Networks and Systems 179,
https://doi.org/10.1007/978-981-33-4687-1_4

Multipliers are utilized in a wide scope of digital signal processing and other different applications. As per the modern technology requirements, multipliers play an important role in design applications. These researchers mainly focus on the design factors like high speed, accuracy, area, and low power consumption. Digital applications have different computational blocks. To perform computational operations of these blocks, speed of execution should be compared with older techniques to get new advancement. Vedic mathematics is a set of techniques or sutras for simple and faster solving of mathematical arithmetic. The word Veda is derived from Sanskrit which means 'knowledge' [1]. In Vedic mathematics, there are 16 sutras and 13 sub-sutras to solve complicated problems involved in arithmetic, calculus, geometry, algebra, and conics. Using these sutras, arithmetic operation like addition, subtraction, multiplication, and division can be solved immediately with great simplicity compared to the conventional methods. Vedic multiplication plays a key role in most signal processing applications. It has many advantages compared to conventional multipliers, like it increases the speed of the system, improves efficiency of the system, and helps in reducing the time delay and path delay, and it reduces the complexity of the system. In this paper, we used the Vedic multiplier in terms of improving the area and power utilization of the system. The memory and power requirement of the Vedic multiplication is much less as compared to the array and add and shift multiplier technique [2, 3]. The performance in terms of area, speed, and power of Vedic multiplier with conventional multiplier [4] was discussed.

To generate a random sequence of numbers, following techniques are used: (1) pseudorandom number generators (PRNGs) and (2) true random number generators (TRNGs). The distinction between true random number generator and pseudorandom number generator is that TRNGs use an unpredictable physical means to produce numbers (like atmospheric noise), and PRNGs use mathematical algorithms. The TRNGs technique provides high amount of entropy that makes it impossible to predict the value. In terms of efficiency, it is less efficient as compared to the PRNGs. The TRNGs is aperiodic, whereas PRNGs is periodic in nature with increased efficiency.

There are various techniques used to generate random number such as linear congruential generator, lagged Fibonacci generator, and linear feedback shift registers (FSRs). In linear congruential generator, a recurrence relation si + 1 = (a* si + c) mod m is used to generate random sequence, but the problem in this method the period is limited by m. The additive lagged Fibonacci generator is defined by si = si − p ± si − p + q mod m which provide much larger period. In this paper, linear feedback shift registers are used to generate a random sequence as it has a good statistical property, minimum implementation cost, and long period sequence. Linear feedback shift register (LFSR) is generally used to produce pseudorandom sequence. The pseudo-noise (PN) sequences are used to create white random noise to produce an unpredictable binary sequence [5]. It provides a strong correlation when the sequence is matched in time with a copy of itself. It is also used for training patterns to equalize a channel. Usually, pseudorandom sequences are often used for scrambling and in direct-sequence spread-spectrum schemes.

This paper consists of five sections. Section 2 describes Vedic mathematics and PN sequence generator, followed by implementation of PN sequence generator and

Vedic multiplier. Section 4 elaborates the simulation result, and Sect. 5 concludes this paper.

2 Multiplier and PN Sequence Generator

2.1 Array Multiplier

There are two different ways for a multiplication, i.e., serial multiplication and parallel multiplication. In a serial multiplication executed by finding partial products and adding partial products together. In parallel multiplication, parallel products are produced at the same time.

The general multiplication method is the add and shift algorithm. Let us consider the X and Y are multiplicand and multiplier, respectively. To generate partial products, AND gates are utilized, with N-bits multiplicand and M-bits multiplier. The partial products thus generated are $N*M$. Different multipliers like booth multiplier, combinational multiplier, sequential multiplier, Wallace tree multiplier, and array multiplier can be used.

$$X = x_{n-1}x_{n-2}\ldots x_2x_1x_0$$
$$Y = y_{n-1}y_{n-2}\ldots y_2y_1y_0$$

The array multiplier circuit based on add and shift principle is shown in Fig. 1. For 4*4-bit multiplication 16 AND gates, 8 full adders, and 4 half adders are used. The partial products are generated by using AND gates, and addition is performed by full adders. As shown in Fig. 1, the input bits are $x_0x_1x_2x_3$, and the output bits are $z_0z_1z_2z_3z_4z_5z_6z_7$. The array multiplier is less complex, easy to scale, and easy to place and route, but the power consumption is more.

2.2 Vedic Mathematics

The Shri Bharati Krishna Tirthji has recreated sixteen mathematical sutras from the Atharva Vedas between 1911 and 1918. Such sutras were derived from 'The Ganit sutras' which is also known as 'Sulabh sutras' or 'mathematics' basic sutras. The Vedic mathematics consists of collecting the sutras to solve the operations of Vedic mathematics very simply and quickly. Vedic mathematics lowers the complexity and increases circuit reliability. When compared to the traditional multiplier, it demands less memory. The techniques of Vedic multiplication solve the mathematical problems in two or three simple steps.

The Vedic multiplication provides mainly two approaches: (1) Nikhilam and (2) Urdhva Tiryagbhyam. Literally, Nikhilam sutra means 'all from nine and last from

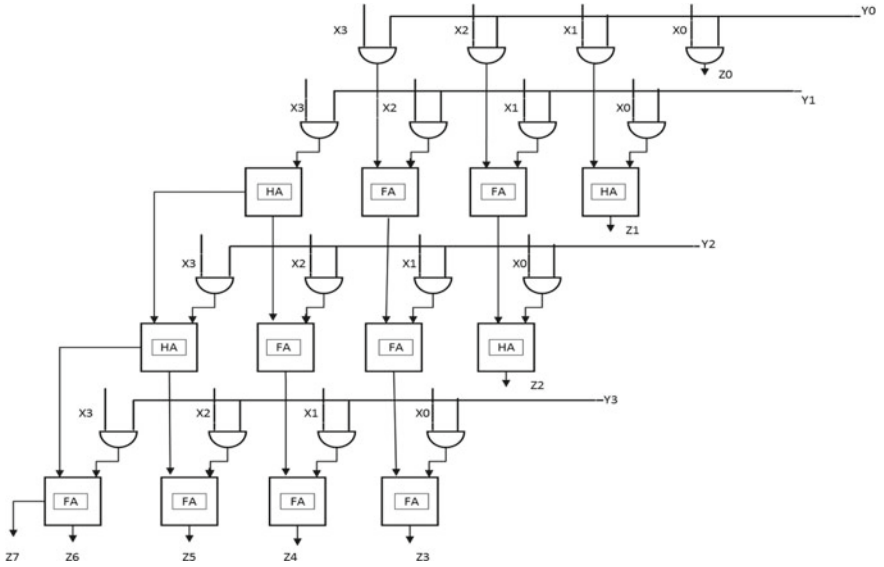

Fig. 1 Array multiplier

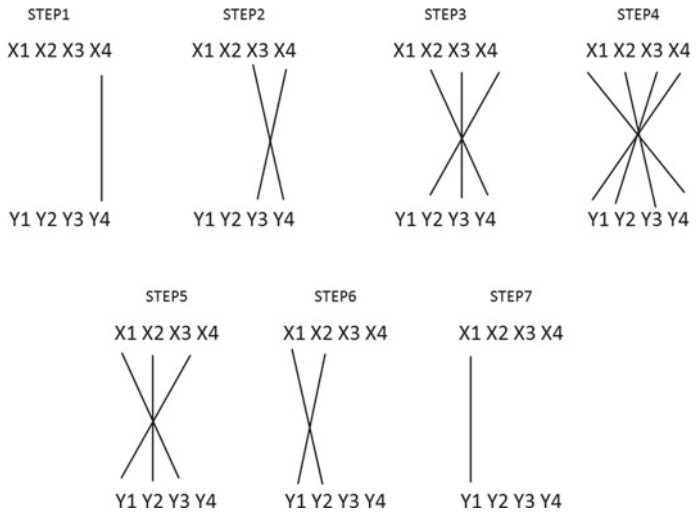

Fig. 2a Four-bit Vedic multiplication technique

ten'. It is more efficient for large numbers. It tries to find the compliment of the large number from its nearest base to execute the multiplication. Urdhva Tiryagbhyam sutra is a general formula that extends to all cases of multiplication. This method contains vertical and cross-multiplication between the digits. The digits at both ends of the line are multiplied, and the result is added with the previous carry. If more

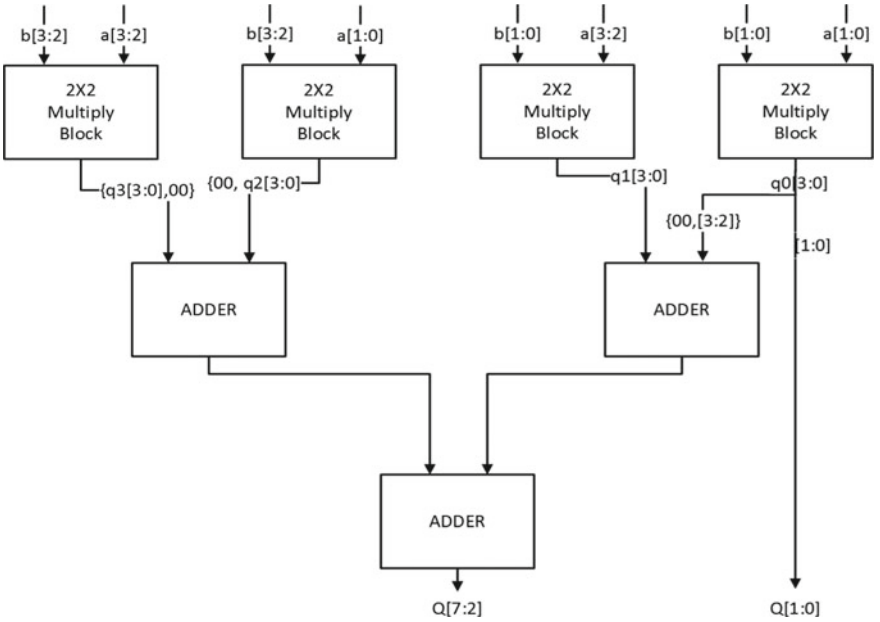

Fig. 2b 4*4-bit architecture Vedic multiplier

lines are added in one step, then all results are added to the previous carry. The least significant digit of the number thus obtained acts as one of the result digits. The rest of the value acts as carry for the next step. Initially, the carry is considered to be zero. In this paper, we have used Urdhva Tiryagbhyam method. Figures 2a and 2b show the 4-bit multiplication Vedic technique (Urdhva Tiryagbhyam) and architecture of Vedic multiplier, respectively [6, 7]. The architecture of 4 × 4 Vedic multiplier is designed using four 2 × 2 Vedic multiplier and three half adders. The 2 × 2 Vedic multiplier can be designed literally by vertically and cross-wise method using the Urdhva Tiryagbhyam sutra. Figure 2c depicts the 8 × 8 Vedic multiplier. It comprises of four 4*4 Vedic multiplier and three adders. The least four significant bit q [3:0] of resultant 16 bit is directly transferred to the output and remaining 12 bit q [15:4] of is forwarded through the adders.

2.3 PN Sequence

It will be difficult to find a difference between a noise and the signal if the bandwidth of the original message signal is higher while maintaining the same signal power. Spectrum spreading accomplishes it using direct-sequence spread-spectrum (DSSS) codes which are considered as pseudo-noise sequence. Since the power density amplitude of the spread-spectrum output is similar to noise, the message

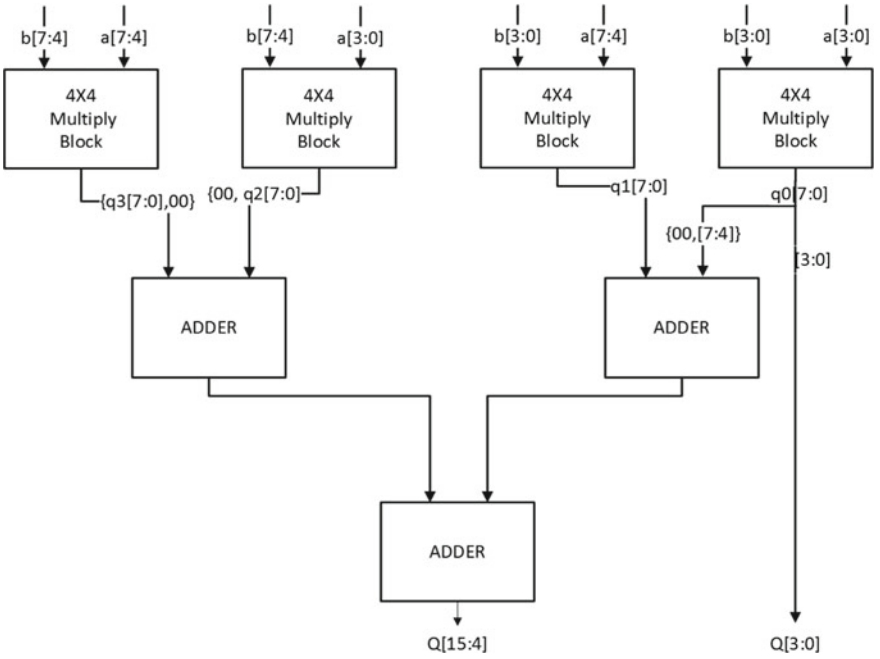

Fig. 2c 8*8-bit architecture Vedic multiplier

signal is hidden. Same code is used at the receiver to dispread the original data. One of the most popular codes is pseudo-noise sequence or pseudorandom sequence. It is used for spreading and dispreading. Pseudo means not exactly noise or not exactly random. It appears like random, but actually, it is a deterministic sequence. If it is purely random, receiver cannot regenerate the code to dispreads the data so that PN sequence is not a purely random, but it looks like random.

There are few techniques to generate the PN sequence. Here, we used the linear feedback shift register concept, i.e., LFSR to generate the random sequence. LFSR is a shift register that has n number of flip-flops connected to it in a feedback mechanism (Fig. 2). An LFSR generates a periodic sequence with the input to LFSR being given as a linear function of its previous state. The length of the PN sequence (N) is given by $2^m - 1$ where 'm' denotes the number of states. It is used to generate pseudo-random number, pseudorandom sequence, and whitening sequence. Mathematically, this polynomial equation can be given as

$$x^p = x^{p-t}1 + \cdots + x^{p-t}n + x^0$$

where x is the bit string, length as n, and t indicates index positions [8]. Two XOR gates in the feedback path perform a modulo-2 operation. The final output taken from the third XOR gate acts as an input to the first MUX.

3 Implementation of PN Sequence Generator

The initial value of the LFSR is called as seed which obtains its input from the output of Vedic multiplier (Fig. 3). The selector lines of multiplexers receive its bit value from load. In this paper for implementation, 8 states are considered in LFSR with an 8-bit Vedic multiplier. For designing the 8-bit LFSR, eight flip-flops are considered and before each flip-flop multiplexer (MUX) is inserted. The feedback path is given as input from the output to the first state through the MUX. So, each MUX will receive two inputs, one from the *seed* and the other input from the feedback. Based on the *load*, the output from the MUX will be given to flip-flops. The MUX is connected before the flip-flop to make the LFSR more randomized. The feedback path comprises of three XOR gates. For feedback path, the characteristic polynomial is given by $f(x) = x^8 + x^6 + x^5 + x^4 + 1$, representing the length of a sequence. In this paper, XOR gate connected in feedback is replaced with XOR, and XNOR gate along with a MUX is designed in the feedback path as shown in Fig. 4. The advantage of MUX -based LFSR is that it reduces the switching activity and hardware as compare to XOR-based LFSR [9].

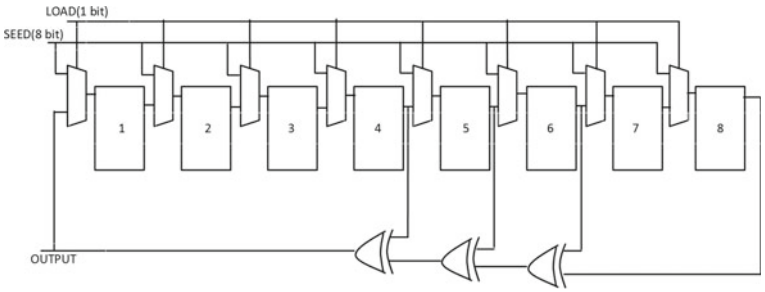

Fig. 3 Linear feedback shift register

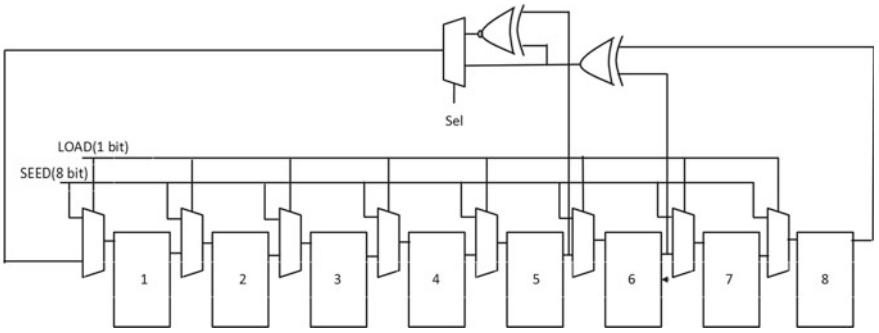

Fig. 4 MUX -based linear feedback shift register

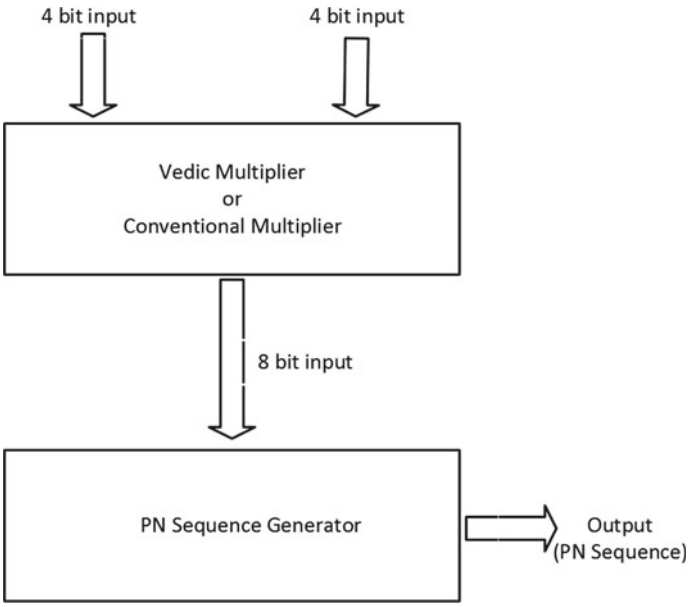

Fig. 5 Basic structure of PN sequence generator using Vedic multiplier

The complete block diagram for PN sequence generator using multiplier is shown in Fig. 5. Two 4-bit inputs are given to the multiplier, and the 8-bit output of the multiplier is given as input to PN sequence generator. This PN sequence generator block uses the LFSR to generate a random sequence. By this method, the two message signals which are given as an input to the Vedic multiplier are masked to generate random sequence of numbers using PN sequence generator.

4 Simulation Results

Experiments were evaluated using Altera FPGA. The simulation results for 4*4 and 8*8 Vedic multiplier and conventional multiplier are shown in Figs. 6, 7, and 8,

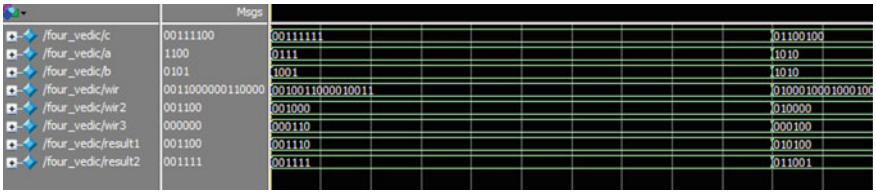

Fig. 6 Simulation result of 4*4 Vedic multiplier

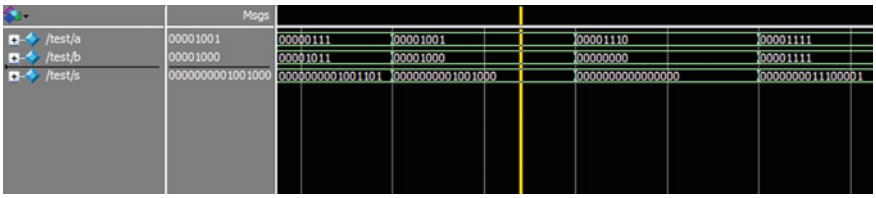

Fig. 7 Simulation result of 8*8 Vedic multiplier

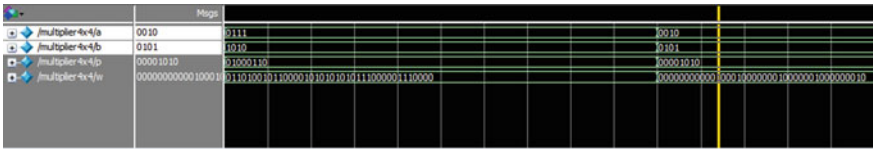

Fig. 8 Simulation result of conventional multiplier

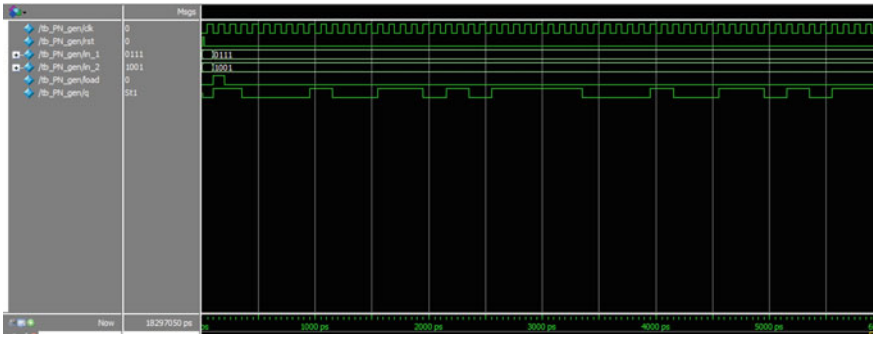

Fig. 9 Simulation result of PN sequence

respectively. We have observed that the PN sequence generates the random output as shown in Fig. 9. The technology schematic of 4*4 array multiplier and 8*8 Vedic multiplier is shown in Figs. 10 and 11. Vedic multiplier consumes 134.19 mV, and conventional multiplier consumes 130.46 mV. The comparison of Vedic multiplier with conventional multiplier shows the Vedic multiplier utilizes less power compared to conventional one.

5 Conclusion

The architecture and design of Vedic multiplier have high operating speed. The performance of the proposed multiplier using Vedic sutra proved to be efficient in terms of speed and space. The results of 4-bit Vedic multiplier are compared with the

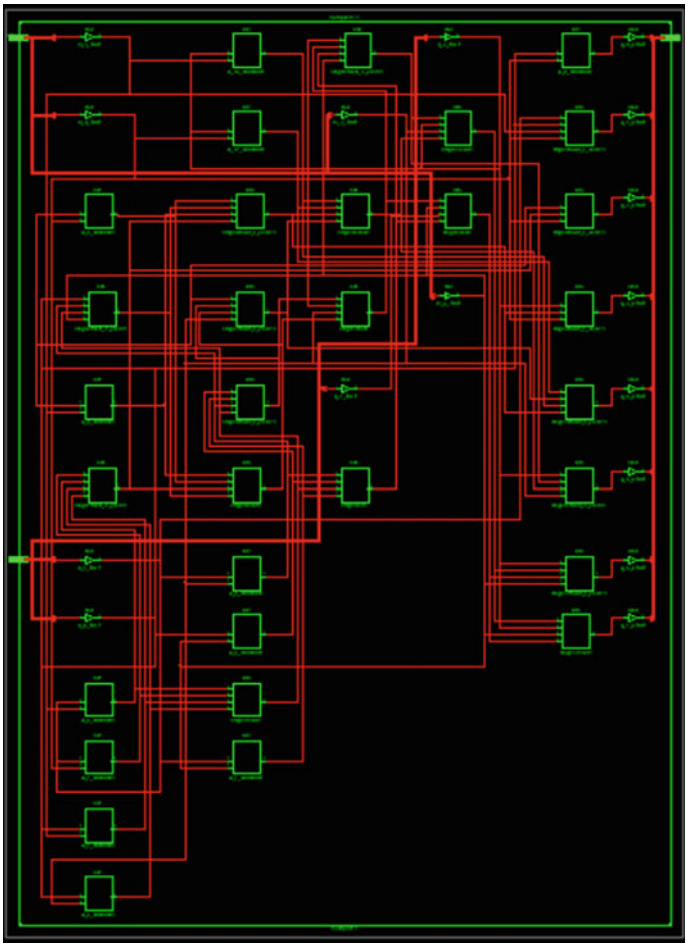

Fig. 10 Technology schematic of 4*4 array multiplier

4-bit add and shift multiplier, i.e., conventional multiplier. The main advantage of the Vedic multiplier is the reduced delay. The power comparison shows that the Vedic multiplier consumes less power compared to conventional multiplier. The random number was generated using PN sequence generator and Vedic multiplier where the message signal is hidden effectively.

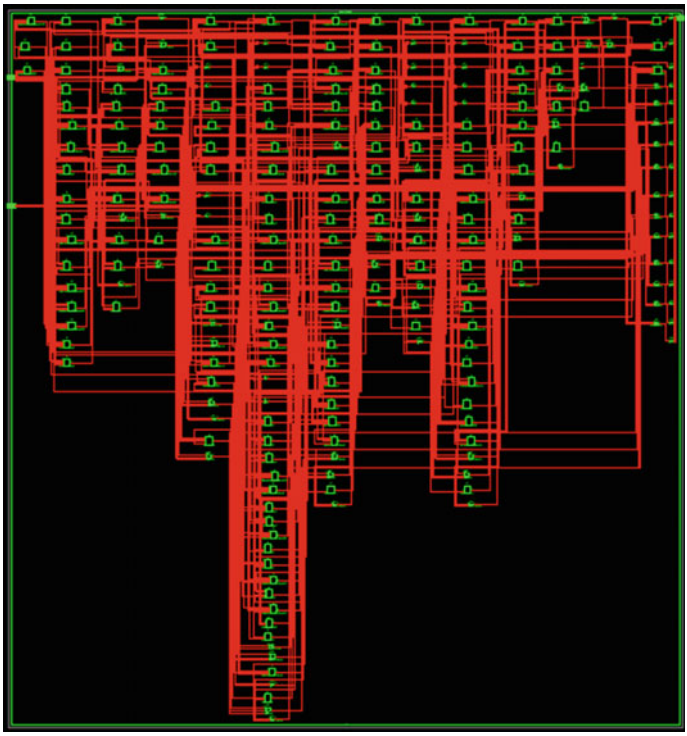

Fig. 11 Technology schematic of 8*8 Vedic multiplier

References

1. Bhat GM, Mustafa M, Parah SA, Ahmad J (2010) Field programmable gate array (FPGA) implementation of novel complex PN-code-generator- based data scrambler and descrambler. Maejo Int J Sci Technol. ISSN 1905–7873
2. Rudagi JM, Ambli V, Munavalli V, Patil R, Sajjan V (2011) Design and implementation of efficient multiplier using vedic mathamatics. In: Proceedings of international conference on advances in recent technologies in communication and computing 2011
3. Saha P, Banerjee A, Bhattacharyya P, Dandapat A (2011) High speed ASIC design of complex multiplier using Vedic mathematics. In: Proceeding of the 2011 IEEE students' technology symposium 14–16 Jan 2011
4. Ma X, Olama MM, Kuruganti T, Smith SF (2013) Security of classic PN spreading codes for hybrid DS/FH Spread Spectrum System, 2013 IEEE
5. Inventor; Brian C_ Banister, San Diego, Calif, Banister BC, inventor; LSI Corp, assignee. PN sequence hopping method and system, Patent Number: 5,987,056, United States Patent
6. Deodhe Y, Kakde S, Deshmukh (2013) Design and implementation of 8-Bit Vedic multiplier using CMOS logic, 1st international conference on machine intelligence and research advancement-ICMIRA-2013 Katra, India, 978–0–7695–5013–8/13, 2013 IEEE
7. Bansal Y, Madhu C, Kaur P (2014) High speed Vedic multiplier designs. In: Proceedings of 2014 RAECS UIET Panjab University Chandigarh

8. Jamgade R, Ambatkar S, Kakde S, HDL Implementation of PN sequence generator using vedic multiplication and add and shift multiplication. In: 2015 5th international conference on communication systems and network technologies
9. Krishna BM, Madhumati GL, Khan H (2019), FPGA based pseudo random sequence generator using XOR/XNOR for communication cryptography and VLSI testing applications. Int J Innovative Technol Exploring Eng (IJITEE), 8(4) Feb 2019

High-Performance Disease Prediction and Recommendation Generation Healthcare System Using I3 Algorithm

P. J. Sathish Kumar, V. Auxilia Osvin Nancy, N. Sathish, K. Kajendran, N. Pugazhendi, and S. Balaji

Abstract The increase in number of disease challenges medical practitioner in making right decisions. As most diseases have the same set of symptoms, the medical practitioner struggles to take decision on recognizing disease as well as right treatment methods. A number of approaches are available for the disease identification and providing treatment, but finding the right approach is what matters. To solve this issue, an inter-/intra-disease impact, the disease-based prediction and recommendation generation method, is presented. The method first reads the input data set and produces a series of clusters with the samples obtained. In the second level, the method estimates inter-disease impact measure and intra-disease impact measure on various disease classes for every data point of the data collection. Using these two measures, the method computes I2-Disease weight for each data point in assigning a label to the data points. For the classification, the method estimates symptomatic disease weight based on inter-/intra-symptom correlation assessment. Based on the selected disease class, a set of treatment samples is populated and ranked according to their curing rate.

P. J. Sathish Kumar (✉) · N. Sathish · K. Kajendran · N. Pugazhendi · S. Balaji
Panimalar Engineering College, Chennai, Tamil Nadu, India
e-mail: sathishjraman@gmail.com

N. Sathish
e-mail: nsathishme@gmail.com

K. Kajendran
e-mail: kajendran@yahoo.com

N. Pugazhendi
e-mail: pughazendi@yahoo.com

S. Balaji
e-mail: balajiit@gmail.com

V. A. O. Nancy
S. A. Engineering College, Chennai, Tamil Nadu, India
e-mail: auxiliaosvinnancy@saec.ac.in

D. K. Sharma et al. (eds.), *Micro-Electronics and Telecommunication Engineering*,
Lecture Notes in Networks and Systems 179,
https://doi.org/10.1007/978-981-33-4687-1_5

Keywords Classification · Disease prediction · High-dimensional clustering · Medical data · I3 · I2 weight · IISS · Artificial intelligence · High performance

1 Introduction

Our human culture is deeply centered on the numerous illnesses that come to light every day. However, there are many precautionary activities taken by the medical society and the health ministry of any country, and the entry of modern disease could not be stopped. Even though the diseases are identified earlier in this decade, concluding the disease affected based on the symptoms is highly difficult for the medical practitioner. The medical practitioner could not say that the person has affected by a disease '*X*', based on a symptom set *S*, where *S* contains a number of symptoms. Because, in most cases, the symptoms identified are more common, they would appear in many diseases. For example, the stomach pain would be found in general for food poison but would also identify on stomach cancer, typhoid and many more even at higher body temperature [1, 2]. Medical data has a wide range of dimensions, and each dimension represents a symptom. In order to group the data points under a certain class of disease, it is necessary to identify or compute the impact of each symptom in each disease. I3: Inter-/Intra-disease impact measures. I3 represents impact of dimension and quality on pieces of data holding class c considered. Even though the dimension or symptom s present in the disease class c, the value of s would not be much influencing than the value of s in other class data points. In general, the temperature value of typhoid class is different from the temperature value of generic fever. The typhoid disease would produce higher temperature more than 102 °C where the general fever would not cross than 101 °C [3, 4]. The I3 measure would be used to determine the illness group to which the piece of data belongs. To obtain and generate the metadata from the medical data and cluster available, the fuzzy rule can be used.

2 Study Work

Usage of data mining techniques to predict diabetes [5], address various conventional approaches, focused on physical and chemical tests, for diagnosing diabetes. Methods that are strongly focused on data mining techniques can be used effectively to predict high blood pressure risk. This paper discusses early diabetes prediction through five different data mining approaches, including GMM, SVM, logistic regression, ELM, ANN.

Study of various data mining techniques for predicting diabetes mellitus [6, 7] discusses early diabetes prediction using a range of data mining techniques. 768 instances of the data set were taken from the PIMA Indian data set to evaluate the quality of prediction machine learning techniques. The study reveals that the modified J48 classifier has the maximum performance according to other approaches.

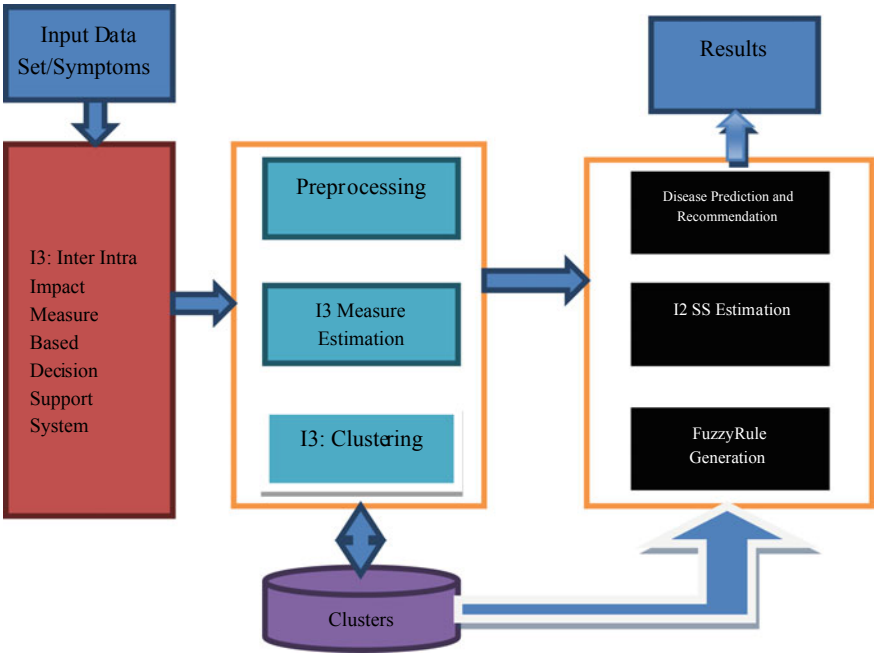

Fig. 1 Architecture of proposed I3 decision support system

Prediction of glucose data analytics for diabetic patient monitoring [8, 9] provides a thorough critical analysis concentrating on current glucose predictive models and recommends the best match model based on an assessment to perform data analytics in a wireless body area network environment.

3 I3: Inter-/Intra-Impact Measure-Based Decision

See Fig. 1.

4 Support System

The I3 approach reads the input data set *D* initially. The input data set has been preprocessed to remove the noisy records based on their dimensional coverage and their values. The preprocessed data set is then used to perform I3 clustering.

Instead, for each data point *d* of *D*, the method calculates the I3 measure and is determined on the basis of the I2 disease weight. A single class is defined and indexed based on the value of I2Dw. Throughout the test process, the I2 symptom

similarity measure is calculated to classify the disease class. Figure 1 demonstrates the architecture of the I3 decision support system and its different phases and components.

5 Data Preparation

The input medical data set would contain an N number of dimensions and the K number of data points. The data preparation algorithm reads all the data points, and for each data point d, the completeness of all dimension and value will be verified in this stage. The data point identified incomplete either in their dimension or the value was excluded from the data collection [10, 11]. The data set extracted from the noise was used to perform clustering in the next step.

6 I3 Measure Estimation

The I3 measure represents the impact of the symptom in various classes of diseases. The I3 metric was projected on the basis of the side effect and the value of the same configurations in different categories. It is performed by counting the number of data points being a match or the distance fall within a threshold. Inter-impact measure is estimated by computing the impact of the dimension in the other classes. Similarly, the intra-impact measure represents the impact of the dimension or symptom in the same class.

Algorithm:
Input: Cluster Set Cs, Data Point Dp, Dimension Dim, Class C
Output: I2DW
Start
Read cluster set Cs, Dp, Dm.
Compute Intra Disease Impact Measure IDIM.

$$IDIM = \int_{i=1}^{size(C)} \frac{\sum C(i)(Dm) == Dp(Dm)}{size(C)} \quad \text{-- (1)}$$

For each other class Oc
Compute inter disease impact measure InDIM.

$$InDim = \int_{i=1}^{No\ of\ other\ Class} \frac{\sum_{i=1}^{size(Ck)} Ck(Dm) == Dp(Dm) \Big/ size(Ck)}{Number\ of other\ class} + \mu \text{--(2)}$$

End
μ - impact constant and value is 0.1
Compute Inter-Intra-Disease-Weight I2DW = IDIM×InDim –(3)
Stop

7 Clustering Using I3

To perform clustering, the method first preprocesses the input data set, and with the preprocessed data set, the method generates initial clustering with random sampling. Then for each data point *D* of the data set, the method computes I2DW measure for different classes.

Algorithm:
Input: Ds named as data sets.
Output: Cs named as clusters
Start
Understand Pds.
Pds = Preprocess(Ds).
Initialize Cluster set Cs.
For each cluster Ci
Initialize with random samples.
End
For each data point Di
For each class ci
For each Dimension Dim
I2Dw = I3-Estimation(Di, Cs, Dim)
End
Compute Disease Support Measure Dsm.

$$\text{Dsm} = \frac{\sum_{i=1}^{size(Di)} I2Dw(Dim) > Th}{size(Di)} \quad \text{-- (4)}$$

End
Choose the class with higher disease support measure Dsm.
Class c = Max(Dsm)
End
Stop

The proposed algorithm performs clustering of data points based on the inter- and intra-impact measures and disease support measure.

8 Fuzzy Rule Generation

The fuzzy rule generation algorithm conducts a variety of illnesses for different league predicated on the I2DW measurement calculated by the I3 measure assessment algorithm.

Algorithm:
Input: Cluster Set Cs
Output: Fuzzy Rule Set Frs.
Start
Read cluster set Cs.
Initialize fuzzy rule set Frs.
For each disease class c
Select a random sample from cluster.
Di = Random(Cs©)
For each dimension Dim
Compute I2DW = I3Estimation(Di)
If I2DW>Th then
Add to Dimension set Dims.
Dims = $\sum(\text{Dimesion} \in \text{Dims}) \cup \text{Dim}$
End
For each dimension Dim $_i$
Compute minimum value Minx = $\int_{i=1}^{size(c)} \text{Min}(\forall(C\,(i))(\text{Dim})$
Compute maximum value Maxx = $\int_{i=1}^{size(c)} \text{Max}(\forall(C\,(i))(\text{Dim})$
End
Generate Fuzzy rule Fr = $\int_{i=1}^{size(\text{Dims})} \{\text{Minx}(\text{Dims}(i)), \text{Maxx}(\text{Dims}(i))\}$
Add to rule set Frs.
End
Stop

The proposed method computes range values to produce fuzzy rule. Generated rule set has been used to perform disease identification in the next stage.

9 Fuzzy Rule Generation

At this point, the inter-/intra-symptom similarity measure is determined for the disease class given. For the specified set of symptoms, the method calculates I2SS measurements for the particular class.

Algorithm:
Input: Fuzzy Rule Fr, Symptoms S
Output: I2SS
Start
Read Fr, S.
Initialize count C.
For each symptom s
If $\int s.\text{value} < Fr(s).\text{value} >$ then
C = c+1.
End
Compute I2SS = $\frac{Count}{size(s)}$ --(5)
End

The suggested method calculates the I2SS calculation for the symptom of the disease class and the law. The calculated I2SS formula was used to make disease predictions.

10 Disease Prediction and Recommendation Generation

For any input symptoms given, the method performs disease prediction based on the result of preprocessing, clustering and fuzzy rule generation. Initially, the method performs preprocessing and I3 clustering. Using the result, the method generates the fuzzy rule for a separate class of diseases.

Algorithm:
Input: Data Set Ds, Symptom Set S
Output: Recommendation R
Start
Dps = Preprocessing(Ds)
Cluster Set Cs = Clustering(Dps)
Rule Set Rs = Fuzzy-Rule-Generation(Cs)
For each disease D
Compute I2SS Measure.
End
Choose Disease with Maximum I2SS value.
Disease Dis =Disease(Max(I2SS))
Identify list of all drugs given for Dis.
Drug set Drs = $\int_{i=1}^{\text{size}(\text{Ds})} \sum \text{Ds.Disease} == \text{Dis}$
For each drug Dr
Compute Drug Curing rage Cr = $\frac{\sum_{i=1}^{size(Ds)} Ds(i).Drug==Dr \;\&\&\; Ds(i).Status==Success}{\sum_{i=1}^{size(Ds)} Ds(i).Drug==Dr}$ --(6)
End
Recommendation R = Sort the drugs with curing rate
Stop

The above-discussed algorithm computes the I2SS measure to find the most impacting disease and computes the drug curing rate to generate recommendation to the medical practitioner.

11 Experimental Results

The proposed I3 approach has been evaluated for its efficiency in disease prediction and recommendation generation. The data set plays a vital role in evaluating the performance of the algorithm. For the clarification, the snapshot of the data set being used is presented here (Tables 1 and 2).

Table 1 Description of data set used

Parameter	Value
Name of data set	KMD
Dimensions	200
Data points	1 million
Classes	25

Table 2 Data's belongs to typhoid disease

Patient									
Widal	Tiredness	tr	Pressure	Sugar	Cholesterol	hp	tc	dc	Puzcells
2	2	102	0	0	22	8	0	0	0
3	4	100	0	158	33	7	0	0	0
4	3	101	0	0	0	6	0	0	0
1	2	102	0	168	0	8	0	0	0
3	4	100	0	156	0	7	0	0	0
0	1	97	160	270	190	7	0	0	0
0	1	98	145	220	210	8	0	0	0
0	1	97	160	270	190	7	0	0	0
0	1	98	145	220	210	8	0	0	0
0	1	97	160	270	190	7	0	0	0

Patient							
Salt	Albumin	Vomit	Headache	Stomach pain	Wheezing	Cold	Disease
0	0	0	1	1	0	2	typhoid
0	0	0	0	1	0	4	typhoid
0	0	0	1	1	0	5	typhoid
0	0	0	1	1	0	2	typhoid
0	0	0	0	1	0	4	typhoid
0	0	0	0	0	0	0	Diabetic
0	0	0	0	0	0	0	Diabetic
0	0	0	0	0	0	0	Diabetic
0	0	0	0	0	0	0	Diabetic
0	0	0	0	0	0	0	Diabetic

The inter-/intra-disease impact measure has been computed based on the above input table. Consider the input symptom values as follows.

Widal	Tiredness	tr	Pressure	Sugar	Cholesterol	hp	tc	dc
2	2	102	0	0	22	8	0	0

Puzcells	Salt	Albumin	Vomit	Headache	Stomach pain	Wheezing	Cold
0	0	0	0	1	1	0	2

From the above input symptom set and values, the value 0 shows the absence of the symptom where 1 represents the presence of the symptom. If it is greater than 1, then it shows the value of the symptom.

According to the above-mentioned input symptoms, the inter-/intra-impact measures can be estimated in (Table 3).

Intra-Impact Measure for widal 1 is.

InIM = 10/10 = 1.

Here consider, the value in the data set represents that the value > 0 shows the presence of viral in the blood sample. According to this, all the 10 rows show the presence and it matches with the input symptom value also.

Intra-Impact measure for Tiredness = 9/10 = 0.9

Here if the tiredness value is > 1, then consider the patient has higher tiredness.

Intra-Impact Measure for Temperature = 7/10 = 0.7. Here consider the temperature should be greater than 100.

Intra-Impact measure for headache = 7/10 = 0.7

Intra-Impact Measure for stomach pain = 10/10 = 1.0

Table 3 Values of Typhoid disease and it contains totally 10 number of rows

Widal	Tiredness	tr	Pressure	Sugar	Cholesterol	hp	tc	dc
2	2	102	0	0	22	8	0	0
3	4	100	0	158	33	7	0	0
4	3	101	0	0	0	6	0	0
1	2	102	0	168	0	8	0	0
3	4	100	0	156	0	7	0	0
4	1	101	0	320	0	6	0	0
2	2	102	0	0	33	8	0	0
3	4	100	0	158	0	7	0	0
4	3	101	0	0	0	6	0	0

Puzcells	Salt	Albumin	Vomit	Headache	Stomach pain	Wheezing	Cold	Disease
0	0	0	0	1	1	0	2	typhoid
0	0	0	0	0	1	0	4	typhoid
0	0	0	0	1	1	0	5	typhoid
0	0	0	0	1	1	0	2	typhoid
0	0	0	0	0	1	0	4	typhoid
0	0	0	0	1	1	0	5	typhoid
0	0	0	0	1	1	0	2	typhoid
0	0	0	0	0	1	0	4	typhoid
0	0	0	0	1	1	0	5	typhoid

Intra-impact measure for cold = 10/10 = 1.0.

The remaining symptoms are not present in the input sample so that they are not necessary.

Using these values computed, IDIm can be measured as follows:

$$\text{IDim} = (1.0 + 0.9 + 0.7 + 0.7 + 1.0 + 1.0)/6 = 5.3/6 = 0.88$$

These values are computed to the Typhoid class, and according to this, the intra-disease impact measure can be computed as follows:

$$\text{InDim} = \int_{i=1}^{\text{No of other Class}} \frac{\sum \sum_{i=1}^{\text{size(Ck)}} \text{Ck(Dm)==Dp(Dm)/size(Ck)}}{\text{Number ofother class}} + 0.1 \quad (1)$$

InDim on widal is estimated as = 0/10 = 0.0 Here from the diabetic class, no tuple has the value greater than 0, whereas the input sample has the value 2. So it matches for 0 rows.

In Dim on Tiredness = 0/10 = 0.0

InDim on Temperature = 0/0.0. Because all the records have the temperature value less than 98.4 which shows nobody has fever.

InDim on Headache = 0/10 = 0.0

InDim on Stomach Pain = 0/10 = 0.0

InDim on cold = 0/10 = 0.0

In cumulative InDim = (0.0 + 0.0 + 0.0 + 0.0 + 0.0 + 0.0)/6 = (0.0 + 0.1) = 0.1

Similarly, the InDim measure can be estimated for different other classes and based on that a cumulative InDim measure can be computed.

Using these two values, the disease weight can be measured.

$$\text{I2Dw} = 0.88 \times 0.1 = 0.88$$

Based on the value, the data points have been clustered and produces efficient results.

Consider after the clustering, the fuzzy rules have been generated in (Table 4).

Table 3 shows the fuzzy rule being generated for the typhoid class and can be generated for any other disease class.

Table 4 Fuzzy rule generated for Typhoid class

Widal	Tiredness	Temperature	Headache	Stomach pain	Cold
2–4	2–6	101–104	1	1	2–8

Table 5 Comparison on time

Method	No of data points of data set		
	3 lakhs	5 lakhs	1 million
Neuro-fuzzy	21	31	65
DTM	18	27	48
HDPS	15	21	34
MLSS	11	15	26
I2DM	7	12	21

Table 6 Comparison on disease prediction accuracy versus no of data points

Method	No of data points of data set versus disease prediction accuracy %		
	3 lakhs	5 lakhs	1 million
Neuro-fuzzy	76	77	79
DTM	84	86	89
HDPS	87	89	91
MLSS	92	97.6	98.4
I2DM	94.5	98.7	99.3

Inter/Intra-Disease Symptom Similarity = 6/6 = 1.0.

Because for the input pattern, all the symptoms are falls within the range value of all the symptoms of Typhoid class.

The inter-/intra-disease symptom similarity for diabetic class is = 0/0 = 0.0.

12 Results and Discussion

The proposed method has produced efficient results than other methods. The efficiency of the method is measured in various parameters. Classification time and prediction time were calculated. It was calculated based on the time value taken with X number of samples for prediction. With another set of samples, it has been approximated.

The methods have been analyzed with various varying number of samples. Table 5 shows the comparison result on time complexity produced by different methods on varying size of data set. The proposed algorithms MLSS and I2DM have produced only negligible hike in the time compared to other methods (Table 6; Fig. 2).

13 Conclusion

An I3 disease impact measure-based approach to the problem of disease prediction and recommendation generation is presented using artificial intelligence (fuzzy rules). The method preprocesses the input medical data set to remove the noisy data.

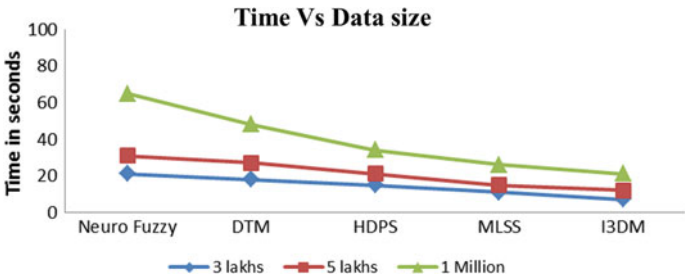

Fig. 2 Comparison on time versus data size

Then the data set has been clustered into different disease class using I3 clustering algorithm. Using the clusters generated, the method generates a fuzzy rule for each disease class. The rule has a different dimension and range value according to the symptoms selected for any disease class. Using the fuzzy rule, the method calculates I2SS test to classify the input symptom class collection for the disease. The system selects a list of medicinal products based on the established disease which has higher curing rate and they will be popped to the MP as a recommendation. The proposed method improves the performance of disease prediction up to 99.3%, and the false ratio has been reduced up to 0.6% with reduced time complexity.

References

1. Huzooree G, Khedo KK, Joonas N (2017) Glucose prediction data analytics for diabetic patients monitoring. In: IEEE conference on next generation computing applications (NextComp)
2. Gandhi M, Singh SN (2015) Predictions in heart disease using techniques of data mining. In: IEEE conference on: futuristic trends on computational analysis and knowledge management (ABLAZE)
3. Begam SS, Selvachandran G, Ngan TT, Sharma R (2020) Similarity measure of lattice ordered multi-fuzzy soft sets based on set theoretic approach and its application in decision making. Mathematics 8:1255
4. Vo T, Sharma R, Kumar R, Son LH, Pham BT, Tien Bui D, Priyadarshini I, Sarkar M, Le T (2020) Crime rate detection using social media of different crime locations and twitter part-of-speech tagger with brown clustering 4287–4299
5. Selkar RG, Thakare M (2014) Brain tumor detection and segmentation by using thresholding and watershed algorithm. Int J Adv Inf Commun Technol 1:321–324
6. Komi M, Li J, Zhai Y, Zhang X (2017) Application of data mining methods in diabetes prediction. In: IEEE conference on image, vision and computing (ICIVC)
7. Beulah R, Punithavalli M (2017) Prediction of sugarcane diseases using data mining techniques. In: IEEE conference on advances in computer applications (ICACA)
8. Renuka DM, Shyla JM (2016) Analysis of various data mining techniques to predict diabetes mellitus. Int J Appl Eng Res 11(1):727–730
9. Sharma R, Kumar R, Singh PK, Raboaca MS, Felseghi R-A (2020) A systematic study on the analysis of the emission of CO, CO_2 and HC for four-wheelers and its impact on the sustainable ecosystem. Sustainability 12:6707
10. Kavakiotis I (2017) Machine learning and data mining methods in diabetes research. Comput Struct Biotechnol J 15:104–116
11. Rajan A, Ramesh GP (2015) Automated early detection of glaucoma in wavelet domain using optical coherence tomography images. Biomed Pharmacol J 8(2)

Performance Analysis of ISOWC Link Considering Different Modulation Schemes

Naina Dahiya, Anuranjana, and Sanmukh Kaur

Abstract The development of optical communications systems from long fibers to compact wireless networks has led to the possibility of linking two satellites using a wireless optical link. The optical communication systems have been upgraded to use of wireless systems. The two satellites can be connected using optical wireless link. The optical wireless communication allows the exchange of information between two satellites at a higher speed. To act as a source of light, laser can be used and as an optical link, and a high-frequency light signal can be used. In this paper, we are analyzing and optimizing the different aspects of an optical communication link by selecting different modulation scheme. The IS-OWC link has been analyzed using PSK, DPSK, and OQPSK. The bit error rate (BER) and *Q*-factor have been used as the main determinant to analyze the performance of optical link between two satellites.

Keywords Inter-satellite optical wireless communication (IS-OWC) · Differential phase shift keying (DPSK) · Phase shift keying (PSK) · Offset quadrature phase shift keying (OQPSK)

1 Introduction

There are different types of wireless communication media used in satellite communication in the modern era to transmit and receive data in the form of radio frequency (RF), microwave frequency, but these techniques suffer from various limitations such

N. Dahiya (✉) · Anuranjana · S. Kaur
Amity School of Engineering and Technology, Amity University Uttar Pradesh, Noida, India
e-mail: nainadahiya054@gmail.com

Anuranjana
e-mail: aranjana@amity.edu

S. Kaur
e-mail: sanmukhkaur@gmail.com

D. K. Sharma et al. (eds.), *Micro-Electronics and Telecommunication Engineering*,
Lecture Notes in Networks and Systems 179,
https://doi.org/10.1007/978-981-33-4687-1_6

as license requirements, fixed bandwidth, and high cost [1] Thus, the link is established between satellites through optical wireless communication (OWC) channel called as inter-satellite optical wireless communication (IS-OWC) system [2]. There is consecutive increase in number of satellites which revolve around the earth, henceforth increasing the payloads and cost of the system. Hence to reduce the satellite traffic and cost of inter-satellite link (ISL) provides excellent network for transmitting the high data rate with global coverage at lower cost [9]. The advantage of using a high-frequency light signal is that it supports high data rate with minimum transmission delay because outer space is vacuum; therefore, lasers are minimum. Antenna required is small as opposed to several meters wide used in conventional RF links [10, 11]. Small antenna means a decrease in cost of satellite which is one of the greatest advantages. Smaller wavelength of light signal is therefore used. The only major limitation of inter-satellite optical wireless communication is that a highly accurate tracking system is required to make sure that the communicating satellites are signed with strict line of sight (LOS) [9].

2 Literature Review

A OWC system faces less signal power loss as compared to RF system. The regulation and license to frequencies that can be used for satellites communication using RF links are not applicable in case of optical system. The work focuses on various challenges faced by FSO communication system from ground-to-satellite/satellite-to-ground and for inter-satellite links [1]. The comparative analysis of three modulation techniques is carried out in inter-satellite optical wireless system (ISOWC system), namely chirped, AMI, DPSK modulation. The optimizing modulation techniques are used through wavelength division multiplexing to achieve an advance system [2].

The result shows that the AMI modulation shows high *Q*-factor (Quality factor) at 40 Gbps as compared to DPSK and chirped modulation technique while DPSK modulation shows best performance at 20 and 10 Gbps with less bit error rate (BER) and better *Q*-factor (quality factor). The best *Q*-factor (quality factor) and minimum bit error rate (BER) are reported at 10 Gbps [3]. The inter-satellite optical communication wireless system is designed using variety of techniques, and the analysis of the effects of the space and polarization technique is carried out on the system performance improvement. The parameters used for performance are bit error rate (BER), *Q*-factor (quality factor), and eye diagram [4].

The analysis of the performance of the optical link between satellites is using parameters link quality factor and bit error rate (BER). High-frequency light signals are used as a carrier for optical link in which the common source of light is lasers. The result shows the optical link is better when compared to RF link in terms of distance and speed. The purported system employs 4×4 transceiver system over 6000 km so that it can support a data rate of 10 Gbps, and in order to achieve a higher data rate of 40 Gbps in inter-satellite optical wireless system (ISOWC system), QPSK modulation technique is used [8]. The inter-satellite optical wireless system (ISOWC

system) performance analysis is carried out using advance modulation formats like CSRZ, RZ, DRZ, DPSK, NRZ and modulation schemes like CSRZ-DPSK, NRZ-DPSK over wavelength spectrum. It is observed that the reception of power decreases with increase in the magnitude of the wavelength [6].

The performance of mode division multiplexing (MDM) inter-satellite optical wireless system (ISOWC system) using DQPSK, DPSK, and Manchester modulation technique is carried out. The result shows till 40 Gbps DQPSK has best performance while Manchester shows least. It is noticed that the quality factor decreases with the increase in bit rates which from 10 to 40 Gbps. It is observed that at 2500 km DQPSK shows best performance as compared to the other two modulation formats of DPSK and Manchester modulation format. The system of mode division multiplexing inter-satellite optical wireless system proposed in this paper is cost-effective, flexible, reliable as well as useful to be used in long distances [7]. Impact of variation of internal parameters of the system on the performance of FSO link has been studied in this work. At different values of beam divergence and wavelength at bit rate 10 Gbps and 15 Gbps, *Q*-factor of link has been analyzed [9].

3 Proposed Configuration

The proposed model is shown in Fig. 1, and schematic configuration is shown in Fig. 2: The system consists of a transmitter, communication channel, a PIN photodetector, and a low-pass filter (Bessel Filter). The wavelength used is 850 nm, and power has been taken to be 15 dBm. The detailed description of the parameters and their values has been given in Table 1. OptiSystem-16 has been used as the tool for simulation of the model.

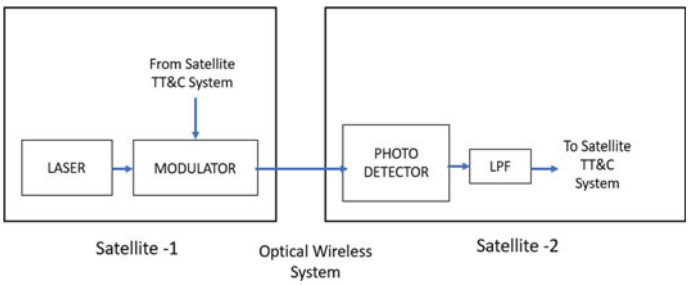

Fig. 1 General free space optical communication system

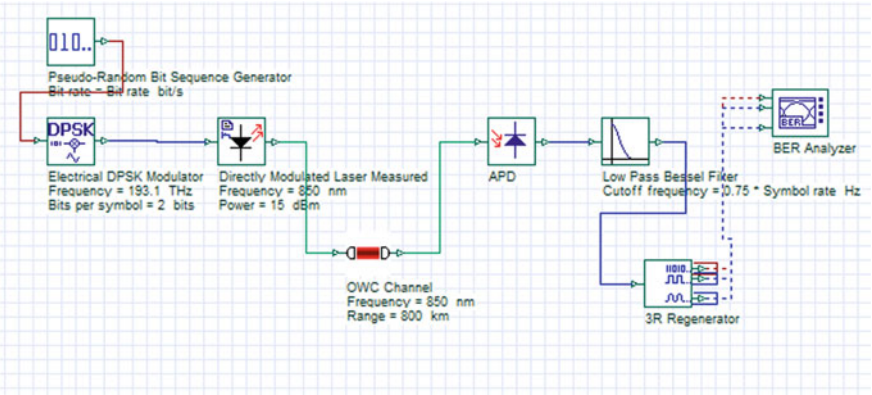

Fig. 2 IS-OWC system model

Table 1 System parameters and values

Parameter	Value
Power	15 dBm
Attenuation	0 dB/km
Range	800 km
Wavelength	850 nm
Transmitter aperture diameter	15, 25, 35 cm
Receiver aperture diameter	15, 22, 29, 36 cm
Bit rate	1 Gbps
Modulation formats	DPSK, PSK, OQPSK

4 Results and Discussion

4.1 Optimization of Different Modulation Formats with Varying Range

Three types of modulation techniques have been analyzed for the performance of IS-OWC link which has been described in Fig. 3. The analysis of PSK, DPSK, and OQPSK has been performed in terms of *Q*-factor for transmission range of upto 800 km. Figure 3 shows that DPSK modulation format provides better *Q*-factor in comparison with PSK and OQPSK. Also, from Table 2 we infer that DPSK modulation scheme provides better *Q*-factor; hence, better link availability is possible than PSK and OQPSK schemes. ISOWC system with use of DPSK modulation can cover range of 800 km distance and provides a *Q*-factor of 50.38 which is better than other schemes. Therefore, DPSK modulation format is optimized for the further simulations.

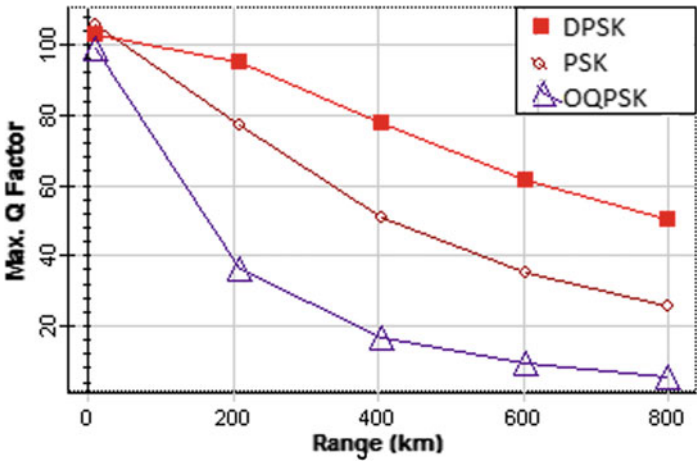

Fig. 3 *Q*-factor versus transmission range for different modulation formats

Table 2 *Q*-factor with varying range for various modulation formats

Range (km)	Bit rate (Gbps)	*Q*-factor DPSK	*Q*-factor PSK	*Q*-factor OQPSK
10	1	102.87	105.41	98.86
202.5	1	94.91	76.85	35.98
405	1	77.68	50.58	16.36
602.5	1	61.32	34.87	9.07
800	1	50.38	25.46	5.64

4.2 Optimization of Wavelength Considering DPSK Modulation Scheme

Different wavelengths have been compared and analyzed using DPSK modulation format shown in Fig. 4. The three wavelengths that have been used here are 850, 1300, and 1550 nm. From Fig. 4 and Table 2, we infer that DPSK modulation format performs better with 850 nm than PSK and OQPSK in terms of *Q*-factor as it provides better quality at longer range than PSK and OQPSK. With the use of 850 nm, it is observed that IS-OWC link covers a distance of 650 km and gives *Q*-factor of 9. Therefore, for DPSK modulation 850 nm wavelength is optimized and used for further simulations (Table 3).

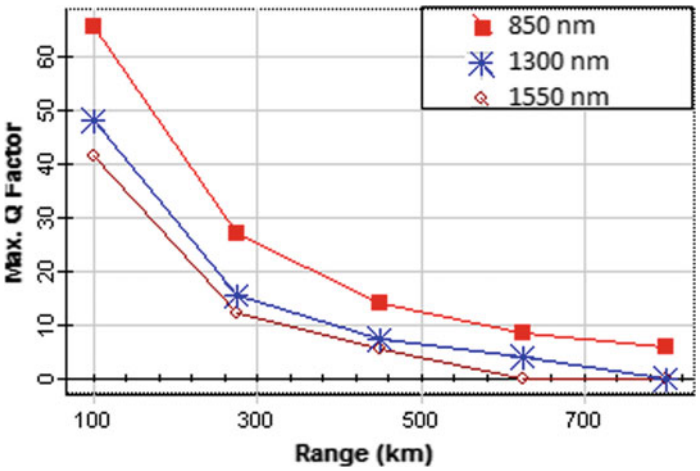

Fig. 4 *Q*-factor versus range with varying wavelength using DPSK modulation format

Table 3 *Q*-factor variation with range considering different wavelengths

Range (km)	Bit rate (Gbps)	*Q*-factor	*Q*-factor	*Q*-factor
		850 nm	1300 nm	1550 nm
100	1	65.4	48.13	41.28
275	1	26.83	15.58	12.06
450	1	14.11	7.3	6.42
625	1	8.54	9.13	0

4.3 Optimization of Data Rate with Varying Range Using DPSK Modulation Scheme

In the plot shown in Fig. 5, three values of data rate have been analyzed using DPSK modulation format for performance of Is-OWC link. The analysis of data rate at 5 mbps, 50 mbps, and 1 gbps has been performed in terms of *Q*-factor, and eye diagrams for the transmission range of 800 km have been considered. Figure 5 shows that while using low value of data rate, i.e., 5 mbps, the better *Q*-factor is achieved, and system performs better for long distance. While using high data rate, i.e., 1 gbps, lower *Q* value is achieved, and system performs for better at 625 Km. The eye diagrams for low and high data rates of 5 Mbps and 1 Gbps at a transmission range of 800 km have been shown in Figs. 6 and 7, respectively.

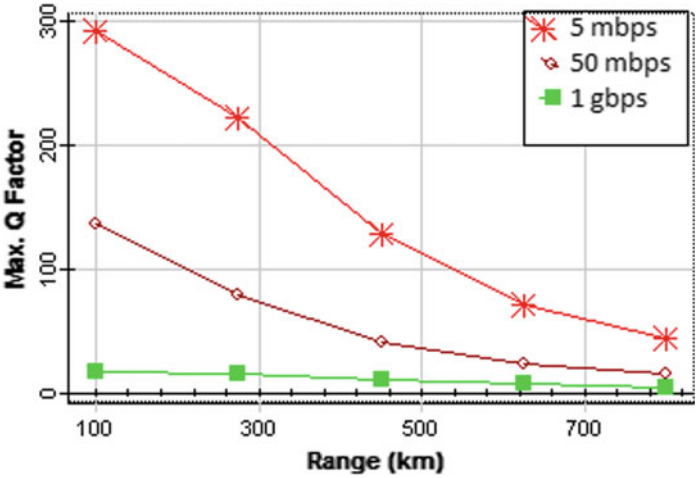

Fig. 5 *Q*-factor versus range with varying data rate for DPSK scheme

Fig. 6 Eye diagram for data rate of 5 Mbps at a distance of 800 km

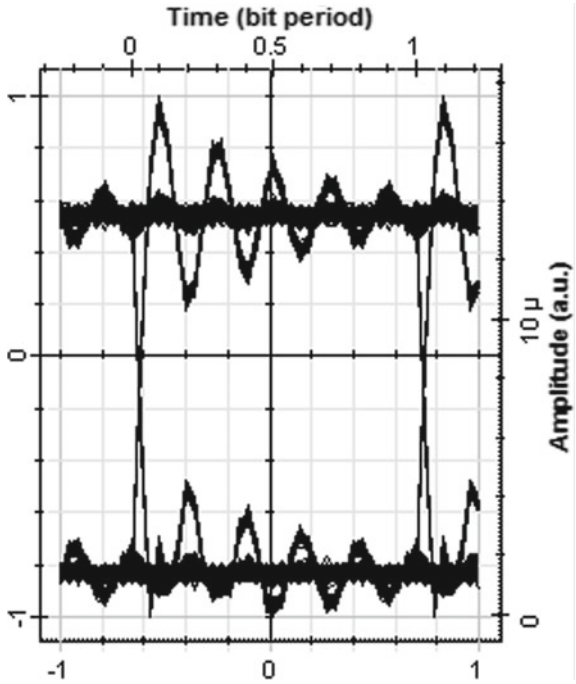

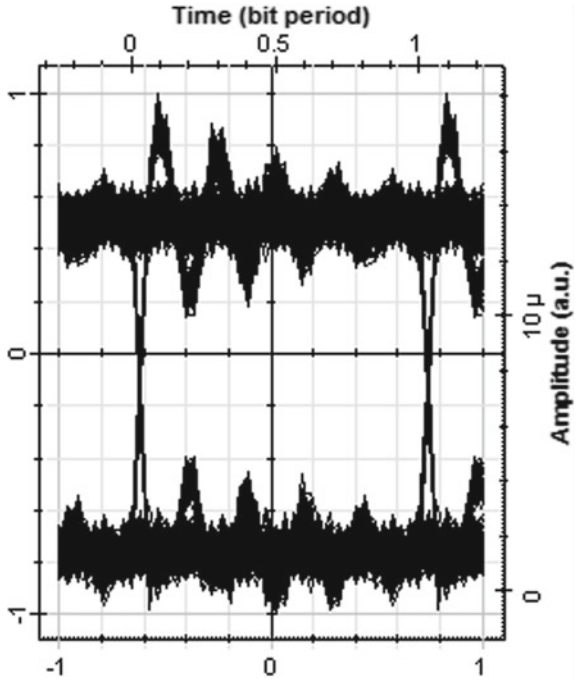

Fig. 7 Eye diagram for data rate of 1 Gbps at a distance of 800 km

4.4 Optimization of Power Levels with Varying Range Using DPSK Modulation Scheme

In Fig. 8, DPSK format has been realized with different power levels such as 10, 20, 30 dBm. The graph *Q*-factor versus range shows that increase in power increases the *Q*-factor value and decreases the BER. The system gives better result at power of 30 dBm. Table 4 gives details of the variation of *Q*-factor at various power levels. It has been analyzed that DPSK performs better at a power of 30 dBm.

4.5 Optimization of Transmitter Aperture Diameter with Varying Range Using DPSK Modulation Scheme

Different values of transmitter aperture diameter have been used to analyze the performance of IS-OWC link, which is observed in Fig. 9. It is observed that when small transmitter aperture diameter is used, i.e., 15 cm, then lower *Q*-factor is obtained and the system performs for smaller distance. While using higher receiver aperture diameter, the better *Q*-factor is achieved, and system performs better for long distance

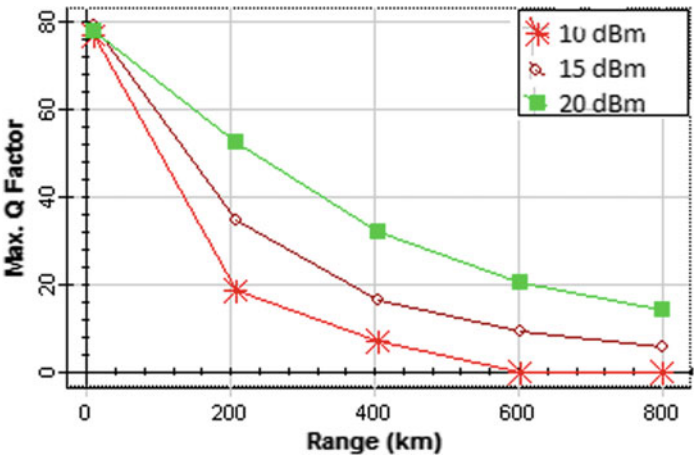

Fig. 8 *Q*-factor versus range with varying power for DPSK scheme

Table 4 *Q*-factor variation with range considering different power levels

Range(km)	Power	Power	Power
	10 dBm	20 dBm	30 dBm
10	77.07	78	78.96
207.5	18.39	34.75	52.54
405	6.77	16.24	31.72

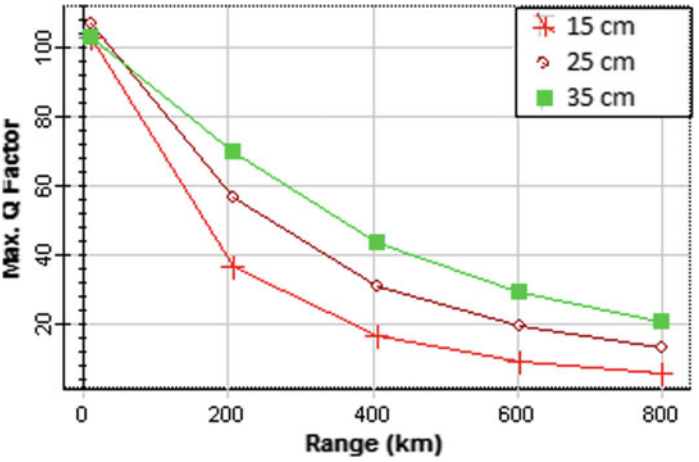

Fig. 9 *Q*-factor versus range with varying transmitter aperture diameter

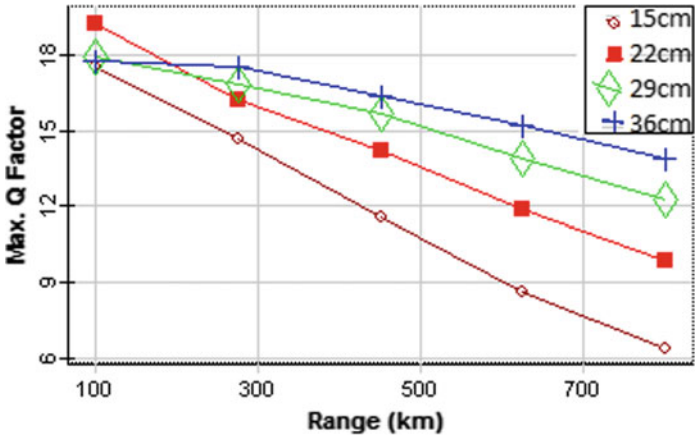

Fig. 10 *Q*-factor versus range considering different values of receiver aperture diameter

than at lower aperture diameter. It is clear from the graph that as the transmitter aperture diameter increases, the *Q*-factor also increases. Transmitter aperture diameter of 35 cm has been optimized for the further simulation.

4.6 Optimization of Receiver Aperture Diameter with Varying Range Using DPSK Modulation Format

Here in this section, Fig. 10 shows that 3 different values of receiver aperture diameter have been used to analyze the performance of IS-OWC link. It is observed that when small receiver aperture diameter is used, i.e., 15 cm, then lower *Q*-factor is achieved and also the system performs for smaller distance and while using higher receiver aperture diameter, the better *Q*-factor is achieved and system performs better for long distance than at lower receiver aperture diameter. It is clear from the graph that as the receiver aperture diameter increases; the *Q*-factor also increases. Receiver aperture diameter of 36 cm has been optimized for the further simulation.

5 Conclusion

In this work, we perform the optimization of inter-satellite optical wireless communication link considering different modulation schemes. There are various system parameters that have been analyzed and simulated to get better results for the link availability. ISOWC link has been designed for 800 km of range. Among three

advance modulation techniques analyzed DPSK, PSK, and OQPSK, the DPSK technique provides better results than other two modulation formats. DPSK modulation technique has been optimized for the further analysis. The system performs better at 15 dBm, and the wavelength at which ISOWC link covers longer transmission range is 850 nm. In this work, transmitter and receiver aperture diameters have also been analyzed and it is concluded that with use of 36 cm receiver aperture diameter and with use of 35 cm transmitter aperture diameter the system gives better. For the future work, the designed ISOWC link can be implemented for practical use in various communication applications.

References

1. Kaushal H, Kaddoum G (2016) Optical communication in space: Challenges and mitigation techniques. IEEE Commun Surv Tutor 19(1):57–96
2. Kaushal H, Jain V, Kar S (2017) Free-space optical channel models. Free space optical communication optical networks. Springer, India, pp 41–89
3. Kaur R, Kaur H (2018) Comparative analysis of chirped, AMI and DPSK modulation techniques in IS-OWC system. Optik 154:755–762
4. Pradhan S, Sahu PK, Giri RK, Patnaik B (2015) Inter-satellite optical wireless communication system design using diversity techniques. In: 2015 international conference on microwave, optical and communication engineering (ICMOCE), IEEE, pp 250–253
5. Ganga SS, Asha RS, Shaija PJ (2016) Design of a standardized inters satellite optical wireless communication (IsOWC) system with minimum input power. Procedia Technol 25:567–573
6. Poonam L (2015) Performance Analysis of IsOWC system using advanced modulation formats and schemes over wavelength spectrum. Int J Eng Develop Res 3(3)
7. Gill HK, Walia GK, Grewal NS (2019) Performance analysis of mode division multiplexing IS-OWC system using Manchester, DPSK and DQPSK modulation techniques. Optik 177:93–101
8. Vinod KK, Sarath VS, Kumar V, Turuk AK, Das SK (2017) Performance analysis of inter-satellite optical wireless communication. Int J Comput Netw Inf Secur 9(4):22
9. Kaur S (2019) Analysis of inter-satellite free-space optical link performance considering different system parameters. Opto-Electron Rev 27:10–13. https://doi.org/10.1016/j.opelre.2018.11
10. Kaur AS, Goyal R (2019) Analysis of terrestrial FSO link performance considering different fog conditions and internal parameters of the system. In: 2019 6th international conference on signal processing and integrated networks (SPIN), Noida, India, pp. 552–557. doi: https://doi.org/10.1109/SPIN.2019.8711577
11. Kaur S, Kakati A (2018) Analysis of free space optics link performance considering the effect of different weather conditions and modulation formats for terrestrial communication. J Opt Commun (published online ahead of print). doi: https://doi.org/https://doi.org/10.1515/joc-2018-0010

Different Diagnostic Aids and the Improved Scope of Establishing Early Breast Cancer Diagnosis

K. Venkata Ratna Prabha, D. Vaishali, Pallikonda Sarah Suhasini, K. Subhashini, and P. Ramesh

Abstract A good prognosis of cancer therapies mainly depends on how early the condition is being diagnosed and hence the initiation of appropriate treatment measures. In view of availability and affordability of a wide array of diagnostic approaches and methods, an attempt is made to provide a brief insight into each technique that leads to a noninvasive mode of determining the cancerous condition at an early stage. Many of these modern methods utilize radioisotopes to determine the extent of the condition in three-dimensional anatomical manners unlike the invasive histological examination of biopsies. A sound knowledge of these modern methods and understanding the importance of early diagnosis and treatment response are much needed for the better prognosis and well-being of the condition. This paper presents the detailed review of types of cancer, its diagnosis, treatments and also the recent methods of diagnosis using deep learning techniques.

Keywords Breast cancer · Biopsy · Chemotherapy · Deep learning · LABC · MRI · Mammography · PET scan · Staging · Tomography

K. V. R. Prabha (✉) · D. Vaishali · K. Subhashini
Department of ECE, SRMIST, Vadapalani Campus, Chennai, Tamil Nadu, India
e-mail: ratnaprabhakv@gmail.com

D. Vaishali
e-mail: vaishali.b@vdp.srmuniv.ac.in

P. S. Suhasini
Department of ECE, Velagapudi Ramakrishna Siddhartha Engineering College, Vijayawada, Andhra Pradesh, India
e-mail: pallikondasuhasini@gmail.com

P. Ramesh
Department of Conservative Dentistry and Endodontics, Drs Sudha and Nageswara Rao Siddhartha Institute of Dental Sciences, Chinoutpalli, Andhra Pradesh, India
e-mail: ramesh51endo@gmail.com

D. K. Sharma et al. (eds.), *Micro-Electronics and Telecommunication Engineering*,
Lecture Notes in Networks and Systems 179,
https://doi.org/10.1007/978-981-33-4687-1_7

1 Introduction

Cancer the world's leading cause of death accounted for some 9.6 million deaths in 2018 [1]. Infectious agents such as human papilloma virus (HPV) and hepatitis are responsible for up to 25% of cancers. The other causes include exogenous agents, genetic changes, and any physical or chemical chronic irritation also leads to cancer. Cancer may spread through vascular and lymphatic channels to distant body parts [1]. Commonly occurring cancer types that are diagnosed with greater frequency are breast cancer, lung cancer, kidney cancer, bladder cancer, pancreatic cancer, blood cancer, thyroid cancer, etc. [1, 2]. The most common cancer types seen are: among females—lung, breast, colorectal; among males—lung, colorectal, prostate; among children—leukemia, lymphoma, brain tumors. Features of breast cancer include a lumpy breast mass, a shift in breast shape, reddish or scaly skin patch dimpling off the skin. Factors like obesity, alcoholism, hormonal replacement therapy during menopause, lack of physical exercises, etc., increase the breast cancer risk. 5–10% of cases are due to genetic predisposition. About 80% are noticed by palpating such a lump with finger tips [1, 2]. In 2018, global breast cancer accounts for 25.4 percent of newly diagnosed cases among women. The top three cancers were breast, colorectal and lung cancers accounts for 43.9% of all cancer's types.

1.1 Breast Cancer Types

Most often breast tumors arise in the cells lining ducts of mammary glands, known as **ductal cancers which** accounts 80% of all breast cancers [1–3].

i. Invasive Ductal Carcinoma (IDC): Also called as infiltrating ductal carcinoma. It originates from cells lining the ducts that drain the mammary glands, leading to infiltration of breast tissue.
ii. Ductal Carcinoma in Situ (DCS): It originates in the skin or tissue other than mammary glands. This type does not spread or infiltrates to breast tissue.
iii. Invasive Lobular Carcinoma (ILC): Also called infiltrating lobular Carcinoma. It originates in the cells lining the lobules of mammary glands and invades the walls of lobules. It is second most common breast cancer.
iv. Lobular Carcinoma in Situ (LCS): It originates in the cells lining lobules of mammary glands and won't spread to adjacent tissues. Poses the increased risk of having invasive breast cancer.

Rarely seen breast cancer types include: i. Inflammatory Breast Cancer: An aggressive kind of cancer presenting with no lumpy tissue masses and causes a, red, swollen or inflamed appearance of the breast or breasts. ii. Paget's Disease of Breast: It involves areolae surrounding the nipple, usually the dark skin circle around the nipple.

1.2 Locally Advanced Breast Cancers (LABC)

20% among newly diagnosed breast cancer cases per year were locally advanced breast cancers (LABC). It includes tumor size more than 5 cm or tumor spread invading the skin or inflammatory type of breast cancer. Spread to infraclavicular, supraclavicular, internal mammary or fixed or matted axillary lymph nodes were also included. Subset of stage IIB and all stage III tumors are designated as locally advanced. Standard treatment protocol for LABC consists of multimodality treatment including neoadjuvant chemotherapy. LABC has poor survival rates (5 years survival rate of approximately 55% cases).

Various treatment modalities available:

1. **Chemotherapy**: Drug treatment in which powerful chemicals is administered either oral route or intravenous route to kill fast growing cells in our body and used primarily to reduce the total count of cancer cells, reduce the cancer spread, shrink tumor size, and reduce current symptoms.[1, 4, 5].
2. **Hormonal Therapy**: Hormones like progesterone and estrogen act upon the breast tissues. Cancerous cells have receptor proteins on their cell membrane for estrogen and progesterone, which causes them to develop. Medicines that impede these hormones from binding to these receptors come under hormonal or endocrine therapy [1, 4, 5]. Agents of hormonal therapy act by adding or blocking or removing the hormones to retard or stop the cancer cell growth that requires hormones for their growth. At hormone-receptor binding sites, they act in two ways i. By reducing the quantity of estrogen production in the body, ii. By blocking the action of estrogen on breast cancer cells.
3. **Radiation Therapy**: Radiotherapy treats cancer by utilizing high-frequency radio waves to damage tumor cells. Objective is to obliterate the malignant growth without harming an excessive number of healthy cells. High radiation dosages destroy cancerous cells or retards their multiplication process by damaging their DNA [1, 4, 5].
4. **Targeted Therapy**: It is different from traditional chemotherapy which also uses drugs to treat cancer and acts by targeting specific genes or proteins or the tissue ambiance that owes to cancer growth and survival. Targeted therapies are often cytostatic (i.e., they block tumor cell proliferation).
5. **Surgery**: Most breast cancer patients have some kind of surgery as a part of their treatment plan, to remove physically as much tumor masses as possible, provide possibility to find the metastatic spread to auxiliary lymph nodes, breast re-construction, and relieve symptoms of advanced cancer.

2 Related Work -Advanced Methods

To detect cancer at early stage, mammography screening is an effective method. For the radiologists, it is difficult to interpret as there are wide variations in the appearance

of normal and abnormal tissue of the breast in mammogram. To detect suspicious tissue in mammograms, in devising automatic methods, different feature extraction methods are proposed in the literature like template matching, gradient-based methods, independent component analysis, wavelets, fractal analysis, and support vector machines are used in segmentation of tissue. Classification methods like *K*-nearest neighbors (KNN), Markov models and neural networks are proposed [3]. Recently, machine learning techniques are used widely to for segmentation and classification [6, 7]. Cellular neural networks are investigated on magnetic resonance imaging (MRI), computed tomography (CT images), and fluorescent DNA microarray images [8]. Cellular neural networks are also used for segmenting the regions in mammogram images in which for detection of mass, geostatistical functions are used as texture signatures [9]. Deep learning is a non-representation of learning method that uses feature learning to discard a separate step of extraction of feature. Here, the computation models learn data representations with multiple levels of abstraction. Deep learning approaches such as convolutional neural networks have brought enormous development in state-of-the art domains, such as image and video object recognition, speech recognition, natural language processing. In the fields of medical image processing, such as MRI image segmentation, image fusion and CNN registration, significant improvements are reported in research [10]. In the recent research, deep learning techniques are used in cancer diagnosis [2, 10–13]. Following table illustrates summary of different research publications for density estimation, detection and classification with deep learning techniques (Table 1).

3 Existing Methods for Early Screening and Diagnosis

1. **Clinical Examination**: Both subjective and objective symptoms required to be concerned are swelling or lumpy mass in the breast, differences in size and shape of the two breasts, color differences of the breast skin and discharge from the nipples. Common risk factors include above 40 years, hereditary, hormonal therapy, and obesity [4, 12, 19, 20].
2. **X-Ray Mammography**: Low dose amplitude X-rays are used in examination of any calcium deposits which appears to be brighter in mammography. Mostly used for detecting early stage of the breast cancer, regarded as standard method. This is done prior to the lesions become clinically palpable favouring early diagnosis and hence reduces the breast cancer mortality. Very recent development is contrast enhanced digital mammography (CEDM). It uses standard iodinated intravenous (IV) contrast agent in conjunction with mammography [4, 12, 19, 20].
3. **Ultra Sound Imaging**: The breast lump under examination may be of solid mass or a fluid filled cyst. This imaging will determine these variations effectively. On the other hand, 3D images can be obtained with 3D ultrasound formats [4, 12, 19, 20].

Table 1 Breast density estimation, breast mass detection, and classification with convolutional neural networks—summary

Reference	Method used	Image type	Task
Xie et al. [14]	Multi-task CNN architecture	Histopathology images	Classification
Wei et al. [15]	Mixture ensemble of convolutional neural networks (ME-CNN)	DCE-MRI	Classification
Nahid et al. [16]	Combination of Convolutional Neural Network (CNN) and a Long Short-Term-Memory(LSTM)	Break His breast image dataset	Classification
Zuluaga-Gomez et al. [17]	CNN	Thermal Images	Classification
Wang et al. [18]	BiCNN model with transfer learning and fine-tuning method	Histopathological image	Classification
Savelli et al. [9]	CNN	Mammogram images	Detection
Wang et al. [10]	CNN	Breast imaging and Reporting Data System (BI-RADS) breast density categories	Density estimation
Ionescu et al. [6]	CNN	Mammographic images	Density estimation
Wu et al. [7]	CNN	Breast cancer screening exams images	Density estimation

4. **Breast Thermography**: As the metabolic rate in cancerous and pre-cancerous tissue will be high, there will be high-temperature changes surrounding these tissues as compared to normal breast tissue temperature, based on which it can detect cancer. The breast cancer can be diagnosed at least 10 years in advance, with this promising screening tool called thermograph [4, 12, 19, 20].
5. **MRI – Breast Magnetic Resonance Imaging**: To capture pictures of interior of breast, MRI machines use a magnet and radio waves. Radiation is not used in MRI [8, 11].
6. **Position Emission Tomography (PET) Scan**: PET scan is an imaging technique, where 3D images are captured. By introducing radio nuclide into the human body, pair of Υ rays emitted, by which images are formed. Compared with normal tissues, malignant tumors are characterized by increased glucose metabolism. Thus, between cancerous and non-cancerous cells, a good contrast would be observed in PET images. Fluorodeoxyglucose is useful in the detection and staging of recurrent breast cancer and assessing its response to chemotherapy [4, 12, 19].

7. **Scintimammography**: It is an imaging test to detect cancer cells in the women, who had abnormal mammograms, as well as women with dense breast tissue, breast implants and with suspected multiple tumors [4, 12, 19, 20].
8. **Optical Imaging**: Near-infrared (NIR) wavelength light is used to detect the lesions in the breast. Diffuse optical imaging (DOI), diffuse optical tomography, and optical mammography are different types of optical imaging. Without the need of harmful radiations and at less cost, this method also characterizes permeability, plethora of contrast agents, and vascularization [[4, 12, 19, 20].
9. **Electrical Impedance-Based Imaging**: Breast tissues which are cancerous will have low impedance. The two different impedance-based imaging methods are electrical impedance scanning [EIS] and electrical impedance tomography [EIT]. In this method, electrodes are kept around the surface of the breast circularly. By doing this, 2D or 3D images are captured with number of impedance values obtained from these electrodes. On the other hand, in EIS method which is simple as compared to EIT, a planar array of electrodes is used.
10. **Computer Tomography (CT)**: X-rays are used to capture 2D images; subsequently by using different algorithms, corresponding 3D-images are generated which provide lesions' anatomical information like location. For better visualization of tumors, iodinated contrast media is injected as intravenous, which improves image contrast. While observing the patients with breast cancer, the CT perfusion's accuracy of diagnosis in discriminating metastatic from inflammatory enlarged auxiliary lymph nodes demonstrated CT to be an effective tool. PET and CT combination is valuable for staging potential metastatic cancers.
11. **Tissue Biopsy**: A definitive diagnosis of breast cancer can be concluded at histological level using tissue biopsy. Specialized needle device guided by X-ray or some other imaging technique is used for the extraction of a core of tissue from the suspicious area. Subsequently, histological analysis is done. Sometimes, a tiny metal-marker is left within the tissues, so as to identify the area for future imaging tests [4, 12, 19, 20].
12. **Machine learning and Deep Learning**: Machine learning in diagnosing breast cancer helps in improving diagnosis of cancer, quality of care, and unnecessary biopsies. There is a break through with deep learning which demonstrated high performance beyond the state of the art in different tasks of machine learning like classification and object detection. In conventional machine learning methods, feature extraction stage is vital which require domain knowledge. Thus, feature extraction task is very challenging. Contrary to machine learning, in deep learning methods the feature extraction process is learned from the input data with respect to the output. Thus, the laborious process of extracting multiple features is thus eliminated with deep learning techniques. [5, 14, 15]

4 Conclusion

Although histological examination of biopsy samples remains the only definitive way of diagnosing the cancer, it is invasive and contributes to spread of the lesion locally. Many modern noninvasive methods give a close diagnosis of the condition at an early stage contributing to good prognosis and provide for the assessment of treatment response, which helps in either continuation or modification of treatment plan. Thermography provides diagnosis much earlier than subjective and objective symptoms appear. PET scan in conjugation with MRI can be of great value for the assessment of treatment outcome. The recent machine learning and deep learning techniques are robust in detection of cancer.

In light of these new noninvasive methods and their combinations, the future scope of cancer therapy seems promising in rendering early detection and monitoring prognostic responses, thereby providing utmost care and reducing the morbidity and mortality. Further, research work is needed in this area for a better combination of newer diagnostic aids in confronting the prognostic and therapeutic hurdles.

References

1. https://www.cancerresearchuk.org/what-is-cancer/how-cancer-starts/types-of-cancer
2. Dey B, Arun K (2018) A review article on breast cancer. Int J Pharm Pharm Res 11:284–298
3. Mao N, Yin P, Wang Q et al (2019) Added value of radiomics on mammography for breast cancer diagnosis: a feasibility study. J Am Coll Radiol 16(4):485–491
4. All Cancer Globo can (2019) 2018-International Agency for Research on Cancer WHO. https://gco.iarc.fr/today/data/factsheets/cancers/39-All-cancers-fact-sheet.pdf
5. Mohame AA, Berg WA, Peng H et al (2018) A deep learning method for classifying mammographic breast density categories. Med Phys 45(1):314–321
6. Ionescu GV, Fergie M, Berks M, et al (2019) Prediction of reader estimates of mammographic density using convolutional neural networks. J Med Image 6(3)
7. Wu N, Geras KJ, Shen Y, Su J, Kim SG, Kim E, Wolfson S, Moy L, Cho K (2018) Breast density classification with deep convolutional neural networks. In: 2018 IEEE international conference on acoustics, speech and signal processing (ICASSP). IEEE, pp 6682–6686
8. Tripathi PC, Bag S (2020) CNN-DMRI: a convolutional neural network for denoising of magnetic resonance images. Pattern Recogn Lett 135:57–63
9. Savelli B, Bria A, Molinara M, Marrocco C, Tortorella F (2020) A multi-context CNN ensemble for small lesion detection. Artif Intell Med 103:101749
10. Wang H, Feng J, Bu Q et al (2018) Breast mass detection in digital mammogram based on Gestalt psychology. J Healthc Eng 2018:13. (Article ID 4015613)
11. Rasti R, Teshnehlab M, Phung SL (2017) Breast cancer diagnosis İndce-MRI using mixture ensemble of convolutional neural networks. Pattern Recog 72:381–390
12. Yassin NI, Omran S, El Houby EM, Allam H (2018) Machine learning techniques for breast cancer computer aided diagnosis using different image modalities: a systematic review. Comput Methods Prog Biomed 156:25–45
13. Valvano G, Santini G, Martini N et al (2019) Convolutional neural networks for the segmentation of micro calcification in mammography imaging. J Healthc Eng 2019:9. (Article ID 9360941)
14. Xie J, Liu R, Luttrell J IV, Zhang C (2019) Deep learning based analysis of histopathological images of breast cancer. Front Genet 10:80

15. Wei B, Han Z, He X, Yin Y (2017) Deep learning model based breast cancer histopathological image classification. In: 2017 IEEE 2nd international conference on cloud computing and big data analysis (ICCCBDA). IEEE, pp 348–353
16. Nahid A-A, Mehrabi MA, Kong Y (2018) Histopathological breast cancer image classification by deep neural network techniques Guided by local clustering. Biomed Res Int 1–20s
17. Zuluaga-Gomez J, Masry ZA, Benaggoune K, Meraghni S, Zerhouni N (2019) A CNN-based methodology for breast cancer diagnosis using thermal images.ArXiv, abs/1910.13757
18. Wang Z, Li M, Wang H, Jiang H, Yao Y, Zhang H, Xin J (2019) Breast cancer detection using extreme learning machine based on feature fusion with CNN deep features. IEEE Access
19. Mambou SJ, Maresova P, Krejcar O, Selamat A, Kuca K (2018) Breast cancer detection using infrared thermal imaging and a deep learning model. Sensors 18(9):2799
20. Gonçalves CB, Leles AC, Oliveira LE, Guimaraes G, Cunha JR, Fernandes H (2019) Machine learning and infrared thermography for breast cancer detection. Multidisciplinary Digital Publishing Institute Proceedings 27(1):45

Deforestation Mapping Using MODIS Tree Cover Mask and Sentinel-1 Images

Prachi Kaushik and Suraiya Jabin

Abstract Forests are an essential resource that needs to be conserved. Excessive cutting of trees for urbanization and growth has led to rapid deforestation in parts of Haryana and its neighboring areas. In this study, tree cover mapping is done over a period of five years (2015–2019) using Sentinel-1 ground range detected band-C images. To distinguish between the land cover classes, a rich set of features play an important role. Based on the second-order statistics, gray level co-occurrence (GLCM) features are extracted from the image to study the uniformity between the pixels. A binary classification of the study area into tree and non-tree area is carried out by supervised random forest algorithm. According to the analysis, the net rate of reduction of the tree cover in parts Haryana and its neighboring areas, i.e., parts of New Delhi, is calculated as 3.1% in successive years.

Keywords Deforestation · SAR · Random forest · GLCM · Sentinel-1 · MODIS

1 Introduction

Deforestation and forest degradation are a result of the urban development in the state of Haryana. Haryana's economic development has led to the increase in the number of industries, construction of high-rise buildings for residential use, especially in districts of Gurugram and Faridabad. New industries have been set up by cutting large number of trees thereby thinning the tree cover. Due to the deforestation, the amount of rainfall has also been reduced. There has been substantial fall in the ground water level in the past twelve years which has adversely affected the farmers for irrigation of crops. The farmers in Haryana depend on the freshwater from the

P. Kaushik (✉) · S. Jabin
Department of Computer Science, Jamia Millia Islamia, New Delhi 110025, India
e-mail: prachikaushik.4@gmail.com

S. Jabin
e-mail: sjabin@jmi.ac.in

D. K. Sharma et al. (eds.), *Micro-Electronics and Telecommunication Engineering*,
Lecture Notes in Networks and Systems 179,
https://doi.org/10.1007/978-981-33-4687-1_8

wells and rainfall for irrigation purpose. Over the years, Haryana has witnessed a sharp fall in annual production of crops such as cotton, bajra, basmati rice, and paddy.

In this study, some parts of Haryana and New Delhi are analyzed over a period of five years (2015–2019) using Sentinel-1 images to map the extent of deforestation in these areas. There have been various studies on the deforestation mapping using different bands of the synthetic aperture radar. To enlist few studies, Rahman et al. [1] mapped the tropical forest cover and deforestation using SAR-C (band-C) and ALOS PALSAR (band-L) images classifying forest and non-forest areas by maximum likelihood classifier. Delgado et al. [2] derived the degradation status of Sumaco Biosphere Reserve Ecuador due to deforestation with the use of Terra SAR (band-X) and Sentinel-1 (band-C). The backscatter from the active radar is fed as input to the random forest algorithm to classify the areas as forest and non-forest. The fusion of RADAR data and optical data (Sentinel-2, Landsat, MODIS) has been used to produce accurate forest maps. Ritchiee et al. [3] used a combination of Sentinel 1, ALOS2 PALSAR, and Landsat time series to detect near real-time deforestation. In another paper, Ritchiee et al. [4] also used a combination of Landsat and ALOS PALSAR (band-L) to extract relevant feature for decision tree classifier.

Saatchi et al. [5] used L- and C-band SAR data for the classification of the deforestation area by the Bayesian classifier with an accuracy of 87%. This study also highlights the comparison between the data acquired in the wet and dry season. Almeida Filho et al. [6] shows an analysis based on the stages of deforestation (slashing, burning, terrain, and clearing) using Landsat images. The wood pieces left after cutting the trees initially act as corner reflectors, but as the debris is removed the backscatter decreases. Kuntz et al. [7] talks about the capability of the ESA ERS satellite for the land monitoring applications. The texture features are created which discriminates among various land cover classes in tropical rain forests. Barreto et al. [8] proposes the use of the two segmentation approaches like iterative clustering and object correlation image segmentation for the X-band synthetic aperture radar images. A. Bouvet [9] in his paper has exploited a new indicator of the shadows which form due to the acquisition of images in slant range to detect deforestation by the use of Sentinel-1 images.

In the proposed work, we present a robust method to find deforestation mapping using Sentinel-1 images. The next section discusses the methodology for calculating the rate of deforestation.

2 Material and Methods

2.1 Acquisition of Image Dataset

Five Sentinel-1A level-1 ground range detected (GRD) products for a period of Aug 2015 to June 2019 are downloaded from Copernicus Open Access Hub [10] for the study area which comprises some parts of Haryana and New Delhi. The time series

dataset from Aug 2015 to June 2019 cover parts of Haryana (Panipat, Hisar, Rohtak, Bhiwani, Rewari, and Gurugram) and New Delhi. The SAR-C synthetic aperture radar instrument operating at a central frequency of 5.404 GHz fitted on the Sentinel-1 Satellite has all weather, day, and night imaging capability. It can capture high-resolution remote-sensing images for land and ocean monitoring. Interferometric wide swath (IW) mode with a swath of 250 km at 5 m by 20 m spatial resolution is preferred as it is suitable for land cover classifications as it acquires the image with detail and resolution. Five datasets with the same geographical coordinates and orbit number (136), VV and VH bands but different time frames (2015 to 2019) are used to map the change in the tree cover using the Sentinel-1A images as given in Table 1.

2.2 Methodology

The reduced percentage of tree covers is due to rapid growth in urban development. It has been observed that National Capital Region (NCR) has a larger rate of deforestation. The methodology for the derivation of tree cover to analyze the rate of deforestation in major parts of Haryana and New Delhi is divided into several steps. The initial step requires preprocessing of Sentinel-1 data, calculation of GLCM features, derivation of training samples using land cover MODIS 2007 mask, classification using random forest algorithm, and change detection to calculate the change in forest cover from August 2015 to June 2019.

Preprocessing of Sentinel-1A images
Level-1 Sentinel-1 GRD multi-temporal images are preprocessed using the SNAP Tool box (Version 6) [11]. To improve the geo-coding and the SAR processing results, the first step of preprocessing [12] is to apply orbit file correction. The next step is calibration to Sigma naught values to map the pixel values directly to the backscatter of the radar. After calibration a 7*7 window size Lee speckle filter is applied to reduce the amount of the grainy noise in the images to further improve the classification results. The last preprocessing step is to convert the data type of the product into int8 for both bands (Sigma0_VH, Sigma0_VB). The converted product is an input parameter for the GLCM texture analysis.

Texture Analysis
A rich set of features in the high-resolution images are essential for understanding the correlation between the sigma backscatter return and texture signatures by landforms in the image. Second-order descriptive statistical features from the image are calculated by the gray level co-occurrence matrix (GCLM) operator available in the SNAP [11] tool. The texture information like mean, variation, contrast, and energy is calculated for the image. It calculates the frequency of the occurrence of the pair of pixels with the particular value in spatial domain. For the analysis purpose, only six GLCM features are calculated, i.e., SigmaVH_Contrast,

Table 1 Image dataset in classification study

Year	Data product	Date of acquisition
2015	S1A_IW_GRDH_1SDV_20150308T005141_20150308T005207_004933_0062A3_5838	08/03/2015
2016	S1A_IW_GRDH_1SDV_20161004T005151_20161004T005216_013333_01542A_4C79	04/10/2016
2017	S1A_IW_GRDH_1SDV_20171128T005158_20171128T005223_019458_02103B_D789	28/11/2017
2018	S1A_IW_GRDH_1SDV_20180819T005203_20180819T005228_023308_0288EB_FEA8	19/08/2018
2019	S1A_IW_GRDH_1SDV_20190603T005205_20190603T005230_027508_031AA0_C615	03/06/2019

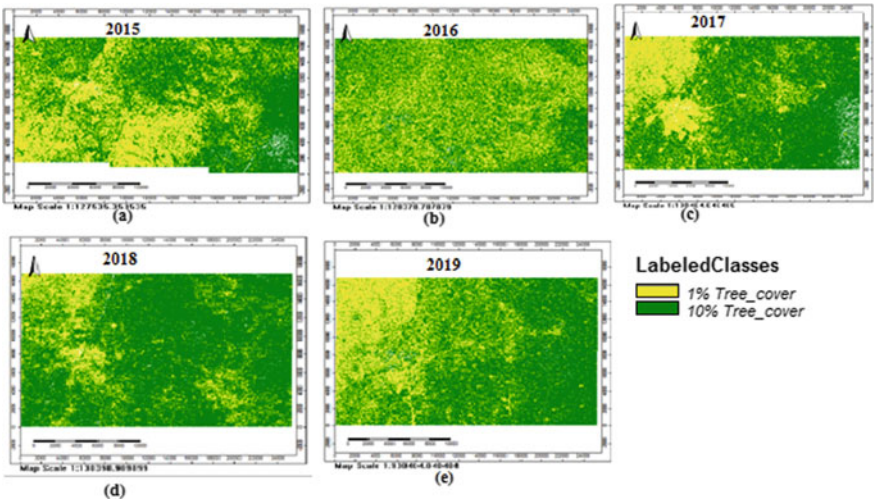

Fig. 1 Classification results from 2015–2019

SigmaVH_Mean, SigmaVH_Variance, SigmaVV_Contrast, SigmaVV_Mean, and SigmaVV_Variance, with respect to each band VH and VV. This information is used for the image classification done in the next step. These features are widely used to compute the second-order statistical features in the satellite images.

Training Samples and Classification

The GLCM features calculated in the previous steps are used as an input in the classification using random forest algorithm. The training sample for 1% tree cover and 10% tree cover are used for supervised classification. The land cover mask, MODIS 2007 Tree cover percentage as shown in Fig. 1, is added on the preprocessed image. The training vectors are selected for the regions having tree cover percentage ranging from 1 to 3% under the label of 1% tree cover. This percentage gives an idea that an area has only 1–3% of area covered by trees, and there is increase in deforestation. The other areas having tree cover percentage more than 35% (median value of the data) are named with the label of 10% tree cover to give an area that the area has more than 35% of the tree cover. These shape files are used as training samples for random forest algorithm. The random forest algorithm is effective in mapping the deforestation in the area on the basis of the training samples as shown in Fig. 1.

3 Experiments and Results

Table 2 presents detailed results for the classification of the study area in two classes of 1% and 10% tree cover in form of percentage change and area change by random

Table 2 Classification results using random forest algorithm

Year	1% tree cover	10% tree cover	1% area cover (Km^2)	10% area cover (Km^2)
2015	60.309	39.691	23,466	15,377.120
2016	65.703	34.297	25,421	13,297
2017	69.642	30.358	27,651	12,080
2018	82.235	17.765	33,026.102	7146
2019	68.205	31.795	27,427	12,809

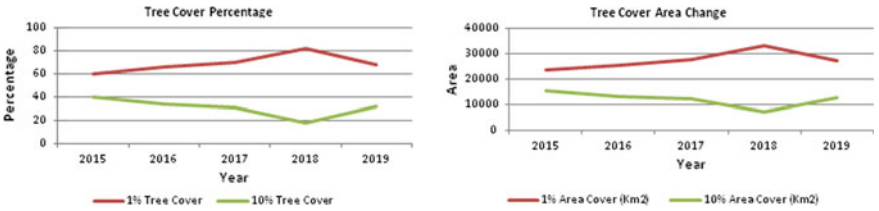

Fig. 2 Graphical representation of tree cover random forest results

forest algorithm. The results are visually represented in the line graphs to show the time series change (see Fig. 2).

The analysis of the results is done on the basis of Formula (1) given in Eq. (1):

$$P_n = P_0(1 + r)^n \tag{1}$$

where P_n is the percentage value after n year.

P_0 is the initial percentage value and r is the rate of growth.

Formula Used for Finding NET Average Rate

$$G = \text{AntiLog}\left(\frac{\sum \log X}{n}\right) \tag{2}$$

where G is the average rate, $x = 100 + r$

$$\text{NET Rate} = G - 100 \tag{3}$$

Table 3 presents the results of random forest algorithm in the form of frequency of the labeled classes (1% tree cover, 10% tree cover). The classifier is trained by the training samples and the GLCM features which classifies the input image of each year into two classes (1% tree cover and 10% tree cover). It is clearly evident from Table 3 that the percentage of 1% tree cover is growing successively every year from 2015 to 2019. The deforestation rate is increasing at a rapid rate. The percentage of tree cover with more than 10% of the trees is decreasing with an alarming rate. For

Table 3 Chain-based method

Year	1% tree cover		1% tree cover	
	Rate %	Rate % (Area)	Rate %	Rate % (Area)
2016	8.94	8.33	– 13.59	– 13.53
2017	6.00	8.772	– 11.48	– 9.152
2018	18.08	19.43	– 41.48	– 40.8
2019	– 17.06	– 16.95	78.98	79.24
NET	3.1	4	– 5.39	– 4.46

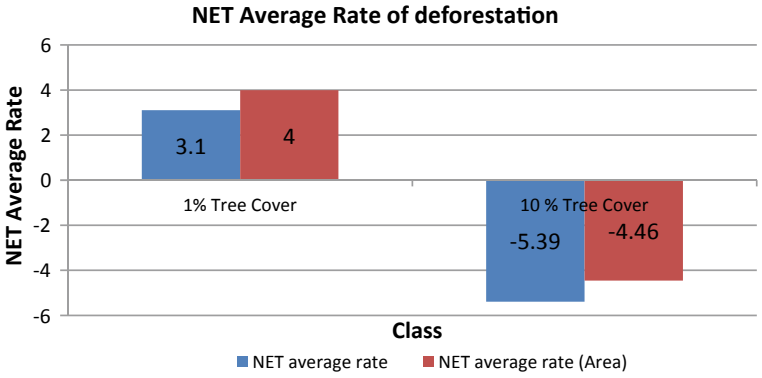

Fig. 3 Net rate of deforestation

analysis, the net rate of deforestation has been calculated using chain-based method described in the next subsection.

Chain-Based Method

This method computes the relative difference in the growth of deforestation. The net rate of growth for the year 2016 is calculated with respect to year 2015; year 2017 is calculated with respect to year 2016 and so on using Eq. (1). The total net growth of deforestation in five years is calculated as 3.1%, and the decrease in the area under 10% tree cover is 5.39% using Eqs. (2) and (3). The rate of deforestation is increasing day by day as it can be clearly seen from Fig. 3 that a considerable decrease in the tree cover is observed from the year 2015–2018. So, some efforts are made by the government agencies to check this alarming situation of deforestation.

4 Conclusion

The results presented in this study suggest that dual polarization (HV and VV) of Sentinel-1 can be used for mapping change in tree cover over a time-series data. The

analysis show that in many parts of Haryana, the tree cover is decreasing at a rate of 3.1% successively every year. Hence, there is a need to plan out some strategies to improve the tree cover in some of the parts of Haryana and New Delhi.

References

1. Rahman MM, Sumantyo JT (2010) Mapping tropical forest cover and deforestation using synthetic aperture radar (SAR) images. Appl Geomatics 2(3):113–121
2. Delgado-Aguilar MJ, Fassnacht FE, Peralvo M, Gross CP, Schmitt CB (2017) Potential of TerraSAR-X and sentinel 1 imagery to map deforested areas and derive degradation status in complex rain forests of Ecuador. Int Forest Rev 19(1):102–118
3. Reiche J, Verbesselt J, Hoekman D, Herold M (2015) Fusing Landsat and SAR time series to detect deforestation in the tropics. Remote Sens Environ 156:276–293
4. Almeida-Filho R, Shimabukuro YE, Rosenqvist A, Sanchez GA (2009) Using dual-polarized ALOS PALSAR data for detecting new fronts of deforestation in the Brazilian Amazônia. Int J Remote Sens 30(14):3735–3743
5. Saatchi SS, Soares JV, Alves DS (1997) Mapping deforestation and land use in Amazon rainforest by using SIR-C imagery. Remote Sens Environ 59(2):191–202
6. Almeida-Filho R, Rosenqvist A, Shimabukuro YE, Silva-Gomez R (2007) Detecting deforestation with multitemporal L-band SAR imagery: a case study in western Brazilian Amazonia. Int J Remote Sens 28(6):1383–1390
7. Kuntz S, Siegert F (1999) Monitoring of deforestation and land use in Indonesia with multitemporal ERS data. Int J Remote Sens 20(14):2835–2853
8. Barreto TL, Rosa RA, Wimmer C, Nogueira JB, Almeida J, Cappabianco FAM (2016) Deforestation change detection using high-resolution multi-temporal X-Band SAR images and supervised learning classification. In: 2016 IEEE international geoscience and remote sensing symposium (IGARSS). IEEE, pp 5201–5204
9. Bouvet A, Mermoz S, Ballère M, Koleck T, Le Toan T (2018) Use of the SAR shadowing effect for deforestation detection with Sentinel-1 time series. Remote Sens 10(8):1250
10. European Space Agency Copernicus Open Access Hub. https://scihub.copernicus.eu/. Online Accessed on date 14 Mar 2020
11. Matthieu Bourbigot Sentinel-1. https://sentinel.esa.int/documents/247904/1877131/Sentinel-1-Product-Definition. Accessed on 14 Mar 2020
12. Kaushik P, Jabin S (2018) A Comparative study of pre-processing techniques of SAR images. In: 2018 4th international conference on computing communication and automation (ICCCA). IEEE, pp 1–4. doi: https://doi.org/10.1109/CCAA.2018.8777710

Assessing the Suitability of DMG-HK Trapezoidal FinFET for High Temperature Applications

Priyanshi Goyal and Harsupreet Kaur

Abstract In this paper, we have developed a temperature-dependent analytical model to study the effectiveness of DMG-HK Trapezoidal FinFET for high temperature operation. It is demonstrated that the proposed device with incorporation of dual material gate and high K layer leads to less degradation in device performance at high temperature as compared to conventional devices. The improvement is seen in terms of reduced threshold voltage sensitivity and DIBL with change in temperature along with suppressed hot carrier effects and improved subthreshold slope.

Keywords Gate stack · Short channel effects (SCEs) · Multigate · High temperature operation

1 Introduction

Since the conventional MOSFET dimensions have been pushed in nanoscale regime and it is extremely important to overcome short channel effects like threshold voltage roll off, drain-induced barrier lowering (DIBL), subthreshold swing, etc., various novel device designs such as multigate geometry devices [1], channel engineering, gate electrode, and gate dielectric engineering techniques [2–4] have been widely reported in the last few years. In view of this, we had proposed an analytical model for DMG-HK Trapezoidal FinFET which incorporates the advantages of the DMG design as well as high K layer [5]

However, it is a well-known fact that device performance degrades at high temperatures, and temperature variations can also cause reliability issues in the circuit. Hence, thermal characterization is necessary when the device is scaled down and operated over a large temperature range [6, 7]. Therefore, in the present work, an

P. Goyal · H. Kaur (✉)
Department of Electronic Science, University of Delhi South Campus, New Delhi 110021, India
e-mail: harsupreetkaur@gmail.com

P. Goyal
e-mail: priyanshigoel.31@gmail.com

D. K. Sharma et al. (eds.), *Micro-Electronics and Telecommunication Engineering*,
Lecture Notes in Networks and Systems 179,
https://doi.org/10.1007/978-981-33-4687-1_9

analytical model has been developed to examine the suitability of DMG-HK Trapezoidal FinFET for high temperature applications. Its effectiveness for high temperature applications has been comprehensively analyzed by comparing various device characteristics with conventional trapezoidal FinFET (C-trapezoidal FinFET) device and dual material gate trapezoidal FinFET (DMG-trapezoidal FinFET) device.

The paper is organized as follows. In Sect. 2, model formulation has been presented followed by Sect. 3 which presents results and discussion. Finally, conclusion is presented in Sect. 4.

2 Model Formulation

Figure 1 shows cross-sectional view of dual material gate-high k trapezoidal FinFET (DMG-HK trapezoidal FinFET).

Using the same methodology as discussed in [5], the 3D scaling Poisson's equation is solved to obtain various characteristics, and the equation is given as

$$\frac{d^2\emptyset_i(z)}{dz^2} - \frac{1}{\lambda_s^2}(\emptyset_i(z) - \emptyset_i(T)) = 0 \tag{1}$$

where $i = 1, 2$ for regions with lengths $L_1(0 \leq Z \leq L_1)$ and $L_2(L_1 \leq Z \leq L_g)$, respectively. L_1 and L_2 are lengths of gates with higher ($\Phi_{M1} = 4.9\,\text{eV}$) and lower ($\Phi_{M2} = 4.4\,\text{eV}$) workfunctions, respectively, and $\emptyset_i(z)$ corresponds to the bottom central potential. λ_s is scaling length and is given as

$$\frac{1}{\lambda_s^2} = \frac{8\varepsilon_{ox}}{(4W_{eff}\varepsilon_{si}t_{oxeff} + \varepsilon_{ox}W_{eff}^2)} \tag{2}$$

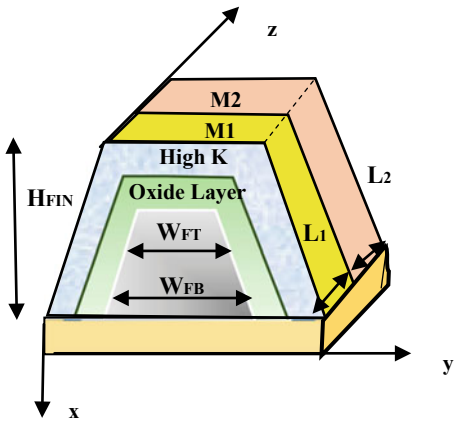

Fig. 1 DMG-HK trapezoidal FinFET

where W_{eff} is the effective fin width [8], t_{oxeff} is effective oxide thickness of gate stack [5] ε_{si}, and ε_{ox} are the permittivity of silicon and oxide.

$\emptyset_i(T)$ denotes the bottom central potential in the two regions and the equation is given as [8]

$$\emptyset_i(T) = V_{\text{gs}} - V_{\text{fbi}}(T) - (qN_{\text{ch}}/\varepsilon_{\text{si}})\lambda_s^2 \tag{3}$$

where $V_{\text{fbi}}(T)$ denotes the flat band voltage in the two regions and N_{ch} denotes doping concentration of channel.

In order to account for temperature dependence in the model, the following parameters have been obtained [7],

$$E_{\text{g}}(T) = 1.179 - \left(9.025\left(10^{-5}\right)T - 3.050\left(10^{-7}\right)T^2\right) \tag{4}$$

$$n_i(T) = 3.34\left(10^{25}\right)(T/300)^{0.5}\text{e}^{-E_{\text{g}}(T)/2kT} \tag{5}$$

$$\Phi_{\text{si}}(T) = E_{\text{g}}(T)/2 - q\Phi_f(T) \tag{6}$$

$$\Phi_f(T) = (KT/q)\ln(N_{\text{a}}/n_i(T)) \tag{7}$$

where $E_{\text{g}}(T)$, $n_i(T)$, $\Phi_{\text{si}}(T)$, and $\Phi_f(T)$ denote band gap, intrinsic carrier concentration, workfunction, and fermi potential of silicon, respectively.

Incorporating Eqs. (4)–(7), considering the boundary conditions [8] and solving Eq. (1), following solutions for channel potential have been obtained.

$$\emptyset_1(z) = C_1 e^{\frac{Z}{\lambda_s}} + C_2 e^{\frac{-Z}{\lambda_s}} + \emptyset_1 \tag{8}$$

$$\emptyset_2(z) = D_1 e^{\frac{(Z-L_1)}{\lambda_s}} + D_2 e^{\frac{-(Z-L_1)}{\lambda_s}} + \emptyset_2 \tag{9}$$

where

$$\begin{aligned}
C_1 &= c_1 V_{\text{gs}} + d_1,\ C_2 = c_2 V_{\text{gs}} + d_2,\\
D_1 &= C_1 \exp(L_1/\lambda_{\text{s}}) - (\emptyset_2 - \emptyset_1)/2\\
D_2 &= C_2 \exp(-L_1/\lambda_{\text{s}}) - (\emptyset_2 - \emptyset_1)/2,\\
c_1 &= \left(\exp\left(-L_{\text{g}}/\lambda_{\text{s}}\right) - 1\right)/2\sinh\left(L_{\text{g}}/\lambda_{\text{s}}\right)\\
c_2 &= \left(1 - \exp\left(L_{\text{g}}/\lambda_{\text{s}}\right)\right)/2\sinh\left(L_{\text{g}}/\lambda_{\text{s}}\right),\\
d_1 &= V_{\text{bi}}(T) + V_{\text{fb1}}(T) + qN_{\text{ch}}/\varepsilon_{\text{si}} - d_2\\
d_2 &= (-V_{\text{ds}} + Y_1 - \left(V_{\text{bi}}(T) + V_{\text{fb2}}(T) + (qN_{\text{ch}}/\varepsilon_{\text{si}})\lambda_{\text{s}}^2\right)\\
&\quad - Y_2)/2\sinh\left(L_{\text{g}}/\lambda_{\text{s}}\right)
\end{aligned}$$

$$Y_1 = (V_{\text{bi}}(T) + V_{\text{fb1}}(T) + qN_{\text{ch}}/\varepsilon_{\text{si}})e^{L_g/\lambda_s},$$
$$Y_2 = (\emptyset_2 - \emptyset_1)\cosh(-L_2/\lambda_s)$$

where V_{gs}, $V_{\text{bi}}(T)$, and V_{ds} denote gate to source voltage, built-in voltage, and drain voltage, respectively.

Threshold voltage has been obtained by equating the minimum bottom potential to twice of bulk potential [8] and solving the resultant equation. Furthermore, subthreshold swing can be obtained using the following expression

$$\text{SS} = 2.3V_t(T)\left(\frac{\text{d}\emptyset_{\text{min}}}{\text{d}V_{\text{gs}}}\right)^{-1} \tag{10}$$

where $V_t(T)$ is thermal voltage and $\emptyset_{\text{min}}(z)$ is minimum bottom potential.

3 Results and Discussion

In this section, various parameters such as surface potential, electric field, threshold voltage, DIBL, and subthreshold swing have been obtained, and a comparison has been drawn out between DMG-HK trapezoidal FinFET (device 1), DMG trapezoidal FinFET (device 2), and conventional trapezoidal FinFET (device 3) for a wide temperature range (200–300 K). Various parameters used in present work are: N_{ch} has a value 10^{16} cm^{-3}. The fin height, top fin width, and bottom fin width are denoted as H_{FIN} (20 nm), W_{FT} (15 nm), and W_{FB} (20 nm), respectively. The gate stack comprises oxide layer and high K layer. The thickness of oxide layer is denoted by t_1 (1 nm), and high K layer thickness is denoted by t_2 (2 nm).The gate stack thickness of device 3 is kept same as physical thickness of SiO_2 layer for device 1 and device 2.

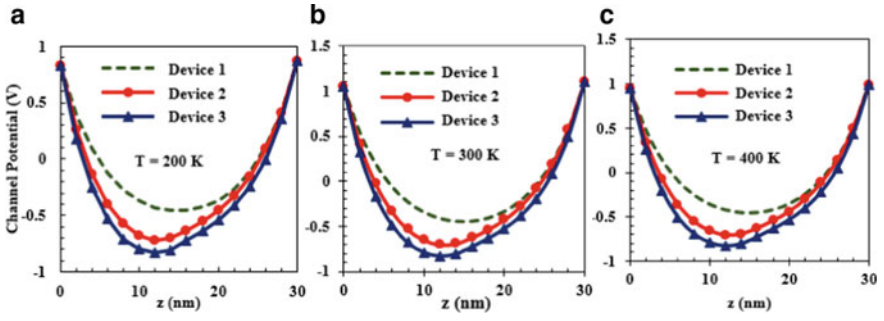

Fig. 2 **a–c** Channel potential along channel at 200, 300, and 400 K for all devices

Figure 2a–c show the change in channel potential along channel length for all devices at different values of temperatures. It can be seen that an increase in temperature leads to lowering of potential barrier. However, it is evident that degradation is minimum for device 3 in comparison with device 1 and device 2. This is because the layer with higher dielectric constant in gate stack of proposed device along with DMG design results in improved capacitive coupling which leads to less degradation with increase in temperature.

Figure 3a–c show the variation in electric field along channel length for all devices at different values of temperature. It can be seen that electric field at drain side increases with increase in temperature for both device 1 and device 2, whereas the increase is much less for device 3. This implies that device 3 is more immune to hot carrier effects apart from offering improved transport efficiency and immunity to SCEs.

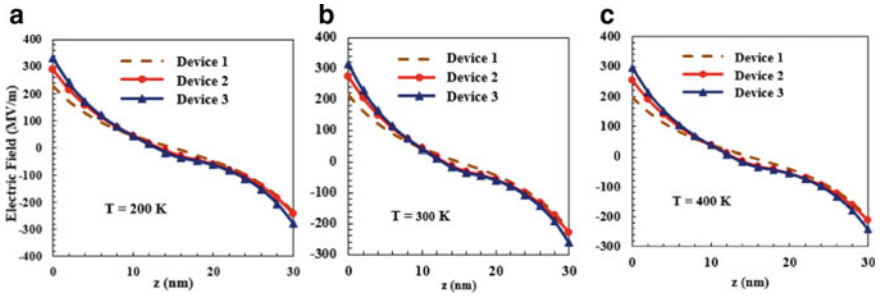

Fig. 3 **a–c** Electric field along channel at 200, 300, and 400 K for all devices

Fig. 4 Threshold voltage with temperature for all devices

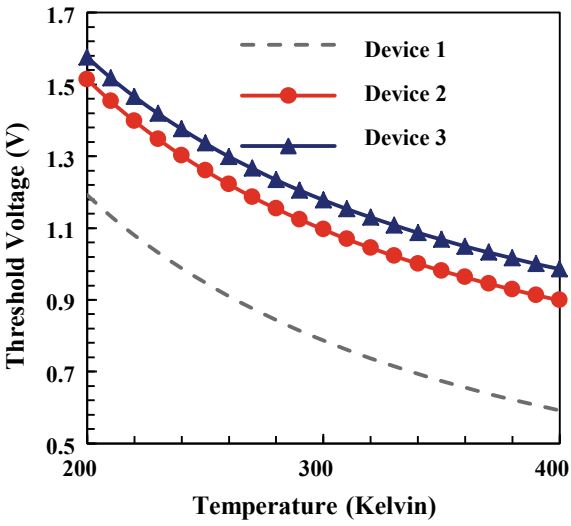

Figure 4 shows the variation in threshold voltage with temperature for all devices. It can be seen that threshold voltage reduces with increase in temperature for all devices. However, there is less degradation in device 3 compared to device 1 and device 2. This is because the decrease in potential barrier is minimum in device 3 in comparison with other two devices.

Figure 5 shows DIBL variation with temperature for all devices. It can be observed that as compared to device 1 and device 2, device 3 exhibits least value of DIBL, and it shows almost no change in DIBL with increase in temperature.

Furthermore, in Fig. 6a–c, the same trend can be seen. The value of subthreshold swing is deteriorating with increase in temperature for all three devices. But device 3 shows minimum degradation in comparison with other two devices. This implies that incorporation of dual material gate and high k dielectric reduce the amount of leakage current in the device and also reduce the subthreshold swing.

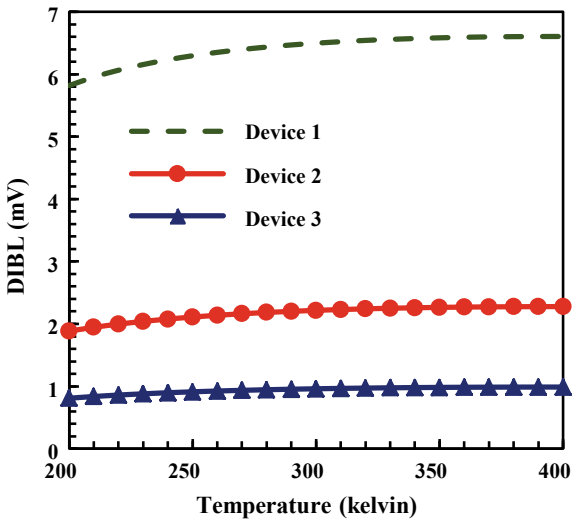

Fig. 5 DIBL with temperature for all devices

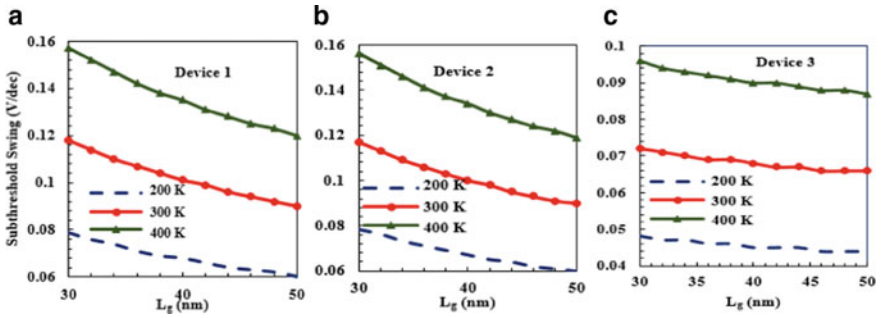

Fig. 6 **a–c** Subthreshold with channel length (nm) at different values of temperature for all devices

4 Conclusion

In summary, we have presented an analytical model to study the suitability of DMG-HK trapezoidal FinFET for high temperature applications. The work demonstrates that integration of gate electrode workfunction engineering along with the presence of high K dielectric layer in the gate stack of proposed device helps in achieving improved device performance in comparison with conventional device even at elevated temperatures. The substantial improvement noticed in threshold voltage roll off, DIBL as well as subthreshold swing corroborates this. It is anticipated that the work will pave the way to further explore the potential of the device for analog and high-frequency applications.

References

1. Brendler LH, Zimpeck AL (2020) Multi-level design influences on robustness evaluation of 7 nm FinFET technology. IEEE Trans Circ Syst 67(2)
2. Kailasam M, Govindasamy M (2020) Impact of high-K gate dielectrics on short channel effects of DG N-finfet. Int J Sci Technol Res 9(03)
3. Kasthuri Bha JK, Aruna Priya P, Bijio Joseph H, John Thiruvadigal D (2019) 10 nm trigate high K underlap FinFET: scaling effects and analog performance. Springer, New York
4. Narendar V, Mishra RA (2015) Analytical modeling and simulation of multigate FinFET devices and the impact of high-k dielectrics on short channel effects (SCEs). Superlattices Microstruct 85:357–369
5. Goyal P, Kaur H (2020) Superior performance of gate workfunction and gate dielectric engineered trapezoidal FinFET in the presence of trap charges, microelectronics, circuits and systems. Micro
6. Jeon DS, Burk DE (1991) A temperature-dependent SOI MOSFET model for high-temperature application (27 °C–300 °C). IEEE Trans Electron Devices 38(9):2101–2111
7. Kranti A, Haldar S, Gupta RS (1999) Temperature-dependent threshold voltage analysis of surrounding/cylindrical gate fully depleted thin film SOI MOSFET in the range 77 to 520 K. Microelectr Eng 49(3–4):273–286
8. Banerjee P, Sarkar SK (2018) Comprehensive analysis of Subthreshold short channel behavior of a Dual-material gate strained trapezoidal FinFET. Superlattices Microstruct 117:527–537

Optimization of the CNN Model for Hand Sign Language Recognition Using Adam Optimization Technique

Simrann Arora, Akash Gupta, Rachna Jain, and Anand Nayyar

Abstract To communicate with someone, hand signs prove to be more effective than just words to emphasize and structure the conversation and give more clarity. Some machines, like a driving car or a robot, are also operated by hand gestures as they are more convenient to interpret, but devising the recognition of hand gesture system is an extremely arcane commission since the model should be clever enough to recognize the hand gestures in distinct positions and orientation. In this research, the convolution neural network (CNN) model of deep learning (DL) is utilized for training the hand sign language image dataset. In addition to this, the Adam optimization technique, which is known to leverage the adaptive learning technique for figuring out the learning rate for every parameter, is utilized here for determining the optimized values of hyperparameters. The dataset is taken from GitHub and is contributed by the *Turkey Ankara Ayrancı Anadolu High School* students. The dataset consists of 218 hand sign sample images of each of the ten digits ranging from 0–9. After determining the optimized values of various hyperparameters, the proposed framework is then validated upon the validation dataset. The training and validation loss over the optimized number of epochs comes out to be 0.021 and 0.064, respectively. Conclusively, the investigational outcomes depict that the anticipated optimized CNN model displays an increased accuracy of 98%.

S. Arora · A. Gupta · R. Jain
Department of Computer Science and Engineering, Bharati Vidyapeeth's College of Engineering, New Delhi, India
e-mail: simrann2099@gmail.com

A. Gupta
e-mail: akashgupta752000@gmail.com

R. Jain
e-mail: rachna.jain@bharatividyapeeth.edu

A. Nayyar (✉)
Graduate School, Faculty of Information Technology, Duy Tan University, Da Nang 550000, Vietnam
e-mail: anandnayyar@duytan.edu.vn

D. K. Sharma et al. (eds.), *Micro-Electronics and Telecommunication Engineering*,
Lecture Notes in Networks and Systems 179,
https://doi.org/10.1007/978-981-33-4687-1_10

Keywords Hand sign recognition · CNN · Adam optimization · Root mean square error · Stochastic gradient descent · Gesture recognition · Sign language

1 Introduction

The hand gesture is a quotidian way of communication among people. It is the process of interpreting and categorizing the legitimate movements performed by the hands of a person. The hand gestures are language-independent and hence also allow us to communicate with the people speaking different languages. Also, it is the one and the only way of communication among the people who are deaf or people with a combination of disabilities. The hand gestures not only play an important role in communication but also have many applications apart from that, for instance, hand gesture recognition plays a crucial role in the human–computer interaction due to its extensive usage in the virtual reality arena as well as the sign language recognition domain. Figure 1 shows the hand gesture letter for American Sign Language.

Many machines like a driving car or a robot also operated upon the hand gestures. But designing a full-hand gesture recognition system is a very complex task and is one of the active research topics. Gesture recognition systems attain a certain structure and have two processes that are the process of acquisition, which transforms the actual gesture into quantitative form, and the process of comprehension, which lends

Fig. 1 Hand gesture letters for American Sign Language [5]

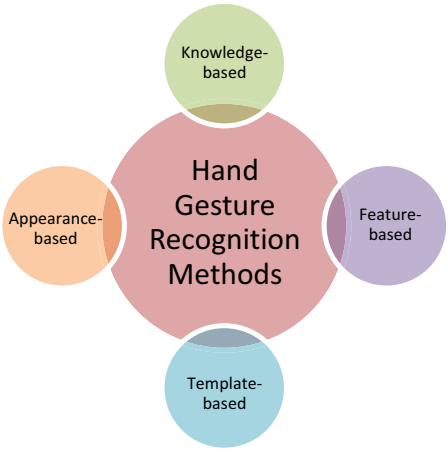

Fig. 2 Hand gesture recognition methods

credence to the sequence of tokens coming from the evaluation process. The system must also be able to detect the hand gestures in diverse sites and alignments as well.

Numerous methods have been anticipated for hand gesture recognition. All these methods can be largely classified into four categories [1–4]. These are knowledge-based, feature-based, template-based as well as appearance-based methods. It is represented in Fig. 2.

In this research, we build a deep CNN model and determine the optimized value of its hyperparameters by utilizing the Adam optimization technique. The Adam optimization technique will lead to increased accuracy of 98%. This research has the following objectives to be carried out and focused on in detail:

- To implement hand sign recognition using the convolutional neural network model which is extensively used in deep learning for problems including image classification, pose estimation, face recognition and scene labeling.
- To focus on the optimization technique after the application of the CNN model using the Adam optimization algorithm which includes the best properties of AdaGrad and RMSProp algorithms, thus making it the best choice for optimization.
- To explore the domain of hand gesture recognition which is mostly applicable in trending research areas such as human–computer interaction, augmented and virtual reality and communication systems.

Apart from this, the paper is presented as follows: Sect. 2 provides a detailed review of various researches taking place in the world for the development of hand gesture recognition systems. Section 3 provides an overview of the Adam optimization technique used for the optimization of the proposed CNN model. Section 4 discusses the methodology part in which various steps of our proposed model are discussed in detail. Later, Sect. 5 discusses the experimental results and simulations

along with various evaluation plots used in this research. Finally, Sect. 6 concludes the entire work and suggests the future areas of study.

2 Related Work

Hand gestures are one of the most common and lucid ways for communication, and many people find it convenient to communicate through this means, and it also plays a key role in helping people with disabilities to interact and communicate with each other. Thus, hand sign/gesture recognition becomes an important aspect to be considered. Many types of research are being done on this issue. Here are some of the researches listed below from all over the world.

Vaitkevičius et al. performed gesture recognition in a virtual reality (VR) environment using data produced by the leap motion device. Leap motion generates a virtual three-dimensional (3D) hand model by recognizing and tracking the user's hands. From this model, the leap motion application programming interface (API) provides hand and finger locations in the 3D space. Authors present a system that is capable of learning gestures by using the data from the leap motion device and the hidden Markov classification (HMC) algorithm. In the result, they achieved that the gesture recognition accuracy (mean $\pm$ SD) is 86.1 $\pm$ 8.2% and gesture typing speed is 3.09 $\pm$ 0.53 words per minute (WPM) when recognizing the gestures of the American Sign Language (ASL) [31].

Patel et al. discussed a complete survey of different techniques for gesture recognition. Some tools are also involved here for recognition such as HMM, ANN, particle filtering and condensation algorithm and many more. The whole recognition process is also covered here. Comparison of various approaches related to the recognition process is also included like glove-based approach, visual approach and color marker approach. The benefits and limitations of all methods for hand gesture recognition were covered efficiently. Human–machine interaction process works very smoothly just because of gesture recognition. For sign language recognition, for controlling robots and for graphical editor control, gesture recognition is very important. The main challenge of this recognition process is to collect input raw data. For that, two different techniques are used which we already discuss as glove-based and vision-based approach. Both approaches have their advantages and limitation. Recognition process includes tracking hand and segmenting it from the background, and then, features are extracted using various techniques, and finally, after applying classification, gestures are recognized. Many methods and tools are used for hand recognition. The hand gesture recognition models such as hidden Markov model, YUV color space model, 3D model and appearance model, 3D model and hidden Markov model FSM approach and ANN distinguish the input and process them for acknowledgement [32].

Alzubi et al. worked on various data analytics methodologies and an overview of it to enable the learning from experience approach for machines as well. An in-depth study has been carried out in the domain of machine learning, beginning from its

definition to advanced paradigms like supervised/unsupervised, ensemble learning and instance-based learning. The technical aspects of machine learning are discussed and interpreted its effect in the industrial space [33].

Ahlawat et al. worked on several design techniques such as the kernel size, number of layers, padding, stride size along with dilution for the handwritten digit recognition through CNN. Along with this, in order to improve the performance, distinct SGD optimizers were also evaluated. A CNN architecture was introduced for achieving a better accuracy as compared to the ensemble architectures and providing better operational complexity. An amalgamation of certain learning parameters in CNN was also presented that brought in an exceptional accuracy of 99.87% for the MNIST dataset [34].

Cui et al. worked on a weak supervised approach with deep neural networks for the recognition of vision-based incessant sign language. The approach deals with the mapping of segments of video to glosses by the introduction of recurrent convolutional neural network for sequence learning and spatiotemporal feature extraction. A three-stage escalation procedure was developed for architecture, which included an end-to-end order learning approach, a better alignment proposal and improved feature representations. The results obtained were analogous to state of the art [8].

Kumar and Manjunatha worked on a novel approach for the recognition of hand gestures for the American Sign Language (ASL), the task of which is the perception of techniques of communication through the signals of gesture. The algorithms used in this research are support vector machine and k-nearest neighbor for the hybridization of an individual marked alphabet. The parameters of evaluation that were utilized for this work are sensitivity, accuracy, precision along with false discovery and negative rate [7].

Zimmerman and Brox proposed a deep network that was capable of learning a network-implicit 3D enunciation prior. This network yielded an appreciable estimate of the 3D pose. A wide-scale 3D hand pose dataset was introduced which included synthetic models involving networks for training [9]. Ma et al. worked on the efficacy of depth image in which the entire partitions are devised for the extraction of the region of gestures, whereas the support vector machine, as well as CNN, has been utilized to extract features and recognition of gestures [10].

R.F Pinto et al. anticipated a method for the identification of gestures by using CNNs. The entire process involved morphological filters, the polygonal estimation, generating the contours as well as partitioning while preprocessing. The training, as well as testing, was done on distinct CNNs, and comparison was done with various architectures [11]. Islam et al. worked on the stationary hand gesture recognition method by using CNNs. The data augmentation techniques such as zoom, rotation, shear as well as the shifting of height and width were applied on the dataset. Training of model was done on eight thousand images, and testing was performed on sixteen thousand images that were segregated in ten classes. The accuracy achieved was 97.12% which was higher than the sans model [30].

Lahiani and Negi researched on the oriented gradient histogram along with the local binary pattern (HOG-LBP) method for the recognition of hand gestures and distinct poses. By the combination of these two features, an accuracy of 92% was

achieved, and it depicted that the amalgamation of HOG-LBP depicted better results than utilizing the features individually [2]. Ma et al. devised an image recognition approach which is based on the feature learning that is unsupervised and majorly utilized in the sparse auto-encoding model of neural networks for the extraction of image features. Then, sorting and recognition of gesture image were performed [3].

Zhu et al. devised a method that learns the short-term features (spatiotemporal) by the 3D CNN, and along with that, it learns long-term features through convolutional LSTM networks which are based on the extricated short-term features. Along with this, the evaluation of fine-tuning amidst the multimodal data is done which is found to prevent the main issue of overfitting when the existence of pre-trained model is undefined [4].

Côté-Allard et al. applied transfer learning on the accumulated data from multiple users and utilizing the power of deep learning algorithms to recognize the features that are discriminant from huge datasets. The datasets used in this work are nineteen and seventeen able-bodied participants by utilizing the Myo armband. The third dataset is gathered from the NinaPro database and contains 10 able-bodied participants. Three distinct deep learning networks were used here for carrying out the training [13].

After discussing various researches, the inference that is drawn is that there was not a great focus on the optimization of algorithms used above and more focus was laid on the processing of data and the ensemble or hybridization of certain algorithms; however, this study is more focused on the optimization of the CNN model for hand sign recognition by using the Adam optimizer and achieves an accuracy of 98%.

3 Adam Optimization Technique

The major issue that has been addressed most of the times in deep learning is the optimization of model performance along with the loss function value by tweaking the training model epochs [13]. Adam optimization is an algorithm to achieve the same.

The name Adam is an abbreviated form of the adaptive moment estimation algorithm. The role of this algorithm is to do the estimation of the moments as well as employing them for the optimization of a function [14]. It is an extension to the stochastic gradient descent and helps in updating of weights more efficiently. More specifically, it is a merger of gradient descent with moment algorithm as well as the root mean square (RMS) prop algorithm [15]. Figure 3 shows Adam optimizer.

The benefits of this algorithm, when applied to non-convex optimization problems, are as follows [16]:

- It is computationally very efficient
- Requires little memory
- It is quite suitable for problems having large data/parameters
- It is also appropriate for problems having sparse gradients or is extremely noisy.
- The hyperparameters, in this case, require very little tuning.

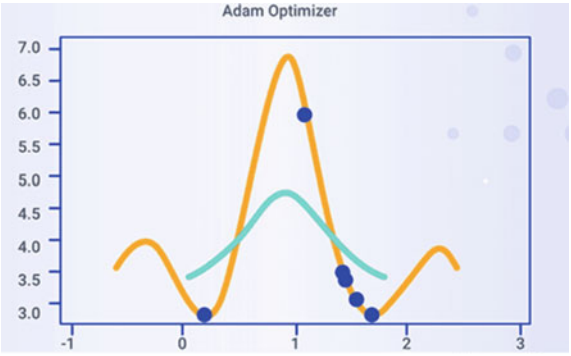

Fig. 3 Adam optimizer [12]

Working

This algorithm calculates the exponential weighted moving average of gradient and then finds the square of the computed gradient [17]. The above algorithm uses two parameters of decay, momentum as well as adaptive learning rates, which regulates the rate of decay of these calibrated moving averages [18].

The mathematical formulation is shown in Eqs. (1), (2), (3) and (4).

$$v_t = \beta_1 * v_{t-1} - (1 - \beta_1) * g_t \tag{1}$$

$$s_t = \beta_2 * s_{t-1} - (1 - \beta_2) * g_t^2 \tag{2}$$

$$\Delta w_t = -\eta \frac{v_t}{\sqrt{s_t + \varepsilon}} * g_t \tag{3}$$

$$w_t + 1 = w_t + \Delta w_t \tag{4}$$

where
w^j: parameter,
η: initial learning rate,
g_t: gradient at time t along with w^j,
$\boldsymbol{v_t}$: the exponential average of gradients along w^j,
β_1, β_2: hyperparameters.

Here, the exponential mean of gradient and the squares of the gradient for every parameter are totaled [19]. For deciding the learning step, the learning rate is multiplied by gradient mean, and its division is carried by root mean square of the exponential mean of the square of gradients along with updating process [20]. The β_1 hyperparameter is typically maintained around 0.9, whereas β_2 is held at 0.99. Epsilon is generally kept at $1e^{-10}$ [21].

4 Proposed Methodology

In this section, the research methodology of this work is discussed in detail. Initially, the sign language digits dataset is provided as an input to the model. After that, the dataset is analyzed and fragmented into the training and the validation dataset. After that, the CNN model of DL is trained and the optimized values of hyperparameters are determined using the Adam optimization technique. At last, the model is validated upon the validation set. Finally, the performance of the proposed model is measured by validation accuracy and validation loss metrics. Figure 4 represents the proposed model of our research work.

4.1 Dataset Description

The dataset for this research is obtained from the GitHub repository [6]. It is made available by the *Turkey Ankara Ayrancı Anadolu High School* Students. The dataset consists of hand sign language images of all the ten digits ranging from 0 to 9. Hence, the dataset consists of a total of 10 classes. All the images provided in the dataset are of 100 × 100 pixels. A total of 218 students had contributed to the generation of this. The sample images of all the ten classes (0–9) are represented in Fig. 5.

4.2 Dataset Analysis and Fragmentation

The dataset is already well organized, and there is no need for any preprocessing of the images used in the dataset. However, the analysis needs to be performed to get some more insights about the dataset. After the analysis, we find out that there are a total of 2062 images provided in the dataset with the uniform distribution of all the ten classes. Here, we fix the validation data size equals to 10% (around 206 samples) of the entire dataset. This splitting is performed randomly. Then, from the training set, we have utilized 50 images for the testing of the model. Hence, the sizes of training, test and validation data are as follows:

- **Total Images** 2062
- **Training Data** 1806
- **Testing Data** 50
- **Validation Data** 206.

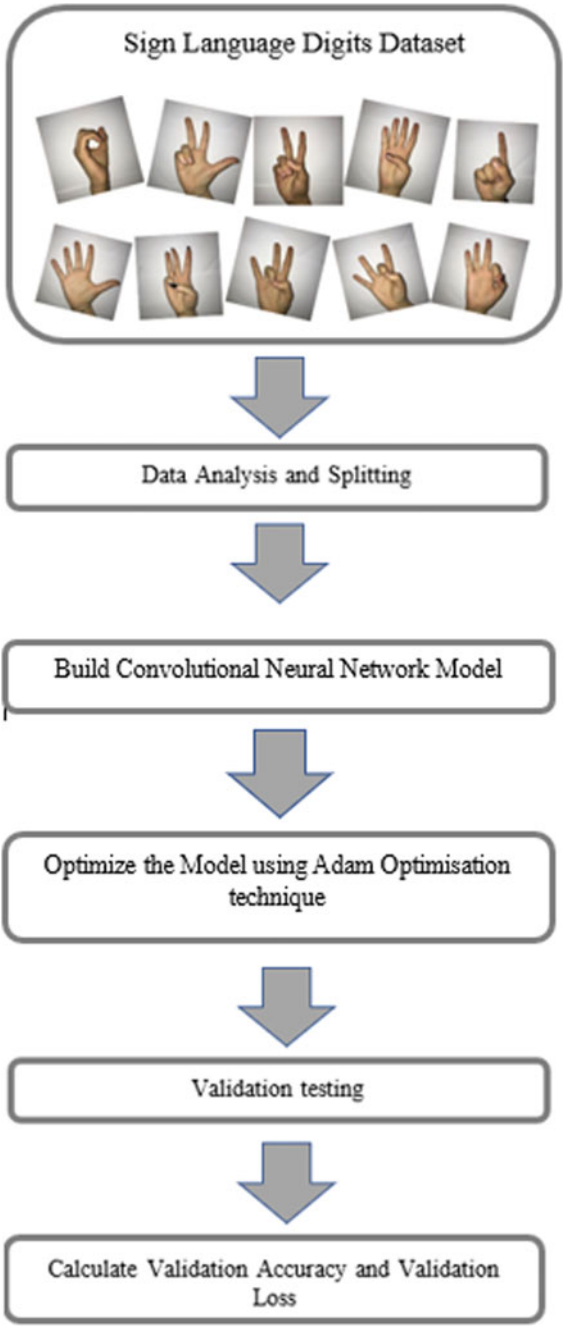

Fig. 4 Proposed research model

Fig. 5 Sample images of all the ten classes (0–9) of the dataset

4.3 Build CNN Model

After the analysis and fragmentation of the dataset, the deep learning model is trained. In this proposed work, we proposed an optimized CNN model for the hand sign language recognition using Adam optimization technique. In this model, the convolution 2D layer is chosen as the input layer and the max pool layer is chosen as the output layer. Here, three hidden layers, namely ReLU, convolution 2D and ReLU, are used in this model. Initially, the values of hyperparameters are chosen randomly and the model is tested on the testing dataset. Then, the variations are made in the values of hyperparameters until a level of accuracy is reached.

4.4 Optimization Using Adam Optimization

The model is further optimized by using Adam optimization technique. The optimized values of hyperparameters are then determined. The optimized values are as follows:

- **Learning rate** 0.0001
- **Number of epochs** 25

After determining the optimal values of the hyperparameters, the model is then validated upon the validation set and corresponding validation accuracy and loss are evaluated and plotted. The results and simulations are discussed in the following section.

5 Experimental Results and Analysis

In the following section, simulation and results of our research work are discussed and analyzed in detail. This section also provides a brief insight into the evaluation metrics utilized in the following research work.

5.1 Evaluation Plots

A learning curve is a plot of model learning progress over context or duration. They are a commonly used screening tool for algorithms which increasingly acquire through a training dataset [22]. This model can be assessed on the training dataset and retained validation dataset after every modification during training, and the calculated output plots can be generated to illustrate the learning curves [23]. The evaluation plots that are used for showing the accuracy and loss are described below:

Accuracy Curve. It generally refers to the plot of the assertion accuracy versus the training set size (it explains how the model gets better predicting the target as the figure of instances applied for training it is increased). Figure 6 shows the accuracy curve [24].

Loss Curve. The loss can be logged into two periods, after every iteration and after every epoch, where the plotting of loss across epochs is considered to be better [25]. The loss function is computed for a data item during an epoch, and the quantitative loss estimate is assured at the specified epoch [26], whereas, in the case of iterations, plotting curves give the loss only on a subset rather than the entire dataset [27]. Figure 7 shows the loss curve.

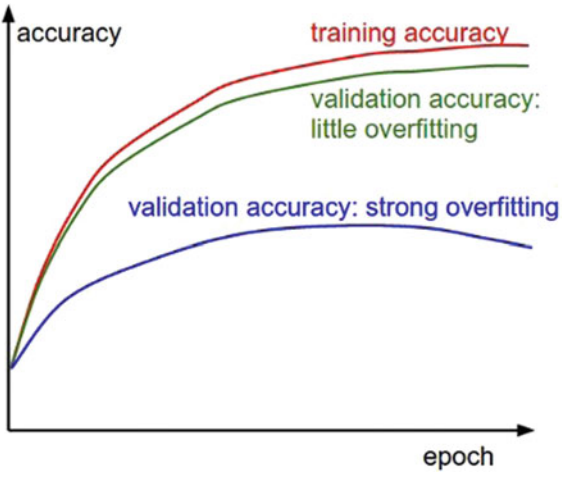

Fig. 6 Accuracy curve [28]

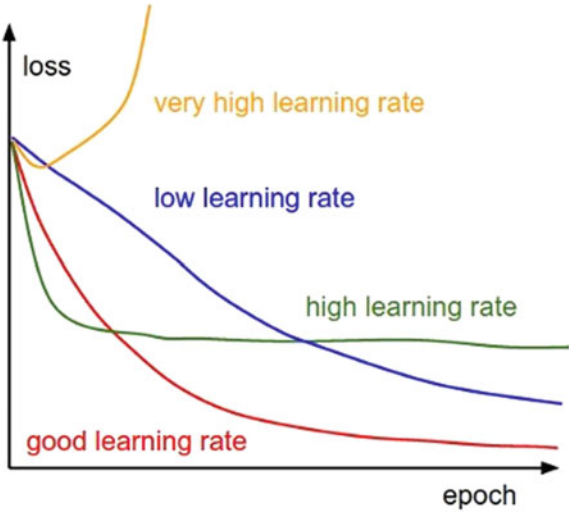

Fig. 7 Loss curve [29]

5.2 Simulation and Results

As discussed in the proposed methodology, initially, the sign language digits dataset is imported and analyzed in detail. After that, the model is split into the training (90% part) and the validation (10% part) set. After that, the CNN model is build using various convolutional layers as discussed in the previous section.

Figures 8 and 9 represent the predicted and the actual values for the two sample images of the test dataset.

By selecting the value of learning rate as 0.0001, the accuracy curve for the validation set is plotted over the 25 epochs. It is represented in Fig. 10. It can be examined from Fig. 10 that accuracy considerably upsurges with the surge in the epoch numbers. At 25, it achieved its maximum value.

The training and the validation losses with the rise in the epoch numbers are also determined and are represented in Fig. 11. From the figure, it can be analyzed that both pieces of training, as well as the validation loss values, are decreased with the growth in the number of epochs. Although the loss value of the training set has a slightly lower value than the loss rate of the validation set, the complete accuracy of the model is still very high. The final values of training and validation loss come out to be 0.021 and 0.064, respectively.

6 Conclusion and Future Enhancement

This research work is carried out to propose an optimized CNN model for hand sign language recognition using Adam optimization technique. Here, Adam optimization

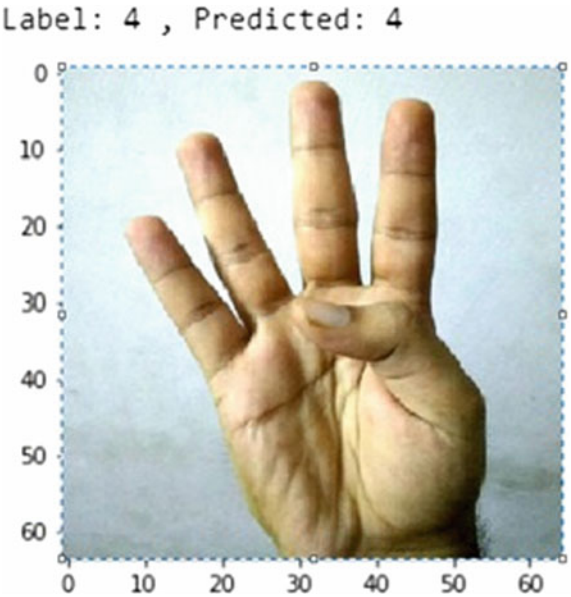

Fig. 8 Predicted value for label 4

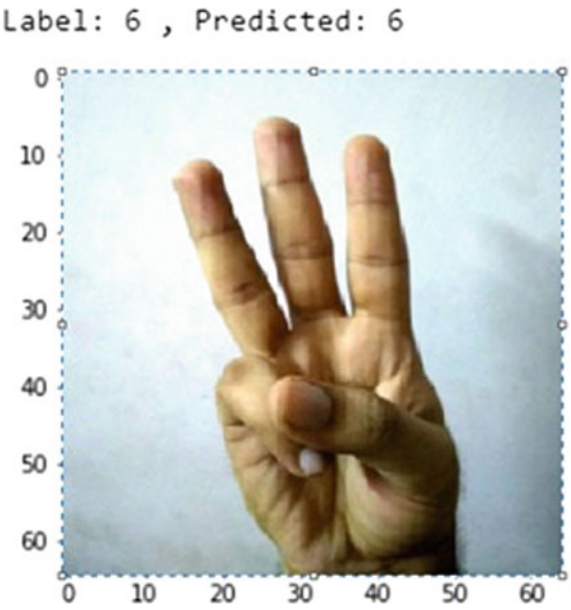

Fig. 9 Predicted value for label 6

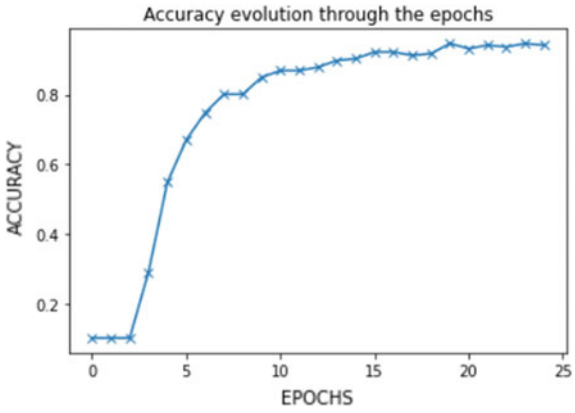

Fig. 10 Accuracy curve for the validation set

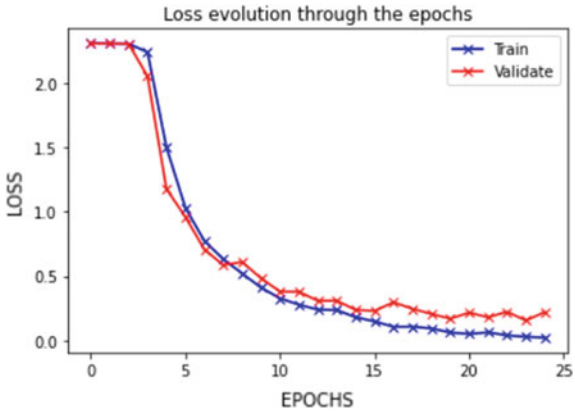

Fig. 11 Training and validation loss

technique is used for calculating the optimized value of the hyperparameters required to build up the deep CNN model. The efficacy of the proposed model is gauged by plotting accuracy as well as the loss curve with the rise in the epoch numbers. Here, the concluding values of training and the validation loss come out to be 0.021 and 0.064, respectively. Ultimate results demonstrate that the anticipated optimized CNN model shows an increased accuracy of 98%.

The dataset used in this research is limited to the hand sign language digits. So, in future, the proposed model can be enhanced by also taking the other hand sign language datasets in the account and study various ways for the optimization of parameters to increase the recognition rate. Also, the model can be further optimized by either applying image data augmentation technique or by developing a deeper network topology for better results.

References

1. Zhang Y, Chen Y, Yu H, Yang X, Lu W, Liu H (2018) Wearing-independent hand gesture recognition method based on EMG armband. Pers Ubiquit Comput 22(3):511–524
2. Lahiani H, Neji M (2018) Hand gesture recognition method based on HOG-LBP features for mobile devices. Procedia Comput Sci 126:254–263
3. Ma L, Huang W (2016) A static hand gesture recognition method based on the depth information. In: 2016 8th international conference on intelligent human-machine systems and cybernetics (IHMSC), vol 2. IEEE, pp 136–139
4. Zhu G, Zhang L, Shen P, Song J (2017) Multimodal gesture recognition using 3-D convolution and convolutional LSTM. Ieee Access 5:4517–4524
5. Sign Language MNIST: Drop-In Replacement for MNIST for Hand Gesture Recognition Tasks (2017). Accessed from https://www.kaggle.com/datamunge/sign-language-mnist
6. Sign Language Digits Dataset by Turkey Ankara Ayrancı Anadolu High School Students (2017). Accessed from https://github.com/ardamavi/Sign-Language-Digits-Dataset
7. Kumar BP, Manjunatha MB (2017) A hybrid gesture recognition method for American sign language. Indian J Sci Technol 10(1):1–12
8. Cui R, Liu H, Zhang C (2017) Recurrent convolutional neural networks for continuous sign language recognition by staged optimization. In: Proceedings of the IEEE conference on computer vision and pattern recognition, pp 7361–7369
9. Zimmermann C, Brox T (2017) Learning to estimate 3D hand pose from single RGB images. In: Proceedings of the IEEE international conference on computer vision, pp 4903–4911
10. Ma M, Chen Z, Wu J (2016) A recognition method of hand gesture with CNN-SVM model. International conference on bio-inspired computing: theories and applications. Springer, Singapore, pp 399–404
11. Pinto, R. F., Borges, C. D., Almeida, A., & Paula, I. C. (2019). Static Hand Gesture Recognition Based on Convolutional Neural Networks. *Journal of Electrical and Computer Engineering*, *2019*.
12. Jiang S, Chen Y (2017) Hand gesture recognition by using 3DCNN and LSTM with Adam optimizer. Pacific Rim conference on multimedia. Springer, Cham, pp 743–753
13. Côté-Allard U, Fall CL, Drouin A, Campeau-Lecours A, Gosselin C, Glette K, Laviolette F, Gosselin B (2019) Deep learning for electromyographic hand gesture signal classification using transfer learning. IEEE Trans Neural Syst Rehabil Eng 27(4):760–771
14. Jais IKM, Ismail AR, Nisa SQ (2019) Adam optimization algorithm for wide and deep neural network. Knowl Eng Data Sci 2(1):41–46
15. Feng J, Wang Z, Zha M, Cao X (2019) Flower recognition based on transfer learning and adam deep learning optimization algorithm. In: Proceedings of the 2019 international conference on robotics, intelligent control and artificial intelligence, pp 598–604
16. Reddi SJ, Kale S, Kumar S (2019) On the convergence of Adam and beyond. arXiv preprint arXiv:1904.09237
17. Bai J, Zhang J (2019) BGADAM: Boosting based genetic-evolutionary ADAM for convolutional neural network optimization. arXiv preprint arXiv:1908.08015
18. Jalal A, Kim K (2020) Wearable inertial sensors for daily activity analysis based on Adam optimization and the maximum entropy markov model. Entropy 22(5):579
19. Mohsin M, Li H, Abdalla HB (2020) Optimization Driven Adam-Cuckoo search-based deep belief network classifier for data classification. IEEE Access 8:105542–105560
20. Huang H, Wang C, Dong B (2018) Nostalgic Adam: Weighting more of the past gradients when designing the adaptive learning rate. arXiv preprint arXiv:1805.07557.
21. Zhang Z (2018) Improved adam optimizer for deep neural networks. In: 2018 IEEE/ACM 26th international symposium on quality of service (IWQoS). IEEE, pp 1–2
22. Hestness J, Narang S, Ardalani N, Diamos G, Jun H, Kianinejad H, Patwary M, Ali M, Yang Y, Zhou Y (2017) Deep learning scaling is predictable, empirically. arXiv preprint arXiv:1712.00409.

23. Nachmani E, Bachar Y, Marciano E, Burshtein D, Be'ery Y (2018). Near maximum likelihood decoding with deep learning. arXiv preprint arXiv:1801.02726
24. Litjens G, Sánchez CI, Timofeeva N, Hermsen M, Nagtegaal I, Kovacs I, Hulsbergen-Van De Kaa C, Bult P, Van Ginneken B, Van Der Laak J (2016). Deep learning as a tool for increased accuracy and efficiency of histopathological diagnosis. Sci Rep 6:26286
25. Spieker H, Gotlieb A (2019) Towards testing of deep learning systems with training set reduction. arXiv preprint arXiv:1901.04169
26. Salehi SSM, Erdogmus D, Gholipour A (2017) Tversky loss function for image segmentation using 3D fully convolutional deep networks. International workshop on machine learning in medical imaging. Springer, Cham, pp 379–387
27. Huang C, Zhai S, Talbott W, Bautista MA, Sun SY, Guestrin C, Susskind J (2019) Addressing the loss-metric mismatch with adaptive loss alignment. arXiv preprint arXiv:1905.05895
28. Abeshu A, Chilamkurti N (2018) Deep learning: the frontier for distributed attack detection in fog-to-things computing. IEEE Commun Maga 56(2):169–175
29. Tran GS, Nghiem TP, Nguyen VT, Luong CM, Burie JC (2019) Improving accuracy of lung nodule classification using deep learning with focal loss. J Healthc Eng 2019
30. Islam MZ, Hossain MS, ul Islam R, Andersson K (2019) Static hand gesture recognition using convolutional neural network with data augmentation. In 2019 joint 8th international conference on informatics, electronics & vision (ICIEV) and 2019 3rd international conference on imaging, vision & pattern recognition (icIVPR). IEEE, pp 324–329
31. Vaitkevičius A, Taroza M, Blažauskas T, Damaševičius R, Maskeliūnas R, Woźniak M (2019) Recognition of American sign language gestures in a virtual reality using leap motion. Appl Sci 9(3):445
32. Patel N, He JS (2018) A survey on hand gesture recognition techniques, methods and tools. Int J Res Advent Technol 6(6). E-ISSN: 2321–9637.
33. Alzubi J, Nayyar A, Kumar A (2018) Machine learning from theory to algorithms: an overview. J Phys Conf Ser 1142(1):012012
34. Ahlawat S, Choudhary A, Nayyar A, Singh S, Yoon B (2020) Improved handwritten digit recognition using convolutional neural networks (CNN). Sensors 20(12):3344

Hybrid Spectrum Access Strategy for Throughput Enhancement of Cognitive Radio Network

Indu Bala, Kiran Ahuja, and Anand Nayyar

Abstract Recently, cognitive radio technology has gained worldwide attention due to its potential to overcome spectrum scarcity. The technology allows unlicensed users to use licensed spectrum in a manner such that minimum or no interference may be experienced by licensed users. To do so, the conventional scheme divides the time frame into two slots i.e. sensing slot and data transmission slot. In this scenario, the achievable throughput of unlicensed user fundamentally depends on the accuracy of sensing results since the sensing error in terms of miss detection and false alarm results into collision and spectrum underutilization, respectively. To overcome this bottleneck, an improved frame structure is proposed in this paper with two sensing slots and one data transmission slot. Based on the sensing results of the current and previous frame, the proposed scheme allows unlicensed users to switch between underlay and interweave mode of communication to enhance secondary user's throughput. It is shown that proposed scheme has a potential to achieve 50% more throughput as compare to the conventional schemes, when channel is occupied by primary user. The simulation results are presented to illustrate the effectiveness of the proposed scheme. Moreover, the performance of proposed scheme is also compared with the conventional schemes to validate the results.

Keywords Sensing · Hybrid spectrum access · Frame structure · Throughput · Data loss

I. Bala
Lovely Professional University, Phagwara, Punjab, India
e-mail: i.rana80@gmail.com

K. Ahuja
DAV Institute of Engineering Technology, Jalandhar, Punjab, India
e-mail: askahuja2002@gmail.com

A. Nayyar (✉)
Graduate School, Faculty of Information Technology, Duy Tan University, Da Nang 550000, Viet Nam
e-mail: anandnayyar@duytan.edu.vn

D. K. Sharma et al. (eds.), *Micro-Electronics and Telecommunication Engineering*,
Lecture Notes in Networks and Systems 179,
https://doi.org/10.1007/978-981-33-4687-1_11

1 Introduction

From last few decades, we all have witnessed the tremendous growth in wireless communication that has increased the bandwidth requirement manifolds. However, with traditional spectrum allocation policies, it has become extremely difficult to assign spectrum for new services/applications. The traditional spectrum allocation policies in use provide spectrum access rights exclusively to the user who purchased the spectrum (known as primary user i.e. PU) for long term use. The unlicensed user (known as secondary user i.e. SU) is refrained from transmission in this channel even if it is not in use by PU. Thus, whole wireless industry is facing spectrum shortage to deploy new services/applications. On contrary to the spectrum scarcity issue, the recent FCC report has revealed that spectrum allocated for different services, is being used sporadically [1]. Thus, the existing spectrum scarcity problem is mainly due to the improper use of the spectrum rather than actual shortage of the spectrum. This fact has pushed regulatory authorities to explore the new communication paradigms to overcome spectrum scarcity issue. Recently, cognitive radio technology has evolved as the most promising technology with a potential to overcome this issue by allowing secondary users to utilize vacant or partial utilized spectrum whenever primary users are not using it [2]. Thus, the basic requirement of the technology is that SU should remain all time updated with the spectrum occupancy level by primary users through spectrum sensing. Many spectrum sensing techniques have been proposed for cognitive radio networks in this regard. However, due to the ease in implementation and no prior knowledge requirement about primary user, energy detection (ED) is most commonly used spectrum sensing scheme [3, 4]. The performance of the energy detector is measured in term of probability of detection (P_d) and probability of false alarm $\left(P_f\right)$ and must be high and low, respectively. To meet these requirements, the spectrum sensing time must be high for the accurate detection of primary user in a channel. However, the main drawback with long sensing duration is that it reduces the data transmission time and therefore SU throughput also. To overcome this issue, many researchers have proposed solutions like parallel sensing and transmission [4], improvement in frame structures [5], hybrid spectrum access [6], threshold adaptation [7] and dedicated channel for spectrum sensing [8] etc. However, to our best knowledge, hybrid spectrum access scheme with improved frame structure has not been analyzed much to improve the secondary throughput. Therefore, a hybrid spectrum access scheme with an improved frame structure has been proposed in this paper, to enhance secondary user's throughput and to reduce the data loss due to sensing errors.

The rest of the paper is organized as follows: The dynamic spectrum access schemes are discussed in Sect. 2. The system model and frame structures are discussed in Sect. 3. In Sect. 4, the conventional and proposed spectrum access scheme is discussed and analytical expression for SU throughput, effective SU throughput and data loss have been derived. Simulation results are presented in Sect. 5 followed by conclusion in Sect. 6.

2 Dynamic Spectrum Access Schemes

The dynamic spectrum access is a mechanism to increase the spectrum efficiency by the real time adjustment of the radio resources [1]. It allows SUs to use licensed spectrum bands dynamically for transmission. Figure 1 illustrates various spectrum access schemes reported in literature [9–20].

Figure 2 shows various spectrum sharing paradigms for cognitive radio network (CRN). The underlay approach allows both PU and SU to transmit simultaneously over a same channel as long as the interference from SU to PU is below interference temperature [9]. Similar to the Ultra Wide Band (UWB) technology, this approach allows SU to spread its signal over a wide frequency range, and the signal level remains below noise level. Thus, the scheme is able to provide seamless connectivity and limited data rates for short range communication [10].

Similar to the underlay scheme, the overlay scheme also allow SUs to transmit over the licensed band along with PU such that the performance of PU may not be affected. The two main approaches used in this paradigm are (i) Channel coding, and (ii) network coding. In the channel coding approach PU transmits a packet that is known the SU. The SU splits its transmission power into two parts to transmit its own (SU) packet along with the PU packet such that the signal to interference and noise ratio (SINR) at PU receiver is not affected much. In addition to this, the SU transmitter can also exploit dirty paper coding to transmit the SU packet to cancel out the interference at SU receiver [11]. The network coding scheme allows SU to encode its packet onto the PU packet while relaying it. Thus, SU does not require

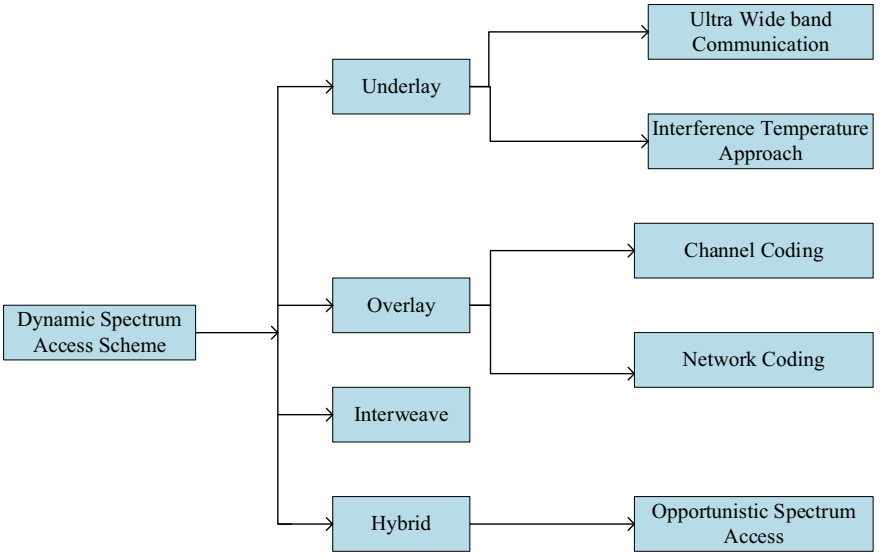

Fig. 1 Classification of spectrum access schemes

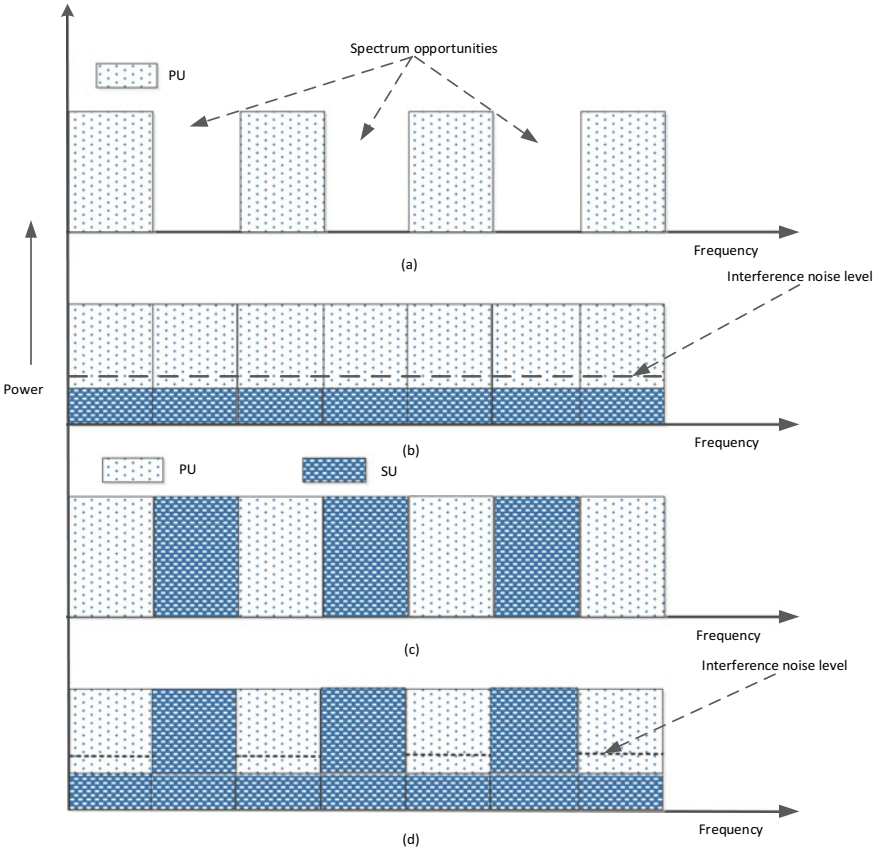

Fig. 2 Spectrum sharing paradigms **a** spectrum opportunities/holes. **b** Underlay paradigm. **c** Interweave paradigm. **d** Hybrid paradigm

separate spectrum access to transmit its own packets and therefore PU transmission remains unaffected [12].

On contrary to the previously discussed approaches, Interweave approach does not allow SU to transmit in licensed frequency band when PU is active on it. The spectrum sensing is mandatory to this approach and it is also known as opportunistic spectrum access (OSA) in a sense that SU can exploit the spectrum opportunities in time, space, and/or frequency domain [13]. In comparison to the underlay scheme, this scheme allows high transmission power level to support high data rates. However, the transmission is truncated abruptly on the emergence of PU in the channel. To overcome all these drawbacks, a hybrid spectrum access scheme is proposed in this paper that switches between interweave and underlay mode of communication based on the channel occupancy level by PU. The proposed scheme not only offers seamless connectivity but high data rates also. In addition to this, transmission frame structure is also improved to achieve high secondary throughput.

The main contributions of this paper are as follows:

(i) A hybrid spectrum access scheme is proposed with an improved frame structure to access idle channels using interweave approach and busy channels using underlay approach.
(ii) The proposed scheme has a potential to overcome sensing errors with the help of two sensing slots.
(iii) The analytical expressions for SU's effective throughput and data loss are derived for the proposed spectrum access schemes.

3 System Model and Frame Structure

3.1 System Model

Consider a communication scenario with one primary transmitter (PU Tx) that uses its allocated licensed frequency band to transmit information to the primary receiver (PU RxN) with power P_P as shown in Fig. 3. The secondary communication system comprises of SU Tx–SU Rx pair that shares the licensed frequency band with PU. The SU Tx is equipped with an energy detector that constantly monitors the channel variations to know the presence or absence of the PU in a licensed frequency band.

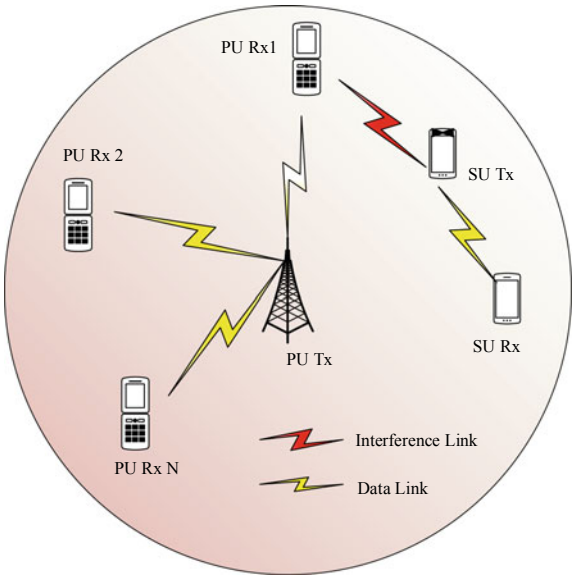

Fig. 3 Proposed communication system scenario

3.2 *Frame Structure*

For given communication scenario, the conventional schemes discussed in [3] and [5] divides time into equal sized frames, where each frame consists of two time slots: the sensing slot and the transmission slot as shown in Fig. 4a. According to this frame structure, SU senses for τ units of time to know PU presence/absence from the channel and decides for transmission/no transmission or mode of transmission for the remaining frame duration of $T - \tau$ units of time. Generally, there exists tradeoff between these two as excessive long sensing duration reduces the transmission time and short sensing duration may leads to the miss detection of PU. Both situations affect primary and secondary users adversely. Moreover, the spectrum sensing by the SU is assumed to be imperfect, and thus sensing errors (i.e., miss detection and false alarm) limits the SU throughput.

Figure 4b shows the proposed frame structure for hybrid spectrum access in which transmission frame is divided into three slots i.e. two sensing slots and one data transmission slot. The basic notion of adding second sensing slot is to enhance the accuracy of sensing results and thus to increase the secondary throughput. In this frame structure, the second sensing slot is optional and it depends on the sensing results of current and previous frame. For example, if the spectrum sensing results of

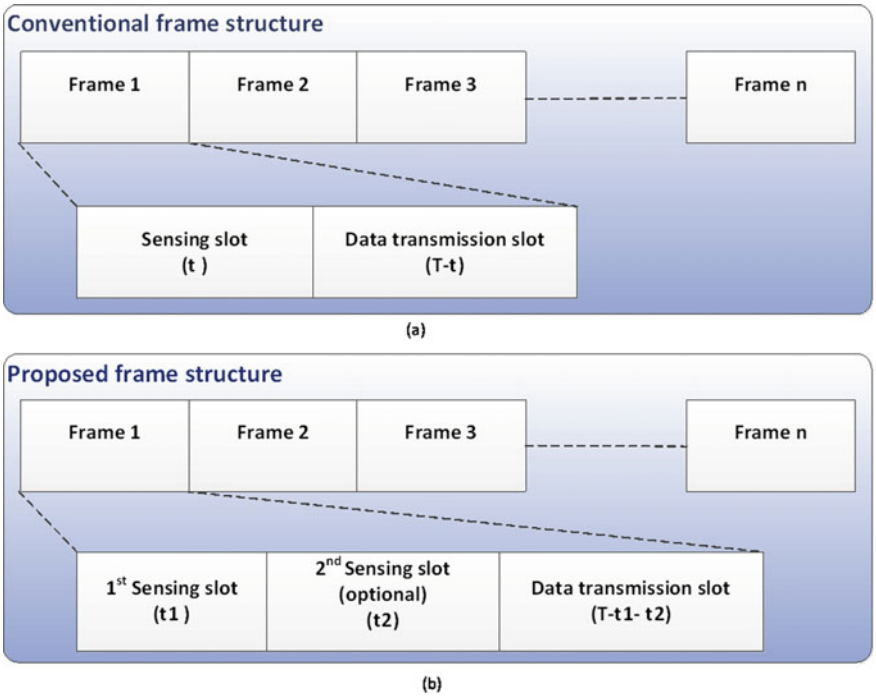

Fig. 4 **a** Conventional frame structure. **b** Proposed frame structure

current and previous frame are same, the secondary user performs spectrum sensing only once for the current frame. However, if the sensing results of the current frame are different from the previous frame, the SU will sense the channel again to avoid ambiguity in sensing results. In case of second sensing, the results of the second sensing slot will be considered final even if they are wrong.

4 Performance Analysis

In this section, we study the conventional and proposed spectrum sharing schemes in detail. The closed form of expression for effective throughput and data loss are derived for each scheme. For spectrum sharing scenario presented in Sect. 3, the sensing results of the received signal $r(t)$ by SU follows the binary hypothesis H_1 and H_0 to represents the presence and absence of the primary user, respectively.

$$r(t) = \begin{pmatrix} h \cdot x(t) + w(t), H_1 : \text{PU is present} \\ w(t), H_0 : \text{PU is absent} \end{pmatrix} \tag{1}$$

where, h, $x(t)$ and $w(t)$ represents channel gain, primary transmitted signal and additive white Gaussian noise (AWGN), respectively. The description of the parameters is given in Table 1.

Table 1 Parameters description [3, 5, 6]

S. No.	Parameter	Description
1	T	Total time frame
2	τ_1	Time duration of 1st sensing slot
3	τ_2	Time duration of 2nd sensing slot
4	$T - \tau_1$	Data transmission time with one sensing slot
5	$T - \tau_1 - \tau_2$	Data transmission time with two sensing slot
6	P_d	Probability of detection
7	P_f	Probability of false alarm
8	P_1	SU transmission power in Interweave mode
9	P_2	SU transmission power in Underlay mode
10	P_P	PU transmission power
11	N_p	Noise power at SU receiver
12	h_{ps}	Channel gain between PU Tx and SU Rx
13	h_{ss}	Channel gain between SU Tx and SU Rx
14	$P(H_0)$	Probability of channel being Idle
15	$P(H_1)$	Probability of channel being busy

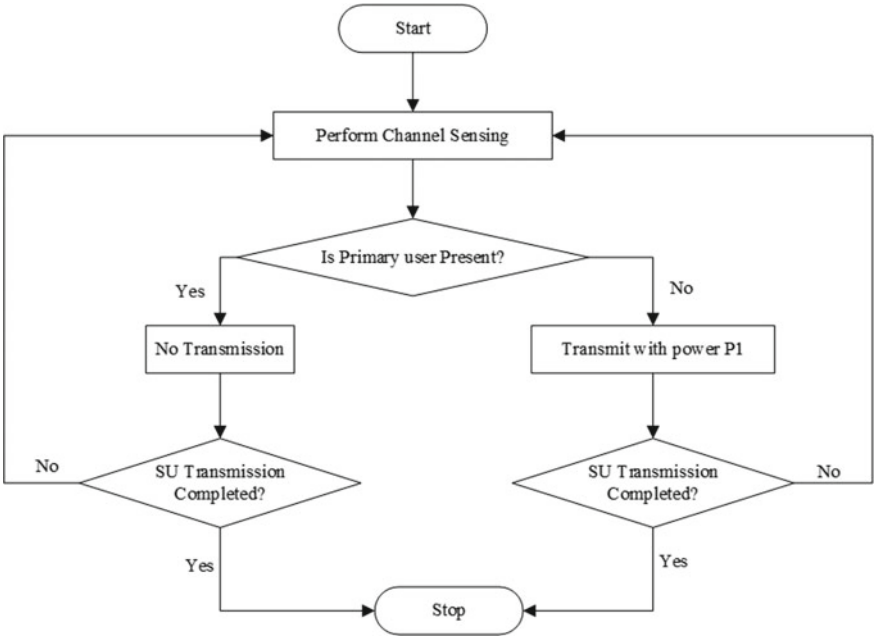

Fig. 5 Conventional spectrum access scheme with one sensing slot (Conv-I)

Figure 5 shows the conventional spectrum access approach with one sensing slot (Conv-I) in which sensing is done at the beginning of the frame. Based on the sensing results, four data transmission cases are possible (Refer Table 2).

Since SU is allowed to transmit with power P_1 whenever channel is sensed idle, the secondary user is allowed to transmit in case 1 and 2 as given in Table 2. Thus, SU throughput will be given by (2)

$$TP_1 = \frac{T-\tau}{T}\left[P(H_0)\left(1-P_f\right)C_{00} + P(H_1)(1-P_d)C_{01}\right] \tag{2}$$

Table 2 Data transmission scenarios for Conv-I scheme [3]

Sensing state	Actual state	Transmission type	Transmission duration	SNR	Capacity
Idle	Idle	Interweave	$T-\tau$	$\frac{P_1 h_{ss}}{N_p}$	C_{00}
Idle	Busy	Interweave	$T-\tau$	$\frac{P_1 h_{ss}}{N_p+P_p \cdot h_{ps}}$	C_{01}
Busy	Idle	No transmission	X	0	C_{10}
Busy	Busy	No transmission	X	0	C_{11}
Where, $C_{xx} = B\log_2(\text{SNR})$					

where C_{xx} represents capacity with first subscript representing sensed state and second subscript representing actual channel state. However, the effective SU throughput is when SU is able to sense the channel accurately and decides the transmission power level accordingly. Under imperfect sensing situation, when SU is not able to sense PU n a channel and transmits using interweave mode, whole transmission results into data loss. Thus, the effect SU throughput and data loss for Conv-I scheme will be given by (3) and (4), respectively.

$$TP_1^E = \frac{T-\tau}{T}\left[P(H_0)\left(1-P_f\right)C_{00}\right] \tag{3}$$

$$DL_1 = \frac{T-\tau}{T}[P(H_1)(1-P_d)C_{01}] \tag{4}$$

Figure 6 shows conventional hybrid spectrum access scheme with one sensing slot (Hybrid-I) in which based on the sensing results, SU transmits with transmission power P_1 in interweave mode, when channel is idle and with transmission power P_2 in underlay mode when channel is busy. Based on this, four possible data transmission scenarios are given in Table 3.

The SU throughput, effective throughput and data loss for Hybrid-I scheme will be given by (5), (6) and (7), respectively.

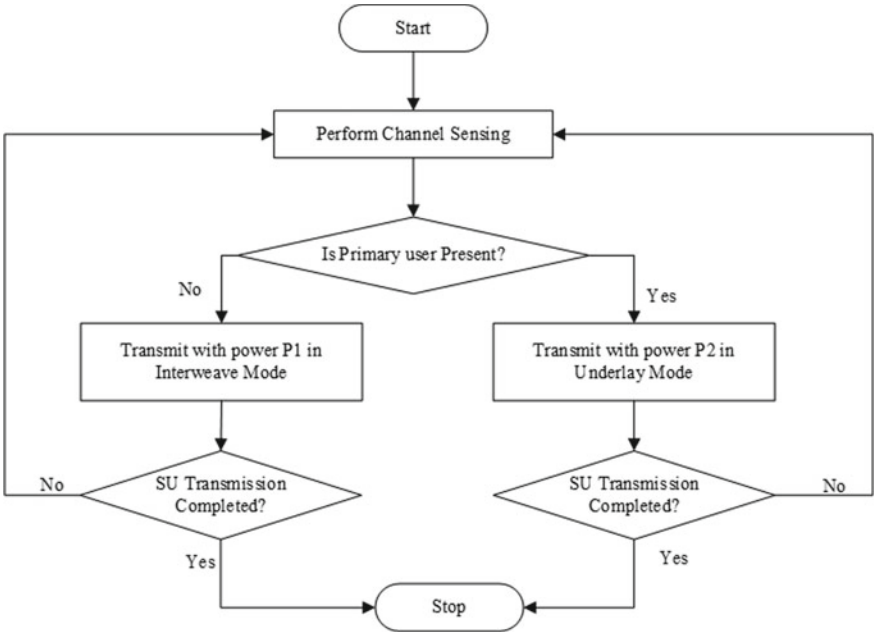

Fig. 6 Conventional hybrid spectrum access scheme single sensing slot (Hybrid-I) [6]

Table 3 Data transmission scenarios for hybrid-I scheme [6]

Sensing state	Actual state	Transmission type	Transmission duration	SNR	Capacity
Idle	Idle	Interweave	$T-\tau$	$\frac{P_1 h_{ss}}{N_p}$	C_{00}
Idle	Busy	Interweave	$T-\tau$	$\frac{P_1 h_{ss}}{N_p+P_p.h_{ps}}$	C_{01}
Busy	Idle	Underlay	$T-\tau$	$\frac{P_2 h_{ss}}{N_p}$	C_{10}
Busy	Busy	Underlay	$T-\tau$	$\frac{P_2 h_{ss}}{N_p+P_p.h_{ps}}$	C_{11}
Where, $C_{xx} = B\log_2(\text{SNR})$					

$$TP_2 = \frac{T-\tau}{T}\left[P(H_0)\big(1-P_f\big)C_{00} + P(H_1)\begin{matrix}(1-+P_d)C_{00}P(H_0)\big(P_f\big)C_{10}\\ +P(H_1)(P_d)C_{11}\end{matrix}\right] \tag{5}$$

$$TP_1^E = \frac{T-\tau}{T}\big[P(H_0)\big(1-P_f\big)C_{00} + P(H_0)\big(P_f\big)C_{10} + P(H_1)(P_d)C_{11}\big] \tag{6}$$

$$DL_2 = \frac{T-\tau}{T}[P(H_1)(1-P_d)C_{01}] \tag{7}$$

Figure 7 illustrate conventional spectrum access scheme with two sensing slots (Conv-II) in which sensing is performed once only if the sensing results of current and previous frame are same. In case the sensing results of current frame and previous frame are different, sensing is performed again to avoid ambiguity in sensing results. Based on this, twelve possible data transmission scenarios are given in Table 4.

The SU throughput, effective throughput and data loss for Conv-II scheme will be given by (8), (9) and (10), respectively

$$\begin{aligned} TP_3 = {} & \frac{T-\tau_1}{T}\big[P(H_0)^2\big(1-p_f^1\big)C_{000x} + P(H_1)P(H_0)\big(1-p_d^1\big)C_{010x}\big] \\ & + \frac{T-\tau_1-\tau_2}{T}\begin{bmatrix} P(H_0)^2 p_f^1\big(1-p_f^2\big)C_{0010} \\ +P(H_0)P(H_1)p_d^1\big(1-p_d^2\big)C_{0110} \\ +P(H_1)P(H_0)\big(1-p_f^1\big)\big(1-p_f^2\big)C_{1000} \\ +P(H_1)P(H_1)\big(1-p_d^1\big)\big(1-p_d^2\big)C_{1100}\end{bmatrix} \end{aligned} \tag{8}$$

$$\begin{aligned} TP_1^E = {} & \frac{T-\tau_1}{T}\big[P(H_0)^2\big(1-p_f^1\big)C_{000x}\big] \\ & + \frac{T-\tau_1-\tau_2}{T}\begin{bmatrix} P(H_0)^2 p_f^1\big(1-p_f^2\big)C_{0010} \\ +P(H_1)P(H_0)\big(1-p_f^1\big)\big(1-p_f^2\big)C_{1000}\end{bmatrix} \end{aligned} \tag{9}$$

$$DL_3 = \frac{T-\tau_1}{T}\big[P(H_1)P(H_0)\big(1-p_d^1\big)C_{010x}\big]$$

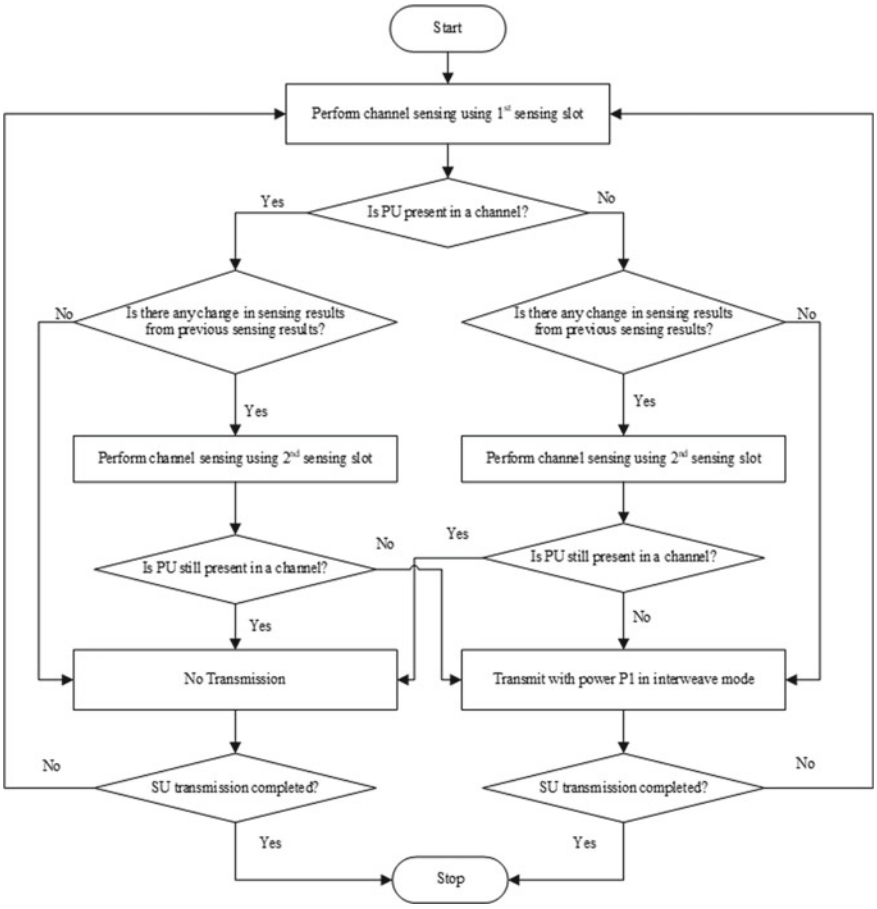

Fig. 7 Conventional spectrum access scheme with two sensing slots (Conv-II) [6]

$$+\frac{T-\tau_1-\tau_2}{T}\begin{bmatrix} P(H_0)P(H_1)p_d^1\left(1-p_d^2\right)C_{0110} \\ +P(H_1)P(H_0)\left(1-p_f^1\right)\left(1-p_f^2\right)C_{1100} \end{bmatrix} \tag{10}$$

The term C_{xxxx} in (8), (9) and (10) represents capacity and first subscript represents sensing state of previous frame, second subscript represents sensing state of current frame, third subscript represents first sensing results and fourth subscript represents sensing results of second sensing.

Figure 8 shows the proposed hybrid spectrum access scheme in which the frame length is divided into three slots i.e. two sensing slots and a data transmission slot. However, unlike Conv-II scheme, the proposed scheme allows the SU to transmit in interweave mode with power P_1 on finding the channel idle and in underlay mode with power P_2 on finding channel busy. Based on the access behavior; twelve possible data transmission scenarios are enlisted in Table 5.

Table 4 Data transmission scenarios for Conv-II scheme [5]

Last state	Current state	1st sensing result	2nd sensing result	Tx type	Tx duration	SNR	Capacity
Idle	Idle	Idle	X	Interweave	$T-\tau_1$	$\frac{P_1 h_{ss}}{N_p}$	C_{000x}
Idle	Idle	Busy	Idle	Interweave	$T-\tau_1-\tau_2$	$\frac{P_1 h_{ss}}{N_p}$	C_{0010}
Idle	Idle	Busy	Busy	Underlay	$T-\tau_1-\tau_2$	0	C_{0011}
Idle	Busy	Idle	X	Interweave	$T-\tau_1$	$\frac{P_1 h_{ss}}{N_p+P_p.h_{ps}}$	C_{010x}
Idle	Busy	Busy	Idle	Interweave	$T-\tau_1-\tau_2$	$\frac{P_1 h_{ss}}{N_p+P_p.h_{ps}}$	C_{0110}
Idle	Busy	Busy	Busy	Underlay	$T-\tau_1-\tau_2$	0	C_{0111}
Busy	Idle	Idle	Idle	Interweave	$T-\tau_1-\tau_2$	$\frac{P_1 h_{ss}}{N_p+P_p.h_{ps}}$	C_{1000}
Busy	Idle	Idle	Busy	Underlay	$T-\tau_1-\tau_2$	0	C_{1001}
Busy	Idle	Busy	X	Underlay	$T-\tau_1$	0	C_{101x}
Busy	Busy	Idle	Idle	Interweave	$T-\tau_1-\tau_2$	$\frac{P_1 h_{ss}}{N_p+P_p.h_{ps}}$	C_{1100}
Busy	Busy	Idle	Busy	Underlay	$T-\tau_1-\tau_2$	0	C_{1101}
Busy	Busy	Busy	X	Underlay	$T-\tau_1$	0	C_{111x}

where, $C_{xxxx} = B\log_2(\text{SNR})$

Thus, the analytical expression for secondary throughput, effective SU throughput and data loss of the proposed scheme will be given by (11), (12) and (13), respectively.

$$
\begin{aligned}
TP_4 = \frac{T-\tau_1}{T}&\left[\begin{array}{l} P(H_0)^2\left(1-p_f^1\right)C_{000x} + P(H_1)P(H_0)\left(1-p_d^1\right)C_{010x} \\ +P(H_1)P(H_0)\left(1-p_d^1\right)C_{101x} + P(H_1)^2\left(p_d^1\right)C_{111x} \end{array}\right] \\
+\frac{T-\tau_1-\tau_2}{T}&\left[\begin{array}{l} P(H_0)^2 p_f^1\left(1-p_f^2\right)C_{0010} + P(H_1)P(H_0)p_d^1 p_d^2 C_{0111} \\ +P(H_1)^2\left(1-p_d^1\right)\left(1-p_d^2\right)C_{1100} + P(H_0)^2 p_f^1 p_f^2 C_{0011} \\ +P(H_1)P(H_0)p_d^1\left(1-p_d^2\right)C_{0110} + P(H_1)P(H_0)p_f^2\left(1-p_f^1\right)C_{1001} \\ +P(H_1)^2\left(1-p_d^1\right)p_d^2 C_{1101} + P(H_1)P(H_0)\left(1-p_f^1\right)\left(1-p_f^2\right)C_{1000} \end{array}\right]
\end{aligned}
\tag{11}
$$

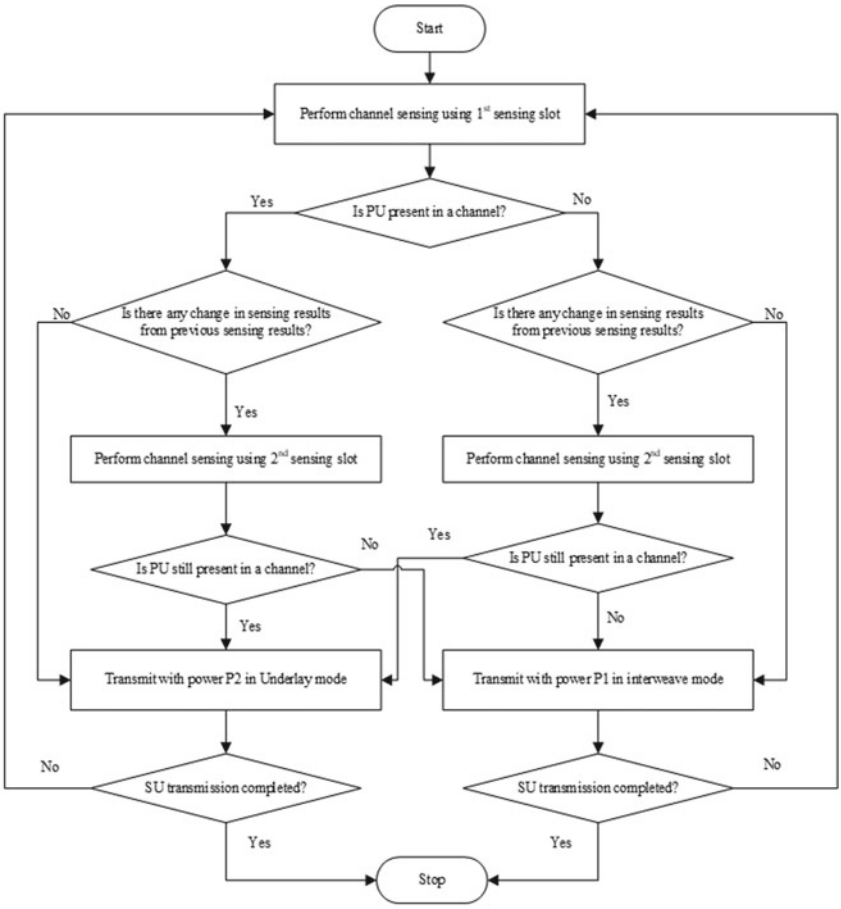

Fig. 8 Proposed hybrid spectrum access scheme with two sensing slots

$$
\begin{aligned}
T P_4^E = \frac{T-\tau_1}{T}\begin{bmatrix} P(H_0)^2\left(1-p_f^1\right)C_{000x} + P(H_1)P(H_0)\left(1-p_d^1\right)C_{101x} \\ +P(H_1)^2\left(p_d^1\right)C_{111x} \end{bmatrix} \\
+\frac{T-\tau_1-\tau_2}{T}\begin{bmatrix} P(H_0)^2 p_f^1\left(1-p_f^2\right)C_{0010} \\ +P(H_1)P(H_0)p_d^1 p_d^2 C_{0111} + P(H_0)^2 p_f^1 p_f^2 C_{0011} \\ +P(H_1)P(H_0)p_f^2\left(1-p_f^1\right)C_{1001} \\ +P(H_1)^2\left(1-p_d^1\right)p_d^2 C_{1101} \\ +P(H_1)P(H_0)\left(1-p_f^1\right)\left(1-p_f^2\right)C_{1000} \end{bmatrix}
\end{aligned} \tag{12}
$$

Table 5 Data transmission scenarios (proposed approach)

Last state	Current state	1st sensing result	2nd sensing result	Tx type	Tx duration	SNR	Capacity
Idle	Idle	Idle	x	Interweave	$T-\tau_1$	$\frac{P_1 h_{ss}}{N_p}$	C_{000x}
Idle	Idle	Busy	Idle	Interweave	$T-\tau_1-\tau_2$	$\frac{P_1 h_{ss}}{N_p}$	C_{0010}
Idle	Idle	Busy	Busy	Underlay	$T-\tau_1-\tau_2$	0	C_{0011}
Idle	Busy	Idle	X	Interweave	$T-\tau_1$	$\frac{P_1 h_{ss}}{N_p+P_p.h_{ps}}$	C_{010x}
Idle	Busy	Busy	Idle	Interweave	$T-\tau_1-\tau_2$	$\frac{P_1 h_{ss}}{N_p+P_p.h_{ps}}$	C_{0110}
Idle	Busy	Busy	Busy	Underlay	$T-\tau_1-\tau_2$	0	C_{0111}
Busy	Idle	Idle	Idle	Interweave	$T-\tau_1-\tau_2$	$\frac{P_1 h_{ss}}{N_p+P_p.h_{ps}}$	C_{1000}
Busy	Idle	Idle	Busy	Underlay	$T-\tau_1-\tau_2$	0	C_{1001}
Busy	Idle	Busy	X	Underlay	$T-\tau_1$	0	C_{101x}
Busy	Busy	Idle	Idle	Interweave	$T-\tau_1-\tau_2$	$\frac{P_1 h_{ss}}{N_p+P_p.h_{ps}}$	C_{1100}
Busy	Busy	Idle	Busy	Underlay	$T-\tau_1-\tau_2$	0	C_{1101}
Busy	Busy	Busy	X	Underlay	$T-\tau_1$	0	C_{111x}
where, $C_{xxxx} = B\log_2(\text{SNR})$							

$$DL_4 = \frac{T-\tau_1}{T}\left[P(H_1)P(H_0)\left(1-p_d^1\right)C_{010x} + P(H_1)^2\left(p_d^1\right)C_{111x}\right] + \frac{T-\tau_1-\tau_2}{T} + \begin{bmatrix} P(H_1)^2\left(1-p_d^1\right)\left(1-p_d^2\right)C_{1100} \\ +P(H_1)P(H_0)p_d^1\left(1-p_d^2\right)C_{0110} \end{bmatrix} \tag{13}$$

5 Simulation Results

In this section, numerically simulated results are presented to validate the proposed scheme over other conventional schemes. These conventional schemes are: (i) Conventional spectrum access with single sensing slot (Conv_I) [3] (ii) Conventional spectrum access with two sensing slots (Conv_II) [5], and (3) Hybrid spectrum access with single sensing slot (Hybrid_I) [6]. The simulation environment considers one PU and multiple SUs placed randomly within the communication range of PU. The parameters used in simulation are given in Table 6. The values of the simulation parameters are same as considered in [3, 5, 6] and the values of P_d and P_f are considered as per IEEE 802.22 standard [21].

Figure 9 shows comparison of the secondary throughput for proposed hybrid spectrum access scheme with other three conventional schemes. It has been observed that the secondary throughput achieved Conv-I scheme is less as compared to the

Table 6 Simulation parameters [3, 5, 6, 21]

S. No.	Parameter	Value
1	T	100 ms
2	$P(H_0)$	0.1
3	$P(H_1)$	0.9
4	$P_f = p_f^1 = p_f^2$	0.1
5	$P_d = p_d^1 = p_d^2$	0.9
6	P_p	4 W
7	P_1	6 W
8	P_2	0.5 W
9	T	5 ms
10	N_p	0.04 W
11	f_s	6 MHz

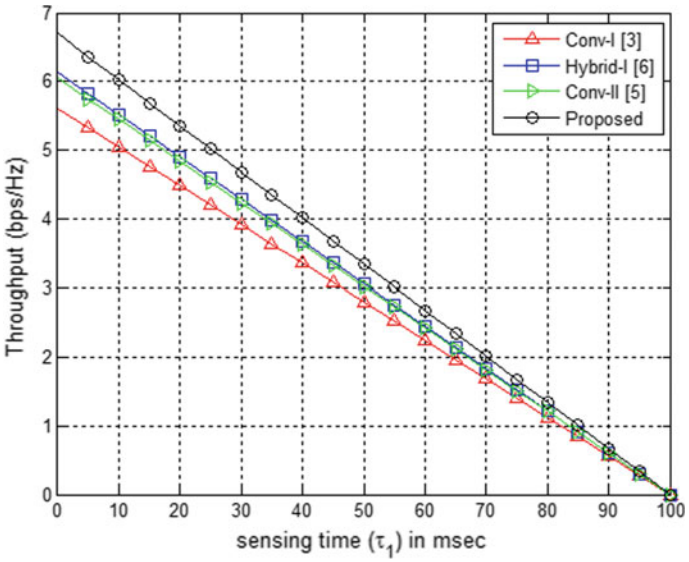

Fig. 9 SU Throughput comparison with respect to sensing time

other three schemes. This is due to the reason that conventional method allows SU to transmit in a channel on detecting PU absent from it. To overcome this bottleneck, Hybrid-I scheme allows SU to transmit in underlay and interweave mode based on the presence and absence of PU from channel, respectively. The scheme improves secondary throughput significantly however, similar to [3], no attempt has been made to correct the sensing error. To overcome uncertainties in sensing results, Conv-II scheme uses two sensing slots. Since, data transmission is allowed on detecting channel idle only and both sensing slots are of equal duration, the total transmission

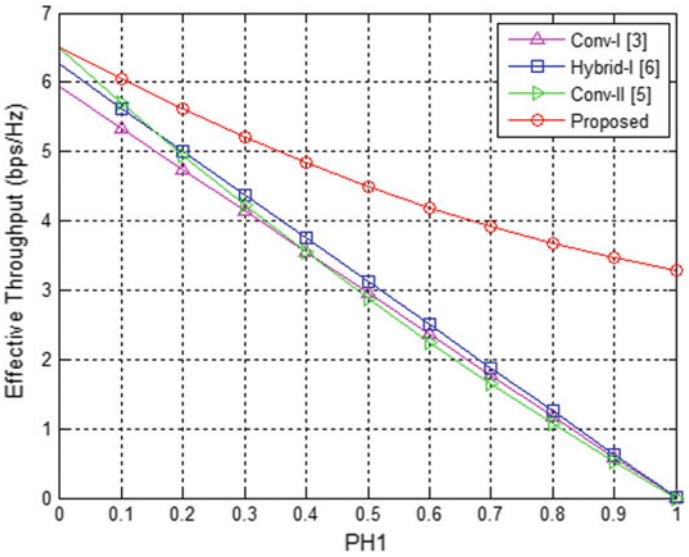

Fig. 10 Comparison of effective SU throughput with respect to PH1

time reduces significantly. However, the scheme performs equally well as Hybrid-I scheme and effective throughput of both the schemes is same. It has also been observed that proposed hybrid spectrum access scheme has a potential to improve effective SU throughput significantly by exploiting transmission opportunities more accurately with the help of two sensing slots.

The comparison of effective secondary throughput with respect to the probability of channel occupancy by primary user is shown in Fig. 10. It has been observed that for the parameters given in Table 5, the effective throughput of the proposed scheme is significantly high as compare to the other conventional schemes. For example when primary user is absent from a channel, the performance of the proposed scheme and Conv-II scheme is same and effective throughput is 5% and 8% more as compare to the Hybrid-I and Conv-I scheme, respectively. When channel is partially occupied by primary user, the proposed scheme improves SU throughput by 23% as compare to the other conventional schemes. It can also be observed that when channel is fully occupied by PU, proposed scheme has potential to achieve 50% more throughput as compare to the schemes proposed in [3, 5, 6].

In dynamic spectrum sharing scenario, when SU is not able to sense PU in a channel and transmits in interweave mode, the whole transmission results into data loss. Figure 11 shows the comparison of data loss with respect to PH1 for the proposed scheme with conventional schemes studied in this paper. It has been observed that for Conv-I and Hybrid-I scheme, data loss increases significantly with the probability of PU being active in channel increases. However, for Conv-II scheme and proposed scheme data loss is equal and decreases with the probability of PU being in a channel increases. For example, when PU is present in a channel, data loss of Conv-II and

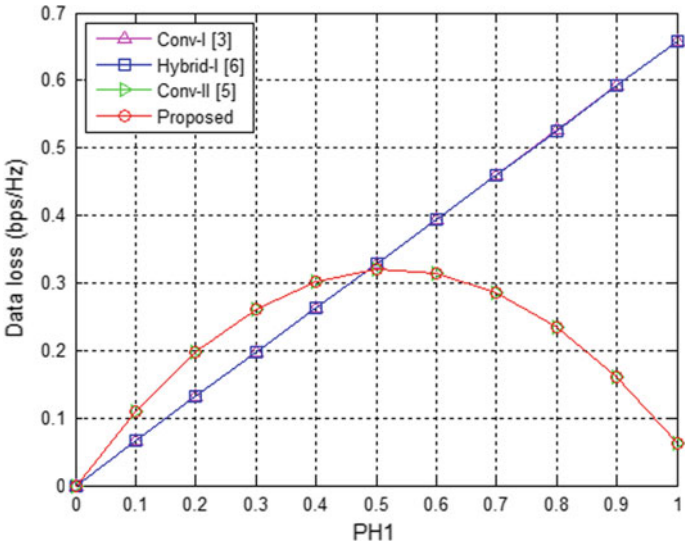

Fig. 11 Data loss comparison as a function of PH1

proposed scheme is 89% less than Conv-I and Hybrid-I scheme. Comparing Figs. 9 and 10, it is clear that proposed scheme has a potential to increase SU throughput significantly without increasing data loss as compared to Conv-II scheme discussed in this paper.

6 Conclusion and Future Scope

In this paper, hybrid spectrum access scheme is proposed for the efficient utilization of frequency spectrum. The scheme utilizes two sensing slots for the accurate detection of PU in a channel to improve SU throughput and to reduce the data loss. The analytical expression for the achievable secondary throughput and data loss have been derived and compared with other existing schemes with one and two sensing slots. Based on the results, it is concluded that the proposed scheme has a potential to increase SU throughput by 50% with zero data loss in comparison with other conventional schemes when PU is present in a channel. In future, the work may be extended further to evaluate the impact of adding second sensing slot in modified frame structure on the energy efficiency of the secondary communication system.

References

1. Akyildiz, I.F., Lee, W.Y., Vuran, M.C., Mohanty, S.: NeXt generation/dynamic spectrum access/cognitive radio wireless networks: a survey. Comput. Netw. **50**(13), 2127–2159 (2006)
2. Zheng K, Liu X, Liu X, Zhu Y (2019) Hybrid overlay-underlay cognitive radio networks with energy harvesting. IEEE Trans. Commun. 67(7):4669–4682
3. Liang, Y., Zeng, Y., Peh, E.C.Y., Hoang, A.T.: Sensing-throughput tradeoff for cognitive radio networks. IEEE Trans. Wirel. Commun. **7**(4), 1326–1337 (2008)
4. Urkowitz, H.: Energy detection of unknown deterministic signals. Proc. IEEE**55**(4), 523–531 (1967)
5. Kong, F., Cho, J., Lee, B.: Optimizing spectrum sensing time with adaptive sensing interval for energy-efficient CRSNs. IEEE Sens. J. **17**(22), 7578–7588 (2017)
6. Thakur, P., Kumar, A., Pandit, S., Singh, G., Satashia, S.N.: Advanced frame structures for hybrid spectrum access strategy in cognitive radio communication systems. IEEE Commun.. Lett.**21**(2), 410–413 (2017)
7. Tang K, Shi R, Dong J (2018) Throughput analysis of cognitive wireless acoustic sensor networks with energy harvesting. Future Gener. Comput. Syst. 86:1218–1227
8. Liu, P., Qi, W., Yuan, E., Wei, L., Zhao, Y.: Full-duplex cooperative sensing for spectrum-heterogeneous cognitive radio networks. Sensors **17**(8), 1773–1793 (2017)
9. Rahayu, Y., Rahman, T.A., Ngah, R., Hall, P.S.: Ultra wideband technology and its applications. In: Proceedings of International Conference on Wireless and Optical Communications Networks (WOCN '08), pp. 1–5 (2008)
10. Mehmeti, F., Spyropoulos, T.: Performance analysis, comparison, and optimization of inter-weave and underlay spectrum access in cognitive radio networks. IEEE Trans. Veh. Tech. **67**(8), 7143–7157 (2018)
11. Liang, W., Ng, S.X., Hanzo, L.: Cooperative overlay spectrum access in cognitive radio networks. IEEE Commun. Surv. Tutor. **19**(3), 1924–1944 (2017)
12. Naeem, M.H. Rehmani, Y. Saleem, Y., Rashid, L., Crespi, N.: Network coding in cognitive radio networks: a comprehensive survey. IEEE Commun. Surv. Tutor. **19**(3), 1945–1973 (2017)
13. Huang, S., Liu, X., Ding, Z.: Opportunistic spectrum access in cognitive radio networks. In: Proceedings of IEEE Conference on Computer Communications, pp. 1427–1435. Phoenix, AZ (2008)
14. Rebato, M., Boccardi, F., Mezzavilla, M., Rangan, S., Zorzi, M.: Hybrid spectrum access for mm wave networks. In: Mediterranean Ad Hoc Networking Workshop (Med-Hoc-Net), Vilanova i la Geltru, pp. 1–7 (2016)
15. Bansal, G., Duval, O., Gagnon, F.: Joint overlay and underlay power allocation scheme for OFDM-based cognitive radio systems. In: Proceedings of 71st IEEE Vehicular Technology Conference, Taipei, pp. 1–5 (2010)
16. Yao, H., Zheng, Z., Liu, H., Zhang, L.: Optimal power allocation in joint spectrum underlay and overlay cognitive radio networks. In: Proceedings of International Conference on Cognitive Radio Oriented Wireless Networks and Communications, Hannover, pp. 1–5 (2009)
17. Zheng, K., Liu, X., Zhu, Y.: Hybrid overlay-underlay cognitive radio networks with energy harvesting. IEEE Trans. Commun. **67**(7), 4669–4682 (2019)
18. Li, X., Zhao, H., Cao, L., Sun, A.: Stable channel allocation in hybrid overlay/underlay cognitive radio networks. In: Proceedings of International Conference on Computer Science and Network Technology (ICCSNT), pp. 1016–1020. Harbin (2015)
19. Manosha, K.B.S., Rajatheva, N., Latvaaho, M.: Overlay/underlay spectrum sharing for multi-operator environment in cognitive radio networks. In: IEEE Vehicular Technology Conference (VTC Spring), pp. 1–5. Yokohama (2011)
20. Yu, R., Zhang, C., Zhang, X., Zhou, L., Yang, K.: Hybrid spectrum access in cognitive-radio-based smart-grid communications systems. IEEE Syst. J. **8**(2), 577–587 (2014)
21. Stevenson, C.R., Chouinard, G.,. Lei, Z., Hu, W., Shellhammer, S.J., Caldwell, W.: IEEE 802.22: the first cognitive radio wireless regional area network standard. IEEE Commun. Mag. **47**(1), 130–138 (2009)

Speech Emotion Recognition Through Extraction of Various Emotional Features Using Machine and Deep Learning Classifiers

Kunal Jain, Anand Nayyar, Lakshay Aggarwal, and Rachna Jain

Abstract Identification of emotions along with the semantics from the speech signals is still one of the most challenging tasks because of the arising difficulty in the extraction and selection of the appropriate emotion features. The speech emotion recognition (SER) system has become one of the active research topics in recent years. Many researchers proposed various models to enhance the machine responses during the man–machine interactions by identifying the emotional state of the customer. This research work aims to propose a multi-class classification model to extract and classify the emotional state of the speaker into eight classes, namely happy, sad, surprised, disgust, neutral, calm, angry, and fearful. In this research work, two machine learning classifiers, namely k-nearest neighbors and random forest, are used along with the multi-layer perceptron classifier of deep learning for determining the emotional features from speech signals. The dataset for this research is obtained from the RAVDESS. Along with the audio speeches of 24 actors, the audio song dataset is also utilized for the better training of the proposed model. The performance of all three algorithms is compared and evaluated by using the confusion matrix and accuracy plots. The empirical results show that the KNN classification model of ML has performed better than other proposed algorithms with increased accuracy of 76.25%.

K. Jain · L. Aggarwal · R. Jain
Department of Computer Science and Engineering, Bharati Vidyapeeth's College of Engineering, New Delhi, India
e-mail: jainkunal286@gmail.com

L. Aggarwal
e-mail: lakshayagg5@gmail.com

R. Jain
e-mail: rachna.jain@bharatividyapeeth.edu

A. Nayyar (✉)
Graduate School, Duy Tan University, Da Nang 550,000, Vietnam
e-mail: anandnayyar@duytan.edu.vn

Faculty of Information Technology, Duy Tan University, Da Nang 550,000, Vietnam

D. K. Sharma et al. (eds.), *Micro-Electronics and Telecommunication Engineering*,
Lecture Notes in Networks and Systems 179,
https://doi.org/10.1007/978-981-33-4687-1_12

Keywords Speech emotion recognition · RAVDESS · Automatic speech recognition system · Multi-class classification · KNN

1 Introduction

The automatic speech recognition systems only focus on the semantics of the speech and not on the emotions of the speaker. The performance of speech recognition systems can be enhanced if it incorporates the ability of emotion recognition as well. The most difficult part of the construction of the SER systems is the extraction of emotional features from the speech signal [1]. SER has become one of the most active research topics, and a lot of challenges are involved in it. It aims to recognize the emotions of people from their speeches. It would enhance the responses of the machines if the machines already know about the emotional state of the user [2]. Since a badly interpreted message or can say, a message without the emotions can lead to a lot of misunderstandings. Figure 1 represents the SER system that anticipates the emotion in real time.

SER systems are used in many applications. Safety is one of the primary objectives associated with the development of these systems and recently gains so much interest in the last year. For instance, the emotional state of the drivers is directly associated with their safety and hence always needs to be analyzed before driving. The risk of the accident increases ten times if the driver having strong emotions during the driving [4, 5]. It is also used to identify the state of dissatisfied customers in various remote call centers. In the e-learning domain, SER systems help the teachers to enhance the lesson plan in case the students are found to be dissatisfied with the current lesson plan [6]. It also found application in the entertainment industry by enhancing the

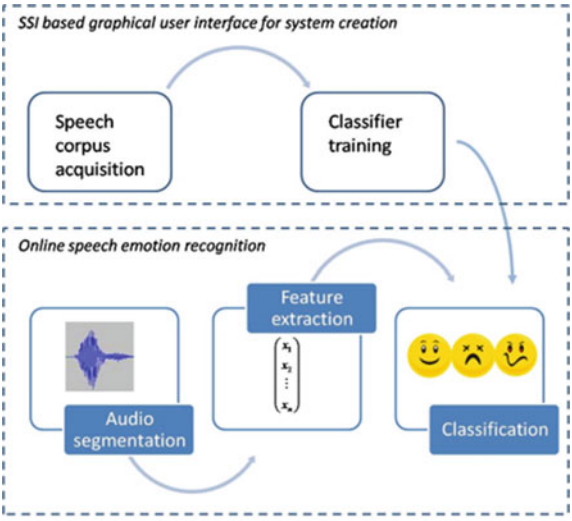

Fig. 1 Real-time SER system [3]

Fig. 2 Application domains of SER systems

quality of the content if the audience reviews find to be dissatisfied with the original content. Other applications of SER systems include alerting systems, lie detection systems, and psychiatric aid [7–11]. Figure 2 represents various industrial domains in which SER systems find useful applications.

This research seeks to carry the extraction and classification of the emotional state of the speaker into eight classes, namely happy, sad, surprised, disgust, neutral, calm, angry, and fearful.

- We extract various features such as MFCC from the dataset, which will be given as input to train the model.
- Here, two machine learning classifiers, namely KNN and random forest, are used along with the multi-layer perceptron classifier of deep learning for determining the emotional features from speech signals.
- The dataset for this research is obtained from the RAVDESS.
- The performance of the three algorithms is compared by using the confusion matrix and the accuracy score.

The rest of the paper is presented in the following way. Section 2 provides a detailed review of various researches which takes place using various approaches for the extraction of various emotional features from the speech signals. Then, the research methodology is discussed in Sect. 3. It discusses the classification algorithms and evaluation metrics used along with the proposed research model. Later, Sect. 4 deals with the data analysis and preprocessing along with the experimental results and simulations of the proposed algorithms. Finally, Sects. 5 concludes the entire paper and suggests future areas of research.

2 Literature Survey

The speech signal is the most common mode of communication among human beings. The messages can be interpreted badly without a proper understanding of other's emotions. Therefore, it is very important to develop the machines (for increasing the man–machine interactions) that can identify the human's emotional state very well and react accordingly [12]. In recent years, SER has got high attention and has become one of the favorite topics of researchers. Here, some of the researches are listed below from all over the world depicting various methods proposed to recognize human emotions through speeches.

In [13], Zhao et al. designed two CNN-LSTM based networks. One is 1D CNN-LSTM and the second one is the 2D CNN-LSTM network. The networks were constructed to understand local as well as global emotional features. Both the networks have a similar working, and each consists of a single LSTM layer and four local feature learning blocks. The fusion of CNN and LSTM made the network to overcome the limitations of each other and increase the strength of the network. The proposed networks were tested on two benchmark datasets. And the comparative analysis of the proposed networks with the traditional deep belief network and CNN networks has also been provided. Results have shown the outstanding performance of both the proposed networks in emotion recognition in comparison with the other network models.

Badshah et al. [14] suggested a new strategy of using deep CNN and spectrograms for emotion recognition. Spectrograms are given as input to the model. The proposed model was made up of the three convolutional and three fully connected layers for extracting the features from spectrograms and predicts output for seven emotions. The model was trained on the Berlin emotion dataset, and the comparison with the pre-trained AlexNet model was also provided in the study. Results show that the proposed approach dependent on the newly prepared model is better than the adjusted model and is equipped for predicting feelings effectively as well as precisely.

Sun et al. [15] proposed an algorithm by combining the decision tree and support vector machine algorithm with fisher feature selection. Fisher features are incorporated to eliminate the feature parameters with higher recognizing capacity. The proposed algorithm was tested on two datasets to approve the viability of the model. The exploratory outcomes showed that the proposed algorithm can viably decrease the emotional confusion and enhance the accuracy in speech emotion recognition.

Fayek et al. [16] presented a study on the topic "Evaluating deep learning architectures for Speech Emotion Recognition." The study proposed the SER system based on feed-forward and recurrent neural network architectures. Experiments were conducted to enlighten the favorable circumstances and confinements of these structures in paralinguistic discourse acknowledgment and feeling acknowledgment specifically. Subsequently, the proposed technique presents quantitative and subjective appraisals of the models' performances.

In [17], Lu et al. proposed a method in integrating automatic speech recognition by giving character-level recurrent neural networks for sentimental analysis. The model

was applied to the Multimodal Corpus of Sentimental Intensity. The method was built with incorporating noise realistic scenarios by using human–robot interaction. The accuracy obtained was 73.6% with binary sentimental analysis.

In [18], Kumar et al. classified the real-time tweets based on truth value by using facilitating rumor analysis. The authors collected 14 k tweets on suspected child-lifters in the Indian continent (#moblyncing) and classifies as true, false, and unspecialized using 13 attributes (features). The empirical analysis validates that the proposed implementation of particle swarm optimization (PSO) for feature subset selection in rumor veracity classification outperforms the baseline supervised learning algorithms.

In [19], Kumar et al. apply data mining on social media sites on big platforms like Instagram, Facebook, Tweeter, etc. The research proposed to overcome the problem of large datasets by enhancing the program. The results are validated on different various applications. By using SWAT analysis, authors tried to find out weaknesses, opportunities, threats, etc. They proposed a model cyberbullying as the name represents, and they try to find out the peoples who bully peoples on social media sites.

In [20], Kumar et al. proposed research to analyze social media to classify different aspects of people which includes emotion, sarcasm, rumor, and even hate speeches posted by them. In the research, a deep learning model named sAtt-BLSTM convNet has been designed which is based on the integration of soft attention-based bidirectional long short-term memory (sAtt-BLSTM) and convolutional neural network by applying GLoVe. The proposed model was tested and compared with other deep learning algorithms by utilizing both balanced and an unbalanced dataset which consists of sarcastic and non-sarcastic tweets. The experimental results have proven that the proposed model surpasses other models in terms of accuracy and can be effectively used in the respective field.

3 Algorithms Used

In this work, the model is trained on three classification algorithms, namely RF, KNN, and MLP classifier [21] for recognizing the human sentiments through audios.

3.1 Random Forest (RF) Classifier

It is a grouped learning algorithm that functions admirably with both the regression and classification problems. It consists of several decision trees [22].

Steps to Build the Random Forest Classifier

1. Starts with the random sample selections of the audio dataset by setting the value of the random_state parameter.

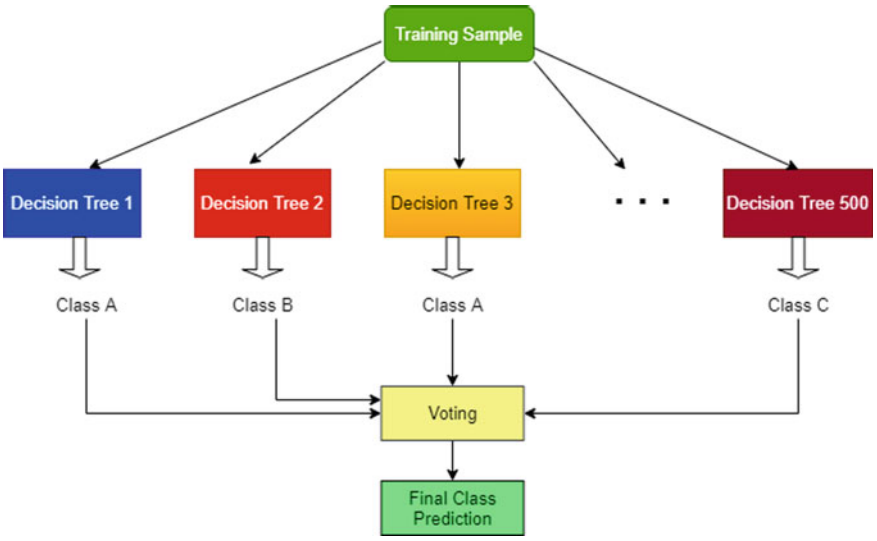

Fig. 3 Random forest classification algorithm [23]

2. Provide the number of decision trees to be constructed through the n_estimator parameter.
3. A decision tree is constructed for every sample to get the expected outcomes for every possible tree.
4. For every predicted outcome, averaging is performed.
5. The most voted (averaged) prediction outcome is selected as the outcome.

Figure 3 represents the procedure involved in building the random forest classification model.

4 K-Nearest Neighbor (KNN) Classifier

KNN is a non-parametric and lazy learning algorithm utilized for regression as well as for classification problems. It uses the distance measures of its neighbors' classes to predict the class of new data samples [24].

Steps to Build the KNN Classifier

1. Load the dataset
2. Set the value of k (number of nearest neighbors).
3. Calculate the distance between the test sample data point and all the training sample data points through one of the distance approaches discussed above by providing the value of p.
4. Sort the distance values in ascending order.
5. Now, it will select the first k entries from the sorted array.

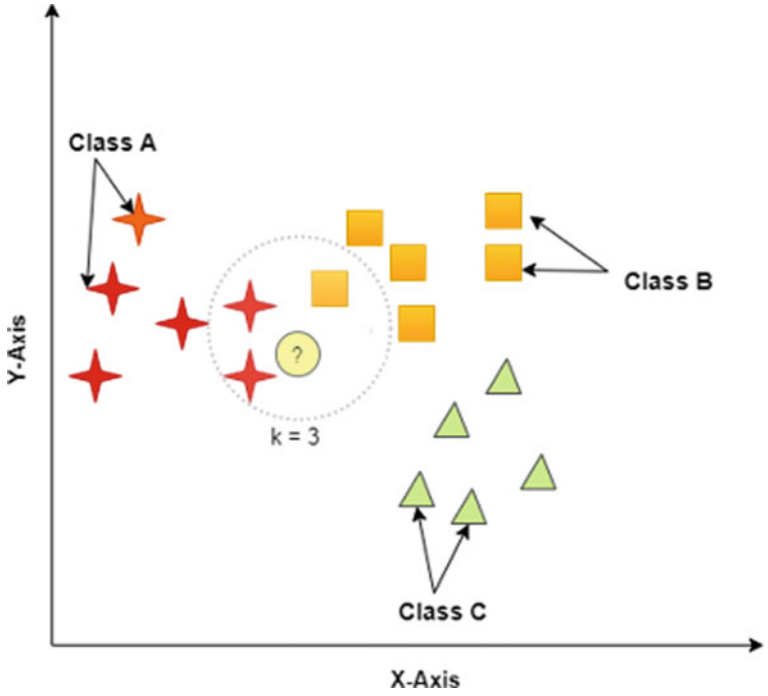

Fig. 4 Classification using KNN algorithm [25]

11. Predict the class of test sample based on the most frequent class of these entries.

Figure 4 represents a general idea of predicting the class of a new item using the KNN algorithm.

5 Multi-layer Perceptron (MLP) Classifier

MLP classifier of the deep learning interfaces with a neural network. Dissimilar to other classifiers, MLP classifier depends on a hidden neural network to perform the classification task [26]. MLP classifier is similar to other scikit-learn's classifiers in the manner that the implementation of MLP classifier does not require the implementation of Naïve Bayes or support vectors or some other classifiers from scikit-learn [27].

Figure 5 represents the basic multi-layer perceptron structure with the input layer of four perceptrons and a hidden layer of three perceptrons.

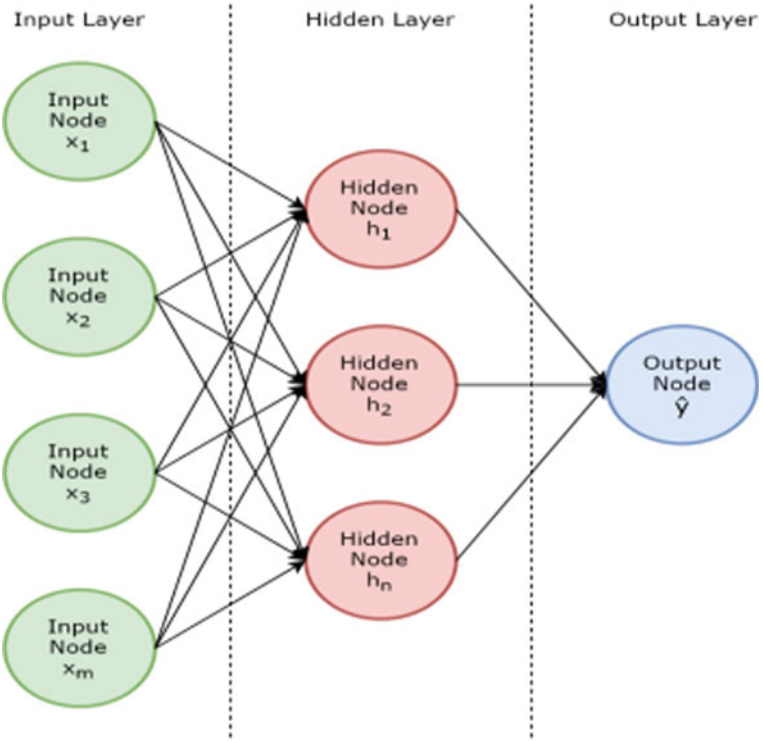

Fig. 5 Multi-layer perceptron classification [28]

6 Proposed Methodology

In this section, the research methodology of this work is discussed in detail. Initially, both the audio speech and the audio song dataset are provided as an input to the model. After the analysis of data, the data gets preprocessed and split for the training (80%) and the validation (20%) purpose. After that, all three proposed models get trained by tuning the values of its hyperparameters. After the training, the validation is performed and the validation set is classified into eight classes. Finally, the models are compared using the confusion matrix and accuracy score as the evaluation metrics. Figure 6 represents the proposed model of our research work.

6.1 Dataset Description

The audio dataset for this research is taken from RAVDESS. The complete dataset consists of recordings of 24 actors (12 males and 12 females), vocalizing two simple sentences (in the form of audio speeches, audio songs, video speeches, and video

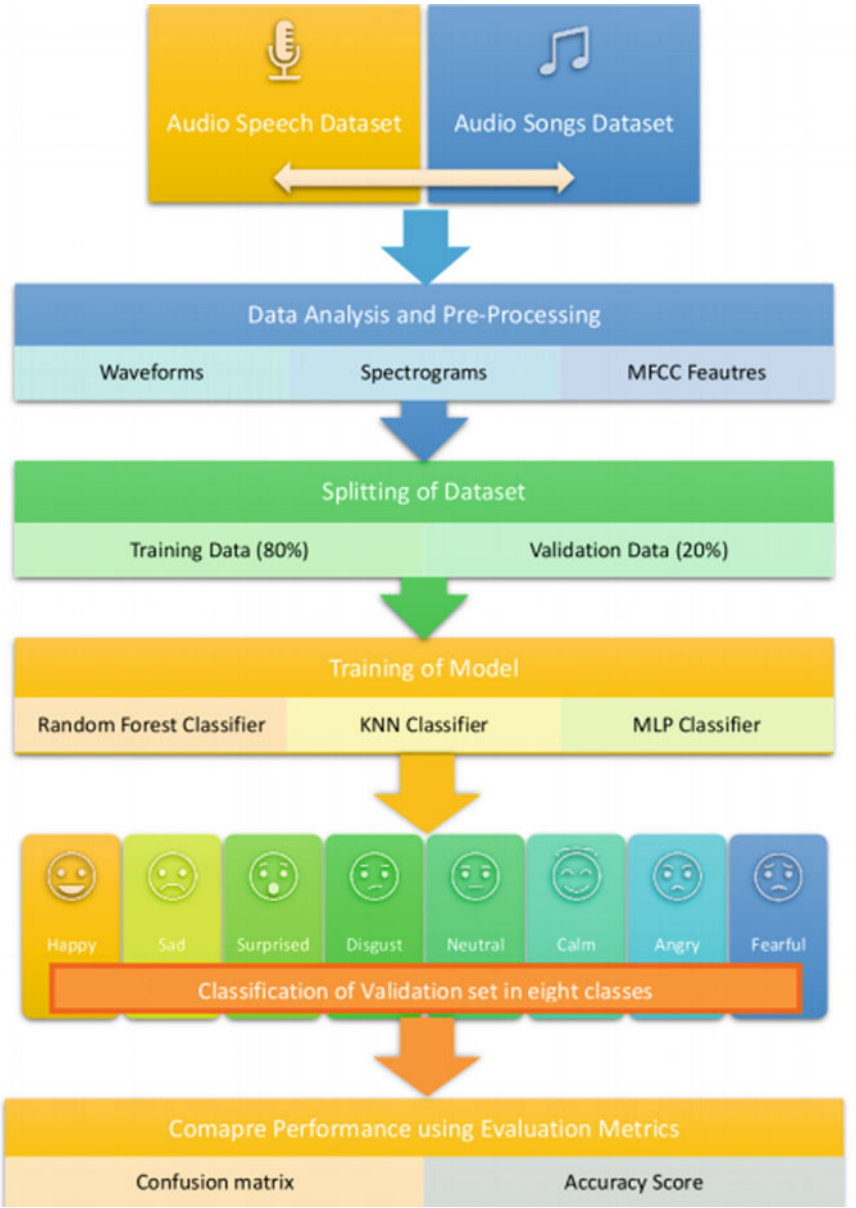

Fig. 6 Proposed research model

songs) with eight different emotions [29]. The two sentences that are used in the dataset are "Dogs are barking by the door," and "Kids are playing by the door." However, for this study, the model is trained only on audio speech and audio song data. The eight emotions considered for constructing this dataset were happy, sad, surprised, disgust, neutral, calm, angry, and fearful.

6.2 Data Analysis

This section will describe the basic concepts of the audio data and signal processing. Specifically, the section will cover aspects like: how to visualize the waveform, how to apply the Fourier transform (FT), how to perform short-term Fourier transforms (STFT) for getting spectrograms, and lastly, how to extract the MFCC features from the spectrograms.

Waveform

The waveform is the graphical representation of audio wave which describes how air molecules get displaced with time. The displacement of the air molecules is determined with the help of amplitude. The higher the amplitude is, the more the air molecules get displaced [30].

Figure 7 represents the waveform generated by actor_01 by delivering a sentence in neutral emotion.

Fourier Transform (FT)

It is a process of decomposing the complex periodic sound into a sum of sine waves which oscillates at different frequencies. When we apply the FT, we are particularly interested in the amplitude. It is because amplitude tells how much a specific frequency contributes to the complex sound. The higher the amplitude, the more that specific frequency contributes to the complex sound [31].

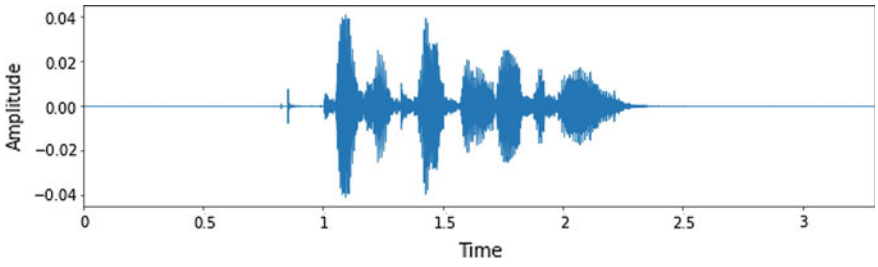

Fig. 7 Waveform generated by actor_01 with neutral emotion

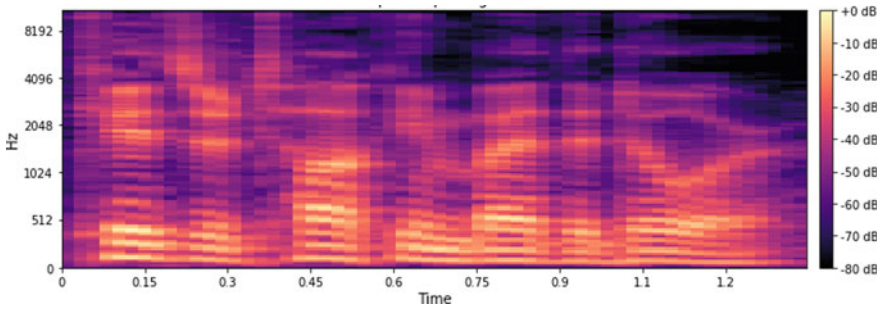

Fig. 8 Spectrogram corresponds to the waveform shown in Fig. 7

Short-Term Fourier Transform (STFT)

STFT computes several FTs at different time intervals. In doing so, it preserves the information about time. Different intervals at which FT is performed are given by the frame size. A frame is a bunch of samples and should be fixed [32].

After performing the STFT, the spectrogram is generated that gives information about magnitude as a function of frequency and time. In spectrograms, the Y-axis represents the frequency, X-axis denotes the time, and the color bar represents the third axis that tells how much a given frequency is present in a sound at a given time [33].

Figure 8 represents the spectrogram obtained after applying STFT to the signal whose waveform is shown in Fig. 7.

Mel Frequency Cepstral Coefficient (MFCC)

MFCC is a fundamental feature of spectrogram which can be used with both machine learning and deep learning algorithms. It is a frequency-domain feature. The advantage of using MFCC over spectrogram is that they approximate the human auditory system, i.e., they try to model the way humans process the audio. The result obtained by extracting the MFCCs is a bunch of coefficients called MFCC coefficients. And for the audio data, the coefficients should be between 13 and 40. These coefficients are calculated at each frame to get an idea of how the MFCCs are evolving with time [34].

Figure 9 represents the MFCC plot corresponding to the spectrogram shown in Fig. 8.

6.3 Model Formulation

After splitting the dataset, all the three models are trained by initializing some random value of the hyperparameters. The models get under continuous training and testing process until the optimized value of the hyperparameters is achieved. After achieving

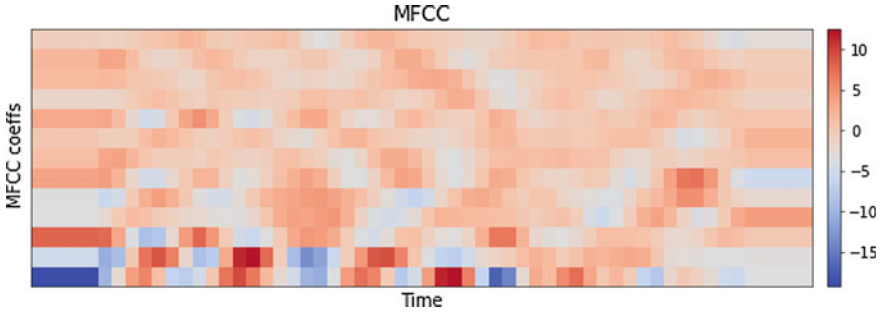

Fig. 9 MFCC plot with 13 MFCC coefficients

the maximum accuracy in each model, the performances are compared using the confusion matrix and accuracy score as the evaluation metrics.

RF Classifier

Initially, the RF model is trained by considering 100 decision trees. After that, the model undergoes in continuous training and testing process until the optimized value of the hyperparameters is achieved. After further increase in the value of the n_estimator parameter (number of decision trees), the accuracy starts decreasing. Hence, the optimized value of n_estimator is chosen to be 500. The rest of the parameters are taken with their default values.

KNN Classifier

Initially, the number of nearest neighbors is evaluated by determining the mean score by modifying the value of k from 1 to 50 and the optimized value of k parameter comes out as 1. Also, the power parameter p is chosen to be 1. The rest of them are set as defaults.

MLP Classifier

In the MLP classification model, various hyperparameters are initialized with some base values. The model is then undergoing continuous training and testing process until the optimized value of the hyperparameters is achieved. The optimum values of various parameters are determined as follows:

- The optimized value of alpha: 0.01
- The batch size: 230
- The activation function: logistic
- Number of neurons in an initial hidden layer: 150
- Maximum number of iterations: 600.

7 Experimental Results and Analysis

In the following section, simulation and results of our research work are discussed and analyzed in detail. This section also provides a brief insight into the evaluation metrics utilized in the following research work.

8 Evaluation Metrics

The evaluation metrics used in this work are confusion matrix and accuracy scores. These are discussed in detail below.

Confusion Matrix

It is a table that is used to describe the performance of the classification model. The total number of true and false outcomes is summed up with count values and grouped separately into two classes, i.e., actual and predicted. Table 1 represents the basic structure of the confusion matrix.

Here,

- True Positives (TPs): Both the actual and predicted results are positive
- False Negatives (FNs): Actual results are positive but predicted are negative
- True Negatives (TNs): Both the actual and predicted results are negative
- False Positives (FPs): Actual results are negative but predicted are positive.

Figure 10 shows the confusion matrix for the random forest model.
Figure 11 represents the confusion matrix for the KNN classification model.
Figure 12 represents the confusion matrix for the MLP classification model.

Accuracy Score

It is defined as a ratio of accurately anticipated observations to the total observations. It is the best method for measuring the performance in case of the symmetric results, i.e., values of FP and FN should be nearly the same [36]. It is described below by Eq. 1.

$$\text{AccuracyScore} = \frac{\text{TP} + \text{TN}}{\text{TP} + \text{FN} + \text{FP} + \text{TN}} \tag{1}$$

Table 2 represents the average accuracy score and the individual accuracy scores of all the eight emotion labels obtained through the three proposed models.

Table 1 Confusion matrix [35]

	Class A predicted	Class B predicted
Class A actual	TP	FN
Class B actual	FP	TN

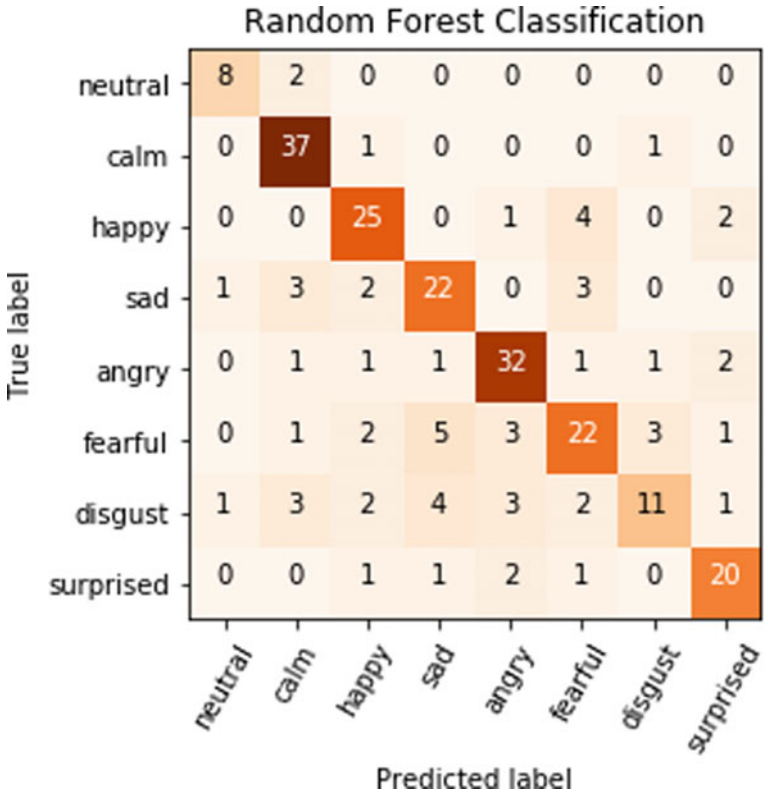

Fig. 10 Confusion matrix for random forest classifier

9 Comparative Analysis

It can be concluded from Table 2 that the average accuracy scores obtained with RF classifier, KNN classifier, and MLP classifier are 73.75%, 76.25%, and 75.42% respectively.

RF classifier achieved the highest accuracy of 94.87% in the prediction of calm emotion in speakers. It also predicted neutral, angry, and surprised emotional states with a significant high accuracy of 80% and above.

KNN classifier achieved the highest accuracy of 90.00% in the prediction of neutral emotion in speakers. It also predicted a happy, calm, and angry emotional state with a significant high accuracy of nearly 80% and above.

MLP classifier achieved the highest accuracy of 92.31% in the prediction of calm emotion in speakers. It also predicted a happy and angry emotional state with a significant high accuracy of 78% and above.

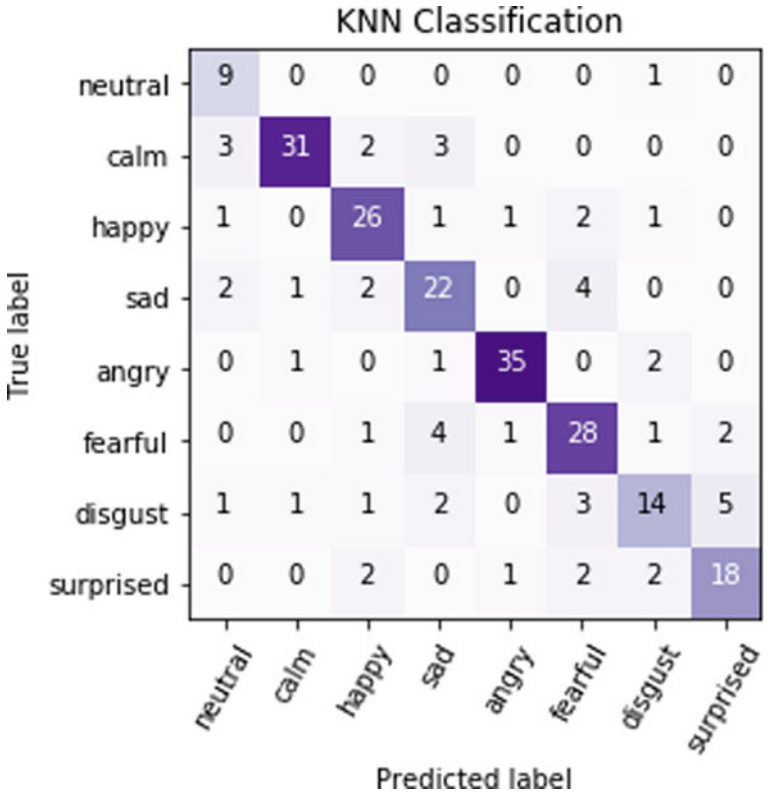

Fig. 11 Confusion matrix for KNN classifier

10 Conclusion and Future Scope

This research work is carried out to build an SER system to extract and identify the emotional state of the people from the speeches and songs. The project would help in a better understanding of people's words and also increase the efficiency of the machines involved in the interaction with humans. This research is performed on the RAVDESS dataset. Two machine learning classifiers, namely k-nearest neighbors classifier and random forest classifier along with the multi-layer perceptron classifier of deep learning are used in this research for determining the emotional features from the speech signals. After the determination of the optimized values of hyper-parameters, the results are evaluated using the confusion matrix and accuracy score graphs. After the evaluation and comparison of the accuracy scores of the proposed algorithms, we conclude that the KNN algorithm of machine learning shows the optimum performance among all proposed algorithms with increased accuracy of 76.25%.

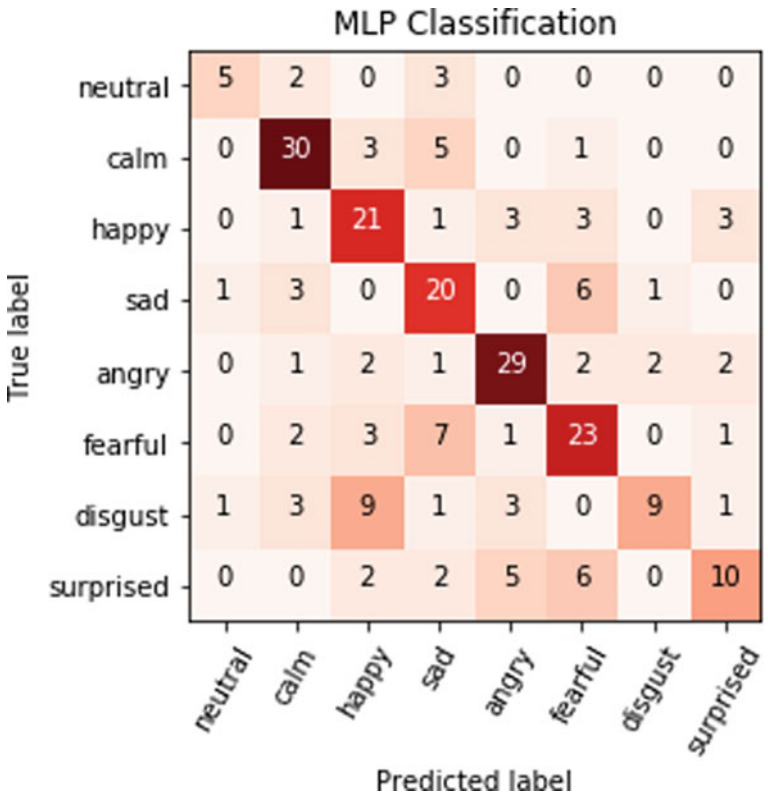

Fig. 12 Confusion matrix for MLP classifier

Table 2 Accuracy scores with three proposed algorithms

	RF classifier (%)	KNN classifier (%)	MLP classifier (%)
Neutral	80.00	90.00	70.00
Calm	94.87	79.49	92.31
Happy	78.12	81.25	78.12
Sad	70.97	70.97	74.19
Angry	82.05	89.74	82.05
Fearful	59.46	75.68	72.07
Disgust	40.74	51.85	55.56
Surprised	80.00	72.00	64.0
Average	73.75	76.25	75.42

The accuracy of the proposed model would possibly be enhanced in the future by utilizing other classification models, namely LSTM, Bi-LSTM, stochastic gradient, and RNN models. Also, along with audio speeches and music, video speeches and songs can be utilized for the training of the model, which would possibly increase the efficiency of the proposed model. The model can also be used to predict the gender and age of the speaker.

References

1. Han K, Yu D, Tashev I (2014) Speech emotion recognition using deep neural network and extreme learning machine. In: Fifteenth annual conference of the international speech communication association
2. Nwe TL, Foo SW, De Silva LC (2003) Speech emotion recognition using hidden Markov models. Speech Commun 41(4):603–623
3. EmoVoice—real-time emotion recognition from speech. Accessed from https://www.informatik.uni-augsburg.de/lehrstuehle/hcm/projects/tools/emovoice/ (2005)
4. Mayou R, Bryant B, Duthie R (1993) Psychiatric consequences of road traffic accidents. BMJ 307(6905):647–651
5. Schuller B, Rigoll G, Lang M (2004) Speech emotion recognition combining acoustic features and linguistic information in a hybrid support vector machine-belief network architecture. In: 2004 IEEE international conference on acoustics, speech, and signal processing, vol 1. IEEE, pp I-577
6. Li W, Zhang Y, Fu Y (2007) Speech emotion recognition in e-learning system based on affective computing. In: Third international conference on natural computation (ICNC 2007), vol 5, pp 809–813. IEEE
7. Saste ST, Jagdale SM (2017) Emotion recognition from speech using MFCC and DWT for security system. In: 2017 international conference of electronics, communication and aerospace technology (ICECA), vol 1, pp 701–704. IEEE
8. Cowie R, Douglas-Cowie E, Tsapatsoulis N, Votsis G, Kollias S, Fellenz W, Taylor JG (2001) Emotion recognition in human-computer interaction. IEEE Signal Process Mag 18(1):32–80
9. Schuller B, Rigoll G, Lang M (2003) Hidden Markov model-based speech emotion recognition. In: 2003 IEEE international conference on acoustics, speech, and signal processing, 2003. Proceedings. (ICASSP'03), vol 2. IEEE, pp II-1
10. Nogueiras A, Moreno A, Bonafonte A, Mariño JB (2001) Speech emotion recognition using hidden Markov models. In: Seventh European conference on speech communication and technology
11. Schuller B, Lang M, Rigoll G (2002) Multimodal emotion recognition in audiovisual communication. In: Proceedings. IEEE international conference on multimedia and expo, vol 1. IEEE, pp 745–748
12. Lalitha S, Tripathi S, Gupta D (2019) Enhanced speech emotion detection using deep neural networks. Int J Speech Technol 22(3):497–510
13. Zhao J, Mao X, Chen L (2019) Speech emotion recognition using deep 1D & 2D CNN LSTM networks. Biomed Signal Process Control 47:312–323
14. Badshah AM, Ahmad J, Rahim N, Baik SW (2017) Speech emotion recognition from spectrograms with deep convolutional neural network. In: 2017 international conference on platform technology and service (PlatCon). IEEE, pp 1–5
15. Sun L, Fu S, Wang F (2019) Decision tree SVM model with Fisher feature selection for speech emotion recognition. EURASIP J Audio Speech Music Process 2(1)
16. Fayek HM, Lech M, Cavedon L (2017) Evaluating deep learning architectures for speech emotion recognition. Neural Netw 92:60–68

17. Lu Z, Cao L, Zhang Y, Chiu CC, Fan J (2020) Speech sentiment analysis via pre-trained features from end-to-end ASR models. In: ICASSP 2020–2020 IEEE international conference on acoustics, speech and signal processing (ICASSP). IEEE, pp 7149–7153
18. Kumar A, Sangwan SR, Nayyar A (2019) Rumour veracity detection on twitter using particle swarm optimized shallow classifiers. Multimed Tools Appl 78(17):24083–24101
19. Kumar A, Sangwan SR, Nayyar A (2020) Multimedia social big data: mining. In: Multimedia big data computing for IoT applications, pp 289–321
20. Kumar A, Sangwan SR, Arora A, Nayyar A, Abdel-Basset M (2019) Sarcasm detection using soft attention-based bidirectional long short-term memory model with convolution network. IEEE Access 7:23319–23328
21. Alzubi J, Nayyar A, Kumar A (2018) Machine learning from theory to algorithms: an overview. J Phys. Conf. Ser. 1142(1):012012
22. Hastie, T., Tibshirani, R., Wainwright, M.: Statistical learning with sparsity: the lasso and generalizations. CRC press (2015).
23. Liaw A, Wiener M (2002) Classification and regression by randomForest. R News 2(3):18–22
24. Song Y, Huang J, Zhou D, Zha H, Giles CL (2007) Iknn: informative k-nearest neighbor pattern classification. In: European conference on principles of data mining and knowledge discovery. Springer, Berlin, Heidelberg, pp 248–264
25. Yong Z, Youwen L, Shixiong X (2009) An improved KNN text classification algorithm based on clustering. J Comput 4(3):230–237
26. John Lu ZQ (2010) The elements of statistical learning: data mining, inference, and prediction. J R Stat Soc Ser A (Statistics in Society) 173(3):693–694
27. Hastie T, Tibshirani R, Friedman J (2009) The elements of statistical learning: data mining, inference, and prediction. Springer Science & Business Media
28. Ramchoun H, Idrissi MAJ, Ghanou Y, Ettaouil M (2016) Multilayer perceptron: architecture optimization and training. IJIMAI 4(1):26–30
29. Livingstone SR, Russo FA (2018) The ryerson audio-visual database of emotional speech and song (RAVDESS): a dynamic, multimodal set of facial and vocal expressions in north American English. PLoS ONE 13(5):e0196391
30. Yang Z, Hirschberg J (2018) Predicting arousal and valence from waveforms and spectrograms using deep neural networks. In: INTERSPEECH, pp 3092–3096
31. Bracewell RN, Bracewell RN (1986) The Fourier transform and its applications, vol 31999. McGraw-Hill, New York
32. Xu Y, Zhao Y (2011) Identification of power quality disturbance based on short-term Fourier transform and disturbance time orientation by singular value decomposition. Power Syst Technol 8
33. Shen J, Pang R, Weiss RJ, Schuster M, Jaitly N, Yang Z, Saurous RA (2018) Natural its synthesis by conditioning wavenet on mel spectrogram predictions. In: 2018 IEEE international conference on acoustics, speech and signal processing (ICASSP). IEEE, pp 4779–4783
34. Han W, Chan CF, Choy CS, Pun KP (2006) An efficient MFCC extraction method in speech recognition. In: 2006 IEEE international symposium on circuits and systems. IEEE, pp 4-pp
35. Santra AK, Christy CJ (2012) Genetic algorithm and confusion matrix for document clustering. Int J Comput Sci Issues (IJCSI) 9(1):322
36. Sokolova M, Japkowicz N, Szpakowicz S (2006) Beyond accuracy, F-score, and ROC: a family of discriminant measures for performance evaluation. In: Australasian joint conference on artificial intelligence. Springer, Berlin, Heidelberg, pp. 1015–1021

Fusion-Based Biometric Identification Using Palmprint Images

K. Vidhya and T. R. Ganesh Babu

Abstract Higher identification accuracy is obtained in multibiometrics than single biometrics. The proposed work improves accuracy in personal identification for achieving high standard security in real-world applications. Among numerous biometric technologies, palmprint recognition drives more attention due to its virtuous performance. It is easy to implement, and better results can be obtained by combining the left palmprint images with that of right. The proposed method executes multibiometrics by systematically combining the palmprint images of left hand and right hand. Fusion is performed using scores generated from palmprint images for performing fusion. The proposed algorithm considers the nature of left palmprint image and right palmprint image to deed the resemblance of palmprints of both hands of same subject. Perfect identification performance is obtained which gives better results while comparing with the previous identification methods.

Keywords Palmprint recognition · Biometrics · Multibiometrics · Image fusion · Edge detection

1 Introduction

One of the most important personal identification technologies which engrosses more attention is palmprint identification. It comprises rich texture and miniscule points in addition to principle curves and wrinkles. Palmprint contains amusing information so that high accuracy can be attained [1–4]. Coding and principle curve techniques are some of the palmprint identification methods. Subspace techniques can also be included for palmprint identification.

K. Vidhya (✉)
Department of Electronics and Communication Engineering, Saveetha School of Engineering, SIMATS, Chennai, Tamil Nadu, India
e-mail: kvidhyasri@gmail.com

T. R. Ganesh Babu
Department of Electronics and Communication Engineering, Muthayammal Engineering College, Rasipuram, Tamil Nadu, India

D. K. Sharma et al. (eds.), *Micro-Electronics and Telecommunication Engineering*,
Lecture Notes in Networks and Systems 179,
https://doi.org/10.1007/978-981-33-4687-1_13

The limitation of unimodal biometric technique is that they cannot meet all requirements, so multimodal biometric methods are developed to improve the performance. They are designed by multiple modals of same biometric feature or by multiple biometrics.The method using palmprints is presented by Han et al. for personal identification [5] with image-level fusion method based on wavelets. Combining and integrating multiple biometric traits give feature-level fusion. Zhang et al. proposed [6] a fusion for matching score level using joint palm vein and palmprint system for personal identification. Different traits are treated independently by using conventional multimodal biometrics methods [7, 8]. Similarity between several kinds of biometric traits exists which cannot be exploited.

Special biometric traits have similarity between them. There is no specific method to discover the correlation between the left and right palmprints for biometric identification. A unique content is proposed for combining left with that of right palmprint at the matching score level. There are various types of match scoring, namely left palmprint image (LPI) matching, right palmprint image (RPI) matching and cross-matching. The final decision is obtained by fusing the left query and training palmprint. Wide range of experiments shows that palmprint identification methods can be integrated for identification with higher accuracy.

The proposed work aims to improve the accuracy of identity by validating the possibility of ill-using the cross-matching score of LPI and RPI of the considered subject which have some similarities between them.

The relevant features of palmprint are principle lines and texture. Widely used palmprint identification ways are principal line-based methods, coding-based methods, subspace-based methods and SIFT-based methods.

In line-based method, palmprint identification and verification are performed by extracting palmprint lines using lines or edge detectors. Three principal lines of palm are heartline, headline and lifeline.Those lines give stable presentation to palmprint check.

Gabor filter, Sobel operation and morphological operation are the methods used to obtain palmprint principal lines. Coding techniques include competitive code, ordinal and palmcode methods and binary orientation co-occurrence vector (BOCV) method [9]. Orientation features from palmprint are extracted using six Gabor filters with six directions, and they are combined with palmprint images. Palmprint texture features are extracted using Gabor filter.

Subspace methods use PCA, LDA and ICA. Subspace method preserves maximum variance of the given input data if found using PCA. The distance is minimized for the samples of identical class in LDA, and Euclidean distance is maximized in case of different classes.

SIFT-based method initially dealt with object classification [10] applications, and in recent years, they are introduced in contactless palmprint identification [11–13]. Severe disparities in scales, rotations and translations are made by contactless palmprint images. Satisfactory results are not provided in case of the existing methods.SIFT-based method is desirable for contactless identification methods. To identify potential interest points, difference-of-Gaussian function is used [14, 15].

Based on the stability, the proper parameters are selected to determine finite location and scale. Depending upon the gradients, the keypoints are assigned with required number of orientations, and they are valuated at appropriate scale around each keypoint. The identification of the query image can be determined by Euclidean distance at the identification stage. The similarity is high between the images for smaller Euclidean distance.

2 Methodology

The correlations existing between the LPI and RPI are illustrated here. Figure 1 shows five LPI of these five subjects. Figure 2 shows five RPI of those subjects. Figure 3 depicts the images obtained after undergoing edge detection operation of LPI of those subjects given in Fig. 1. Figure 4 shows the images obtained after undergoing edge detection operation of RPIof five subjects of Fig. 2.

Comparative principal lines of LPI and RPI from different persons have altogether different shape and position, which is clearly represented in figures. Palmprint verification can also be done with principal lines of the right and reverse left palmprints. Preprocessing step involves noise removal by median filtering.

In the proposed method, palmprint identification method is applied to the left palmprint images and the scores are calculated for the given sample. Similarly, the calculations are done for right palmprint images, and finally, the cross-matching scores between LPI and RPI for each class are obtained. Then, score-level fusion is performed to combine cross-matching scores and to attain the results of identification.

Consider H subjects, in which each has p LPIs and p RPIs for training [1]. X_i^k X_{ik} and Y_i^k Y_{ik} denote the ith LPI and ith RPI for kth subject, where $i = 1, \ldots p$, $k = 1$,

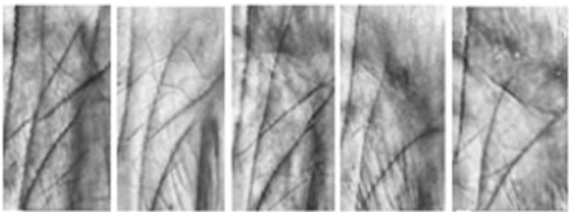

Fig. 1 Left palmprint images of five persons

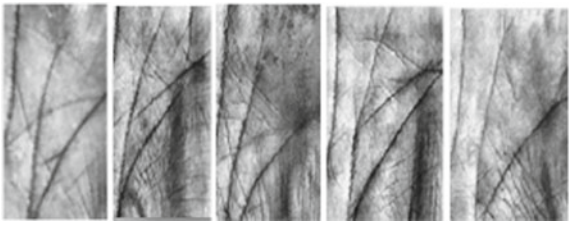

Fig. 2 Right palmprint images of five persons

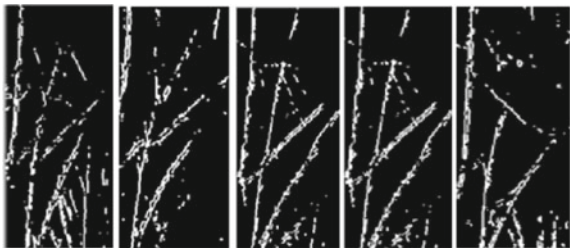

Fig. 3 Edge detection images of five persons left palmprint images

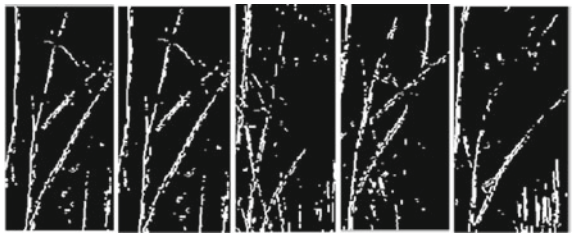

Fig. 4 Edge detection images of five persons right palmprint images

… H. Sim_score(Y, X_k) is

$$\text{Sim\_score}(Y, X^k) = \sum_{t=1}^{T} (S(\hat{Y}_t, X^k))/T \tag{1}$$

$$S(\hat{Y}_t, X^k) = \max(\text{Score}(\hat{Y}_t, \hat{X}_i^k)) \tag{2}$$

where $s_i = \{1 \ldots p\}$ and Y is LPI/RPI image. XK are LPIs/RPIs of the kth subject and X_i^k is one of the image from Xk. $\widehat{X}$ *ik* and $\widehat{Y}$ are the principal line of the LPI/RPI and t represent tth principle line. Score is assigned with zero when it is smaller than the given threshold, which is empirically assigned 0.151.

The ultimate decision depends on LPI, RPI and the correlation between the LPI and RPI. Fusion in the proposed biometric system can be evaluated using weight-sum score-level fusion that improves the performance of the discussed identification method. The weight is allotted to the obtained score, which enhances the strength of match of an individual. The procedure of combining/fusing is simple, which makes matching by score-level fusion a desirable choice.

Figure 5 shows the technique of fusion of the method presented. The resultant matching score is generated from those various matching (LPI, RPI and cross-matching) scores. Two matching scores are obtained from the LPI and RPI. The third score is evaluated from cross-matching, i.e., cross-correlation between LPI and RPI.

The proposed technique is superior to regular strategies by appropriately modifying the weight coefficients.

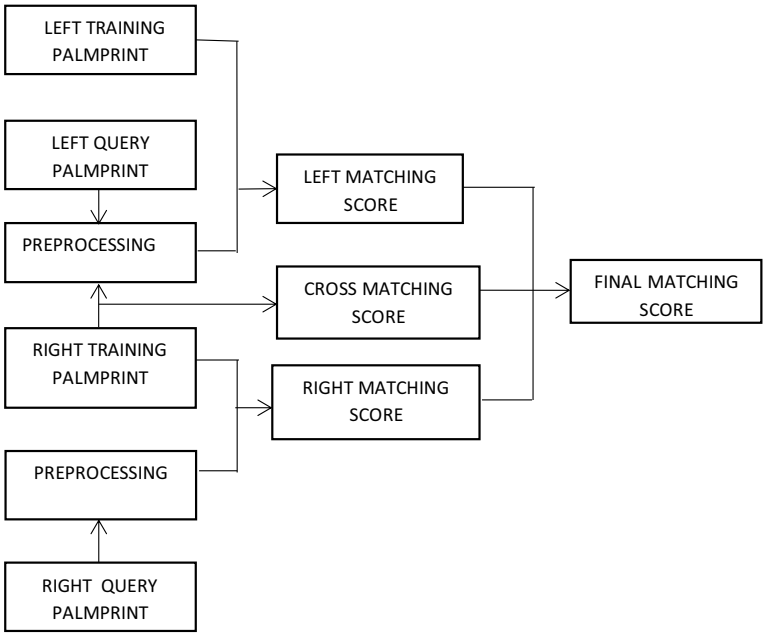

Fig. 5 Block diagram of the proposed system

3 Results and Discussion

In this work, five palmprint images of different persons are stored in the database. Score-level fusion is the fusion method used.

Figure 6 shows the similar fusion images of the corresponding images shown in Figs. 1 and 2. Figure 7 shows the cross-matching images of the corresponding images shown in Figs. 1 and 2.

Comparing to the existing method, this fusion method is performing in an efficient way which is illustrated in terms of accuracy, specificity and sensitivity and is shown in Table 1.

The existing method gives an accuracy of 50.7, sensitivity of 60.8 and specificity of 66.2. It involves the similar fusion dataset images and gives the results either

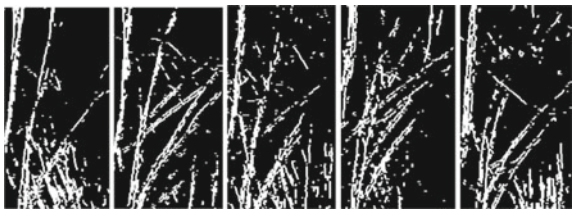

Fig. 6 Fusion images of the corresponding images shown in Figs. 1 and 2

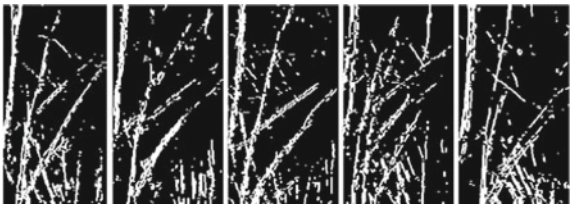

Fig. 7 Cross-matching images of the corresponding images shown in Figs. 1 and 2

Table 1 Performance measures

Parameters	Existing method	Proposed method
Accuracy	50.7	77.6
Sensitivity	60.8	86.1
Specificity	66.2	80.5

authenticate or unauthenticated. Therefore, this method gives less accuracy when compared to the proposed system (Fig. 8).

In the proposed system, score-level fusion method is used to process LPI and RPIof the subjects. The proposed technique not only involves the normal fusion technique but also cross-matching technique. The use of cross-matching technique provides improved performance than the previous methods. This system gives more accuracy of 77.6, sensitivity of 86.1 and specificity of 80.5.

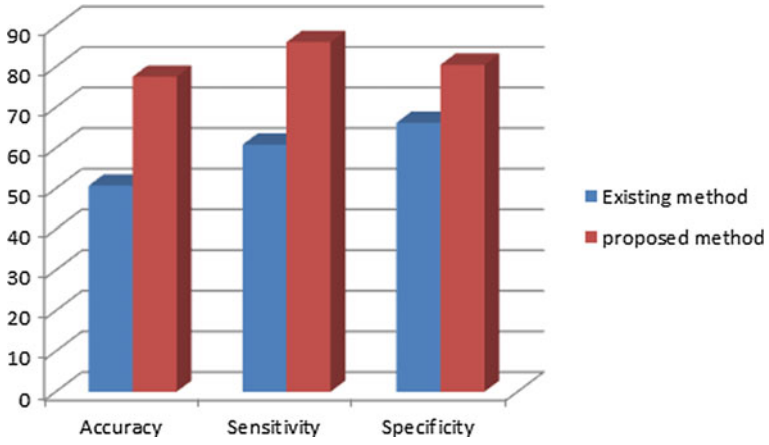

Fig. 8 Comparison of the proposed method with the existing method

4 Conclusion

The proposed system shows the similarity between LPI and RPI. The performance of this system is improved depending on the utilization of closeness between the LPI and RPI. The proposed technique combines the scores obtained from LPI and RPI. Because of the matching score, high accuracy is achieved in the proposed method. This method seems to be helpful in improving the bimodal biometric issues.

References

1. Xu Y, Fei L, Zhang D (2015) Combining left and right palmprint images for more accurate personal identification. IEEE Trans Image Process 24(2)
2. Kong AWK, Zhang D, Kamel MS (2009) A survey of palmprint recognition. Pattern Recogn 42(7):1408–1418
3. Zhang D, Zuo W, Yue F (2012) A comparative study of palmprint recognition algorithms. ACM Comput Surv 44(1):1–37
4. Chu R, Liao S, Han Y, Sun Z, Li SZ, Tan T (2007) Fusion of face and palmprint for personal identification based on ordinal features. Proc IEEE ConfComput Vis Pattern Recogn (CVPR), 1–2
5. Han D, Guo Z, Zhang D (2008) Multispectral palmprint recognition using wavelet-based image fusion. Proc IEEE 9th IntConf Signal Process, 2074–2077
6. Zhang D, Guo Z, Lu G, Zhang D, Zuo W (2010) An online system of multispectral palmprint verification. IEEE Trans Instrum Meas 59(2):480–490
7. Dai J, Zhou J (2011) Multifeature-based high-resolution palmprint recognition. IEEE Trans Pattern Anal Mach Intell 33(5):945–957
8. Thanh V, Rohit S, Raghvendra K, Hoang SL, Thai PB, Dieu TB, Ishaani P, Manash S, Tuong L (2020) Crime rate detection using social media of different crime locations and twitter part-of-speech tagger with brown clustering, pp 4287–4299
9. Nguyen PT, Ha DH, Avand M, Jaafari A, Nguyen HD, Al-Ansari N, Van Phong T, Sharma R, Kumar R, Le HV, Ho LS, Prakash I, Pham BT (2020) Soft computing ensemble models based on logistic regression for groundwater potential mapping. Appl Sci 10:2469
10. Sharma R, Kumar R, Sharma DK, Son LH, Priyadarshini I, Pham BT, Bui DT, Rai S (2019) Inferring air pollution from air quality index by different geographical areas: case study in India. Air QualAtmos Health12:1347–1357
11. Manahoran N, Srinath MV (2017) K-means clustering based marine image segmentation. Int J MC Square Sci Res 9(3):26–29
12. Rajan A, Ramesh GP Automated early detection of glaucoma in wavelet domain using optical coherence tomography images. Biomed Pharmacol J 8(2), 2105
13. Morales A, Ferrer MA, Kumar A (2011) Towards contactless palmprint authentication. IET Comput Vis 5(6):407–416
14. Satpathy RB, Ramesh GP (2020) Advance approach for effective EEG artefacts removal. In: Balas V, Kumar R, Srivastava R (eds) Recent trends and advances in artificial intelligence and internet of things. Intelligent systems reference library, vol 172. Springer, Cham
15. Wu X, Zhao Q, Bu W (2014) A SIFT-based contactless palmprint verification approach using iterative RANSAC and local palmprint descriptors. Pattern Recogn 47(10):3314–3326
16. Hemalatha RJ, Vijaybaskar V, Thamizhvani TR (2019) Automatic localization of anatomical regions in medical ultrasound images of rheumatoid arthritis using deep learning. Proc Inst Mech Eng [H] 233(6):657–667

PHY Layer Design for MIH in GNU Radio

Akshada Bhosale, Ganesh Rahate, and Nilkanth Chopade

Abstract Handover is an essential process in wireless networks where mobile node changes its access points during the call. Due to heterogeneity in the networks and coexistence of various wireless technologies like wireless fidelity (WiFi), long-term evolution (LTE), wireless interoperability for microwave access (WiMAX), etc., the vertical handover is essential for mobile unit. Vertical handover (VHO) happens to be amongst heterogeneous technologies. Media-independent handover (MIH) is an IEEE 802.21 framework that defines the horizontal and vertical handover process amongst IEEE and non-IEEE standards. MIH suggests an intermediate layer in the technology stack just above physical and media access control (PHY-MAC) layer and greatly relies on PHY-MAC for events and triggers for handover. The handover delays and subsequent packet loss decide quality of service in heterogeneous networks. The various triggers received from PHY-MAC layer rely on hardware/software design of underlying technology. The PHY layer of technologies like WiFi, WiMAX, and LTE relies on orthogonal frequency division multiplexing (OFDM). OFDM is an advanced version of multicarrier modulation system with high spectral efficiency, resistant to inter-symbol interference, high data rate, and less complex in design. In this paper, we propose design of OFDM transreceiver in GNU radio from our future perspective of MIH implementation in software defined radio (SDR) platform like Universal Software Radio Peripheral (USRP).Our design is based on various signal processing blocks and can successfully transfer the text in GNU radio platform.

Keywords MIH · OFDM · Vertical handoverhandover · SDR

A. Bhosale (✉) · G. Rahate · N. Chopade
Department of Electronics and Telecommunication, Pimpri Chinchwad College of Engineering, SPPU, Pune, India
e-mail: akshadabhosale122@gmail.com

G. Rahate
e-mail: ganesh.rahate@pccoepune.org

N. Chopade
e-mail: nbchopade@gmail.com

D. K. Sharma et al. (eds.), *Micro-Electronics and Telecommunication Engineering*,
Lecture Notes in Networks and Systems 179,
https://doi.org/10.1007/978-981-33-4687-1_15

1 Introduction

In recent times, wireless networks have undergone enormous technological changes, and they are reflected in exponential growth in subscriber base. At the same time, multiple wireless technologies like WiFi, WiMAX, and LTE are also evolved and widely accepted too due to their improved features. Manufacturers are also providing the multi-interfaced gadgets so that one can get access of desired technology as per the need, viz. data rate, cost, bandwidth, user preference, etc. For outdoor coverage, devices can have access of wide area networks like LTE and WiMAX, while for indoor usage they can rely on local area networks like WiFi. This leads to coexisting scenario for heterogeneous networks. Due to heterogeneity amongst the networks, the handover between them is a crucial issue. This handover is termed as vertical or heterogeneous or intersystem handover. There are various methods proposed in literature, and their comparison shows that MIH is a choice for implementation on the reconfigurable platform like SDR [1].

MIH (IEEE 802.21) is a scalable framework designed to support seamless mobility amongst networks. MIH has defined the common set of MIH services that can be offered to higher layers protocols like mobile IP and SIP for handovers. Figure 1 shows the MIH function introduced between PHY-MAC and higher layers of protocol stack. The information collection from the client/server is the key of MIH handover.

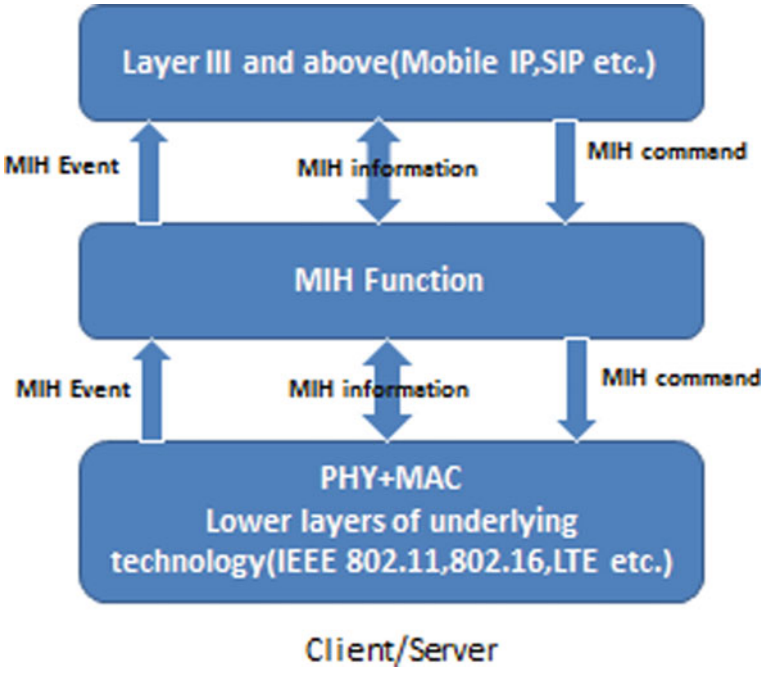

Fig. 1 MIH services

It defines three basic services, viz. MIH event service, MIH command service, and MIH information service. The link type, link quality, and link ID are the information received by MIH function from PHY/MAC layer and update the layer III for further action [1]. The PHY layer of most of the said technologies (WiFi, WiMAX, LTE) is based on OFDM.

High data rates, typically varying between 100 Mbps and 1 Gbps, are the key feature of existing heterogeneous networks. As data rate increases, symbol duration decreases. Channel dispersiveness causes the inter-symbol interference (ISI). If symbol duration is less than delay spread across the channel, then inter-symbol interference occurs. This degrades the performance of communication system. In OFDM, symbol duration is increased by dividing larger bandwidth into small sub-bands and reduces ISI. OFDM allows adaptive modulation and coding of carrier and due to its various advantages is used in Digital Video Broadcasting (DVB), WiFi, and LTE, etc.

OFDM and its implementation are explored in different research papers. Rihani et al. [2] have proposed an implementation of an adaptive OFDM transmitter performing VHO. Authors implemented the unified PHY layer for WiFi and WiMAX and tested it on Zed board. Hwang [3] has elaborated OFDM basics, mathematical equations ,and OFDM system design rules. Arun Kumar [4] has used the partially reconfigurable approach for the implementation of OFDM transmitter using MATLAB Simulink and FPGA and reconfigured BPSK and QPSK modulation technique. Mecwan and Shah [5] have proposed the implementation of OFDM transreceiver on FPGA vertex using MATLAB Simulink. This implementation did not consider channel between transmitter and receiver. In the paper, Muslimin et al. [6] have proposed the validation of robustness of OFDM by considering random data transfer using OFDM through various channels like Rayleigh, Rician, and white Gaussian noise channel in GNU radio. Authors Simanthi and Rahate [7] designed binary phase shift keying (BPSK) and quadrature phase shift keying (QPSK) modulator in MATLAB Simulink and proposed further FPGA implementations. Sung and Hsu [8] proposed the OFDM baseband processor using FPGA and designing of processor is Verilog based.

This paper proposes the MIH-PHY design for WiFi in GNU radio to be further extended on SDR platform like universal software radio peripherals (USRP). GNU radio is an open-source framework to design user-defined communication system. GNU radio supports various hardware platforms. It has larger inbuilt libraries. This tool allows researcher to write own signal processing block using Python. Software defined radio overcomes the challenges with traditional research approach using fixed radio hardware. It had opened opportunities for researcher to study and experiment communication protocols. Rapid prototyping and testing of various communication protocols with low cost and time are possible due to software defined radio. Initially, we are focusing on low data rate traffic, i.e. text. We are using different signal processing blocks to implement the design in GNU radio with suitable channel conditions. In this paper, Sect. 2 OFDM is discussed in brief. Section 3 describes the modular design of OFDM system, design parameters, transmitter, and channel

model and receiver flowgraph module in GNU radio. Section 4 contains the results and analysis of design.

2 Orthogonal Frequency Division Multiplexing

In orthogonal frequency division multiplexing, data is transmitted by using narrow and orthogonal subcarriers. Due to overlapping of subcarriers, OFDM has high spectral efficiency. Fast Fourier transform and cyclic prefix are core blocks of OFDM.

Mathematical expression of OFDM modulation can be given as follows:

$$s_n(t) = \sum_{k=0}^{N-1} s_{n,k} * e^{j2\pi k \Delta f t} \tag{1}$$

where $s_{n,k}$, Ts, Δf, and N are the complex symbols, symbol duration, the subchannel spacing, and N be the number of subchannels. IFFT and cyclic prefix are core block of OFDM transmitter. Cyclic prefix adds guard interval. Due to cyclic prefix, transmitted symbols get circularly convolved with channel. Receiver is designed by arranging opposite blocks as that of transmitter. In first step, cyclic prefix is removed after that fast Fourier transform is applied so to get complex symbols transmitted by transmitter. At receiver, autocorrelation and cross-correlation are used to get the symbol transmitted. Channel estimation is knowing about channel properties such as dispersive fading and delay. Pilot-aided channel estimation, blind channel estimation, and decision directed channel estimation are three methods used for channel estimation.

3 Flowgraph Modules

Complete OFDM system is designed in one flowgraph using three modules. These modules are three sections of communication system. The diagrammatic representation of flowgraph is shown in Fig. 2. Flowgraph in this paper is designed by using GNU radio maint 3.7.

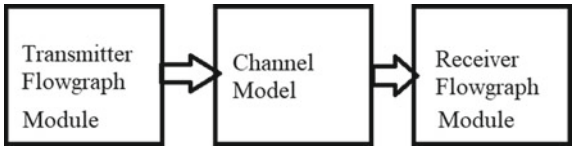

Fig. 2 Flowgraph module

Table 1 Parameters of design

Parameters	Values
Number of FFT points	64
Number of subcarriers	52
Number of data carriers	48
Number of pilot symbols	4
Bandwidth	20 MHz
Header modulation	BPSK
Payload modulation	QPSK
Packet length	96

3.1 Design Parameters

The IEEE 802.11 [9] standard is referred to decide the parameters of design. In Table 1, various parameters of design are shown.

3.2 OFDM Transmitter

In packet data transmission, packets carry header and payload information. Header contains the metadata while payload carries the actual data. Figure 3a shows the header and payload creation. The header and payload are BPSK and QPSK modulated, respectively. File source block reads text data from file (filename.txt). The output of file source is taken in bytes format and given to tagged stream block. By using tagged stream tag is added after every 96 bits. Tagged stream output is given to cyclic redundancy check (CRC) block. Protocol formatter is used to generate header. Protocol formatter requires formatter object. Formatter objects call the C++ constructor of digital header of OFDM. In formatter object, constructor calls various arguments such as occupied carriers, header modulation per bits, payload modulation per bits, length tag and scramble. Repack bit is used to repack the data bytes. There is no data loss at repack bits. Virtual sink and source are used to divide design into sub-modules. Header and payload are applied to respective chunk to symbol block. Chunk to symbol blocks are acts like modulators. Header and payload are mapped with respect to constellation points of binary phase shift keying and quadrature phase shift keying, respectively.

After the modulation of header and payload, these symbols are multiplexed by using tagged stream multiplexer. Figure 3b shows the multiplexing process. Output of tagged stream block is given to virtual sink name as pre-OFDM. Virtual source which contains complex symbols feeds to OFDM carrier allocator block. This block contains various parameters such as occupied carriers, pilot carriers, pilot symbols, and sync words. Pilot symbols are training symbols which are used for channel state estimation. Pilot carriers are used to carry pilot symbols. Sync word1 and

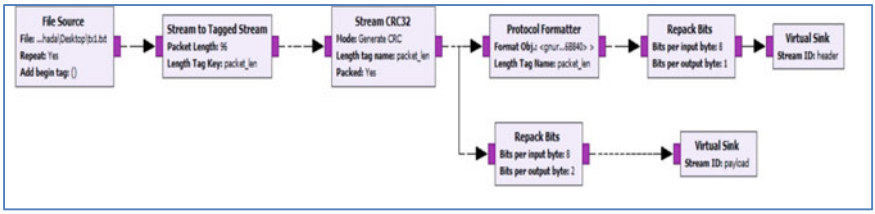

(a) Header and payload creation

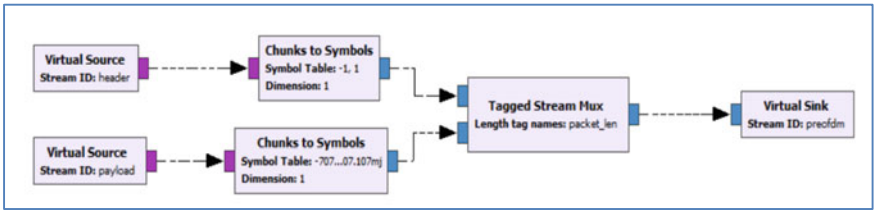

(b) Pre OFDM (Multiplexing)

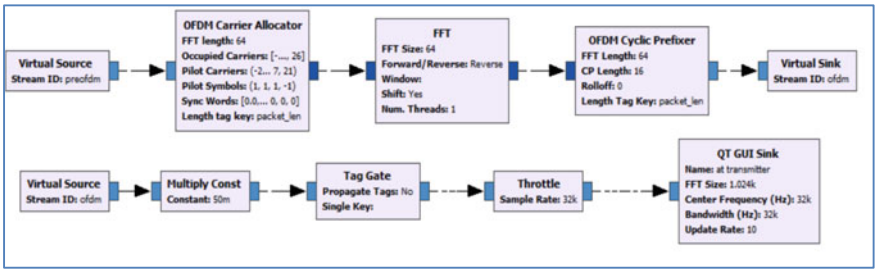

(c) OFDM transmission

Fig. 3 **a** Header and payload creation. **b** Pre-OFDM (multiplexing). **c** OFDM transmission

sync word2 are short and long preamble sequence. These sequences are used to have synchronization between transmitter and receiver. Output of OFDM carrier allocator block is given to fast Fourier transform block which apply inverse fast Fourier transform. Cyclic prefixer block is used to add cyclic prefix. Due to cyclic prefix, transmitted signal gets circularly convolved with channel. After adding cyclic prefix, the OFDM modulated signal is transmitted into channel by using QT GUI sink. QT GUI sink is used to observe the waveform. Along with QT GUI sink, it can be also given to UHD sink if USRP is used for hardware design. UHD is application package interface available for USRPB210. The flowgraph of packet data transmitter using OFDM is shown below in Fig. 3c.

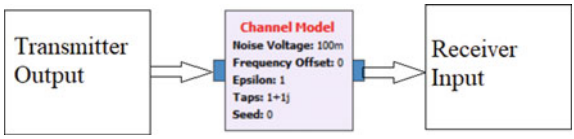

Fig. 4 Channel model

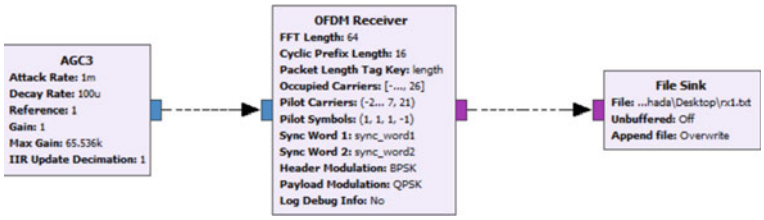

Fig. 5 Text file OFDM receiver flowgraph

3.3 Channel Model

Channel model allows user to set noise voltage, timing offset, frequency offset, randomization of noise, etc. Here in this OFDM system noise voltage is set to 100 mV. Channel will add AWGN noise to OFDM modulated signal of transmitter and pass on to OFDM receiver module. Block of channel Model is given below in Fig. 4.

3.4 OFDM Receiver

The channel output is noise contained and is an input to receive block set. At receiver, for gain controlling automatic gain control (AGC) block is used with attack rate of 1 m, decay rate of 100 μ, and min–max gain of 1–65 k. Output of AGC is given to OFDM receiver block. OFDM receiver block requires various arguments such as occupied carriers, header modulation method, payload modulation method, pilot carriers, and information about pilot symbols. At receiver, maximum likelihood and autocorrelation are used to retrieve the data. In OFDM receivers, first channel state is estimated by using pilots. After this, data is retrieved from data carrier. File sink is used to write text data into text file. The flowgraph of packet data receiver using OFDM is shown in Fig. 5.

4 Results

In packet data transmission, BPSK and QPSK are the preferred modulation in the design for header and payload, respectively. Time domain waveform of payload and

header is given in Fig. 6. The top waveform is the time domain complex payload while the bottom wave is header. Payload contains actual data. Payload waveform is denser than header waveform.

Digital modulation is represented in terms of constellation points. Chunk to symbol mapped header and payload with respect to constellation points of QPSK and BPSK. QPSK and BPSK modulations have four and two constellation points. Figure 7 sets forth constellation plot of payload and header. First plots show payload constellation points, while second plot shows header constellation points.

Transmitted complex symbols are mapped to one constellation point. For 64 complex symbols, 64 constellations points are observed at transmitter. Constellation plot of OFDM transmitter is given in Fig. 8.

Channel adds noise to the signal transmitted. Due to noise constellation, points get spread and also the amplitude value increases. The increase in amplitude value at receiver is observed in time domain plot. As channel noise voltage increases, amplitude at receiver increases. It is also observed in constellation plot at input of OFDM receiver in Fig. 9.

As text file is transmitted repeatedly at transmitter, so at receiver multiple copies of text file is received as shown in Fig. 10. Text file is successfully transmitted and received by using the OFDM transmitter and receiver using channel model in GNU radio software.

Complexity of any GNU radio flowgraph is measured in Balint unit. As design complexity increases, this value is also increased. Different combination of BPSK and QPSK as modulation for header and payload is considered in the design. The bit error rate (BER) and complexity of flow graph with varying payload modulation

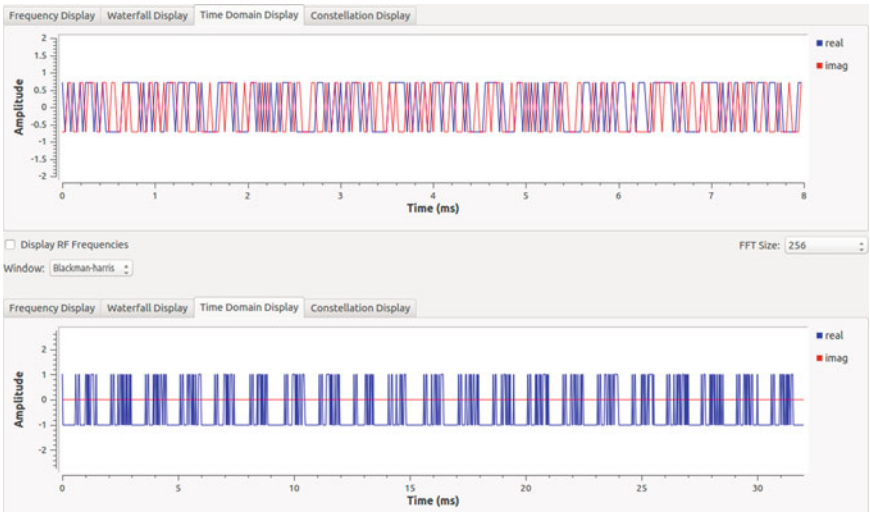

Fig. 6 Time domain plot of payload and header

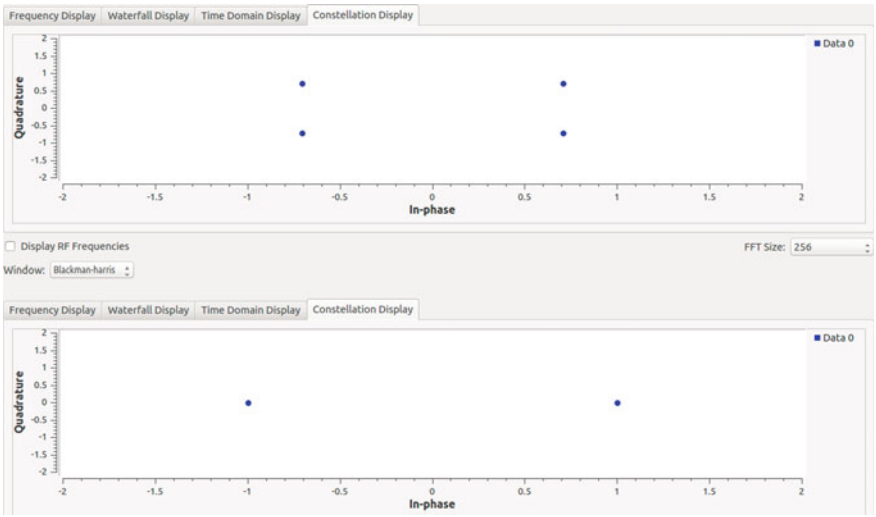

Fig. 7 Constellation plot of payload and header

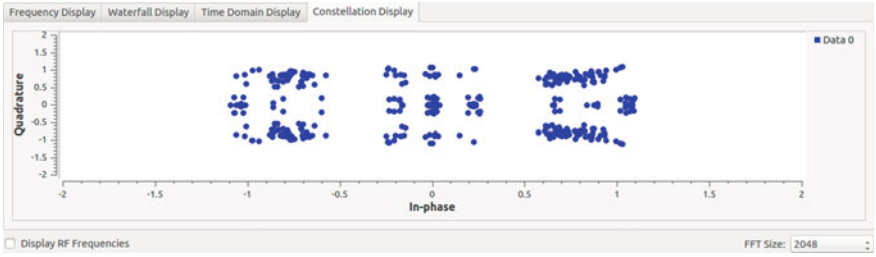

Fig. 8 Constellation plot of OFDM transmitter

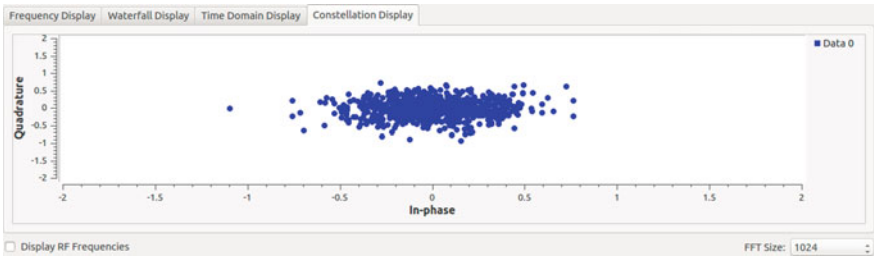

Fig. 9 Constellation plot at input of OFDM receiver

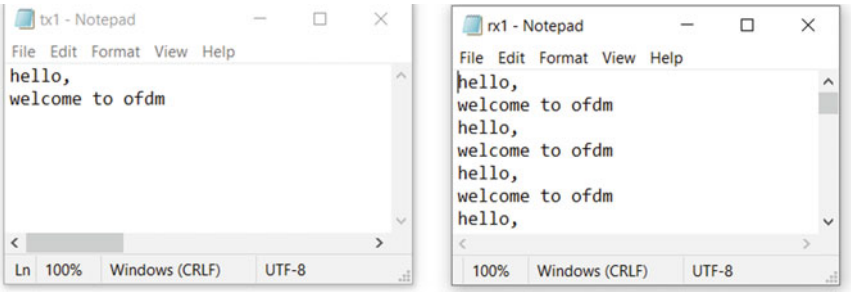

Fig. 10 Text file at transmitter and receiver

Table 2 Analysis of design

Modulation method for header–payload	Bit error rate	Complexity of flowgraph (Balint) (m)
BPSK-BPSK	0.283	2.275
BPSK-QPSK	0.369	2.349

technique are given in Table 2. It is obvious that BPSK-BPSK combination results in lower BER and complexity.

5 Conclusion

MIH-PHY layer is important from various triggers point of view in VHO process. The next generation networks have PHY layer based on OFDM due to its high spectral efficiency, more resistant to ISI and simplicity in design. In the process of MIH implementation on SDRs, we have implemented PHY layer using OFDM for 802.11 and successfully transmitted and received the text data in GNU radio. Due to vast scope in the MIH-based VHO implementation, in near future immediate phase will be the transfer of design on USRP B210 and testing for text. There will be two USRP modules: one will act as transmitter while the second as receiver. We will test the system for high bit rate traffic like audio and video. Due to similarity between WiFi and WiMAX, design of unified PHY can be proposed. Further by using reconfiguration algorithm, design optimization can be achieved to improve upon the VHO QoS parameters like latency and packet loss.

Reference

1. Chaudhari S, Rahate GR (2015) Survey paper on partially reconfigurable PSK modulators on FPGA. Int J Eng Educ Technol

2. Rihani M-A-F, Mroue M, Prévotet J-C, Nouvel F, Mohanna Y (2017) ARM-FPGA-based platform for reconfigurable wireless communication systems using partial reconfiguration. EURASIP J Embed Syst 2017(1):35
3. Hwnag T, Yang C, Wu G, Li S (2009) OFDM and its wireless application: a survey. IEEE Trans Veh Technol
4. Mecwan A, Shah D (2013) Implementation of OFDM transceiver on FPGA. In: Nirma University international conference on engineering
5. Jusnaini Muslimin AL, Asnawi AF, Ismail, Mohd Ramli HA, Jusoh AZ, Noorjannah S, Azmin NFM (2015) Basic study of OFDM with multipath propagation model in GNU platform. In: EEE conference on wireless sensors
6. Rahate GR, Chopade NB (2019) Vertical handoff solution on software defined radio for next generation wireless networks. In: 2019 international conference on innovative trends and advances in engineering and technology (ICTAET). Shegoan, India. https://doi.org/10.1109/ICITATE47105.2019.917045
7. Sung K, Hsu T-Y (2017) FPGA implementation of OFDM baseband processor. In: IEEE conference on dependable and secure computing
8. GNU Radio Companion Tutorials, https://wiki.gnuradio.org/index.php/Tutorials
9. IEEE 802.11 Standard Website, https://standards.ieee.org/standard/802_11-2016.html

Machine Learning Technique for Target-Based Sentiment Analysis

Jyoti Srivastava and Neha Katiyar

Abstract The study covered with machine learning strategies utilized in the analysis of sentiments at both the sentence and viewpoint levels. It likewise tended to the advantages and inconveniences of the different condition of-the-craftsmanship procedures. This paper perceived that the arrangements viability contrasted by the technique. As far as estimation system, there is an absence of institutionalization. Accordingly, it is beyond the realm of imagination to expect to reach determinations from the present condition of-the-workmanship approaches where strategy gives the best result to every area. In any case, a move from the customary word-based way to deal with semantic-based idea driven methodology is obviously apparent in the measurement level sentiment analysis. Machine learning approaches alongside semantic idea driven methodology can create another age of calculations that can react to language and significant level settings. This gap will likewise leave an enormous region for the scientists to find out experimental and emotional views of a human

Keywords Machine learning · Semantic orientation · Deep learning · Sentiment analysis · Twitter · Literature review

1 Introduction

In the era of yottabyte, social networking development has expanded the degree to which thought or belief is shared on a public platform. At the same time, people's growing interest in obtaining more and more knowledge about various perspectives and details about any subject available online is boosting the need to develop effective techniques for evaluating sentiments. The literature offers some significant form of machine learning for sentiment analysis, in addition to information about the sites visited by users in day to day life, etc. They are understanding their thoughts as conveyed through posts on different areas in predicting people's opinions on a

J. Srivastava (✉) · N. Katiyar
Madan Mohan Malviya University of Technology, Gorakhpur, India
e-mail: sriv.jyoti1996@gmail.com

D. K. Sharma et al. (eds.), *Micro-Electronics and Telecommunication Engineering*,
Lecture Notes in Networks and Systems 179,
https://doi.org/10.1007/978-981-33-4687-1_16

particular topic—a ubiquitous way of classifying a text's polarity for user happiness, frustration, or neutrality. The polarity may range from positive to negative in terms of marking or amount of rates, but it usually signifies the emotions of a book that contrast from glad to troubled mode. The methodologies used to dissect sentiments are various and depend on different common language handling strategies and machine learning systems to extricate sufficient highlights and group content into proper extremity marks. With the attention achieved by deep learning techniques, numerous deep neural networks have been widely used on the market for some years. In particular, the convolutionary neural networks (CNN) and long short-term memory (LSTM) networks have proven to be efficient for tasks related to sentiment analysis. Different studies have demonstrated their efficacy either alone or in combination. Among the most popular methods in the field of natural language processing are Word2Vec and the global vectors for word representation (GloVe), which are used to remove features from terms. The precision obtained with the above approaches is good but still unsatisfactory, rendering sentiment analysis a topic of continuing, open study. That is why we are attempting to construct new methods or to improve existing ones. Since the existing methods have a wide variety in terms of network setup, tuning, etc. (Fig. 1).

This paper provides synthesis literature of deep learning methods to evaluate opinion at both the sentence and context stages. Remaining construction of this paper as follow: Sect. 2 examines the critical related work and discusses the basic concepts of deep learning and its interaction with machine learning and artificial intelligence and the types of research, and Sect. 3 demonstrates a sample of the machine learning approaches used in the study of sentence-level opinion. Section 4

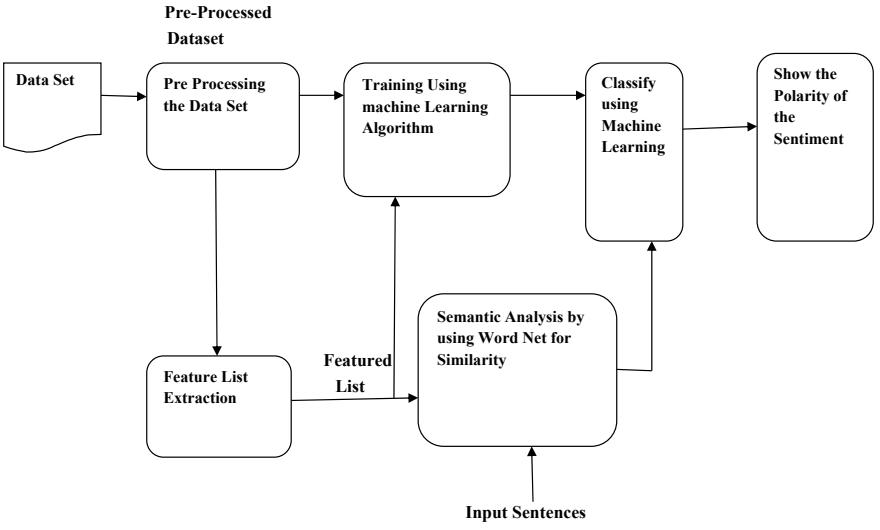

Fig. 1 Sentimental classification process [5]

provides an overview of dimension type feeling, and the article is summarized in Sect. 5.

2 Related Work

The vast number of social platforms allows people to tell about their thoughts, beliefs, and viewpoints have encouraged researchers to research with models of sentiment analysis to extract emotions across these tools. Scientists, though, come up with issue of constantly evolving the vocabulary used digitally in user-generated material; the terms that affect us each day impact the words that we use. Because dialects are generally spoken and not published, only a limited amount of work was done to identify the dialects.

Moon and Assessment et al. [1] of smaller scale blog supposition examples will uncover changes in individuals' emotions that have become a typical point interesting issue of content analysis. There is a critical absence of research on Tibetan. Right now, test the exactness of different calculations on Tibetan small scale blog sentiment discovery, a deep learning calculation is actualized into the Tibetan sentiment analysis. Next, by utilizing the word vector technique, the Tibetan word smaller scale blog is prepared as a word vector; at that point, the scholarly word vectors and the comparing meaning orientation names are explicitly embedded into the different deep learning models to recognize Tibetan miniaturized scale Web journals.

Al-Jawad et al. [2] with the appearance of Web 2.0, there is a tremendous measure of composed substance on the Internet, from news stories and verifiable reports, with a huge increment with the ascent of Web-based life, for example, Facebook. Over the Web and different social channels, more individuals start to communicate their emotions and conclusions. This prompted an expansion in the measure of client produced sentences that contain data with respect to feelings. All things considered, new strategies are tried to acquire different viewpoints into how individuals feel and react to various conditions. This paper differentiates the proficiency of various machine learning and deep learning procedures.

Handkerchief et al. [3] and different thoughts and remarks have constantly formed human instinct. Individuals are constantly quick to know the assessments of others for their advantage, yet every site incorporates an exceptionally enormous measure of survey message, the normal human client would think that its hard to find explicit pages. Extracting and abstracting input with the goal that the correct choice can not be made in less time is the reason programmed sentiment analysis frameworks are required. Heterogeneous innovations, for example, machine learning ward and lexicon-based highlights and directed learning calculations, for example, Naive Bayes (NB) and linear support vector machine (LSVM) utilized in the recommended strategy.

Umarani Srikanth et al. [4] this article gives a point by point audit of the techniques utilized in sentiment analysis for deep learning. Sentiment analysis is one of the fields of regular language preparing which is generally examined. Regular language

preparing has a wide scope of uses, for example, voice acknowledgment, machine interpretation, item assessment, angle situated item analysis, feeling analysis, and archive recognition, for example, email arrangement and spam sifting. The traditional strategies utilized for an understanding of feelings are portrayal centered around dictionaries. Besides, with the advancements of computerized reasoning, the machine learning models kept on assuming a significant job in applications for sentiment analysis.

Kaushal et al. [5] Evaluation of feelings is a developing region with numerous applications. In view of the consequence of the sentiment analysis, not exclusively are buyer needs met, yet additionally providers, merchants and so forth get a comprehension of the client's or client's response, accordingly guaranteeing they will make the vital changes. We have considered all PC and deep learning systems.

Khine et al. [6] Sentiment analysis is a common field for NLP research that seeks people's opinions on a given product, services, movie reviews, etc. It was used extensively in advisory systems, market research, and social media predictions. Sentiment analyzes are a concern in the field of science. It needs many NLP tasks such as text normalization, POS labeling, text chunking, lemming, detection of subjectivity, sarcasm detection, look-ups, and detection of polarity. Among them, the key role in sentimental research is aspect mining. If we do not know, the accuracy of the classification will decrease.

Indhra om Prabha et al. [7] The analysis of sentiments can be based on the granularity of the textual aim, such as document, phrase or aspect, being analyzed. The analysis of document sentiment gives the polarity of feeling over a large part of text such as a paragraph or the entire document. The emotion polarity of each sentence is determined by the sentence level. The measurement of sentiment levels in the aspects decides the polarities of the different aspects addressed. The various characteristics of the product or the context are characteristics or goals.

Seo et al. [8] The purpose of a classification of feelings is to assess the positive or negative meaning of a particular text. Sentiment classification is widely used in many business fields by understanding the views of customers about these products in order to improve products or services. In various challenging fields, deep learning results state-of-the-art. With the success of profound learning, many studies have proposed model classification models for deep learning and achieved improved achievements compared to conventional models for machine learning.

Wadawadagi et al. [9] The current decade has witnessed the remarkable developments in artificial intelligences and has changed the entire artificial intelligence field by the explosion of deep learning. Finally, in today's world of computing, deep learning techniques have become essential components of any model. Nevertheless, profound techniques of learning promise high degree of authorization for text and feeling classification tasks with general rule extraction.

Yadavet al. [10] Social media is a powerful medium for people's communication and offers an overwhelming amount of unstructured knowledge in the form of views and opinions about every subject and post. Business entities need to analyze and research these emotions to examine data and to obtain market insights. In the past, different machine learning and natural language approaches have therefore been

used to analyze these sentiments. Even so, in recent times, high performance in deep learning methods has become extremely popular.

3 Sentiment Analysis Method

The convolutionary neural system essentially takes care of the issue of spatial arrangement, while the repetitive neural system basically takes care of the issue of time arrangement. In Tibetan smaller scale blog conclusion, displaying a multi-arrange model was created and explored for the Tibetan framework. The engineering is involved three convolutionary neural systems and two LSTM layers. The explanation the CNN-LSTM model performs well is on the grounds that the deep learning model can get the content's deeper semantine structure information. The convolutionary neural system is situated toward worldwide estimation. The RNN centers around reestablishing any neighboring subtleties. LSTM systems are increasingly successful in putting away deep-content literary information than customary RNNs. The CNN-LSTM model can ensure each microblog's worldwide measurements, yet can likewise gather more inside and out semanthetic subtleties, change distinctive model parameters, make the calculation locate the best state, and make feeling arrangement progressively exact. In the zone of normal language handling, word vectors have brought trust in deep learning. It will anyway be exceptionally languid to utilize SGD to prepare expansive neural systems. This post was utilizing Adam and getting great outcomes. There are still issues to over-fit. Utilizing the three-layer CNN in the convolutionary layer to realize the Tibetan small scale blog term vectors' spatial area relationship, utilizing the 128-dimensional execution of the CNN's third layer as information, and afterward getting to the LSTM layer utilize 128-hub LSTM layers for every space layer. The presentation of the last cell of the subsequent layer is appended to a completely associated layer to know the worldly relations between powerful edges, disposing of information is utilized between the LSTM layer and the completely associated layer, and the last Tanh highlight figures the microblog emotional arrangement labels.

4 Classification Algorithms

Assessment of the conclusion incorporates grouping content remarks into classifications dependent on extremity of sentiment. Extremity suggests the state of hearing two distinct thoughts in the assessment record. The extremity could be either positive or negative. Here, the characterization of report level analysis of sentiment utilized in the proposed strategy and executed heterogeneous highlights to regulated machine learning calculations, for example, Naive Bayes (NB) and linear support vector machine (LSVM) to learn and dole out content criticism into a positive and negative

gathering. Here, a directed learning calculation was picked for this strategy, since we can without much of a stretch get enough informational index to prepare.

5 Sentiment Analysis Procedure

a. Information Collection
   The job of information assortment is the primary period of the sentiment analysis process. Information might be gathered from any of the Web journals or from the different considerations and remarks informational collections accessible on the Web.
b. Preprocessing
   This is the cleanup phase of the outcomes. Words and images are precluded which are not required. This is done to additionally rearrange the handling. This move incorporates evacuating hyperlinks, rehashed expressions, emojis and unique characters. There is additionally lemmatization and stemming. A diminished assortment of highlights is at last taken out and given to the classifier.
c. Grouping
   A classifier is the most basic segment of a framework for sentiment analysis. Order is led into negative, idealistic or impartial sorts. 33% of the database is typically utilized as the preparation set to make the classifier. The classifier's precision depends to an enormous degree on the course set. Machine learning classifiers, for example, SVM, Bayes classifier, greatest entropy classifier and so forth can be utilized for order. By the by, for the classifiers of machine learning, include extraction is directed before the classifier is prepared and approved where Deep Neural Networks can likewise be utilized to order the information. Characterization should likewise be possible by essentially utilizing a deep learning calculation. There are various sorts of deep systems which can be utilized with regards to neural systems, for example, convolutionary neural system (CNN), probabilistic neural system (PNN), intermittent neural system, and so on.

6 Machine Learning Approach for Sentimental Data Classification

Machine learning is utilized to show a machine the capacity to learn without being designed straightforwardly. This requires factual and prescient analysis to empower the machine to recognize various examples and to utilize this data to get mystery bits of knowledge into the information gave. The two calculations for machine learning are classified into supervised machine learning and unsupervised machine learning. Managed machine learning calculations are those used to test forecasts. Such calculations conjecture the impact or ward variable from a given arrangement of indicators or free factors, which is accomplished by watching the present pattern and finding

Table 1 Comparative analysis different machine learning model [8]

Sample target-based sentiment analysis	Model	Accuracy (%)
Dataset 1	SVM	88.90
Dataset 2	Naive bayes	90.66
Dataset 3	Naive bayes (NB) and linear support vector machine (LSVM)	95.77

how to apply it on another model. Then again, unaided machine learning calculations are utilized for the most part for gathering diverse interesting information types and are applied in various fields where information arrangement is fundamental. Arrangement assumes a significant job in the field of sentiment analysis. A pregrouped database object, called a preparation assortment, is utilized to prepare and create a classifier in the arrangement phase of sentiment analysis utilizing a machine learning procedure. The classifier rather denotes the beforehand unlabeled information after the pattern has been distinguished. However, the precision of any classifier additionally relies vigorously upon the information used to prepare it. So, we see that supervised machine learning strategies are the most proper for an understanding of feelings. Coming up next are the key classifiers for sentiment analysis utilized in machine learning.

Results Analysis

We performed the experiment using Python and selected the target-based sentiment analysis. Data accuracy for classification models is one of the most widely applied indicators. It is the sum of the accurate forecasts divided by the total number of forecasts. For an imbalanced dataset, we can get a high degree of precision that is mostly class-oriented. In an extreme case, each test case could be added to the large class by the classified to obtain a consistency equivalent to that of the most frequent marks in the test set. Precision can therefore be a deceptive measure of performance. The controlled precision is a better measure of generalizability. Where l is the class count, the average accuracy obtained on each class can be calculated (Table 1).

$$\frac{\sum_i^l (\mathrm{TP}_i + \mathrm{TN}_i)(\mathrm{TP}_i + \mathrm{FP}_i + \mathrm{TP}_i + \mathrm{FN}_i)}{l}$$

7 Conclusion

We show that utilizing emojis as boisterous identifiers to prepare information is an effective method to perform remote directed learning. Utilizing this methodology, machine learning calculations (Naive Bayes, most extreme entropy characterization) can accomplish high exactness while ordering sentiment. This paper introduces

a three-classifier machine learning sentiment analysis model and contrasts the efficiency of the three classificators. The model is split into four stages: data collection, preprocessing, abstraction, and classification of the vector properties. The efficiency of the all classifier is however important, and therefore, it can be inferred that the machine learning method has great potential for classification of emotions. Hence, discovering this experiment would make a meaningful contribution to knowing the experience of different products by individuals. For all three methods, a greater sample is believed to perform better in emotion classifications. The research can be improved by deleting Internet slang and adding certain classifiers for machine learning.

References

1. Sun B, Tian F, Liang L (2018) Tibetan micro-blog sentiment analysis based on mixed deep learning. In: 2018 international conference on audio, language and image processing (ICALIP). https://doi.org/10.1109/icalip.2018.8455328
2. Abd El-Jawad MH, Hodhod R, Omar YMK (2018) Sentiment analysis of social media networks using machine learning. In: 2018 14th international computer engineering conference (ICENCO). https://doi.org/10.1109/icenco.2018.8636124
3. Bandana R (2018) Sentiment analysis of movie reviews using heterogeneous features. In: 2018 2nd international conference on electronics, materials engineering & nano-technology (IEMENTech). https://doi.org/10.1109/iementech.2018.8465346
4. Prabha MI, Umarani Srikanth G (2019) Survey of sentiment analysis using deep learning techniques. In: 2019 1st international conference on innovations in information and communication technology (ICIICT). https://doi.org/10.1109/iciict1.2019.8741438
5. Jain K, Kaushal S (2018) A comparative study of machine learning and deep learning techniques for sentiment analysis. In: 2018 7th international conference on reliability, infocom technologies and optimization (trends and future directions) (ICRITO). https://doi.org/10.1109/icrito.2018.8748793
6. Goularas D, Kamis S (2019) Evaluation of deep learning techniques in sentiment analysis from twitter data. In: 2019 international conference on deep learning and machine learning in emerging applications (Deep-ML). https://doi.org/10.1109/deep-ml.2019.00011
7. Govindarajan M (2013) Sentiment analysis of movie reviews using hybrid method of Naive bayes and genetic algorithm. Int J Adv Comput Res (ISSN (print): 2249-7277 ISSN (online): 2277-7970) 3(4, 13)
8. Biswas SK, Bordoloi M, Heinsnam RS, Purkayastha B (2016) A neuro-fuzzy rule-based classifier using important features and top linguistic features. Int J Intel Inf Technol 12(3) IGI Global
9. Che W, Zhao Y, Guo H, Su Z, Liu T (2015) Sentence compression for aspect-based sentiment analysis. IEEE/ACM Trans Audio Speech Lang Process IEEE 23(12)
10. Korenek P, Imko M (2014) Sentiment analysis on microblog utilizing appraisal theory. In: World Wide Web, Springer, vol 17, pp 847–867
11. Vinodhini G, Chandrasekaran RM (2016) A comparative performance evaluation of neural network based approach for sentiment classification of online reviews. J King Saud Univ Comput Inf Sci Elsevier 28:212
12. Singh Y, Bhatia PK, Sangwan OP (2007) A review of studies onmachine learning techniques. Int J Comput Sci Sec 1(1):70–84
13. Liu CL, Hsaio WH, Lee CH, Lu GC, Jou E (2012) Movie rating and review summarization in mobile environment. IEEE Trans Syst Man Cybern Part C 42(3):397–407

14. Poriaa S (2017) Ensemble application of convolutional neural networks and multiple kernel learning for multimodal sentimentanalysis. Elsevier, pp 217–230
15. Seo S, Kim C (2019) Comparative study of deep learning-based sentiment classification, Received December 13, 2019, accepted December 21, 2019, date of publication January 1, 2020, date of current version January 14, 2020. https://doi.org/10.1109/ACCESS.2019.2963426
16. Singh Rajawat A, Jain S (2020) Fusion deep learning based on back propagation neural network for personalization. In: 2nd international conference on data, engineering and applications (IDEA). Bhopal, India, pp 1–7. https://doi.org/10.1109/IDEA49133.2020.9170693
17. Yadav A, Vishwakarma DK (2019) Sentiment analysis using deep learning architectures: a review. Artif Intel Rev https://doi.org/10.1007/s10462-019-09794-5
18. Wadawadagi·R, Pagi V (2020) Sentiment analysis with deep neural networks: comparative study and performance assessment. Artif Intel Rev https://doi.org/10.1007/s10462-020-09845-2
19. Rajawat AS, Upadhyay P, Upadhyay A (2020) Novel deep learning model for uncertainty prediction in mobile computing. In: Arai K, Kapoor S, Bhatia R (eds) Intelligent systems and applications. IntelliSys 2020. Advances in intelligent systems and computing, vol 1250. Springer, Cham. https://doi.org/10.1007/978-3-030-55180-3_49
20. Indhra om Prabha M, Umarani Srikanth G (2019) Survey of sentiment analysis using deep learning techniques, IEEE
21. Rajawat AS, Upadhyay AR (2020) Web personalization model using modified S3VM algorithm for developing recommendation process. In:2nd international conference on data, engineering and applications (IDEA). Bhopal, India, pp 1–6. https://doi.org/10.1109/IDEA49133.2020.9170701
22. Khine WLK, Aung NTT (2019) Applying deep learning approach to targeted aspect-based sentiment analysis for restaurant domain. https://foursquare.com/toledonews/list/restaurant-reviews
23. Khine WLK, Aung NTT (2019) Applying deep learning approach to targeted aspect-based sentiment analysis for restaurant domain. In: 2019 international conference on advanced information technologies (ICAIT). https://doi.org/10.1109/aitc.2019.8920880

Performance Improvement in Target Detection Using Various Techniques in Complex Matched Filter in Radar Communication

Ajay Suri, Soham Gautam, and Ridhi Aggarwal

Abstract The term radar was coined in 1940 by the United States Navy and is derived from three terms, radio detection and ranging. Radar transmits electromagnetic (EM) waves of radio frequency (RF). Radar is also helpful in classifying targets as known or unknown; a known target may be monitored to check the progress of the respective target. An unknown target may be a theft unit; it may or may not be with the intentions of causing harm. Radar also faces interferences while its operation, namely clutter or some intentional/unintentional jammers (Han C et al, Multimed Tools Appl 1–16, 2018 [Han C, Guangyu G, Yu Z (2018) Real-time small traffic sign detection with revised faster-RCNN. Multimed Tools Appl 1–16]). Moreover, radar also faces obstruction by its own thermal noise. Nowadays, radar is advanced enough to implement the two-dimensional and three-dimensional mapping. Radar is also widely used for collision avoidance and earth resource monitoring (Hu et al, IEEE Sens J 18:3152–3162, 2018 [Hu et al. in IEEE Sensors J 18:3152–3162, 2018]).

Keywords Clutter · Jammers · Thermal noise · Mapping · Monitoring

1 Introduction

The evolution of radar system has been tremendous since its early days when it was just limited to functions such as target range detection and target detection. The term radar was coined in 1940 by the United States Navy and is derived from three terms, radio detection and ranging. The main objective of this project is to understand radar from its basics, the functionalities, and develop an understanding to be able to know its operations and analysis. This project focuses on the main issues in radar design, its operation and calculation. It also focuses on the received radar data and its processing. It gives an idea about the signal processing basic terms, signal detection techniques and clutter rejection in signal detection. To add on, it gives meaning to the terms such as data acquisition and digitization, also the concept

A. Suri (✉) · S. Gautam · R. Aggarwal
ABES Engineering College, Ghaziabad, Uttar Pradesh, India
e-mail: suriajay21@gmail.com

D. K. Sharma et al. (eds.), *Micro-Electronics and Telecommunication Engineering*,
Lecture Notes in Networks and Systems 179,
https://doi.org/10.1007/978-981-33-4687-1_17

of discrete Fourier transform analysis, having windowing and interpolation methods. Other parts included the important digital filters like matched filter concepts and its relation to data integration. Furthermore, resolution of range targets was enhanced by pulse compression, which was vital in range detection. Target speeds were offered with the help of Doppler concepts, through which the velocities of targets were accurately measured and reported further to classify them as friendly or foe. Radar cross section is also considered while discussing radar received power strength. Finally, the Doppler shifts were measured for the targets so as to classify them as stationary or moving targets, with their respective distances from the radar [1]. Doppler processing means Doppler shift information to attain two certain goals. The first one is to enable detection of targets in environment having clutter in it. Other is to measure Doppler shift, in general radial velocity of targets. Now, we will discuss: moving target indication (MTI) and pulse Doppler processing. MTI processing is used to achieve first goal; but pulse Doppler processing works for both the goals to accomplish. Now to understand clutter when signal returns by reflecting targets, the clutter signals act as echoes of external objects present in the surroundings, thus increasing radar power which ultimately does not improve the signal-to-clutter ratio (SCR) because it is caused in the signal-to-clutter form of the given radar range equation. Doppler processing is the principal means of improving SCR. Doppler effect in radar systems is observed by pulsed radar.

Our main aim here is to detect the moving targets along with its range by using various filters and analysis techniques. Apart from that, ambiguity resolution and blind zones are also included.

2 Literature Review

Complex matched filter is used for data processing for dealing with real as well complex data for getting the distance, direction and velocity of the target. Methods like windowing for reducing relative side lobe level that are unwanted and often not needed signal and pulse compression for finer resolution are used for generating accurate results. For further improvement, the Doppler concepts are also used which are known for improving the resolution of the range. Hence, it produces less ambiguity and losses.

2.1 Doppler Shift

Whenever a transmitted wave is reflected of a target which is radially in motion to the radar, be it in opposite direction or the same direction, there is always a difference in the frequency of the transmitted wave and the received wave. If the target is moving radially away from the receiver, then there is a decrement in the frequency hence

negative Doppler frequency, while if the target is moving toward the radar, there is an increment in frequency, hence positive Doppler frequency [2].

2.2 Clutter

A return of a non-target from the radar is which is legitimate but is unwanted in the received radar data is called clutter. In other words, unintentional and unwanted but unwanted return from the receiver of radar is clutter. Among the three noises that we discussed earlier, clutter plays a dominant rule and is by far the most difficult to remove [3].

Noise in the atmosphere is at a set threshold and can be removed by increasing the threshold above that threshold noise power, but such is not the case with clutter which has variable power at different Doppler frequency levels [4]. The Doppler output of the receiver signal is all the combination of all the above-mentioned noises. Among all, there is white noise spread across all of the range bins. This white noise is of varying amplitude and is of non-uniform power [5].

2.3 Pulse Compression

As we are aware that the major function of the radar is to detect the radar range detection. This is one of the most important features of the radar. So to get a finer resolution of range bins from the radar, we implement pulse compression. Originally, the radar received signal comprises the high power response of the whole CPI, but this is not the case in pulse compression [6]. Pulse compression is carried out by using the matched filter technique. The matched filter technique is used to essentially increase the SNR of the target's range bin so as to differentiate the specific range bin of the specific dwell that corresponds to the target echo. The matched filter technique is actually the correlation of the received radar data with the transmitted data. The received radar data is nothing but the delayed version of the same transmitted signal, with attenuated amplitude but with only linearly shifted phase, and hence, when a time shifted signal is auto-correlated to its own self, we receive a peak at a delay sample of the signal. This is the principle of using matched filtering, to get finer resolution in the range bin spectra of the analysis [7].

2.4 Windowing

Windowing is a method to suppress the relative side lobe level of the signal. The main lobe of the signal carries the desired response of a signal, while the side lobe level is made up of undesired response. This undesired side lobe level when competes with

main lobe level can lead to incorrect results. So, the difference between the main lobe level and side lobe level is enhanced by using the windowing technique [8]. The windowing is in fact the gain introduced in a filter to maximize the central response and deplete the side levels of the filters [9]. There are many windows that can be used that give different responses, but custom Chebyshev window of 50 dB relative side lobe level has been used in the signal processing of this project were overcome in the pulse Doppler processing.

Although the clutter is dominant at range bins that are closer to the radar due to high clutter power that competes with the target echo power. It was also observed that pulse Doppler processing is difficult when the target has velocities corresponding to zero Doppler shifts due competition with the clutter's Doppler response, hence velocity detection is difficult in that case [10].

2.5 Matched Filter

Matched filter (MF) is conception based on the waveform of the sender radar signal. When the white noise is present, it gives maximum SNR. With MF, we can attain very thin pulses from low power long signals. As not all signals have achieved faithful matched filters, new waveform designs were created. Based on the requirement and nature of clutter noise, the waveform design must follow certain requirements. Also, correlation function between the senders and receivers signal can be utilized in place of MF. This filter is inactive in colored-noise. Thus, when colored-noise is present, a whitening filter has to be applied before the matched filter or you can say the correlation function, to reduce the spectrum of noise and avoid mismatch between the signals. Integration is a subpart of matched filter process which is used in radar signal processing (RSP) to improve the SNR of the output echo. The integrator used in this stores the energy of consecutive echo pulses which are reverted by the same target. At the IF stage of the output, pre-detection integration occurs that gives improved SNR in comparison with post-detection integration [11].

2.6 Doppler Processing

The process of Doppler processing of radar signals is used to set aside the unmovable objects and effectively increase the signal-to-clutter ratio (SCR). In recent times, there are two main techniques to boost the SCR in radar, i.e., moving target indication (MTI) for short pulses in radar and moving target detection (MTD) for pulse Doppler. Suppose the wavelength of signal is λ, the frequency shift will be the received from a target which is moving with a relative velocity (v_r). An MTI filter unstays the blind speeds issue with the help of a staggered PRF, in place of using the common PR. Now, the chances of a target moving with blind speeds will eventually reduce [12]. In case of pulse Doppler, a bank of filters is made into use to get larger dynamic range in the

Doppler frequency domain. This whole process avoids filtering out moving targets due to blind speeds and reduces errors to the least when the velocity is measured.

2.7 Drawbacks of the Existing System

- It does not do pulse compression.
- No function for windowing.
- They handle only real data.
- Not using Doppler concepts for accuracy.

3 Proposed Architecture

- Resolution of range targets was improved with Doppler concepts.
- It is a complex matched filter for complex data processing.
- More accurate results were produced.
- Here, one filter is overlapping two other filters. So, it produces less ambiguity and losses.
- Windowing is also done to suppress the relative side lobe level of signal.
- We will be concluding that when velocity corresponds to zero Doppler shifts, then velocity detection is difficult.

4 Results

4.1 Radar Range Plot

Radar Position = [0; 0; 0;] in x, y, z coordinates, respectively.

Target Positions:

1st target = [10,000 m; 0; 0;] which corresponds to 334th bin (=30 m) after the pulse transmission bins, i.e., 120, so the target echo is received at 120 + 334 = 454th range bin at a power of 70.81 dB.

2nd target = [16,000 m; 0; 0;] which corresponds to 654th range bin at a power of 74.15 dB.

3rd target = [22,000 m; 0; 0;] which corresponds to 854th range bin at a power of 76.8 dB.

Radar Range Plot with Clutter:

Due to clutter, the peak power of range bins 120–1000 is higher than the case of without clutter.

Radar Position = [0; 0; 0;] in x, y, z coordinates, respectively.

Target Positions:

1st target = [10,000 m; 0; 0;] which corresponds to 454th range bin at a power of 70.81 dB.

2nd target = [16,000 m; 0; 0;] which corresponds to 654th range bin at a power of 74.15 dB.

4.2 Complex Bandpass Filter

Ten complex bandpass filters used with relative side lobe level of 50 dB. This side lobe level is achieved by using a custom Chebyshev window. Figure 1 shows the ten filters with equally spaced central frequencies, ranging from-to frequencies (in radians).

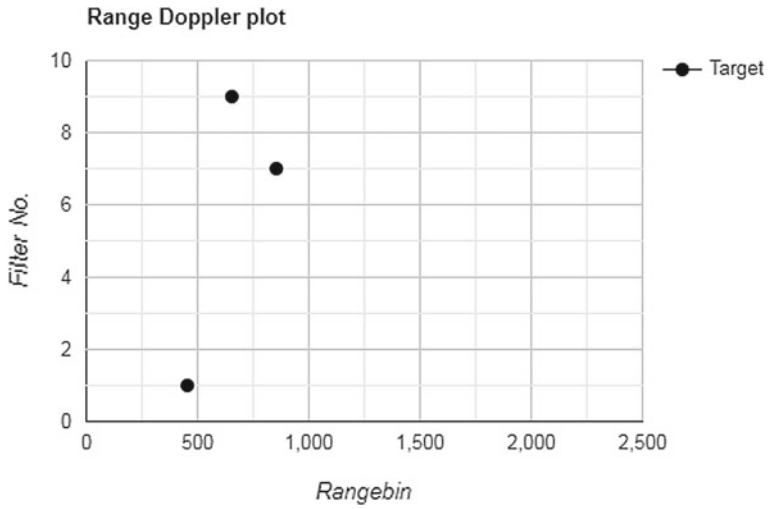

Fig. 1 Range doppler response

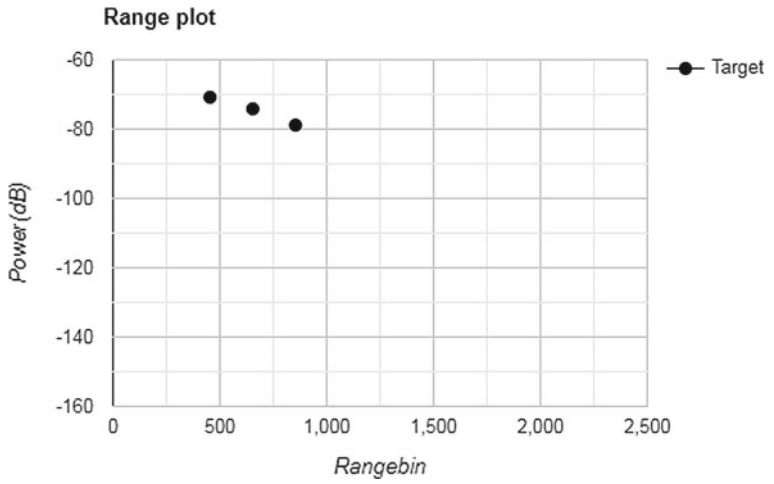

Fig. 2 Radar range plot

4.3 Range Doppler Response

As discussed above, the range of the targets is plotted according to their respective range bins. Targets 1, 2 and 3 having velocities in x, y, z coordinates as (100 m/s, 0, 0), (125 m/s, 0, 0) and (112 m/s, 0, 0), respectively, have been detected at 1st, 9th and 7th filter, respectively, and hence, there doppler frequencies have been calculated.

Range Doppler Response with Clutter:

As seen above in the range Doppler plot without clutter, the targets were detected with relative ease. Such is not the case in presence of clutter, especially when the clutter power competes with the target echo power. This happens in the range bins following the transmission of radar pulse. In other words in presence of clutter, the targets having near zero Doppler shifts are hard to detect using pulse Doppler processing (Fig. 2 and Table 1).

5 Conclusion

The range detection and Doppler shift calculated with the pulse radar processing technique have been duly verified with the theoretical results. The pulse Doppler processing model accurately fits the results of the actual target functions such range and Doppler shift, which in turn is used to calculate the speed of the target. Effects of clutter were duly considered for both range detection and Doppler measurement and were overcome in the pulse Doppler processing. Although the clutter is dominant at range bins that are closer to the radar due to high clutter power that competes with

Table 1 Comparison between the existing models and the proposed model based on several parameters

S. No.	Parameters	Existing method	Proposed method
1	Works on	Only real data [6, 10]	Real as well as the complex data
2	Clutter	The peak power of range bins is 120–1000 is higher. Also, unwanted distortions can occur in the results [5]	The peak power of range bins is correct. No distortions are present
3	Accuracy	Theory and practical results vary with each other [1, 2, 7]	The practical and theoretical results are identical
4	Side lobe level	Side lobe level of the signal was comparable with the main lobe [10]	Ten complex bandpass filters used with relative side lobe level of 50 dB achieved by using a custom Chebyshev window
5	Resolution	Standard resolution [9]	Improved by taking suitable pulses

the target echo power. It was also observed that pulse Doppler processing is difficult when the target has velocities corresponding to zero Doppler shifts due competition with the clutter's Doppler response, hence velocity detection is difficult in that case.

References

1. Weicheng Z, Xuewei L, Hongzhe L (2018) Overview of target detection algorithms based on deep learning. In: Proceedings of the 22nd network new technology and application conference of the network application branch of China computer users association
2. Yang H, Li N, Li T, Liu QH (2018) Least-square-based non uniform borehole SAR imaging for subsurface sensing. IEEE J Sel Top Appl Earth Observ Remote Sens 11(5):1545–1555
3. Sharma R, Kumar R, Sharma DK, Son LH, Priyadarshini I, Pham BT, Bui DT, Rai S (2019) Inferring air pollution from air quality index by different geographical areas: case study in India. Air Qual Atmos Health12**:**1347–1357
4. Nguyen PT, Ha DH, Avand M, Jaafari A, Nguyen HD, Al-Ansari N, Van Phong T, Sharma R, Kumar R, Le HV, Ho LS, Prakash I, Pham BT (2020) Soft computing ensemble models based on logistic regression for groundwater potential mapping. Appl Sci 10:2469
5. Al-Ashwal WA, Woodbridge K, Griffiths HD (2014) Analysis of bistatic sea clutter-part I: average reflectivity. IEEE Trans Aerosp Electron Syst 50(2):1283–1292
6. Li C, Zhao H, Wu F et al (2018) Digital self-interference cancellation with variable fractional delay FIR filter for full-duplex radios. IEEE Commun Lett 99:1–1
7. Abouelfadl et al (2016) Performance analysis of LFM pulse compression radar under effect of convolution noise jamming. In: 2016 33rd national radio *s*cience conference (NRSC) Aswan, pp 282–289
8. Cho J, Jung J, Kim S (2018) Analysis of cross-borehole pulse radar signatures on a terminated tunnel with various penetration lengths. IEEE Trans Geosci Remote Sens 56(2):799–807
9. Shuhua L, Hua B, Yu S, Mengyu Z, Yang F Method for detecting Chinese texts in natural scenes based on improved faster R-CNN. Int J Pattern Recogn Artif

10. Xiang Z, Chen B, Yang M (2018) Transmitter/receiver polarisation optimisation based on oblique projection filtering for mainlobe interference suppression in polarimetric multiple-input–multiple-output radar. IET Radar Sonar Navig 12(1):137–144
11. Wilden H, Kirchner C, Peters O, Ben Bekhti N, Brenner A, Eversberg T (2016) GESTRA-a phased-array based surveillance and tracking radar for space situational awareness. In: IEEE international symposium on phased array systems and technology (PAST)
12. Thanh V, Rohit S, Raghvendra K, Hoang SL, Thai PB, Dieu TB, Ishaani P, Manash S, Tuong L (2020) Crime rate detection using social media of different crime locations and twitter part-of-speech tagger with brown clustering, pp 4287–4299
13. Han C, Guangyu G, Yu Z (2018) Real-time small traffic sign detection with revised faster-RCNN. Multimed Tools Appl 1–16
14. Hu X, Tong N, Guo Y, Ding S (2018) MIMO radar 3-D imaging based on multi-dimensional sparse recovery and signal support prior information. IEEE Sensors J 18(8):3152–3162

Unhindered Safety Monitoring System for Underground Workers

G. Shanmugaraj, B. V. Santhosh Krishna, S. SriSahithya, M. Sandhya, and T. H. Monikca

Abstract Though the earth is heading toward automation, there are still many works which could be performed only by mankind. Such jobs always tend to be dangerous and life demanding. Even today, jobs like sewage cleaning and mining fall under this category. In such cases, real-time health monitoring systems for these workers will be helpful. In this paper, the device presented will monitor the heart beat rate, the body temperature, the methane concentration and also the atmospheric oxygen concentration and provides alert to the worker and the exterior unit. When parameters deviate from the safe limit range, it will alert the workers to stay safe and detect toxic gases before any harm.

Keywords Health sensing · Pulse oximetry sensor · Arduino nano · Arduino uno · Inter-integrated circuit communication · Gas sensor · Beats per minute · Temperature sensor · Occupational health hazards · Wearable in underground

G. Shanmugaraj (✉) · B. V. Santhosh Krishna · S. SriSahithya · M. Sandhya · T. H. Monikca
Department of Electronics and Communication Engineering, Velammal Institute of Technology, Chennai, India
e-mail: gsraj76@gmail.com

B. V. Santhosh Krishna
e-mail: Santhoshkrishna1987@gmail.com

S. SriSahithya
e-mail: srisahithya.s@gmail.com

T. H. Monikca
e-mail: monikcahari@gmail.com

B. V. Santhosh Krishna
New Horizon College of Engineering, Bangalore, Karnataka, India

D. K. Sharma et al. (eds.), *Micro-Electronics and Telecommunication Engineering*,
Lecture Notes in Networks and Systems 179,
https://doi.org/10.1007/978-981-33-4687-1_18

1 Introduction

Generally, sewage cleaning and mining are the most risky jobs. Year after year, many such workers die due to health-related problems. They are not given any safety equipment. Many cities have bought safety equipment worth lakhs for the workers. Every equipment costs around 4–5 lakh rupees [1]. But, due to negligence, the underground safety equipment distribution program is not being effectively implemented. Within the context of mining, many operators are employed in various extraction actions such as drilling, care of the roof support, transport of mined ores, and review of various mined fields. In addition, the deep mining was deemed heavy stress workplace situations because of its specific characteristics known as high humidity, temperature, toxic gas concentration, low visibility disturbance and dirt. These challenges make working in underground environment very difficult and toilsome.

This paper aims to develop a device which would monitor the health of the worker working underground and provides the health parameters in real time to the members outside or to the display unit. The device is designed to provide a low-cost solution to the existing problems related to the health issues of the workers [2]. The system also has emergency safety system, which work, if the electronics fails. The main problems for the workers include explosion, falls or fire, oxygen depletion, gas poisoning, asphyxiation from gases and fumes inside the sewer. In all of the above cases, the problem involving gases are easily overlooked which can lead to health risks or even cause death. Harmful gases, which are mainly composing methane (CH_4), carbon monoxide (CO) and ammonia (NH_3), are released during the cleaning of sewage. Methane displaces atmospheric oxygen at a fast rate and forms rapidly in moist places with temperatures higher or lower than room temperature. CH_4, CO and NH_3 are released in large amounts in closed sewage areas like manholes, gutters, closed drains, etc. Methane is an asphyxiant; i.e., it replaces oxygen easily and gets trapped in confined spaces easily. This methane displaces atmospheric oxygen present in the air gap. Many toxic gases are released during any sort of work in the sewage. This may cause several health problems to the workers. These gases are also responsible for bad odor and fire explosion in the sewer and mines.

2 System Description

A. Arduino Microcontroller

Arduino is one of the fastest growing and vastly used microcontrollers in the world of electronics. There are many different microcontrollers available. Arduino is based on the ATMEGA AVR series microcontrollers from ATMEL. Arduino has both analog and digital pins. Although the processing is done in digital format, the analog values are converted to digital values by a 10-bit ADC. Arduino has its own integrated

Fig. 1 MAX30100 pulse oximetry sensor

development environment. The Arduino [3] microcontrollers used in this device are Arduino Nano and the Arduino Uno [4].

B. Max30100 Pulse Oximetry Sensor

The MAX30100 [4] is a heart rate monitoring Fig. 1 and an integrated pulse oximetry sensor [5]. It is a combination of two LEDs, a photodetector and low-noise analog signal processing to detect pulse oximetry and heart rate signals and optimized optics. The MAX30100 breakout operates from 1.8 to 5.5 V.

The circuit diagram of MAX30100 is shown in Fig. 2. The system takes benefit of the varying visual attributes between oxygenated and deoxygenated blood. When red led is fired in the blood vessels, then the deoxygenated and blood and oxygen consume varying amounts of light and reflect back different amount of lights.

A photodetector measures the level of distorted light. A small batch collects which extracts the outputs and then implements correct signal processing. Finally, the output is taken by the microcontroller via an inter-integrated circuit communication.

C. LM35 Temperature Sensor

LM35 is a temperature regulating unit with an analog out volt corresponding to heat (shown in Fig. 3). It gives voltage output in °C. No external calibration circuit may be needed. LM35 has a frequency of 10 mV/°C [6]. To measure the temperature through signals, it requires a thermocouple or resistance temperature detectors (RTD).

Two dissimilar materials producing the electricity volt implicitly corresponding to temperature changes are used for the preparation of a thermocouple [7]. The voltage that reads across the diode constitutes the working base of the sensors. The temperature rises, if the voltage increases. When the voltage varies, the sensor transmits the temperature to the Arduino microcontroller which displays the temperature of the sewer or any other underground working environment.

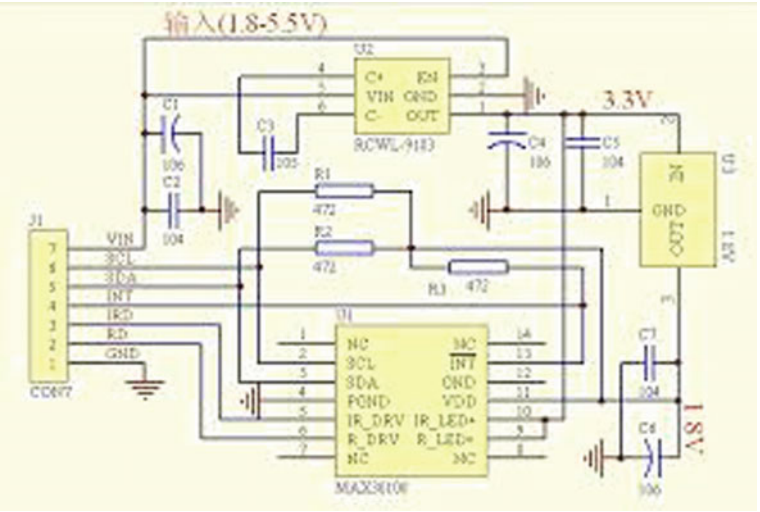

Fig. 2 Circuit diagram of MAX30100

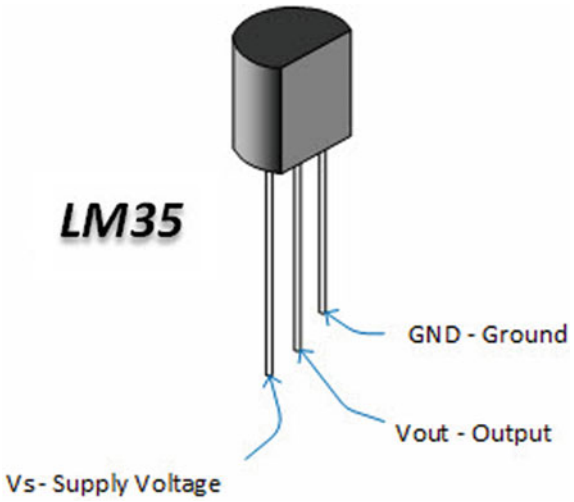

Fig. 3 LM35 temperature sensor

D. MQ-4 Natural Gas Sensor

The MQ-4 natural gas sensors are commonly used in gas leakage detecting equipment Fig. 4. Natural gas is mainly composed of methane, but commonly including small percentage of carbon dioxide, nitrogen, carbon monoxide and other hydrocarbons [8]. Here, we are using MQ-4 natural gas sensor which is sensitive to the toxic gases which are harmful for life and are present inside the sewer and the mines.

Fig. 4 MQ-4 natural gas sensor

MQ-4 responsive gas detector layer has SnO_2, which has reduced capacitance in breathable air. When the target gas is present, the conductivity rises with the concentration of the target gas. This voltage is fed to the microcontroller as an input [3]. The limitations on the sensor, posed due to other corrosive gases, may be overcome by suitable screening from gases as H_2S and CL_2. The output is obtained in the form of a voltage developed across a load resistor (RL). The MQ-4 gas sensor requires a preheating time of 48 h in a clean environment, free from any toxic gases.

E. **SO 110-Oxygen Sensor**

Oxygen sensor is the electronic device (Fig. 5.) which is used to measure the oxygen level present in the gas or liquid analyzed. Here, the sensor we used is SO 110 which is manufactured by Apogee Instruments [9]. This oxygen sensor is specially used to measure the oxygen in closed environment or in an indoor laboratory. The top layer of the sensor can be heated to prevent water from condensing on the sensor layer and blocking the diffusion path. The heater is typically used only when sensors are placed in environment where relative humidity is most probably equal to 100%.

Fig. 5 SO 110—oxygen sensor

3 Overview of the Device

The working of this device may be categorized into two halves. The first unit comprises the sensing unit and another display unit. The sensor unit consists of various sensors such as MQ-4 natural gas sensor, an oxygen sensor, MAX30100 pulse sensor, temperature sensor, vibration motor and buttons. The system can be powered with a 5 V supply, which is sufficient for working of every device connected to the sensor assembly. The sensor assembly may be worn by the person while working, on the hand. The sensor assembly will communicate with the display set using an UART communication [10].

The other highlighting feature that is provided on the sensing part of the system is the emergency switch. The emergency switch can be used to give inputs from the display unit, whenever immediate actions like moving out from the underground surface are required. The emergency switch will work even if the system stops functioning due to any fault and the underground environmental conditions.

The display unit comprises an OLED display, buttons, LEDs and a vibration motor. It consists of three LEDs. The green LED signals indicate that all levels are below the threshold levels. The red LED is used to alert if any parameter is above or below the critical/threshold level. The yellow LED signals are used to alert when the emergency switch is pressed. The display unit communicates with the sensor unit by the UART communication [11]. The OLED display is mostly preferred because it works in sunlight better than other technologies. Figures 6 and 7 show the block diagram and design flow of the project.

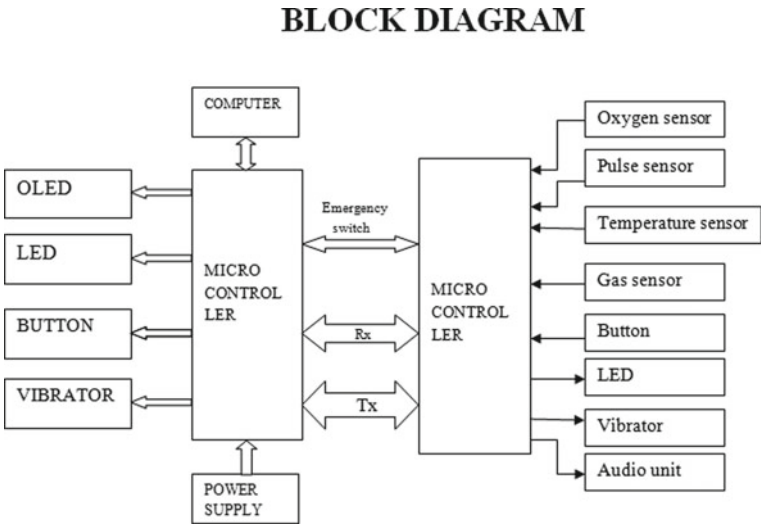

Fig. 6 Block diagram

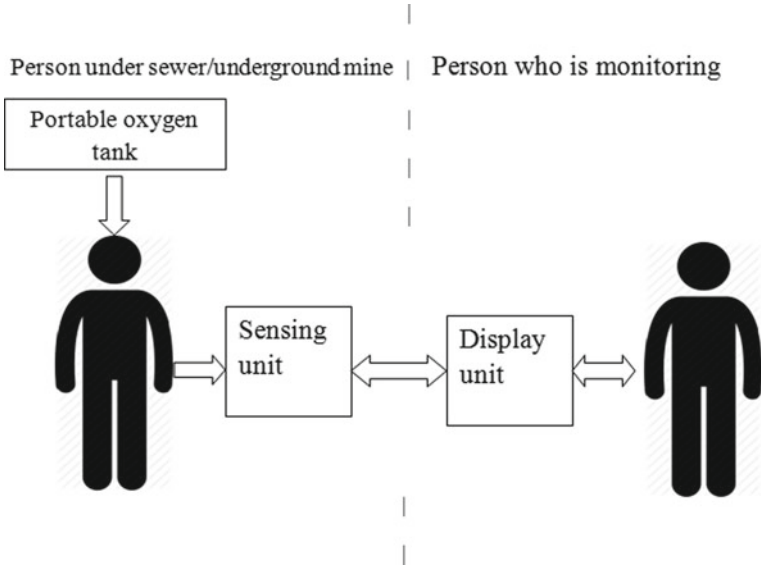

Fig. 7 Design flow

4 Experimental Results

The complete experimental setup for the system is shown in Fig. 8.

Tests were performed on two individuals for sewage workers. The test area had a bad odor, and temperature was higher than normal. The natural gas sensor was tested in two different conditions, an open sewer and a closed sewer. The analog values

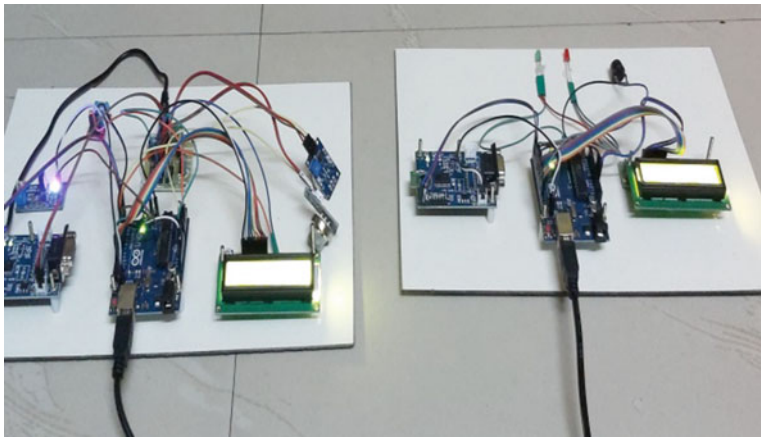

Fig. 8 Experimental setup

Table 1 Pulse rate of every individual under normal conditions

Person	Heart beat rate (beats per minute)
1	71
2	75

Table 2 Test the result of two different persons in an open sewer

Person	Average oxygen concentration (%)	Average methane concentration (ppm)	Average beats per minutes for 2 min
1	20.10	643	86
2	20.00	659	78

Table 3 Test result of person 1 in varying depth

Person	Horizontal surface depth (m)	Concentration of O_2 (%)	Concentration of methane (ppm)	Sum of beats per minute
1	1	20.20	900	77
	3	20.16	945	83
	5	20.14	1099	95
	7	19.92	1235	103

Table 4 Test results of person 2 in varying depth inside the sewer

Person	Horizontal surface depth (m)	Concentration of O_2 (%)	Concentration of methane (ppm)	Sum of beats per minute
2	1	20.12	916	81
	3	20.05	984	85
	5	19.85	1097	95
	7	19.78	1251	99

were converted to parts per million. The heart beat rate test was performed on two different individuals, and the results are shown in the Tables 1, 2, 3 and 4.

Figures 8, 9 and 10 show the oxygen concentration, methane concentration and average beats per minute.

5 Conclusion

This device is designed, especially for monitoring and measuring the necessary parameters, which is needed for the safety of the underground workers. The system finds its application in household sewage systems, municipal manholes, sewage,

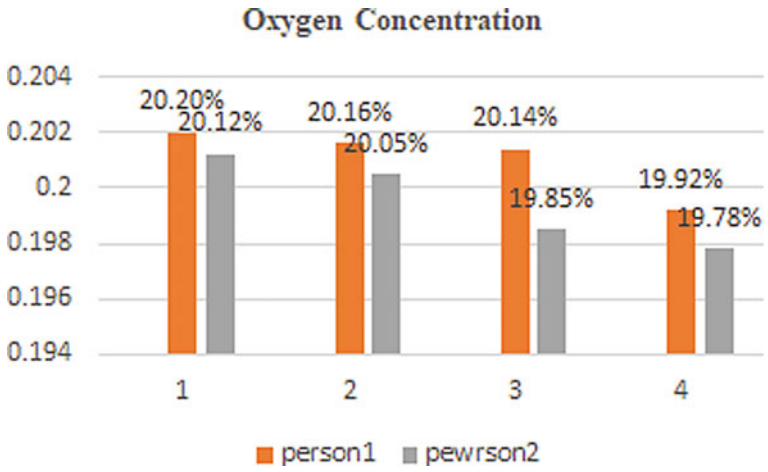

Fig. 9 Oxygen concentration

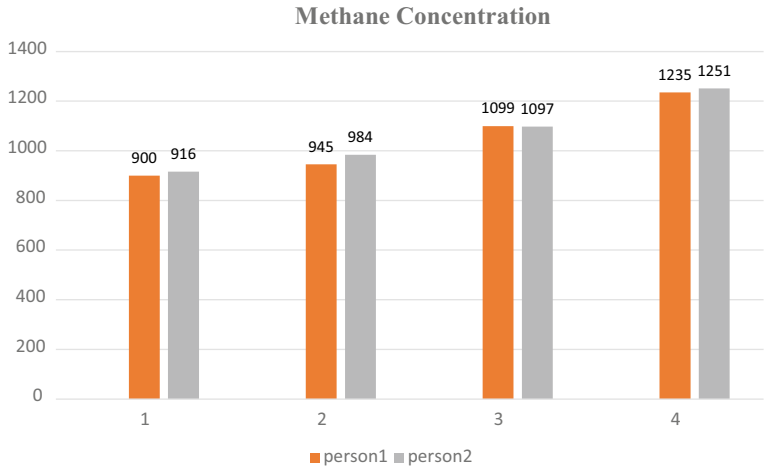

Fig. 10 Methane concentration

gutters, mines, etc. This device can be widely used in countries where sewage is mostly cleaned by humans and also in places where mining is a major occupation.

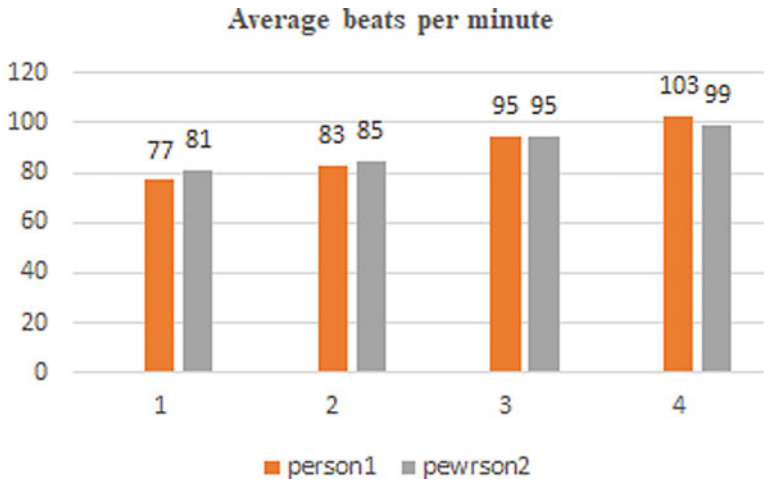

Fig. 11 Average beats per minute

References

1. Misra P et al (2010) Safety assurance and rescue communication systems in high-stress environments: a mining case study. IEEE Commun Mag 48(4):66–73
2. Ranjan A, Sahu HB, Misra P (2016) Wireless sensor networks: an emerging solution for underground mines. Int J Appl Evolut Comput (IJAEC) 7(4):1–27
3. Jun X, Wen-Bin W (2016) Design of sewage treat controller. IEEE
4. Onubeze A (2016) Developing a wireless heart rate monitor with MAX30100 and nRF51822. BE thesis, Helsinki Metropolia University of Applied Sciences
5. Casilari E, Luque R, Mor MJ, Gzquez JA (2005) A Wireless monitoring system for pulse-oximetry sensors. In: 2005 systems communications (ICW). Montreal, Quebec, Canada, pp 79–84. https://doi.org/10.1109/ICW.2005.20
6. Apogee Instruments, A web article on Oxygen Sensor, https://www.apogeeinstruments.com/oxygensensor/. Accessed on 13 Jan 2019
7. Hanwei Electronics, Data Report on "Technical Data MQ-4 Gas Sensor. https://www.sparkfun.com/datasheets/Sensors/Biometric/MQ-4.pdf. Accessed on 11 Jan 2019
8. Arduino, Web article on different types of Arduino Board and its features, https://www.arduino.cc/. Accessed on 10 Jan 2019
9. Maxim Integrated, A Web article on "UART Communication", https://www.maximintegrated.com/en.html. Accessed on 12 Jan 2019
10. Digital humidity sensor with temperature output. Accessed on 12 Jan 2019
11. Occupational Safety and Health Administration, United States of Department of Labor, a web article of exposure and quantity of methane. https://www.osha.gov/. Accessed on 11 Jan 2019

Design and Fabrication of Flexible Antenna Using Foam Substrate for WiMAX Applications

M. Pandimadevi and R. Tamilselvi

Abstract In present scenario, world interoperability for microwave access (WiMAX) is gaining great momentum among broadband wireless technologies. Employing flexible antenna will enable high-performance of radio frequency transmission as well as cost effective for such wireless applications. In this work, a flexible antenna is designed, simulated, and fabricated using foam substrate material for world interoperability for microwave access (WiMAX) band applications. The operating frequency is chosen as 3.5 GHz. The proposed antenna is bendable, wearable, low cost, and smaller in size, reduced reflection co-efficient, greater directivity, and wider bandwidth. The antenna is simulated using computer simulation technology software and is fabricated using vector network analyzer. The return loss value obtained in measurement is −24.95 dB which is in good agreement with simulated value of −34.6 dB. The gain and directivity obtained are 3.096 and 4.93 dBi, respectively. The radiation pattern obtained is omnidirectional. Thus, the designed antenna is compact enough with the dimensions of 50 × 36 × 2.2 mm^3 to place inside any new technology wireless device. Since the directivity of the antenna under bending condition is 4.672 dBi, it can also be used for wearable applications.

Keywords Flexible antenna · Foam substrate · Directivity · Returns loss · Bending

1 Introduction

Currently, the development of radio equipment in various shapes and immediate progress in flexible electronics [1, 2] needs the antennas employed on wireless devices to be manufactured in different shapes. Moreover, improved studies of wearable equipment, RFID tags [3], and flexible displays have sparked on more interest to the flexible antenna. Notably, there are rising necessities of flexible antennas with low-profile, small size, and multiple operating bands including the wireless local area network (WLAN) [4–6] band 2.4/5.2/5.8 GHz and the world interoperability

M. Pandimadevi (✉) · R. Tamilselvi
Sethu Institute of Technology, Virudhunagar, Tamil Nadu, India
e-mail: devidevi64@gmail.com

D. K. Sharma et al. (eds.), *Micro-Electronics and Telecommunication Engineering*,
Lecture Notes in Networks and Systems 179,
https://doi.org/10.1007/978-981-33-4687-1_19

for microwave access (WiMAX) [7–9] band 3.5 GHz due to the enormous increase of demand for wireless data communication. Antennas used in wearable systems and RFID tags are susceptible to the proximity of the material itself, so they usually degrade performance due to the resonant current on the ground plane and their compact size.

Because of their low profile, simple feeding, low manufacturing cost, and easy-to-integrate functionality, microstrip patch antennas [10, 11] are ideal candidates for wireless applications. The antenna size has a major impact on the overall design of wireless networks, and there is usually a trade-off between the antenna size and efficiency as the antenna's characteristics are closely related to its size. Compared to traditional antennas, microstrip antennas have many advantages and have also been used in a wide variety of applications ranging from mobile communication to satellite, aircraft, and other applications.

The aim of the latest generations of wireless mobile radio networks is to provide the mobile devices with flexible data rates and a wide variety of applications while supporting as many devices as possible. The key goal for today's networking network is to provide high bandwidth [12–14]. Nowadays, flexible antennas have been employing for wireless applications with better efficiency.

Even though previous works have employed patch antenna using rigid substrate materials such as RT/duroid 5880 [15], glass epoxy [16], Getek-ML 200M [17] Roger R04003C [18], RogersRO4350 [19], and FR-4 [20] for WLAN/WiMAX applications. However, the usage of those substrates will result in high cost, high design complexity, and easily breakable. This issue can be easily overcome by using flexible materials.

Gupta et al. [21], proposed an assembled design of textile antenna employing foam and jeans substrate at triple band frequencies. The substrate has the thickness of 3 mm. The dimension of the antenna is $41.6 \times 61.6\,mm^2$. The maximum directivity obtained is 6.123 dBi and return loss obtained is −21.33 dB at 3.667–4.4 GHz.

Pauria et al. [22] designed a flexible antenna for wideband applications. The size of the antenna is 60 X 60 mm2. The maximum gain obtained is 7.79 dB at 13.15 GHz. Saeed et al. [23] proposed flexible reconfigurable antenna using a flexible polyethylene terephthalate (PET) substrate at 2.36 GHz and 3.64 GHz for WLAN and WiMAX applications, respectively. The size of the antenna is 59×31 mm2. The maximum gain obtained is 1 dB. The return loss obtained is around −20 dB. In the above works mentioned, even though the directivity and gain obtained are higher, the return loss is high [21, 23] and the size is also little bit heavy [21, 22]. These drawbacks should be addressed and rectified by correctly choosing the substrate materials.

The objective of the work is to design a compact antenna that operates at 3.5 GHz frequency for WiMAX application. The antenna to be designed must be very small enough to place inside any compact new technology wireless device. Main aim is to achieve greater directivity to have higher efficiency even under bending position.

In this work, a flexible square patch antenna is presented with H-shaped slot which is aimed for wearable as well as WiMAX applications. Foam is used as a substrate due to its flexible nature, in expensive, readily available, eco-friendly, etc. Its main

advantage is its easy coming back to its original position after the exhibition of any bending or twisting its structure.

The organization of this paper is as follows: Sect. 2 deals with design of the proposed antenna. Section 3 details the simulation and fabrication of the proposed antenna. Section 4 discusses the results obtained from the testing of the fabricated antenna and compares it with simulation results. The conclusion is provided in Sect. 5.

2 Design of the Proposed Antenna

Microstrip patch antenna is a type of planar antennas which have more merits and better anticipation when compared to other conventional antennas. It can have any shape, but rectangular, square, circular, and elliptical are commonly used. The square shape is chosen because it has equal dimension in all sides. Due to this, the analysis is also simple when compared to rectangle shape patch. The inclusion of the slot in the patch antenna will improve the overall performance of the antenna.

Figure 1 represents the structure of the proposed antenna. Using the standard equation of the patch antenna, parameters are calculated. The calculated parameters are listed in Table 1. The copper is used for the patch element, ground plane, and stripline. As the patch is square in shape, each side of the patch is 16 mm in length and 0.1 mm in thickness.

The H-shaped slot is present in the square-shaped patch. The slot is 14 mm in length and 1 mm in thickness. The presence of slot in the patch will reduce the area of the patch. The length and width of the stripline are 22 mm and 3 mm, respectively. The thickness of stripline is 0.1 mm. The foam material is used as the substrate whose properties are listed in Table 2. The substrate is 50 mm and 36 mm in length and width, respectively. The thickness of the substrate is 2 mm. The copper is used as

Fig. 1 Antenna structure

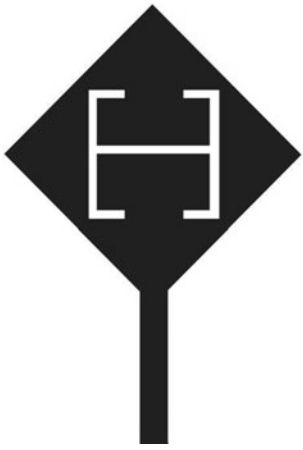

Table 1 Parameters of the proposed antenna

Parameters	Dimension (mm)
Patch length	16
Stripline	22 × 3
Substrate and ground plane	50 × 36
Patch and stripline thickness	0.1
Ground plane thickness	0.1
Substrate thickness	2
Slot thickness	1
Slot length	14

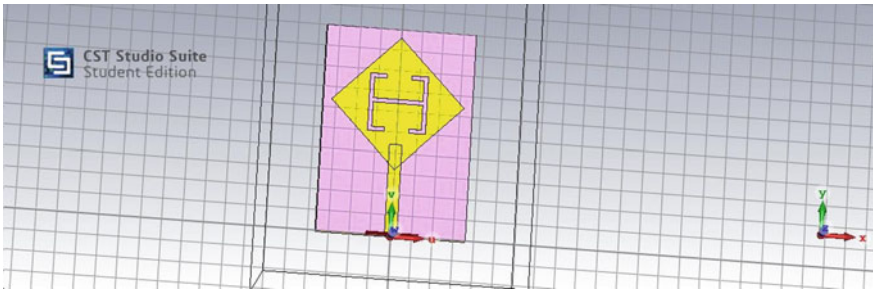

Fig. 2 Proposed antenna structure in CST software

Table 2 Properties of foam

Properties	Value
Dielectric permittivity	1.03
Loss tangent	0.00001
Thermal conductivity	0.033 W/K/m
Young's modulus	2.76 kN/mm^2
Poisson's ratio	0.3333

the ground plane. The ground plane's length and width are as same as the substrate length and width.

3 Simulation and Fabrication of the Proposed Antenna

The antenna is designed using CST Studio suite software, as shown in Fig. 2.

CST MICROWAVE STUDIO® (CST MWS) [24] is a professional tool for 3D EM simulation of high-frequency components. CST MWS can quickly and accurately analyze high-frequency (HF) equipment, such as antennas, filters, couplers, planar

and multilayer structures, and SI and EMC effects. The designed antenna is simulated to get the output parameters such as S_{11} parameters (return loss), voltage standing wave ratio (VSWR), gain, directivity, and radiation pattern.

The most widely cited parameter with respect to antennas is S_{11} in operation. The S-parameter computes the quantity of power that the radiator reflects itself. That's what, it is otherwise known as the reflection co-efficient. It can be also referred as return loss [25]. Figure 3 shows the return loss measurement. For antenna to be effective, the return loss should be less than −10 dB. In this proposed antenna, the simulated value of S_{11} parameter is −34.64 dB at 3.5 GHz. Most of the values are below −10 dB ranging from 3.35 GHz to nearly 4 GHz. Thus, the bandwidth obtained is more than 1 GHz.

Voltage standing wave ratio (VSWR) is a calculation of how effectively radio frequency power is transmitted from a power source to a load. The full amount of energy is transferred in an optimal device [25]. Figure 4 shows the VSWR measurement of the proposed antenna. For any antenna to be effective, VSWR should be between the values of 1 and 2. In this work, VSWR value obtained is 1.04 which is easily acceptable.

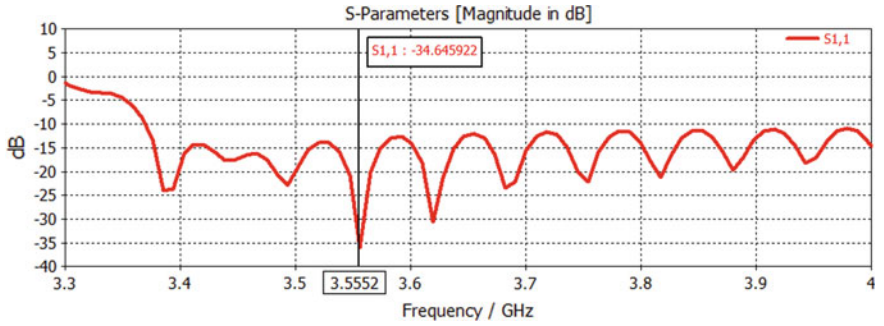

Fig. 3 S_{11} parameter measurement

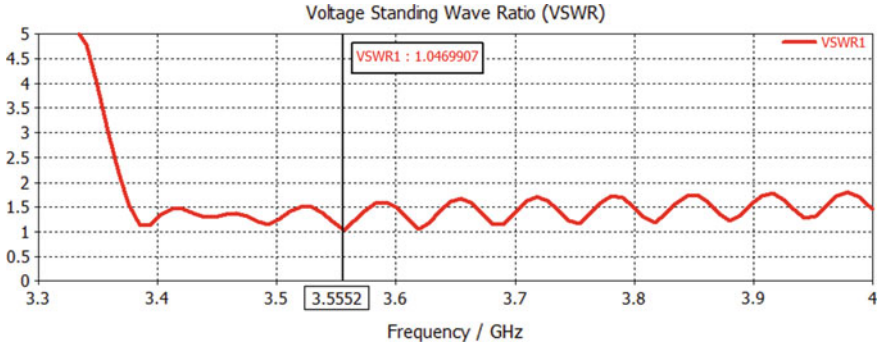

Fig. 4 VSWR measurement

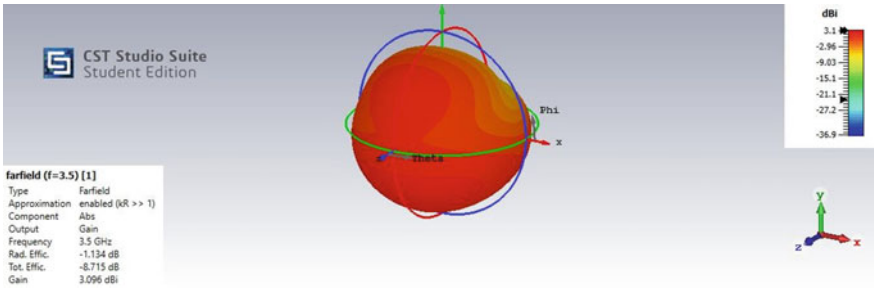

Fig. 5 Gain measurement

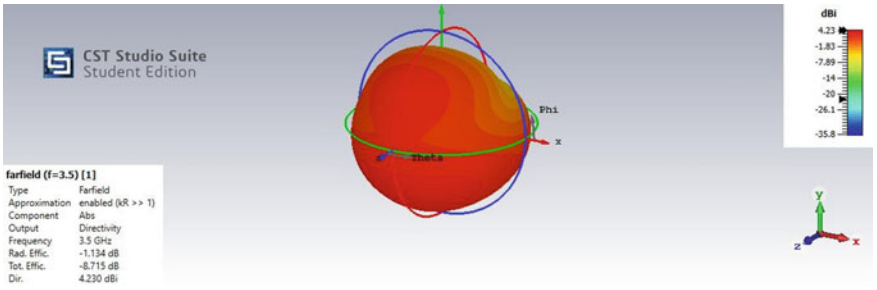

Fig. 6 Directivity measurement

Antenna gain [25] shows how strongly an antenna can radiate or receive a signal in a desired direction. The intensity of the signal will reach further in a narrower direction when the antenna has higher gain. Figure 5 shows the simulation result of gain measurement. The value obtained is 3.096 dBi.

Directivity is the calculation of the radiation pattern collection of an radiator element in a desired direction [25]. The higher directivity implies higher the beam radiated by an antenna in the desired direction. Figure 6 shows the simulation result of directivity measurement. The value obtained is 4.23 dBi.

An antenna's radiation pattern plays an important role in the functioning of the antenna element as it implies how far the energy transmission of the antenna will radiate in space [25]. The pattern includes a number of lobes. It would not depend on distance that is measured far from the antenna. Figure 7 shows the simulation result of radiation pattern of the proposed antenna. The pattern is mostly omnidirectional which is required for an antenna to employ in WiMAX applications.

The designed antenna is bent at an angle of 20′ in the simulation software as shown in Fig. 8. The results show better efficiency with directivity of 4.672 dBi as shown in Fig. 9 which is very near to 5 dBi. This implies that the antenna can be readily used for wearable applications.

The proposed antenna is fabricated as shown in Fig. 10, the ground plane and patch of the antenna were made by copper sheet of 0.1 mm thickness. The substrate

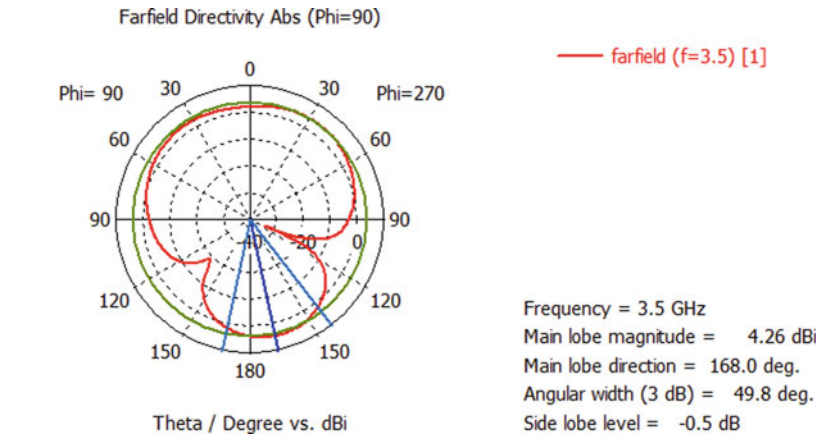

Fig. 7 Radiation pattern measurement

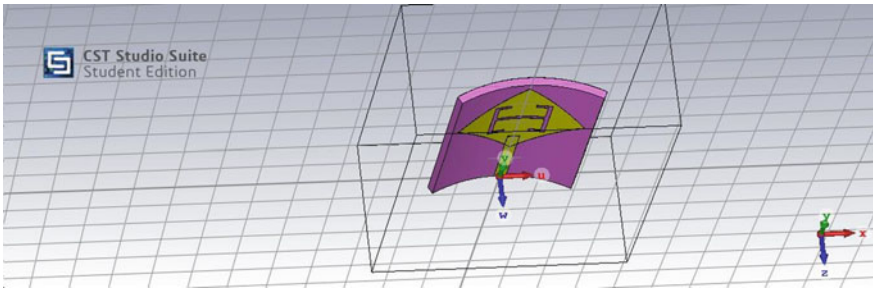

Fig. 8 Antenna under bending condition

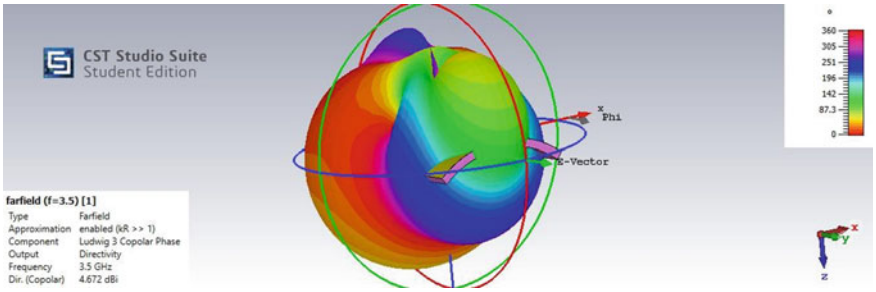

Fig. 9 Directivity measurement—under bending

Fig. 10 Structure of fabricated antenna

is made use of foam material of 2 mm. All the layers are stacked and are connected with the SMA connector via coplanar waveguide (CPW) feed.

4 Results and Discussion

The fabricated antenna is tested using Vector Network Analyzer Agilent Technologies N99223A [26] as shown in Fig. 11. The S_{11} parameter and VSWR measurement of the fabricated antenna are shown in Figs. 12 and 13, respectively. The result shows that the return value VSWR is measured as −24.95 dB and 1.24 at 3.4 GHz frequency, respectively.

From the results, the S_{11} of the simulated antenna is measured as −34.6 dB, where the S_{11} of the fabricated antenna is measured as −24.95 dB. The VSWR of the simulated antenna is measured as 1, where the VSWR of the fabricated antenna is measured as 1.2.

Comparing the simulated antenna and fabricated antenna measured results as shown in Table 3; the values of S_{11} parameter and VSWR are very much matched and satisfactory. The proposed antenna has compact size (50 mm × 36 mm) and low thickness (2 mm) when compared with work [21] whose antenna size is 62.6 mm × 41.6 mm and substrate thickness of 3 mm and work [22] whose antenna size is 60 mm × 60 mm. Due to its compact, it can also be fit with any kind of new wireless

Fig. 11 Testing of antenna using vector network analyzer

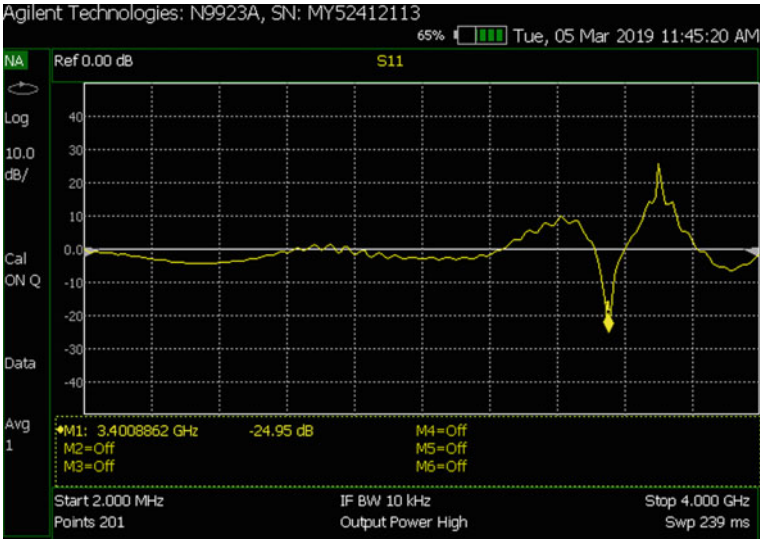

Fig. 12 S_{11} parameter measurement of fabricated antenna using vector network analyzer

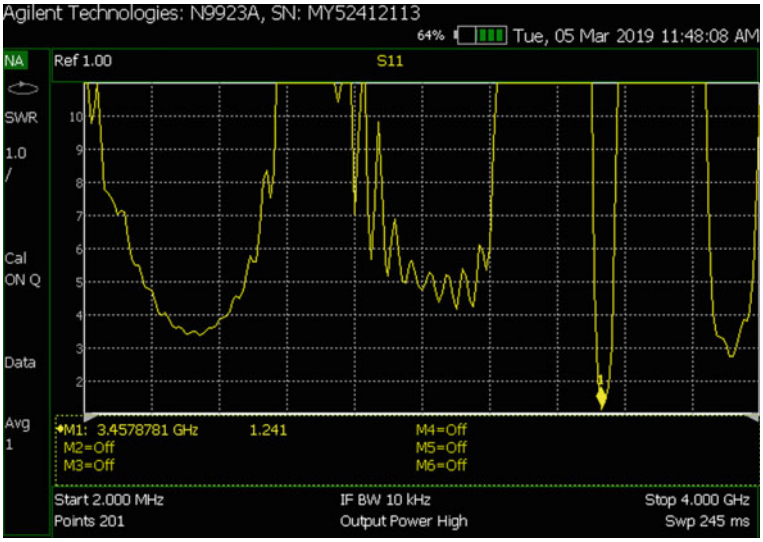

Fig. 13 VSWR measurement of fabricated antenna using vector network analyzer

Table 3 Comparison of simulated and measured values of the antenna

Parameters	Simulated	Measured
Return loss	−34.6 dB	−24.95 dB
VSWR	1	1.2

communication device. The foam substrate also does not absorb water content which makes it to employ in outside environment appliances also. Moreover, the directivity is satisfactory for both flat and bending conditions.

5 Conclusion and Future Scope

The proposed antenna is the key approach to use foam fabric as flexible substrate. The simulated (−34.6 dB) and measured (−24.95 dB) values of reflection co-efficient, S_{11} is in good agreement. The directivity obtained under flat (4.23 dBi) and bending (4.67 dBi) conditions is also satisfactory. Thus, the overall results show that foam fabric act as an acceptable candidate for flexible applications. Due to lightweight, long durability, washable, water resistant, and low cost, it is possible to take over the rigid board substrate materials. Therefore, the satisfactory performance and compactness of the antenna prove it to be deserved for diverse portable wireless applications particularly for wearable medical application and WLAN/WiMAX applications. Further, reducing the dimension will employ the antenna inside the cellular devices for 5G applications.

Reference

1. Huang H Flexiblewirelessantennasensor—areview.iEEESensJ 13(10):3865–3872 (2013). https://doi.org/10.1109/JSEN.2013.2242464
2. Pandimadevi M, Tamilselvi R, Parisa Beham M Design issues of flexible antenna—a review. Int J Adv Trends Comput Sci Eng 1386–1394 (2019). https://doi.org/10.30534/ijatcse/2019/55842019
3. Want R An introduction to RFID technology.IEEE Pervasive Comput 5(1):25–33 (2006). https://doi.org/10.1109/MPRV.2006
4. Asnani V,Bauda S (2019) TriplebandmicrostrippatchantennausefulforWi-Fi andWiMAX. IETEJ Res. https://doi.org/10.1080/03772063.2019.1582365
5. Desai A, Upadhyaya T, Patel J, Patel R, Palandoken M (2020) Flexible CPWfedtransparentantenna for WLAN and sub-6 GHz 5G applications, vol 62, Issue 5, pp2090–2103
6. Sekkal S, Canale L, Asselman A (2020) Flexible textile antenna design with transparent conductive fabric integrated in OLED for WiMAX wireless communication systems. In: 2020IEEEinternationalconferenceonenvironmentandelectricalengineeringand2020 IEEE industrial and commercial power systems Europe (EEEIC/I&CPS Europe). Madrid, Spain, pp. 1–4. https://doi.org/10.1109/EEEIC/ICPSEurope49358.2020.9160757
7. Reis P, Virani HG(2020) Designofacompactmicrostrippatchantennaofflame resistant-4substrate forwirelessapplications. In:2020internationalconferenceonelectronicsandsustainable communication systems (ICESC).Coimbatore, India, pp 713–716. https://doi.org/10.1109/ICESC48915.2020.9156024
8. Kumar Y, Gangwar RK, Kanaujia BK (2020) Characterization of CP radiations in a planar monopole antenna using tuning fork fractal slot for LTE band13/Wi-Max and Wi-Fiapplications. In: IEEEAccess, vol 8, pp127123–127133.https://doi.org/10.1109/ACCESS.2020.3008285
9. Nouri L, Yahya S, Rezaei A (2020) Design and fabrication of a low-loss microstrip low pass-bandpass diplexer for WiMAX applications. In: China communications, vol 17, no 6, pp 109–120. https://doi.org/10.23919/JCC.2020.06.009
10. Bansal A, Gupta R (2018) A review on microstrip patch antenna and feeding techniques.IntJInfTechnol.https://doi.org/10.1007/s41870-018-0121-4
11. Carver K,Mink J(1981) Microstripantennatechnology.IEEETransAntennas Propag 29(1):2–24. https://doi.org/10.1109/TAP.1981.1142523
12. Legay H, Shafai L (1994) New stacked microstrip antenna with large bandwidth and high gain. In:IEE proceedings—microwaves, antennas and propagation, vol 141, no 3, pp 199–204. https://doi.org/10.1049/ip-map:19941041
13. Mao CX, Zhou Y, Wu Y, Soewardiman H, Werner DH, Jur JS (2020) Low-profile strip-loaded textile antenna with enhanced bandwidth and isolation for full-duplex wearable applications. IEEE Trans Antennas Propag 68(9), 6527–6537. https://doi.org/10.1109/TAP.2020.2989862
14. Dwivedi S, Rawat A, Yadav RN (2013)Design of U-shape microstrip patch antenna for WiMAX applications at 2.5 GHz. In:2013 tenth international conference on wireless and optical communications networks (WOCN). Bhopal, pp. 1–5. https://doi.org/10.1109/WOCN.2013.6616214
15. Parashar K, Singh V (2014) Microstrip patch antenna for WiMAX/WLAN applications. Appl Phys Lett 1:34–37 (ISSN: 2349-1108)
16. Bah AO, Gucuyetkin G (2020) Design of microstrip patch antenna for wimax applications. Int J Electric Electron Data Commun 6(6). ISSN(p): 2320-2084, ISSN(e): 2321-2950
17. Baabdullah F, Affandi A, Dobaie AM (2016) Design microstrip patch antenna for WiMAX applications at 8.5 Ghz. Int Org Sci Res (IOSR) J Electric Electron Eng 11(3): 74–78. p-ISSN: 2320-3331, e-ISSN: 2278-1676, Version IV
18. Prahlad RA, Prasanna KM, Jugale AA, Ahmed MA (2019)Microstrip patch slot antenna design for WiMAX and WLAN applications. In: ICOEI-third international conference on trends in electronics and informatics. Tirunelveli, India, pp 810–814. https://doi.org/10.1109/ICOEI.2019.8862578

19. Osklang P, Charoenpanich CP, Akkaraekthalin P (2019) Triband compactprintedantennafor2.4/3.5/5 GHzWLAN/WiMAXapplications.Int J Antennas Propag Article ID 8094908. https://doi.org/10.1155/2019/8094908
20. Dey AB,Talukdar B,Debnath S, Arif WDesignofflexibleanddualwideband antenna for compact wireless devices. In: 2019 IEEE international conference on advanced networks and telecommunications systems (ANTS). GOA, India, pp 1–6. https://doi.org/10.1109/ANTS47819.2019.9118120
21. Gupta N, Singh VK, Ali Z, Ahirwar J (2016) Stacked textile antenna for multi band application using foam substrate. In: CMS-2016 international conference on computationalmodelingandsecurity,Elsevier,ProcediaComputer Science85:871–877
22. Pauria IB, Kumar S, Sharma S (2012) Design and simulation of E-shape microstrip patch antenna for wideband applications. Int J Soft Microstrip Patch Antenna Wideband Appl; Int J Soft Comput Eng (IJSCE) 3(2). ISSN: 2231-2307
23. Saeed SM, Balanis CA, Birtcher CR (2016) Inkjet-printed flexible reconfigurable antenna for conformal WLAN/WiMAX wireless devices. IEEE Antennas Wirel Propag Lett 15:1979–1982. https://doi.org/10.1109/lawp.2016.2547338
24. CST homepage,https://www.3ds.com/products-services/simulia/products/cst-studio-suite/
25. Balanis CA (2016) Antenna theory: analysis and design, 4th edn. Wiley publications. ISBN: 978-1-118-64206-1
26. Key sighthomepage, https://literature.cdn.keysight.com/litweb/pdf/5968-5260E.pdf

Breast Cancer Prediction Through Multilayer Artificial Neural Network

Kumari Alka and Rajeev Kumar Gupta

Abstract In the current era, neural networks are playing a significant role in many sectors, especially in health care. In this work, the neural networks will be used for the diagnosis of disease, i.e., cancer. The proposed work designs a multilayer deep neural network to predict whether the person is a cancer patient (malign) or a healthy person (benign). This work evaluates the performance of the two-layer neural network and multilayer neural network with diverse activation functions like rectified linear unit (ReLU), softmax, and sigmoid. The proposed model uses ReLU activation function in the hidden layer and sigmoid activation function in the output layer. After evaluating the result, it can be stated that a multilayer neural network is performing better as compared to the two-layer neural network and achieved an accuracy of 97.7%.

Keywords Sigmoid · Rectified linear unit (ReLU) · Multilayer · Artificial neural network · Accuracy

1 Introduction

Nowadays, cancer is one of the main causes of death in the world today. The death rate is rising regularly. The levels of death from cancer over the next few days are predicted to increase. In 2017, 1,688,780 cancer new cases have been diagnosis, whereas 600,920 deaths cases were identified in the USA. The study says that male having 20% higher than the probability of cancer as compared to females, and the death rate for males was 40% higher [1]. Through 2030, more reports are likely to be published. We need smart diagnostic tools for this type of disease, and this type of illness can be significantly lowered. This can lead to decreased cash

K. Alka · R. K. Gupta (✉)
Sagar Institute of Science & Technology, Bhopal, India
e-mail: rajeevmanit12276@gmail.com

K. Alka
e-mail: alkasingh582@gmail.com

D. K. Sharma et al. (eds.), *Micro-Electronics and Telecommunication Engineering*,
Lecture Notes in Networks and Systems 179,
https://doi.org/10.1007/978-981-33-4687-1_20

losses and injuries, resulting in medical errors. We have to be vigilant when implementing this kind of smart program. The big issue with the system design is that growth in the proportion of patients increases the number of cases. Predicting is very straightforward, but when the number of patients rises, is difficult. Suppose we have smaller patients or criteria. Even by observing several advanced and experienced professional people, the relationship is complicated to determine in several parameters. That's the only explanation we saw in recent decades that computer detection equipment has been rapidly growing and allowing doctors to eliminate design errors effectively. This equipment minimizes human error and provides precise medical information. Machine learning technology has dramatically improved in the identification of diseases in the last few regions. Even such machine learning algorithms have rapidly increased with substantial predictions [2] in the area of scientific studies.

There are several cancer-related works of literature are available, and most of the literature is on cancer diagnosis [3]. The time estimation method is used for the identification of cancer and patients without cancer. They do use hybrid classification schemes, primarily associated with the current classification scheme. We have found that none of us, even in the report, discussed the cost of misclassifying this disease. This is mainly because we have regular algorithms such as Naïve Bayes [4], SVM [5], and K-NN [6]. But in this article, we introduced the idea of a comprehensive learning approach in order to differentiate between cancer patients and cancer-free patients. Deep learning is just part of machine learning, but here we use our term artificial comprehension. We will also see how this profound principle works better than the regular algorithm of classification.

ANN is among the most advanced automated data mining techniques, such as classification and regression (monitored learning) [7]. Many articles found that the diagnosis of breast cancer by ANN was extremely accurate. This process involves initially building the system for the model, modifying the parameters in the training period, such as the set of sample nodes, remote nodes, initial weights and output nodes, the level of learning, and the activation function.

2 Algorithm and Dataset

The key aim of this paper is to identification or prediction of a malignant or benign tumor in breast cancer.

2.1 Dataset

The Kaggle competition diagnostic data was taken from the Wisconsin Breast cancer dataset and can be found at the UCI learning repository [8]. The dataset has 569 × 32 dimensions, 30 real attributes, and one numerical attribute (field Id), and one

categorical name. This dataset has two class values to be classified as M (malignant) and B (benign) since this is a two-class classification problem, also called the binary classification problem. For each cell nucleus, 10 real-life characteristics are calculated as radius, texture, perimeter, area, smoothness, compactness, concavity, concave points, symmetry, and fractal dimension.

2.2 Classifiers

The classification technique used in the learning process is discussed in this section. The algorithms of classification, we will be tackling, are Naive Bayes, random forest [9], logistic regression [10], and SVM, and drive them toward the neural network and deep learning algorithm [11], which includes CNN [12].

2.2.1 Naïve Bayes

This is one of the most standard algorithms for classification and it can also be used when the probability estimation is of some distance. It has a less training time because data samples are predicted based on the probability only. Although it has less training time, but we cannot trust the accuracy of the Naïve Bayes classifier because it assumes that all features in the given dataset are independent. It is generally used for big datasets. It is a linear, classifying, predictive, and estimated algorithm. There are different kinds of algorithms to distinguish between the healthy and unhealthy person.

Nevertheless, there are other algorithms with different variations, processing times, and continuous binning statements. There is no other way to define them. Naïve Bayes faced several problems and one of the easiest to submit for large datasets. The likelihood is considered its predictive factors for the party when provided.

The prediction contains the following steps:

Naïve Bayes knows that the training set has no class value. The predictive test package is now available. Only if Cx and Cy fulfill the criteria is consistent for a test set T

$$P(Cx) > P(Cy) \quad \text{for } 1 = y = m,\ y! = x$$

P represents probability, and both $P(Cx|T)$ and $P(Cy|T)$ are considered the higher probability as the predicted class for T.

2.2.2 K-Nearest Neighbors (K-NN)

K-NN is one of the most common algorithms for machine learning for distance-based classification [13]. There should be no learning mechanism focused on instances only. The entry set we thought was a training set, and the selection or estimation of the new object was mixed with a remote feature. It takes a '*n*' value that is a number integral and the new objects are grouped into *n*. If the distance between the objects is smaller, the current object is of the previously resident object class and is removed from the other object of different classes until the new object is called. We also use Euclidean approach for distance measurement. As this figure illustrates:

Class A and class B are of two categories which are shown in Fig. 1, class A is represented by blue and class B is represented by purple. Now, a new object X that must be anticipated to the class. For example, $n = 3$ shows that the distance to that particular new object from the nearest 3 is calculated. This equation takes less of the calculated distance, since this function focuses on our expected function and the new object x. Therefore, it is clearly shown in the Fig. 1 that class A consists of x.

Simple K-NN algorithm

i. Consider the neighbor's worth *n*.
ii. The number of S samples is known as their class input.
iii. Take the sample class t as c(t).
iv. A new sample x was entered for the class to be predicted.
v. The distance of x is now established from the neighbors.
vi. Combine the class of x samples in one class c.
vii. The class c consists of x.

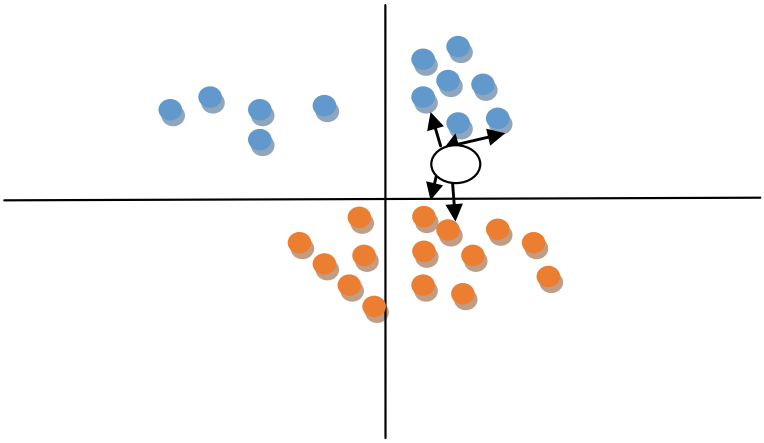

Fig. 1 Representation of K-NN

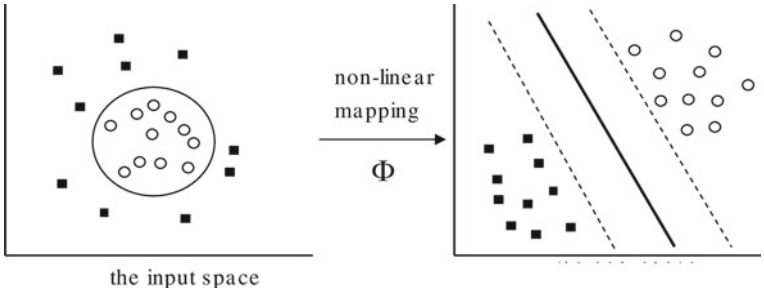

Fig. 2 Representation of SVM

2.2.3 Support Vector Machine

SVM is a linear classification which works as a binary classification. Vapnik presented it for the first time and demonstrated its effectiveness in the field of pattern recognition [14]. Even for a small dataset, this has been proved many times better than other classification. If dataset consists of m samples and x_i represents the feature matrix and y_i represents the target vector then

$$(x_1,\ y_1),\ (x_2,\ y_2), \ldots,\ (x_m,\ y_m)$$

The kernel that plots nonlinear input space into the new linear space is based on a linear SVM technique as shown in the Fig. 2. All vectors are shown to be -1 on one side of the hyperplane and $+1$ on that other. Trained zones next to the hyperplane are called support vectors in the transformed space. The supporting vectors are smaller in size than the training set, so people determine the hyperplane margin and the decision.

3 Proposed Methodology

The ANN with a backpropagation algorithm was implemented, and it showed how nerve network-based algorithms could be better than traditional machine learning algorithms such as Naïve Bayes, SVM, and K-NN. This project involves two main steps:

1. Preparing of data
2. Model building
3. Preparation of data.

This is an essential step in the purification, processing, and non-structuring of the data. The phase is essential for the model building, it should be noted that useful data are more important than a good model. There are 569 samples of 33 features in

Model

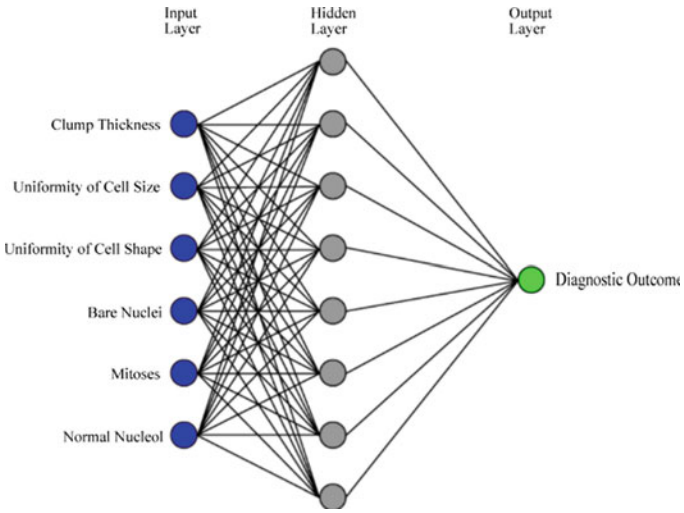

Fig. 3 Artificial neural network

the dataset. The last unnamed column: 32 is a vacant, useless column, so I delete it. Next, the function and label data are separated (target). The typical data is that the models are educated and that the target data are a test showing the tumor is malignant or benign. Since the true labels are (M, B), I decrypted them to 1, 0. Then, I divided the information in two groups, i.e., training and test sets. It is because of my random collection of data for the entire system that the strongly correlated, randomly sampled system has been divided into 70:30.

We cannot train the whole model on the entire data, because it results in an overlap. After all, we separate data between training sets and test sets. In other words, the model is good at training data and struggles with new invisible data (i.e., a low exercise error and a high and high testing error).

In the data processing phase, the final task is to scale features; here, we convert data to make it within a single range for every value. This makes forecasting and executing easier for our model. The standard scalar function converts the mean = 0 and the standard deviation = 1 of each variable of the results. We have used dispersion to see the similarity of the function selection features.

Model.

Artificial neural networks (ANNs) are part of artificial intelligence, which evolves and learns from data using different optimization techniques and predicts new invisible information (tests).

Steps:

1. Architecture of network

2. Forward propagation
3. Backward propagation
4. Weights updation
5. Testing and calculation of performance.

Network parameters like input, output, hidden, rates, and epochs are defined by network architecture. Advanced propagation is the first step in network growth, multiplying the input node by weight, and providing value from [0 to 1]. For the next step, the values are entered and multiplied by the weight of the next step.

$$h_j = \sum_{k=1}^{p} w_{jk} x_k \tag{1}$$

$$v_{j=} \frac{1}{1 + e^{-h_j}} \tag{2}$$

$$g_i = \sum_{j=1}^{m} w_{jk} v_j \tag{3}$$

Building the model

In this work, the activation function, the first is sigmoid, and the second is ReLU [15]. Both functions are used at hidden layers and in the output layers. The next function is ReLU [15]. This new approach also shows how these functions perform in the neural two-layer and neural multilayer networks. This also showed improvement compared to other cutting-edge algorithms. The two proposed work as follows.

Algorithm-1 Network with two layers

A two-layer neural network is completely connected. The system has a loss function and cross-entropy. A ReLU or sigmoid activation function [16] is used for the input layer. At the output layer, sigmoid is the only activation function used. The second fully connected layer output varies from 0 to 1.

1. Two-layer network class
2. A fit function is calculated for the forward and backward step
3. Computation of weight and gradients
4. Defining the predict function
5. Implementation of predict function.

Algorithm-2 Network with multi layers

1. Multilayer network class
2. A pre-activation linear function of the layer is computed
3. Computation of backward propagation and gradients
4. Defining the predict function
5. Implement the predict function.

4 Results

We use Python 3 as a simulation language and TensorFlow library to create ANN. Table 1 shows the accuracy for two-layer ANN for different number of epoch, learning rate, and activation function (AF).

Figures 4–7 have shown the accuracy comparison of the two-layer networks based on a different epoch, activation function, and learning rate.

The table above contains more than two layers with multiple functions, but only two activation functions have been listed.

Figures 8–11 have shown the performance based on multilayer model. The measurements of the hidden layer increase marginally and improve the precision of the sigmoid activation. The accuracy is comparable to the maximum accuracy

Table 1 Comparison of accuracy for two layers

Designed model	AF hidden layer	Epoch	Learning rate	Accuracy
ANN with two-layer	Sigmoid	300	0.01	96.1
ANN with two-layer	ReLU	300	0.01	97.0
ANN with two-layer	Sigmoid	400	0.02	96.4
ANN with two-layer	ReLU	400	0.02	94.7

Table 2 Comparison of accuracy for multilayers

Designed model	AF hidden layer	Epoch	Learning rate (LR)	Accuracy
ANN with multilayer	Sigmoid	300	0.01	94.9
ANN with multilayer	ReLU	300	0.01	95.6
ANN with multilayer	Sigmoid	400	0.02	96.01
ANN with multilayer	ReLU	300	0.002	97.7

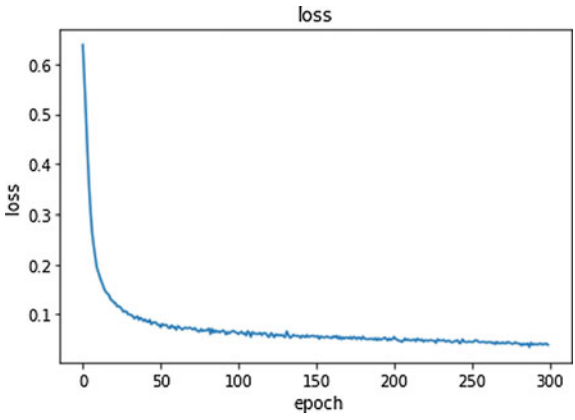

Fig. 4 Sigmoid epoch—300, learning rate—0.01

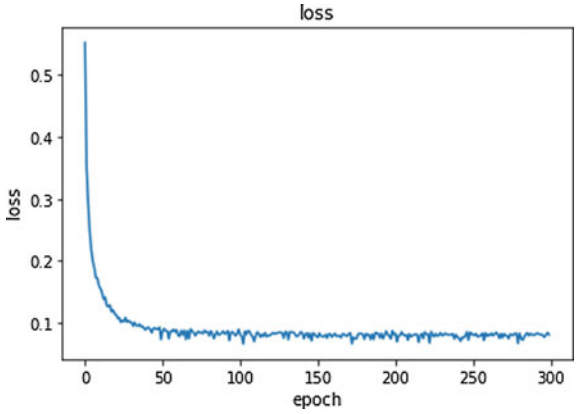

Fig. 5 ReLU epoch—300, learning rate—0.01

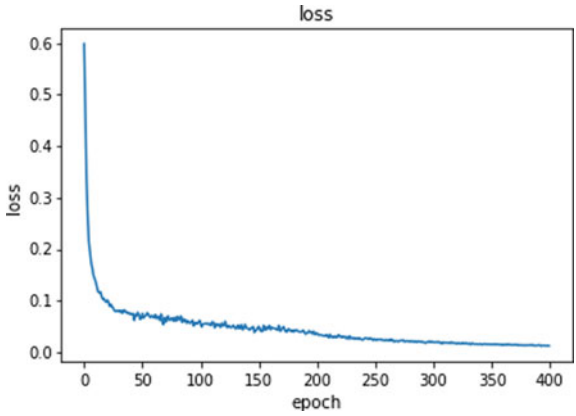

Fig. 6 Sigmoid epoch—400, learning rate—0.02

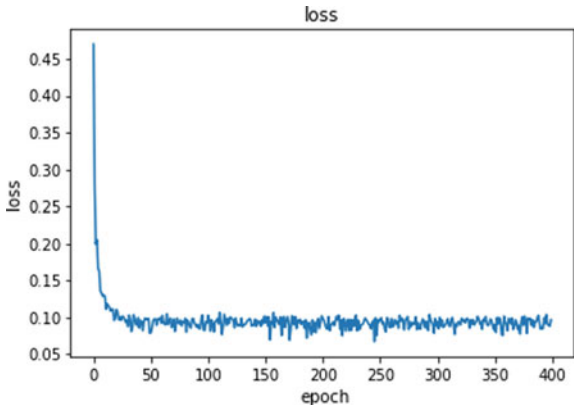

Fig. 7 ReLu epoch—400, learning rate—0.02

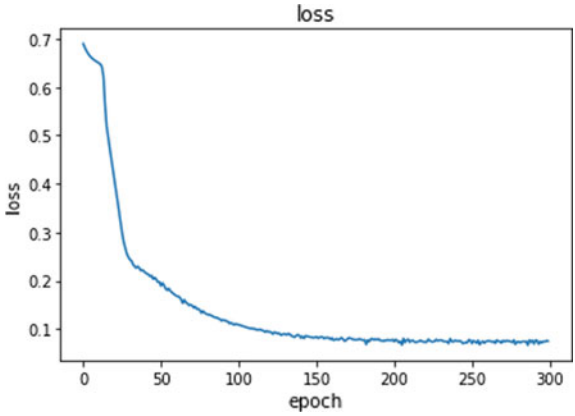

Fig. 8 Sigmoid, epochs = 300, LR = 0.01

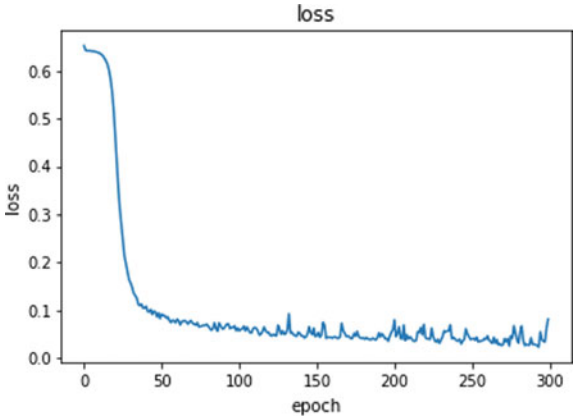

Fig. 9 ReLU, epochs = 300 LR = 0.01

achieved by sigmoid for ReLU activation and is relatively consistent. Activation of ReLU thus can give high accuracy in comparison with the lower hidden layer dimensions of activation of sigmoid.

5 Conclusion

In this paper, single layer and multilayer artificial neural network was designed to predict whether the person is a patient of cancer of not. In order to train model, Wisconsin breast cancer dataset is used which has two classes namely M (malignant) and B (benign). Experiment results say that multilayer neural network with back-propagation gives better result as compare to the single layer neural network. This paper shows the comparative analysis of two-layer and multilayer neural network for different number of epoch, activation function, and learning rate. The multilayer

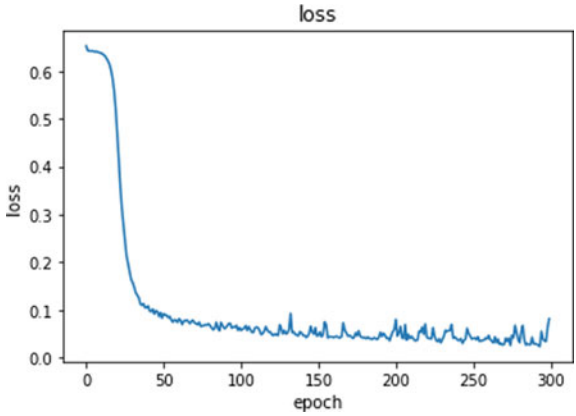

Fig. 10 Sigmoid, epochs—400 learning rate = 0.02

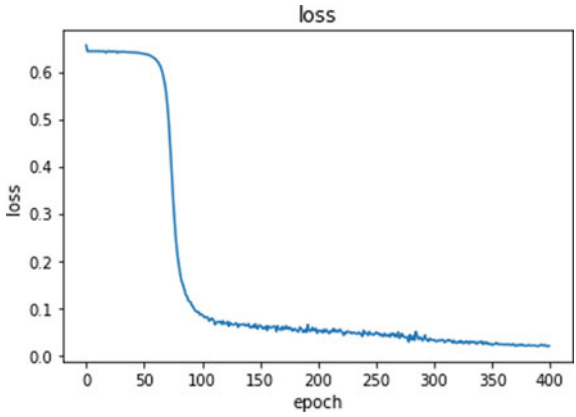

Fig. 11 ReLU, epochs—400, learning rate = 0.02

model with ReLU activation function, 300 epoch, and 0.002 learning rate achieved 97 percent accuracy.

References

1. Newswire PR (2019) Global cancer immunotherapy market: focus on pharmaceutical products, therapeutic indication, competitive landscape and region—analysis and forecast, 2018–2028, NY-REPORTLINKER
2. Spring ML (2015) Machine learning in action
3. Schneider KA (2011) All about breast cancer. In: Counseling about cancer
4. Asri H, Mousannif H, Al Moatassime H, Noel T (2016) Using machine learning algorithms for breast cancer risk prediction and diagnosis. Proc Comput Sci 83, Fams:1064–1069
5. Akay MF (2009) Support vector machines combined with feature selection for breast cancer diagnosis. Expert Syst Appl

6. Li R, Sun Y (2010) Diagnosis of breast tumor using SVM-KNN classifier. In: Proceedings—2010 2nd WRI global congress on intelligent systems, GCIS 2010
7. Amato F, López A, Peña-Méndez EM, Vaňhara P, Hampl A, Havel J (2013) Artificial neural networks in medical diagnosis. J Appl Biomed
8. Worlberg W, Street WN, Mangasarian O (2011) UCI machine learning repository: breast cancer wisconsin (diagnostic) data set. https://archive.ics.uci.edu/ml/datasets/Breast+Cancer+Wisconsin+%2528Diagnostic%2529
9. Rigatti SJ (2017) Random forest. J Insur Med
10. Davis LJ, Offord KP (2013) Logistic regression. In: Emerging issues and methods in personality assessment
11. Lecun Y, Bengio Y, Hinton G (2015) Deep learning. Nature
12. Krizhevsky A, Sutskever I, Hinton GE (2017) ImageNet classification with deep convolutional neural networks. Commun ACM
13. Hu LY, Huang MW, Ke SW, Tsai CF (2016) The distance function effect on k-nearest neighbor classification for medical datasets, Springerplus
14. O'Rourke J, Toussaint GT (2017) Pattern recognition. In: Handbook of discrete and computational geometry, 3rd edn.
15. Li H, Wang J, Tang M, Li X (2017) ReLU. J Opt Soc Am A Opt Image Sci Vis
16. Kalman BL, Kwasny SC (2003) Why tanh: choosing a sigmoidal function

Smart Model for Big Data Classification Using Deep Learning in Wireless Body Area Networks

Pradeep Bedi, S. B. Goyal, Rohit Sharma, Dileep Kumar Yadav, and Monika Sharma

Abstract Deep learning is an innovative set of machine learning algorithms and requires human engineering effort in data collection. It can find the optimum set of parameters for network layers by means of a back-propagation algorithm and thereby model complex data distribution structures. In addition, the deep learning architecture has led to enormous achievements in the most recent challenges of machine learning involving sequential information such as text and series data. Big data technology is an asset in this context for modern companies. Smart automation is useful if it is used. The big data consists of large datasets which can, for example, be analysed by machine learning to find comprehensive models and trends. Thanks to new machine learning and big data techniques, businesses are far more effective than ever before in creating long-term market value. Big data's potential real-life applications are not confined to medical, retail, financial and automotive industries. This makes a great impact of the profound learning on the analysis of patient data generated by wireless body area network (WBANs). WBAN is the emerging healthcare technology to help monitor essential signs of the use of biomedical sensors for patients. The tracked data is forwarded to the doctor for an optimum processing under life risks. We need to develop an intelligent model for the classification of large data using deep learning on wireless body networks.

Keywords Big data · Machine learning · Deep learning · Wireless body area networks

P. Bedi (✉)
Graphic Era Hill University, Dehradun, India
e-mail: bedipradeep1983@gmail.com

S. B. Goyal
City University, Petaling Jaya, Malaysia
e-mail: drsbgoyal@gmail.com

R. Sharma
SRM Institute of Science and Technology, Ghaziabad, India

D. K. Yadav · M. Sharma
Galgotias University, Greater Noida, India

D. K. Sharma et al. (eds.), *Micro-Electronics and Telecommunication Engineering*,
Lecture Notes in Networks and Systems 179,
https://doi.org/10.1007/978-981-33-4687-1_21

1 Introduction

As a traditional concept of artificial neural networks, deep learning has developed as well as converging wireless and wire-less networks communication systems. We have carried out a detailed analysis into the use of deep learning methods for analyzing e-health sensitive data and have implemented important deep learning techniques including deep feed networks, auto-coders, convergence neuro trans-parent networks, deep faith networks, the Boltzmann system and the Boltzmann restricted computer.

We have classified Techniques of sensory data acquisition focused on current data generation technology in order to provide as well as emerging deep learning tools is used to accurately interpret sensory data. In addition, we have discussed in depth the open problems and challenges in the smart health sector of large sensed information, with a particular focus on the acquisition of Data and processing considerations from a deep learning technology point of view. The Big data are classified as the data is to be completely analysed to the partially utilising Standard techniques for sampling. Big data were described in the most recent paper [1] as a dataset of mathematical points representing three independent variable, Length, Pace and Variety. The traffic data for the network that is stored on a distributed network intermediate system displays huge volumes of data with large variations of high-speed traffic types [2, 3]. The big data classification of network traffic has two main problems. It is possible to tackle this problem through emerging large-data platforms, such as the Hadoop Distributed File System (HDFS) [4]. The HDFS uses the two concepts called Map and Reduce to take input data to a task, dividing them in smaller fragments (data and tasks). It then distributes tasks and information in a cluster to several nodes and performs those tasks in those nodes. This distribution system contributes to bandwidth and a fault-tolerant system. The second difficulty is to find a strong representation of the data in order to learn the traffic distribution characteristics. You can use the training data set to develop classification and validate classifiers using trial data. This problem of data representation can be dealt with by techniques of representative learning used in ML research [5]. Representational training can help to learn robust data representation that can be used with Big Data Platforms to classify regular and intravenous traffic. The intruder datasets are large-scale, so representational learning can serve as a means to select traffic type classification features (i.e. feature selection). Although Representation-learning does not provide a full answer for classification of big data, the suitability for developing the network intrusion detection method of the new design Unit-Circle Algorithm (UCA) must be examined [6].

This article proposes a special, class separate representation learning platform objective that characterizes the intrusion traffic's geometric representation properties using the unit-circle method that distinguish for intrusions and normal traffic through the network. This technique is called the unit ring machine (URM), since it uses the unit circles and defines the distribution of the unit ring where the unit ring consists of a unit-circle set. It offers a theory and findings based on the extraction of features and distance metrics for a default pair of features, so the feature option is not addressed.

However, to understand function selection variables, a simple selection approach has been presented.

2 Related Work

As the people of humanity are rising, medical jobs are hard to find, frustratingly long waiting times crowd emergency rooms and demand for doctors and staff seems never to be met. Bora [7] had analyze big data trends and deep learning techniques for handling large volumes of data and explore how they are applied while handling wireless stochastic channels. We develop some methods of learning that are expected to help preserve spectrum and to achieve better connectivity reliability. This paper focuses on several current topics related to big data, the positions played by 5 G skills and the advantages that deep learning can offer [7]. Lin [8], then a set of DT and NBC-based models with different configurations of features, the number of SINRs continually and the decision function are generated [8]. Davenport [9], whilst AI can do many healthcare tasks better than or more frequently than human beings, factors for implementation prevent major automation of occupational healthcare for a significant period. Mouzehkesh [10], throughout our suggested MAC solution, these conditions are achieved by evaluating network activity, taking into consideration the cumulative impact of two separate parameters that would represent the equal allocation of the channel to each sensor unit.

3 Advance Deep Learning

Supervised or Unsupervised learning techniques consist in DL for based on many layers of Artificial Neural Networks (ANNs) that are capable of learning for the show in deep architectures [11]. Subsequently, a number of AI fields, including object detection, pattern analysis and material learning as well as natural language processing, demonstrated the state-of-the-art success of such technologies. Besides technical dimensions and complexity of DL designs as hardware advanced, DL approaches have gained from developments in the successful deep-network algorithm are trained including: Addressing deg. One benefit of DL architectures relative to conventional ANN architectures is DL techniques can benefit from raw data hid-den functions.

4 Proposed Methodology

We focused on creative Big Data Analytics tools and tested several health systems with approaches for patients with a range of diseases. There are known critical problems with the large data generated by the user. Now that we have learned a number of data mining method of machine learning for their advantages and disadvantages in the various health research systems, we conclude that we must focus on a single disease in future. We would limit the scope of data collected from diabetic patients and the diseases they are likely to be liver cirrhosis. It will allow us to reduce the limits faced in previous research with a more centered approach. We'd like to develop a cloud-based, context-based Smart Health application [12] integrated with IoThNet embedding medical analysis to help diagnose diabetic patients with inherent liver cirrhosis disease. Our system focuses on high intelligence while taking on the positive aspects of previous systems examined in this paper. We would like to create this framework in accordance with the latest HIP A standards with support from organisations, such as the World Health Organization (WHO) in order to achieve a high level of user acceptability. Our program aims to become an integral part of LHS [13].

5 Analysis of Sensory Data in E-Health

5.1 Convolutional Neural Networks (CNNs)

For vision-based tasks, dense layer-to-layer DNNs are difficult to train and do not scale well. The translation-invariance property of these models is an significant factor. This is not understandable of characteristics that could be transformed in the image (e.g. hand rotation in pose detection). CNNs (as shown in the diagram of [4]) have solved this issue by promoting translation equivariance computing. CNN (as shown detailed CNN process in [5]) provides 2-D feedback (e.g. photo or voice signal). The concentration layer is central to the CNN and is made up of a collection of learn-ing parameters called philtres which, however, have less measurements than the input object [14]. The entire input layer (e.g. if an image is displayed, the philtre transcends the width and length of the image) of each CNN layer during the training phase, and determine the inner value of the input and philtre. Max pooling is a standard method that splits the input space in fields that do not converge and selects the optimal parameter for each section The last significant part of CNN is ReLU, which consists of neurons with activation mechanism in the form of $f(x) = \max(0, x)$. The key distinction between CNNs and completely linked networks is that any neuron in CNNs is related only to a limited subset of data.

5.2 Conventional Machine Learning on Sensed Health Data

Since the implementation of the WSN model, Method of Machine Learning is describe as a feasible option for reducing the cost of capital and network architecture, as well as for improving network life. Currently, Many machine learning techniques incorporate the extraction of features with modality-specific algorithms for manual writing and/or speech recognition [15]. Applications on sensory data for machine learning algorithms are diverse, for example, telemedicine monitoring of air quality, indoor localization and intelligent transport.

5.3 Deep Learning on Sensed Health Data

In deep learning the algorithmic methods'mimic, the brain' are defined. These problems can be resolved through experience learning rather than rule-based learning through a bottom-up approach. The labelled data are used to provide training for the system that builds on previous experiences during the training process [16]. Experience learning is ideal For spam filtering apps. The problem is therefore properly defined, In particular where there are multi-dimensional elements, which in turn raises spatial volumes such that the data accessible become sparse and sparse data training does not produce substantial results. These problems make it clearly show that deep learning is necessary as a deep learning algorithm to address difficult and/or intuitive problems that have little or no high dimensions characteristics. Acharya [17] used deep learning (especially CNN) techniques to diagnose and detect Coronary Artery Disease from the Electrocardiogram (ECG) signals and achieved 94.95% precision.

The authors proposed that the active and automated classification of ECGs should be made possible by the use of deep neural networks (DNN) Acharya et al. [17]. Furthermore, deep learning can view as a border computing for epileptogenicity localization using electroencephalographic (EEG). In this context, authors use deep belief networks (DBN) and EEG data to distinguish positive and negative emotions. Their work resulted in a rating accuracy of 8762%. The writers created a BGMonitor for blood glucose levels to interpret and process the data and make further observations through a deep learning approach. Compared to traditional approaches, study revealed an exactness of 8214%.

The Boltzmann machine (BM) is a special type of neural network consisting of nodes symmetrically connected as shown by neurons which help a BM make decisions on/off. Firstly, the node calculates the z_i input total as the b_i (bias) sum and Both weights for other device links as defined.

$$z_i = b_i + \sum_j s_j s w_{ij} \tag{1}$$

$$P_r(s_i = 1) = \frac{1}{1 + \mathrm{e}^{-z_i}} \tag{2}$$

The network should be a delivery of BM with a status Probability for vectors q and control E (q are show below Eqs. (3) and (4), respectively, when all the neurons are updated in the following sequence:

$$P_r(q) = \frac{1\mathrm{e}^{-E_{(q)}}}{1 + \mathrm{e}^{-E_{(u)}}} \tag{3}$$

$$E(q) = -\sum_i s_i^q b_i - \sum_i s_i^q s_j^q w_{ij} \tag{4}$$

$$E(v, h) = -\sum_i c_i v_i - \sum_i \mathrm{d}_i h_j - \sum_i v_i w_j h_i \tag{5}$$

$$\rho \mathrm{d} f(\vartheta, h) = \frac{1}{Z} \mathrm{e}^{-E(\vartheta, h)} \tag{6}$$

Equation (2) W_{ij} refers in the equation to the weights of the relations between j and i. In order to eliminate the local optima, weights of the connections could be so selected that each energy from each of the vector represents these vectors' costs. The probability is as shown in Eq. (4). Two formations of BM are trained, either in units hidden or without units concealed. There are numerous BM forms, several mentioned below: Boltzmann systems Conditional Create and dispense data vectors in many ways that extend leads to conditional distributions. Mean field Boltzmann machines use the true values of mean fields to calculate the unit status based on the current condition of other units in the network. In RBMs with no two similar connections two layer types (i.e. visible versus hidden) are included. The secret units h should be independent conditionally from the visible unit, to obtain unbiased elements from the set HSI sjidata; strong calculations are, however, necessary to obtain unbiased samples of Hsi sjidata. Function of RBM to energy is mathematically determined as defined by Eq. (4) and is distributed by probability as shown in Eq. (5). d_j and h_j represent the partial weights in the equations of the hidden and visible units, whereas Z refers to the partition factors system in the probability function. The nature of the data required for health care quality assurance and the methods employed to data acquisition are responsible. This phenomenon of sensory data acquisition in medical applications has resulted in the nature of new data acquisition techniques in order to complement "already in use". Because of this data collection process changes, sensory data processing and interpretation have also improved. Recently, these changes have contributed to increased health care quality. In this segment, we address briefly the methods used to collect and process sensory health data in connection with profound learning. In addition, we talk about how deep learning techniques process the created sensory data types. A short taxonomy of data acquirement and processing is explained through diagram in [5]. Most of the

data acquisition is done through wearable and sample sensors as dedicated sensors and mobile device integrated sensors as non-dedicated sensors.

When one layer is started learning, the results can be considered as the input data needed to train another RBM. Sensory Data Acquisition and processing The accurate acquisition and processing of data using Smart Health deep learning is key to the effective of healthcare. A review of the technologies and the deep learning techniques used in three categories: medical imaging, bioinformatics and prediction. It is a very useful for selecting the relevant profound Deep learning techniques while deep learning with problems and challenges in the preceding point. In addition [18], deep learning has also helped with images of MRI, MRI and other sources 3D brain building with Broad CNN and autoencoders, neuronal cell division DNN tube diagnostics and Alzheimer's DNN Diagnosis. Bioinformatics: The deep learning applications in bioinformatics are again being applied in Most terminal diseases diagnosis and treatment. gene selection and gene variants using the deep belief network to sequencing the micro-array data. Predictive analysis: The prediction of diseases has gained popularity as learning technologies have come into being. It is also worth mentioning that sensory data monitoring of health phenomena must be linked to sensory data monitoring of human behaviour in order to improve prediction accuracy. Two sets of experiments were completed.

6 Experimental Results and Analysis

The proposed runtime analysis is performed with OPPORTUNITY. It contains 75% samples for training and 25% testing, and each sample consists of a sequence. The models are run on a GPU with a clock speed of 25 MHz and a RAM speed of 8 GB. The system proposed was based on the model of VGG-16 and the system proposed was composed of the model of AlexNet. In both cases, the classificator was the SVM with the RBF kernel [19].

Human activity data sets are often imbalanced between classes in natural scenes Certain classes which have several specimens, while other classes have just a few specimens; more than 70% of all data were in the null type. The consistency and warning of the class are taken into consideration to measure the ranking, and the formula should be higher than the quality. The weighting classes in line with their survey proportion mitigate class imbalance:

$$F_1 = \sum_j 2w_i \frac{\text{Precision}_i - \text{recall}_i}{\text{Precision}_i + \text{recall}_i}$$

where $w_i = \frac{n_i}{N}$ is the proportion od sample of the ith class, with n_i being the number od samples of the ith class and N being the total number of samples (as shown in Table 1).

Table 1 Existing Model and Proposed Model Value

Model	Training time (s)	Testing time (s)
Existing model	11234.01	7.025
Proposed model	10456.01	3.512

Table 2 show the Comparative Study between different machine learning model

Machine learning	Accuracy	Sensitivity	Specificity
Restricted boltzmann machines (RBMs)	76.9	74.3	82.10
Deep connet	86.6.6	76.2	95.2
VGG approach	86.59	78.91	95
Proposed approach	90.32	80.60	95.70

Table 2 show the comparative analysis the existing model and proposed model Restricted Boltzmann machines (RBMs) models have reached a device sensitivity of 74.3% and 78.57% and a speciality of 82.10% and 76.9%. Displays precision, sensitivity and system specificity using both models. The Deep Connet device achieved an accuracy of 86.6.6%, and achieved an sensitivity of 76.2%.

The system accuracy is 86.59%, while the system was sensitivity % precise in with the use of VGG approach (as shown in Fig. 1). The corresponding records received these 78.91 accuracies. The table indicates that the proposed method obtained greater accuracy for both versions than the other three systems. The system was also more sensitive and specific than the other three. This showed that the proposed method is effective in comparing the method's output [20].

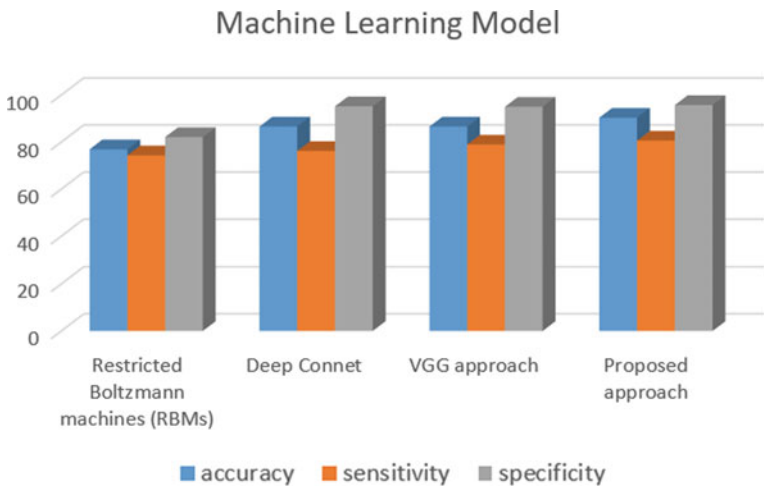

Fig. 1 Show the comparative study between different machine learning model

Precision as the other two systems did. The system proposed was also more adaptive and more precise than the other two. This shows the success of the system proposed.

7 Conclusion and Future Work

Wireless network utilization and the constant miniaturization of electrical devices have enabled Wireless Body Area Network (WBANs) development. Various sensors on the clothes or on the body or even under the skin are connected in these networks. Numerous new, practical and innovative applications enhance the network's wireless nature and the widespread range of sensors. WBAN sensors measure the heart beat, body temperature, or record an extended electrocardiogram, for example. We analyzed the latest research on the Wireless Body Area Networks in this study. In this paper, you will find an overview of human body research, WBAN MAC protocols, WBAN challenges and the various uses in WBAN. In future we will used deep learning based application provided positive feedback, however, but due to the sensitivity of healthcare data and challenges, we should look more sophisticated deep learning methods that can deal complex healthcare data efficiently. Lastly we conclude that there are unlimited opportunities to improve healthcare system.

References

1. Ullah F, Islam IU, Abdullah AH, Khan A (2018) Future of big data and deep learning for wireless body area networks. SpringerBriefs in Comput Sci 53–77. https://doi.org/10.1007/978-981-13-3459-7_5
2. Shafqat S, Kishwer S, Rasool RU, Qadir J, Amjad T, Ahmad HF (2018) Big data analytics enhanced healthcare systems: a review. J Supercomput https://doi.org/10.1007/s11227-017-2222-4
3. Suthaharan S (2013) In: A Single-domain, representation-learning model for big data classification of network intrusion. Lecture notes in computer science, pp 296–310. https://doi.org/10.1007/978-3-642-39712-7_23
4. Ravindran S, Aghila G (2019) A data-independent reusable projection (DIRP) technique for dimension reduction in big data classification using k-Nearest neighbor (k-NN). National Acad Sci Lett https://doi.org/10.1007/s40009-018-0771-6
5. Anthopoulos LG (2017) The rise of the smart city. In Understanding smart cities: a tool for smart government or an industrial trick? Springer, Cham, Switzerland, pp 5–45
6. Chen M, Hao Y, Hu L, Hossain MS, Ghoneim A (2018) Edge-CoCaCo: Toward joint optimization of computation, caching, and communication on edge cloud. IEEE Wireless Commun 25(3):21–27
7. Bora A, Sarma KK (2018) Big data and deep learning for stochastic wireless channel. Studies in computational intelligence, pp 307–334. https://doi.org/10.1007/978-3-662-57277-1_13
8. Lin K-C, Zhang K-Y, Huang Y-H, Hung JC, Yen N (2016) Feature selection based on an improved cat swarm optimization algorithm for big data classification. J Supercomput 72(8):3210–3221. https://doi.org/10.1007/s11227-016-1631-0

9. Davenport T, Kalakota R (2019) The potential for artificial intelligence in healthcare. Future healthcare J 6(2):94–98. https://doi.org/10.7861/futurehosp.6-2-94
10. Mouzehkesh N, Zia T, Shafigh S, Zheng L (2015) Dynamic backoff scheduling of low data rate applications in wireless body area networks. Wireless Netw 21(8):2571–2592. https://doi.org/10.1007/s11276-015-0929-9
11. Sharma R, Kumar R, Singh PK, Raboaca MS, Felseghi R-A (2020) A systematic study on the analysis of the emission of CO, CO_2 and HC for four-wheelers and its impact on the sustainable ecosystem. Sustainability 12:6707
12. Begam SS, JV, Selvachandran G, Ngan TT, Sharma R (2020) Similarity measure of lattice ordered multi-fuzzy soft sets based on set theoretic approach and its application in decision making. Mathematics 8:1255
13. Vo T, Sharma R, Kumar R, Son LH, Pham BT, Tien BD, Priyadarshini I, Sarkar M, Le T (2020) Crime rate detection using social media of different crime locations and twitter part-of-speech tagger with brown clustering. pp 4287–4299
14. Nguyen PT, Ha DH, Avand M, Jaafari A, Nguyen HD, Al-Ansari N, Van Phong T, Sharma R, Kumar R, Le HV, Ho LS, Prakash I, Pham BT (2020) Soft computing ensemble models based on logistic regression for groundwater potential mapping. Appl Sci 10:2469
15. Sharma R, Kumar R, Sharma DK, Son LH, Priyadarshini I, Pham BT, Bui DT, Rai S (2019) Inferring air pollution from air quality index by different geographical areas: case study in India. Air Qual Atmos Health 12:1347–1357
16. Jha S et al (2019) Deep learning approach for software maintainability metrics prediction. IEEE Access 7:61840–61855
17. Acharya UR, Oh SL, Hagiwara Y, Tan JH, Adeli H (2018) Deep convolutional neural network for the automated detection and diagnosis of seizure using EEG signals'. Comput Biol Med 100:270–278
18. Jin Y (2019) Low-cost and active control of radiation of wearable medical health device for wireless body area network. J Med Syst 43(5). https://doi.org/10.1007/s10916-019-1254-0
19. Zhen Y, Liu H (2019) Distributed privacy protection strategy for MEC enhanced wireless body area networks. Digital Commun Netw. https://doi.org/10.1016/j.dcan.2019.08.007
20. Latha R, Vetrivelan P (2020) Wireless body area network (WBAN)-based telemedicine for emergency care. Sensors 20(7):2153. https://doi.org/10.3390/s20072153

Automated Rocker Rover for Terrain Surface Surveillance

R. Vallikannu, B. Meenakshi, Venkata Subhash, Basha, and Chandra KiranKumar

Abstract The methodology used in the Mars exploration and curiosity rover by Mars Science Laboratory is rocker bogie. The term rocker derives from the suspension system with large forward leg on each side of the vehicle chassis on either side which exhibits automated wheel movement, henceforth when one side of the vehicle rocker goes up, the other side goes down and maintain an average pitch level. Earlier research has envisaged that the Rocker-Rovers are much suitable for conducting scientific experiments like travelling to many meters to tens of kilometres. However, the recent mobility designs are complex, using many wheels or legs. Moreover, such rocker bogies can achieve only minimum distance transverse on field like agriculture land, rough land, inclined, stairs and obstacle surfaces which concludes that greater mobility experiments need to be conducted. There are most cases noted that mechanical failures were caused due to harsh environment. Hence, for surveillance in rough terrains, a robust design of rover is required. This paper focused on development of an efficient high mobility suspension system that is capable of travelling through rough terrain using a four wheeled rover. The primary mechanical feature of the rocker bogie design is arrived by using only two motors for mobility and drive line easiness. Motors are located inside the body for increased reliability and efficiency, while considering the thermal variation to be minimum. Increased stability requires both front wheels to be climb first, put forth the necessity of four wheels for driving the rover. The Rocker-Rover suspension system has a vigorous capability to overcome the uneven terrain because of its equal distribution of the pressure over its six wheels. Moreover, this article has implemented a rover with TSM (Total Surveillance Manager) which is an intelligent surveillance and security robot system, designed for monitoring behaviours and activities in the region of interest. The proposed prototype

R. Vallikannu (✉) · V. Subhash · Basha · C. KiranKumar
Electronics and Communication Engineering, Hindustan Institute of Technology and Science, Chennai, TN, India
e-mail: vallikannu@hindustanuniv.ac.in

B. Meenakshi
Electronics and Electrical Engineering, Sairam Engineering College, Chennai, TN, India
e-mail: meenakshi.eee@sairam.edu.in

D. K. Sharma et al. (eds.), *Micro-Electronics and Telecommunication Engineering*,
Lecture Notes in Networks and Systems 179,
https://doi.org/10.1007/978-981-33-4687-1_22

utilizes multiple types of surveillance devices including robots, CCTV cameras, and sensors

Keywords Control · Robotics · Suspension · Webserver

1 Introduction

In the current generation the need for mobile robots are increasing which are used to operate in uneven environments with highly uneven terrain. These robots are especially used in the areas where humans can't interfere and which are not safe for humans. To achieve the task, the mobile robots have to adjust its mobile system according to situation. Mars Rover Sojourner is the mobile robot which is the first kind of suspension design used with rocker—bogie. The current NASA's wheel suspension is different and favourable than the first model. The rocker—bogie suspension is a mechanism which consists of six wheels to able to keep all the six wheels attached to the ground while moving on the severe uneven terrain surfaces. There are two advantages in the rocker—bogie suspension. First advantage of the vehicle is that the pressure on the ground will be equally spread. The vehicle shrinking into the driving surface in soft terrain where excessive ground pressure can be resulted. All the six-wheels will usually remain in contact with the ground surface over the hard and uneven surfaces is the second advantage. The vehicle's motive force capability can be maximized by using drive actuator connected with each wheel, which exploration rovers takes over the advantage. The major disadvantage of rocker-bogie is that they are slow in order to be able to climb or cross the uneven surface without significant risk of flipping the vehicle or damaging of the vehicle, these rovers operate at slow and climb over obstacles by lifting the suspension each piece at a time. On rough surfaces, obstacles are most important, it should consider the situation whether the surface is even or gradual obstacles, accordingly the rover should increase or decrease its rapidity to arrive faster from starting point to ending point. The past space rovers are most commonly used in the development which are reviewed. The mobility, navigation, the design features and capabilities that made the rovers successful in reaching their goal on the Martian or lunar surfaces were explored by researchers.

The mobility challenges of ground compliance and hazard avoidance are reviewed on both hardware and software design choices. NASA current research, testing analogy and evaluation is more focused with planetary rovers on earth. In a variety of grating earth environments are examined for their appropriateness in analog testing based how the rovers are performing on Martian and lunar environments some NASA organized competitions are also observed, as they can often provide different opportunities for analog testing at NASA facilities.

2 Related Work

In Mars path finders and sojourner rover implemented the Rocker-Bogie suspension system by NASA. In the even or un even surfaces the Rocker-Bogie suspension system keep all the wheels of the rover on the ground and increase the traction. Mars Path finder is an American robotic space craft that landed at a base station on mars in 1997. It consists of light weighted wheeled robotic mars rover named sojourner, which became first rover to operate outside the earth moon system [1].

This article is deals with the chain linkage instead of the wheel based. The wheeled-based robots using a linkage mechanism are more stable than caterpillar-based robots. Example Rocker bogie have linkage structure containing of six wheels and a pair of passive joints. By the help of passive joints, the wheels can get contact to the ground while travelling. In the same way shrimp and bogies also demonstrates high stability for example wheel mechanisms cannot travel over holes with large length than its wheel diameter or steps without frontal side.to overcome the limits of wheel-based robots, Shuroetal proposed the RT-Motors, which is a wheel-legged robot consisting of four wheels and a linkage structure. This robot adopts a leg-like axle structure it can move its legs either horizontally or vertically and control them individually. An alternative to the before mentioned are two types of robot mechanisms a new mobile robot is proposed in this project one that has high mobility and stability performance called the *ROCKER—PILLAR* this robot is made up of two caterpillar tracks, four wheels and four linkage structures, so it can maintain its body stability without any actuator while travelling [2].

The dynamic rocker bogie suspension has the same structure of the rocker bogie with six-wheels has been demonstrated. The rocker arm are has divided into two arms which is attached to the gear and can be moved according through dynamically. The rocker arms are moved according to the left or right accordingly and over the upcoming obstacles. The transverse of the wheels is occurred through the high–speed transversal configuration. The Dynamic rocker bogie is mainly done to achieve a greatest stability margin over the high-speed transversal without losing the original configuration, it can be done in two modes by switching between original configuration and high–speed transversal configuration [3].

The analysis about the capability of obstacle climbing ability over the uneven surfaces was presented. It also deals with the planetary exploration i.e., the continuous monitoring over the surface of the planet. It also deals with the space feasible region which is known as is the set of all possible points (sets of values of the choice variables) of an optimization problem that satisfy the problem's constraints, potentially including inequalities, equalities, and integer constraints [4, 5].

Design of a wheel chair using Rocker-bogie suspension for all-terrain was focused primarily. This Six-wheel Rocker Bogie suspension of the wheel chair, make it to move accordingly to the control instruction given by the patient through the joystick attached to the handle of the wheel chair. This work mainly aims at the safety of the patient while shifting from one place to another without any risk, with a speed of 10 km/hr [6].

This work could be further blended to remote real-time monitoring using LoRaIoT which was found more suitable for industrial environment monitoring [7–9].

3 Proposed Method

Firstly, the chassis suspension of the robot is designed by using the FUSION 360 software in which the simulation is done. Later, using this software design the construction of the hardware chassis is constructed. Later the process of the rover is initiated by giving conditions to the rover like detection of ultrasonic sensor 2 which is attached near the wheels of the rover. Then the microcontroller needs to give command to the microcontroller as to go forward and just climb the obstacle which comes in the path of the rover and go continuously. If the ultrasonic sensors 1 and 2 are detected then the rover decides to move in either to the left and if no obstacles detected again it should work accordingly, otherwise the rover should move right and move forward continuously. In this process the PIR sensor attached to the rover is detected then the microcontroller allows the rover to stop and make LED which is attached over the rover to blink. The rover is mainly constructed on these basis:

TSM (Total Surveillance Manager) is an intelligent surveillance and security robot system, which is designed for monitoring behaviors and activities in a wide area utilizing multiple types of surveillance devices including robots, CCTV cameras, and sensors. The proposed work deals with the wheel friction over the surface and make the rover to be fractionized and make the rover strong. It mainly focus on the speed control of the rover on the uneven surfaces, how the motion should be present on the flat and smooth surfaces.

The continuous surveillance of the surface using Quad camera attached to the rover. The starting and stopping of the rover is done by the webpage created [10]. Automatic motion of the rover is set according to the conditions sataed so as to avoid the obstacles whenever necessary, else to climb the obstacles.

4 Implementation

The proposed methodology consists of Ultrasonic Sensors, PIR sensor, Raspberry Pi 3 Microcontroller, Motor Driver L293D, Motors, Camera, LED, Webpage (Fig. 1).

The ultrasonic sensors which is used to find the distance between the rover and the obstacles in the way, the PIR sensor is used to detect the variation of the room temperature is known to the moment of the human or the animal [11]. The power supply required for the every components is 5v but the power supply is outcomes is 12v to convert the 12v power supply to 5v supply a voltage regulator which is fixed in the power supply board converts into 5v. the microcontroller receives 5v. but the motors required 12v to run so the voltage regulator fixed in the motor driver is used to convert 5–12v. The camera which is known as quantum web camera which I

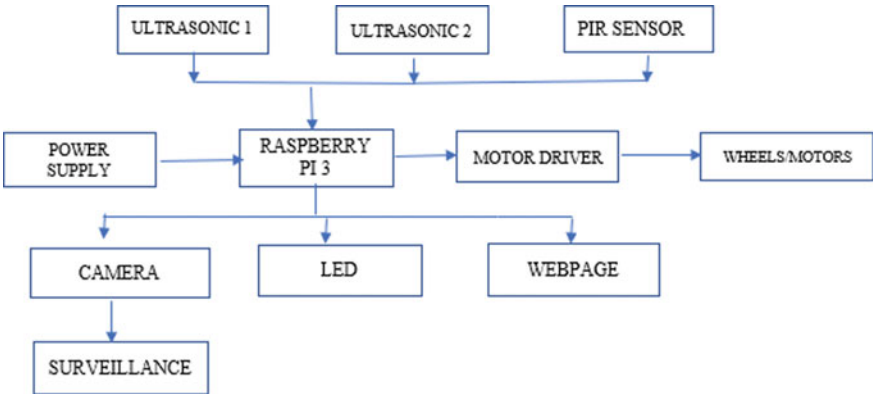

Fig. 1 Block diagram

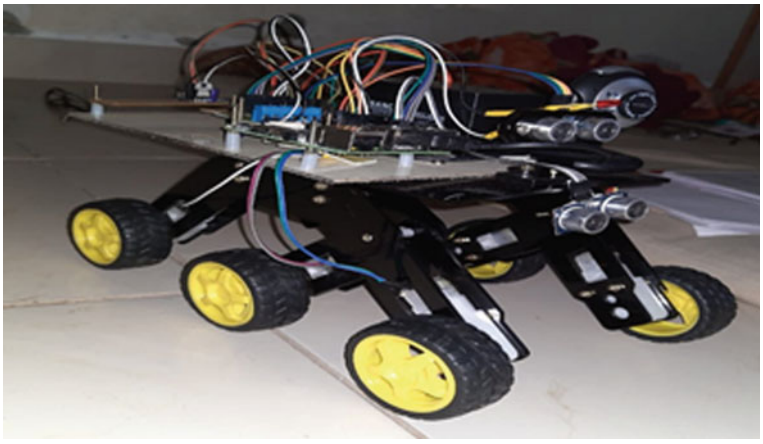

Fig. 2 Hardware kit construction

attached with 6 light sensors results in the surveillance of image in the range of 4 cm to 5 m (Fig. 2)

4.1 Website Development

The website development mainly consists of the Three Buttons Robo, Distance 1, Distance 2, the robo buttons deals with the starting and stopping of the robot [12]. The distance 1, distance 2 are known as the time taken to the rover to reach the obstacle (Fig. 3).

Fig. 3 Rover's webpage design

Fig. 4 Forward and stopping button

When the Robo button is clicked there are two other buttons visible they are forward and stop. The forward button is used to turn ON the rover and it will be displayed as the robot has been turned ON. The stop button is used to turn robot OFF and it will be displayed as the robot has been turned OFF (Fig. 4).

4.2 Hardware Setup

The interfacing of hardware includes connection with the Raspberry pi module is done by using the same internet connection of the mobile hotspot or the WIFI router. And the IP address of the mobile or the router is copied and pasted into the interfacing code which is in build to the Raspberry pi microcontroller and this would allow the connection between the webpage and the rover.

4.3 Mobility

The rover's capacity to overcome varying terrains, slopes, and obstacles relates to mobility. The automated design including the chass is, suspension, and wheel components are the reason for mobility. While moving the rover over the obstacles the rover makes the movement of each piece at one portion at a time. The connection of passive pivot attached to the main bogie are connected distinctive on the other side of the rocker—bogie. This leads to wheel displacement, thereby smoothening the ride of the rocker bogie. Either wheels of the rover are driven independently. To remove asm any dynamic effects as possible the maximum speed of the robots performed in this way. The Rover while crossing over the obstacle, the back wheels forced the front wheels over the obstacles [13]. The rotation of the front wheels forces the wheel to the obstacle to move up and make the rover to cross the obstacle. The middle wheel is forced down until the body is forced to move over the obstacle. Finally, by the help of the two front wheels the rear wheel is grabbed. During this process of climbing the obstacle, the motion of the vehicle's front wheels makes the front wheels to move up is slowed or halted. The same ideology is used in the six-wheeled independent drive to cross the obstacles without any differential method. We choose each individual motor to make the process of overcoming the obstacle easily. However, having one motor for each wheel reduces the need for a difficulty in power transfer system

4.4 Flowchart

See Fig. 5.

4.5 Construction

There are two arms fixed on each side of the rover called as the rocker and the bogie (Fig. 6).

Here AC is the Rocker and the AB is the Bogie. The length of the Bogie is given as the square of the length of the robot is equal to the length of the rocker and the square of the length of the bogie. Here in this application the length of the rocker and the bogie will be same. It is given by Eq. 1,

$$(BC)^2 = (AC)^2 + (AB)^2 \tag{1}$$

Length of the swing arm will be given as the length of the half base is equal to the sum of the length of the Bogie side and square of the length of the half of the swing arm.it is given as Eq. 2,

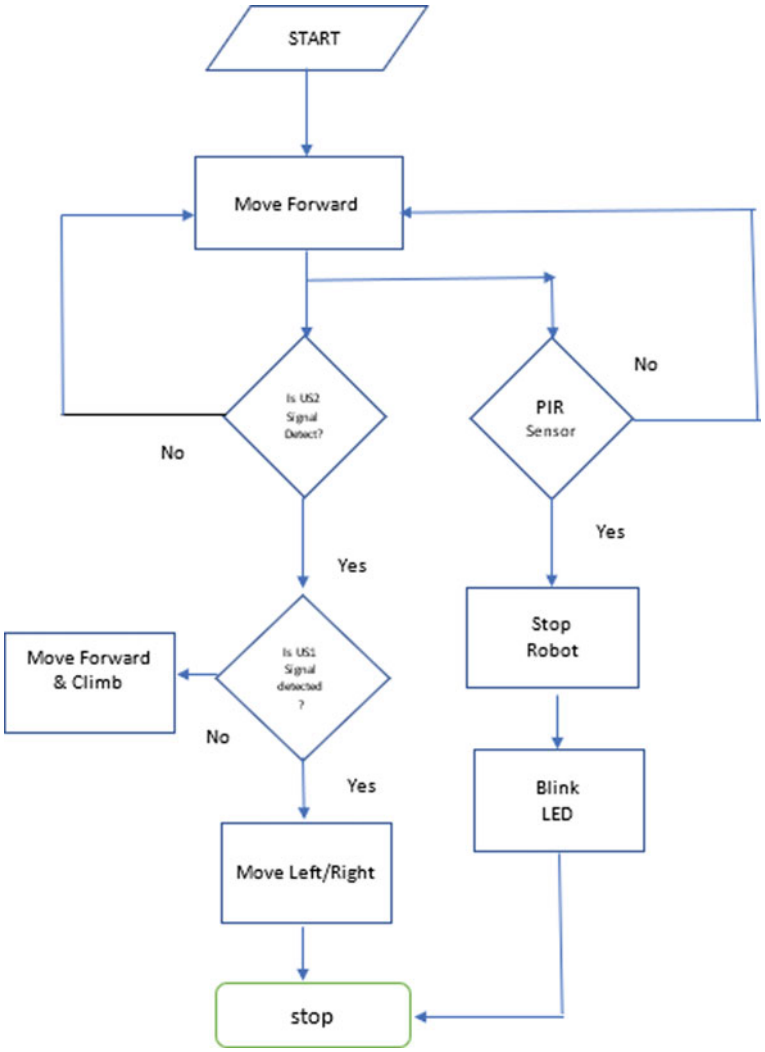

Fig. 5 Rover mobility flow chart

Fig. 6 Bogie design construction sketch

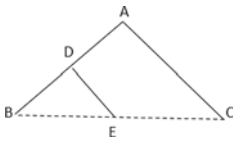

$$(BE)^2 = (DB)^2 + (ED)^2 \tag{2}$$

The angle between the Rocker arm and the Bogie arm is approximately 90 degrees. The swing arm angle with respect to the Bogie arm is 90 degrees.

The height of the Robot will be given as the difference between the square of the bogie arm and square of the half of the base. It is given as Eq. 3,

$$(H)^2 = (AC)^2 + (EC)^2 \tag{3}$$

The net height of the robot will be given as the sum of the height and radius of the wheel. It is given as Eq. 4,

$$(NH) = (H) + (R) \tag{4}$$

where *NH*—Net Height,
H—Height and
R—Radius of the wheel.

The strength to the weight ratio of the proposed rover is defined as the if the weight is given as 1, then the strength of the rover is given as 1.5. Therefore, the ratio of strength to weight is given as 1.5: 1

5 Results

The project designed has overcome the problem identified in the existing system and satisfy the conditions to achieve the objectives such as to overcome the obstacle that comes in the middle of the path and to turn when the both the sensors signals fused detection along with the camera monitoring captured and monitored through webpage that depicts the visual path. Thereby, the concept of autonomous robot is successfully implemented. The webpage Fig. 3 deals with the connectivity of the rover to the webserver. In this screen there are 3 options mentioned over that in that 1. Robo, 2. Distance_01 3. Distance_02. The Robo acts as a link which connects the other page. And there are two things the Distance_01 which detects the distance through the ultrasonic sensor 2. The Distance_02 is detected by the ultrasonic sensor 1. Figure 4 the page deals with the starting and stopping of the robot can be accessible with the web page. When the start button is pressed the robot will start. And the stop button is pressed the robot will be stopped. Figure 2 deals with the Hardware setup of the project with all components attached and which is represent the working model and the process which is acquired is explained below.

In the proposed work there are three modes available they are:

- Firstly, maintaining stability of the rover without flipping.

- Secondly is calculating the distance using the ultrasonic sensors and finding the presence of obstacles on the way and move the Rover Autonomously.
- Thirdly is presence of PIR sensor which detects the presence of human and makes the rover to stop.

The function of the robot is mainly done by using the ultrasonic and the visual screen can be monitored in the output screen in the PC which is used to control the starting and stopping of the rover

6 Conclusion

The proposed prototype with the standard usage of rocker rover in the uneven surfaces has improved stability without slipping or losing control. Thereby using all the six wheels the traction will be given to the rover to move without falling. The developed model of the rover overcomes flipping and may travel a little faster too and make it less cost with maximum possible rigidity and ruggedness. The rocker rover the weight can be manageable while climbing or the coming down by tilting according to the objects occurred on the way.

- Designed and implemented Rocker Rover moves in the uneven surfaces without slipping or losing control by using all the six wheels with traction that helps the rover to get hold with the ground surface without slipping.
- The developed rover doesn't flip and is able to travel a little faster.

It is cost effective with maximum possible rigidity and ruggedness.

7 Future Works

As modular research platform the rover developed by this project is designed specifically to facilitate future work. With the development in technology the rover can be used for exploration (the use of soldiers or aircraft to go into an area and get information about an enemy) purpose of the cameras installed on the rover and minimizing the size of rover. By doing small modifications by attaching arms to the rover it can be used as the bomb diffusing squad by using it for the cutting the wires of the bomb. By development of the project into bigger size it can be used for the transferring of the patients or shifting the people through stairs. We could develop it into a wheel chair too. It can be used for the substitute for the humans in the places like valleys, jungles or such places where people can face danger. It can also be developed into low cost exploration rover that could be send the data collecting information about the environment of some celestial bodies

References

1. Erickson JK (2006) Living the dream-an overview of the mars exploration project. IEEE Robot Autom Magaz 13(2):12-18
2. Chen B, Wang R, Jia Y, Guo L, Yang L (2009) Design of a high performance suspension for lunar rover based on evolution. Acta Astronaut 64(9–10):925–934
3. Nagatani K, Yamasaki A, Yoshida K, Adachi T (20017) Development and control method of six-wheel robot with rocker structure. In: 2007 IEEE International workshop on safety, security and rescue robotics, IEEE, pp 1–6
4. Thomas B, Gold G, Sertic N (2011) Dark rover rocker-bogie optimization design
5. Kumar GH, Ramesh GP (2018) Novel gateway free device to device communication technique for IoT to enable direct communication between homogeneous devcies. Int J Pure Appl Mathemat 118(16):565–578
6. Manik MD, Chauhan AS, Chakraborty S, Tiwari VR (2016) Experimental analysis of climbing stairs with the rocker-bogie mechanism 2(2)
7. Sharma R, Kumar R, Singh PK, Raboaca MS, Felseghi R-A (2020) A systematic study on the analysis of the emission of CO, CO_2 and HC for four-wheelers and its impact on the sustainable ecosystem. Sustainability 12:6707
8. Begam SS, JV, Selvachandran G, Ngan TT, Sharma R (2020) Similarity measure of lattice ordered multi-fuzzy soft sets based on set theoretic approach and its application in decision making. Mathematics 8:1255
9. Vo T, Rohit S, Raghvendra K, Hoang SL, Thai PB, Dieu TB, Ishaani P, Manash S, Tuong L (2020) Crime rate detection using social media of different crime locations and twitter part-of-speech tagger with brown clustering. 4287–4299
10. Kavitha BC, Vallikannu R, Sakthidasan K (January 2020) Delay-aware concurrent data management method for IoT collaborative edge computing environment. J Microprocess Syst 9(2):167–174
11. Ohya A (1998) In: Kosaka A, Kak A (eds) A Vision-based navigation by a mobile robot with obstacle avoidance using single-camera vision and ultrasonic sensing. Robotics and Automation, IEEE Transactions, Institute of Information Science and Electronics, Tsukuba University, Ibaraki, Japan
12. Kavitha BC, Vallikannu R (2018) The Internet of Things model architectures for customized applications: a review. Int J Simul Syst Sci Technol 19(6):32.1–32.6. https://doi.org/10.5013/IJSSST.a.19.06.32
13. Bhole A, Turlapati SH, Rajashekhar VS, Dixit J, Shah SV, Krishna KM (2019) Design of a robust stair-climbing compliant modular robot to tackle overhang on stairs. Robotica 37(3):428–444

Study of MIMO Antenna Design and Challenges—State of Art

Rasika Verma, Rohit Sharma, and Dhirendra Kumar Diwedi

Abstract This paper discusses about the Design and challenges associated with multiple input multiple output (MIMO) antenna. Additional degree of freedom is provided by MIMO with multiple antenna placed near to each other. As UWB technology suffers from Multipath fading, this problem is easily resolved with MIMO technology. Mutual coupling is another problem associated with MIMO systems, this reduces antenna efficiency. MIMO technology is advantageous for data transmission problems so there are great challenges in this technology In this paper study of various parameters like isolation, ECC, peak gain, mutual coupling etc. has been done. Here we present a comprehensive survey on MIMO antenna for wireless communication. Another important issue related with compact MIMO (multiple input multiple output) is space constraint and structure of antenna array. as MIMO antennas are closely spaced, performance of MIMO antenna is reduced due high signal correlation as well as antenna efficiency is reduced. The main aim of the work is to give an idea regarding the recent trends and technologies used in MIMO antenna design and challenges.

Keywords MIMO UWB antenna · Isolation · Mutual coupling · ECC (envelop correlation coefficients)

1 Introduction

MIMO antennas were evolved in year 1993 [1]. This technology is used in wireless communication due to improved bandwidth efficiency and capacity. Federal communications commission (FCC) have provided a frequency band from 3.1 to 10.6 GHz so ultrawide band technology is used for high data rates for easy fabrication and for

R. Verma (✉) · R. Sharma
SRM Institute of Science and Technology, Ghaziabad, India
e-mail: rashikaverma@gmail.com

D. K. Diwedi
RKG Group of Institutions, Ghaziabad, India

D. K. Sharma et al. (eds.), *Micro-Electronics and Telecommunication Engineering*,
Lecture Notes in Networks and Systems 179,
https://doi.org/10.1007/978-981-33-4687-1_23

small distance communication [2], but it suffers from multipath fading. The ultra wide band technology with MIMO technology reduces multipath fading and provides high data rates [2]. So for this problem, a MIMO (multiple input multiple output) antenna was introduced [3]. Whenever two or more antenna's are placed nearer to one another, problem of mutual coupling between them becomes strong so high isolation is very difficult to attain. Due to high mutual coupling antenna performance, efficiency of antenna is reduced so it is necessary to reduce mutual coupling [4, 5]. Mutual coupling is reduced by adopting different techniques. Now a day's research is rapidly moving towards voice to data services as WLAN, Wi-Max, IOT etc. The MIMO system increases various parameters like spectrum efficiency, channel capacity range and link reliability [2]. Major work is done in this area for ultrawide band antennas for wide bandwidth, improved isolation, improved radiation pattern. Multipath fading is a big issue in UWB communications systems, MIMO technology provides less multipath fading and improved channel capacity by improving multiplexing gain and diversity gain. Whenever multiple antennas are placed near to each other, problem of mutual coupling arises and it can be reduced by using different decoupling structure and without using decoupling structure. One major problem with MIMO technology is that for lower frequency, wavelength increases so small size is a big challenge. But if the size is small, fading increases this is also a challenge in MIMO technology. As we already know that antenna spacing is half the wavelength ($\lambda/2$), to achieve good performance it should be taken into account. If further spacing is reduced then again problem of mutual coupling arrises. Here we will emphasize upon problem of coupling and will present different ways to overcome the problem coupling. As well as this paper presents study and evaluation of various antennas designed with good isolation, reduced mutual coupling, good diversity gain and improved channel capacity. Different design and techniques are used for this purpose.

Now a days, due to increasing number of frequency bands design of single antenna is always a research topic for mobile terminals. Without increase antenna implementation or increase in the space given these frequency bands should be covered. For this MIMO Technology is adopted in all major wireless communication standards.

As devices are increasing day by day for high data rates wireless communication is highly supportive [6]. So mostly researchers and subscribers are shifting from 4G to 5G network which is expected to be launched in 2020. In near future most of devices like home appliances, clothes, vehicles will be connected to the internet to communicate with each other through radio frequency. MIMO technology is the best technology to achieve high data rates, high through put and connection of various users. MIMO technology gives low ECC, high isolation and high throughput. In order to achieve better isolation antenna orientation is important and it can be changed to get better isolation and gain in MIMO technology. For independent wireless channel low mutual coupling among different elements of antenna is required. As there is limited space for mobile terminals and increasing number of operating devices there is a great challenge to provide MIMO technology in compact area of mobile phone. So, now a day's building multiple antennas into small volume of a smart phone for 5G communication is a big challenge for researchers as frequency bands for 5G are not issued formally. The major topic of concern for all the countries is sub 6 GHz

bands. For realization of massive MIMO 5G technology most of the countries are focusing on the 3400–3800 MHz band (a combination of LTE band 42 and LTE band 43). This band is important for both traditional and non traditional applications and is key to various broadband 5G applications like internet of things (IoT), Automation and business purposes.

Development in wireless systems and 1G–5G technology, still suffers from various problem. Day by day various advancements are done in engineering and research field to overcome these problems.

2 Review of MIMO Antenna

2.1 Coupling Effects

There is a great impact of coupling in MIMO antenna. As the antenna spacing in terms of wavelength is reduced there is degradation in performance of antenna in terms of diversity and capacity for limited surfaces and frequencies. As there is lack of references for diversity and capacity that is why capacity is based on SNR (dB) and diversity on probability level. Capacity is based on SNR (db) and diversity on probability level.

2.2 Decoupling Techniques for MIMO Antenna

Different strategies have been adopted to achieve decoupling, these techniques are mainly adopted to improve isolation among the antenna which are in close proximity to each other. The performance of MIMO antenna are greatly effected by mutual coupling.

In broader sense decoupling techniques are classified as: (1) Antenna decoupling (2) Circuit decoupling.

Antenna decoupling [7] can be achieved by modifications in structure of antenna by various ways and this can be achieved by implementing different approaches. These different approaches are modifications in plane of ground, neutralization of line, parasitic scatters and diversity in polarization. The most attractive circuit for decoupling is parasitic scatter and this decoupling technique replaces circuit used for decoupling with loaded parasitic antenna which is relatively very efficient.

Another way to achieve good orthogonaltiy (better isolation) at antenna level is to use dielectric resonator antenna structure for the realization of diversity in polarization with in antenna ports. To prove this concept a Maltese shaped DRA Design is used for ultra wideband applications. here antenna is designed with trapezoidal shaped strip. With this structure high bandwidth is achieved(111%). With defected ground structure good isolation is achieved.

Circuit decoupling can be attained by using a matching network(realizes conjugate match) for antenna impedence. Circuit decoupling approach is very efficient as it does not require antenna structure to be modified. This approach requires only knowledge about antenna impedence but is limited by size of matching circuit. On the other hand minutarisation of circuit is achieved by equivalent circuit of lumped circuits. One drawback associated with decoupling circuits is low efficiency at decoupled ports (analysis not yet done).

So perfect decoupling of MIMO antenna, which uses coupled matching network and parasitic scatter can be achieved by compromising for low bandwidth and additional complexity. According to statistics of channel performance of MIMO can be optimised. So for some channel conditions, the performance of uncolupled matching network approaches nearly to coupled matching network.

Coupling in MIMO Antenna increases as spacing among the antenna increases. However when more than one antenna are exploited on ground plane as radiator more dominant coupling mechanism can be achieved. Detailed study of parametric characterstics mode analysis indicates that isolation can be improved if antenna type and location both are optimized. Generally improvement in isolation is of worth if it gives improvement in capacity and diversity gain.

However when antenna element uses shared ground plane for radiation, the ground can contribute to higher coupling.

3 Related Work

Here different methods to reduce coupling in order to increase the isolation by various researchers are presented.

A. Metamaterial technology in MIMO

(1) Metamaterial antenna with spiral shaped resonator isolator: If arrays of metamaterial isolator are used in between two antenna arrays it reduces coupling effect [8]. Metamaterial have negative permeability and permittivity with geometrical sizes less than operating wavelength and it is feasible for small MIMO antenna.

(2) Metamaterial antenna and coupler: It has been found that signals have different route of transmission by using directional coupler. Here metamaterial directional coupler is placed between elements of antenna for enhancing isolation between antenna elements.

B. Multi mode metallic ring MIMO antenna: Here for multimode operation four ports are used symetrically by using this technology. As a result with the introduction of capacitive loading has improved return loss characterstics in comparison with original antenna. It has also been analyzed that by using capacitive loading all modes resonates on single frequency, to achieve this rings are placed at different angles.

C. MIMO Antenna with equilateral patch array: Here the design is optimized for resolving the problem of channel capacity and also different diversity techniques are used. To get particular radiation pattern, diversity in polarization and bandwidth, equilateral triangular patch is used.
D. MIMO antenna used for mobile applications.: In this MIMO antenna system operating at 2.4 GHz is proposed. Initially measurement of return loss and design of single element is done and it is observed that field radiation pattern are functions of the physical location, orientation and polarization.
E. MIMO antenna for Multiband: Here PIFA i.e. printed inverted F antenna which has property to resonate at single frequency is discussed. PIFA employs J shaped slot due to which original PIFA is divided into two parallel PIFA's. Here performance is evaluated on Total active Reflection Coefficient [TARC]. TARC ranges from -6 to -9 dB.Then enhancement is done in a from of four element. From here it is concluded both the MIMO antenna for multiband which is proposed here and array of four monopole antennas with half of wavelength spacing between elements has same channel capacity.
F. MIMO antenna element isolation using Band stop filter: Here a technique for obtaining enhanced isolation between antennas has been proposed. For improving isolation characterstics a band stop filter is placed at corner of each antenna. Due to High coupling between the feeding and shorting lines through the slot, size reduction and bandwidth improvement are achieved. Further it is found that antenna is narrow band for LTE have satisfactory bandwidth at WCDMA/HSDPA and WiMAX. Both antennas have Omni directional pattern over the entire range.
G. MIMO antenna with circular polarization: Here RFID systems uses circularly polarized MIMO antenna system. The elements of antenna have different orientation with respect to each other and air gap substrate for wide bandwidth antenna design is carried out using air gap substrate. Further resonant frequency and bandwidth are measured for antennas.
H. H.Monopole MIMO antenna with decoupling structure: Here researchers designed monopole antenna with two folds which are placed parallel to each other for LTE band. Here the decoupling network used, have two transmission lines which are individually connected to two input ports. The performance is evaluated by determining the correlation coefficient between two ports of antenna and calculated ECC is less than 0.2 over the hole LTE band.
I. UWB MIMO antenna with *F*-Shaped Stubs: In this article, antenna with two radiating elements and shared ground plane have been discussed. Here *F* shaped stubs are inserted in shared ground thus produces high isolation between elements of MIMO. This design results in very low mutual coupling, Low Envelop correlation coefficient and high diversity gain.
J. UWB MIMO Antenna with pattern diversity and Band Rejection: Here researcher proposes a compact size CPW fed ultra wide band MIMO antenna having two elements with notch behavior. It has patch radiator which is semi elliptical and have asymmetric ground plane where notch characterstics are inserted by a folded stub into patch radiator. Here single stop band can be

achieved from 3.3 to 3.9 GHz. (Wi MAX).In this two elements are placed orthogonal to achieve diversity in patterns with improved system performance and omproved isolation ith out decoupling structure. The size of antenna is 50 $\times$ 28 mm^2 and return loss is lower than -10 dB with low insertion loss.

K. UWB MIMO diversity antenna ith dual band characterstics: Here the size of proposed antenna 18 $\times$ 34 mm^2. Notches at WLAN and IEEE Insat/super extended C bands is introduced with the help of inverted L shaped slits used in single radiating element and anteena used is microstrip slot fed. The mutual coupling achieved is less than -22 dB (2.93–20 GHz.). The desirable value of TARC is < 0 dB. The performance of MIMO systems is evaluated in terms of radiation pattern, efficiency, gain, ECC, MEG and TARC.

A detailed survey of MIMO antennas is presented here

In the article discussed by Kedar Trivedi, Dhaval Pujara [9] DRA (Dielectric resonator antenna) antenna for MIMO applications is discussed; here Maltese shaped DRA Design is used for ultrawideband. Antenna is designed with trapezoidal shaped strip. High bandwidth is achieved (111%).here defected ground structure is taken with this mutual coupling < -18db is achieved.

In the work done by Deepika et al. [10] four element planer antenna array is designed for ultrawideband applications. This array does not require decoupling circuit and array can be extended in size. Here slotted annular ring monopole antenna is used for improved impendence matching and high isolation in the range of 3–15 GHz.Without decoupling structure although small size can results but current variations problems occur. It results in Return loss < -10db and coupling is less than -20db.Here ECC (Envelope correlation coefficient) is < 0.05 with channel capacity loss (CCL) < 0.4 b/s/Hz.

In the litreture presented by, Chandrasekhar Rao et al. [11] a compact size (22 $\times$ 26 $\times$ 0.8 mm3) MIMO antenna with dual notched band is designed. here antenna is microstrip feed with T slot and narrow slot (for improving isolation between 3 and 4 GHz) for enhancing impedence matching performance and also provides isolation above 4 GHz. The frequencies that are notched are 5.4–5.86 GHz and 7.6–8.4 GHz. it has return loss greater than 10 db as well as mutual coupling > 20 dB for full bandwidth but not on notched band.

In a work proposed by Li et al. [12] a dual polarised MIMO UWB antenna is designed. Here two antennas are sharing ground plane one is microstrip line which is stepped and other is circular planer monopole. Good isolation is achieved by slotting in the ground plane in different formats like tapered slot, circular slot and L shaped slot. With this impedence bandwidth is improved. Size of 30 $\times$ 30 mm^2 is achieved. Return loss and mutual coupling covers the range from 3.4 to 13.6 GHz and 2.8–19.2 GHz with an isolation > 20 dB for entire range and peak gain variation is of 3.7–9.8 dbi [13].

In the work done by Shobhit et al. [14] a small MIMO (multiple input multiple output) antenna or UWB applications is designed. It incorporates circular polarization for frequencies (5.5 GHz, 5 GHz, 5.2 GHz). By introducing the rectangular arm vertically in ground plane, AR(axial ratio) bandwidth of 34.38% is achieved. For

Table 1 Work comparison in the field of MIMO systems

S. No	Reference	Size of antenna	Substrate used	Return loss/mutual coupling(MC)	ECC	Peak gain
1	[15]	23*18 mm^2	FR4	S11, S21 <−10db	Below 0.1	NA
2	[9]	60*60 mm^2	Roger	MC <−18db	NA	NA
3	[10]	18*18 mm^2	Neltec	S11 <−10db, MC <−20db	ECC < 0.5	0.5–5 dBi
4	[12]	30*30 mm^2	FR4	S11 < -10db	–	3.7–9.8 dBi
5	[11]	22*26*0.8 mm^2	FR4	S11 > 10db, MC > 20db	ECC < 0.03	3.6–6 dBi

enhancement of isolation L shaped radiators were used. Impedence bandwidth of 112.05% and isolation greater than 17 db is achieved. ECC is less than 0.01 and gain is 1.2–4.9 dBi.

4 Comparative Analysis

Here comparison of various work already been done in the field of MIMO systems is shown. This table (Table 1) indicates about different parameters used in antenna design viz size, substrate used, return loss, isolation, ECC and peak gain. This gives an idea, how different design and technology used influences antenna performance.

5 Conclusion

This paper presents a brief review on recent research findings concerning antenna design for MIMO systems. From here it is seen that antenna vary in their design, size, technology, decoupling structure u used, so different design results in enhancement of performance of a practical MIMO system. It is not feasible to carry out an efficient comparison among the antennas. since they vary widely in operating frequency, bandwidth, area, material used etc. There is a need of optimizing the antenna parameters and design procedure for enhanced performance so it is a great challenge for MIMO systems. So from here it is concluded that as we are moving towards 5G and upper 5G this technology had shown lot of scope for research and development in the arena for antenna design.

References

1. Begam SS, JV, Selvachandran G, Ngan TT, Sharma R (2020) Similarity measure of lattice ordered multi-fuzzy soft sets based on set theoretic approach and its application in decision making. Mathematics 8:1255
2. Nguyen PT, Ha DH, Avand M, Jaafari A, Nguyen HD, Al-Ansari N, Van Phong T, Sharma R, Kumar R, Le HV, Ho LS, Prakash I, Pham BT (2020) Soft computing ensemble models based on logistic regression for groundwater potential mapping. Appl Sci 10:2469
3. Sharma R, Kumar R, Sharma DK et al (2019) Inferring air pollution from air quality index by different geographical areas: case study in India. Air Qual Atmos Health 12:1347–1357
4. Biswas AK, Chakraborty U (2019) Compact wearable MIMO antenna with improved port isolation for ultra-wideband applications. IET Microwaves Antennas Propagation **13.4**:498–504; Saxena S et al. (2017) A compact dual-polarized MIMO antenna with distinct diversity performance for UWB applications. IEEE Antennas and Wireless Propagation Letters 16 (2017): 3096-3099
5. Sharma R, Kumar R, Singh PK, Raboaca MS, Felseghi R-A (2020) A systematic study on the analysis of the emission of CO, CO_2 and HC for four-wheelers and its impact on the sustainable ecosystem. Sustainability 12:6707
6. Dioum I et al. (2018) Miniature MIMO antennas for 5 g mobile terminals. In: 2018 6th International conference on multimedia computing and systems (ICMCS), IEEE
7. Lau BK Ying Z (2011) Antenna design challenges and solutions for compact MIMO terminals. In: 2011 International workshop on antenna technology (iWAT), IEEE
8. Jamil A, Yusoff MZ, Yahya N (2010) Current issues and challenges of MIMO antenna designs. In: 2010 International conference on intelligent and advanced systems, IEEE
9. Trivedi K, Pujara D (2018) Mutual coupling reduction in UWB modified maltese shaped DRA array for MIMO applications. In: 2018 48th European microwave conference (EuMC), IEEE
10. Deepika S, Abegaonkar MP, Koul SK (2017) Easily extendable compact planar UWB MIMO antenna array. IEEE Antennas Wireless Propag Lett 16:2328–2331
11. Chandrasekhar Rao J, Nandanavanam VR (2018) Trident-shape strip loaded dual band-notched UWB MIMO antenna for portable device applications. AEU-Int J Electron Commun 83:11–21
12. Li Z, Zhu X, Zhang J (2018) Compact dual polarized MIMO antenna for UWB communication applications. In: 2018 8th International Conference on Electronics Information and Emergency Communication (ICEIEC). IEEE
13. Vo T, Sharma R et al (2020) Crime rate detection using social media of different crime locations and twitter part-of-speech tagger with brown clustering, pp 4287–4299
14. Jha S et al (2019) Deep learning approach for software maintainability metrics prediction. IEEE Access 7:61840–61855
15. Tao J, Feng Q (2017) Compact ultrawideband MIMO antenna with half-slot structure. IEEE Antennas Wireless Propag Lett 16:792–795

FPGA Based Implementation of Hamming Encoder and Decoder

K. Umapathy, S. A. Yuvaraj, K. Gunasekaran, and D. Muthukumaran

Abstract Communication is among the vast and fast-growing engineering fields. Improving communication efficiency by overcoming external electromagnetic and noise sources is a difficult task. Different methods for detecting and resolving errors are implemented to reduce data loss during transmission. A novel approach that uses cyclic redundancy tests is proposed in this paper. In the field of communication, there have been many developments in the digital world. In most fields of communication, the input message or data is encoded and transmitted through a medium of transmission. Data are obtained at the receiver and the original data is successfully retrieved after decoding the received data. The paper aims to explain the hammer code design cycle with VLSI, as FPGA is cheaper than the other device. The hamming algorithm for encoding and decoding was discussed in this paper and the results were obtained by implementing hamming error detection and the correction code. Compared to the traditional Narayanan and Ramesh (Journal of Engineering and Applied Sciences 12:6281–6285, 2017 [1]) hamming parity checking process, hamming code is an improved version and used in Verilog to transmit n-bit information with redundancy bits. A hamming to find out how important these redundant bits.

Keywords Hamming encoder · Hamming decoder · Bit error · Redundant bits · Parity

K. Umapathy (✉) · D. Muthukumaran
Department of ECE, SCSVMV, Kanchipuram, Tamilnadu, India
e-mail: umapathykannan@gmail.com

D. Muthukumaran
e-mail: sarvamkumaran@gmail.com

S. A. Yuvaraj
Department of ECE, GRT Institute of Engineering and Technology, Tiruttani, Tamil Nadu, India
e-mail: akmraja007@gmail.com

K. Gunasekaran
Electronics and Communication Engineering, GRT Institute of Engineering and Technology, Tiruttani, Tamil Nadu, India
e-mail: guna.k77@gmail.com

D. K. Sharma et al. (eds.), *Micro-Electronics and Telecommunication Engineering*,
Lecture Notes in Networks and Systems 179,
https://doi.org/10.1007/978-981-33-4687-1_24

1 Introduction

In the telecom field, the key issue is the smooth and seamless data transmission from the transmitter to the receiver. A variety of technologies are currently available to ensure the transmission of flawless data. One Hamming Code technology is used to identify and correct errors in order to access error-free data at the intended destination. With Hamming code data, data is encrypted with a standardized and unlike parity method until information is transmitted to the recipient end at source [2, 3]. Hamming codes will correct one mistake each word. Memories or registers are most widely used to defend against soft errors. The communication channel will introduce noise. Noise. The noise affects the data input, and during transmission it could be corrupted. It is therefore important that the recipient has used certain functions which can locate the error on the recipient's end data. The forward error-fixing code exists in many ways. One of them is the hamming code that has a number of applications. A variety of modern computer applications including optical storage, random access memory, high-speed modems and the wireless communication network can be used for code identification and correction. A soft error occurs when the device is sludged by an active radiation and then changes or registers the logical significance of a memory cell. ECC can add block code to a block and stream-code data store. Examples of ECC include hamming, Reed Solomon, Bose-Chaudhuri-Hocquenghem Code (BCH) and cyclical redundancy check codes. Examples of ECC are: For any word length, hamming codes are simple to construct, so coding and decoding can be done easily. SEC code can be expanded to cover all bits to execute the SEC-DED code [4] with a parity bit. Thus, they are ideal for the security of the digital circuit registry, not just RAM and ROM applications. Now, the digital communication device is used for different forms of channel noise-based error—correcting code. These include: the Hocquenghem Code for Bose-Chaudhuri (BCH) [5], the Salomon Code for Reed [6], the LDPC [7], the Turbo Code [8], and the Hamming Code [9]. The hamming codes are based on the 1950s bell laboratory work by R.W.Hamming. Hamming has found certain errors that can cause bits to be altered and even corrected to obtain the original data by taking an algorithm-based data word and adding bits to it. Parity, which is the most common way of recognizing errors, may only record an mistake[10–13]. Word algorithm codes are very complex, but the circuit to execute the method turn out to be very simple combination logic. The first program is Verilog to construct hamming codes and the second produces Verilog code for decoding hamming codes. There are two programs C. Both of them certainly give a word-size input parameter and build the appropriate Verilog function[14–16]. Below is the architecture proposed by the Hamming computer system: encoding, decoding, replication and bit decode.

2 Proposed Method

Hamming code is a linear code that fixes mistakes. There are up to two bit equal errors and a one-bit mistake can be corrected. Therefore, precise communication is possible if Ter1 is the difference between the transmission and receiving bit patterns. The only thing that can detect an extraordinary number of confusion is simple parity code. The hamming code cycle uses only two methods to generate a bit of redundant systems (even and odd parity). In general, The basic concept of hamstring codes is based on a Hamming distance (Hd) concept, which is the difference between two binary codes, that is to say. Total bits vary in size. For example, since the bit number is three different places, the hamming distances from both 100,010 and 1,010,100 are 3 For the general word formulation which can be used to overcome x errors and detect y errors, the continuity Formula can be used.

$$2x + y + 1 \leq Hd \tag{1}$$

Each Data Word must be mapped into a series of Codes for data transfer, detection and correction of errors. To do this, you can insert bits of every data word to increase the distance. The smallest matrix H must first be set for both features when the code bit number is n and the data bit number is m, so the section number matrix H is $n + m$, the shortest n in a matrix is 2n − 1. This is achieved in the beginning. The number of the Matrix H line n corresponds to the number of bits. Vector H is a vector of identity to the left. The current columns matrix H give a special binary representation. In order to construct matrix H to satisfy a matrix, H to pT, where p is the code for adding most essential bits to a hamming code, hamming coding bits can only be used for each Data Word. T is the translated p-vector. On each zero from the right side, the n-bit vector is 0. Syndrome rule If all nullifications are not correlated with the syndrome, the matrix column that represents the syndrome is the same as the error bit. To get the correct data, you need to set the bit in the receiver data, then delete the code bits. The redundancy is based on the bits of data. The method of encoding and encoding is as follows.

3 Hamming Code

3.1 Encoding

Advanced bug fixes are usually used to move a data or bit pattern from a binary database source to a communication system encoder. In this connection, the encoder's inserts contain redundant (or parity) bits and therefore result in a longer sequence, known as the coded word. An adequate 1010 A. H. M.-H. M. The recipient section of the original data sequence must be using the decoding system.

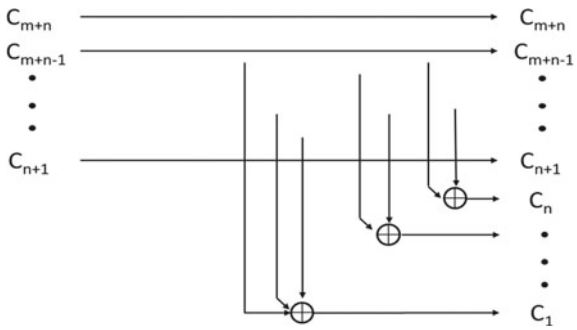

Fig. 1 Encoder

The code (x, d, t) refers to a'd' block of bits of data that can be corrected 't' bits in the error, mapping to an x-bit-code word (where $d < x$) and 'br' $(= x - d)$ error-check bits. In the case of 'x'$(= d + br)$,"br' must have different statuses for at the very least '$x + 1$' $(= d + br + 1)$, The number of bits in the transmitter segment is the sum. Therefore, state '$n + 1$' should be detected by bits 'br;' and the specific state of '$2br$' must be detected by bits 'br.' Accordingly, $2br$ would have been equal to, or greater than '$n + 1$. The determination of 'br' can be made by replenishing 'd' (where d is the original length for data sent); The determination of 'b' must be achieved by replacing 'b' with bits 'br;' and the difference between bits 'br.' For example, if the value 'd' is '7,' the lowest value 'r,' which can reach the limit (Fig. 1).

3.2 Channel Coding

Even in the presence of noise and interferences, digital communications systems, Especially used in defense systems, the channel must function accurately and reliably. Advanced correction of errors is very agile and cost effective, as transmission errors are reduced. A digital network transmitter end (also known as the "channel coding") helps the receiver to correct the errors. Usually FEC detects and corrects errors by bits of redundancy. FEC is one of the digital systems, the use of filters, the reception of varieties and the equalization processes within its communication systems.

3.3 Redundancy

Duplicate bits are the kind of extra bits that can spot or fix fault bits. They are placed at the end of the transmitter and removed at the end of the destination. This same compensation bit lets the receiver detect totally corrupt bits or correct them. In any coding scheme it is necessary to connect redundant bits to transmitted data as well as the strength of the operation. So the correct sync can be achieved even if the redundant bits contain errors in the correctly framed word code

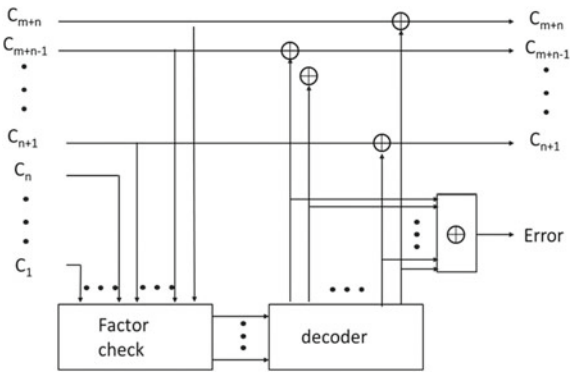

Fig. 2 Decoder

3.4 Decoding

The circuit of the Hamming decoder can be set k, n, where n and k are both encoded bits and message bits. 48-bit encrypted data (input) is divided in four 12-bit sets, each set will then be sent to the internal decoder area. An internal decoder decodes every 12-bit–8-bit error detection. The error is fixed by a corrector mechanism [17]. When a single-bit fault is found. When a dual bit error has been detected, an error flag is produced. That 8-bit data is composed of 4-bit information and 4-bit parity. To order to achieve a natural structure, this information and parities can be separated and given to the data block and the parity of the leaver block. Every 8-bit data is provided in the external decoder portion. The 8-bit message is decoded into a 4-bit data stream by correcting a 1-bit fault while recognizing a 2-bit fault. Therefore the subsequent output of the decoder gives the original data Fig. 2).

The generation of the parity check matrix is based on the different matrix generated according to the Hamming encoding principle. The generated parity check matrix can be obtained, resulting in a calibration factor that can be obtained by encoding the matrix for logical parity check.

4 Results and Discussions

The stroke pixel region detection method stated in this paper is applied on the BrainWeb dataset images in order to evaluate the effectiveness of the proposed stroke detection method. This stroke detection method detects 153 stroke region free brain MRI images over 156 stroke region free brain MRI images, which reaches 98% of stroke detection rate for normal MRI brain images. This stroke detection method detects 121 stroke affected brain MRI images over 125 stroke affected brain MRI images, which reaches 96.8% of stroke detection rate for normal MRI brain images. The average detection rate for stroke detection system is about 97.4%.

Table 1 Slices comparisons

Method	Number of slices	Number of 4 inputs luts
Conventional	876	1450
Proposed	806	1340

Table 1 shows the performance of stroke detection rate of the proposed method with other state of art methods achieved 90.7% of stroke detection rate.

The data word is usually increased until it is wrapped back up to zero in the simulation. For small budget analysis functions, field Programmable Arrays can be used. In Verilog HDL, the recommended method is to logically verify and to synthertize the timing, device utilization analysis, and hamming code synthesis report with the use of Xilinx 14.7 and SPARTAN 3 platform using XST synthesizer tools.

5 Conclusion

Hamming code is the correcting code for an error. It is useful to communicate without errors. It can not only be used to detect bits or burst errors, but can also be used to correct bits that occur when numeric information is forwarded from device to device. In this document Xilinx program imitated Hamming's encoder and decoder in FPGA. FPGA is less than a fixed device IC and more versatile than alternative medium-volume approaches. So, skilful use. The diagram was followed in simulation. Also found were a chronological outline and summary of device use Area of the method proposed is minimized by conventional. The How many locks, multipliers and digital logic circuits were designed with Hamming decoder. FPGA was always covetable for the complex design of the circuit, since less hardware is required for a given system.

References

1. Narayanan KL, Ramesh GP (2017) VLSI Architecture for multi-band wavelet transform based image compression and image reconstruction. J Eng Appl Sci 12:6281–6285
2. Forouzan AB (2007) Data communications and networking (sie), Tata McGraw-Hill Education
3. Parvez M, Shahariar AHM et al. (2019) Design and implementation of hamming encoder and decoder over FPGA. In: International conference on computer networks and communication technologies, Springer, Singapore
4. Pedroni VA (2008) In: Digital electronics and design with VHDL, Morgan Kaufmann
5. Berrou C, Glavieux A (1996) Near optimum error correcting coding and decoding: turbo-codes. IEEE Trans Commun 44.10:1261–1271
6. Gross WJ, Kschischang FR, Koetter R, Gulak PG (2006) Applications of algebraic soft-decision decoding of Reed-Solomon codes. IEEE Trans Commun 54(7):1224–1234
7. Ashenden PJ (2007) In: Digital design (verilog): An embedded systems approach using verilog, Elsevier

8. Panda AK, Sarik S, Awasthi A (2012) FPGA implementation of encoder for (15, k) binary BCH code using VHDL and performance comparison for multiple error correction control. In: 2012 International conference on communication systems and network technologies, IEEE, pp 780–784
9. Goss Y, Paul E, Strasser-Weippl K, Lee-Bychkovsky BL, Fan L, Li J, Chavarri-Guerra Y, Pedro ERL et al (2014) Challenges to effective cancer control in China, India, and Russia. Lancet Oncol 15(5):489–538
10. Cohen DB (2002) Real chip design and verification using verilog and VHDL, vhdlcohen publishing
11. Ramesh GP (2020) Design of digital FIR filters for low power applications. In: Intelligent computing in engineering, Springer, Singapore, pp 433–440
12. Podder P, Hasan MM, Khan TZ (2014) FPGA implementation of high performance fast page mode dynamic random access memory. In: The 8th international conference on software, knowledge, information management and applications (SKIMA 2014), IEEE, pp 1–7
13. Mathew B, Neepa P, Anith M (2016) Matrix code based error correction for LUT based cyclic redundancy check. Proc Technol 25:590–597
14. Paul A, Khan TZ, Podder P, Hasan MM, Ahmed T (2015) Reconfigurable architecture design of FIR and IIR in FPGA. In: 2015 2nd International conference on signal processing and integrated networks (SPIN), IEEE, pp 958–963
15. Shamir MA, Safran I, Ronen E, Dunkelman O (2019) A simple explanation for the existence of adversarial examples with small hamming distance. arXiv preprint arXiv:1901.10861
16. Rajavelu T (2012) Implementation of umhexagons motion estimation algorithm for video coding standard. Int J MC Square Sci Res 4(1):42–47
17. Pedroni VA (2008) In: Digital electronics and design with VHDL, Morgan Kaufmann

Spatial Specification of Grid Structures by Petri Nets

Dmitry A. Zaitsev, Tatiana R. Shmeleva, and Werner Retschitzegger

Abstract To deal with models in grid computing (and systems biology as well), two basic ways of specifying spatial structures with Petri nets are considered—a colored Petri net and a parametric expression. We present a composition of hypertorus grid models in a form of parametric expression and colored Petri net, their mutual transformations, and unfolding into a place/transition net; the parameters are the number of dimensions and the size. The rules of mutual transformations of Petri net spatial specifications are studied. Colored Petri nets are convenient for the state space analysis. The main advantage of parametric expressions is the ability to obtain linear invariants and other structural constructs of Petri nets, for instance, siphons and traps, in parametric form that allows us to draw conclusions on Petri net properties for any values of parameters. Thus, we say that infinite grids (Petri nets) with definite spatial structure are investigated.

Keywords Infinite Petri net · Parametric expression · Colored Petri net · Spatial specification · Grid structure · Hypertorus

D. A. Zaitsev (✉)
Odessa State Environmental University, St. Lvivska 15, Odessa 65016, Ukraine
e-mail: daze@acm.org

T. R. Shmeleva
A.S.Popov Odessa National Academy of Telecommunications, St. Kuznechnaya 1, Odessa 65023, Ukraine
e-mail: t.shmeleva@onat.edu.ua

W. Retschitzegger
Johannes Kepler University Linz, Computer Science Building, Altenberger Str. 69, 4040 Linz, Austria
e-mail: werner@bioinf.jku.at

D. K. Sharma et al. (eds.), *Micro-Electronics and Telecommunication Engineering*,
Lecture Notes in Networks and Systems 179,
https://doi.org/10.1007/978-981-33-4687-1_25

1 Introduction

When studying complex networking protocols of parallel and distributed computer systems [1], especially, computing grids and clouds [2, 3], and interconnects of supercomputers [4], hypercube [5] and hypertorus [6] Petri net models were constructed. In structural biology, similar structures [7, 8] appear. The structures of triangular, square, and hexagonal grids on a plain or a hypercube, for an arbitrary number of dimensions, are similar in grid computing and systems biology though the nature of a cell is different. A thorough study reveals that even a cell function has traces of similarity. A communication (computing) device transmits packets, forwarding them to one of its neighbors, while bioplast transmits substance and impulses.

There are two basic approaches to specify spatial structures with Petri nets: via parametric expressions (PE) of infinite Petri nets [9, 10] and via colored Petri nets (CPN) [7, 8]. Both approaches represent concise specification of place/transition nets (P/T-nets); they have their advantages and deficiencies. Sometimes the source net is not an elementary one [11], for instance, it specifies continuous processes via associated differential equations [7]. Moreover, parameterization of colored Petri nets occurs useful: a colored Petri net in [12] declares a set of colored Petri net models of a switched network; it uses parameters to specify the network topology.

PE designates a mathematical concept that allows us to apply algebraic transformations and rules of composition. On a given PE, a linear Diophantine system for calculation of place and transition invariants is directly obtained. A parametric solution of the system represents results valid for any values of parameters [9, 10]. Based on this fact, we ascertain that properties of infinite Petri nets have been studied with regard to definite spatial structure [13] composed of definite cell model. The model design can be represented as composition of clans [14].

CPN [15] represents a graphical simulation language considered as an algorithmic concept. Laconic and powerful specifications of spatial structures are based on the application of CPN ML language [16] features such as abstract data types (colors), a Cartesian product, list, and union, combined with recursive functions. A CPN produces an elementary P/T-net via unfolding [15] that is considered as an additional advantage providing conceptual unity of formalisms.

For producing P/T-nets on a PE, special program generators [9, 10] are composed requiring further formalization of the process. Note that CPN regular unfolding is possible for simple finite sets of colors; moreover, mathematical investigation of CPN properties is hampered save a brute force construction of the entire state space.

The transformations [17, 18] of PEs and CPNs into P/T-nets have been studied in detail [15]. In the present work we consider mutual transformations of PEs and CPNs and compare tools and techniques for their analysis. We demonstrate that PEs and CPNs are complimentary approaches, they both specify spatial structure of Petri net models though using different facilities. In the present paper, we develop further 2-dimensional case results [19] generalizing then on transformations of hypertorus specifications in d-dimensional lattice.

2 A D-Dimensional Rectangular Grid (Hypercube or Hypertorus)

Let us study a unit-sized hypercube in d-dimensional space [19] considering it as a spatial model of a cell with von Neumann neighborhood, generalized neighborhood [20] can be considered as well.

We compose PE with variable number of dimensions given as an external parameter and transform it into CPN using the list data structures to specify variable length indices. We consider a d-dimensional rectangular grid—a hypercube of size $k_1 \times k_2 \times \ldots \times k_d$. Closing the rectangle in each dimension via connection of its opposite edges, a hypertorus is obtained [6]. Hypercube and hypertorus applications, especially in thermonuclear physics, are studied in [21, 22].

We specify the following rules for the grid composition:

(a) an upper index i is added to the device model [19] to specify its location within the grid; the device model is copied into each cell of a multidimensional matrix of size $k_1 \times k_2 \times \ldots \times k_d$; the obtained structure is specified with the following PE

$$\left(\left(\begin{array}{l} (to^i_{j,n} : pb^i_{j,n}, pol^i_{j,n} \to po^i_{j,n}, pbl^i), \\ (ti^i_{j,n,j',n'} : pi^i_{j,n}, pbl^i \to pb^i_{j',n'}, pil^i_{j,n}) \end{array} \right) : \right.$$
$$\left. \begin{array}{l} i = (i_1, \ldots, i_d),\ 1 \le i_j \le k_j, \\ 1 \le j \le d,\ 1 \le n \le 2,\ 1 \le j' \le d,\ 1 \le n' \le 2,\ (j', n') \ne (j, n). \end{array} \right)$$

that describes a grid of unconnected devices.

(b) then we merge contact places of neighboring devices, renaming them to avoid duplicity in accordance with the following PEs:

$$\left\{ \left(\begin{array}{l} pi^i_{j,1} := po^{ri(i,j)}_{j,2} \cup pi^i_{j,1}, \\ pil^i_{j,1} := pol^{ri(i,j)}_{j,2} \cup pil^i_{j,1}, \\ po^i_{j,1} := pi^{ri(i,j)}_{j,2} \cup po^i_{j,1}, \\ pol^i_{j,1} := pil^{ri(i,j)}_{j,2} \cup pol^i_{j,1} \end{array} \right) : \ i = (i_1, \ldots, i_d),\ 1 \le i_j \le k_j,\ 1 \le j \le d, \right.$$

$$ri(i, j) = i',\ i'_l = \begin{cases} i_l,\ l \ne j, \\ rij(i_l, j),\ l = j. \end{cases}$$

$$rij(i, j) = xij(i, j) = \begin{cases} i - 1,\ 1 < i, \\ 1,\ i = k_j. \end{cases}$$

We denote the obtained model as $H_{d,k}$:

$$\left(\begin{array}{l}\left(\begin{array}{l}(to^i_{j,1}:\ pb^i_{j,1}, pol^i_{j,1} \to po^i_{j,1}, pbl^i)\\ (ti^i_{j,1,j',n'}:\ pi^i_{j,1}, pbl^i \to pb^i_{j',n'}, pil^i_{j,1})\\ (to^i_{j,2}:\ pb^i_{j,2}, pil^{xi(i,j)}_{j,1} \to pi^{xi(i,j)}_{j,1}, pbl^i)\\ (ti^i_{j,2,j',n'}:\ po^{xi(i,j)}_{j,1}, pbl^i \to pb^i_{j',n'}, pol^{xi(i,j)}_{j,1})\end{array}\right):\\ i=(i_1,\ldots,i_d),\ 1\le i_j\le k_j,\\ 1\le j\le d,\\ 1\le j'\le d,\\ 1\le n'\le 2,\ (j',n')\ne(j,n).\end{array}\right)$$

$$xi(i,j)=i',\quad i'_l=\begin{cases}i_l,\ l\ne j,\\ xij(i_l,j),\ l=j.\end{cases}$$

$$xij(i,j)=\begin{cases}i+1,\ i<k_j,\\ 1,\ i=k_j.\end{cases} \tag{1}$$

(c) the initial marking is described as follows

$$\left(\left(\begin{array}{l}\left(nf^*pb^i_{j,n},\ bl*pbl^i\right):\ 1\le n\le 2,\\ \left(pil^{ii}_{j,n},\ pol^i_{j,n}\right):\ n=1\end{array}\right)\right.$$
$$\left.:i=(i_1,\ldots,i_d),\ 1\le i_j\le k_j,,\ 1\le j\le d\right)$$

As a result, we obtain a connected grid. Further we use only names of contact places having the direction number $n = 1$ to avoid ambiguity. Auxiliary functions notation uses letter "r" that denotes the previous element (derived from "previous"). For instance, a function ri calculates index of the previous cell, and a function rij calculates the previous cell coordinate in dimension j. Note that, in each dimension, there is only one previous cell. As for functions xi and xij, their meaning is the same as for *2*-dimension case—they give indices of the next cell, but their new specifications work for any number of indices.

We transform (1) into CPN which graphical representation coincides with $H_{2,k}$ [19] for 2-dimensional case, though they differ in declarations of color sets, variables, and functions (2). The model is constructed for a particular case $k_1 = k_2 = \ldots = k_d = k$; modeling separate limitations for each dimension leads to cumbersome declarations.

$$
\begin{array}{ll}
val\ d = 2; & fun\ xij(i) = if\ i < k\ then\ i + 1\ else\ 1; \\
val\ k = 2; & fun\ xi(i : hk, j) = List.take(i, j - 1)^{\wedge\wedge} \\
colset\ dd = int\ with\ 1..d; & [xij(List.nth(i, j - 1))]^{\wedge\wedge} List.drop(i, j); \\
colset\ v = int\ with\ 1..2; & var\ i, ii : hk; \\
colset\ f = product\ dd * v; & var\ u : f; \\
colset\ dk = int\ with\ 1..k; & var\ j : dd; \\
colset\ hk = list\ dk\ with\ d..d; & val\ bl = 6; \\
colset\ hkf = product\ hk^* f; & val\ nf = 1; \\
colset\ hkd = product\ hk^* dd; &
\end{array}
\tag{2}
$$

An index within a hypercube is declared as a list *hk*; the declaration works for any given number of dimensions *d*. Function *xi* uses auxiliary standard functions *List.take, List.nth,* and *List.drop* which give the list head, specified element, and list tail, respectively; it allows the modification of a single element given by index *j*. Function *xij* is simplified because of pure hypercube structure with equal size *k* on all the dimensions.

Using specifier "*with d..d*" for list structure when declaring color set *hk* allows the application of the standard function *all()* to generate initial marking of the model. Note that, function *all()* works for small color sets of CPN Tools [23] besides its application is hampered when using separate size limitations in each dimension. For generating the initial marking in the general case, special recursive functions were composed. Visual representation of unfolded P/T-nets for number of dimensions greater than two is rather difficult but it is possible to work with them in logical format of modeling system Tina [24] without graphical binding.

3 Composition of Hypertorus via Connection of Cells by Dedicated Transitions

In the previous section, we considered composition of the neighboring cells via merging their corresponding contact places situated on the common facets. The obtained grids abstract from the technical peculiarities regarding the way of neighboring devices connection. Similarly, the composition can be implemented via merging of contact transitions using dual parametric expressions [9, 10]. Sometimes, packet transmission channels should be modeled as well. Moreover, a series of models studied in [8] consider a single place as a model of a biological cell and its connections with neighbors by dedicated transitions.

Let us implement a transformation from a CPN to PE when composing a hypertorus via connection of cells by dedicated transitions and denote this model as $HC_{d,k}$. Each added transition represents a simple model of some entity transmission (a packet, impulse, matter, etc.) between cells without loss. In more complex cases, a transmission can imply either partial or entire loss, represented by a token loss

with certain probability or changing its attributes – decreasing mass, energy etc., respectively.

To start the CPN composition, we consider an example of P/T-net, for instance, shown in Fig. 1 for $d = 2, k = 2$. As opposed to $H_{d,k}$, in $HC_{d,k}$ all contact places of each H_d are present that simplifies the model description because it does not require specifying ports 2 and 3 separately from ports 1 and 4.

CPN model of $HC_{d,k}$ is shown in Fig. 2; the declarations are mainly compatible with (2), excepting the next indices functions given with (3). The model is constructed for a particular case $k_1 = k_2 = \ldots = k_d = k$. The basic principle of its composition consists in that each indexed (both upper and lower indices) node of P/T-net is represented by a single CPN node.

Color set *hkf* of contact places *po, pol, pi, pil*, as well as of sections of the internal buffer *pb*, describes all facets of all cells combining color sets of upper index *hk* and lower index *f*; the available buffer size *pbl* has only upper index represented with color set *hk*. The model contains three CPN transitions: *to* represents all transitions, which take packets from the sections of the internal buffer; *ti* represents all transitions, which put packets to the sections of the internal buffer; and *tc* represents all transitions,

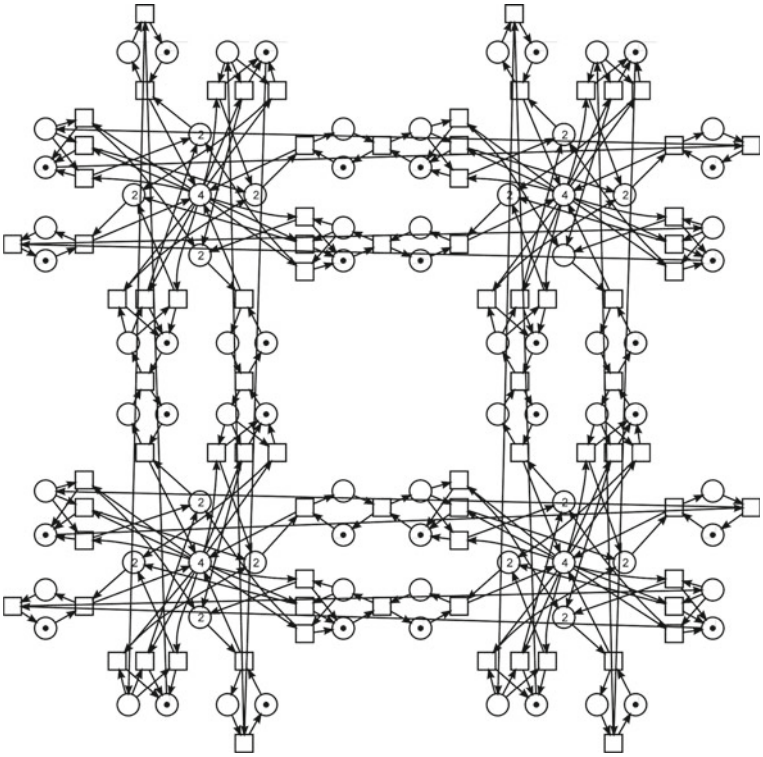

Fig. 1 An example of $HC_{d,k}$ for $d = 2$ and $k = 2$

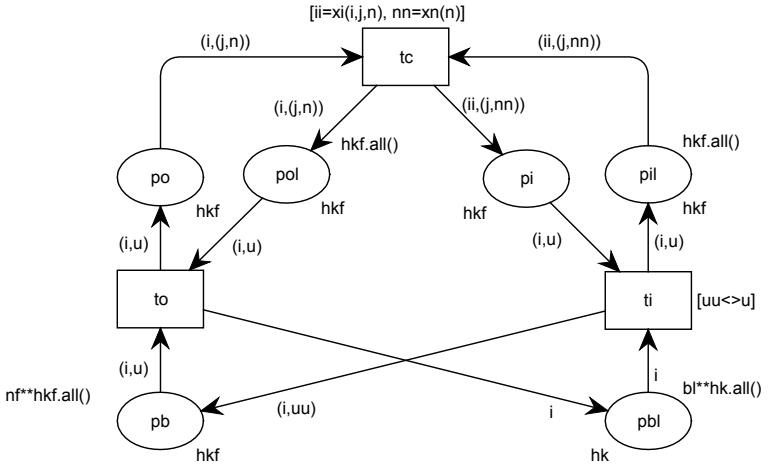

Fig. 2 CPN model $HC_{\mathrm{d},k}$ of d-dimensional grid with connection of cells via dedicated transitions

which connect cells, taking a packet from the output port buffer of a cell and putting it to the input port buffer of a neighboring cell.

From the conceptual point of view, $HC_{d,k}$ seems simpler than $H_{d,k}$ because the initial scheme of a cell is preserved; only its color sets are extended with cell index represented as color set *hk*. Thus, model $HC_{d,k}$ resembles H_d shown in [19] supplied with CPN transition *tc* and 4 arcs connecting it with places *po, pol, pi, pil*. The additional grid index (color set *hk*) stays unchanged within a cell model represented with CPN transitions *ti* and *to*; only CPN transition *tc*, which describes connections of cells, changes it using functions *xi* and *xn* specifying the next cell index and surface number, respectively. Function *xi* changes only one component of index *i*, corresponding to dimension number *j*, with auxiliary function *xij* and returns it to the variable *ii*; function *xij* depends on the direction of transmission and provides connection of the first and the last cells in dimension *j*. As opposed to (2), functions xi, xij use the number of direction n as an additional parameter.

$$
\begin{aligned}
&fun\, xi(i : hk, j, n) = List \cdot take(i, j-1)^{\wedge\wedge} \\
&[xij(List.nth(i, j-1), n)]^{\wedge\wedge} List \cdot drop(i, j); \\
&fun\, xij(i, n) = if\, n = 1\, then\, (if\, i > 1\, then\, i-1\, else\, k) \\
&else(if\, i < k\, then\, i+1\, else\, 1); \\
&fun\, xn(n) = if\, n = 1\, then\, 2\, else\, 1;
\end{aligned} \tag{3}
$$

Now we transform CPN model of $HC_{d,k}$ into PE (4). Each PE row directly corresponds to a CPN transition; names of nodes are supplied with indices, which correspond to the arcs inscriptions. Index *i* is written as an upper index, and index *u*, split into a pair *(j, n)*, is written as a lower index; repeated letters are denoted with a stroke symbol. The rest of expression (4) represents mathematical description of

functions *xi*, *xij*, and *xn*.

$$\left(\left(\begin{array}{l}(to^i_{j,n} : \ pb^i_{j,n}, pol^i_{n,1} \to po^i_{j,n}, pbl^i),\\ (ti^i_{j,n,j',n'} : \ pi^i_{j,n}, pbl^i \to pb^i_{j',n'}, pil^i_{j,n}),\\ (tc^i_{j,n} : \ po^i_{j,n}, pil^{xi(i,j,n)}_{j,xn(n)} \to pi^{xi(i,j,n)}_{j,xn(n)}, pol^i_{j,n})\end{array}\right)\right.$$
$$\left.\begin{array}{l} i = (i_1, \ldots, i_d),\ 1 \le i_j \le k_j,\\ : \ 1 \le j \le d,\ 1 \le j' \le d,\\ n \in \{1, 2\},\ n' \in \{1, 2\},\ (j', n') \ne (j, n).\end{array}\right),$$

$$xi(i, j, n) = i', \quad i'_l = \begin{cases} i_l,\ l \ne j,\\ xij(i_l, j, n),\ l = j.\end{cases}$$

$$xij(i, j, n) = \begin{cases} i - 1,\ i & gt; 1 \wedge n = 1,\\ k_j,\ i = 1 \wedge n = 1,\\ i + 1,\ i & lt; k_j \wedge n = 2,\\ \\ 1,\ i = k_j \wedge n = 2.\end{cases}$$

$$xn(n) = \begin{cases} 2, n = 1,\\ 1, n = 2.\end{cases} \tag{4}$$

The $HC_{d,k}$ initial marking specification is also simpler comparing $H_{d,k}$ because all the contact places are present after connection of cells by transitions and we can specify them using the same row as for the internal places:

$$\left(\left(nf^* pb^i_{j,n},\ bl^* pbl^i,\ pil^i_{j,n},\ pol^i_{j,n}\right) : \ i = (i_1, \ldots, i_d),\ 1 \le i_j \le k_j,,\ 1 \le j \le d,\ 1 \le n \le 2\right).$$

4 Transformations of Spatial Specifications

Based on the case study of spatial specifications for hypertorus, presented in Sect. 3, we propose the following rules for transformations of a PE into a CPN and vice versa. We give their *verbal* description because a CPN unites a Petri net graph with a functional programming language which *formal* semantic definition is rather cumbersome.

4.1 Rules of Transformation of PE into CPN

Each place of CPN corresponds to all places of PE with the same name, a place index is given as a color of a corresponding color set. A color set of a place specifies the complete range of valid indices.

Each transition of CPN models a row of PE; a transition index is composed as a combination of ranges for variables which are inscribed on input and output arcs of the transition. When a PE contains separate rows for definite values of indices, they are modeled by separate transitions. Limitations on transitions' indices are inscribed as a transition guard function.

For brevity, a color set with a unit type is not modeled in combination with other color sets. A fixed-length vector of indices is represented as a Cartesian product; a variable-length vector of indices is represented as a list. When describing a regular initial marking, special (recursive) functions are constructed for generating all the tokens within a definite color set and a given number of tokens of each color.

4.2 Rules of Transformation of CPN into PE

A precondition of the transformation is a definite enumeration of all colors of used color sets, which is expressed with either integer numbers, vectors of integer numbers, or lists of integer numbers.

Each CPN place is represented as a place of PE, which enters rows corresponding to incidental transitions. If a CPN place belongs to a unit color set it is represented with a single (unindexed) PE place, otherwise, it is represented with an indexed PE place which index corresponds to the place color set. The index range of each entry is defined with arcs' inscriptions and the transition guard function.

Each CPN transition is represented as a separate row of PE. Its input and output places are listed before and after an arrow symbol, respectively. Indices of the places correspond to the color sets. The indices range is defined with arcs' inscriptions and the transition guard function.

Aggregation of the similar expressions is done via brackets using the same relations defining the indices range.

4.3 Motivation for Transformations

Transformation PE-> CPN is advisable for visual representation of a PE and working with the model state space [23]. Transformation CPN-> PE is advisable for analytical investigation of model properties for any values of parameters (infinite P/T-net abstraction) via p/t-invariants and auxiliary graphs [9, 10]. Moreover, transformation CPN-> PE is useful as an intermediate step for CPN unfolding into a P/T-net for a given values of parameters [6] as distinct from complex direct transformations [18].

5 Conclusions

To deal with models in such application areas as grid computing and systems biology, two basic ways of Petri net spatial specification have been studied and compared—a colored Petri net and a parametric expression which are considered as a form for finite specification of infinite sets of place-transition nets. We unfold either of them into sets of place-transition nets. It was shown in the paper, that CPN and PE mutually complement each other having their advantages and deficiencies. When colors of a colored Petri net are enumerated, it is possible its direct transformation into a parametric expression. Besides, a parametric expression is easily transformed into a colored Petri net.

As a future research direction, we considers studying transformation rules for subclasses of colored Petri nets, building reachability graph in parametric form, and developing formal methods for solving infinite Diophantine systems of linear equations and inequalities.

References

1. Kurose JF, Ross KW (2009) In: Computer networking: a top-down approach, 5th edn, Addison-Wesley
2. Preve NP (Ed) (2011) In: Grid computing: towards a global interconnected infrastructure, Springer
3. IGI-Global (2012) In: Grid and cloud computing: concepts, methodologies, tools and applications, vol 4, Information Resources Management Association (USA), IGI-Global
4. Ryan (2020) Whitwam Japan's new ARM-based supercomputer is the fastest in the World, ExtremeTech, June 23
5. Zaitsev DA, Shmeleva TR (2010) Verification of hypercube communication structures via parametric Petri nets. Cybern Syst Anal 46(1):105–114
6. Zaitsev DA (2013) Verification of computing grids with special edge conditions by infinite petri nets. Autom Control Comput Sci 47(7):403–412
7. Gao Q, Liu F, Tree D, Gilbert D (2011) Multi-cell modelling using coloured petri nets applied to planar cell polarity. In: Proceedings of the 2nd international workshop on biological processes and petri nets (BioPPN2011), pp 135–150
8. Gilbert D, Heiner M, Liu F, Saunders N (2013) Colouring space-a coloured framework for spatial modelling in systems biology. In: Proceedings PETRI NETS 2013, Milano, Springer, LNCS, vol 7927, pp 230–249
9. Zaitsev DA, Zaitsev ID, Shmeleva TR (2017) Infinite petri nets: Part 2, modeling triangular, hexagonal, hypercube and hypertorus structures. Complex Syst 26(4):341–371
10. Zaitsev DA, Zaitsev ID, Shmeleva TR (2017) Infinite petri nets: part 1, modeling square grid structures. Complex Syst 26(2):157–195
11. Giavitto J-L, Klaudel H, Pommereau F (2010) Qualitative modelling and analysis of regulations in multi-cellular systems using petri nets and topological collections. In: Ciobanu G, Koutny M (eds), Membrane computing and biologically inspired process calculi 2010, (MeCBIC 2010) EPTCS 40, pp 162–177
12. Zaitsev DA, Shmeleva TR (2011) A parametric colored petri net model of a switched network. Int J Commun Netw Syst Sci 4:65–76
13. Zhang JX, Atkinson P, Goodchild MF (2014) In: Scale in spatial information and analysis, CRC Press, Taylor and Francis Group

14. Zaitsev DA (2006) Compositional analysis of petri nets. Cybernet Syst Anal 42(1):126–136
15. Kordon F, Linard A, Paviot-Adet E (2006) Optimized colored nets unfolding. In: Najm E et al. (eds) FORTE 2006, LNCS 4229, pp 340–356
16. Zaitsev DA, Shmeleva TR, Retschitzegger W, Pröll B (2016) Security of grid structures under disguised traffic attacks. Cluster Comput 19(3)
17. Kusel A et al (2013) Reuse in model-to-model transformation languages: are we there yet?. Softw Syst Model
18. Song A, Wang MZ (2012) Model transformation of coloured petri nets into place/transition nets. J Comput Info Syst 8(12):5025–5034
19. Shmeleva TR (2018) Transformations of models of 2-dimensional grids colored petri nets into infinite petri nets and vise versa. In: 2018 International conference on information and telecommunication technologies and radio electronics (UkrMiCo), Odessa, Ukraine, pp 1–6. https://doi.org/10.1109/ukrmico43733.2018.9047513
20. Zaitsev DA (2017) A generalized neighborhood for cellular automata. Theoret Comput Sci 666:21–35
21. Miyamoto K (2005) In: Plasma physics and controlled nuclear fusion, Springer
22. Roosta SH (2000) In: Parallel processing and parallel algorithms, Springer
23. Jensen K, Kristensen LM (2009) In: Coloured petri nets: modelling and validation of concurrent systems, Springer
24. Berthomieu B, Vernadat F (2006) Time petri nets analysis with TINA. In: Proceedings of 3rd international conference on the quantitative evaluation of systems (QEST 2006), IEEE Computer Society

Enhanced Spanning-Tree Adder Structures Using Carry Increment Adders

D. Muthukumaran, K. Umapathy, S. A. Yuvaraj, and K. Gunasekaran

Abstract This paper is aimed primarily at reducing the overall amount of time and increasing efficiency on FPGA platforms. They are proving their applicability in high-performance computing to decide the field of FPGA's use. The paper defines the tree adder with variable data path sizes of eight bits to 64 bits, which is the parallel implementation prefix. VHDL was used to develop P.P.A. topology, and Xilinx was synthesized with the FPGA chip machine. Intensive experiments and measurements have been performed, and design costs such as total path delay time and the use of hardware have been checked and assessed. The results for code synthesis demonstrated the best values of delays for spanning tree adder, which was suggested over the existing method Price and Stine (IEEE 62nd International Midwest Symposium on Circuits and Systems (MWSCAS), pp 223–226, 2019 [1]), which has brought new creativity in the field of digital arithmetic. Such designs take the best part of many applications and improve performance in terms of area and delay. This work implements a 64-bit hybrid adder with the carrying increment algorithm using a spanning tree structure. In contrast to an existing design, the results showed promising data.

D. Muthukumaran (✉) · K. Umapathy
Department of ECE, SCSVMV, Kanchipuram, Tamilnadu, India
e-mail: sarvamkumaran@gmail.com

K. Umapathy
e-mail: umapathykannan@gmail.com

S. A. Yuvaraj · K. Gunasekaran
GRT Institute of Engineering and Technology, Tiruttani, Tamilnadu, India
e-mail: akmraja007@gmail.com

K. Gunasekaran
e-mail: guna.k77@gmail.com

D. K. Sharma et al. (eds.), *Micro-Electronics and Telecommunication Engineering*,
Lecture Notes in Networks and Systems 179,
https://doi.org/10.1007/978-981-33-4687-1_26

1 Introduction

The field of arithmetic holds importance to current and future advancement in processing and measurement as technology advances over time. The basic functioning of the inserting data path block is at the heart of modern arithmetic. More advanced features are provided by addition. In other key areas of the processor architecture, improvements in adder designs may also be further promoted. Therefore, it is essential to develop the digital arithmetic design as feature sizes decrease in order to adapt to technical requirements. Two strings of bits complement every digital circuit to its basic purpose. Counting is the cornerstone of mathematics, and additional calculations provide the basis [1, 2]. The adders allow circuits, including hardware, to increase signal, change address positions and perform arithmetic. The core of the optical circuitry is these adders. The rapid developments in technology in the modern era are partly responsible. The introduction of carrying propagate (C.P.A.) is made more relevant by looking at more complex arithmetic algorithms. The adder system is used, among other features, in subtraction, multiplication, and division. When major implementations are more efficient, more supplements are also included in the model. Consequently, it is important to start improving at the most basic organizational levels and then boost the hierarchy at higher levels [3–5]. Emphasizing these underlying hierarchy structures offers a bottom-up optimization strategy, which enables engineers to spend more time on different design stages. Optimizing the adder design, therefore, improves the overall arithmetic design. With the optimization of the design, the designer will concentrate on more critical aspects of practical execution while avoiding lower-level time-consuming tasks. Due to changes in efficiency, other designs may be differently designed for area, power, or delay [6–8]. Basic designs must, therefore, be revised and optimized as transistor sizes decrease in functional size constantly. Early on, progress was dominated with a view to exploring digital arithmetic, dedicated architecture, and new architecture; however, recent improvements led to the combination of several designs and paradigms to create hybrid blocks [9–12]. These hybrid designs often take advantage of two or more models and attempt to compensate for the disadvantages by providing an integrated approach to solve key problems associated with their implementation.

2 Study Work

The transmission-propagated adder configuration is typically configured based on the volume and output delay. Early adopted digital arithmetic practitioners realized that propagation supplementation is useful, but it is expensive. In other words, the propagation of the signal from one cell to the next has caused much of this delay across the entire adder [4]. The Ripple Carry Adder is an early solution for digital additions. The R.C.A. is a concatenation of the full adder cells from a bit point of view. Every bit of carrying and each bit of sum are measured as:

$$sk = ak\_bk\_ck$$
$$ck + 1 = ak\_bk + ak\_ck + bk\_ck \tag{1}$$

The delay can be approximated by a gate delay for any complete adder in the R.C.A. Because the transmission signal passes through 5 gates. The sum is spread over six gates. The name "Ripple Carry Adders" implies that signals are expected to ripple from one cell to the next cell's input.

With R.C.A. growing, the option of wind is growing. After each cell, each cell depends on the sum and the bits. A significant delay in R.C.A.'s becomes an issue in modern architectures that require 32 and 64-bit implementation. A minimal delay in the formulation of the carrying signal, therefore, occurs so that any full transmitter can transmit both signals very quickly

As shown in Fig. 1, carrying-select adders are useful in dramatically increasing R.C.A. rpm. In tandem with many R.C.A., the algorithm uses descriptions and signals easily. Because the least important R.C.A. measures the first quantities and transfers the two R.C.A.s that are hard-coded with a '0' bit and a '1' bit, respectively. The total output is sent to a 2–1 multiplexer by each of the hard-coded adders. When the signals from the first adder are ready, the select signal of the multiplexer is used, one of the two identical carryings in values is essentially chosen.

$$c8 = g7 : 4 + p7 : 4\_c4 \tag{2}$$

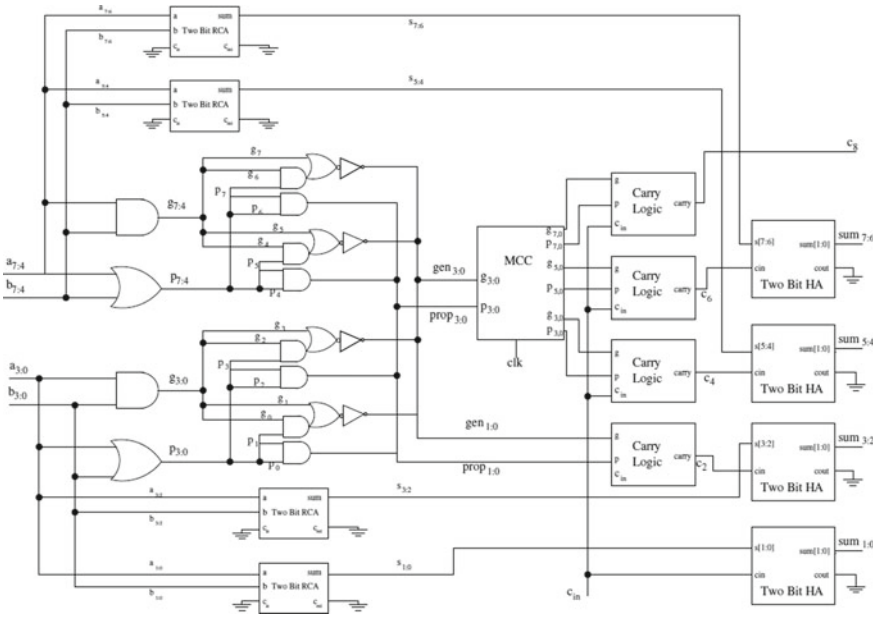

Fig. 1 Proposed ripple carrying-select adder

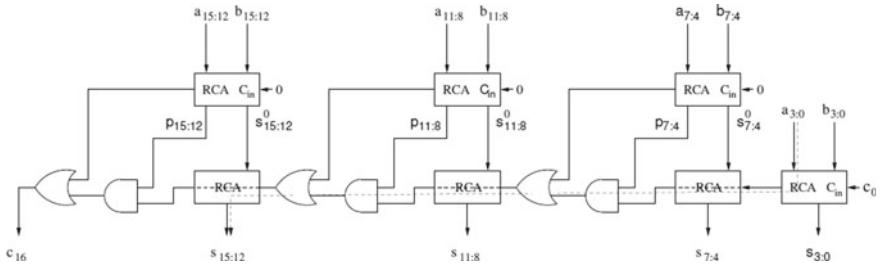

Fig. 2 Enhanced carry increment adder

More bits can be added by combining more segments into the design. Enhanced carry increment adder shown in Fig. 2. It functions smoothly as each block exits a carrying signal that is ready for use as the next multiplexer pick signal. This leads to high amounts that are ready fast and wait for the correct carrying bits to select the sum that can be used. However, multiple R.C.A.s are required for each block. It means an improvement in overall energy dissipation.

3 Results

The proposed uses Verilog that establishes the desired implementation. As Verilog modules, 8-bit blocks were produced and merged into a 64-bit architecture. Logical components are created within each block by means of a sub-module representing the necessary logic for each component. Appropriate input and outputs and inner signals called\wires are added to the design. The simulated waveform is shown in Fig. 3. Because bits from each block spanned between modules have been performed, these connecting signals have been designated as wire.

The area of the connecting signals is low compared to the traditional procedure shown in Table 1. The area to be implemented is low, and the congestion of the cables is low. The additional modules are implemented in Xilinx ISE 14.7 architecture suite in Verilog HDL and then tested using Xilinx spartan 3 FPGA.

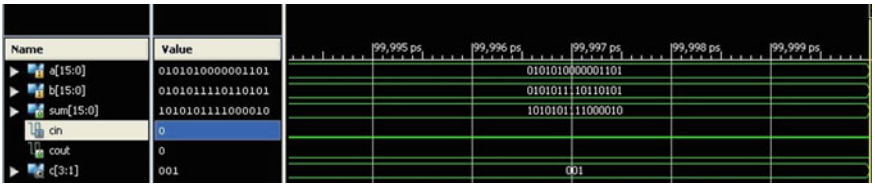

Fig. 3 The simulated waveform of proposed method

Table 1 Comparison with the existing method

	#Cells	Delay[ps]
Proposed method	1006	135.4
Existing method	1099	146.29

4 Conclusion

As device dimensions tend to decrease, the building blocks of commonly used designs are more important to consider. General changes to fundamental automated arithmetic units can have significant cumulative impacts. Furthermore, modular designs such as hybrid adders allow fast and scalable deployments in changing environments. The modules for these hybrid models offer various advantages in the area, delay of the desired limitations. Finally, we should note that the use of multiple branches in modular tree designs allows for very customized results. The designer can prefer to optimize for a particular constraint, but the use of alternation will find a balance. The presented supplements conducted a comparative analysis of parameters and simulation results. Research has also shown that the improved adder in the study has a benefit compared with the current device in terms of hardware complexity. Besides, the proposed parallel prefix adder has an advantage over the traditional system in terms of speed.

References

1. Price K, Stine JE (2019) Using carry increment adders to enhance energy savings with spanning-tree adder structures. In: 2019 IEEE 62nd international midwest symposium on circuits and systems (MWSCAS) August, IEEE, pp 223–226
2. Harish B, Sivani K, Rukmini MSS (2019) Design and performance comparison among various types of adder topologies. In: 2019 3rd International conference on computing methodologies and communication (ICCMC) March, IEEE, pp 725–730
3. Vykuntam HB, Chennaiah M, Sudhakar K (2018) Design and implementation of high speed area efficient carry select adder using spanning tree adder technique
4. Raghavaiah B, Prakash O, (2017) Quaternary logic based high recital spanning tree parallel prefix adder. In: 2017 International conference on energy communication data analytics and soft computing (ICECDS) August, IEEE, pp 686–691
5. Sajwan N, Sharma I, Kumar A, Balyan LK (2020) Performance of multiplierless FIR filter based on directed minimal spanning tree. A comparative study. Circ SystSignal Process
6. Bindima T, Elias E (2017) A novel design and implementation technique for low complexity variable digital filters using multi-objective artificial bee colony optimization and a minimal spanning tree approach. Eng Appl Artif Intell 59:133–147
7. Shalymov D, Granichin O, Klebanov L, Volkovich Z (2016) Literary writing style recognition via a minimal spanning tree-based approach. Expert Syst Appl 61:145–153
8. Gunasekaran, Ramesh GP (2020) Design of digital FIR filters for low power applications. In: Solanki V, Hoang M, Lu Z, Pattnaik P (eds) Intelligent computing in engineering. Advances in intelligent systems and computing, Springer, Singapore, vol 1125
9. Biswas P, Goel M, Negi H, Datta M (2016) An efficient greedy minimum spanning tree algorithm based on vertex associative cycle detection method. Proc Comput Sci 92:513–519

10. Sendhilkumar NC (2017) Design and implementation of power efficient modified russian peasant multiplier using ripple carry adder. Int. J MC Square Sci Res 9:154–165
11. Ramesh GP (2020) Design of digital FIR filters for low power applications. In: Intelligent computing in engineering, Springer, Singapore, pp 433–440
12. Gunasekaran K, Regan D (2016) Design of enhanced half ripple carry adder for vlsi implementation of two-dimensional discretewavelet transform. Int J MC Square Sci Res 8(1):50–59

Design and Implementation of High Value Itemsets from Online Trade

Hare Ram Singh, S. K. Yadav, and Sheo Kumar

Abstract Data mining, a technique to understand and change over unrefined data into supportive information, is dynamically being used in an arrangement of fields like publicizing, business information, intelligent revelations, biotechnology, Internet look, and blended media. Data mining is an interdisciplinary field merging considerations from bits of knowledge, AI, and standard language getting ready. High utility itemsets mining (HUIM) is an intriguing subject with regards to datamining which may be important in a numeral of vocations, for instance, in online disclosure of sold items giving high compensation, low rate, etc. Before long, High utility itemsets mining just examinations utility estimations of itemsets/things that may be inadequate to watch mentioning behavior of customers. To address this issue, here we present an Algorithm to incorporate consistency basic into high utility itemsets mining. Grounded on these lines, sets of co-occasion things with high utility characteristics and standard occasion, named high utility-uncommon itemsets (HURIs), are viewed as fascinating itemsets. We have so many algorithms available for deferent purposes, but The Sh_Ku algorithm is intended to propose customer interesting from different itemsets.

Keywords Data mining · Itemsets · Frequent itemset mining algorithms · High utility mining

H. R. Singh · S. K. Yadav
JJTU, Raj, India
e-mail: hresingh.2000.2000@gmail.com

S. K. Yadav
e-mail: drskyadav@hotmail.com

S. Kumar (✉)
CSE, CMREC, Hyderabad, India
e-mail: sheo2008@gmail.com

D. K. Sharma et al. (eds.), *Micro-Electronics and Telecommunication Engineering*,
Lecture Notes in Networks and Systems 179,
https://doi.org/10.1007/978-981-33-4687-1_27

1 Introduction

The Information mining is the investigation of gathering, cleaning, handling, dissecting, and increasing valuable bits of knowledge from information. A wide variety exists as far as the issue areas, applications, details, and information portrayals that are experienced in genuine applications. Along these lines, "information mining" is a wide umbrella term that is utilized to depict these various parts of information preparing.

In the cutting edge age, for all intents and purposes every single robotized framework produce some type of information either for demonstrative or investigation purposes. This has brought about a downpour of information, which has been arriving at the request for petabytes or exabytes. A few instances of various types of information are as per the following:

World Wide Web: The quantity of archives on the recorded Web is currently on the request for billions, and the undetectable Web is a lot bigger. Client gets to such archives make Web get to logs at servers and client conduct profiles at business locales. Besides, the connected structure of the Web is alluded to as the Web diagram, which is itself a sort of information. These various kinds of information are helpful in different applications. For instance, the Web archives and connection structure can be mined to decide associations between various themes on the Web. Then again, client get to logs can be mined to decide frequent examples of gets to or uncommon examples of conceivably outlandish conduct.

Financial collaborations: Most normal transactions of regular day to day existence, for example, utilizing a mechanized teller machine (ATM) card or a charge card, can make information in a computerized way. Such transactions can be dug for some helpful bits of knowledge, for example, extortion or other bizarre action.

User collaborations: Many types of client cooperations make enormous volumes of information. For instance, the utilization of a phone ordinarily makes a record at the media transmission organization with insights regarding the term and goal of the call. Many telephone organizations routinely break down such information to decide important examples of conduct that can be utilized to settle on choices about system limit, advancements, estimating, or client focusing on Sensor innovations and the Internet of Things: An ongoing pattern is the improvement of minimal effort wearable sensors, cell phones, and other savvy gadgets that can speak with each other. By one gauge, the quantity of such gadgets surpassed the quantity of individuals on the planet in 2008. The ramifications of such gigantic information assortment are critical for mining calculations.

The storm of information is an immediate aftereffect of advances in innovation and the computerization of each part of present day life. It is, in this way, common to inspect whether one can extricate compact and conceivably significant experiences from the accessible information for application–explicit objectives. This' is the place the assignment of information mining comes in. The crude information might be self-assertive, unstructured, or even in an arrangement that isn't promptly appropriate for mechanized preparing. For instance, physically gathered information might be drawn from heterogeneous sources in various configurations but then in some way or another should be prepared by a computerized PC program to pick up bits of

knowledge. To address this issue, information mining investigators utilize a pipeline of preparing, where the crude information are gathered, cleaned, and changed into an institutionalized arrangement. The information might be put away in a business database framework lastly handled for bits of knowledge with the utilization of scientific strategies. Actually, while information mining regularly evokes the idea of logical calculations, actually by far most of work is identified with the information readiness segment of the procedure. This pipeline of preparing is thoughtfully like that of a genuine mining process from a mineral metal to the refined finished result. The expression "mining" gets its underlying foundations from this relationship.

Frequent Itemset Mining Algorithms

Various famous algorithms for frequent itemset age will be explained. Since there are an enormous number of frequent itemset mining algorithms, these stunts are regularly reusable across various algorithms in light of the fact that a similar identification tree structure is utilized by essentially all frequent example mining algorithms.

Problem Statement

As a product of a Transactional D with internal and external objects, level of regularity and usefulness levels (Ţu), high-use abnormal products should be mined to find a full collection of abnormal high-value items with a μu and a no less frequency than βr.

Proposed Method: SU_KU Algorithm

A single-pass algorithm is implemented in this section, called Su_Ku. The definition of transaction weighted utility (TWU), residual usefulness and closely overestimated usefulness was used by Su_Ku for pruneing search space. For the I efficient management of event details, the system structure named the New Modified Utility System (NUL) is used.

A transaction database and the thin utility threshold are inputs to the main procedure (algorithm 1). Initially, the algorithm considers that α is the current itemset (line 1). The algorithm will then scan the database once to calculate each itemw.r.t.α's local utility, by using the binarray(line 2).

TWU. Then, thelocalutilityofeachitemiscomparedwithminutil

To get w.r.t to α secondary items I e. Articles to be considered in the α (line 3) extensions. Such objects must then be ordered by TWU ascendant, and this sequence will be used as the sequence afterwards (line 4). The archive is checked to delete all documents there are no secondary elements from rt to α since they are unable to be part of any extremely valuable posts. Each each of the transactions, objects are concurrently categorized according to them and deleted from the database if a transaction is null. In order to facilitate a convergence of O(nw) transactions, The archive is checked to delete all documents there are no secondary elements from rt to α since they are unable to be part of any extremely valuable postsPer operation, whenever an operation is null, items are classified by themselves simultaneously and removed from the database. The index is then screened back to organize the transactions in T order in order to enable aggregation of O(nw) transactions. The algorithm searches the database using a utilities list (lines 7 and 8) with each secondary variable

w.r.t. α to determine the subtree utility. The first depth scan from the algorithm is named by the remedial search protocol (line 9). In order to calculate the subtree and its locality w.r.t. β of each itemz that could extend β(the secondary items w.r.t to β)—the data base is searked by means of two utility-bin arraies again (line 5).The first and secondary β items (line 6 and 7) are therefore determined. Next, the quest method is recurrently named by β to expand the first-in-depth test by β (line 8). On the basis of theorems and properties, it can be shown that all and only high-use itemsets from deferential datasets are generated at Sh Ku termination. By using the Sh Ku algorithm, one can suggest itemsets for customers.

2 A Detailed Explanation

This segment offers a comprehensive description of how the Sh Ku algorithm should be used for the current test. Please take the current database illustration and minutil = 30. It is the key (Algorithm 1) process. The α-line is ˆ (line 1) and the table is searched using the functionality list for calculating lu(α, I of all items. It contains the Lu values of the lu(all, a) = 65, lu(all, b) = 61, lu(all, c),96, lu(all, d) = 58, lu(all, e) = 88, lu(all, f) = 30 and lu(all, g) = 38. The Lu values are the following. These values refer to the TWU as the upper limit of lu is the α-bis TWU. This segment offers a comprehensive description of how the Sh Ku algorithm should be used for the current test. Taking the present illustration and the minutil table = 30. It is the key (Algorithm 1) process. Originally, α is set to¯ (line 1) and a database is used to calculate lu(α I for all items by a collection of tools which refers back to the Lu of the paper lu(all, a) = 65, lu(all, b) = 61, lu(all, c), 96, lu(all, d) = 58, lu(all, e) = 88, lu(alle, f) = 30 and lu(all, g) = 38. Lu(all, d) Such values are same since the TWU, since α = bis is the TWU upper limit (Tables 1, 2, 3, 4).

Table 1 External utility values

Item	a	B	c	d	e	f	g
Profit	5	2	1	2	3	1	1

Table 2 Strong Utility Minutil itemsets = 30

Itemset	Utility
{b, d}	30
{a, c, e}	31
{b, c, d}	34
{b, c, e}	31
{b, d, e}	36
{b, c, d, e}	40
{a, b, c, d, e, f}	30

Table 3 Database D with objects sorted according to/a

TID	Transaction
T_3	(f,5) (b,2) (d,6) (a,1) (e,1) (c,1)
T_2	(g,5) (a,2) (e,2) (c,6)
T_4	(b,4) (d,3) (e,1) (c,3)
T_5	(g,2) (b,2) (e,1) (c,2)
T_1	(d,1) (a,1) (c,1)

Table 4 The expected {a}-D database (when the transaction is merged)

TID	Transaction
T_3	(e,1) (c,1)
T_2	(e,2) (c,6)
T_1	(c,1)

The set Primarily (all) = {b, a, c} (line 8), which implies that a first search examines only b, a and c substrates. The first depth scan (Alga-Rithm 2) in the subtree is then called to execute. In descendant nodes (as they are in secondary(α)), the items f, g, d, b, a, e, c can be found. Parameters are given for the Primary(α) and Secondary(α) collection. This process is preceded in line 1 by loops on primary objects b, a and c. Here we conclude that item a, initially handled, is more important for item a than item b. Therefore, find the analysis of $\beta = \{a\}$ (line 2). The database is then searched for {a}-D (line 3), the predicted version. The corresponding estimated sample will be as seen in Fig, if only the data base analysis were carried out. 1. However, the transaction merging is done in conjunction with database projection, which is explained previously. Therefore, during database creation transactions $T2$ and $T3$ are combined into a new Transaction T23. In addition, u({a}) is estimated during the estimation phase of the database, and u({a}) = 20 is found. Since {a} is not a HUI = 20 (u({a}).

Let l be the amount of quest itemsets. Then O(nw log(nw) + l(nw + nw + nw) is the regional time complexity of the Su_Ku. The word Nwlog(nw) may be overlooked, however then the difficulty is similar to O(lnw). Because the sorting is only completed once.

The efficiency of the algorithm therefore corresponds to the number of items in the search field. A search space determines the number of objects by the upper boundaries for the search field. Su_Ku suggests two narrow upper limits. The preceding section showed that the proposed upper (revised) sub-tree utilities for one step of HUI mining are tighter than the rest of the upper-bound utility at the cutting-edge stage. Nevertheless, in the experimental assessment portion, the utility of the upper limit is also measured. The usage of a pattern-growth method, which only considers elements occurring in data banks, is another feature which enhances Su_Ku's efficiency (unlike algorithms like the HUI-Miner, FHM and HUP-Miner which take patterns not in the database into consideration).

The room utilized for service binaries and the location for preservation of planned repositories are the main costs in terms of their resource sophistication. When required O() space is generated for utility bin arrays. For each α primary itemset, the data base projection operation requires a maximum O(nw) room for each database projected. This is not enough, in practice, since larger items are examined and the databases are projected using offset pointers. The projection of the database is small. Generally, Su_Ku's space complexity is O(+ lnw) since the amount in the quest range l defines the expected base value.

Experimental Results

In order to determine the efficiency of the Su_Ku algorithm, we carried out multiple checks. On a 4th generation 64-bit core i7 cpu operating Windows 8.1 and 64 GB of RAM tests have been conducted. We contrasted Su_Ku's efficiency to five state-of-the-art algorithms: UP-Growth+ , HUP-Miner, d2HUP, HUI-MinerandFHM. We also deactivated the impact of the architecture decisions in Su_Ku and space-search pruning using the subtree. Both algorithms read the database first, then scan for high-use itemsets and write to disk the output. The expense for disk exposure has little effect on the outcome of the tests since the inputs and performance are the same with all the algorithms (Table 5 and 6).

Su_Ku Algorithms were implemented on Java and the stan-dard Java API memory measurements were performed on the basis of a series of standard data sets for evaluation of HUIM algorithms in HUIM literature, specifically: accidents. Foodmart is a small, fast transaction dataset. Chainstore is a small, fast transaction dataset. Mushroom is a thick, relatively long data package. Chainstore and Foodmart are customer transaction databases that contain real values for external/internal utilities. External/internal utility values were created for other datasets, as in previous stateof the art HUIM studies, in [1, 1,000] and [1,5] intervals in the form of a lognormal

Table 5 Attributes of the dataset

Dataset	# Distinct items	# Transactions	Avg. Trans. Length
Food mart	1559	4141	4.4
Accident	468	340,183	44.8
Chess	75	3196	37.0
BMS	497	59,601	4.8
Connect	129	67,557	43.0
Kosarak	41,270	990,000	8.1
Pumsb	2,113	49,046	74
Mushroom	119	8124	23.0
Chainstore	46,086	1,112,949	7.2

Table 6 Dataset types

Dataset	Type
Food mart	Sparse, short transactions
Accident	Moderately dense, moderately long transactions
Chess	Dense, long transactions
BMS	Sparse, short transactions
Connect	Dense, long transactions
Kosarak	Very sparse, moderately short transactions
Pumsb	Dense, very long transactions
Mushroom	Dense, moderately long transactions
Chainstore	Very sparse, short transactions

distribution. You will access the data sets and the source code of comparable algorithms as part of the SPMF open-source data mining library. The effect of minuti threshold on the duration of the sprint. We have managed to reduce the algorithms of each dataset until we have noticed algorithms that are too lent or that are out of memory or a clear winner. As it is shown in the figure execution time 4. Notice that no Connect or Pumsbdataset results are seen for UP-Growth+ , and that any Chess data set result is absent, as UP-Growth + has a ram cap of 16 GB. Results on Pumsb and Kosarak are not shown because it took too long to finish the EFIM(lu) algorithm, too.

Su_Ku is particularly good for dense and medium dense datasets. Su_Kuis typically has about 2–3 magnitude orders quicker than any other algorithms. For BMS, Chess, Connect, Foodmart, Mushroom and Pumsb, and for accident events, EFIMs, Chess, Connect, FOODmart, and Pumsb shall be included, respectively, up to 15334,2,33028,–,17,3855 and—times FASTRATHAN-Grown + ,154,741,323,22636,2,85 and 12 times FASTRATHanHUP-Min-Er,89,1490,109,2587,1,15 times and 65 times Faster than HUI-Min–Su_Ku is approximately 10 times lighter on the Chainstore dataset than D2HUP, but more fast and similar in speed to FHM than UPGrowth + and HUI-Miner. EFIM(nop) in the Kosarak dataset is faster than other algorithms with the exception of HUP-Miner although d2HUP, and the variations are small (1 or less) for these two algorithms. The triggers of Su_Ku's strong running time are four occasions, and in the next tests are studied in greater depth.

- The proposed sub tree method & the local-usefullness upper limits usually allow Su_ Ku to prune, since the sub tree is the upper limit of previous one phase algorithm in Contrast to the other algorithms. The high-use itemsets therefore required fewer objects.
- The second point is to avoid time spent looking at the element sets not contained in the database in comparison with algorithms like HUI-Miner, FHM and HUP-Miner, Su_Kuonlysiders itemsets included in the database.

- Thirdly, it is feasible to substitute a variety of transactions with one transaction, which dramatically reduces the expense of database surveys, utilizing the current HTM transaction mixing methodology. The combination of transaction functions with database of a large amount of transaction are thick data sets. Su_Ku fits well for these datasets in terms of execution time.
- Fourthly, the effective measurements of the suggested upper limits within a lineary time utilizing the service bin arrays often add to the reliability of Su_Ku's period.

The previous study also documented the resource use of Su_Ku and contrasted them using the same parameters for the same algorithms. Tables 7 and 8 illustrate the findings.

Typically speaking, UP-Growth+ is worst, as the Chess dataset also reaches the 16 GB capacity cap. It is interesting that Su_Ku is also with the Kosarak data sets, where Su_Ku is slower than d2HUP. Their resource capacity is perhaps most significant. The tradeoff given by Su_Ku for such data sets is useful for programs with minimal memory. One factor Su_Ku is so effective in memory is that it uses a straightforward database model that does not allow any knowledge to be processed

Table 7 Comparison of Su_Ku, FHM, UP-Growth+ and HUI-Miner's full memory usage (MB)

Dataset	Su-Ku	FHM	UP-Growth+	HUI-MINER
Foodmart	64	211	819	808
Accident	895	1480	765	1656
Chess	65	305	–	405
BMS	64	590	64	210
Connect	385	3141	–	2565
Kosarak	576	1409	1207	1163
Pumsb	986	1436	–	1221
Mushroom	71	224	1507	194
Chainstore	460	1270	1058	1164

Table 8 Comparison of HUP-Miner and d2HUP's maximum memory usage (MB)

Dataset	HUP-Miner	d2HUP
Foodmart	68	84
Accident	1787	1691
Chess	406	970
BMS	758	282
Connect	1204	1734
Kosarak	712	1200
Pumsb	1021	2046
Mushroom	196	468
Chainstore	1034	878

only in pseudo-projections. It is more complicated structures, Such as tree structure, are used to support. Up-Growth + and list structures for example. hyper-link structures e.g. d2HUP, HUI-Miner and FHM; It is interesting that Su_Ku is also with the Kosarak data sets, where Su_Ku is slower than d2HUP. Their resource capacity is perhaps most significant. The tradeoff given by Su_Ku for such data sets is useful for programs with minimal memory. One factor Su_Ku is so effective in memory is that it uses a straightforward database model that does not allow any knowledge to be processed only in pseudo-projections. More complicated structures, such as tree structures, are used to support other algorithms. Up-Growth+ and list structures for example. hyper-link structures e.g. d2HUP, HUI-MinerandFHM; Therefore, several entries are substituted by one by implementing transaction merging. Therefore, for large datasets or datasets where transaction merger has a more efficient impact (in the next paragraph the impact of combining transactions will be explored), the memory distance between Su_Ku and other algorithms appears to increase. Because Su_Ku's numbers of expected bases are below the amount of utility list lists, Su_Ku uses the suggested upper border subtrees to reach fewer search tree nodes in the search set, given the objects that exist inside the index, as a possible explanation for Su_Ku's high memory utilization relative to the utility set bases. Su_Ku are also stronger algorithms for than two phase, for example UP-Growth+ , because it is a one-phase algorithm (the memory does not need to be preserved by other applicants).

Finally, a further important feature of Su_Ku is that it re-use some of its data structures in terms of memory efficiency. As explained, Su_Ku utilizes a highly effective Fast Array Counting system for upper bound calculations. Su_Ku uses the proposed upper border subtree service to visit fewer search-enumeration tree nodes and only to consider itemsets that appear in the database. Su_Ku are also stronger algorithms for thantwophase, for example UP-Growth+ , because it is a one-phase algorithm (the memory does not need to be preserved by other applicants).

Finally, a further important feature of Su_Ku is that it re-use some of its data structures in terms of memory efficiency. As explained, Su_Ku utilizes a highly effective Fast Array Counting system for upper bound calculations.

Transaction influence merging with execution time

In terms of enhancements, Su_Ku often improves its efficiency in terms of deployment time considerably in the suggested transaction mixing technique. Table 9 indicates the total number of transactions in scheduled repositories when Su_Ku is performed on an active transaction merging (Su_Ku) when the transaction merging is conducted, and when it is performed on a deactivated transaction merging mechanism. The mix of transactions helps to decrease the scale of More than 90% of the proposed database in terms of the amount of transactions in the Accident, Chess, Link and Mushroom and Pumsb datasets.

That is one of the reasons Su_Ku performs exceptionally effectively in small or medium compressed datasets (Chess, Link, Mushroom and Pumsb). Su_Ku terminates in three seconds for Connect and minutil = 13 M when HUP-Miner, d2HUP, HUI-Miner or FHM operate for 22, 2, 10, or 6 h respectively. Transaction fusion on dense datasets is highly effective because the planned transactions are more likely to

Table 9 Database average (number of transactions) predicted

Dataset	Su-Ku	EFIM	Size reduction(%)
Foodmart	1.12	1.21	7.1
Accident	784	113.304	99.3
Chess	2.6	1363.9	99.8
BMS	112.6	204.1	44.8
Connect	1.4	43687	99.9
Kosarak	1.727	3.653	53
Pumsb	1.075	22.326	95.2
Mushroom	1.3	573	99.7
Chainstore	1,085	1.326	18.1

be the same. Transaction fusion also reduces execution times for accidents, BMS and Foodmart, but up to 90, 2 or 2 times the amount of Su_Ku by a lower amount than the EFIM(no) on accidents, BMS and Foodmart. It is also important to remember that because of the vertical data foundation and hyperlink-based algorithms like the d2HUP algorithm it is also possible to interpret it. In utility lists based algorithms such as HUPMiner, HUI-Miner and FHM, the proposed transaction merger process can not be effectively implemented. For such datasets, EFIM(nop) is faster than Su_Ku. The costs of the contract fusion thus outweigh their advantages and should be eliminated for such datasets.

Number of visited nodes while compared

In order to equate Su_Ku's capacity to prun with other algorithms, we performed an experiment. Tables 10 and 11 display the amount of nodes visited byEFIM, UP-Growth+ ,HUPMiner, d2HUP for analysis enumerationtree(itemsets),

The lowest minutil value on the same datasets is HUI-Miner and FHM. It should be remembered that, due to its sub treetop and local utility upper-bound features, Su_Ku is usually more efficient at cutting search space than other algorithms. For

Table 10 Comparison of HUI-Miner, FHM and Su_Ku node counts visited

Dataset	Su-Ku	HUI-Miner	FHM
Foodmart	233,231	55,172,950	1,880,740
Accident	52,883	131,300	128,135
Chess	2,875,166	6,322,753	6,271,900
BMS	323	2,205,782,168	212,800,883
Connect	1,366,893	3,444,785	3,420,253
Kosarak	2073	4,794,819	135,874
Pumsb	56,267	74,050	68,050
Mushroom	2,453,683	3,329,191	3,089,819
Chainstore	3,005	4,422,322	8,285

Table 11 Comparison for d2HUP, HUP-miner and UP-growth+ of visited node count

Dataset	d2HUP	UP-Growth+	HUP-Miner
Foodmart	233,231	233,231	1,258,820
Accident	119,427	3,234,611	113,608
Chess	3,052,789	–	3,385,134
BMS	220,323,377	91,195	205,556,936
Connect			
Kosarak	9,257	2,292	57,706
Pumsb	62,361	–	1,029,702
Mushroom	2,919,842	13,779,114	3,054,253

an illustration, the Su_Ku's visit to UP-Growth+ , HUP-Miner, d2HUP, HUI-miner and FHM could be as big as 282, 636000, 682000, 6000800 and 658000.

Effect of the volume of executive transactions

In conclusion, we equate Su_Ku's run-time with UP-Growth+ , HUPMiner, d2HUP, HUI-Miner and FHM and adjust the scalability of the algorithms in each dataset through separate transactions. In previous studies on similar datasets, the algorithms for this experiment used the lowest minutil values, with transaction numbers variable of 25–100%. Results are shown in figures below 1. Su_Ku's runtime increases w.r.t in linear numbers. For example, the results of Su_Ku are presented in Fig. 1. Therefore, Su_Ku can be concluded that the data sets have the best overall scalability.

The scalability of essentially all of the algorithms is exponentially increased for the last three datasets, Chainstore, Pomsb and Kosarak, and Su_Ku is comparable to other algorithms on these datasets. The explanation why algorithms are operating at an increasing pace is that the maximum is defined on all three data sets and thus, further objects can not be tapped at the minute threshold for a larger amount of transactions. And as if the storage capacity of any object is increasing in their search area, its time is decreasing, similar to the other data set algorithms.

3 Conclusion

For several applications, high-use entity mining is a key data mining activity. It still takes a lot of time, though. The new high-use itemset mining algorithm named Su_Ku was proposed to improve HUIM's efficiency in the memory and deployment era. However, Su_Ku uses two methods, including HDP and Mer-gin (High Usage Transaction) for the prediction and processing of the database. A detailed check on various databases reveals Su_Ku is usually two or three orders of magnitude rapidly, using and utilizing the advantage of the data base scans to minimize the expenses of the database search. Su_Ku can be more sluggish than any other algorithms with very small datasets. Nonetheless, it still surpasses the other algorithms when it comes to memory utilization. In fact, the findings suggest that Su_Ku is very flexible on both

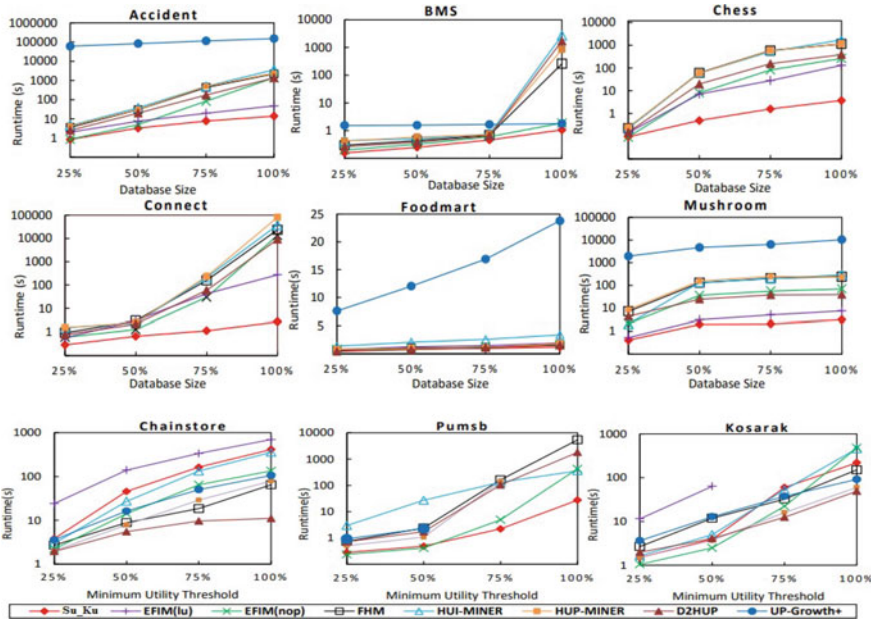

Fig. 1 Scalability on different datasets

dense and spartan datasets. In order to further boost Su_Ku performance, additional optimizations may also be created. For illustration, the Su_Ku algorithm was used in the main database. An fascinating potential is to rewrite Su_Ku as a distributed algorithm such that very broad datasets can be mine.

All rules with help greater than a defined threshold are generated by established association mining algorithms. Nonetheless, in order to find uncommon objects, we will aim further at unique things. (FournierViger et al. 2016) and (Fournier-Viger et al. 2015) frequent, strong usefulness itemsets. In order to further boost Su_Ku performance, additional optimizations may also be created. For illustration, the Su_Ku algorithm was used in the main database. An fascinating potential is to rewrite Su_Ku as a distributed algorithm such that very broad datasets can be mine.

All rules with help greater than a defined threshold are generated by established association mining algorithms. Nonetheless, in order to find uncommon objects, we will aim further at unique things.

Future Scope the research work

The architecture of Su_Ku needs to be modified to enable resource broker to be introduced into the device dynamically. This will enable Su_Ku to investigate the effect of different plans for job planning on the use of the resource and on the quality of service of the cluster. Such parameters are typically configured manually and based on practice with true Hadoopcluster environments. Nevertheless, a pilot program may be developed and deployed to operate on one example of cluster nodes, to

enable Su_Ku to under-experienced users. Instead you select the strongest parameter values to be applied to Su_Kusimulator from the pilot code. For this paper a limited cluster of participant nodes are used to test Su_Ku algorithm efficiency, for future research algorithms will be tested for a far bigger cluster like Amazon Elastic. Similar approach is used for other simulators such as DiskSim simulators.

References

1. Agrawal R, Imieliński T, Swami A (1993) Mining association rules between sets of items in large databases. In: Proceedings of the 1993 ACM SIGMOD international conference on Management of data, pp 207–216
2. Agarwal R, Srikant R (1994) Fast algorithms for mining association rules. In: Proceedings of the 20th VLDB conference, pp 487–499
3. Cheng J, Ke Y, Ng W (2008) A survey on algorithms for mining frequent itemsets over data streams. Knowl Info Syst 16(1)
4. Farzanyar Z, Cercone N (2013) Efficient mining of frequent itemsets in social network data based on MapReduce framework. In: Proceedings of the 2013 IEEE/ACM international conference on advances in social networks analysis and mining, pp 1183–1188
5. Han J, Cheng H, Xin D, Yan X (2007) Frequent pattern mining: current status and future directions. Data Mining Knowl Discovery 15(1)
6. Das A, Bhattacharyya DK (2004) Rule mining for dynamic databases. In: International workshop on distributed computing, Springer, Berlin, Heidelberg, pp 46–51
7. Huang C-H, Leu Y (2019) Multi-level dataset decomposition for parallel frequent itemset mining on a cluster of personal computers. Cluster Comput 22(2)
8. Irshad SM, Ramesh GP (2020) ANFIS-Based MPPT control in current-fed inverter for ac load applications. In: Intelligent computing in engineering, Springer, Singapore, pp 459–469
9. Lucchese C, Orlando S, Perego R, Silvestri F (2004) WebDocs: a real-life huge transactional dataset. In: FIMI, vol 126
10. Fournier-Viger P (2014) FHN: efficient mining of high-utility itemsets with negative unit profits. In: International conference on advanced data mining and applications, Springer, Cham, pp 16–29
11. Aggarwal CC (2015) In: Data mining: the textbook, Springer
12. Kumar GH, Ramesh GP (2018) Novel gateway free device to device communication technique for IoT to enable direct communication between homogeneous devices. Int J Pure Appl Math 118(16):565–578
13. Alkan OK, Karagoz P (2015) CRoM and HuspExt: Improving efficiency of high utility sequential pattern extraction. IEEE Trans Knowl Data Eng 27(10):2645–2657
14. Singh HR, Kumar S (2019) A review on algorithms for mining frequent itemsets. In: International conference on recent challenges in engineering and technology (ICRCET–2019)

A New Embedding and Extraction Algorithms for Robust Video Watermarking in Wavelet Domain

Suman Mishra, S. Poongodi, and K. Karthik

Abstract Watermarking is an innovation that is utilized for giving the security to the multimedia/digital information and digital media copyright assurance. Late years, there are numerous scientists who had created watermarking algorithms based on LeaSe noteworthy Bit (LSB), Discrete Fourier Transform (DFT), Discrete Sine Transform (DST), Discrete Cosine Transform (DCT), Discrete Wavelet Transform (DWT) and Principle Component Analysis (PCA) and so on., Here, we proposed "a new embedding and extraction algorithms for robust video watermarking in wavelet domain". In terms of consistency, the proposed algorithm indicates that the proposed algorithm was superior to the current algorithms. such as Structural Similarity Index (SSIM), CoVariance (CV) and Peak Signal To Noise Ratio (PSNR).

Keywords Digital watermarking · LSB · DFT · DCT · DWT · SVD · PSNR and SSIM

1 Introduction

It's a digital world, everything has gotten to be digital in this day and age. Consistently Gega bytes of information have been sharing over web. Subsequently, one must need to give the security to the mutual multimedia/digital information. One conceivable arrangement is watermarking, which is a piece of information covering up otherwise called steganography [1, 2] and [3]. These systems used to install the

S. Mishra (✉) · S. Poongodi
Department of ECE, CMR Engineering College, Hyderabad, India
e-mail: sumancmrec@gmail.com

S. Poongodi
e-mail: poongsvel2005@gmail.com

K. Karthik
Department of ECE, St. Martin's Engineering College, Secunderabad, India
e-mail: kodakarthik@gmail.com

D. K. Sharma et al. (eds.), *Micro-Electronics and Telecommunication Engineering*,
Lecture Notes in Networks and Systems 179,
https://doi.org/10.1007/978-981-33-4687-1_28

information to be covered up into the spread media. Along these lines, if the information is replicated by someone, then the concealed information will be duplicated and. Many techniques for digital picture watermarking were suggested. The vast majority of the analysts have done their examinations on dim scale image which are 2D images. Be that as it may, the greater part of the organization logos are in multi color and information sharing is likewise should be shading as of late. Subsequently, one needs to create RGB image watermarking to give security and copyright insurance. RGB watermarking is likewise same as grayscale watermarking, just distinction is here in RGB images there are three components i.e., red, green and blue though dark scale images have stand out component. Be that as it may, there are a few issues brought up in creating RGB watermarking algorithms. As of late, the interest in security of copyrights has been brought up in different fields [3], for example, military, bio-restorative, common, web and bio-metric and so on. Copyright protection encloses authentication, for instance, of knowledge on ownership of traditional media material and their trademarks without compromising the quality of traditional images [4]. When a debate exists, the public media evokes verified facts that may be seen as definitive documentation to show possession. Watermarking is the procedure that inserts the information to be shrouded which is called as a digital mark into the digital multimedia questions with the end goal that this watermarked information can be evoked later to make an asseveration about the article. All digital watermarking proposals must follow imperceptibility requirements and, in turn, protection against every threats against watermark extraction and expulsion. From the previous decades there are such a variety of algorithms have been executed for digital image watermarking utilizing slightest noteworthy bit (LSB) approach [6, 7] and [8], Separable four transformations (DFT), discrete transforming cosines (DCT) [9] and [10], discrete transforming sines (DST), transforming radons (RdT) [11] and [12] etc., However, every one of them or neglected to create higher imperceptibility and absence of perceptual quality. Here in this letter, an imperceptibility and strong embedding and extraction algorithms have been proposed. DCT, DFT and also separate transformations are more powerful than Wavelet. It is computer-efficient than other strategies of transformation [13]. It is exceedingly rational to classify areas in the RGB picture where imperceptibility may be inserted for the watermark details because of their fantastic spatial frequency limitation properties. We know that any relation among wavelet coefficients also exists after disintegration of the RGB edge using the wavelet transformation.

2 Existing Approaches

2.1 LSB Approach

Minimum Significant Bit (LSB) addition is a typical, straightforward way to deal with installing information in a spread video. Video is changed over into various

edges, and after that change over every casing into an image. Afterwards, a few or most of the bytes inside an image will be replaced to a bit of each part of the Red, Green and Blue shading as each is spoken to by one byte. At the end of the day one can store 3 bit in every pixel. We executed our undertaking with the end goal that it can acknowledge and video of any size.

2.2 Discrete Fourier Transform

Frederic suggests a 2-D DFT solution in 1999 [5] and a secured video protection, which is primarily to reduce the copying and dispersal of proprietary materials. The strategy is based on the DFT of the picture scene borders, which then in existing commitments proposed separately a screen shot. In fact, the details to be contained in the film will be programmed using the private encryption key, to maintain the confidentiality of the frame and placed in the DFT range of the camera edges.

$$F(u, v) = 1/MN \sum\nolimits_{\_} (x = 0)\hat{}(M - 1) \sum\nolimits_{\_} (y = 0)\hat{}(N - 1)$$
$$\left(f(x, y)^{*}\mathrm{e}\hat{}((-j2\pi(ux/M + vy/N)))\right) \quad (1)$$

where, u=0,1,2,…., $M-1$,
$v = 0, 1, 2, \ldots, N-1$ and $j=\sqrt{(-1)}$
The inverse DFT (IDFT) is given by

$$F(x, y) = \sum\nolimits_{\_} (u = 0)\hat{}(M - 1) \sum\nolimits_{\_} (v = 0)\hat{}(N - 1)$$
$$\left(F(u, v)^{*}\mathrm{e}\hat{}((-j2\pi(ux/M + vy/N)))\right) \quad (2)$$

The frame ‘s size is M and N. DFT will help you recognize enough portions of the watermark image to insert the text, which in effect increases perceivability and robustness. It is really helpful as a watermarking algorithm.

2.3 DCT

DCT is one of the ways in which host signal may be decomposed into many frequencies and the insertion into the mid-band watermark becomes much smoother because the host video frames are left without any large optical sections of the bands [14]. The mid-frequency bands were also picked for integrating the details into the recording of the host. That block is inserted in the initial video picture, which is transformed into a spatial domain in motion and is separated into 8×8 pixel sections. The DCT is given in two dimensions

$$C(0,0) = 1/K \sum\nolimits_{\_} (a = 0)\hat{}(L-1) \sum\nolimits_{\_} (y = 0)\hat{}(K-1)(f(a,b)) \quad (3)$$

$$C(i,j) = 1/\left(2K\hat{}3\right) \sum\nolimits_{\_} (a = 0)\hat{}(L-1) \sum\nolimits_{\_} (b = 0)\hat{}(K-1)$$
$$\left(F(a,b)^{*}[\cos(2a+1)i\pi]^{*}[\cos(2b+1)j\pi]\right) \quad (4)$$

where, i=0,1,2,…., $K-1$,
j=0,1,2,…., $K-1$ and $j=\sqrt{(-1)}$
The IDCT is given by

$$f(a,b) = 1/K\, C(0,0) + 1/\left(2K\hat{}3\right) \sum\nolimits_{\_} (a = 0)\hat{}(L-1) \sum\nolimits_{\_} (b = 0)\hat{}(K-1)$$
$$\left(f(a,b^{*}[\cos(2a+1)i\pi]^{*}[\cos(2b+1)j\pi]\right) \quad (5)$$

Many architectures in the watermarking phase have been found by DCT. In certain instances the DCT image coefficient has been applied to watermark coefficients [9] and [10] or other DCT inputs have been selected to be inserted. The DCT scope also contains [15] and [16] articles. Authors in [16] was checked on automated watermarking policies like LSB, DCT and DWT. These methods are applied and measured. The DWT-based algorithm [17] has recently been created. Nevertheless, they both suffer from a loss of imperceptibility, higher computing difficulty and time. Within this letter a modern video watermarking algorithm was introduced to address these drawbacks and increase protection standards. The algorithm suggested has been found to have much superior watermarking algorithms than previous models.

Wavelet analysis: This is a moving window system of different regions. Wavelet analysis enables us to use longer periods, low-frequency comprehensive and shorter areas where information on high frequency is needed (Fig. 1).

Some of the main benefits of wavelets is that it can evaluate the region locally from a wide-ranging signal. Find a slight discontinuity in the sinusoidal signal which is so low that it is hardly noticeable [18]. Throughout the modern world, this signal can easily be produced by a fluctuation of power or a noisy turn.

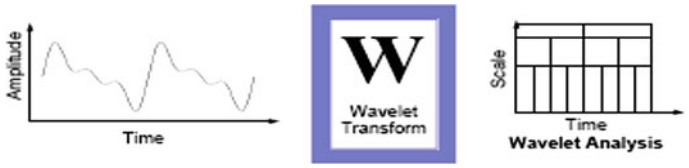

Fig. 1 CWT

3 Proposed Methods

3.1 Wavelet Domain

The wavelet is more main stream in sign handling applications. In the beginning we must disintegrate a video from a host into a variety of frames and then the edges into pictures. One edge would then be selected to mount the information after it has been connected and deteriorated three subtle components, one speculation, across four sub-bands. The guess-coefficients comprise fewer inputs (LL), and the higher precision knowledge (HL), vertical(LH), and corner-to-corner(HH) components is given by the implicit input-coefficients. The most prefered point of view for the wavelet transformation is its consistency with the HVS model portion in comparison to FFT or DCT. For the deployment phase are agreed on the suggested algorithm substrands LL and HH of the wavelet transition level 2 of the event. The accompanying Fig. 2 illustrates how the degradation and leisure tree works.

We anticipated utilizing low frequency substrips here in this document. Since the usage of watermarks in low substrates enhances the strength of different assaults, for instance, RST, distortion, Gaussian clamor, and middle filtering, rendering the design more fragile for shifting variations, gamma alteration, and histogram change. Implanting watermarks in high frequency subbands renders the watermark imperceptible and allows it safer against a range of threats when embedded in low frequencies.

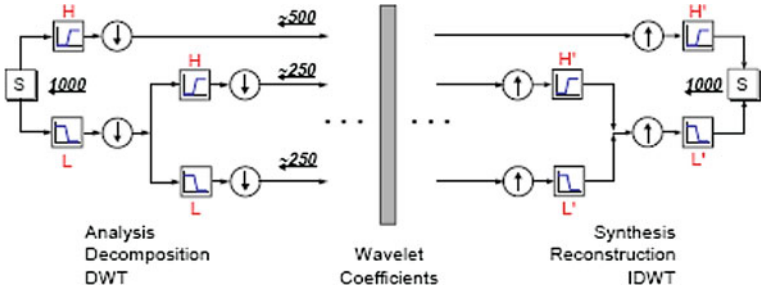

Fig. 2 Wavelet decomposition and reconstruction tree

3.2 Algorithms

Proposed watermarking consists two algorithms, those are

1. RGB image watermarking
2. RGB video watermarking

Both of them consists of embedding and extraction processes.

I. ***RGB image Watermarking***

A. ***Embedding Process***

Step 1: DW is included in the 4 subbands of Cover A: LSLS, HSLS, LSHS and HSHS Figure A.

Step 2: SVD applies to any image of the subband $M\hat{}n = P\_m\hat{}n \sum\_ m\hat{}nJ\_m\hat{}nRn = 1, 2, 3, 4$ where k denotes LSLS, HSLS, LSHS, and HSHS bands, and $\lambda\_g\hat{}n$, $g = 1, \ldots n$ are the singular values of $\sum\_ m\hat{}m$

Step 3: Place the visual watermark on SVD: $P = P\_V \sum\_ V\ S\_P\hat{}R$ where λ_pg, $g = 1, \ldots, n$ are the singular values of $\sum\_ P$

Step 4: Adjust the singular values of the cover picture for the singular values of the graphic watermark of each subband:

$$\lambda\_g\hat{}(*n) = \lambda\_g\hat{}n + \alpha\_n\lambda\_pg,\ g = 1, \ldots, i, \text{and}\, n = 1, 2, 3, 4.$$

Step 5: Get the 4 sets of DWT coefficients changed:

$$M\hat{}(*n) = P\_m\hat{}n \sum\_ m\hat{}(n*)V\_m\hat{}nR,\ n = 1, 2, 3, 4$$

Step 6: To create a watermarked cover image add the reverse DW to the 4 sets of adjusted DW coefficients.

Extraction Process

Step 1: Decompose (and likely attack) picture A^* with a watermark on the DW into 4 subbands: LSLS, HSLS, LSHS and HSHS.

Step 2: Place the visual watermark on SVD: $M\hat{}(*n) = P\_m\hat{}n \sum\_ m\hat{}(*n)V\_m\hat{}nR$, n = 1,2,3,4, where n is, LSLS, HSLS, LSHS, and HSHS bands.

Step 3: Remove special values from any subband: $\lambda\_pg\hat{}n = \left(\lambda\_g\hat{}(*n) - \lambda\_g\hat{}n\right)/\alpha\_n$, g = 1,…, i, and n = 1,2,3,4.

Step 4: Build the four visual watermarks with the same vectors: $P\hat{}n = R\_P \sum\_ P\ S\_P\hat{}R\, n = 1, 2, 3, 4$ (Fig. 3).

II. ***Video Watermarking***

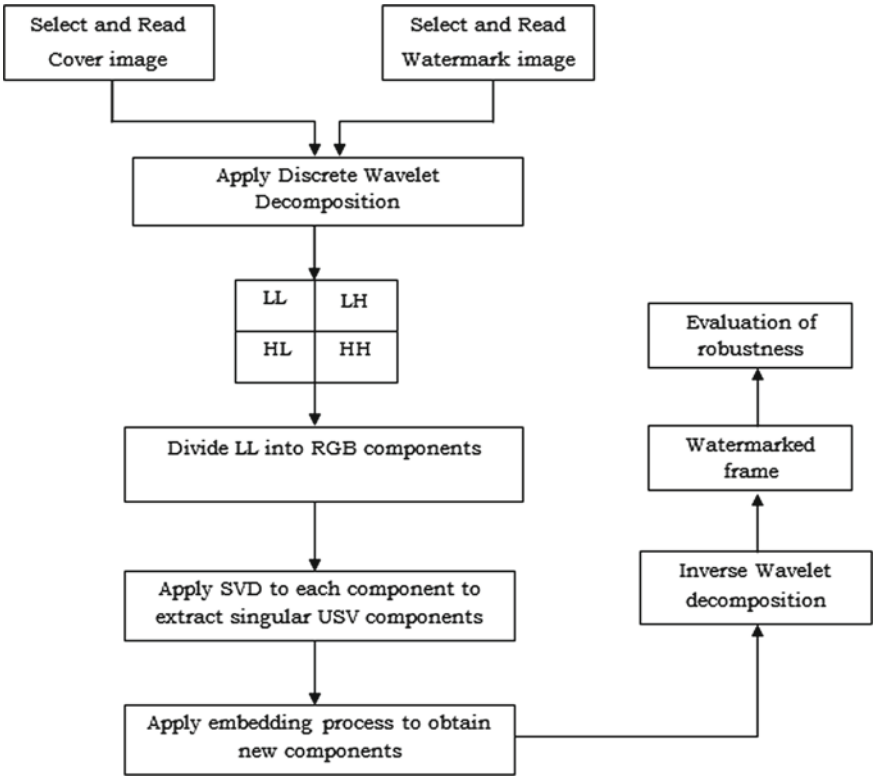

Fig. 3 RGB image watermarking algorithm

Get video frames and camera frames This analysis work applies to video frame steganography. We are separating all the frames from the video until the subject is inserted in the camera frames. We receive video frames by means of a simple algorithm (Fig. 4).

It is very necessary to break the RGB picture into its elements, then continue the cycle, to obtain the very same RGB message picture. The picture of the notification shows us red, green and blue sections in gray scale (Fig. 5).

The proposed Decimated Wavelet (DW) and Singular Value Decomposition (SVD) based video watermarking embedding process on video frame is as follows:

Step 1: Select and read source video from the MATLAB current directory.

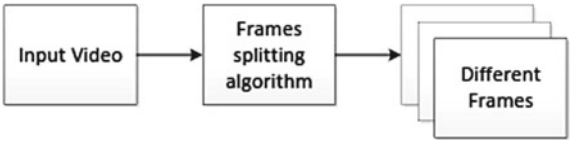

Fig. 4 Split video into frames

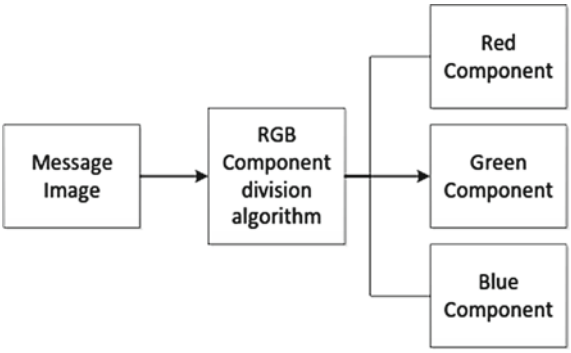

Fig. 5 RGB component of input image

Step 2: Split the input watermarking video into number of frames and select a cover frame in which we want to embed the message
Step 3: Select and read the watermark image
Step 4: With DW, the cover F is broken down into 4 sub-bands: LSLS, HSLS, LSHS, and HSHS.
Step 5: SVD is applied for each surface $H\hat{}nPm\hat{}n == 1.2, 3 - 4$ for every band of LSLS, HSLS, LSHS, and HSHS bands $-g\hat{}n$, g=1,… i are the specific values of $\hat{}\ m\hat{}n$ SVD for every subface of the picture is applied, $H\hat{}n = P\ m\hat{}n\ \hat{}\ m\hat{}n\ R\ m\hat{}nV\ n = 1,2,3,4$ for any subband of the band of the same name, where k is LSLS, HSLS, LSHS and HSHS, and $\mu\ g\hat{}n$, g=1,…
Step 6: SVD is placed in watermark: $P = S\_P \sum\_ PJ\_P\hat{}R$ where λ_pg, $n = 1,\ldots, i$ are the singular values of $\sum\_ P$
Step 7: Adjust the identical picture values with a special watermark for each subband values:

$$\lambda\_g\hat{}(*n) = \lambda\_g\hat{}n + \alpha\_n\lambda\_pg, g = 1, \ldots, i, \text{and}\, n = 1, 2, 3, 4$$

Step 8: Get 4 DWT coefficient sets modified:

$$F\hat{}(*k) = U\_a\hat{}k \sum\_a\hat{}(*k)V\_a\hat{}kT, k = 1, 2, 3, 4.$$

Step 9: Apply the reverse DW to the watermarked cover image with 4 sets of modified DW coefficients.

The proposed Decimated Wavelet (DW) and Singular Value Decomposition (SVD) based video watermarking extraction process on watermarked video frame is as follows:

Step 1: Read watermarked frame
Step 1: Using DW to decompose a designated $F*$ frame into 4 parts of subtrips: LSLS, HSLS, LSHS and HSHS. DW is used for this function.

Step 2: Apply SVD on any image of the subband: $R\hat{}(n*) = P\_m\hat{}n \sum \_m\hat{}(n*) P\_m\hat{}nR$, $n = 1,2,3,4$, where n is LSLS, HSLS, LSHS, and HSHS bands.

Step 3: The every subband is extracted into the singular values: $\lambda\_pg\hat{}n = (\lambda\_g\hat{}(*n) - \lambda\_g\hat{}n)/\alpha\_n$, $g = 1, \ldots, i$, and $n = 1, 2, 3,4$.

Step 4: Build 4 visual watermarks with single vectors: $P\hat{}n = V\_P \sum \_PT\_P\hat{}R\, n = 1, 2, 3, 4$(Fig. 6).

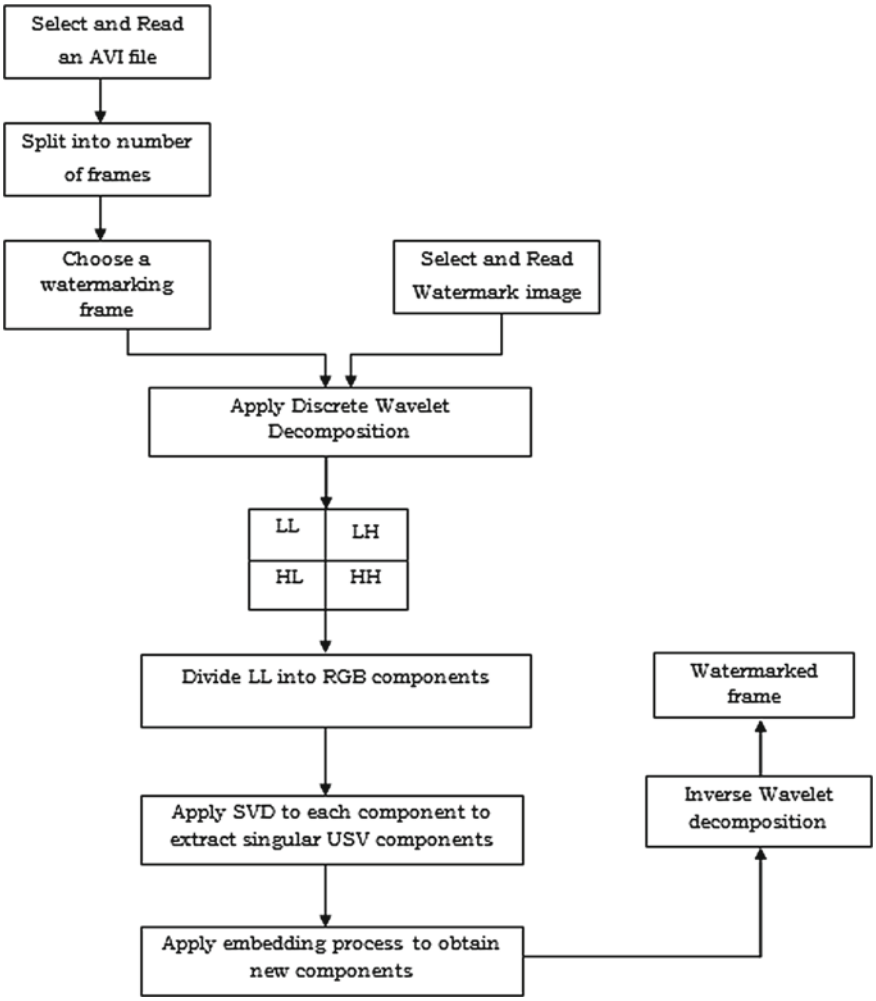

Fig. 6 Proposed video watermarking algorithm

4 Experimental Analysis

The MATLAB 2014 Update has conducted preliminary tests and evaluated various RGB photos and RGB recordings. They used the update 4GBRAM.Our proposed video watermarking algorithm has provided more security and robustness. We also compared the proposed quality metric algorithm with the current DWT method such as PSNR and SSIM. Figures 7 and 8 show that the embedding and extracted simulation results of DWT watermarking process.

Proposed RGB image watermarking outputs has shown in Fig. 9. We can see that the extracted watermark image is more robust and efficient than the DWT process

Fig. 7 **a** Cover image **b** watermark image **c** DWT decomposition of watermark image **d** watermarked image

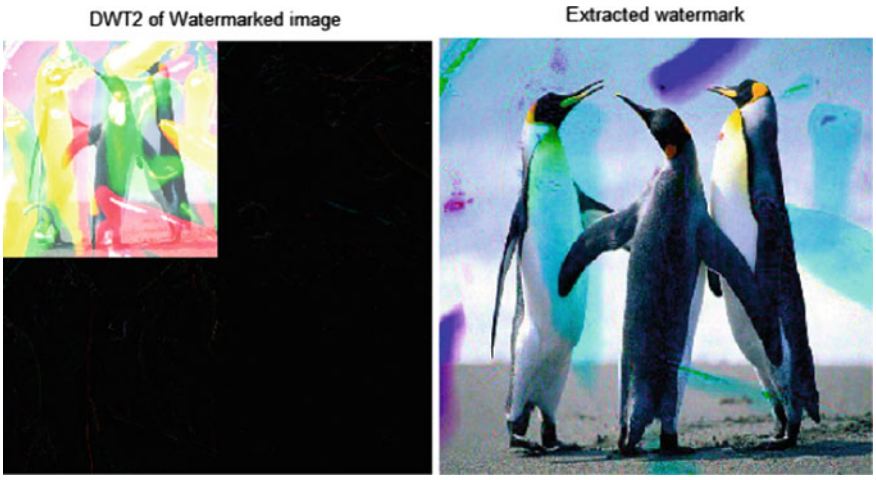

Fig. 8 Decomposition of watermarked image and extracted image

which has been shown in Fig. 9. Our new video watermarking approach has been shown in Fig. 10 and Figs. 11, 12.

5 Conclusion

In order to boost the reliability and stability of traditional watermarking algorithms, built for RGB images, a new encoding and decoding algorithm was suggested to be used for video marking in the wavelet transform domain. Simulation results suggest a higher performance than the traditional systems of the proposed algorithm. We had also measured the quality assessment of images (IQA) to improve the imperceptibility. We got higher imperceptibility for the proposed video watermarking also gained more PSNR value, which indicates that the higher perceptual quality of extracted watermark and watermarked image/frame.

Fig. 9 Proposed RGB image watermarking results

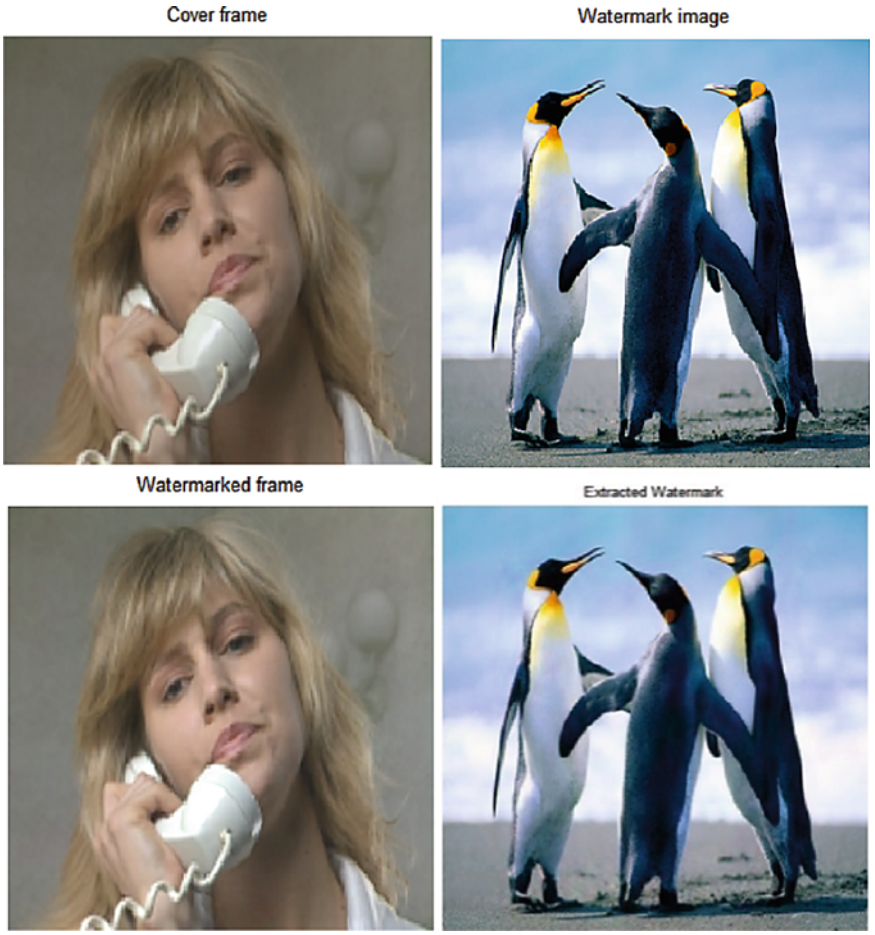

Fig. 10 Proposed video watermarking **a** cover frame **b** watermark image **c** watermarked frame and extracted image

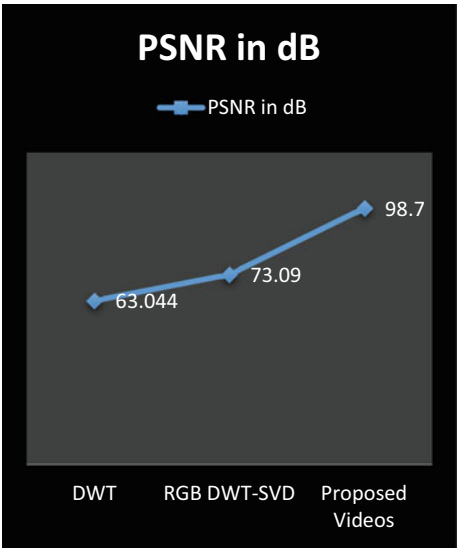

Fig. 11 Comparison of PSNR values

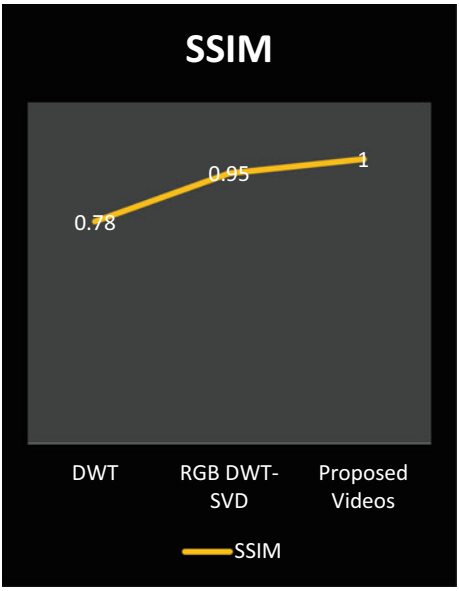

Fig. 12 Comparison of SSIM values

References

1. https://en.wikipedia.org/wiki/Digital_watermarking
2. http://www.alpvision.com/watermarking.html
3. Shih FY (2007) In: Digital watermarking and steganography: fundamentals and techniques, December 17

4. Kedmenec L, Poljicak A, Mandic L (2014) Copyright protection of images on a social network.In: ELMAR (ELMAR), 2014 56th international symposium, pp 1–4
5. Deguillaume F, Csurka G, O'Ruanaidh JJ, Pun T (1999) Robust 3D DFT video watermarking. In: Proceedings SPIE 3657, security and watermarking of multimedia contents, (April 9, 1999), vol 113
6. Keshari S, Modani SG (2011) Dual watermarking based on multiple parameter fractional fourier transform and LSB technique. In: Image information processing (ICIIP) 2011 International conference on, pp 1–5
7. Abdullatif M, Zeki AM, Chebil J., Gunawan TS (2013) Properties of digital image watermarking. In; Signal processing and its applications (CSPA), 2013 IEEE 9th international colloquium on, pp 235–240
8. Kumar S, Yadav AK, Gupta A, Kumar P (2015) RGB image steganography on multiple frame video using LSB technique. In: Computer and computational sciences (ICCCS), 2015 international conference on, pp 226–231
9. Hernandez JR, Amado M, Perez-Gonzalez F (2000) DCT-domain watermarking techniques for still images: detector performance analysis and a new structure. IEEE Trans Image Process 9(1):55–68
10. Zheng J, Zhang Y., Feng D, Zhao R (2002) Color image watermarking based on DCT-domains of color channels. In: TENCON '02. Proceedings 2002 IEEE region 10 conference on computers, communications, control and power engineering, 28–31 Oct. 2002, vol 1 pp 281-284
11. Liu Y, Zhao J (2004) Rotation, translation, scaling invariant image watermarking based on radon transform. In: First canadian conference on computer and robot vision, pp 225–232
12. Cai L, Du S (2004) Rotation, scale and translation invariant image watermarking using Radon transform and Fourier transform. In; Proceedings of the IEEE 6th circuits and systems symposium on emerging technologies: frontiers of mobile and wireless communication, vol 1, pp: 281–284
13. Hernandez-Guzman V, Cruz-Ramos C, Nakano-Miyatake C, Perez-Meana H (2006) Watermarking algorithm based on the DWT. IEEE Latin Am Trans 4(4):257–267
14. Arya RK, Singh S, Saharan R (2015) A secure non-blind block based digital image watermarking technique using DWT and DCT". In: International conference on advances in computing, communications and informatics (ICACI), pp 2041–2048
15. Chandran S, Bhattacharya K (2015) Performance analysis of LSB, DCT and DWT for digital image watermarking application using steganography. In: International conference on electrical, electronics, signals, communication and optimization (EESCO), pp 1–5
16. Sneha K, Naveen C, Satpute VR, Keskar AG (2016) Discrete wavelet transform based video watermarking technique. In: International conference on microelectronics, computing and communications (MicroCom), pp 1–6 J
17. Sendhilkumar NC, Ramesh GP (2020) Analysis of digital FIR filter using RLS and FT-RLS. Advances in intelligent systems and computing
18. Irshad SM, Ramesh GP (2020) ANFIS-based MPPT control in current-fed inverter for AC load applications. Advances in intelligent systems and computing

FPGA Implementation of 3D NOC Using Anti-Hebbian for Multicast Routing Algorithm

G. P. Ramesh and S. Prabhu

Abstract This work shows that a novel 3-Dimensional (3D) vertically incorporated adaptive computing structure. This FPGA for 3D is a mix of best in class dealing with and interconnection development. It includes the vertical joining of two chips of Configurable Array Processor. The Configurable Array Processor is a variety of heterogeneous manufacturing components while the Intelligent Configurable Switch contains a switch controller, on-chip program, and data memory, information outline support alongside a Direct Memory Access controller. The FPGA for 3D architecture for constant communication and mixed media flag preparing as a next-generation computing system and programming execution and check philosophy including abnormal level demonstrating and design investigation of FPGA for 3D utilizing System to decide the ideal equipment detail in the early outline organize. It can deal with a few goals addresses in the meantime, recombine the packages, sent similar information to the diverse goal hubs, and maintain a strategic distance avoid from the congestion. The innovative multicast 3D NoC router performs the proposed algorithm, NoC can be designed in the Verilog HDL, and the operation is computed in the ModelSim software. All these samples and modulation taken and it has been synthesized in FPGA.

Keywords 3D · NoC-Bus hybrid architecture · 3D ICs · Multicast communication

1 Introduction

Network-on-Chip have been the dominant pattern standard as a multi and several—core structures for quite every while, and a functioning field of research for near

G. P. Ramesh (✉)
Department of ECE, St. Peters Institute of Higher Education and Research, Chennai, India
e-mail: rameshgp@yahoo.com

S. Prabhu
Department of Electronics and Communication Engineering, Mahendra Institute of Technology, Namakkal, India
e-mail: vsprabu4u@gmail.com

D. K. Sharma et al. (eds.), *Micro-Electronics and Telecommunication Engineering*,
Lecture Notes in Networks and Systems 179,
https://doi.org/10.1007/978-981-33-4687-1_29

two decades. They give the adaptability required to the correspondence of numerous heterogeneous centers and are a characteristic counterpart for the advances of 3D combination. A fundamental component in the NoC is the switch which advances bundles through the system. Initially, NoC switches were explicitly adjusted from interconnection systems, with no specific thought of the particular conditions forced by the on-chip condition. Figure 1 shows 3D FPGA system where many FPGA chips connected with DRAM chips.

The router parameters that rely upon arrange conditions and impact execution, territory, and power utilization, are flit size, flutters per cradle and number of virtual channels. A steering table or a primary rationale based directing method is utilized for steering computation. Specifically, support association in early NoC executions was restricted to info and input and output queuing which implies that the switch put away approaching or active movement, separately. Each information/yield port had its private supports. The quantity of info and yield ports relies upon the topology. A considerably more radical recommendation was the proposition of entirely buffer less routing, in view of redirecting or misrouting a few flutters that can't be appointed to an output port prompting the most brief way and there are no buffers to store them. This approach exchanges off router area for switch region and power utilization because of the elimination of buffers. The following improvement of 3D coordination prompted adjusting the routers proposed initially for 2D NoCs to 3D topologies. Network-on-Chip (NoCs), has developed as another last decade in the most recent decade to conquer the confinement of customarily on-chip correspondence framework, and are progressively essential in the present System-on-Chip (SoC) designs.

The architecture shown in Fig. 2 incorporates physical interfaces and correspondence instruments, which execute the correspondence between on-chip parts. It can accommodate a substantial number of protected innovation centers, giving separation between the computation and correspondence, and encourage a truly particular and scalable design approach for SoC. The plan of 2D on-chip interconnects been inspected from different viewpoints, for example, execution, circuit area, control utilization and dependability and some commercial contributions as of now send such systems. The approach and expanding suitability of three-dimensional (3D) silicon incorporation innovation give another skyline to interconnect plan on-chip. The 3D NoC has increased more interest and significance at a few colleges and

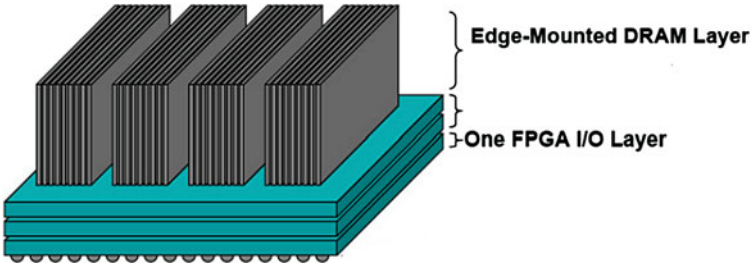

Fig. 1 3D FPGA diagram

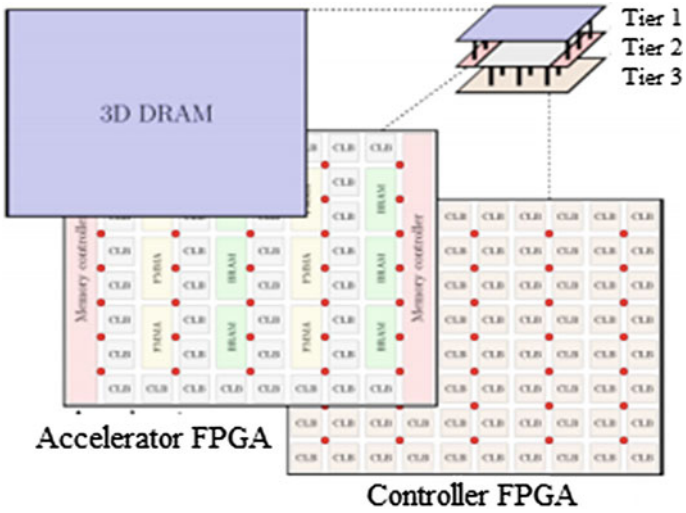

Fig. 2 3D FPGA-DRAM architecture

industry, as it is accepted to be a solution for the future interconnection issues in 3D chip multiprocessors.

2 Related Works

A basic issue in the plan of on-chip systems is the choice of the topology which influences all NoC parameters, for example, organizes dormancy, steering cost, zone and power execution. In writing, on-chip correspondence structures can be outlined as general or custom system topologies. The mesh-based interconnect architecture that comprises of a work of routers interconnecting IP centers set alongside the routers. The 2D Convolutions and Cross-Correlations Using Scalable and NOC for signification execution into a 3-D based FPGAs techniques. This architecture is getting more renowned for its smooth execution, the straightforwardness of the directing methodology and modularity [1–4].

The Cordic Algorithms for Multiplying Quaternion [5].A variety of the torus architecture, which wipes out the utilization of long wraparound wires, called a collapsed torus, is portrayed in the issue of torus and work topologies is the related system idleness. The solution of the NoC routing device is to locate the valid adjust between that territory, data transfer rate, control utilization and additional noteworthy execution records. Every outlined on-chip switch is a fundamental assurance to superior network rk-chip [6, 7]. The Online Set Intersection for Network Processing [8] has the accompanying attributes: its distance across stays sensible the quantity of layer of a system, the topology is adaptable and utilizes few switches for a given

amount of user. It has a characteristic progressive structure which can be helpful in the expansive scale interconnects and system zone networks [9, 10].

An interconnect architecture in light of a butterfly fat-tree for an organized SoC is a broad thought that insinuates the coordination of about all parts of system plot on a singular chip. The SoC diagrams are routinely dictated by the reliably creating enthusiasm for extended structure convenience and conservatives at any rate cost, control usage and time to publicize. These designs outline the purpose behind different novel electronic applications in the blink of an eye in regions, for example, wired and remote interactive media correspondence, and also the plan of required switches and tending to components. As of late, other new topologies, for example, such as a spider on NoC. The routing algorithm and NoC router its meant said by various works are centered around transmission package through a hub to different hub, both of this described as unicast. Nonetheless, among that advancement about the several core chip, the role of conveying a similar bundle over a few hubs is additionally required [11, 12], are proposed as a compromise among the clustering routing [13] and 2D work topologies. In any case, the versatility of the right now proposed arrangements, including a honeycomb structure, and butterfly fat-tree structure is either deficient or unexplored. Up to now the most well-known topologies utilized for on-chip arrange in center/tile based models are 2D work and 2D torus. In any case, rising three-dimensional coordination innovation shows two noteworthy favorable circumstances, in particular, higher execution and lower control utilization.

The dimensional enable chips to work at bringing down voltage with bringing down leakages, an unprecedented mix of upgraded execution and essentials viability stood out from past forefront transistors. The innovation incorporation capacities give chip creators the practicality to plan and fabricate NoCs that will grow in the third measurement. The topology of a NoC indicates the physical association of the interconnection organizes. It characterizes the interconnection between hubs, switches, and connections. One of the kinds of system topology is the roundabout system typologies; every hub has guide point-to-direct connections toward a subset of different hubs in the system called neighboring hubs [14–16].

The NoCs designs are made out of many layers, where each layer is a NoC matrix, where the systems are the same for every one of the layers, framed of components. A few examinations have demonstrated that NoCs can enhance normal correspondence execution, fundamentally in regards to usable data transmission and short bundle conveyance latencies, in light of the likelihood of utilizing the extra dimension [17–19]. A significant diminishment in the number and length of worldwide interconnect using 2D incorporation anticipated. The majority of these examinations found the 2D work most reasonable NoC. Our switch engineering delivers the requirements to help low inertness, and high transmission capacity correspondence administrations for the on-chip 2D work organizes and to give an adaptable and versatile outline for the multiprocessor frameworks on-chips. Our model will be created in the following sections [20].

3 Materials and Methods

The design of expansive gadgets infers radical and effective development in FPGA interconnection structure to enhance control utilization, region, and execution. Present day work FPGA plans depend on a bunched engineering additionally called group-based work FPGA. The proposed work is utilized to investigate the new effective approach to outline interconnection structures for bunch based work FPGA designs. 3D FPGA innovation is used to moderate the extensive ranges of lines effects and enhance that general framework exhibition. Within the case, the 3D network IC advancement should be ascended being a champion among the various assuring responses to crushing the difficulties in interconnection and mix many-sided quality of present-day circuit plans. The 3D design can be effectively used to decrease worldwide interconnect length and enhance the execution of the system.

A novel approach named Augmented Fabric Routing algorithm shown in Fig. 3 is proposed to enhance the execution of FPGA steering by including Traces into

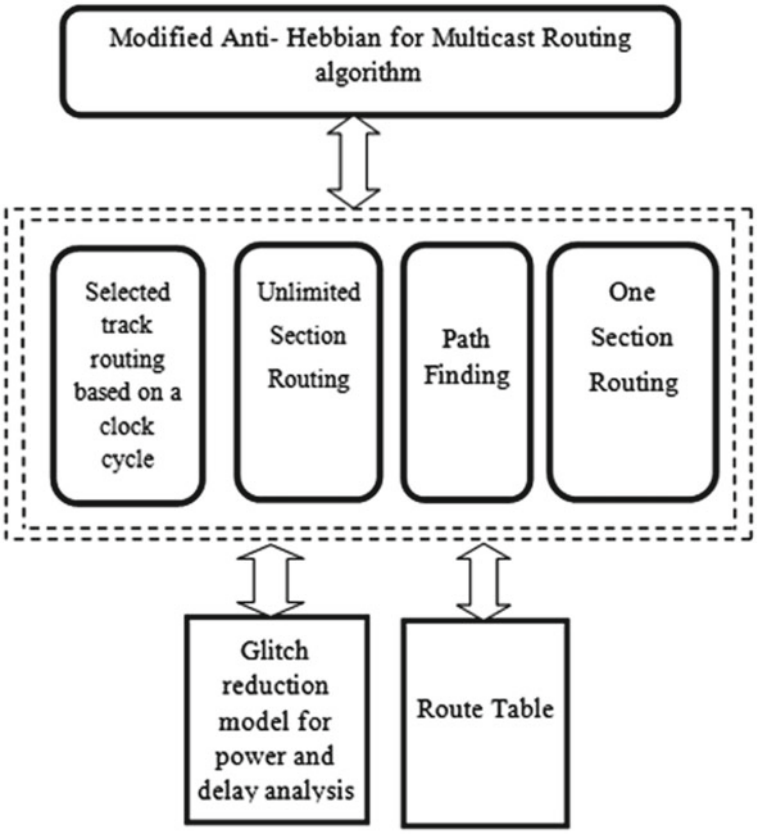

Fig. 3 Proposed system architecture

the current FPGA directing. The proposed work performs way discovery by sending the Sectional course ask for the message and gets the answer, which has the area data of the stations. Likewise, the halfway channels additionally perform learning of different channels area data which enables the choice of a region where the objective to channel finds and where the way identification must be executed. It is propelled to enhance the nature of the administration of on-chip arranges moreover; the spread of glitches in both the control and data route parts of the circuit. In light of the examination, we make frameworks that undertaking to diminish glitching power use by constraining age and expansion of glitches in the circuit.

3.1 Modified Anti—Hebbian for Multicast Routing Algorithm

In the accompanying system, the identification of suspicious fortuitous events is performed by anti Hebbian Multicast Routing inhibitory feedback connections, i.e., data-wise similarities within source components, Even though additionally about Excessive arrange conditions and highlights of the information. A unit that has been inert for quite a while slowly brings down its edge (i.e., ~ limits its Selectivity), observe an often effective system steadily turns out to be more specific by increasing its edge. This system produces m data: $ab, j = 1\ldots M$, to n portrayal units: bi, $I = 1\ldots n$. In light about each input and the non—linearity units, that can't be ascertained in a single advance as on account of one unit, because the criticism from other units impacts the last yield here. Given that the input is symmetric ($w_{ij} = w_{ji}$), the system is ensured to sink into a steady state after an underlying transient. Here transient occurred mimicked by numeric explaining the modified distinctive condition for specific info design:

$$\mathrm{d}Y/\mathrm{d}t = F \sim i\, qibaj + j = \sim 1\, w \sim b^* - ti) - b^*$$

Either j, q both this density for an association from ab toy ~ , w U is a unique association within units yj, nonlinearity y, the units are addressed with that capacity.

$$J(u) = 1/(1 + \exp(-Au)).$$

The system is at that point computed by forming the benefit of y^* in the steady state to 0 or 1 ($bi = 1$ if $b^* > 0.5$, $b \sim = 0$ contrarily). These feedforward data are arising chance, 2 also the feedback substances are 0.

3.1.1 Algorithm

stated m, precision criteria ε, and the most extreme number

of cycles max iter.
Note weights $w = [\alpha ij, \beta i]T$ $(1 \leq j \leq 7,\ 1 \leq i \leq m)$.

Step 1: Initialize: $w =$ Test and estimate $iter = 0$.
Step 2: Deliberate $E(w)$ practice using data. If $E < \varepsilon$ or $iter >$ max iter, then stop.
Step 3: Compute $\dfrac{\partial E}{\partial w}$ using example information.
Step 4: Apply the optimal solution to obtain Δw, renew $w1 = w1 + \Delta w2$, and receive the new model $f\ E(w) \cdot$ Continuous $=$ iteration $+ 1$ and go to Step 2.

Performed efficiency criteria ε, and the highest number of covered node max. Obtain weights $W = [\alpha ij, \beta i]T$ also M.

Step 1: Establish: $W = 0$, $E = 0$.
Step 2: Compute $E(w)$ relating instruction data. If $E < \varepsilon$ or $m >$ max m, when check.
Step 3: Extension a numeral of secret node to one $M = M + 1,\ i = i + 1$.
Step 4: Allow arbitrary data weight αij $(1 \leq j \leq 7)$ to the current ith isolated neuron.
Step 5: Assume that amount weight βi for the modish obscure node based on instruction information, E, and αij, and receive the distinct design $f\,W$new $= f\,W$e preceding $+ \beta iyi$. Go to Step 2.

3.2 A Path Finder Routing Algorithm

The Pathfinder calculation to detect path for every one of the nets. Pathfinder routes one loss at any given moment inside every iteration. Congestion is transiently permitted in the middle of the road steering comes about, and the nets must consult with each other to figure out which one possesses the full asset in ensuing cycles until the point when all blockages are settled, and an entirely legitimate directing outcome is perceived.

3.2.1 The Sequential Pathfinder Algorithm

Step 1: PathFinder(gains $\{Ni\}$, arch $G =$ hV,Ei)
Step 2: while routing deficient or clog exists does.
Step 3: SeqMaze($\{Ni\}$)
Step 4: modified history expenses of the hubs in V
Step 5: close while
Step 6: result Pathfinder
Step 7: finish
Step 8: SeqMaze(nets $\{Ni\}$)
Step 9: during various unrouted or stuffed net Ni do
Step 10: rip-up RTi if exists
Step 11: $RTi \leftarrow \{si\}$

Step 12: for each separated sink *tij* do
Step 13: $Pj \leftarrow$ MazeExpand(*RTi, tij*)
Step 14: $RTi \leftarrow RTi \cup \{Pj\}$
Step 15: end regarding
Step 16: update already takes about that node in *RTi*
Step 17: the purpose of
Step 18: end SeqMaze

3.3 Parallel Pathfinder

The routing of $S-$ and $S+$ don't begin until the point when S0 completes, and the directing of *S*0 in the following cycle does not begin until *the point that* $S-$ and $S+$ wrap up. The nets in every subset are either directed successively or divided similarly and routing in parallel. Plainly our parallel directing calculation is deterministic.

3.3.1 Parallel Pathfinder Algorithm

Step 1: ParRoute(nets {*Ni*}, arch $G =$ h*V,E*i)
Step 2: *pid* $\leftarrow$ producer_id()
Step 3: if *pid* == 0 then
Step 4: while routing incomplete or blockage exists do
Step 5: {*RTi*} $\leftarrow$ ParMaze(0, {*Ni*})
Step 6: update history expenses of the hubs in *V*
Step 7: return {RTi}
Step 8: end *whi*le
Step 9: else
Step 10: *tid* $\leftarrow$ task_id(*pid*)
Step 11: to occumplish $\leftarrow$ owner_pid(parent(tid))
Step 12: receive nets {*Nj*} from *manager*
Step 13: $\{RTj\} \leftarrow$ ParMaze($tid, \{Nj\}$)
Step 14: send {*RTj*} to *manager*
Step 15: close if
Step 16: finish ParRoute
Step 17: finish
Step 18: ParMaze(task id *tid*, nets {*Nj*})
Step 19: if *tid* is at the last level then
Step 20: $\{RTj\} \leftarrow$ SeqMaze($tid, \{Nj\}$)
Step 21: return {*RTj*}
Step 22: else
Step 23: ($S0,\ S-,\ S+$) $\leftarrow$ partition($\{Nj\}$)
Step 24: $\{RTj : Nj \in S0\} \leftarrow$ SeqMaze(*S*0)
Step 25: *operater* = owner_pid(rchild(*tid*))

Step 26: passing $S+$ to *worker*
Step 27: $\{RTj : Nj \in S-\} \leftarrow$ ParMaze(lchild(tid), $S-$)
Step 28: receive $\{RTj : Nj \in S+\}$ from *worker*
Step 29: return $\{RTj\}$
Step 30: end if
Step 31: end ParMaze

4 Results and Discussion

A. Estimation approach

The Proposed method is outlined with in Verilog (HDL), reproduced in Modelsim, also incorporated FPGA separately prototyped. Some multifaceted equipment nature of within planned 3D multicast switch means assessed into regards to territory use, update, and inactivity. To confirm this legitimacy of our 3D Anti-Hebbian For Algorithm, Multicast Routing technique we first utilize the which Modelsim is a standard business reproduction device in the hardware business. To finish the reproduction, activity generators are utilized for creating excitation motion to switch. The signals appeared in Fig. 4 clarify that that information send through to goal yield port in light of the goal tends to which it takes. So our directing calculation can fulfill the necessities of capacity and timing.

At that point, a Mesh NoC is worked to confirm the legitimacy of the entire system and figure the throughput and inertness. In Fig. 5, the condition of the IP centers of various hubs sending and accepting bundles can be seen. So we may presume that our switch likewise can fulfill the prerequisites of capacity and timing in the entire 3D arrange.

B. Everywhere and latency

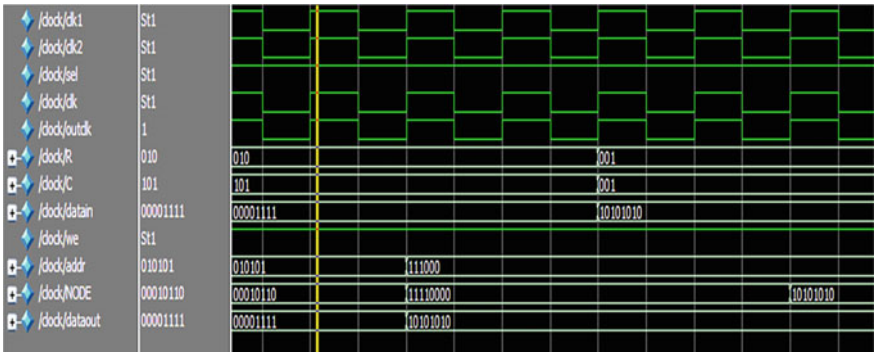

Fig. 4 Simulation waveforms of router

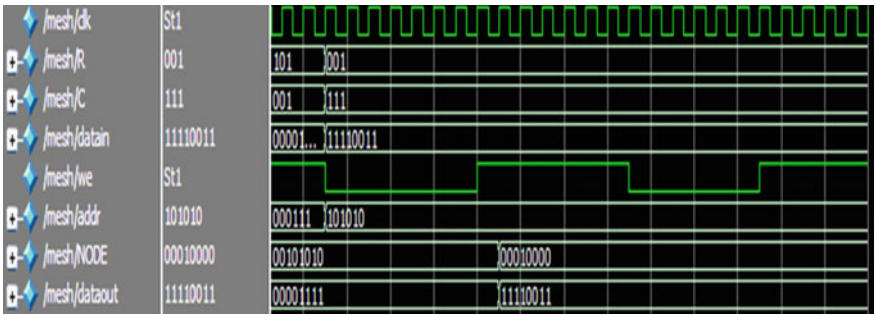

Fig. 5 Simulation waveforms mesh NoC

Throughput implies the rate that packets can be sent over the system.

$$\text{Throughput} = \frac{\text{Total Packets} \times \text{Length}}{\text{IP's number} \times \text{Time}}$$

where the Total bundles is the number of parcels which effectively achieve their goal hubs, Length is the number of bits per packet, IP's name is the quantity of IP squares embroiled in the correspondence, and the Time alludes to the amounts of clock cycles that pass between the principal message sending and the last message accepting [11].

The dormancy implies the average time which keeps going between the head bounce infusion into the system at the source hub and the tail flutter of this parcel gathering at the goal hub:

$$\text{Latency} = \frac{\sum_{i}^{N} \text{Latency}i}{N}$$

where the Latency I allude to the flag inertness and N is the aggregate number of parcels achieving their goal hub.

Figure 6 dropping probability is obtained by calculating the ratio of the count of data having type identifier to the count of the total number of data generated from each source node. Figure 7 shows variation of average throughput with traffic load for various topologies.

5 Conclusion

There is the tremendous number of routing algorithm proposed, and few of them are executed in the system. The choice of routing algorithm exclusively relies on application and system conditions. A deterministic calculation is easy to perform and

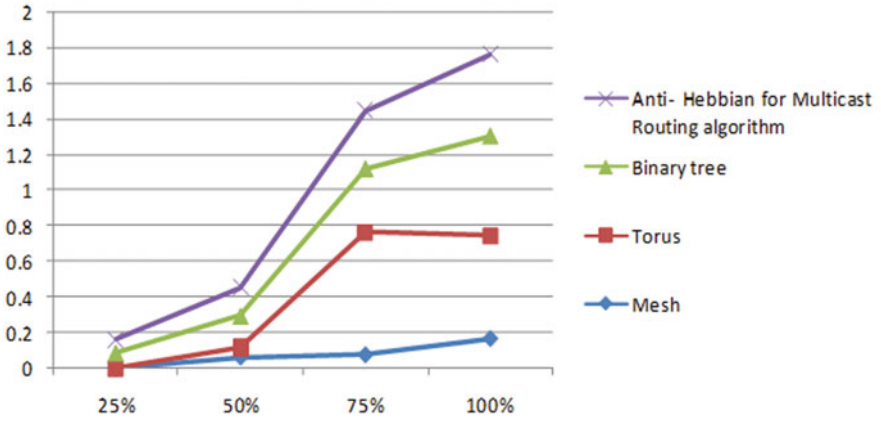

Fig. 6 The variation of dropping probability with traffic load

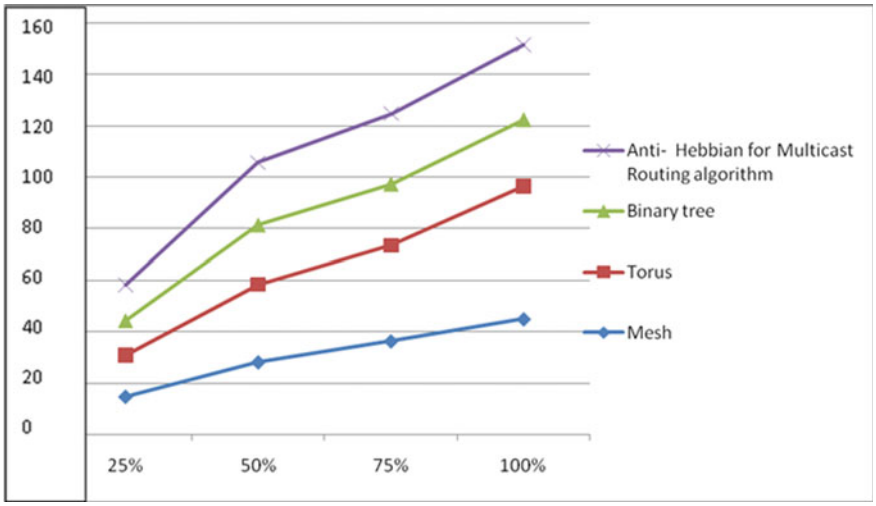

Fig. 7 Variation of average throughput with traffic load for different topologies

has a particular structure of way to take after between the source and the goal hub. In overwhelming rush-hour gridlock, a deterministic calculation may incline to clog and give higher system inactivity. *XY* directing calculation is deterministic and takes after the steering way and has inactivity on the more upper side. Turn model can be sorted as an Anti-Hebbian For Multicast Routing Algorithm. However, it confines a few turns, which makes it somewhat versatile. The basic parameter considered while planning the switch is an exchanging system. There is the quantity of switch engineering proposed before with exchanging procedures. This paper looks at past switches and depicts the outline of the switch utilized for usage of the versatile

calculation on FPGA for 3D. There are not very many completely Anti-Hebbian For Multicast Routing Algorithm was in presence which is appropriate for 3D, and there is the degree for creating one as the above registering situation is advancing progressing every time.

References

1. Coelho D, Cintra R, Rajapaksha N, Mendis G, Madanayake A, Dimitrov V (2017) DFT computation using gauss-eisenstein basis: FFT algorithms and VLSI architectures. IEEE Trans Comput 99:1–1
2. Carranza C, Llamocca D (2017) Fast 2D convolutions and cross-correlations using scalable architectures. Marios Pattichis IEEE Trans Image Process 99:1 – 1
3. Siozios K, Soudris D (2016) A customizable framework for application implementation onto 3-D FPGAs. IEEE Trans Comput-Aided Des Integr Circuits Syst 35(11):1783–1796
4. Firdaus AF, Meribout M (2016) A new parallel VLSI architecture for real-time electrical capacitance tomography. IEEE Trans Comput 65(1):30–41
5. Parfieniuk M, Park SY (2016) Sparse-iteration 4D CORDIC algorithms for multiplying quaternions. IEEE Trans Comput 65(9):2859–2871
6. Pan T, Zhang T, Shi J, Li Y, Jin L (2016) Towards zero-time wakeup of line cards in power-aware routers. IEEE/ACM Trans Netw 24(3):1448–1461
7. Oliveira PAM, Cintra RJ, Bayer FM, Kulasekara S, Madanayake A (2016) Low-complexity image and video coding based on an approximate discrete Tchebichef transform. IEEE Trans Circuits Syst Video Technol 99:1–1
8. Qu YR, Prasanna VK (2016) Fast online set intersection for network processing on FPGA. IEEE Trans Parallel Distrib Syst 27(11):3214–3225
9. Wehbe T, Wang X (2016) Secure and dependable NoC-connected systems on an FPGA chip. IEEE Trans Reliab 65(4):1852–1863
10. Kumar R, Gordon-Ross A (2016) MACS: a highly customizable low-latency communication architecture. IEEE Trans Parallel Distrib Syst 27(1):237–249
11. Trefzer MA, Lawson DMR, Bale SJ, Walker J, Tyrrell AM (2016) Hierarchical strategies for efficient fault recovery on the reconfigurable PAnDA device. IEEE Trans Comput 99:1–1
12. Benson S, Chen CH, Lin DM, Liou LL (2016) Digital linear chirp receiver for high chirp rates with high-resolution time-of-arrival and time-of-departure estimation. IEEE Trans Aerospace Electron Syst 52(3):1146–1154
13. Mukherjee S, Roy S (2016) Nearly-2-SAT solutions for segmented-channel routing. IEEE Trans Comput-Aided Des Integr Circuits Syst 35(1):128–140
14. Moctar YOM, Lemieux GGF, Brisk P (2015) Fast and memory-efficient routing algorithms for field programmable gate arrays with sparse intracluster routing crossbars. IEEE Trans Comput-Aided Des Integr Circuits Syst 34(12):1928–1941
15. Gaillardon P-E, Tang X, Kim G, Micheli GD (2015) A novel FPGA architecture based on ultrafine grain reconfigurable logic cells. IEEE Trans Very Large Scale Integr (VLSI) Syst 23(10):2187–2197
16. Weinberg M, Betz V (2015) Robust optimization of multiple timing constraints. IEEE Trans Comput-Aided Design Integrated Circuits Syst 34(12):1942–1953
17. Jiang SY, Luo G, Liu Y, Jiang SS, Li XT (2014) Fault-tolerant routing algorithm simulation and hardware verification of NoC. IEEE Trans Appl Superconduct 24(5):9002805
18. Peng C-H, Chen B-W, Kuan T-W, Lin P-C, Wang J-F, Shih N-S (2014) REC-STA: reconfigurable and efficient chip design with SMO-based training accelerator. IEEE Trans Very Large Scale Integr (VLSI) Syst 22(8):1791–1802
19. Wang D, Lo C, Vasiljevic J, Jerger NE, Steffan JG (2014) DART: a programmable architecture for NoC simulation on FPGAs. IEEE Trans Comput 63(3):664–678

20. Vansteenkiste E, Al Farisi B, Bruneel K, Stroobandt D (2014) TPaR: place and route tools for the dynamic reconfiguration of the FPGA's interconnect network. IEEE Trans Comput-Aided Des Integr Circuits Syst 33(3):370–383

Wearable Jacket for Posture Correction Using Flexible Fabric Stretch Sensor for Working Age Groups

B. V. Santhosh Krishna, J. Jijin Godwin, A. Aline Gratia, K. Keerthanaa, and B. Kiruthika

Abstract Generally, IT professionals and people who are engaged with working in a long duration sitting postures are affected by musculoskeletal disorder. Our device is designed to help the people who are affected by this kind of health issue. Usually the people suffering from this disorder cannot give attention to their postures due to their full concentration in their respective work. This jacket will help in alerting the patient by the warning or stimulus which is given to them whenever the angle of the bend of the spinal cord has reached the pre-determined value or the threshold value of spinal cord angle in comparison with posture indication position. The sensor used in this device is flexible and thereby can be fixed to the fabrics so that the patients can wear them regularly. The trigger or stimulus given by our system which is done by using IOT will make the people to change their postures to prevent themselves from this disorder. Overall, the analysis performed implements the proposed idea as a monitoring system that can be used to identify body posture variations related to different levels of engaged users while performing cognitive tasks. Our model is also embedded with a pulse monitoring facility for easy diagnosis. Since it is a wearable one it can be used by young age people, middle age people as well as older age people.

Keywords IOT · Postures · Musculoskeletal disorder · Wearable one deflection sensor

1 Introduction

Due to the advancement of IT industry and the rapid increase in the busy hurry world, people loss themselves to give attention to their health especially the youngsters and

B. V. Santhosh Krishna (✉)
New Horizon College of Engineering, Bangalore, Karnataka 560103, India
e-mail: santhoshkrishna1987@gmail.com

J. Jijin Godwin · A. Aline Gratia · K. Keerthanaa · B. Kiruthika
Velammal Institute of Technology, Chennai, Tamil Nadu 601204, India

D. K. Sharma et al. (eds.), *Micro-Electronics and Telecommunication Engineering*,
Lecture Notes in Networks and Systems 179,
https://doi.org/10.1007/978-981-33-4687-1_30

middle aged people. As the working environment are changing into automation nowadays,physical works are reduced and mental works are increased which risks the human lives and their lifestyle. Because of this, the carelessness towards their respective health got increased which leads to sudden death and non-reasonable deaths at a very young ages. One such serious health issue called MUSCULO-SKELETAL DISORDER, a kind of non-communicable syndrome which affects the human's back and posture is increasing day by day. The demand for device-assisted care has been grown day by day. On the other hand, wearable devices such as fitness trackers (e.g., smart bands, smart Wrist watches, Garmin, Apple Watch, MI Band) and many healthcare wearable devices like smart clothes is emerging every day. These innovative electronic devices help the users to monitor and frequently check their physiological parameters and manage their health on their own. This can also help the physician access to the user's health data and receive personalized medical attention care. The proposed system of wearable jacket not only focuses on elderly people but also focuses on young age and middle age too who are affected by many in number by this special kind of health syndrome. As the system alerts and forces them to change their posture frequently they may get adopted to the changing position and make themselves to prevent from these serious health issues. The first section of the paper explains about the existing technology which is already involved in this kind of providence of a solution for the problem digitally. It also explains their features, its working condition in brief, components involved, advancement level along with their advantages and disadvantages and special kind of applications.

The second part of the paper describes the proposed model and the idea and theory involved briefly. The components involved, the advancement it holds, the advantages it overcame with the existing technologies and devices which are compatible. It also holds the comparison of performances of the existing one and the proposed one. Finally the paper got concluded with the advantages and vital applications of the proposed idea.

2 Existing Methods

In most cases, the main motive of this work has been focused in the detection and alteration of the user's posture. In the several literatures, many ideas have been explained to analyse the posture of the person automatically. In most of the methods the bending of the human skeleton is detected by using cameras. Everything is done through a camera like capturing the image, mapping with the predefined postures and then setting the result. This makes the system high in cost due to the use of cameras and it consumes a lot of time for manipulation. There is no intimation for the user if he is in the wrong posture for a longer time. This fails the person from experiencing damage. Most of the Project has been done by fitting the sensors in the chair. The posture of the person will be modified only if he/she is sit in that particular chair and we can't carry that chair wherever we want.It would be a disadvantage, the chair should be designed for each person's physical structure, it

can't be used by another person and if we are building a chair with these equipment it may cost high. Let's discuss by analysing each of these methods briefly.In this approach, the ideology implemented is providing a newly watch type patch which is a wearable one made of sheet sensors [1]. These sensors gets the value from the human body through ECG, body temperature, aspiration and chemical contents of glucose etc., These method also involves in highlighting the angle measurement of spinal cord and is displayed on the patch and nothing is done to detect the posture. In the Intelligent Chair Sensor—Classification and Correction of Sitting Posture, the method of approach mentioned is designated and manipulated for analysis through pressure sensors that are fitted within the adjustable chairs and according to the observed value[2], the posture correction is intimated by notification made by a sound. As this method uses pressure sensors to analyse the sitting posture that is fitted with the chair, the manufacturing is costlier than any other designs. In the Motor Control [3] after Human SCI through Activation of Muscle Synergies under Spinal Cord Stimulation, the approach concentrates only on the SCI i.e. Spinal Cord Injury patients and does not involve with correct intimation of posture correction. They implement the method called real time analysis of angle detection of spinal cord through the help of flex sensor [4–6]. It doesn't involve in creating any preventive technique that can be used for the prevention of any kind of posture correction syndrome. A neural basis for motor primitives in the spinal cord, explains the analysis of the motor control responses of the neurons in the spinal cord and the observed electrical impulses transferred between neurons is analysed through electrodes fixed with the victim [7–11]. By the comparison of observed value with pre-determined value, the angle of the spinal cord is provided as well as the motor activities of the neurons is also analysed. The signal is transmitted to the cloud using a transmission module implemented with a rectangular zigzag antenna [12,13]. Chvatal et al. [6] came up with a solution to posture correction of all age group people by implementing the bending movement analysed by deflection sensor using electrodes attached to the human body and the flexibility of the concern patient is provided by using Euler's formula. From the flexibility of the concerned person's spinal cord [14–16] we can able to give counselling to the person about their posture.

3 Proposed Method

The proposed system helps in breaking the ups and downs and drawback in the existing system. This system involves in the process of examining and intimation of the spinal cord bend movement and the angle measurements of humans while they bend to and fro when the limitation period exceeds the duration for the cause of the disorder. The system uses special kind of sensors to obtain the spinal cord bending movement. When the typical type of event occurs, then a strong intimation of alert is produced to the user with the help of vibrations and buzzer [17]. The vibrations are intimated to the user by the action of Motors. Then their posture status will be monitored by the doctor using the IOT module along with pulse monitoring (Fig. 1).

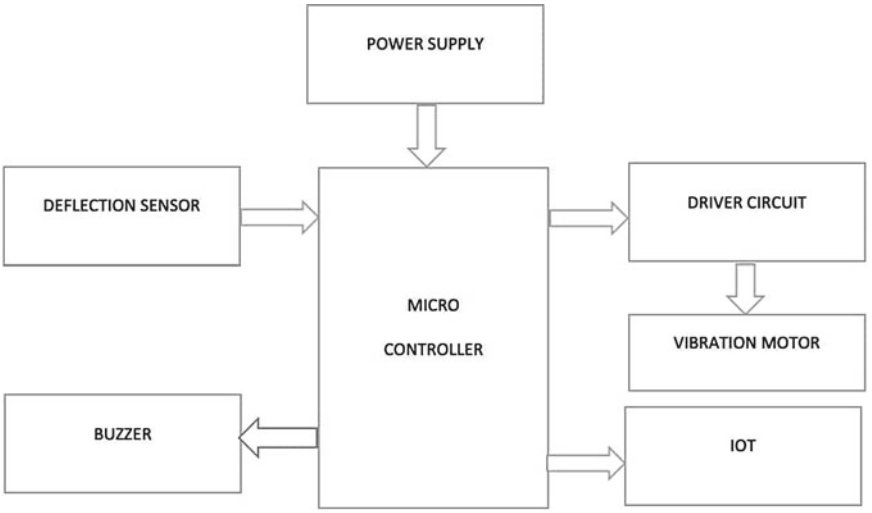

Fig. 1 Block diagram of proposed method

For a long time many attempts have been made to describe tourism as a system. Leiper tried to generate a tourism region consisting of destination and generating regions to construct an efficient system.

3.1 Microcontroller

A microcontroller is an integrated chip that is often part of an embedded system. The microcontroller includes a CPU, RAM, ROM, I/O ports, and timers like a standard computer. They are designed to execute only a single specific task to control a single system. The predominant architecture is CISC (Complex Instruction Set Computer) [18–20]. Some use a RISC (Reduced Instruction Set Computer) architecture, which implements fewer instructions. Here, the micro controller is used to control the entire operations embedded within it. The RISC architecture is used in this micro-controller to embed the perfect working of the model.

3.2 Vibration Motor

A vibration motor is a shaftless vibration motor that is perfect for non-audible indicators. With a 2–3.6 V operating range, these units shake crazily at 3 V. An eccentric rotating mass vibration motor (ERM) uses a small unbalanced mass on a DC motor, when it rotates it creates a force that translates to vibrations. In this model, this

Fig. 2 Vibration motor

vibration motor helps in providing the vibration alert to the user who wear this jacket (Fig. 2).

3.3 Flex Sensor

Flex sensors are passive resistive devices that can be used to detect bending or flexing analysis. It is considered as a bi-directional flex sensor. This flex sensor also can be used as a deflection sensor wherein it helps in sensing the bending movement of spinal cord. By analysing the data sensed from this sensor, we can be able to detect the angle of bending movement of the spinal cord in which the user is engaged with (Fig. 3).

Fig. 3 Flex sensor

3.4 Software Used

Embedded C is designed to bridge the performance mismatch between Standard C and the embedded hardware and application architecture. The Embedded C with MPLAB integrated development environment (IDE) is used here. This programming language which helps to process the hardware with its programming contents commanded to it helps to process the model in a more efficient way. Thus, Embedded C software also helps sensors and micro-controller to work according to our favoured condition and user friendly.

4 Working of the Model

When the power supply is given by using the battery of volts, the system is ready to use and now the analysis of bending movement of the spinal cord of the user is recorded and sensed using deflection sensor. The deflection sensor is available to produce the sensed value according to the analysed position of the angle of the user's spinal cord. The various degrees and position status of the spinal cord is given as follows: (Table 1).

The deflection sensor senses the angle values and send it to the Arduino board to detect the abnormal changes. Initially the Arduino, which is embedded with a LCD display shows the default value which is shown in the Fig. 4.

In Fig. 4, F:195 indicates the angle of spinal cord. HB denotes the pulse calculation value. Finally, POS indicates the posture position of the user. Now when the abnormal position is detected the Arduino automatically takes the count using counter algorithm which is embedded in the coding for almost 7 min. After that the buzzer is provided with sound to alert the user to change their position for 7 s.

Figure 5 indicates the spinal cord angle values and posture of the user when the user is in normal position.

Figure 6 indicates the sensed values which is observed when the user is in abnormal position. If the user change their position, the counter gets restart and the buzzer gets off too. If the user doesn't change their position after the 7 s of the buzzer indication, the vibration motor gets activated and it continuously provides vibration to the user and thus urges the user to change their position immediately. The system is also provided with pulse calculating module which is provided for easy diagnosis. The indication of the position of the posture is indicated to PCs or Personal mobile devices

Table 1 Indication of position of the posture respective to the angle of spinal cord

Angle of degrees	Status of position
180–200	Normal position
150–180	Abnormal position
Less than 150	Over bend position

Fig. 4 The default starting display in the arduino board

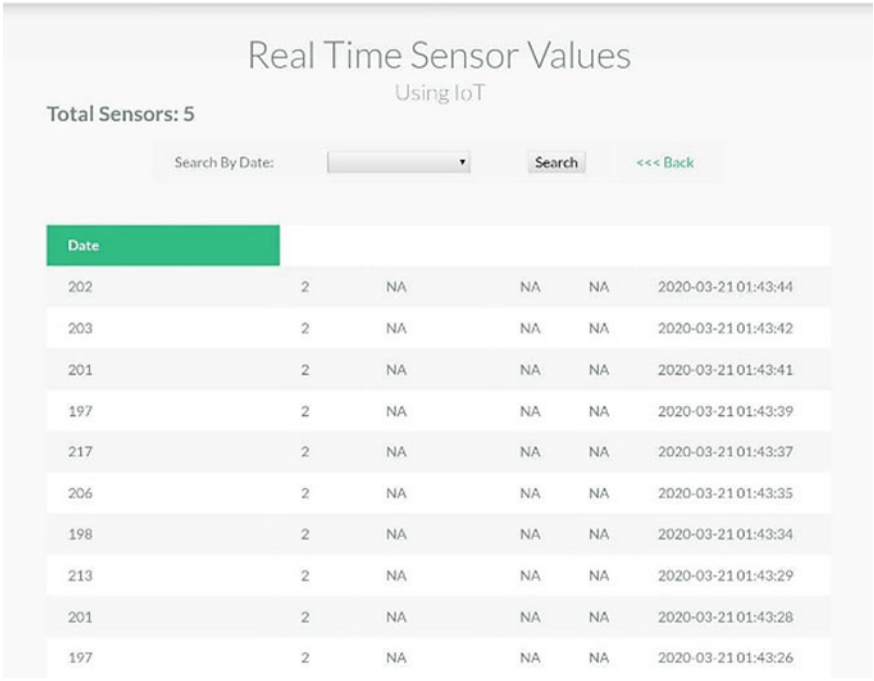

Fig. 5 Sensor value phase 1

Fig. 6 Sensor value phase 2

through IOT for screening of the user's posture information. The entire model will be a wearable one and the full structure is given in Fig. 7.

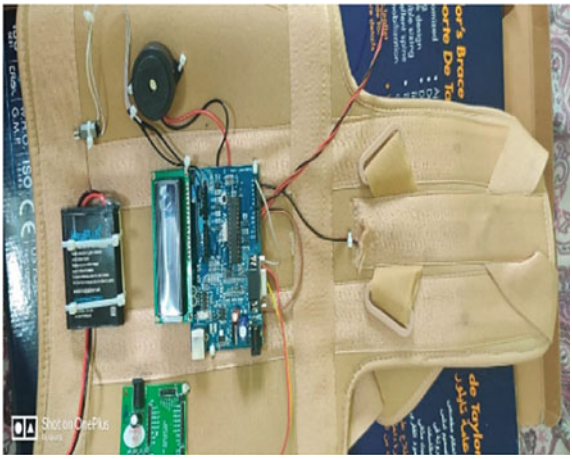

Fig. 7 Complete prototype of wearable jacket

5 Applications and Advantages

- Less weight.
- Can be used by anyone including middle aged persons, juveniles and elderly persons.
- Since it is wearable it can be used in anywhere and anytime.
- Comfortable to wear without any uneasiness.

6 Conclusion

Though the development of technologies has reached its heights, man forgets himself to give attention to his own health nowadays. As the responsibility towards society increases, the responsibility towards health decreases which now leads to the younger deaths due to health issues. This system will overcome all the difficulties in the existing technologies and helps in improving human health in a preventive manner.

References

1. Takei K (2018) Printed multifunctional flexible healthcare patch. In: 2018 International flexible electronics technology conference (IFETC) August, IEEE, pp 1–1
2. Martins L, Lucena R, Belo J, Almeida R, Quaresma C, Jesus AP, Vieira P (2014) Intelligent chair sensor–classification and correction of sitting posture. In: XIII Mediterranean conference on medical and biological engineering and computing 2013, Springer, Cham, pp 1489–1492
3. Cheng R, Sui Y, Sayenko D, Burdick JW (2019) Motor control after human SCI through activation of muscle synergies under spinal cord stimulation. IEEE Trans Neural Syst Rehabil Eng 27(6):1331–1340

4. Gill ML, Grahn PJ, Calvert JS, Linde MB, Lavrov IA, Strommen JA, Beck LA, Sayenko DG, Van Straaten MG, Drubach DI, Veith DD (2018) Neuromodulation of lumbosacral spinal networks enables independent stepping after complete paraplegia. Nat Med 24(11):1677–1682
5. Wenger N, Moraud EM, Gandar J, Musienko P, Capogrosso M, Baud L, Le Goff CG, Barraud Q, Pavlova N, Dominici N, Minev IR (2016) Spatiotemporal neuromodulation therapies engaging muscle synergies improve motor control after spinal cord injury. Nat Med 22(2):138
6. Cheung VC, Turolla A, Agostini M, Silvoni S, Bennis C, Kasi P, Paganoni S, Bonato P, Bizzi E (2012) Muscle synergy patterns as physiological markers of motor cortical damage. Proc Natl Acad Sci 109(36):14652–14656
7. Angeli CA, Boakye M, Morton RA, Vogt J, Benton K, Chen Y, Ferreira CK, Harkema SJ (2018) Recovery of over-ground walking after chronic motor complete spinal cord injury. N Engl J Med 379(13):1244–1250
8. Cheng R, Burdick JW (2018) Extraction of muscle synergies in spinal cord injured patients. In: 2018 40th Annual international conference of the IEEE engineering in medicine and biology society (EMBC), IEEE 2018 July, pp 2623–2626
9. McCrea DA, Rybak IA (2007) Modeling the mammalian locomotor CPG: insights from mistakes and perturbations. Prog Brain Res 165:235–253
10. Hart CB, Giszter SF (2010) A neural basis for motor primitives in the spinal cord. J Neurosci 30(4):1322–1336
11. Chvatal SA, Torres-Oviedo G, Safavynia SA, Ting LH (2011) Common muscle synergies for control of center of mass and force in nonstepping and stepping postural behaviors. J Neurophysiol 106(2):999–1015
12. Kumar GH, Ramesh GP, Avadi C (2018) Novel gateway free device to device communication technique for IoT to enable direct communication between homogeneous devcies. Int J Pure Appl Math 118(16):565–578
13. Ramesh GP, Kumar NM (2019) Design of RZF antenna for ECG monitoring using IoT. Multimedia Tools Appl 1–6
14. Vidhyalakshmi D, Balaji K (2018) Performance of bidirectional converter based on grid application. Indonesian J Electri Eng Comput Sci 12(3):1203–1210
15. Kumar SM, Balakrishnan G (2013) Multi resolution analysis for mass classification in digital mammogram using stochastic neighbor embedding. In: International conference on communication and signal processing, IEEE 2013 April, pp 101–105
16. Hemalatha RJ, Vijayabaskarin V (2018) Histogram based synovitis scoring system in ultrasound images of rheumatoid arthritis. J Clinical Diag Res 12(8)
17. Pendem S, Ramesh GP (2020) 75 GHz 5G Frequency spectrum analysis. In: Recent trends and advances in artificial intelligence and internet of things, Springer, Cham, pp 165–176
18. Ramesh GP, Parasuraman S.: Design and implementation of U-Shape microstrip patch antenna for bio-medical application. Int J Adv Sci Technol 28(12):364–374
19. Fahad AAA (2019) Design and implementation of blood bank system using web services in cloud environment. Int J MC Square Sci Res 11(3):09–16
20. Pattnaik M (2019) Infrastructure of data mining technique with big data analytics. Int J MC Square Sci Res 11(1):23–30

Design of Multistar Fractal Microstrip Patch Antenna for Multiband Application

R. Jothi Chitra, M. Mukesh Khanna, M. Rakesh, A. Praveen Kumar, J. Jerin Godbell, R. Nivetha, and C. H. Amulya Nissy

Abstract A new multistar fractal microstrip patch antenna is introduced in this paper for multiband applications. The proposed antenna is designed to resonate within the frequency range of the WiMAX, WLAN, S and C bands. The action of a multiband is studied by constructing five star-shaped structures in the same Substrate. The proposed antenna uses FR-4 substrate which has a dielectric constant $\varepsilon_r = 4.4$ and loss tangent of 0.02. Increasing the number of iterations will greatly improve the operating bandwidth. By changing the size of the transmitter, the antenna can work for multiband mode by adding additional four star-shaped structures. The parameters of the antenna such as return loss, VSWR, radiation pattern and gain are simulated and then described using CST Microwave Studio.

Keywords Multistar · Multiband · CST · WiMAX · Iteration

1 Introduction

In past years, it is important to design an antenna which resonates for multiband application to meet the required demands in the modern communication system. Microstrip patch antenna is preferred to meet the current trends in wireless communication due to its extraordinary features like small weight, low cost, easily fabricated, less fabrication cost and multiband application support. Fractal antennas are most suitable for multiband operation. Applying fractal to antenna results in size reduction and supports multiband operation. Fractals have space-filled properties of self-uniqueness which is the attractive feature of fractal antenna. Self-similar fractal

R. Jothi Chitra (✉) · M. Mukesh Khanna · M. Rakesh · A. Praveen Kumar · J. Jerin Godbell · R. Nivetha · C. H. Amulya Nissy
Department of Electronics and Communication Engineering, Velammal Institute of Technology, Chennai, India
e-mail: sureshashika@gmail.com

M. Mukesh Khanna
e-mail: mukeshjeyaprakash@gmail.com

D. K. Sharma et al. (eds.), *Micro-Electronics and Telecommunication Engineering*,
Lecture Notes in Networks and Systems 179,
https://doi.org/10.1007/978-981-33-4687-1_31

property raises the diameter of the antenna in a total surface area and facilitates multiband operation by space filling property. These two properties increase the effective radiation of the antenna. The basic concept and design procedure of microstrip patch antenna are described in [1]. In [2], an extensive overview of principle as well as specification of fractal modules was reported. Bandwidth improvement is accomplished in the literature [3] by the presentation of a microstrip line fed scanned fractal shaped port antennas. But this antenna model resonates for 2.4 and 4 GHz. Further in [4], an octagon fractal microstrip antenna for wideband application is presented. This antenna resonates from 10 to 50 GHz and uses coaxial feed. But coaxial feed is difficult for fabricating the antenna hardware model. Consequently in [5], a RFID reader and tag antenna are designed using fractal tree iteration. This antenna model is used only for RFID application. A Koch snowflake fractal antenna for multiband applications like GPS, WiMAX and applications for radar was demonstrated at [6]. A Koch fractal antenna has been addressed in [7] which produces circular polarization and size reduction for RFID application. In [8], a novel Koch fractal antenna was recorded on an octagonal substratum covering 1–30 GHz. In [9] a Koch fractal antenna, coplanar waveguide fed was presented for multiband use. In [10–12], a hybrid fractal antenna is modeled for commercial, science and medical band application based on Giuseppe Peano, Cantor collection and Sierpinski Carpet fractal. This antenna model is used in this literature to realize the artificial neural network (ANN) using the firefly algorithm. The commonly used fractal geometries are Sierpinski, Minkowski and Koch. In this letter, a multistar fractal antenna is proposed for multiband use. The advantage of this proposed antenna is that the antenna resonates for several frequencies, without increasing the size of the antenna. A remainder of the segment is structured as continues to follow Sect. 2 that covers the design of a multistar fractal antenna. The results of the simulation and the discussions are listed in Sect. 3.

2 Antenna Design

This segment deals with the method of constructing the suggested multistar fractal antenna. A suggested fractal antenna is a special structure that is used in this proposed design consisting of multistar-shaped patch with FR4 substrate with permittivity of 4.4. A microstrip fed line is placed at the optimized position and connected to the patch. Impedance matching between feed and patch should be perfectly matched. The antenna characteristics depend on the feed position. Single star antenna is initially constructed as shown in Fig. 1, and the antenna radiation characteristics are analyzed. But this antenna model resonates only for S and C band frequency range. In order to increase the resonate frequency of antenna, a four-star pattern is incorporated inside the single-star major update without increasing the size of an antenna. Multiband property could be accomplished by growing iteration order numbers. Figure 2 depicts the planned multistar fractal antenna. Figure 2a and b displays the front image of the planned antenna and its side view. The measurements of the suggested antenna are

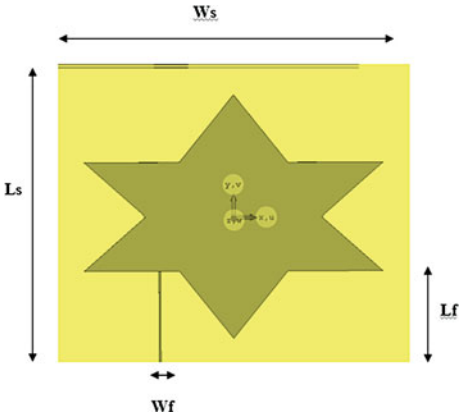

Fig. 1 Initiator—a star-shaped antenna

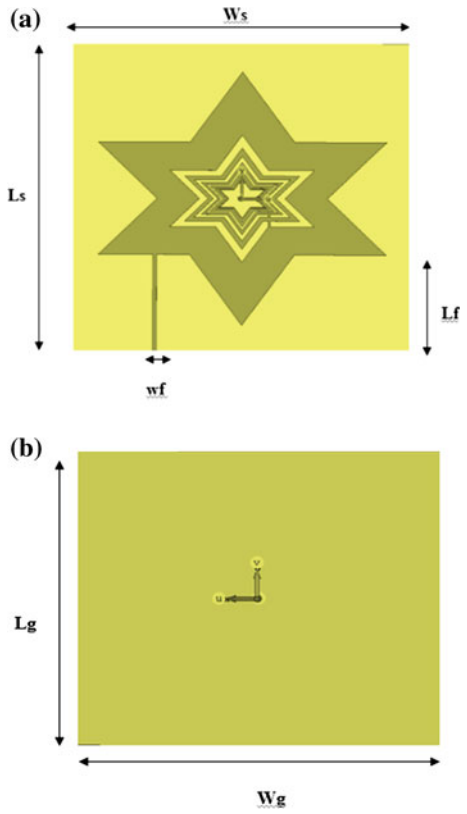

Fig. 2 **a** Front view of the planned fractal multistar antenna, **b** ground plane of proposed antenna

Table 1 Geometrical dimensions of antenna

Design parameter	Description	Dimensions (mm)
L_s	Length of substrate	65
W_s	Width of the substrate	66
L_f	Length of feed line	35
W_f	Width of the feed line	2
L_g	Length of ground plane	65
W_g	Width of the ground plane	66

determined using transmission method [1]. The antenna geometric measurements are measured and represented in Table 1. The antenna size is 65 × 66 mm and substrate height is 1.6 mm.

3 Results and Discussions

This suggested multistar fractal antenna is modeled using the simulation software CST Microwave Studio focused on finite integration technique. VSWR, radiation pattern, return loss and benefit from single-star antennas and multistar fractal antenna are analyzed and discussed. This swept frequency ranges from 1 to 9 GHz is considered in order to analyze the radiation efficiency of the suggested antenna. Figures 3 and 4 show the simulated VSWR value of first iteration and fifth iteration, respectively. For the star-shaped antenna structure (first iteration), the VSWR value for 2.5 and 4.2 GHz is 1.25 and 1.27, respectively. For both the frequencies, the VSWR

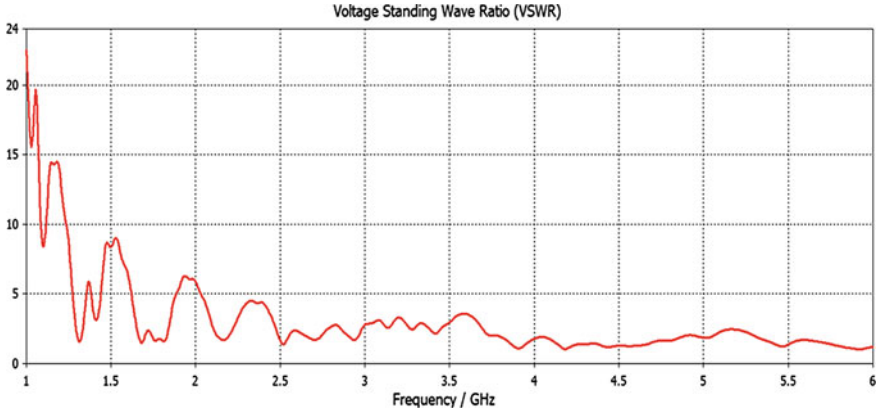

Fig. 3 Simulated VSWR value of Star shaped antenna

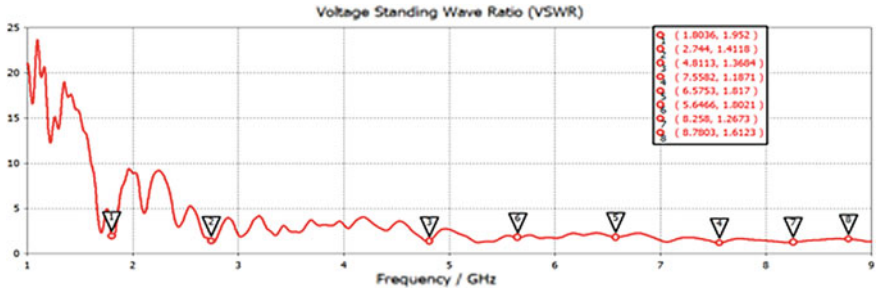

Fig. 4 Simulated VSWR of a fractal multistar antenna

value is optimum. Therefore, the star-shaped antenna resonates for 2.5 and 4.2 GHz only. For multiband operation, multistar fractal antenna (fifth iteration) is designed. The multistar antenna meets the desired value of VSWR for the frequencies 1.8, 2.7, 4.8, 5.6, 6.5, 7.5, 8.2 and 8.7 GHz.

Figures 5 and 6 show first iteration and fifth iteration modeled return loss (S11) value. For the star-shaped antenna structure (first iteration), the return values for 2.5 GHz and 4.2 GHz are −15.6 dB and −43 dB, respectively. For both the frequencies, the value of return loss seems to be more unfavorable. For strong radiator, the optimum value is below −10 dB. Therefore, the star-shaped antenna resonates for 2.5 and 4.2 GHz only. For multiband operation, multistar fractal antenna (fifth iteration) is designed. The multistar antenna meets the desired value of return loss value for the frequencies 1.8, 2.7, 4.8, 5.6, 6.5, 7.5, 8.2 and 8.7 GHz. From the simulation results of VSWR and return loss, it is concluded that the proposed antenna covers Wi-Fi, WiMAX, S and C band frequency bands in Table 2.

Figure 7a, b and c shows the simulated far field radiation pattern of E and H plane patterns for the frequencies 1, 5 and 9 GHz. To all frequency ranges, the radiation distribution is almost omnidirectional.

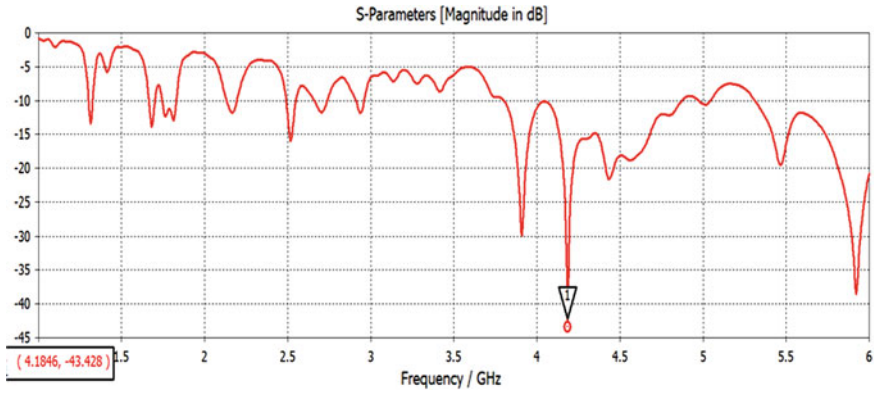

Fig. 5 Simulated return loss of star shaped antenna

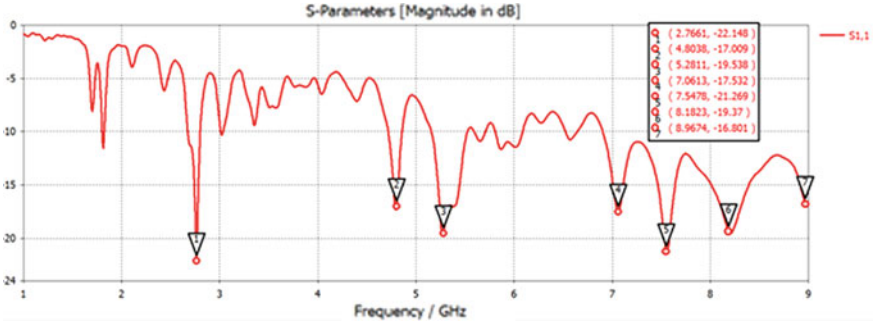

Fig. 6 Simulated return loss of fractal multistar antenna

Table 2 Illustration of the proposed antenna simulated VSWR and return loss value for various frequency ranges

Frequency range (GHz)	VSWR	Return loss (dB)
1.8	1.9	−12
2.7	1.4	−22
4.8	1.3	−17
5.6	1.8	−12
6.5	1.8	−10
7.5	1.1	−21
8.2	1.2	−19
8.7	1.6	−10

The 3D gain plot of star-shaped and multistar fractal proposed antenna is illustrated in Figs. 8 and 9, respectively. The maximum gain obtained for star-shaped antenna is 2 dBi. The maximum gain achieved is 4 dBi. From the figure, it clearly shows that when the quantity of iterations improves, the antenna gain is rising.

4 Conclusion

For multiband application, a new multistar fractal microstrip patch antenna is built. The antenna designed consists of five star-shaped patches on the same substrate. For several frequencies, the antenna resonates. The optimum value of simulated VSWR results and return loss is achieved. For all the frequencies, the radiation distribution is almost omnidirectional. Maximum gain attainable is 4 dBi. The antenna proposed suits remote applications.

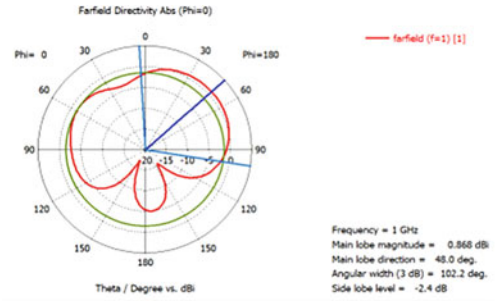

(a) f=1GHz

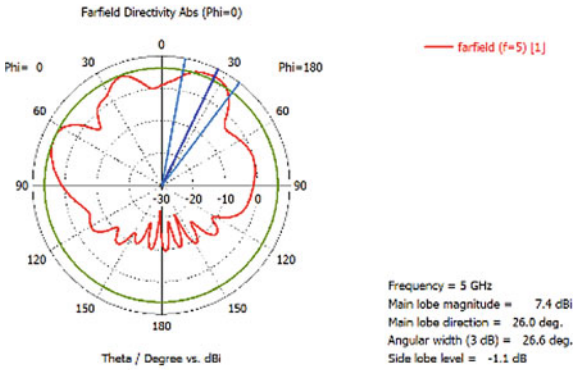

(b) f = 5GHz

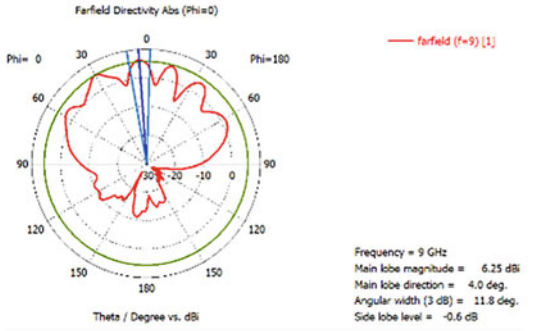

(c) f = 9GHz

Fig. 7 Simulated radiation pattern of proposed *YZ* plane antenna (red) and *XZ* plane (blue) **a** $f = 1$ GHz **b** $f = 5$ GHz **c** $f = 9$ GHz

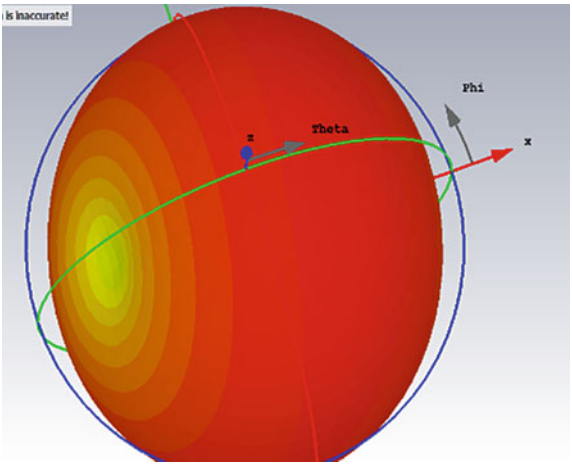

Fig. 8 3D gain plot of star-shaped antenna

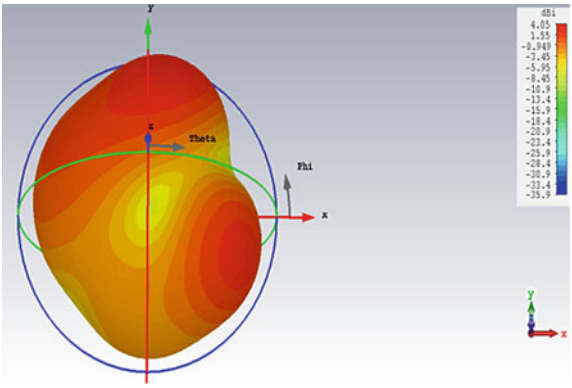

Fig. 9 3D gain plot of multistar fractal antenna

Acknowledgements The writers want to appreciate the Velammal Institute of Technology for supporting the research and development laboratory facilities.

References

1. Balanis CA (1997) Antenna Theory, Analysis and Design. Wiley, NewYork
2. Werner DH, Haup RL, Werner PL (1999) Fractal antenna engineering: the theory and design of fractal antenna arrays. IEEE Ant Propag Mag 41(5):37–59
3. Chen W-L, Wang G-M, Zhang C-X (2009) Bandwidth enhancement of a microstrip line fed printed wide slot antenna with a fractal shaped slot. IEEE Trans Ant Propag 59(9), 1724–1727
4. Azari A (2011) A new super wideband fractal microstrip antenna. IEEE Trans Ant Propag 57(7), 2176–2179

5. Pakkathillam JK, Varadhan C, Kanagasabai M, Sivasamy R, Natarajan R, Palaniswamy S (2013) Triband antenna structures for RFID systems deploying fractal geometry. IEEE Ant Wirel Propag Lett 12, 437–440
6. Sharma R, Kumar R, Singh PK, Raboaca MS, Felseghi R-A (2020) A systematic study on the analysis of the emission of CO, CO_2 and HC for four-wheelers and its impact on the sustainable ecosystem. Sustainability 12:6707
7. Begam SS, Selvachandran G, Ngan TT, Sharma R (2020) Similarity measure of lattice ordered multi-fuzzy soft sets based on set theoretic approach and its application in decision making. Mathematics 8,1255
8. Vo T, Sharma R, Kumar R, Son LH, Pham BT, Tien Bui D, Priyadarshini I, Sarkar M, Le T (2020) Crime rate detection using social media of different crime locations and twitter part-of-speech tagger with brown clustering. 4287–4299
9. da Costa LF, D'Assunção AG, Barreto EL (2018) Simulation and design of koch fractal CPW antennas. In: 11th German Microwave Conference
10. Kaur M, Sivia JS (2020) ANN and FA design of hybrid fractal antenna for ism band applications. Progress In: Electromagnetics Research C, vol. 98, pp. 127–140
11. Ramesh GP, Rajan A (2014) Microstrip antenna designs for RF energy harvesting. In: International Conference on Communications and Signal Processing (ICCSP), pp. 1653–1657
12. Rajan A, Ramesh G.P (2013) RF energy harvesting systems for low power application. Int J Technol Eng Sci. 1(7), 1085–1091
14. Jothi chitra R, Nagarajan V (2016) Design and development of koch fractal antenna. In Proceedings of the IEEE International Conference on Communication and Signal Processing, 2294–2298
15. Wqrner DH, Ganguly S (2003) An overview of fractal antenna engineering research. IEEE Antennas and Propagation Magazine 45(1):38–57
16. Azim R, Islam MT (2013) Compact planar UWB antenna with band notch characteristics for WLAN and DSRC. Progress In Electromagnetics Research 133:391–406
17. Malik J, Kartikeyan MV (2011) A stacked equilateral triangular patch antenna with sierpinski gasket fractal for WLAN applications. Progress In Electromagnetics Research Letters 22:71–81
18. Lin S, Wang LZ, Wang Y, Zhang X-Y, Zhang H-J (2012) Design and analysis of a circular polarization microstrip antenna with koch fractal edges. Progress In Electromagnetics Research Letters 34:9–19

Design of a 48 V BLDC Motor for Military Application

G. Moorthy, G. Shanmugaraj, R. Sankar Raj, J. Swetha, P. Gunavathi, and R. Jeyaprakashini

Abstract Electromechanical actuators are increasingly used in aerospace applications, particularly for all electrical and space aircraft. In the recent years, unmanned aerial vehicles (UAV) have gained widespread applications. Here an electromechanical actuator is used to control the speed and position of the nose landing gear for military purpose. The hydraulic actuators had been replaced into electromechanical actuators (EMA) which has the ability to control and monitor torque. The EMA consists of a BLDC motor which has an advantage of high efficiency and excellent controllability. The main challenge of using BLDC motor in this application is that it should have good size and torque ratio with reasonable efficiency. For this reason, design has to be made analytically and motor FEA analysis has to be done with transient electromagnetic analysis for motor effectively before prototype. In this project, a 48 V BLDC motor is designed by using JMAG-Designer software. This software provides to verify the FEA analysis under transient condition. The JMAG software has the ability to evaluate all the motor characteristics like torque–speed characteristics, loss characteristics, inductance characteristics, etc. Finally, the results are

G. Moorthy (✉)
Department of Mechanical Engineering, Velammal Institute of Technology, Panchetti, India
e-mail: moorthyg1979@gmail.com

G. Shanmugaraj · J. Swetha · P. Gunavathi · R. Jeyaprakashini
Department of Electronics and Communication Engineering, Velammal Institute of Technology, Panchetti, India
e-mail: gsraj76@gmail.com

J. Swetha
e-mail: Swethajayaprakash1998@gmail.com

P. Gunavathi
e-mail: gunavathipalani98@gmail.com

R. Jeyaprakashini
e-mail: prakashinirajavel.r@gmail.com

R. Sankar Raj
Department of Electrical Engineering, Velammal Institute of Technology, Panchetti, India
e-mail: sankar0201@gmail.com

D. K. Sharma et al. (eds.), *Micro-Electronics and Telecommunication Engineering*,
Lecture Notes in Networks and Systems 179,
https://doi.org/10.1007/978-981-33-4687-1_32

inferred how the efficiency is improved with the proposed design, and the graphs generated are used to infer the design proficiency.

Keywords EMA · BLDC motor · FEA analysis · JMAG-designer software

1 Introduction

Linear and rotary hydraulic actuators play an important role in aircraft application. The hydraulic actuators consist of cylinder or fluid motor that uses hydraulic power to facilitate mechanical operation. But the drawback of using hydraulic actuator is that they leak fluids, which leads to a loss in efficiency. The leaks can damage the surrounding area and components and lead to environmental problems. The hydraulic actuators have now been replaced by electromechanical actuators (EMA), which have complete control over the motion profile. They are fitted with encoders which can be used to monitor precisely the velocity and location. It also provides the ability to control and monitor torque using BLDC motor. Thus, a 48 V BLDC motor is designed with the requirements of low inertia, high speed, and high torque and with reliable operations. The BLDC engine has a multi-phase winding stator and a permanent magnet core-fixed rotor. The BLDC motor of the actuator is equipped with a Hall-effect sensor for position sensing to generate required signal for the firing of power semiconductor switches and control switches. The BLDC motor used here has maintenance-free due to lack of mechanical switches and brushes and can operate at a very high speed. A high-speed and low-torque BLDC motor is built, as the size of our modeled motor is small, as will reach the system's high bandwidth at reduced space consumption, also the rotor inertia is kept low.

Brushless DC motors have several advantages over other existing motors such as PMSM, induction motor, PM synchronous motor, and so on and conventional brushed DC motors such as high efficiency, higher-speed ranges, low maintenance, long service life, noiseless operation, improved speed versus torque characteristics, and high dynamic response [1]. The aerospace vehicle under consideration is powered by four rear mounted control surfaces operated by four independently powered actuators. The BLDC motor is the prime mover for the position power actuator [2]. The configuration of the internal rotor permanent magnet form is chosen in the design of the permanent magnet BLDC motor, so that it can be applied to a drive requiring a large torque that can accelerate and decelerate with a good response. The option of 8 poles and 12 slot configuration is aimed at improving motor performances [3]. In this study, the BLDC motor has three Hall-effect sensors embedded in the stator on the non-driving end of the actuator to know the position of the rotor [4]. To meet the performance requirements, the design of a BLDC motor is with a permanent magnet inside and a rotor mounted on the top. Even the design of the 300 and 48 V DC power supply BLDC motor is carried out, and the 300 V DC output is assessed [5]. High-power BLDC closed loop control system includes mainly IR2130 drive circuit design, H bridge drive rotary motor direction control, and speed detection circuit

Table 1 Specification for BLDC motor design

Parameter	Specification
Rated power	0.28
Torque	1
Poles	4
Slots	12
Power supply	48
Maximum current	7
Outer diameter	50
Motor height	105
Line current	10

to enhance engine performance by modifying parameters. [6]. BLDCM is proposed and analyzed for FESS, and eddy current loss and air gap flux density in permanent magnets BLDCM outer rotor ironless are investigated by 2D finite element analysis using different magnetization methods [7]. In the BLDC motor design, the rare earth magnet material example Nd–Fe–B is often used in comparison with any other magnet material due to high flux density [8]. The designed output of the SynRM motors can achieve the same degree of efficiency of the standard BLDC motor where material costs are reduced by up to 50% [9]. The concept equations and effects, such as cogging torque flux patterns and predicted 3D views for 8 poles 27 slots and 0.75 kW PMBLDCM are presented [2]. The proposed design would allow the user to rotate the motor either in the clockwise direction or in the opposite direction [10, 11].

A BLDC engine is an electronically commuted DC engine that does have any brushes or commutators. The brushless DC motor is the one designed for unmanned aerial vehicle (UAV) electromechanical actuator. The brushless DC motor is highly effective in producing a significant amount of torque over a wide range of speeds. BLDC motor is used due to its high efficiency, higher torque value per volume, and a high-speed applications capability (Table 1).

2 Existing Method

Earlier conventional actuator with hydraulic process requires only mechanical engines with fuel which is improved with a motor-driven hydraulic actuators called as electrohydrostatic actuators which are used to actuate the nose landing gear steering mechanism of UAV vehicle. The conventional actuator which uses mechanical engine in aircraft applications causes pollution due to emission of carbon. In the hydraulics system, the cost of the fuel is high and due to the leakage of oil the system efficiency gets affected. Hydraulic actuators may suffer loss of efficiency due to fluid leakage.

They also require many auxiliary, making them bulky and more complicated to maintain. An analysis of some critical mode failures for EMAs and condition indicators has been developed to require detection, identification, and isolation of fault modes [12]. The complicated nonlinear entity was converted into a simple linear structure using the control strategy for linearization feedback. The PID controller was coupled with the linearization feedback technique to perform proper position control [13, 14].

3 Proposed Method

A BLDC motor is designed for electromechanical actuator to actuate the nose landing gear steering system mechanism of UAV vehicle. A BLDC motor is a DC motor which is electronically commuted and has no brushes. Brushless DC motors are highly efficient in producing large amount of torque over a vast speed range. The BLDC motor provides the proper characteristics of size and torque. By increasing its efficiency, the motor is designed with reduced size for reliable aerospace application. The analytical calculations are carried out with finite element analysis using JMAG software. The parameters of the motor are obtained using the calculation with motor constraint. The parameters are used for the design of BLDC motor in JMAG, and the transient analysis is carried out and hence the result is obtained and verified.

4 Finite Element Analysis

Finite element analysis of a BLDC motor's electromechanical field considers speed control and mechanical versatility. Electro-Mechanical transient analysis approach is used for studying the BLDC motor behaviour at each step, nonlinear step finite element analysis of the magnetic field is achieved by taking into account the switching behavior of the time step finite element analysis of the mechanical movement and also taking into account the shaft, rotor and bearing flexibility. A BLDC motor's electromechanical field research consists of two parts: Driver circuit magnetic field analysis and mechanical motion analysis which provided the feasibility for portable structure. The finite element analysis is widely used when designing electric motors in terms of both the theoretical and numerical aspects [15]. With the defined design parameters from calculation, through FEA analysis the design validation purposes, the failure analysis, and analytical methods are effectively involved in fast evaluation of motor performance characteristics.

5 Design Calculations

In order to design a 48 V BLDC motor the parameters like rotor outer diameter, width of the teeth, length of the stator stack, width of stator back iron, number of winding turns, etc., with the gear ratio 96 Torque 2.421 Nm and speed 662.4 RPM, the research is performed using "JMAG-Designer" software.

Output power P0 = ("2.421*2*pi*" 662.4)/60
=167 W
Given, Torque (T) = 2.421 Nm
Speed in R.P.M = 662 RPM
Assuming efficiency 60 %
Motor input power (Pi) = 167/0.6 W
= 278.33 W
Rated Current (I) = 278.33/48 A
= 34.79A
Resistance (R) = (278.33 – 167) / 34.792
= 0.09ohm

MOTOR TORQUE CONSTANT (kt)

Back EMF of the BLDC drive (E) = Vm-Im*Rm
kt= Ke= E/2πNs
where Øm—flux produced by each magnet
Zm—no.of conductors in stator
Pm—no.of poles on the rotor in BLDC Motor
Ns – Synchronous Speed (No Load)
Kt = Ke = E/2πNs = (48∗60)/(2∗pi∗960)
= 0.47V/rad
ØZP = (60*48*3)/(2 * 960) = 4.5

ROTOR PARAMETERS AND DIMENSIONS

ROTOR PARAMERS AND DIMENSIONS
Shaft Torque, T = $\pi D^2 L$ Bav ac/3
Assuming: Bav = 0.75, ac =40,000
We get D^2L = 7.71*7-5
Putting length of stack L = 0.063 m
We get dia. of rotor D = 0.035 m
PØ = 0.75*pi*0.035*0.063, Taking P = 4,
we get Ø = 0.001299
MMF required to produceBav
MMF = 0.75*0.00519*/(4*pi*10-7) =3097.55 AT
MMF to be produced by magnet (MMF)mag = 3097.55*1.2 =3717.06 AT
Length of magnet(Lm)= (MMF)mag/Hmax =3717.06/133.33*103
= 3.79

STATOR PARAMETERS AND DIMENSIONS

ØZP= 2.625
Therefore, Z = 505.78
No. of slots Q = pole * No. of phases
= 4*3
= 12 Slots
Therefore, No.of conductors per slot=505.78/12
= 42.15
Magnet pole area (Outer face) =π*0.035*0.063/4
= 0.0073 mm2
Di=D-2*Lm =35-2*3.79
=27.42 mm
Therefore,Øg=π*27.42*63*10-6*0.75/4
=4.07e-3 wb

STATOR BACK HEIGHT (hbs)

hbs = π*34.58*0.75/2*4*1.6
= 6.37 mm
Height of the slot can be calculated as
hs = 105-(2*6.37)-34.58-(2*1.5)/2
= 54.72 mm
Where, Dos is the outer rotor diameter,
hbs is the stator back height,
Dis is the inner stator diameter,
lg is the air gap between rotor outer diameter and stator
inner diameter
Width of teeth, (Wt) = π*27.42*10^-3*0.75/12*1.6
= 0.0034 mm.

Therefore heat dissipated
= (McuxScu x (T2 - T1)+Mau x Sau x (T2 - T1)+ Ms x Ss x (T2 - T1))
= (0.12* 0.385 * (T2 - T1) + 0.1 * 100*(T2 - T1) + 0.2*92 (T2-T1))= 29*(T2-T1)
Copper loss + Iron losses = 45.625 W.
Energy loss = losses x T (time) =45.625 x 20. (Time for 20sec)
= 925 J.
Since heat dissipated = energy losses.
925 = 29 (T2-T1).

If we take the temperature as 35 °C (ambient), then the final temperature will be around 67 °C and it is the safe limit for all elements.

6 Results and Discussions

The design software uses the parameter constrain used in the calculation, and the calculated parameter values as tabulated in Table 2 are used for motor dimension. JMAG provides 2D and 3D analysis of motor. In this paper, 3D analysis is made for accurate output characteristics of motor.

In JMAG-Designer platform for motor, creation and analysis are available. With motor designed of given size and structure, transient electromagnetic analysis is made and results obtained are represented graphically.

Figure 1 shows the motor geometry model designed in the JMAG editor window. The motor model has been created. Then the materials used for stator core, rotor core, magnet, and coil windings have been given. The materials used for stator and rotor core are steel sheets. The coil windings are made of copper. The rare earth neodymium magnets are used because of its advantages like small size which is available in different shapes. They are less weight and offers high resistance to

Table 2 3D FEA motor model output characteristics

Torque	2.421 Nm
Phase resistance	0.046 O
Flux	0.001299 Wb
Bav	0.75
AC	40,000
Length of the magnet	3.79
Height of the slot	54.72 mm
Stator back height	6.37 mm
Width of the teeth	0.0034 mm

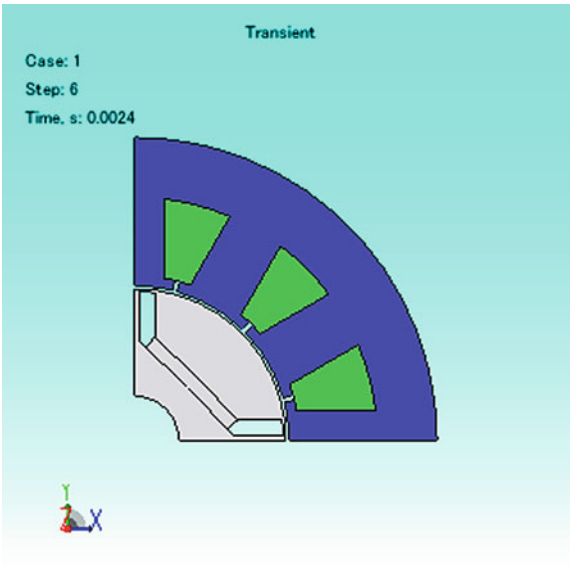

Fig. 1 Front view of 3D model—BLDC motor

demagnetization. It has high power to weight ratio and a high flux density compared to other magnet material.

Figure 2 shows the 3D motor model extracted from the JMAG editor to JMAG-Designer. The FEM coil circuit is formed, and by setting the parameters such as resistance and voltage or current source the FEM coil circuit is built. At the initial stage, the analysis of the engine conditions with no load and the engine armature winding current is assigned to zero. Load analysis is carried out, and a supply of 48 V and 10 A current passes through the winding.

Figure 3 represents the condition for rotation motion, rotation periodic boundary, symmetry boundary, and torque nodal force and FEM coil. After giving the boundary conditions, the mesh analysis is made. The conditions for rotation motion, rotation periodic boundary, symmetry boundary, torque nodal force, and FEM coils are given. The precision that can be obtained from any FEA model is directly related to the

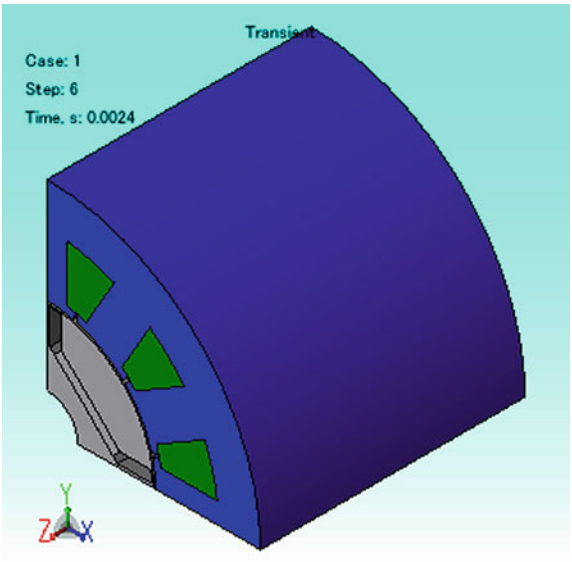

Fig. 2 Isometric view of 3D model—BLDC motor

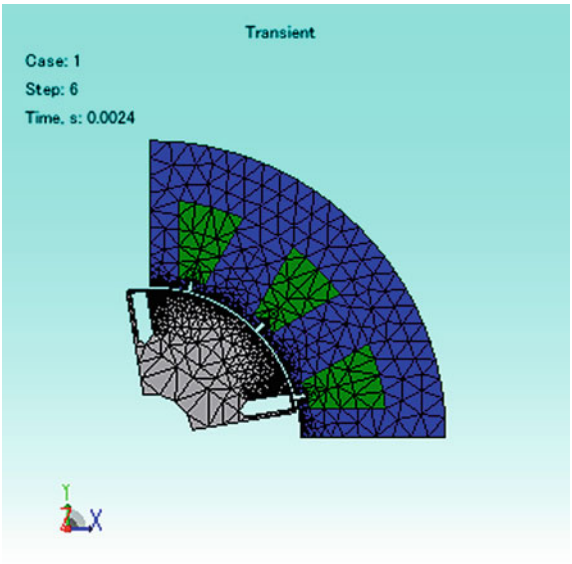

Fig. 3 Front view FEA model view—BLDC motor

mesh used for finite elements. The finite element mesh is used to divide the model into smaller domains called components, which solve a series of equations.

Figure 4 shows the mesh analysis of BLDC motor in JMAG software. The structure is optimized as the components are rendered smaller, and the simulated solution approaches the true solution. The grid optimization method is a crucial step in validating any model of finite elements and the results.

Figure 5 shows that *x*-axis represents torque and *y*-axis represents time. In the initial stage, torque will be at 0.42, then it will gradually increase and reach a peak value of 0.48, and after reaching the peak value the torque reduces gradually with respect to time.

Figure 6 represents joule loss versus time. The maximum loss generated is 75 W at three-phase coil.

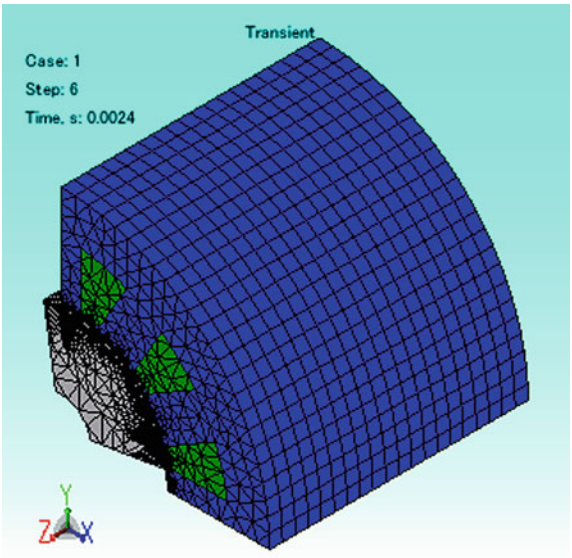

Fig. 4 Isometric view 3D FEA model—BLDC motor

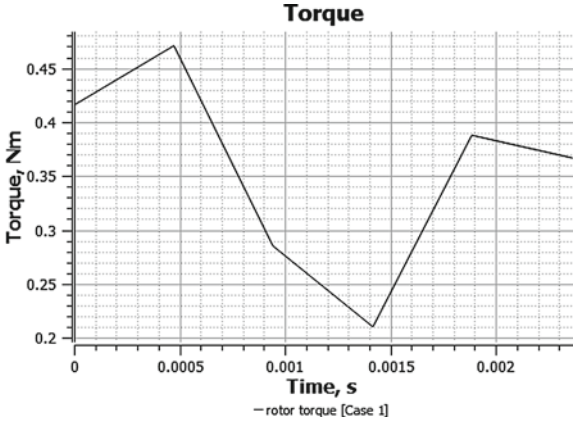

Fig. 5 Torque Vs Time curve of 3D model

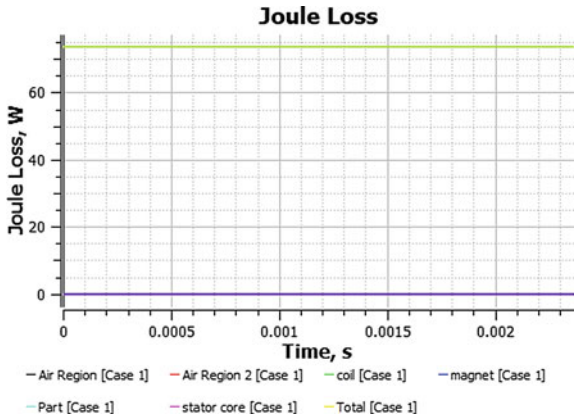

Fig. 6 Graphical representation of Joule loss at different parts of BLDC motor

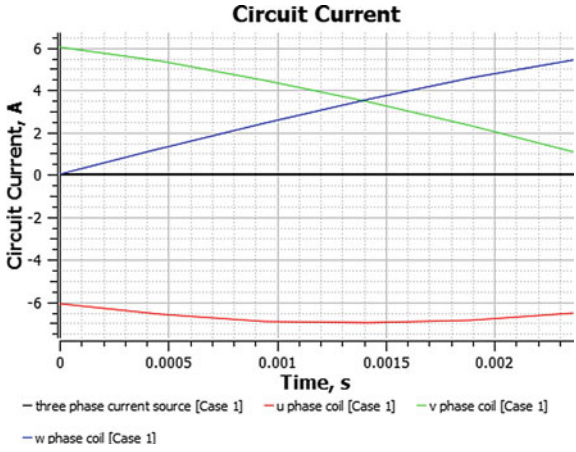

Fig. 7 Three phase current waveform of BLDC motor

Figure 7 represents circuit current versus time. The maximum current at each coil is 5 A.

Figure 8 represents circuit voltage versus time. The maximum voltage at all phases is 7 V.

Figure 9 represents coil flux linkage versus time. The maximum flux linkage at each coil is 0.02 Wb.

Figure 10 represents rotational displacement versus time. The total rotational displacement is 10° at 0.0025 s.

Figure 11 represents circuit electric power versus time. The maximum electric power at the motor is 95 W.

Figure 12 represents rotational velocity versus time. The motor runs at the speed of 670 RPM.

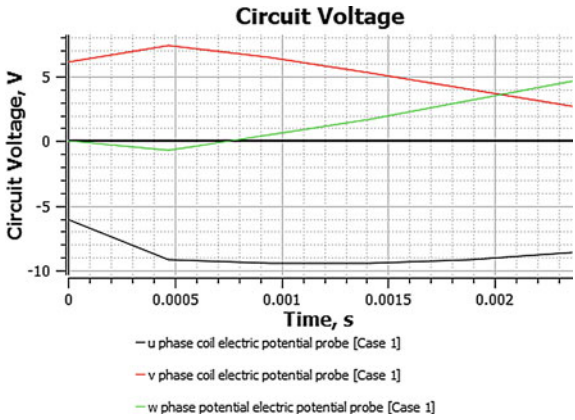

Fig. 8 Circuit voltage at three phases of BLDC motor

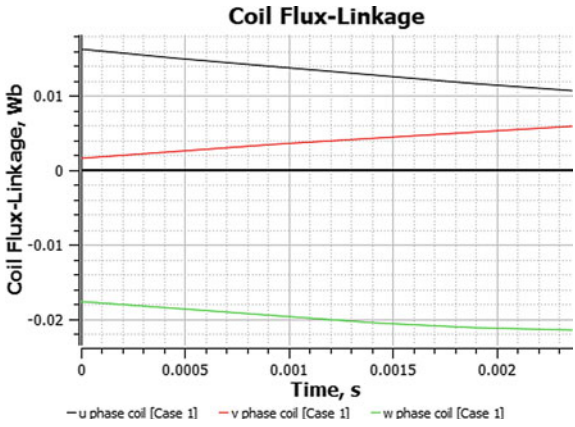

Fig. 9 Coil flux-linkage at the three phase coils

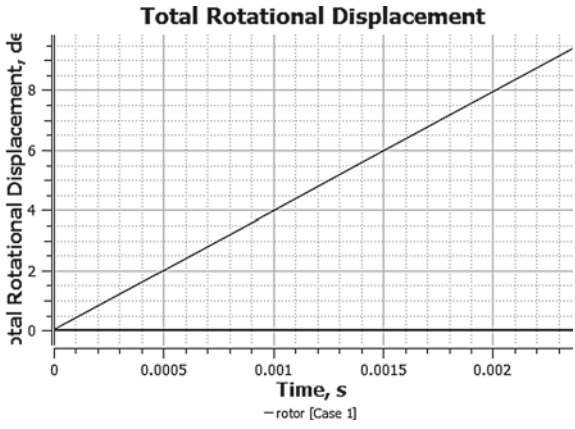

Fig. 10 Total rotational displacement of the rotor in degree

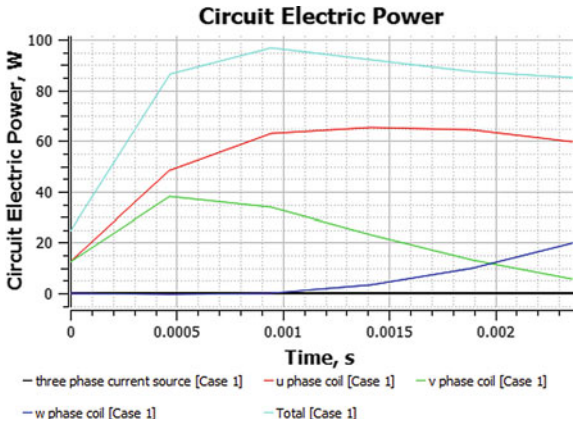

Fig. 11 Electrical power waveform for three phase winding

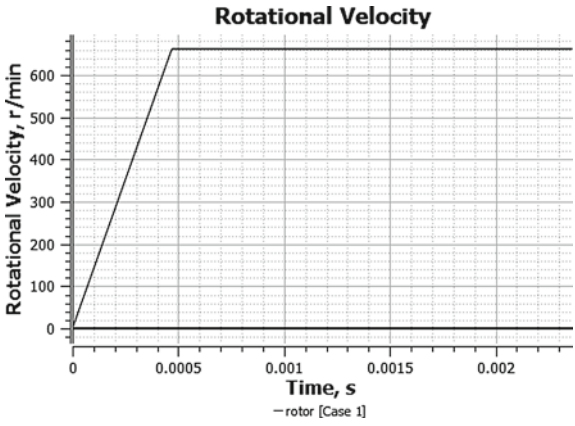

Fig. 12 Rotational velocity of the BLDC motor

From the above graph generated, the torque–speed characteristics are as required and efficiency is improved at given current and consumes less voltage and thus the size and torque ratio are achieved, and conclusions are made in the next section.

7 Conclusion

The hydraulic actuators in aerospace application have been replaced into electromechanical actuators (EMA). The EMA has a BLDC motor which is very effective in controlling the motor speed and torque ripple at low speed. Thus to control the speed of an aircraft for military application, a 48 V BLDC motor is designed in the "JMAG-Designer" software with the specification of the gear ratio 96, torque 2.421 Nm, and speed 662.4 RPM. The result generated verifies that at given size

constrain highly efficient BLDC motor is designed at desired torque speed characteristics and nominal speed. FEA analysis is done successfully as motor sustainability is verified. The obtained output at no load and load condition clearly indicates that the actuator meets the requirement of the system specifications.

References

1. Laxminarayana, Y.: Design of a compact BLDC motor for high power, high bandwidth rotary electromechanical Actuator for aerospace application. In: Annual IEEE India Conference, pp. 1–4. IEEE (2011)
2. Hazari, M.R., Jahan, E., Siraj, M.E., Khan, M.T.I. and Saleque, A.M.: Design of a Brushless DC (BLDC) motor controller. In: International Conference on Electrical Engineering and Information & Communication Technology, pp. 1–6. IEEE (2014)
3. Kamalakannan, D., Singh, N.J., Karthi, M., Narayanan, V., Ramanathan, N.S.: Design and development of DC powered BLDC motor for Mixer-Grinder application. In: First International Conference on Sustainable Green Buildings and Communities (SGBC), pp. 1–6. IEEE (2016)
4. Liu K, Yin M, Hua W, Ma Z, Lin M, Kong Y (2018) Design and analysis of Halbach ironless flywheel BLDC motor/generators. IEEE Trans. Magn. 54(11):1–5
5. Gyeong-Chan L.: Design Comparisons of BLDC Motors for Electric Water Pump. Department of Electrical Engineering (2012)
6. Hasen, R., Salim, K.M.: Design implementation and testing of a three phase BLDC motor controller, In: 2nd International Conference on Advances in Electrical Engineering (ICAEE), pp. 192–196. IEEE (2013)
7. Khalid A.K.: Bridgeless landsman converter based BLDC motor drive using IFOC. Int. J. MC Squ. Sci. Res. **10**(1) (2018)
8. Burin. K., Sangkla, K.: Design of synchronous reluctance motors with IE4 Energy Efficiency Standard Competitive to BLDC Motors used for Blowers in Air Conditioners. National Electronics and Computer Technology Centre (2017)
9. Balaban, E., Bansal, P., Stoelting, P., Saxena, A., Goebel, K.F., Curran, S.: A diagnostic approach for electro-mechanical actuators in aerospace systems, In: IEEE Aerospace Conference, pp. 1–13. IEEE (2009)
10. Apatya, Y.A., Subiantoro, A., Yusivar, F.: Design and prototyping of 3-phase BLDC motor. In: 15th International Conference on Quality in Research (QiR): International Symposium on Electrical and Computer Engineering, pp. 209–214. IEEE (2017)
11. Manikandan G., Anand M.: Radix-2/4 FFT multiplierless architecture using MBSLS in OFDM applications, In: Solanki V., Hoang M., Lu Z., Pattnaik P. (eds) Intelligent Computing in Engineering. Advances in Intelligent Systems and Computing, vol 1125. Springer, Singapore (2020)
12. Zhang, Q., Li, B.: Feedback Linearization PID Control for Electro-hydrostatic Actuator. North Western University, IEEE (2011)
13. Sundaram, A., Ramesh, G.P.: Investigation of Solar Based SL-QZSI Fed Sensorless Control of BLDC Motor, In: Babu V.H., Balaji L (eds.) Intelligent Computing in Engineering, pp. 779–787. Springer. Singapore Survey on Modular Multilevel Inverter Based on Various Switching Modules for Harmonic Elimination. In: Solanki V., Hoang M., Lu Z., Pattnaik P. (eds.) Intelligent Computing in Engineering. Advances in Intelligent Systems and Computing, vol 1125. Springer, Singapore (2020)
14. Vijayabaskar, Kumanan T.: Link quality and energy-aware metric-based routing strategy in WSNS, In: Solanki V., Hoang M., Lu Z., Pattnaik P. (eds) Intelligent Computing in Engineering. Advances in Intelligent Systems and Computing, vol 1125. Springer, Singapore (2020)

15. Sundaram A., Ramesh G.P.: Investigation of solar based SL-QZSI fed sensorless control of BLDC Motor, In: Solanki V., Hoang M., Lu Z., Pattnaik P. (eds.) Intelligent Computing in Engineering. Advances in Intelligent Systems and Computing, vol. 1125. Springer, Singapore (2020)

Enhanced SURF- and Wavelet-Based Underwater Image Stitching

G. Babu, B. Sridevi, T. Divyani, M. Monisha, and D. Pavithra

Abstract Underwater images are used in numerous scientific applications in the fields of marine geology, archaeology, military reconnaissance, finding underwater resources, detection of temporal changes under the sea, environment damage assessment, etc. Stitching these underwater images to obtain a clear view is a challenging and interesting problem for researchers. Several advances have been made to stitch normal images, but the problem of stitching underwater images has been poorly exploded because underwater images suffer from poor visibility conditions. Since underwater images are captured by unmanned underwater vehicles (UAVs), the orientation of the images obtained also introduces an difficult problem. An effective underwater image stitching technique is proposed in this paper. The images obtained from a particular location are oriented in correct angle using self-organizing map (SOM). The features of the oriented images are obtained with the help of speeded-up robust feature (SURF) registration technique. Hessian matrix plays the role of obtaining the feature points because it augments the number of feature points. From the obtained feature points, the overlapping regions in the images are identified. These regions are then eliminated using random sample consensus (RANSAC) algorithm. Finally, the pre-processed images are fused to obtain the overview of that particular area, thus provides a helping hand for researchers in various fields.

Keywords Image stitching · SURF algorithm · Mosaicked image · Fusion

1 Introduction

The image stitching is broadly used in various fields like document mosaicking, medical imaging, video stitching, multiple-image super-resolution imaging, high-resolution mosaicked photos in digital maps and satellite imagery. Many techniques have been employed by researchers for stitching underwater images; still they find

G. Babu (✉) · B. Sridevi · T. Divyani · M. Monisha · D. Pavithra
Department of Electronics and Communication Engineering, Velammal Institute of Technology, Panjetty, Tamil Nadu, India
e-mail: gbu@velammalitech.edu.in

D. K. Sharma et al. (eds.), *Micro-Electronics and Telecommunication Engineering*,
Lecture Notes in Networks and Systems 179,
https://doi.org/10.1007/978-981-33-4687-1_33

the underwater image stitching as quite complicated issue because of low quality. So, the aim of the paper is to get a clear view of a location by orienting the images and to produce a natural quality image.

The first step to obtain a natural mosaicked image is to orient the images in a particular angle for making the image stitching process a bit easy. Orienting the image is performed by self-organizing map (SOM) algorithm. Algorithm for learning features of different resolution in hidden layers in a completely unsupervised manner is established [1].

Second, the oriented images then undergo registration technique. Image registration is the most important step in the underwater image stitching process. It is the action of transforming different sets of data into single coordinate system by using SURF algorithm [2]. Various registration techniques like Oriented FAST and Rotated Brief (ORB) and Scale-Invariant Feature Transform (SIFT) are also available [3, 4].The speeded-up robust feature (SURF) is an advanced image registration technique of SIFT and ORB techniques which identifies the speed at greater speed. This algorithm is also capable of identifying the similar features of images of different sizes. The blob detection focuses in detecting the points in a digital image which are different in color and brightness by comparing it with the neighbouring region. Thus, the feature points are identified.

After identifying the matching features of images, the overlapping region can be determined. The overlapping regions of the images are eliminated with the help of RANSAC algorithm [2].

The last and significant step in the underwater image stitching process is fusing the images. The image fusion is the blending of two or more images for recognition of the image with perfect quality. The image fusion is performed using wavelet transform algorithm thus producing seamless results.

To achieve high-resolution stitched image, an effective image stitching method based on self-organizing map, and SURF algorithm is proposed in this paper.

2 Proposed System

2.1 Block Diagram

The block diagram for enhanced SURF and wavelet based underwater image stitching is as follows (Fig. 1).

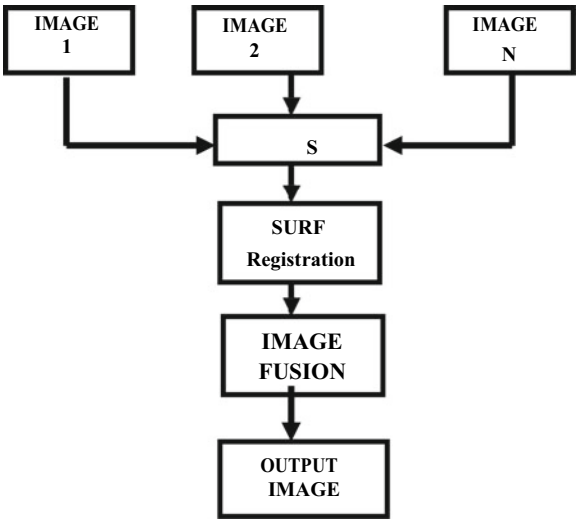

Fig. 1 Block diagram

3 Algorithm

3.1 Self-organizing Map

Map is an artificial neural network, designed for yourself [5]. It is trained by unattended learning to produce the input space for the exercise samples, which is called the map, with a two-dimensional discrete representation. It is the way to reduce dimensions. Instead of error-correction learning, competitive learning is employed in self-organizing map [6, 7].

The network has to be fed with large number of example vectors. These vectors must be as close as possible to the vectors expected during forming map. These example vectors are processed several times recursively [8].

The competitive learning in SOM is whenever a training set is given, the Euclidean distance to all the pixels of the given training images is computed. From the obtained distance, a map is formed [9]. The update formula for an image x with weight vector $W_x(s)$ is,

$$\mathbf{DisplaystyleW_x(sp+1) = W_x(sp) + \theta(u, x, sp) \cdot \alpha(sp) \times (D(i) - W_x(sp))\}}$$

SURF obtains Hessian matrix using blob detector to find the point of interest. Considering a point $m = (x, y)$ in an image I, the Hessian matrix H(pt, s) at point pt and scale s is:

$$\mathrm{H(m, s)} = \begin{pmatrix} Lxx(m,s)Lxy(m,s) \\ Lyx(m,s)Lyy(m,s) \end{pmatrix}$$

where sp is the step index of the sample, i is the index of training sample and u is the index of BMU of the input vector.

The example for orienting the images using self-organizing map is of which 0° orientation is identified as correct by the SOM algorithm.

3.2 SURF Registration

SURF descriptors spot and identify objects, people's faces or reconstruct 3D image by extracting the point of interest. The determinant of hessian blob is computed with 3 integer operations [10].

In SURF method, the image is converted into coordinates using multi-resolution pyramid technique to obtain the same image with reduced bandwidth using Gaussian or Laplacian pyramid shape. This achieves a state called scale-scarp which ensures that the point of interest is scale invariant. The algorithm has three steps: interest point detection, neighbourhood description and matching [11]. The self-organizing map clusters the data without having knowledge about the class memberships of the input data. Since the self-organizing map is used to detect features; it is also called as self-organizing feature map (SOFM). Interest point detection: SURF algorithm uses box filters(square-shaped) as an approximation of Gaussian smoothing [12]. This type of filtering is much faster if integral images is used:

$$S(x, y) = \sum_{K=0}^{x} \sum_{I=0}^{y} I(k, l)$$

3.2.1 Scale-space and point of interest position

The scale-space representation in SURF algorithm is implemented by using square(box) filters of various sizes. The scale space of an image is obtained by up-scaling the filter size to reduce the size of the image. The determinant of Hessian matrix is obtained from which the maxima is interpolated.

3.2.2 Descriptor

The descriptor provides a unique description of an image feature. Thus, the description for every point of interest identified in the previous step is obtained. The descriptor first fixes a reproducible orientation which is done based on the information from a circular region around the point of interest. Then, a square region is constructed around the selected point of interest aligned to the orientation from which the SURF descriptor can be extracted from it.

The area of interest is split into 4*4 smaller sub-regions. The Haar wavelet responses are obtained at 5*5 spaced sampled feature points. Finally, the descriptors obtained from two images are compared so that the matched pair can be found.

3.3 RANSAC Algorithm:

RANSAC is an recursive technique to estimate parameters of mathematical model. The parameters are estimated from a set of observed data which contains outliers. When the outliers are accorded, there will be no influence on the values of the estimates. Hence, this is also called as outlier detection method. RANSAC is a non-deterministic algorithm which produces reasonable result with certain probability.

RANSAC algorithm is used to minimize the error occurring during matching a consensus set. The feature points of the fan zone of the images are removed, and inner feature points are double-checked by this algorithm.

RANSAC is a resampling method that generates user's solutions by using minimum number of observations which are required to estimate the underlying model parameters.

The basic RANSAC algorithm is given as: 1. Select the minimum number of points required to determine the model parameters in random manner. 2. Solve the parameters of the model. 3. Determining how many points from the set of total points fit with predefined tolerance. 4. Re-estimate the model parameters using all the inliers identified, if the fraction of the number of inliers over the total number of points in the set exceeds a predefined threshold. 5. Else, repeat the steps 1–5. The steps are repeated for a maximum of N times.

By solving homography matrix using RANSAC feature points obtained from SURF technique, points of straight line are determined. Two points can determine a straight line. Hence, two points from the data set determine a straight line. Then by setting a given threshold value, the number of points, inliers that meet the threshold range on both sides of straight line, is calculated (Figs. 2 and 3).

Fig. 2 A dataset with many for which RANSAC a linehas to befitted

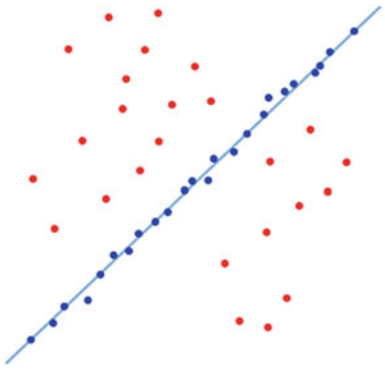

Fig. 3 Fitted line with RANSAC

3.4 Image Fusion Based on Wavelet Transform

Wavelet transform is an important process in image compression because wavelets allow both time and frequency analysis to be carried out at a same time. First, the images are blended using wavelet transform. Then, the images are decomposed, and then the images are fused. To reduce distortion, the wavelet coefficient for the fused image is obtained. This is performed not only by considering the corresponding coefficients but also their close neighbours. The parameters like visual quality, absence of impairments and artifacts are concerned [13].

3.4.1 Image Fusion

Image fusion is the process of combining two or multiple images together to form an image which holds all the common and complementary information from each and every original images. The result of fusion is a higher spatial resolution image which is free from all possible burring effects. To get the details of approximate

components, the original image is passed through high-pass and low-pass filters. Haar wavelet decomposition is employed for subjective analysis.

3.4.2 Fusion Rule

Fusion rules are the set of rules that are used to determine the exact decomposition of the tensor product of two representations of a group into a direct sum of irreducible representations.

The fusion rule employed for image fusion is maximum selection fusion scheme. The largest absolute wavelet coefficient is selected, and this value is replaced with coefficient at that particular location in the fused image.

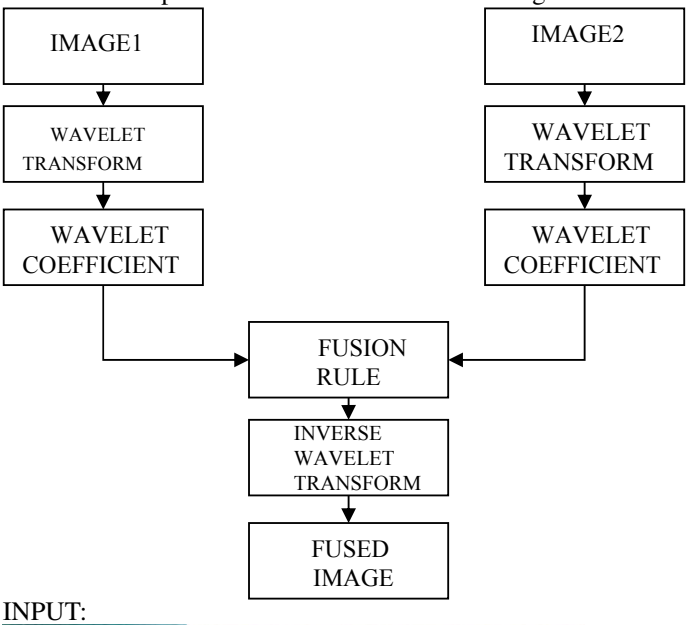

INPUT:

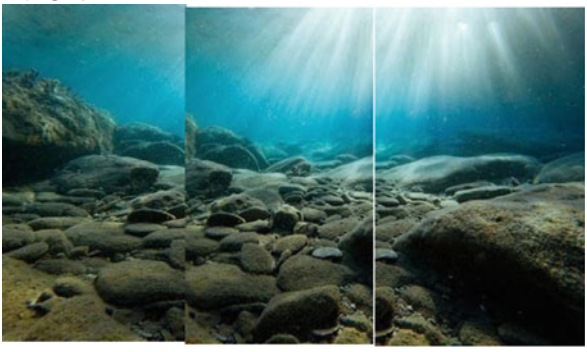

OUTPUT:

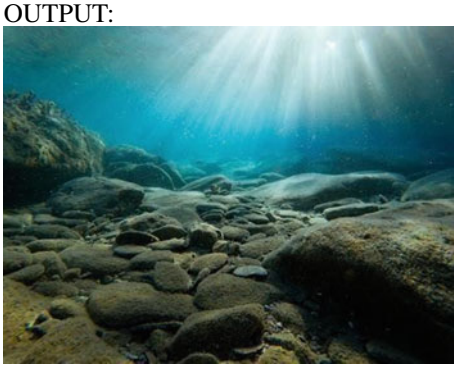

4 Conclusion

An efficient technique for stitching the underwater images using self-organizing map, speeded-up robust feature, random sample consensus and image fusion based on wavelet transformation can be achieved. The experiment results shown in the paper are efficient and satisfy the need of the researchers.

References

1. Wickramasinghe CS, Amarasinghe K, Marino D, Manic M (2018) Deep self-organizing maps for visual data mining. In: 2018 11th international conference on human system interaction (HSI). IEEE, pp 304–310
2. Ferles C, Papanikolaou Y, Naidoo KJ (2018) Denoising autoencoder self-organizing map (DASOM). Neural Netw. 105:112–131
3. Cao L, Jin L, Tao H, Li G, Zhuang Z, Zhang Y (2014) Multi-focus image fusion based on spatial frequency in discrete cosine transform domain. IEEE Signal Process Lett 22(2):220–224
4. Jadhav S (2014) Image fusion based on wavelet transform. Int J Eng Res 3(7):442–445
5. Zhichun Z, Liqun K, Xie H, Xiaowen Y (2014) An improved RANSAC algorithm for image Mosaic. Comput Measur Control 22(6):1856–1858
6. Chew VC, Lian FL (2012) Panorama stitching using overlap area weighted image plane projection and dynamic programming for visual localization. In: 2012 IEEE/ASME international conference on advanced intelligent mechatronics (AIM). IEEE,pp. 250–255
7. Babu VH, Balaji K (2020) Survey on modular multilevel inverter based on various switching modules for harmonic elimination. In: Intelligent computing in engineering. Springer, Singapore, pp 451–458
8. Kumanan T (2020) Link quality and energy-aware metric-based routing strategy in WSNS. In: Intelligent computing in engineering. Springer, Singapore, pp 533–539
9. Manikandan G, Anand M (2020) Radix-2/4 FFT multiplierless architecture using MBSLS in OFDM applications. In: Intelligent computing in engineering. Springer, Singapore, pp 553–559
10. Sundaram, A., Ramesh, GP (2020) Investigation of solar based SL-QZSI fed sensorless control of BLDC motor. In: Intelligent computing in engineering. Springer, Singapore, pp 779–787
11. Snehalatha N, SA TS, Amudha S (2016) Remote display access using remote frame buffer and IO streaming. Int. J. MC Square Sci. Re. 8(1):23–40

12. Rajesh D (2016) Ch panel based routing scheme for mobile wireless sensor network. Int. J. MC Square Sci. Res. 8(1):183–198
13. Rajan A, Ramesh GP (2015) Automated early detection of glaucoma in wavelet domain using optical coherence tomography images. Biomed Pharmacol J 8(2)

Multilevel Inverter-Based Power Quality Improvement in Grid-Connected DVR System

Gundala Srinivasa Rao and S. Sampath Raju

Abstract In the transmission and distribution system, the major issues are power quality which is a concern in recent years. The problems that are occurred in the power system are swell, sag, voltage flickers, harmonics. To compensate such problems, the traditional power devices are used. In this paper, the dynamic voltage restorer is discussed with the multilevel inverter to prevent the equipment failures and protect sensitive loads. The cascaded multilevel inverter is interfaced with the DC link capacitor as a source. In this system, seven levels are achieved with multilevel inverter to compensate the power quality problems. This result is achieving the better quality of power improvement in voltage sags. To control the MLI inverter-based dynamic voltage restorer, the hysteresis control (HC) method is used. The MLI-based system is achieving the compensation in distribution network and which results are analyzed and verified using in Simulink environment.

Keywords DVR · Cascaded multilevel inverter · And hysteresis control

1 Introduction

The power quality problem is increasing very essential one every day due to the improvement in the sensitive loads with huge amount. In the power system, there are three sections as generation, transmission and distribution. In the transmission and distribution network, the PQ problems are occurred such as voltage imbalance and flicker, sag and swells. [1–4] The power quality problem is occurred in both commercial and industrial customers. The under voltage is occurred from various sources [5–8]. The DVR is a compensation device of the flexible AC transmission system (FACTS), and it is used to mitigate the voltage sag which is occurred as a fault in the distribution system [9–11]. The sag fault is compensated through the DVR device by voltage injection in series and provides normal level power supply in which the supply voltage is dropped. The DVR system mainly consists of voltage

G. S. Rao (✉) · S. Sampath Raju
CMR College of Engineering & Technology, Hyderabad, India
e-mail: drgundalasrinivasarao@gmail.com

D. K. Sharma et al. (eds.), *Micro-Electronics and Telecommunication Engineering*,
Lecture Notes in Networks and Systems 179,
https://doi.org/10.1007/978-981-33-4687-1_34

source inverter, stage of measurement, control system unit and transformer of series injection. The various methods are available to control the PQ issues of voltage disturbance compensation. The fast response and flexibility solutions are most perfect solutions based on the power electronics devices. The series-connected VSI is used to provide compensation voltage with the grid terminal line by means of transformer. This operating performance leads to the safe operation of the loads for the sensitive loads. In the DVR circuits, many types are available as the VSI is main system to DVR device [12, 13]. In the existing systems, the multilevel inverters (MLI) are used to the voltage disturbances compensation through the DVR device. This device is controlled by using various controllers. The MLI is controlled through the control of fundamental frequency method. The cascaded multilevel inverters are introduced in sag compensation with dynamic voltage restorer. The basic control methods for the cascaded MLI system lead to the poor power quality output voltage in some points [14]. The PWM control is used for cascaded MLI system which is considering both symmetric and asymmetric systems. In the cascaded MLI, a DC source is required for each of them. The output voltage from the cascaded MLI with levels is compensating the sag voltage through the injection transformer.

2 Proposed System

In the proposed system, the external fault is given to the grid-connected distribution system, and the load voltage is compensated by cascaded dynamic voltage restorer. Normally, the AC source is fed to grid-connected distribution system along transmission system. The external source is used for multilevel inverter to provide three-phase AC supply. In this system, the DC supply is given to the proposed multilevel inverter after that the DC voltage is converted into AC voltage with seven levels.

By this output voltage of multilevel inverter, the harmonics content in the three phase voltage which is converted from DC supply can be reduced. The multilevel inverter output is fed to the transmission line to inject the voltage to compensate the sag issue in grid-connected distribution system. The sensitive loads are performed well while using such kind of compensation devices in industries and commercial areas. The proposed system block diagram is shown in Fig. 1. The load side terminal is decreased due to the events of large loads starting, nonlinear loads running, etc. The network proposed involves AC source, transmission device, grid system and multilevel inverter. The convention systems are using transformers with three-leg bridge inverter to pump the voltage in transmission line. For this method, the cascaded multilevel inverter is suggested to increase the power efficiency of the complete reduction for harmonics. The harmonics in the injection voltage is reduced with the help of MLI, and the output of the inverter is injected in transmission line. The sag is compensated using cascaded multilevel inverter with control strategy.

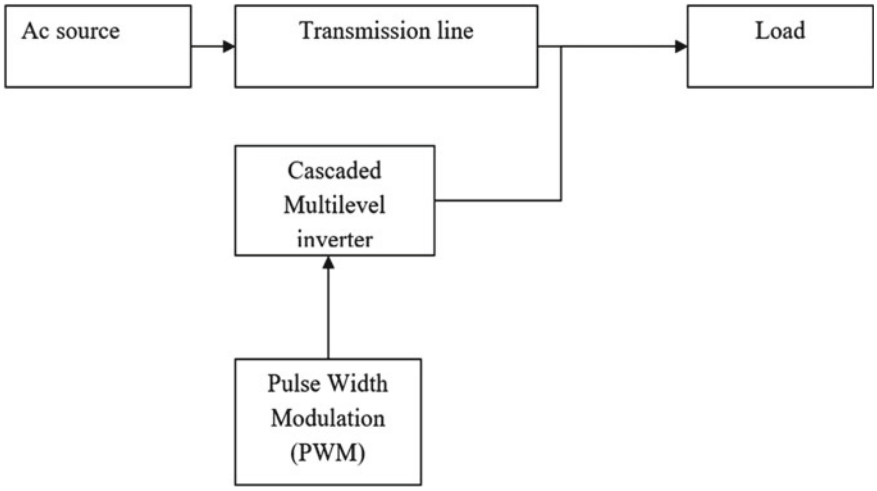

Fig. 1 Proposed system block diagram

2.1 Control Method

Present controller function well only because we are correctly characterizing the two party viz. Present error is fed as controller input and produces gate signals when error is below the limit of the hysteresis band or when the pulse reaches the limit of the band it induces gate signals which are low to power switches. As shown in Fig. 2, if the band limit is preferred, band limit will be held at a lower significance because the pulse's high switching frequency is also high, resulting in high-power electronic switching losses. This hysteresis controller (HC) is PWM-based control of instantaneous compensation, and within the hysteresis band, the command current is tracked by the actual current. The compensation current is varied from the lower and higher limits of the HC. If upper hysteresis limit (ica* + HB/2), then 0 (S1 = 0, S2 = 1). On the other hand, if less than the lower hysteresis limit (ica* - HB/2) then 1 (S1

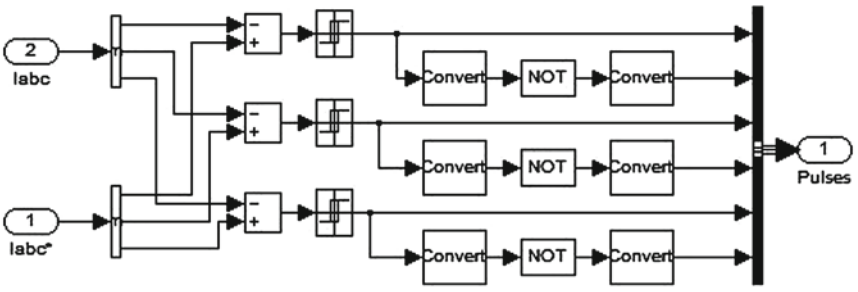

Fig. 2 Proposed system control block diagram

= 0, S2 = 1). HC method is excellent dynamic response, easy implementation and low cost. Instantaneous reactive power theory is used to generate the actual output current which will generate pulses in such a manner that inverter output current will follow the reference current.

3 Simulation and Results

The dynamic voltage restorer proposed is the system to improve the effectiveness of the power. For these devices, the issues in the grid-connected network and industrial as well as commercial sectors can be rectified in the distribution system. The multilevel inverter is interfaced with the inject voltage transmission line, which is compensating energy from the multilevel inverter output. The inverter is used to balance the grid voltage by external DC supply. Seven-stage output voltage is produced from the inverter. This simulation process uses both linear and nonlinear loads. Multilevel inverter is introduced to regulate pulse width modulation. Figure 2 shows the Simulink model of the DVR-based hysteresis controller. Figure 3 shows the transmission line supply voltage during fault occurred in transmission line. The output of the multilevel inverter is 300 V, and its output voltage is seven levels as shown in Figs. 4, 5 and 6.

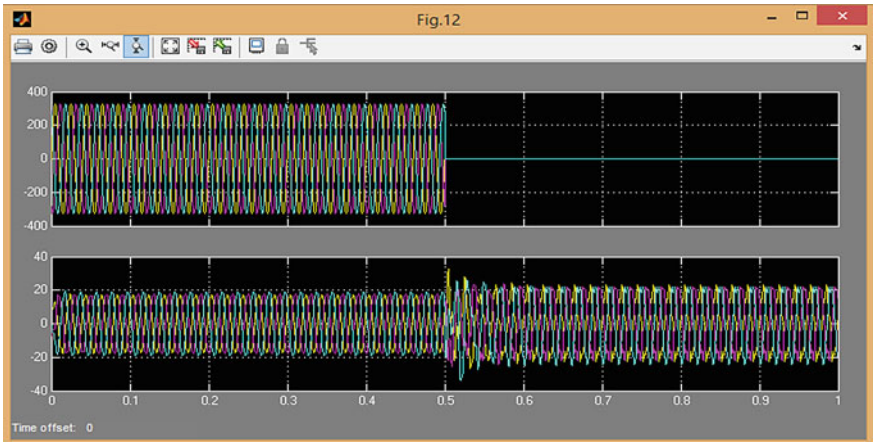

Fig. 3 Sag voltage during fault in transmission line

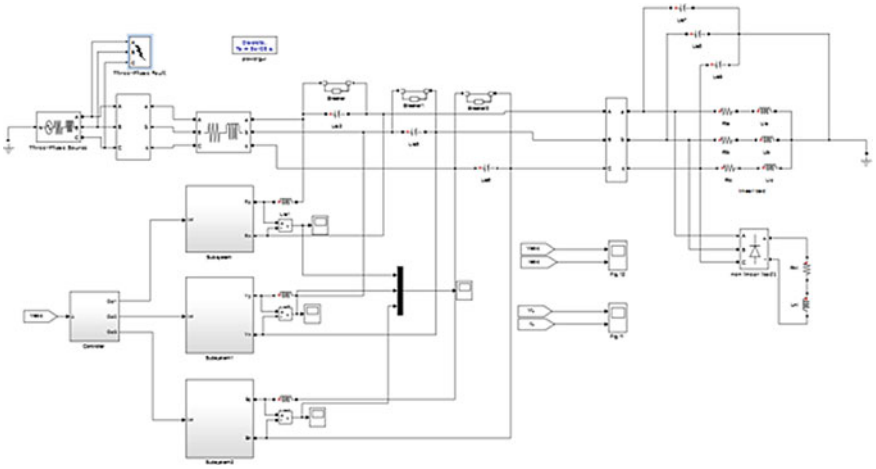

Fig. 4 Simulation model of proposed system

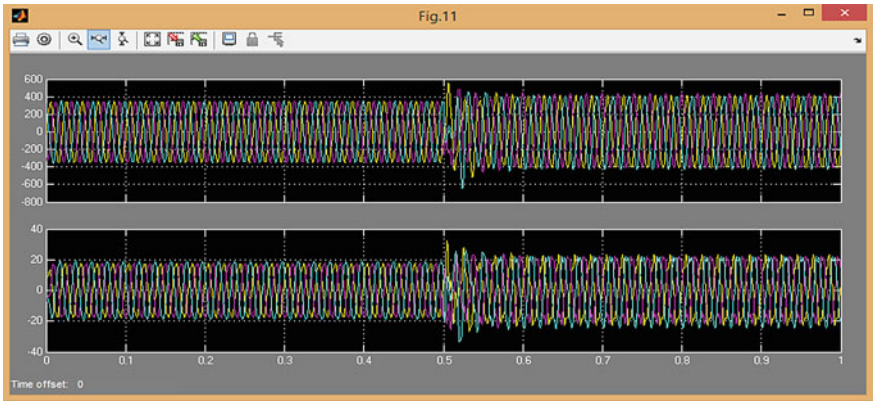

Fig. 5 Proposed system compensation voltage using DVR

4 Conclusion

In this paper, a dynamic voltage restorer is designed to mitigate the voltage sag, and voltage compensation is accomplished by multilevel inverter. The sag voltage in grid-connected transmission system due to external fault occurred in line can be compensated by pulse width modulation control technique. The seven levels are achieved in output voltage of inverter. The supply voltage sag compensation is verified, and results are obtained successfully. The harmonics of the compensation voltage is reduced, and power quality improvement is accomplished. The simulation results are supported to the theoretical analysis, and they show voltage sag compensation of the proposed system and also total harmonics reduction.

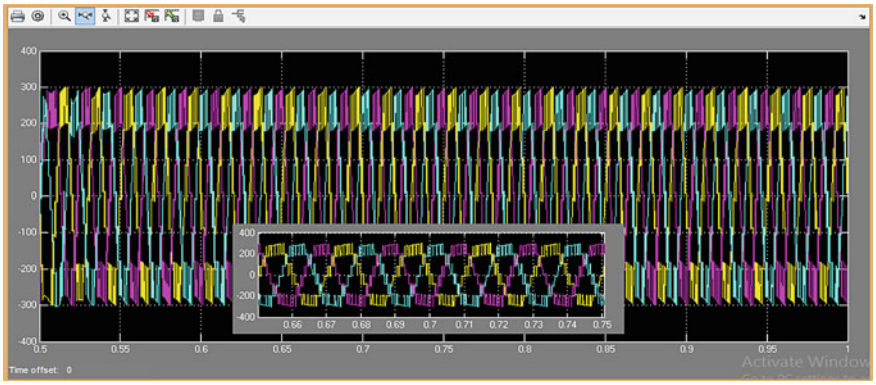

Fig. 6 Multilevel inverter output voltage with 7 levels

References

1. Surendran V, Srikanth V, Subhash T (2014) Performance improvement of dynamic voltage restorer using proportional-resonant controller. In: 2014 power and energy systems: towards sustainable energy (PESTSE). pp 1–5
2. San-Millan A, Russell D, Feliu V, Aphale SS (2015) A modified positive velocity and position feedback scheme with delay compensation for improved nanopositioning performance. Smart Mater Struct 24(7):1–11
3. Gee AM, Robinson F, Yuan W (2017) A superconducting magnetic energy storage-emulator/battery supported dynamic voltage restorer. IEEE Trans Energy Con 32(1):55–62
4. Jiang F, Tu C, Guo Q, Shuai Z, He X, He J (2019) 'Dual-functional dynamic voltage restorer to limit fault current.' IEEE Trans Ind Electron 66(7):5300–5309
5. McDonald A, Jimmy G (2017) Parallel wind turbine powertrains and their design for high availability. IEEE Trans Sustain Energy 8(2):880–890
6. Chen X, Wang L, Sun H, Chen Y (2017) Fuzzy logic based adaptive droop control in multi-terminal HVDC for wind power integration. IEEE Trans Energy Convers 32(3):1200–1208
7. Shen YW, Ke DP, Qiao W, Sun YZ, Kirschen DS, Wei C (2015) Transient reconfiguration and coordinated control for power converters to enhance the LVRT of a DFIG wind turbine with an energy storage device. IEEE Trans Energy Convers 30(4):1679–1690
8. Morshed, MJ, Fekih A (2016) A fault-tolerant control paradigm for microgrid-connected wind energy systems. IEEE Syst J 99:1–13
9. Tuyen ND, Fujita G, Muhtazaruddin MNB, Funabashi T (2014) Shunt active power filter for 3-phase 3-wire nonlinear load under unbalanced and distorted PCC voltage using notch adaptive filter. In: IEEE PES T&D conference and exposition, pp 1–5
10. Komurcugil H, Biricik S (2017) Time-varying and constant switching frequency-based sliding-mode control methods for transformerless DVR employing half-bridge VSI. IEEE Trans Ind Electron 64(4):2570–2579
11. Rajeswari R (2015) Power quality improvement of novel PWM based 15 level inverter for modified unified power quality conditioner (UPQC). Int J MC Square Sci Res 7(1):23–40
12. Balaji K, Ashok Kumar R (2020)Adaptive super-twisting sliding mode controller-based PMSM fed four switch three phase inverter.In: Intelligent computing in engineering. Springer, Singapore, pp 327–337
13. Sivasankar C, Kumanan T (2020)Friend list-based reliable routing in autonomous mobile networks.In: Intelligent computing in engineering. Springer, Singapore, pp 409–415
14. Ramesh GP (2020)Design of digital fir filters for low power applications.In: Intelligent computing in engineering. Springer, Singapore, pp 433–440

Era of Small Satellites: Pico, Nano and Micro-satellites (PNM Sat)—an Over View of Frugal Way to Access Low Earth Orbit

Dušan Radosavljević, Lazar Jeftić, L. V. Muralikrishna Reddy, K. Gopalakrishnan, and S. Mohankumar

Abstract Every nation, be it a small or big, aspires to launch their own satellite to space and wishes to provide an opportunity to their scientists/students, in order to encourage them to continue space research. For the majority of the nations and academic institutions/universities, it is still a distant dream! including former Yugoslavian countries (Bosnia and Herzegovina, Macedonia, Montenegro, Croatia, Serbia and Slovenia). Committee for Space Programme Development (CSPD), Serbia, has been striving hard to provide an opportunity for building and launching satellites for former Yugoslavian countries. In continuation of their sustained efforts since last 2–3 years, CSPD has succeeded in establishing a working relationship with India and paved the way for Indo-Serbian Collaborative Research leading to the realization of the launching of satellites of small nations. This paper highlights the opportunities opened up globally during Space 2.0 era and need for the Pico, Nano and Micro-Satellites (PNM Sat) as a frugal way to access space and sustain space research by academic institutions and small nations to realize their dream in a more frugal way!

Keywords Pico · Nano and Micro-Satellites (PNM Sat) · CanSat · PocketQube · CubeSat · UNITYsat

D. Radosavljević · L. Jeftić · L. V. Muralikrishna Reddy
Committee for Space Programme Development (CSPD), Novi Sad, Serbia
e-mail: cspd.office@gmail.com

K. Gopalakrishnan (✉)
Indian Technology Congress Association and Convener, Consortium of 75 Students' Satellites: Mission 2020, Bengaluru, India
e-mail: profgoki@yahoo.com

S. Mohankumar
New Horizon College of Engineering(NHCE), Bangalore, India

D. K. Sharma et al. (eds.), *Micro-Electronics and Telecommunication Engineering*,
Lecture Notes in Networks and Systems 179,
https://doi.org/10.1007/978-981-33-4687-1_35

1 Introduction

The first man-made object that was launched into space was the Sputnik-1 satellite [1] in 1957. That was fascinating and appealing to all humankind and escalated the space race [2], consequently, developing technologies and bringing attention to space science around the globe. Space became more accessible and opens to not only governmental space agencies and huge companies but also universities and other educational institutions in recent years. Technologies and devices have a tendency of becoming smaller in size and more powerful in performance (an ideal example is the smartphone industry). A similar development has occurred in small satellite design, and they have decreased in size as well as became more of a standard in their build-up.

1.1 Cube Satellite (CubeSat)

A CubeSat is a cubic-shaped satellite identified by the number of units. One unit, more commonly known as 1U, is a cube with a volume equivalent to one liter and a side length of 10 cm. By merging a few cubes on top of each other, the variety of sizes increases (1U, 2U, 3U, 6U…). Satellites can be categorized by their mass. The one with a mass below 1 kg is a picosatellite, which is very often a 1U CubeSat, or a PocketQube (0.25U). The majority of the launched or built CubeSats are nanosatellites with a mass of 1-10 kg, shown in Fig. 1, as per March 14, 2017 [3].

Majority of 3U CubeSats mentioned in Fig. 1 below have a nominal mass limitation equivalent to 4 kg, however, depending on the deployer, the mass can be higher. As in the case of ISIPOD, the maximum allowable mass for 3U is 6 kg [4]. A spacecraft with a mass range from 10 to 100 kg is a microsatellite, below 1 kg a picosatellite and below 0.1 kg a femtosatellite. The smallest publicly known femtosatellite is called a KickSat, which is a 3.5 by 3.5 cm single printed circuit board (PCB) with a microprocessor, gyroscope, magnetometer, radio with antennas and solar cells [5].

As with any piece of hardware (HW), a satellite needs a structure for holding it together or deploying into the orbit, even in the case of KickSat. Moreover, the development process for space structures is somewhat similar to the ground application with more strict requirements and constraints [6].

Development process initiates with the list of requirements and ends up with the product delivering for LV integration; it consists of designing, verification, manufacturing and testing. For the ground applications, one also considers the outer appearance (how it looks like and how it feels like), however, for the space mission the main target in designing is functionality under certain requirements (some exceptions exists for public relations (PR) purposes).

In this particular case, the satellite consists of payloads (which conduct scientific and technologic demonstration and performance) and subsystems or satellite bus

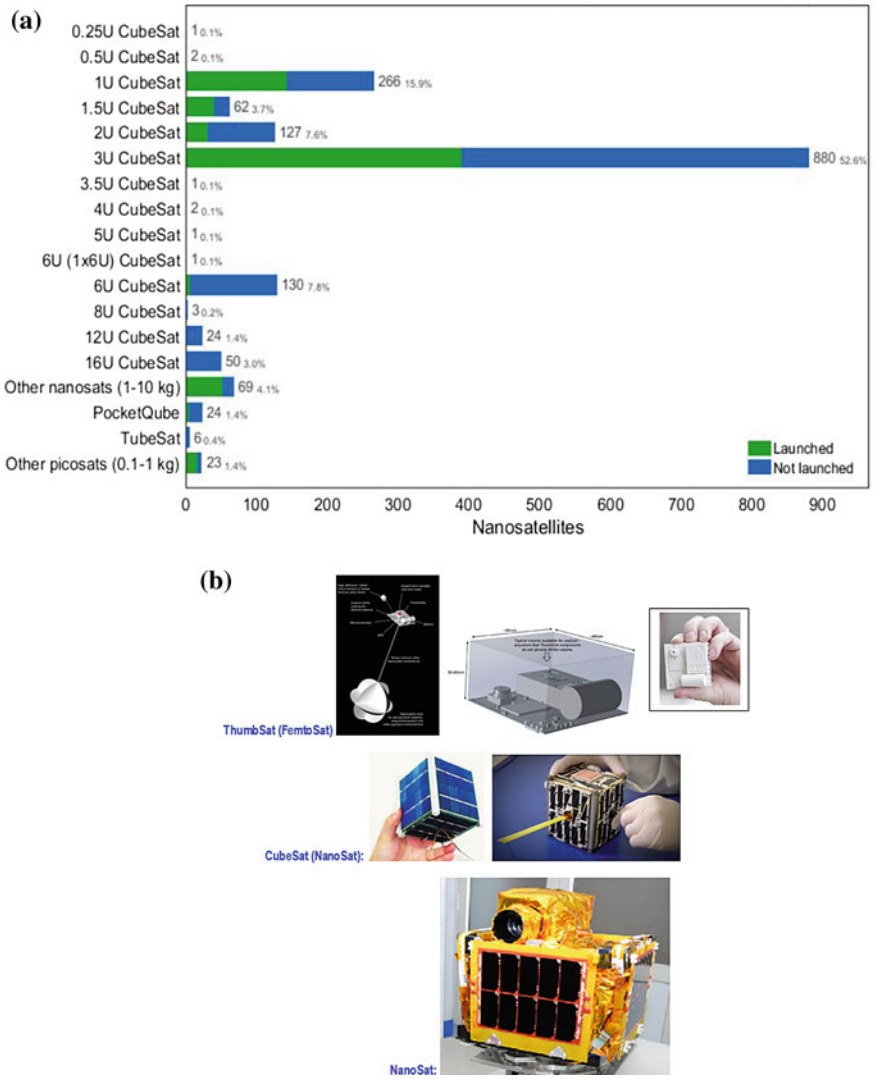

Fig. 1 **a** Nanosatellites launched into orbit and under development, **b** Nanosatellites by type

(which operates the spacecraft). Key requirements consist of functional (what must be done), operational (how well it must be done) and constraints (limit the available sources, schedule or physical characteristics) [7, p. 26]. The risk has to be evaluated and if the elimination is not feasible due to constraints in terms of time, cost or schedule shift, then one has to accept the certain probability of failure or damage. In addition, the level of risk has to be evaluated with its influence on the entire mission—will it cause full mission failure or just minor element deformation that

does not affect the mission success. Any risk evaluation starts with the estimation of failure probability and resolving the consequences of that failure.

2 Space Mission Habitat

After the satellite reaches the specific orbit, it will be exposed to other harmful habitats in the near-Earth space environment. The list consists of, but is not limited to, vacuum, thermal radiation, charged-particles radiation, neutral atomic and molecular particles, micrometeorites and space debris, magnetic fields and gravitational fields [7, p. 61]. Various sources are influencing the man-made objects as a function of orbit (Fig. 2).

The term **vacuum** describes the extremely low pressure in space. A vacuum has various effects on the structure. In vacuum, polymer-based materials (thermal insulators, adhesives and the matrices for advanced composites) release substances in a gaseous form [7, p. 63]. The substance is one of an organic origin or absorbed nitrogen, oxygen and carbon dioxide on the ground. Moreover, the material has issues with water desorption that was absorbed by the material during on-ground processes. The aforementioned effects may degrade certain properties of the material and might cause condensation on critical surfaces (lenses, mirrors and sensors). Another effect is the internal pressure of sealed structures that were assembled at the ambient Earth pressure. **Thermal radiation** is mainly a reference to direct solar flux (1309–1400 W/m^2) which means the intensity of radiation, planetary albedo (global annual average is 0.3) which originates from the reflected solar flux, planetary emission flux (189–262 W/m^2) and the satellite electronics' infrared thermal emission. This results in non-uniform heating of spacecraft which causes materials (especially with various thermal expansion coefficients) to expand differently, resulting in structural stresses. In addition, certain components require a precise operating temperature range (e.g. batteries, propellant tanks). The solution is to implement an active (requires power) and/or a passive (materials and coatings) thermal control system.

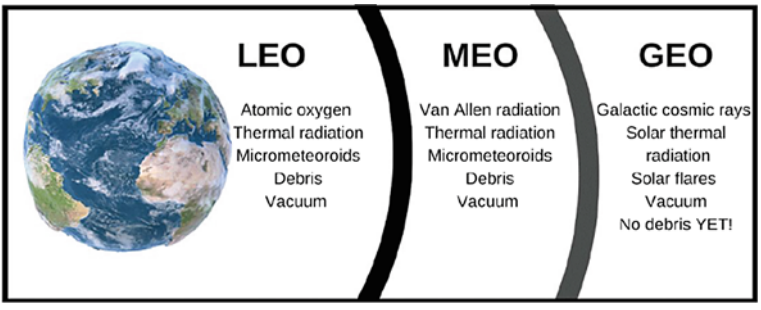

Fig. 2 Space environment as the function of altitude

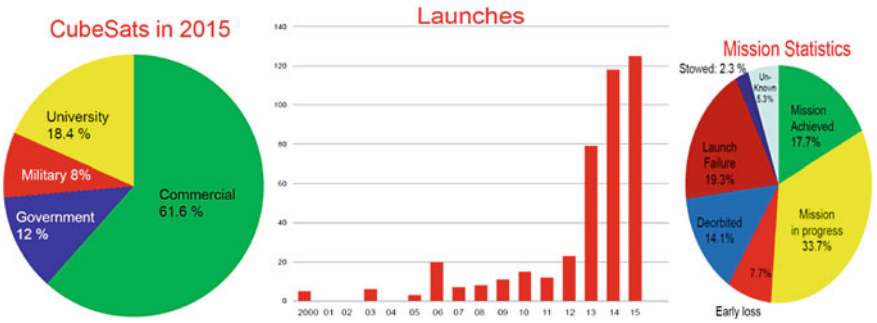

Fig. 3 NanoSats launched till 2015 *Source* M. Swartwout

Charged-particle radiation is a high flux of energetic particles. The major sources are trapped radiation (Van Allen belt) which contains electrons and protons in the MEO, galactic cosmic radiation which contains 90% of protons and 10% of helium nuclei in the GEO and further, and solar radiation which is largely continuous solar wind (electrons, protons and helium nuclei low in energy) and solar flares (high energetic protons and heavy ions) [7, p. 69]. The radiation has a negative effect on the electronic components and may cause damage or failure to the systems. There is no way to predict or to be protected against galactic cosmic radiation, thus electronics have to tolerate it (Fig. 3).

Space Debris

- *Increasing number of nanosatellites imposes a space debris risk*
- *LEO orbit crowded*
- *Orbit to comply with < 25 year orbital life-time*
- *Or: Active De-orbiting Mechanisms*
  - *Deployable sails/structures*
  - *Drag mechanisms*
  - *Propulsion (e.g. micro arc-jets)*

LEO contains relatively stable atomic and molecular particles. When the spacecraft moves at orbital hypervelocity, its surface is struck by particles that cause material recession. The most damaging is atomic oxygen (ATOX) [8]; among other impactors are N_2, O_2, Ar, He, H. The erosion process and rates rely on the material's composition. The most damaging are polymer-based materials, while the impact on metals is not that significant, especially on aluminum (Al) which is commonly used for space structures due to its low density, radiation shielding capabilities and manufacturability. For instance, an exposed Al surface to ATOX at an altitude of 500 km

has an erosion rate of 7.6e–6 mm/year, however, the same parameters applied to silver results in the erosion rate of 0.22 mm/year [9].

Against trapped and solar radiations, shielding is implemented. The structure of the satellite can act as a radiation shield as well. For instance, in order to keep the total radiation dose below 10e4 rads per year at 4000 km, the required thickness of aluminum is 9 mm [7, p. 71].

Micrometeoroids and Space Debris can have a fatal impact on the spacecraft structure at the orbital hypervelocity due to impacts (if the size of impactor is large enough). One can implement shielding against smaller objects. Also, thermal blankets decrease the impact of small objects [10, pp. 10–11].

The **plasma brake** (Fig. 4a) is an end-of-life disposal technique for objects in the LEO. The problems behind already existing debris are upcoming large constellations as shown in Fig. 4b. The probable collisions at orbital hyper-velocities (over 3 km/s) will cause defragmentation which will consequently result in an enormous escalation of small objects, better known as the Kessler syndrome, which will disable access to LEO if the escalated problem is ignored

Space Missions with Few Examples [11–15]

- Astrobiology
- Astronomy
  - BRITE
  - CANIVAL-X (NASA): formation flying, virtual telescope
- Atmospheric science
- Biology
- Pharmaceutical research
- Earth observation
  - Planet Laboratories (commercial)
- Space weather
- Telecommunications
  - AIS (UTIAS, SPIRE-commercial)
  - ADS-B monitoring
  - Messaging
  - Amateur radio
- Material science
- Technology (OPS-SAT)

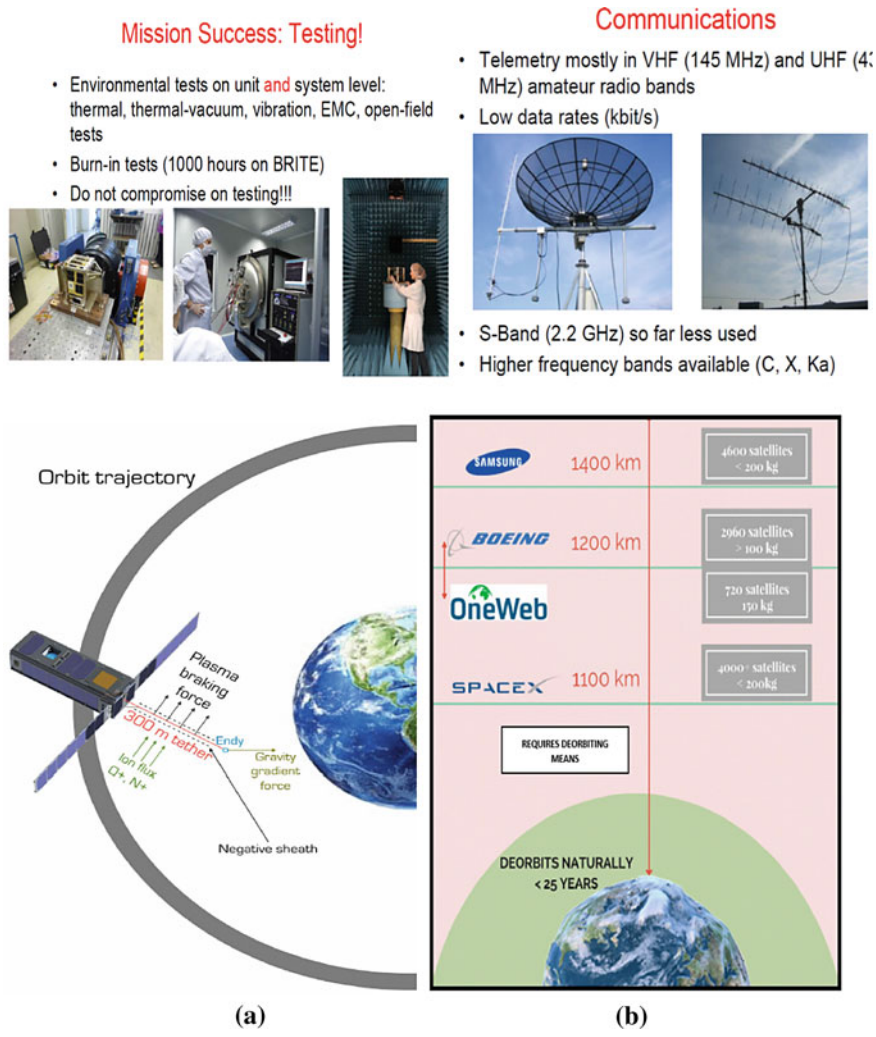

Fig. 4 **a** Plasma brake concept for the gravity-stabilized tether, **b** upcoming large constellations

Commissioning and Operations Support

Work Group	Major Team/Core Activities
Solar Panels	Payload Design and Development Payload Identification/Development
CubeSat Platforms	
System Integration	Payload Integration
Software Programming	Mission Software Development (Programming)
Launch Service	Launch Logistics
Ground Control Station	GCS
Commissioning and Operations Support	Observation
Review of Literature/ Case Studies	Documentation
Testing and Analysis/ Failure Analysis	System-Level Testing

Applications of Satellite Programs

ISISpace has been working on training next generation scientists and engineers, performing small scale science missions or planning a novel application using a globe-spanning constellation, etc. Potential space applications are listed below (but not limited to the following):

1. **Earth Sciences**: Nanosatellites for better understanding of our own planet;
2. **Ship Tracking Services**: Near real-time vessel tracking using satellite-AIS;
3. **Aircraft Tracking**: Keeping track of aircraft on a global scale using ADS-B;
4. **Space Research**: Small scale astronomy and exploration missions;
5. **Climate Monitoring**: Network of satellites to monitor climate change;
6. **Earth Observation**: Provide real-time imaging capability with satellite swarms;
7. **Agriculture Monitoring**: Improve crop production using remote sensing data;
8. **Microgravity Research**: Use the space environment to gain new insights;
9. **Pipeline Monitoring**: Monitor critical infrastructure using satellites;
10. **Signal Intelligence**: Use small satellites to ensure the security of our nation;
11. **Education and Training**: Train the next generation scientists and engineers;
12. **Telecommunications**: Provide global connectivity using small satellites;
13. **Technology Validation**: Test your latest technologies on-board a small satellite.

Various Successful Strategies to Nurture Interest and Mobilize Passionate Workgroups/Team

What is a CanSat?

A CanSat is a simulation of a real satellite. All systems and subsystems are housed in a soft drink “can”-shaped structure which can hold up to 350 ml. Building a CanSat is an economical way to gain basic knowledge and skills in space engineering for

teachers and students, also, to experience engineering challenges, when designing satellites which have to survive in the hostile space environments! Students are able to build a small electronic payload that can fit into the cans of 350 ml. CanSat is launched by rocket, balloon, plane or drone and is carried to apogee. With the parachute, the CanSat slowly descends to the ground and carries out its mission during descent (for example: measures air pressure and temperature and sends telemetry). By analyzing the data collected by CanSat, students will analyze the reasons for its success or failure of the mission. It is an affordable process to keep the passionate students engaged and in the process, and the team acquires adequate fundamentals/knowledge of system engineering along with necessary systems and subsystems to build their CubeSat! Space engineering learning, based on the CanSat/Rocketry concept, gives an opportunity to the students to gain hands-on experience through a specific inter-disciplinary project. Since this is a space engineering project, teachers and students will gain experience from mission definition, conceptual design, through integration and testing, up until launching and actual system operation, i.e., experience from the whole space project cycle and then participate in the CanSat/Rocketry competition with its peers at home country and abroad. One of the main advantages of the CanSat/Rocketry concept is its interdisciplinary and multi-disciplinary in nature: combination of mathematics, physics, informatics/programming, mechatronics, telecommunications, aviation and rocketry, mechanics, etc. Whenever the CanSat/Rocketry teams win or lose in the competitions, they have enough lessons learned in the process to cement their unity with the project and dos and don'ts as well! It helps the team members to get motivated and sustain their interest for learning and doing continuously till they launch their own CubeSat/PocketQube to LEO!

Benefits of CanSat/Rocketry-Based Education
CanSat/Rocketry is an effective educational tool for:

- Learning by doing and also provides an opportunity to "create" new CanSat/Rocket/PocketQube, which is the highest level of learning pedagogy as per Revised Bloom's Taxonomy (RBT);
- Involving students in technology and engineering as a practical complement to other, fundamental, subjects they study, such as mathematics and physics;
- Emphasizing teamwork where each student has a specific task/role that creates a sense of responsibility for him/her;
- Students gain experience of the complete process: defining the mission, design, development/constructing, programming, testing, launching and analysis;
- Simple conducting experiments with balloon/rocket/plane/drone;
- Learning methods can be adapted to the age level of students, or to their needs and abilities;
- Students are able to analyze the reasons for success or failure after descending CanSat and Rocket to the ground;
- Acquired knowledge and experience can be applied to other projects as this concept enables obtaining of ideas and stimulates students' thinking;
- Useful for a further education/career guidance process;

Today, almost every country in the higher education system has a CanSat/CubeSat program, so the initiative to establish CanSat/Rocketry Championship at the Global level is additionally justified.

Facts as of 2020 January 1 (Nanosatellite Database by Erik: https://www.nanosats.eu/)

Companies in database: 467

Forecast: over 2500 nanosats to launch in 6 years

Design and Development of Indo-Serbian PocketQube, CanSat and UNITYsat: TSC PocketQubeV1 (50 mm × 50 mm × 50 mm):

Power Specifications

- Total unit works at 3.3 V.
- Battery specs (planned to use): LiPo 3.6 V @ 1240 mAh.

Board Specifications

- Per board: 44.45 mm (L) × 44.45 mm (W) × 8.5 mm (header height) + desired board thickness.
- Available board thickness 0.4, 0.6, 0.8, 1, 1.2, 1.6, 2.0 in mm.
- 2 layer board.
- 4 M3 mounting holes.
- All boards are interconnected in two rail configurations using stack headers.

Board Description

EPS

- Can plug 3no of 2 V @ 150 mA solar cells (dimension 5 cm x 5 cm x 4 mm).
- Discharge protection circuit.
- 3V3 voltage regulator.
- LiPo fuel gauge (to monitor battery).

Power switch (Figs. 5 and 6).

OBC (with COM)

- Has on-board USB interface for uploading and serial monitoring.
- Uses 8-bit AVR RISC-based microcontroller combines 32kB Flash, 2 KB SRAM
- Uses SX1268 433/868 MHz **LoRa** module. (http://www.dorji.com/products-detail.php?ProId=64)
- Can plug in 16 GB micro-SD Card for data storage.

Contains UFL male connector for antenna extension (Figs. 7 and 8).

Sensor Breakout

- Holds temperature and 9-DOF (BMP280 + MPU9250) sensors on-board
- 4 I2C ports.

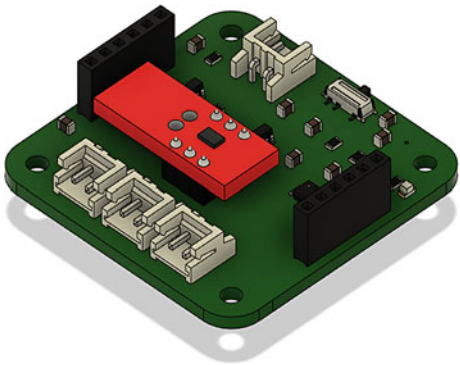

Fig. 5 Snapshot of EPS v1

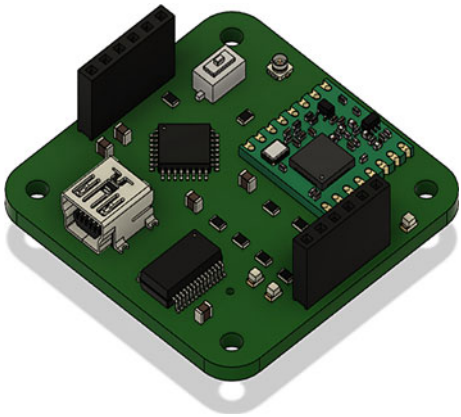

Fig. 6 Snapshot of OBC (isometric top view)

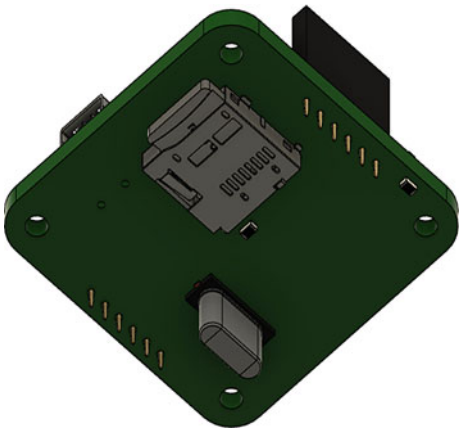

Fig. 7 Snapshot of OBC (isometric bottom view)

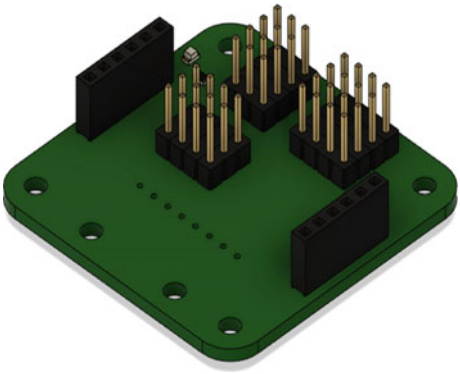

Fig. 8 Snapshot of sensor breakout board (isometric top view)

- 4 analog pinouts
- 4 digital pinouts. (1 PWM).

Complete PocketQube View
Figures 9, 10 and 11.

Indo-Serbian CanSat:
Figures 12 and 13.

Indo-Serbian collaboration has paved the way for Conducting Capacity Building CanSat Workshops in Eastern Europe along with CSPD, Serbia! Also, planned to Organize Continental and Global CanSat/Rocketry Competitions 2020/2021 at Serbia and Other Host Countries by the end of 2020 onwards and Global Finals

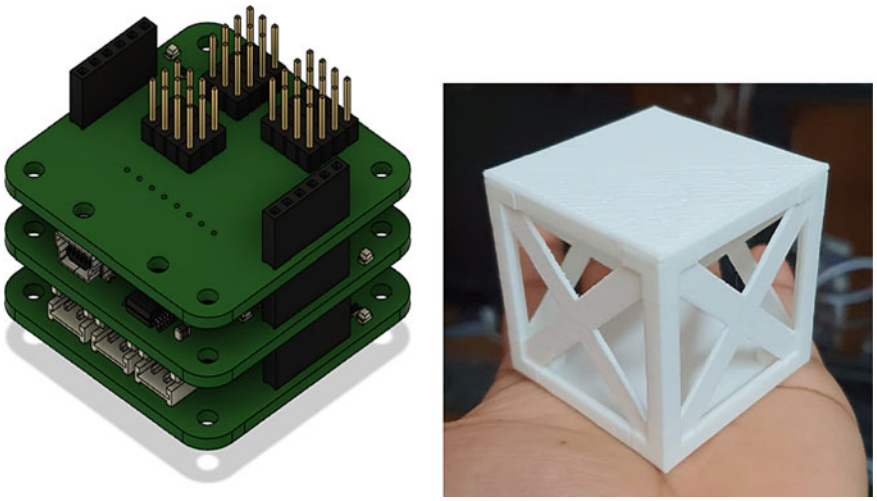

Fig. 9 Isometric view

Fig. 10 Front view

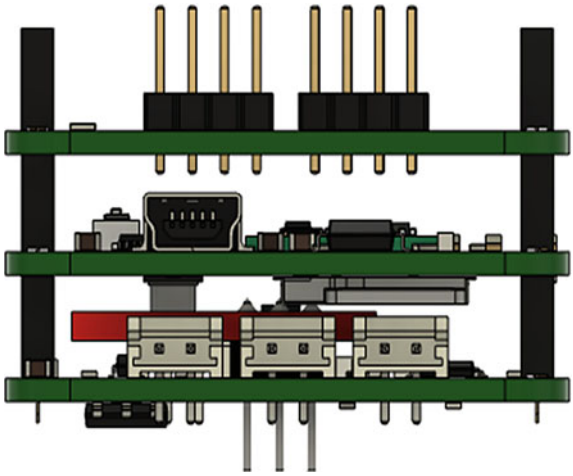

Fig. 11 Right view

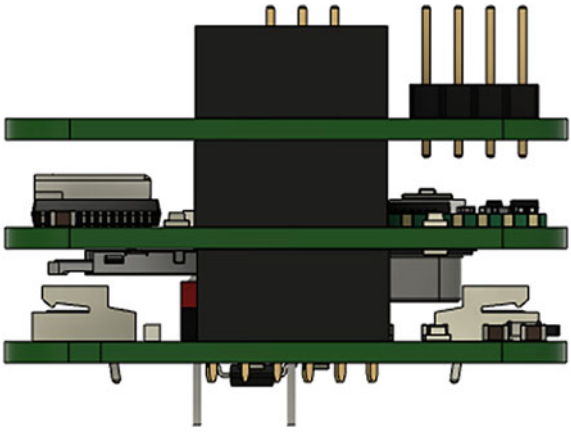

will be held at Serbia! Students' Exchange/Higher Education/Joint Development of Satellites for Former Yugoslavia Regions also have been planned.

Fig. 12 Final assembly of CanSat

3 UNITYsat

The Unity program (originally conceived by CSPD, Serbia has been evolved into Indo-Serbian collaboration) represents a response to the increasing need of people and groups for easier access to space, so as to attain sustainable progress in their work and development of this area.

The main characteristics of the UNITYsat are as follows:

(a) The chassis of every UNITYsat is made by combining of anodized aluminum and 3D printed filament;
(b) Basic dimensions of every UNITYsat are 10.0 cm × 10.0 cm × 2.5 cm or 1.25 cm;
(c) User/developer defines payload of its own UNITYsat with respect of the standards defined in this document;

The price is formed on the one UNITYsat: development kit + launch service. Although the volume of the one UNITYsat is 250 cm^3, the same rules (rights and obligations) are valid as for large satellites. The user/developer can put all the basic

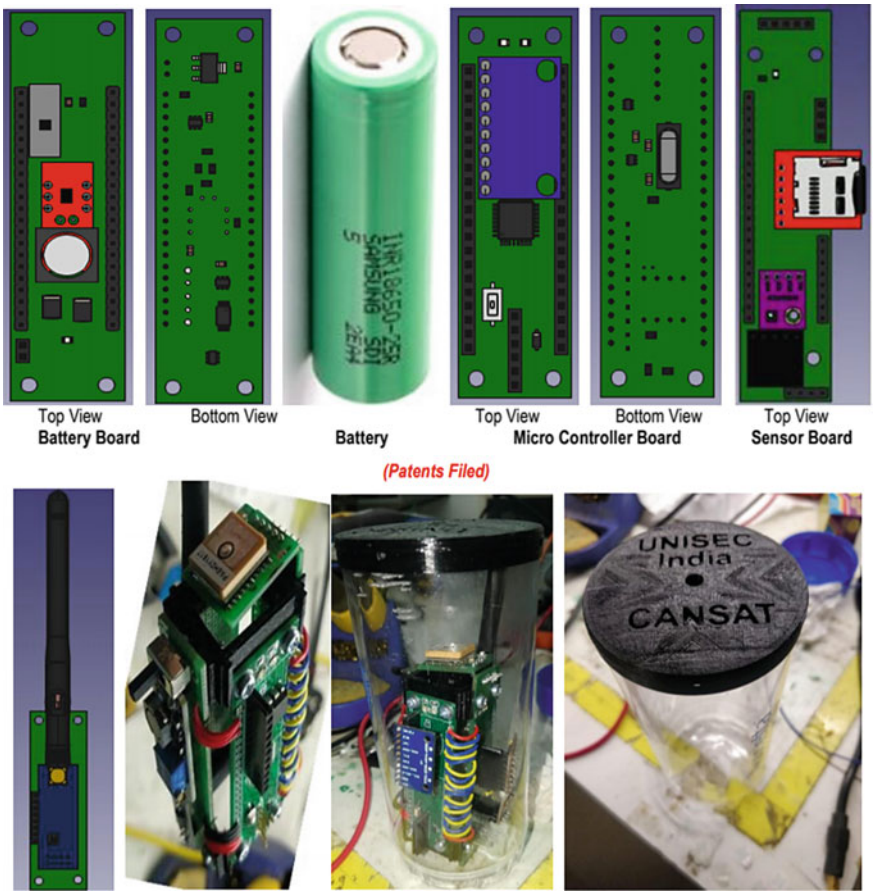

Fig. 13 Battery board

subsystems and payload in its own UNITYsat if meets the defined standards. Testing of each UNITYsat before the launching process is mandatory and this is also defined by mentioned standards.

- Each UNITYsat is sorted one on the other.
- The remove before flight (RBF) must be on designated side of the UNITYsat (yellow side) in the form of switch, which must not exceed the external dimension of the designated side, i.e., it must be in the same plane.
- RBF is a mandatory part of each UNITYsat regardless of whether the user/developer has chosen to power its own UNITYsat only from batteries or uses other solar cells.
- Batteries may be fully charged during launching, but the user/developer must provide a place (port) on a designated (yellow surface in UNITY.skp) side of UNITYsat for external battery charging and diagnostics if desired. External

battery charging and diagnostics will not be allowed after placing UNITYsat in 3U POD Deployer!

The Unity program is an open-source program, which means that all components except the external structure can be designed and standardized by third parties, under a condition that everything complies with the standards defined in program document. This is one of the reasons why this program is called Unity (Fig. 14).

Defined Standards for UNITYsat

(a) **UNITYsat Mechanical Requirements**

The UNITYsat configuration and physical dimensions shall be per UNITY.skp mentioned in program document (which will be shared among interested teams/countries after signing NDA).

- A single UNITYsat (basic dimension) shall be maximum 25.0 mm tall (Z dimension per UNITY.skp), including antennas and solar cells (if exist). (Note: Users/developers should keep in mind that external structure (anodized aluminum) of the UNITYsat will be delivered to each user/developer after additional purchase of structure. It is a prerequisite for participation in the program! In this way, deviations in the external dimensions will be prevented. The internal/core structure which holds electronics can be 3D printed (ABS filament). User/developer can design the internal/core structure as it likes, but with respect of the defined standards in this document. The UNITY.skp is given only an example of internal/core structure and changes are allowed!)
- **Mass**: Each single UNITYsat (basic dimension) shall not exceed 220 g mass; two UNITYsat shall not exceed 440 g mass and three UNITYsat shall not exceed 660 g mass, etc.
- **Materials**: For external structure material, it is an anodized aluminum. For internal/core structure material, ABS (3D printing filament) shall be used (Table 1 and Fig. 15).

(b) **UNITYsat Electrical Requirements**

Electronic systems shall be designed with the following safety features:

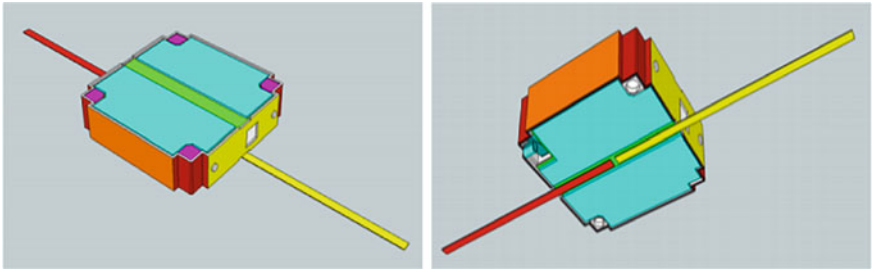

Fig. 14 UNITYsat assembly

Table 1 UNITYsat separation spring characteristics

Characteristics	Value
Plunger material	Stainless steel
End force initial/final	0.5 lbs./1.5 lbs
Throw length	0.05 inches minimum above the standoff surface

Fig. 15 Spring plunger

- No electronics shall be active during launch to prevent any electrical or RF interference with the launch vehicle and primary payloads.
- The UNITYsat shall include deployment switch on the designated place (blue switch on the bottom side in UNITY.skp) to completely turn off satellite power once actuated. The RBF switch shall be accessible from the access port location (yellow surface in UNITY.skp).
- The RBF switch shall cut all power to the UNITYsat once it is OFF.
- Batteries may be full charged during launching, but the user/developer must provide a place (port) on a designated (yellow surface in UNITY.skp) side of UNITYsat for external battery charging and diagnostics if desired. External battery charging and diagnostics will not be allowed after placing UNITYsat in 3U POD Deployer!
- An example of setting the antenna and bending method will be performed live through the workshop during the development process (example of dipole antenna 17.3 cm $\times$ 2). This example is extremely important because based on it must be set up and bend and the antenna(s) with other dimensions. The contact between the antenna and the interior side of the 3U POD Deployer is not allowed!
- Deploying of antennas and/or solar cells, etc., is allowed only by using timer switch (e.g., NiChrome timer switch) which countdown is triggered by separation of UNITYsats after ejection from the 3U POD Deployer in orbit. The timer countdown must last at least 15 min before deploying of antennas and/or solar cells.

(c) **Operational Requirements**

UNITYsats shall meet certain requirements pertaining to integration and operation to meet legal obligations and ensure safety of other UNITYsats.

(d) **Testing Requirements**

Testing shall be performed to meet all requirements deemed necessary to ensure the safety of the UNITYsats and the 3U POD Deployer. Test plans that are not generated

by the CSPD, Serbia and ITCA/TSC, India are considered to be unofficial. Requirements derived in this document may be superseded by launch provider requirements. All flight hardware shall undergo protoflight and acceptance testing.

(e) **Responsibilities**

CSPD and ITCA/TSC responsibilities are to deliver purchased development kit to users/developers, to enable launch (through its LV provider partner) at a contracted price once capacity of 3U POD Deployer is full, to integrate the users/developers UNITYsats with 3U POD 7 Deployer, to ensure the safety of the 3U POD Deployer and protect the launch vehicle (LV), primary payload and other satellites. Responsibility for deploying UNITYsats in orbit is on LV provider. Responsibility for functionality of the UNITYsats is on users/developers.

(f) **Applicable Documents**

The following documents form a part of this document to the extent specified herein. In the event of conflict between the documents referenced herein and the contents of this document, the contents of this document shall take precedence.

- Procedural Requirements for Limiting Orbital Debris (NPR 8715.6)

Frugal Way to Access Low Earth Orbit (LEO): Indo-Serbian Collaborative Efforts as a Case Study

Problems Identified by Space Enthusiasts to Access LEO:

Limited knowledge, insufficient experience, money for launch/cheaper launch, time in general, period of time to launch, etc.

Tools Available to Access LEO:

Acquired knowledge, technology, collaboration/teamwork, motivation.

Let us start with the problems of limited knowledge and insufficient experience using the tool at our disposal. Due to the interdisciplinary nature of space engineering, acquired knowledge allows you to be aware of what you do not know and thus save you time and direct you. Collaboration/teamwork makes up for time and knowledge—because not everyone knows everything, so teams are made up of people from many fields (inter-disciplinary and multi-disciplinary teams). Technology speeds up the process and helps you to gain experience because it allows you to make mistakes that you can easily correct during the process.

Motivation is, of course, the basis of everything and is constantly present when someone is doing most exciting project such as "building their own satellite"! However, you all knew this, let us see specifically; we want to make a satellite, and we have the problems and tools listed. We decided to start gradually, from the beginning. We adapted the CanSat concept to elementary school age and started learning the same way as making a real satellite because CanSat is a replica of a real satellite and contains everything (all systems and subsystems) that has a real satellite, but with limited complexity. We made teams, shared tasks and everyone was given their own scope of work and responsibility. All participants (members of

each team) are equally important. Then, we raised everything to a higher level, high school and started studying rockets. Both rocket engine rockets and water rockets are constantly applying the acquired knowledge of fundamental subjects. We put together CanSat and Rocket and launch CanSat as a true satellite. Then, things got even more interesting. Then, the study at University came, we asked ourselves, what now … it is not a problem to raise CanSat and Rockets to an even higher level, and even accredit space engineering programs, but what is the point if we cannot reach the goal because we are so small, how do we continue to improve ourselves? How can we contribute to development now? Do we have to wait for employment in some big aerospace company or agency?

History has taught us that no one should be underestimated and everyone should be given a chance if possible, if the goal is justified/correct/legitimate/democratic/inclusive. These issues occur even at the very beginning, and therefore we again applied engineering approach and again start with thinking and rethinking… then we realized that we are constantly going around in circles, because new problem that has not been present has now appeared. And that problem is money for the launch/the cost of launch must be cheaper. OK, now we have the knowledge and we have some experience, but how to apply it completely, how to go further during study period. (Digression: The cheapest launch is € 30,000–40,000–60,000 for PQ, which is unrealistic and unaffordable for many institutions/organizations, especially individuals).

Then, we applied a tool that has been used all the time, but in the process of learning, and that is collaboration. India and Serbia have found an optimum solution that big players made possible for small players and beginners (anyone either individuals or institutions who are interested to build and launch their own satellite). The UNITY Program was created, and these big players are from ISRO/Roscosmos, etc. India and Serbia have proposed a new approach in the educational process in which students have the opportunity to apply their theoretical knowledge through the creation of a real satellite during their studies and to motivate one another through competition with their colleagues/students from other institutions and automatically promote this program, which is actually common goal. This is UNITY because you cannot reach the goal easily (and cheaply through a frugal way). You are all independent in your work and will be independent in orbit, but only together you can achieve that goal.

Consider the breadth (wideness) of this program and how much UNITYs, we actually have here and whether it may be a symbolic representation of humanity. Finally, remember the price of € 30 k-40 k-60 k for PQ, our proposed UNITYsat has allowed you to get twice as much (in satellite capacity) for € 25–30 k (Rs.21–26 Lakhs @ 1Euro = Rs. 84), and the whole program applying the open-source principle of development (which means you can save money, too). Cost-effective launch opportunities have been studied extensively by Indo-Serbian collaborative team and they wish to share such knowledge to interested workgroups and teams institutions) of various countries! World CanSat/Rocketry Championship (WCRC) has also been announced under consortium! (For more details, visit: https://wcrc.world/) [17–23].

Hence, the entire project cost will be approx. Rs. 25–30 Lakhs (Euro 27–35 k) to design, fabricate, test and fulfill all the certifications before launching the UNITYsat and also including the cost launch etc.! All this is very important because, the future of space science depends on our ability to attract and engage students into science, technology, engineering and mathematics (STEM) fields.

4 Summary

- Nanosatellites and CubeSats have matured from pure educational projects to in-orbit demonstrators.
- Proof that demanding scientific and technological missions can be carried out with small satellites at low cost and within short timescales.
- Industry and space agencies are increasingly using nanosatellite technology.
- Commercial services are already in place using constellations.
- Reliability increased: professional implementation.
- Tailored PA/QA standards introduced.
- Next astronomy mission can make use of recent developments in processors and communication subsystems.
- Coordinated frequency bands should be used instead of traditional amateur radio bands to avoid interference and to provide higher data throughput.
- Large number of spacecraft require strict adherence to existing rules and procedures to avoid harmful interference and space debris problems.

Turn-key CubeSat and nanosat/picosat missions are possible with the help of Innovative Solutions from Consortium of Space Scientists, MSMEs in Space Programs under the initiative of CSPD/ITCA/TSC.

5 Conclusion

The future of space science depends on our ability to attract and engage students into science, technology, engineering and mathematics (STEM) fields. Authentic, hands-on experience with space applications enhances engagement and learning in the STEM disciplines and can help to attract students to STEM careers [16]. The goal of the UNITY program is to provide interested students and small nations the opportunity to lead and participate in the development of a spacecraft payload through its life cycle in a frugal way. The learning experience will be enhanced with CanSat/Rocketry competitions and development of PocketQube/CubeSat by the team through learning by doing and creating their own “satellite” (which is the highest in RBT level of learning pedagogy) right from manufacturing, environmental testing, satellite integration, spaceport, launch vehicle, range and spacecraft operations, etc. The UNITYsat Program of Serbia will provide a unique and important

STEM opportunity for students/researchers in small countries to develop critical skills in systems engineering and space science that will complement their existing programs and initiatives. It is a cost effective, short-term program that provides students/researchers in small countries with an exciting opportunity to conduct valuable scientific space-based research.

Indo-Serbian collaboration has paved the way for global competitions, starting at continent level to international levels along with various knowledge conferences, workshops and exclusive sensitization seminar/workshop on "Capacity Building for Student Satellites and Rocketry" has been planned with the help of international experts, which will cover and provide overall bird's-eye view of the above major components of satellite programs. Indian Technology Congress Association (ITCA) and Committee for Space Programme Development (CSPD), Serbia have also agreed to network with global leaders to get various opportunities for funding the entire projects on affordable terms and conditions. ITCA has also initiated 75 Students' Satellites Program: Mission 2022 which has envisaged to launch 75 students built satellites to LEO to celebrate India's Freedom 75 Years (1947–2022) in India! Good amount of academic institutions and universities have shown interest and started their own space projects at their campuses enthusiastically, since 2017–2018.

Lead Agencies for 75 Students' Satellites Program: Mission 2022:

Israel: The Herzliya Science Center and Tel Aviv University

India: Indian Technology Congress Association (ITCA)

Opportunities for Launch Support and Technical Collaborations: Identified Agencies:

1. Indian Space Research Organization, ISRO
2. Israel Space Agency and Israel Aerospace Industry
3. French National Space Research Center, CNES
4. United Nations Space Office—UNOOSA
5. GK Launch Services (GK) is an operator of Soyuz-2 Commercial Launches from the Russian Spaceports (Vostochny, Plesetsk) and the Republic of Kazakhstan (Baikonur)
6. World Federation of Engineering Organizations (WFEO)-ICT
7. BRICS Federation of Engineering Organizations
8. World Academy of Engineers
9. CANEUS Small Satellite Sector Consortium, Canada/USA.
10. University Space Engineering Consortium (UNISEC)–Global, Japan; UNISEC-Serbia, India, Samara, Italy.

Acknowledgements to NHCE Students' Satellite Team We acknowledge the contributions of the following Research Engineers of NHCE!

Nikhil Riyaz, Denzel George. A, Hariraj. R, Ashwin. S, Bhavana. S, TarunSai.R, Sainath G, Athira. Ajaykumar, Joshua. Tom Jacob, Sanketh Huddar and Vishwa Gopal

Research Engineers, TSC Technologies Private Limited (TSC), R&D Cell,

New Horizon College of Engineering (NHCE), Bangalore, India

References

1. Origin of the Sputnik project, http://www.russianspaceweb.com/sputnik_origin.html, (visited 31.03.2020)
2. Ilbis, E., Mari-Liis, A., Ervin, O., Johan, K., Pekka, J., Jouni, E., Petri, T., Andris, S.: ESTCUBE-2 Plasma Brake Payload for Effective Deorbiting
3. Nanosatellite database by Erik, Figures: CubeSat type. http://www.nanosats.eu/index.html#figures. Accessed Feb 31 2020
4. ISIPOD CubeSatdeployer, ISIS, https://www.isispace.nl/brochures/ISIS_ISIPOD_Brochure_v.7.11.pdf. (last visited 9.04.2017)
5. KickSat, product description, http://kicksat.github.io. (last visited 9.04.2017)
6. ESTCube-1. The course of mission, https://www.estcube.eu/en/estcube-1. (last visited 10.04.2017)
7. Sarafin, T.P., Wiley J.L.: Spacecraft Structures and Mechanisms–From Concept to Launch (1995)
8. Samwel SW (2014) Low earth orbital atomic oxygen erosion effect on spacecraft materials. Space Res. J. 7(1):1–13
9. Barter NJ (ed) (1982) TRW space Data. S&TG Marketing Communication. TRW Inc., Redondo Beach, CA
10. Iakubivskyi I (2017) Nanosatellite Anatomy Analysis: The Second Generation of ESTCube. Ph.D. Diss, Tartu Ülikool
11. Koudelka, O., Manuela, U., Patrick, R.: Nanosatellites—the BRITE and OPS-SAT Missions. e &iElektrotechnik und Informationstechnik **131**(6), 178–187 (2014)
12. https://www.isispace.nl/. Accessed Feb 31 2020
13. Rosalyn, P.-G., Soli,z J." Study and Selection of Satellite Images of Nano Satellites for the Agriculture Field in Bolivia. Space Fostering Latin American Soc. 27–36 (2020)
14. https://space.skyrocket.de/
15. http://www.unisec-global.org/ and http://www.unisec.jp/flash/index-e.html
16. Dingwall, B., Robert, T., Matt, C., Sean, M., Hank, V., Joyce, W., Dale, N., Brian, C., Matt, O.: Bringing Space to the Classroom Through STEM Education Providing Extreme Low Earth Orbit Missions Using ThinSats
17. http://www.cubesat.org/
18. http://outgassing.nasa.gov
19. http://2comnet.info/komsat/en/unity-program/
20. https://wcrc.world/
21. Hemalatha RJ, Vijaybaskar V, Thamizhvani TR (2019) Automatic localization of anatomical regions in medical ultrasound images of rheumatoid arthritis using deep learning. Proc. Inst. Mech. Eng. 233(6):657–667
22. Narayanan, K.L., Ramesh, G.P.: Vlsi architecture for 2D-discrete wavelet transform (DWT) based lifting method."Indian J. Public Health Res. Develop. **8**(3), 644–649 (2017)
23. Alexander S (2013) Design and implementation of efficient reversible multiplier using tanner Eda. Int. J. MC Squ. Sci. Res. 5(1):15–22

Pulse Shaping Filter for CP-OFDM PAPR Reduction

Rajmohan Madasamy and Himanshu Shekhar

Abstract Cyclic Prefix Orthogonal Frequency Division Multiplexing (CP-OFDM) waveform is emerging as the best candidate for the 5G technology in downlink and uplink transmission due to its spectral efficiency and multiple access capability. In this paper, the modified parametric exponential pulse (MPEXP) filter is used in the CP-OFDM to improve the spectrum efficiency and to reduce the PAPR. The clipping and the filtering PAPR technique are combined together and applied to the proposed system. The result shows that the PAPR of the CP-OFDM system with MPEXP filter along with the combined clipping and filtering reduction technique offers low PAPR value when compared with the selective mapping technique.

Keywords 5G technology · MPEXP · SDR · Clipping and filtering

1 Introduction

The evolution of standards such as 2G, 3G and 4G in the telecom industry and the different wireless standards such as DVB-H, DVB-T, wireless LAN and WiMAX necessitate high data rate with error-free and better reuse of narrow bandwidth. There is a growing need in digital communication to accommodate more number of users and channels within the available bandwidth. Software-defined radio (SDR) is an emerging technology that uses narrow bandwidth and different modulation techniques to replace the hardware by the software configuration. Figure 1 shows the SDR architecture using the pulse shaping filter. The baseband processor handles different modulation and channel coding methods.

The orthogonal frequency division multiplexing (OFDM) transceiver is implemented in baseband processor using field-programmable gate array (FPGA). The

R. Madasamy (✉) · H. Shekhar
Hindustan Institute of Technology & Science, Chennai, Tamilnadu, India
e-mail: mrajmohan@hindustanuniv.ac.in

H. Shekhar
e-mail: himanshus@hindustanuniv.ac.in

D. K. Sharma et al. (eds.), *Micro-Electronics and Telecommunication Engineering*,
Lecture Notes in Networks and Systems 179,
https://doi.org/10.1007/978-981-33-4687-1_36

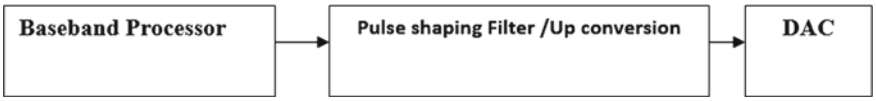

Fig. 1 SDR architecture using pulse shaping filter

serious problem involved in narrow bandwidth is interference among the different user due to intersymbol interference (ISI). The Nyquist's first and second criterions will ensure that the digital data transmitted as a sequence of pulses, sampled at optimum points, will have zero ISI. The Root Cosine (RC) and Square Root Raised Cosine (SRRC) filters satisfy the Nyquist's criteria and are the commonly used pulse shaping filters in 3G standards. The BER rate will vary in the presence of timing error. A better than Nyquist pulse is presented in [1] which produces a lower error rate in the presence of timing error, lower maximum distortion and more eye receiver. Two new ISI-free improved Nyquist pulses are presented in [2]. The flipped hyperbolic secant (FSECH) and the flipped-inverse hyperbolic secant (FARSECH) method offers better error probability and also robust to truncation and root operation when compared to raised cosine (RC) filter. The ISI-free pulses are designed with parametric construction of a Nyquist pulse, which gives more degrees of freedom is explained in [3]. This approach provides a better receiver eye diagram and symbol error rate (SER) when compared to the RC filter.

Three new ISI-free pulses, namely inverse-cosine inverse-hyperbolic sine, inverse-cosine inverse-tangent and sine inverse hyperbolic cosine based on two-parameter design, are presented in [4]. Single carrier frequency division multiple access (SC-FDMA) and the interleaved mode of (SC-IFDMA) scheme use various form of parametric pulse shaping filter to reduce the peak-to-average power ratio (PAPR) [5, 6]. A new linear combinational pulse is obtained by combining RC pulse and parametric exponential pulse (PEX) for the reduction of PAPR in SC-interleaved FDMA [7].

In 5G technology, the choice of the waveform used in wireless and mobile communication for the radio link is crucial for accessing the radio network. The pulse-shaped OFDM is also considered as one of the important waveforms for 5G communication. The latest research findings in 5G suggest that cyclic prefix (CP) OFDM waveform used in downlink will outperform the other waveform due to its support with multi-antenna technologies, time-critical application, spectral efficiency and low complexity structure [8, 9]. The main drawback in the OFDM system is the peak-to-average power ratio (PAPR) value. The previous research finding indicates that the common methods used are pulse shaping (PS), clipping, constellation shaping, partial transmit sequence (PTS), filtering and selective mapping (SM) [7]. In this paper, the CP-OFDM combined with pulse shaping model is proposed for improving the waveform used in the 5G technology New Radio downlink. The existing PAPR reduction techniques are applied to the proposed system, and the PAPR value is analyzed.

Pulse Shaping Filter for OFDM System:

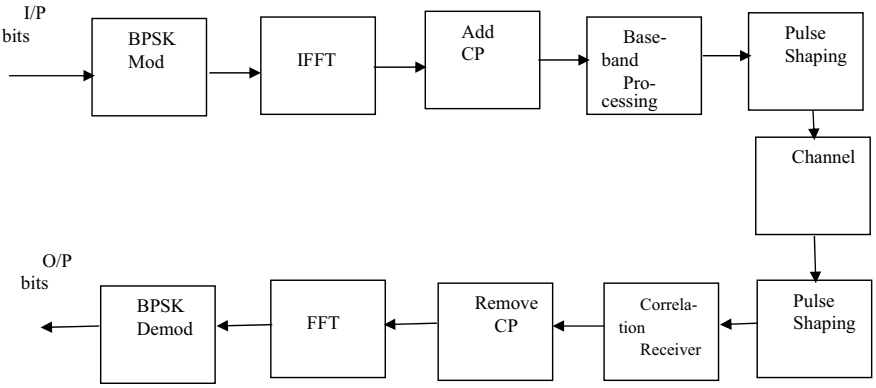

Fig. 2 CP-OFDM with pulse shaping filter block diagram

Orthogonal frequency multiplexing division (OFDM) is a commonly used multi-carrier modulation technique and good waveform choice in various telecommunication standards such as Wi-Fi 802.11a, 4G and 5G technologies. In general, OFDM allows multiple users to share the same bandwidth by allocating different non-overlapping sub-channels. The sub-channels are closely spaced and overlapped to eliminate the guard band, thereby improving the efficiency of the data transmission. The 5G New Radio technology offers improvement in scalability, flexibility, spectrum efficiency and low usage of power for handheld device when compared with 4G LTE. The advantage of 5G New Radio is that it can accommodate higher bandwidth signal and achieves high data throughput rates. The block diagram of the CP-OFDM system is shown in Fig. 2.

In the proposed CP-OFDM system, to avoid inter-symbol interference the last part of the data frame is added in the beginning of the frame and the length of the CP should be more than the channel delay spread [8]. The pulse shaping filter ensures the multiple band-limited signals are not affected by ISI and occupy less bandwidth. Nyquist observed that pulse might spread beyond the symbol period (T_b) and ISI. Nyquist pulse is introduced to avoid ISI and also affects the minimum bandwidth requirement for the modulated signal [4]. The most commonly used pulse is raised cosine (RC) pulse, and the time domain expression is given as [10]

$$\mathrm{RC}(t) = \sin c\left(\frac{t}{T}\right)\frac{\cos\left(\frac{\pi\alpha t}{T}\right)}{1-\left(\frac{2\alpha t}{T}\right)^2} \tag{1}$$

where RC(t) represent the impulse response.

T is the symbol duration.

α is the roll-off factor and typical values lie between 0.3 and 0.5

$T = nTs$, n is the number of samples.

Ts is the sampling frequency.

The Square Root Raised Square (SRRC) pulse shaping filter is most commonly used as a matched filter in digital communication, and the impulse response of the SRRC in the time domain is expressed as [10]

$$\mathrm{SRRC}(t) = \frac{\sin\left(\frac{\pi t}{T}(1-\alpha)\right) + \frac{4\alpha t}{T}\cos\left(\frac{\pi\alpha}{T}(1+\alpha)\right)}{\frac{\pi t}{T}\left(1-\left(\frac{4\alpha t}{T}\right)^2\right)} \tag{2}$$

The parametric exponential pulse (PEXP) shaping filter is more suitable in the application of the peak-to-average power ratio (PAPR) reduction in OFDM-based communication systems. The typical representation of the parametric exponential pulse (PEXP) in the time domain is expressed as [10]

$$\begin{aligned} hp\exp(t) &= \sin c(T)\cdot m(t) \\ m(t) &= \frac{2\{(\pi\alpha t)/(\ln 2)\}T\sin(\pi\alpha t)+2\cos(\pi\alpha t)-1}{((\pi\alpha)/(\ln 2)T)^2+1} \end{aligned} \tag{3}$$

The decay level in PEXP is found to be t^{-2}. The decay rate has a great impact on the reduction of PAPR. The modified form of PEXP is proposed in [11], and the time domain expression for modified parametric exponential pulse (MPEXP) is expressed as

$$\mathrm{hmp}exp(t) = \sin c(T)\frac{2\{(\pi\alpha)\ell n2/3\}T\sin(\pi\alpha t)+2\cos(\pi\alpha t)-\left(\frac{(\ell n2)}{3}\right)^2}{5.63\left(\left((\pi\alpha)/\frac{\ell n2}{3}T\right)\right)^2+\left(\frac{(\lambda n2)}{3}\right)^2}$$

To further minimize ISI, it is necessary to reduce the strength of the side lobes. The side lobes of the MPEXP are decreased compared to PEXP, and the decay rate for both the methods is same. In our research work, the MPEXP is used as a pulse-shaping (PS) filter in CP-OFDM due to the property of lower side lobes for increasing value of α. The PAPR reduction in OFDM systems mainly depends on the type of modulation technique, PS filter and the method of PAPR reduction technique. In our proposed method for CP-OFDM, the MPEXP filter is used along with the quadrature phase shift keying (QPSK) modulation. The PAPR reduction techniques used in CP-OFDM are clipping, filtering and selective mapping [12]. This technique is found to effective and simple method when compared to existing methods.

2 Experimental Result

Figure 3 shows the noise-free signal of CP-OFDM signal. The total sample size is 65536, and the fast Fourier transform (FFT) size is 64. The number of bit in each sample is 256, and the modulation scheme used is QPSK. The clipping, filtering

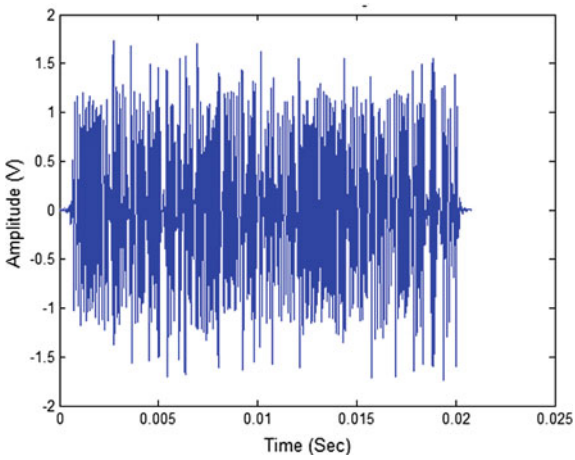

Fig. 3 CP-OFDM noise-free signal

and selective mapping filtering techniques are applied to our proposed CP-OFDM method.

Figure 4 illustrates the CP-OFDM signal after the MPEXP filter is applied. The alpha value considered in our approach is 0.5 based on the experimental values derived from [9].

In our approach, the proposed CP-OFDM with MPEXP filter is analyzed with two filtering approaches. The first method is the selective mapping (SM). PAPR technique is used to analyze the performance of the proposed method. The second method is the clipping technique combined with filtering. The combined PAPR approach is then applied to our proposed system CP-OFDM system, and the PAPR values are calculated. It is observed from Table 1 the combined clipping and filtering technique along with modified parametric exponential pulse (MPEXP) that produce better PAPR reduction when compared with the selective mapping (SM) technique.

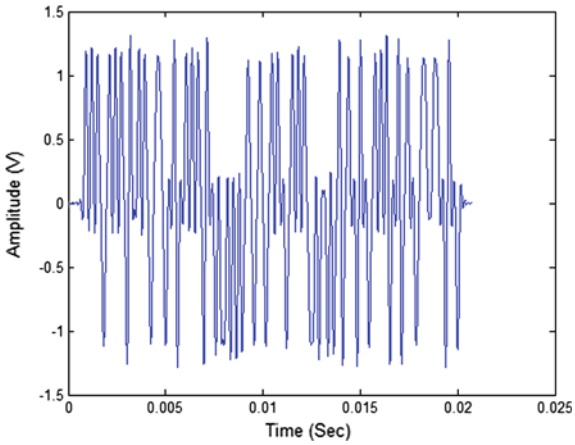

Fig. 4 Waveform of CP-OFDM with PS

Table. 1 Comparison of PAPR

S No.	Method	PAPR technique	PAPR in dB
1	Normal CP-OFDM	–	19.82
2	CP-OFDM	SLM	14.86
3	CP-OFDM	Clipping combined with filtering	10.43
4	CP-OFDM with MPEXP	Clipping combined with filtering	8.69

3 Conclusion

The objective of this paper is to analyze the performance of CP-OFDM system combined with MPEXP pulse shaping filter using QPSK modulation for two PAPR reduction techniques. The proposed CP-OFDM system with the combined clipping and filtering technique achieves less PAPR value when compared with selective mapping technique. In future, the hybrid combination of the pulse shaping filter and the improved PAPR reduction techniques can be designed to improve the performance of the CP-OFDM.

References

1. Beaulieu NC, Tan CC, Damen MO (2001) A better than Nyquist pulse. IEEE Commun Lett 5(9):367–368
2. Assalini A, Tonello AM (2004) Improved nyquist pulses. IEEE Commun Lett 8(2):87–89
3. Beaulieu NC, Damen MO (2004) Parametric construction of Nyquist-I pulses. IEEE Trans Commun 52(12):2134–2142
4. Assimonis SD, Matthaiou M, Karagiannidis GK (2008) Two-parameter Nyquist pulses with better performance. IEEE Commun Lett 12(11)
5. Azurdia-Meza CA, Lee KJ, Lee KS (2012) PAPR reduction in SCFDMA by pulse shaping using parametric linear combination pulses. IEEE Commun Lett 16(12):2008–2011
6. Azurdia-Meza CA (2013) PAPR reduction in SC-IFDMA uplink system using parametric pulses. In: 2013 IEEE Latin-America conference on communications. IEEE, pp 1–5
7. Mohammad A, Abdelhamid B, Hafez IM (2015) A new linearly combined Nyquist pulses for PAPR reduction in IFDMA. Int J Comput Appl (0975–8887)
8. Zaidi AA, Baldemair R (2017) In the race to 5G, CP-OFDM triumphs. ericsson. com, para 5. 29
9. Zaidi AA, Baldemair R, Tullberg H, Bjorkegren H, Sundstrom L, Medbo J, Kilinc C, Da Silva I (2016) Waveform and numerology to support 5G services and requirements. IEEE Commun Magz 54(11):90–98
10. Fowdur TP, Jhengree P (2017) Enhanced pulse shaping filters for IEEE 802.11 OFDM WLANs. J. Electri Eng Electron Control Comput Sci 3(1):21–28
11. Fowdur TP, Doorganah L (2019) Performance of modified and low complexity pulse shaping filters for IEEE 802.11 OFDM transmission. J Inf Telecommun 3(3):361–380
12. Robin B (2020) OFDM with PAPR reduction.zip (https://www.mathworks.com/matlabcentral/fileexchange/46440-ofdm-with-papr-reduction-zip), MATLAB Central File Exchange. Retrieved July 25, 2020

An Intelligent Wheelchair for Disabled Person

S. Prabhu, V. Nagaraju, P. Sailaja, and B. R. Tapas Bapu

Abstract Every new development in sensors and ultrasonic technologies has always been a bonus for electronics traveling aids (ETAs). This sets way to the development of smart vehicles for disabled people. These smart vehicles are used by physically disabled people. This electronic intelligent wheelchair is designed to help disabled people to move independently to any place without a caretaker. It consists of a smartphone app-based operation along with obstacle avoidance, fall detection and narrow way locomotion. An android application is used to control the wheelchair. This smart chair can function in full automatic mode. It uses GPS-guided system and magnetic compass to determine location and stores the location to return back to the location automatically. The fall detection system tilts the seat when it moves around any inclined plane and alerts the nearby caretaker with an SMS when a fall is detected. It has an intelligent collision avoidance system to avoid any type of obstacles including potholes and can move around narrow pathways and doors without being hit or bumped against any obstacle.

S. Prabhu
Department of Electronics and Communication Engineering, Mahendra Institute of Technology, Namakkal, India
e-mail: vsprabu4u@gmail.com

V. Nagaraju (✉)
Department of Electronics and Communication Engineering, Rajalakshmi Institute of Technology, Chennai, India
e-mail: Vankadarinagaraju@ritchennai.edu.in

P. Sailaja
Department of Information Technology, Velammal Institute of Technology, Chennai, India
e-mail: sailajavit@gmail.com

B. R. Tapas Bapu
Department of Electronics and Communication Engineering, S. A. Engineering College, Chennai, India
e-mail: tapasbr@yahoo.com

D. K. Sharma et al. (eds.), *Micro-Electronics and Telecommunication Engineering*,
Lecture Notes in Networks and Systems 179,
https://doi.org/10.1007/978-981-33-4687-1_37

Keywords Smart wheelchair · Fall prevention and detection · Collision avoidance · Smartphone controlled · Disabled · Seat tilting · Automated wheelchair · Pothole detection

1 Introduction

As the world of phone moved to smartphone features, a huge evolution took place in the technological industry. A variety of products and services together with the smartphones are being developed. These new products and services are changing rapidly. Among these is a fully automatic intelligent wheelchair product in combination with smartphones and other researches have been made. The concept of smart wheelchair has been proposed as a hot topic but very few satisfies the definition of smart wheelchair even those which fit are not affordable by common people because of high cost. The technological advancement has made easier to develop a smart wheelchair cost efficient and affordable by common people. Around 1.1 billion people in the world live with at least a small form of disability, among which around two hundred million experience functional difficulties in muscles. In this paper, we present the design of the cost-efficient fully feature-packed wheelchair with safety measures and automation using machine learning algorithms. One of the major advantages of this wheelchair is that it uses sensors to detect narrow spacing and allows to move the wheelchair in places such as in a crowded room, office, auditorium, narrow corridor and doorway where chairs need to be moved carefully without colliding with other obstacles. In such places, wheelchairs are supposed to be pushed and arranged in a line every time whenever the wheelchair is not aligned. So this design proposes a smart way to move around such congested places.

The below bar graph shows the statistics of different types disabilities, among which movement is the highest with 20.28 percentage. In India, around 90 million people are disabled among which most of them are not able to locomote from one place to another. Thus, it is necessary to develop a wheelchair which can be afforded by common people and must be smart enough to fulfill the criteria.

Statistics of Disabilities 2018

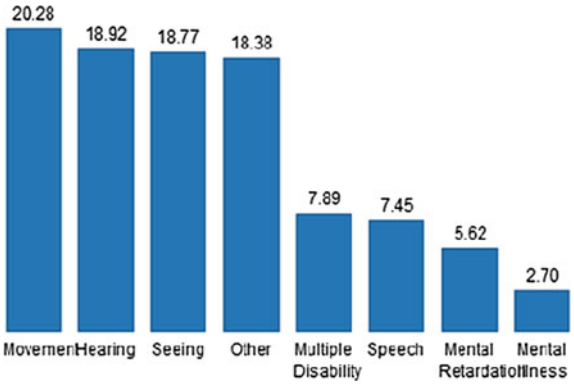

Therefore, the paper mainly focuses on the design of an intelligent wheelchair which is cost efficient and controllable without any difficulty with the help of a smartphone. Automation can be made by GPS-guided system and compass-driven DC motors attached to the wheelchair. The safety measures are the collision avoidance and the fall prevention in case of any emergency, and the red button in the app can be pressed to send SOS signals to the nearby caretaker with the activation of an alarm siren in the chair to seek nearby people's help. Additional system failure prevention system is designed to avoid system failure. This system calibrates each and every component of the system for failures and limits the function of the wheel chair only to the functions which uses the currently usable sensors. Also if the system finds a major failure, it denies access to the control of the wheelchair and can only be manually driven. The complexity is reduced by making use of smart phone so that size of the system is very compact as the smart phone is used to send emergency signals [5]. This eliminates the use of GSM module to the system. Thus, we get a compact system with very less sensors but provide many features.

2 Existing Systems

Due to several kinds of demands in the wheelchair, very many designs and concepts are put forward by researchers. The evolution of the wheelchair started from hand pulled wheelchair which made the user to feel tiredness in his/her arm. Also this needs lots of physical energy which weak people find difficult to use. Later to overcome this problem, electrically controlled wheelchairs had been introduced as the next evolution.

A. Electrical wheelchair

The electrical wheelchair has been a turning point to the wheelchair users as it is very easy and energy conserving and can be used independently. But even though the electrical wheelchairs are made for easy use, the controlling of the wheelchair is very complicated. The common joystick-controlled electrical wheelchair can be

considered. In this joystick-controlled wheelchair, even a small change in the joystick made accidently can lead to a sudden quick turn which is a major difficulty when moving in crowded place.

B. Line follower wheelchair

The line follower wheelchair uses magnetic ferrite markers which are laid on the pathways where the wheelchair has to be moved, and this pathway with laid ferrite markers is followed by the wheelchair like a line follower with a magnetic sensor placed at the bottom of the footrest of the wheelchair [1]. These sensors read the magnetic markers and control the steering and speed of the wheelchair.

To avoid obstacles, two infrared sensors are placed in front of the wheelchair which detects any obstacle placed in front of the wheelchair. To stop the wheelchair at the desired destination, reflective tapes are placed at the destination and the magnetic sensors are made to stop the wheelchair when it detects any reflection [2].

C. Modular wheelchair

The concept of modular wheelchair came into existence after the specific demands made by the users according to their disability. Modular wheelchair comes with modular attachments which can be installed as modules to the wheelchair to control the overall operation in demand of the specific user. The different types of modules are head movement control, voice control, hand gesture control, joystick-controlled wheelchair, etc.

The head movement-controlled wheelchair can be used by people who are not able to use their hands which gives them the ability to control the wheelchair by placing controller near the chin which is moved to steer and accelerate the wheelchair in the desired direction.

The voice-controlled wheelchair is an advantageous method. In this module, several pre-installed voice commands are given to the wheelchair to control the steering and acceleration of the wheelchair. The voice commands are recognized by a separate voice recognition board, and this recognized voice commands are sent to the controller to examine the command and control the wheel chair in accordance with the given command.

3 Proposed System

The proposed system helps to easily operate the wheelchair automatically by using a smartphone to move forward, backward, left and right. Also it can be made use of the GPS guiding system to track down the location as waypoints of the marked places and automatically steer to the marked waypoints using the magnetic compass.

Also the proposed system is assembled with many sensors for every application. These applications are explained in detail. The wheelchair is comprised of collision avoidance system, fall detection and prevention system, self-calibration system, GPS-guided system, compass-driven system, tilting system for the seat to stabilize the

Table 1 Motor rotation for the given command

Commands	Left motor	Right motor
Forward	Anticlockwise	Clockwise
Reverse	Clockwise	Anticlockwise
Right turn	Anticlockwise	Anticlockwise
Left turn	Clockwise	Clockwise
Stop	Stop	Stop

seating position and automatic motor speed control system to give a smooth ride for the user.

D. Motor Control System

There are two motors used in this system, one for the left and one for the right. These two motors are given power supply with a rechargeable battery. The motor's RPM and torque are calculated according to the load of the wheelchair. The power supply is not directly given to the motors, instead they are given through a motor shield to avoid damage of the microcontroller and also to drive the motors in various directions.

The 4 H-Bridges: L293D chipset provides 0.6A per bridge and a maximum of about four bidirectional DC motors with individual 8-bit speed selection. Pull down resistors keep motors disabled during power-up. This chipset-based shield is used to control both the motors by programming the microcontroller. The different commands are activated by the Bluetooth communication. Once the commands are received from the smartphone app, these commands trigger the particular function of the main program set to that particular command.

The main program contains separate function for each command like forward, reverse, left and right. These commands are triggered by the mobile app (Table 1).

Each motor is calibrated before starting the system, if any error in the motors is found the system stops working as it is considered as a major defect. The motor speed can be controlled either manually by the user or automatically when the system detects high speeds while turning to provide a comfortable ride for the user. This speed control is done by limiting the power to the motors. Thus, by limiting the power to the motors, the speed can be varied from 0 to 255 speed levels, this speed level can be adjusted manually by the user in the app, or the system automatically detects sharp turns and adjusts the speed with a predefined speed value set by the developer.

E. SmartPhone App

The android has become the most commonly used mobile platform, so an android app is developed with the help of Android Studio IDE software. This enables to create android applications, and the app has a very simple user interface which can be easily used by anyone. The app's interface is shown in the figure. The app uses Bluetooth connection to the system. When a button is clicked, it sends the

corresponding string to the microcontroller. The microcontroller converts the data into string and recognizes the command and runs the specific operation related to the given command.

The Bluetooth connectivity button is placed on top of all the buttons. Once the Bluetooth is connected, it shows that the Bluetooth is connected in the notification area. The app has been designed to provide a vivid and easy interface to the controls so that the user does not find any difficulty in accessing the app. The cursor placed at the bottom of the app is used to control the speed of the motor. Once the desired speed is set, the "send" button is pressed which sends the speed to the controller to adjust the speed, if not the intelligent system automatically detects sharp turns, over speeds and controls the speed accordingly (Fig. 1).

F. Collision avoidance system

Numerous sensors are available for the application of obstacle detection. Sensors like infrared sensor, ultrasonic sensor, LIDAR and even camera can be used to capture image samples and detect the obstacles by image processing. Since cost efficiency is a very important aspect of the proposed system, the camera cannot be used, but also accuracy is necessary. Therefore, the HC-SR04 ultrasonic sensor is used in this system. The HC-SR04 ultrasonic sensor is very cost efficient and provides a decent accuracy. Also the ultrasonic sensor is able to measure distance even at places

Fig. 1 Android app interface

where the light is highly intense. Sensors like camera and infrared cannot measure in such conditions. To serve the key purpose of cost efficiency and high accuracy, ultrasonic sensors have been selected. The HC-SR04 ultrasonic sensor is equipped to detect objects from a range of 2–400 cm. The module works at 5 V DC power supply and a working current of 15 mA. It requires a 10 μS trigger pulse to initiate the triggering of waves for detection. Upon triggering, the transmitter directs eight cycles of ultrasound waves at 40 kHz frequency. If an obstacle exists in its course, the sound returns backwards to be received by the receiver of the module. The distance is then calculated as follows: Obstacle Distance = [Time between transmitting and Receiving of Signal*Velocity of Sound (340 m/s)]/2

Four ultrasonic sensors are used. One in the left, right, front and bottom. The bottom sensor is used to detect potholes, and it sends signals to the controller about the depth of the pothole. Neural network is used to identify the obstacles and controlling the speed of the wheelchair driving motors according to the obstacle's distance from the wheelchair. The first layer of the neural network is made up of sensors, the second layer is the related self-learning algorithm to control speed and avoid obstacles, and the last layer is made of the control motors. This is how neural networks are implemented in the collision avoidance system. The microcontroller reroutes the wheelchair to the desired destination in both the control modes automatic and in manual (Fig. 2).

G. GPS-guided system

For GPS location, the Neo-6 U-Blox GPS module is used in this system. Instead of using the smartphone's GPS location, we are using a separate module to detect the location of the wheelchair accurately. The NEO-6 module series is a standard pack of

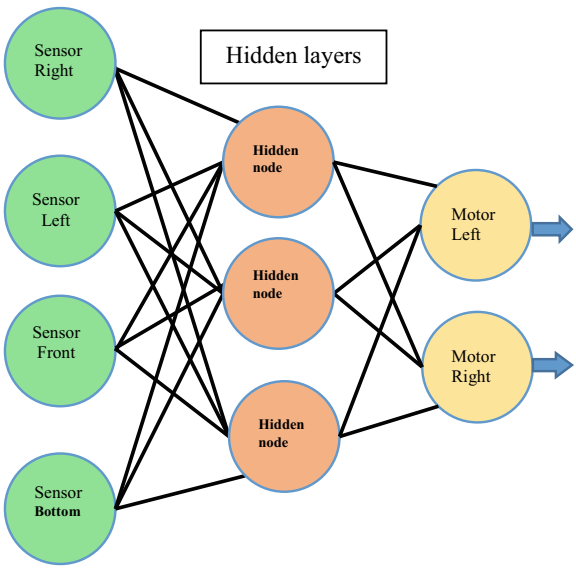

Fig. 2 Flowchart of neural network for collision avoidance

stand-alone GPS receivers which features the high performance u-blox 6 positioning engine with several satellites. These receivers are flexible and cost-effective receivers which offer numerous connectivity options in a miniature 16 × 12.2 × 2.4 mm package. This module is an ideal option for battery-operated mobile devices with very strict cost and space constraints.

The GPS guiding system is focused to deliver a fully automated locomotion of the wheelchair. The GPS receiver continuously sends the latitude and longitude of the current wheelchair location. This continuous data is used when necessary by the microcontroller. The user can store several locations in the app to navigate back to the stored locations automatically. These locations are stored in an array of data, and when the user clicks the button "Go to waypoint" the system drives the wheelchair to all the stored array of locations one by one.

This is how the GPS guiding system works. The compass heading is very important in the GPS navigation. The compass heading makes sure the direction of the wheelchair is headed straight to the GPS navigation, without the compass the GPS navigation is not possible. To ensure the stability of the module, a separate supply is given to the GPS receiver module.

H. Compass drive

The compass drive is used to drive the wheelchair in a preset direction continuously until stopped by the stop button, and the stop button breaks the loop and stops the wheelchair from moving. In this system, we use the QMC5883l magnetometer as the compass sensor. The QMC5883L is a multi-chip three-axis magnetic sensor. This surface-mounted, compact chip has magnetic sensors integrated with signal condition ASIC, and it has the advantages of less noise, very good accuracy, low-power consumption, offset cancelation and temperature compensation.

This application is used by first turning the wheelchair to the desired direction by using the turning buttons. Once turning to the desired direction, the "set heading" button is pressed and the compass heading value is transmitted to the microcontroller which drives the wheelchair in that direction by pressing the compass drive button. The compass readings are needed to make a perfect 90° turn and a 180° turn of the wheelchair. This is how the compass drive feature works.

I. Fall prevention and detection

The fall prevention is a very important feature which helps the user of the wheelchair from not falling down because of the uneven construction of the ways [3]. The wheelchair installed with this feature makes the user more independent regardless of any situation or any place. Although the fall prevention system makes the cost of the wheelchair to raise, this can be a modular feature which can be installed later by the user's request. By making this a modular feature, the cost efficiency is not affected by the idea of the fall prevention.

In this fall prevention system, the seat of wheelchair can be tilted according to the level of the pathway inclination. This can be detected continuously by the help of ADXL335 which is a three-axis accelerometer used to detect even a small change in

Fig. 3 Tilting of wheelchair

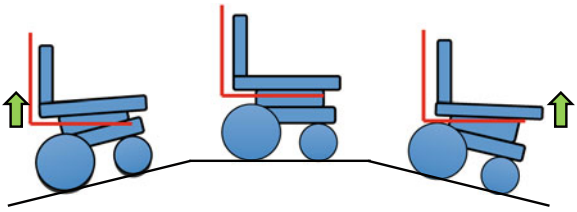

Table 2 Tilt system control protocol

Seat tilting	*X*-axis	*Y*-axis
	−20 ~ 0° (Front Lift): 00–14 +0 ~ 20° (Back Lift): 15–28	−20 ~ 0° (Left Lift): 00– 14 +0 ~ 20° (Right Lift): 15 –28

the inclination of the surface. This is attached to the bottom surface of the wheelchair. The tilting of the seat is carefully done according to the reading from the sensor. The schematic illustration of the seat tilting system is shown in Fig. 3 (Table 2).

4 Working Mechanism

The project uses a microcontroller as the brain, and it is interfaced with an application built for an android smartphone (the most commonly used device) which uses Bluetooth for communication between the autonomy system and the smartphone. It provides high security and a lot of features to the user. It has GPS guiding system, which can be used for automated locomotion of the chair to any pinned location on the map. It has an intelligent collision avoidance system to avoid any type of obstacles and can move around narrow pathways and doors without being hit or bumped against any obstacle. This smart vehicle can also detect pits in the pathway and reroute the vehicle to the shortest distance. The speed of the driving motors can be adjusted to user's preference [6–8].

An emergency button can be used in case of emergency to start the alarm and to send SMS alert to the pre-registered contacts. All the sensors and motors are calibrated automatically before every start of the wheelchair, and it alerts if there is any error in the system. The battery percentage can be monitored from the app or by a LED indicator which is placed near the battery to measure and display the amount of charge left in the battery. Once the charge is drained, it can be recharged several times. There is a charge control system in the charging adapter which limits or stops the charging process once the battery has reached the maximum charge. This helps to keep the battery safe.

The government of United States of America states that there is around four-meter accuracy in horizontal civilian Global Positioning System (GPS) [4]. Therefore, the

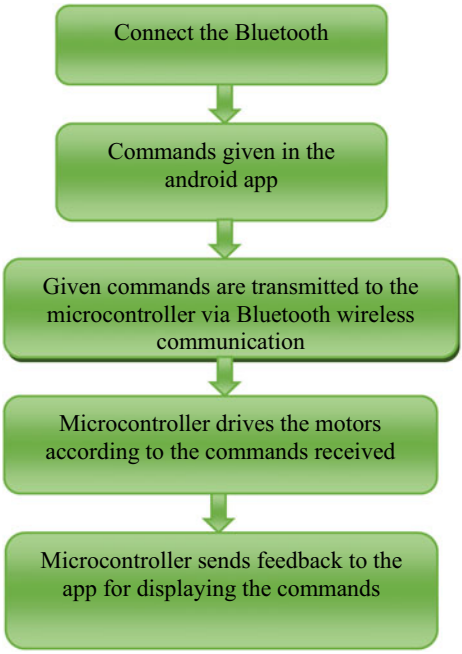

Fig. 4 Working of the system flowchart

current four-meter accuracy is not sufficient enough to map a small room as the GPS coordinates keep changing every time in a 4 m range, but in future advancement the accuracy can be increased which may help in indoor mapping of the wheelchair with only the GPS receiver. Thus, indoor routing can be made more accurate in future (Figs. 4, 5 and 6).

The block shows that the system starts with the smartphone app, and once the user gives commands to the wheelchair in the app it processes the data and transforms the given input into numerical commands and sends the array of numerical values of commands to the pre-programmed microcontroller (ATmega 2056) via wireless communication means of Bluetooth. The microcontroller receives the data from the Bluetooth transmitter. The received numerical value from the Bluetooth module is used to trigger the commands programmed for the dedicated value, and this either accesses the data from the modules or sends commands to the motor shield to drive the motors and simultaneously send data to the smartphone to display the given commands

5 Conclusion

The proposed system is a compact, cost-efficient and feature-packed wheelchair system ever proposed. This proposes a wheelchair with standardized autonomy

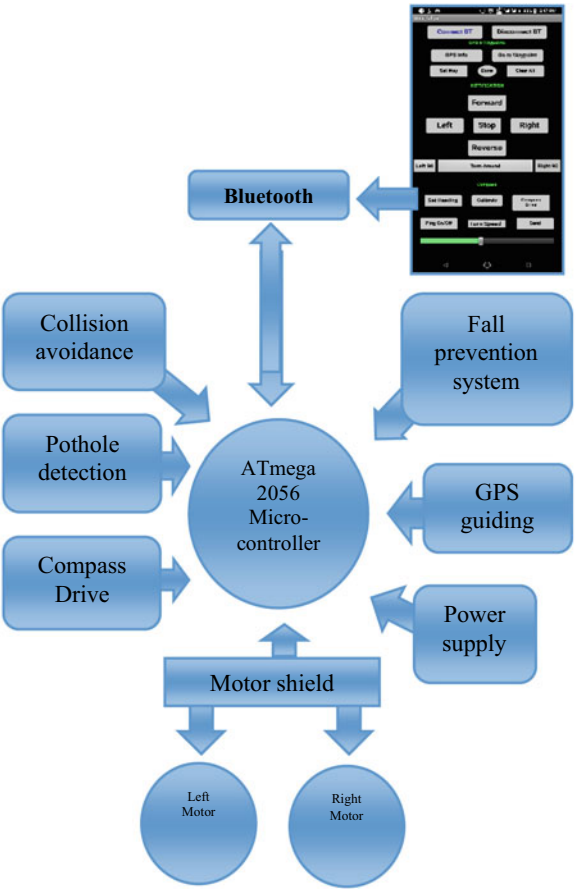

Fig. 5 Working of the system flow chart

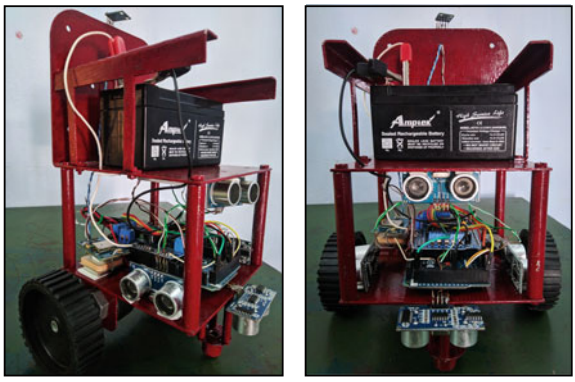

Fig. 6 Working prototype of the wheelchair

system. It is mainly focused to establish sufficient on-board autonomy at minimal cost and material usage, while achieving high efficiency, sufficient safety, smooth experience and future extendibility of the proposed system with further modular addition to the system as per the user-specific demands.

References

1. Hiroo W, Koichi N (1992) Development of an automated wheelchair guided by a magnetic ferrite marker lane. J. Rehabilit. Res. Develop. 29:27–34
2. Ana, C.L., Fernando, M., Urbano, N., Razvan, S.: An Outdoor Guidepath Navigation System for AMRs Based on Robust Detection of Magnetic Markers (2007)
3. Sanghyun, P., Tran, T.T.H., Jadhav, Y.S., Jaehyung, P., Jinsul, K.: Smart Wheelchair Control System using Cloud-based Mobile Device. IEEE (2013). 978-1-4799-2845-3/13
4. T. U. Government: Official US Government Information About the Global Positioning System (GPS) and Related Topics. Accessed March 3 2018 (217)
5. Available: https://www.gps.gov/systems/gps/performance/accuracy/
6. Doshi Siddharth P.: 2016 Symposium on Colossal Data Analysis and Networking (CDAN) Embedded system design for real-time interaction with Smart Wheelchair
7. Sharma R, Kumar R, Singh PK, Raboaca MS, Felseghi R-A (2020) A systematic study on the analysis of the emission of CO, CO_2 and HC for four-wheelers and its impact on the sustainable ecosystem. Sustainability 12:6707
8. Begam S.S., Selvachandran, G., Ngan, T.T., Sharma, R.: Similarity measure of lattice ordered multi-fuzzy soft sets based on set theoretic approach and its application in decision making. Mathematics **8**, 1255 (2020)

Convolutional Neural Network-Based Detection and Classification of Cardiovascular Disease and Diabetic Macular Edema

R. Senthamizh Selvi, S. Bragadesh Bharatwaj, B. Ajith Kumar, V. R. Bharath Raj, and S. Sudha

Abstract Artificial intelligence is one of the most advanced and prominent research areas which is used to solve several worldly problems. Traditional methods take up a lot of the doctor's time and are also prone to human error. The existing techniques utilize separate algorithms to only detect the disease. But their speed and accuracy are very low. The developed novel system utilizes deep learning in which the retinal fundus images are first preprocessed and then sent to a convolutional neural network (CNN) module. The proposed module not only accurately detects the presence of a disease (i.e., diabetic macular edema (DME) or cardiovascular disease) but also determines its severity. The severity is determined by the intensities of the pixels in the eye fundus images. Based on the empirical results obtained on the parameters, accuracy, sensitivity, and specificity, the proposed CNN model is proven to be more efficient and accurate than the previously utilized algorithms such as support vector machine (SVM) and extreme learning machine (ELM).

Keywords Convolutional neural network (CNN) · Diabetic macular edema (DME) · Cardiovascular diseases (CVDs)

R. Senthamizh Selvi (✉) · S. Bragadesh Bharatwaj · B. Ajith Kumar · V. R. Bharath Raj · S. Sudha
Easwari Engineering College, Ramapuram, Chennai, Tamil Nadu 600089, India
e-mail: senthamizhselvir74@gmail.com

S. Bragadesh Bharatwaj
e-mail: s.bragadesh@gmail.com

B. Ajith Kumar
e-mail: ajithkumar2510.b@gmail.com

V. R. Bharath Raj
e-mail: vrbharathraj10@gmail.com

S. Sudha
e-mail: sudha76s@yahoo.com

D. K. Sharma et al. (eds.), *Micro-Electronics and Telecommunication Engineering*,
Lecture Notes in Networks and Systems 179,
https://doi.org/10.1007/978-981-33-4687-1_38

1 Introduction

Diabetic macular edema (DME) and cardiovascular diseases are some of the most common and serious health issues around the world. If not detected, early DME can cause permanent blindness, while cardiovascular diseases can be fatal. Based on the "Vision Problems in the US Database," diabetic retinopathy is highly prevalent in the US population of people above 40, present in 7.68 million people [14]. If not treated early, it will cause permanent blindness, which makes it a primary cause of vision loss in the USA. As per information available in the WHO, CVDs are the chief cause of death around the world, killing an estimated 18 million people every year which includes about 32% of all deaths globally [15]. Several modules have been created in the past using various methodologies to detect DME or cardiovascular diseases separately. In that, the partial least squares (PLS) algorithm was used which provides good generalizability to new inputs when trained on a bounded, pre-segmented dataset [1]. Another approach was [4]; in this, the author utilized minimum distance classifier for macula isolation. Here the distance between the training feature vector and each candidate region's specific feature vector is computed, and thus, the region that has the least distance is chosen as the macula. The more advanced approaches utilized better machine learning algorithms to achieve the desired effect. In [3], the author utilized adaptive thresholding followed by support vector machine algorithm (SVM) for classification. The various features such as orientation, geometrical, and shape features have been utilized to correctly classify the segmented objects as exudates. The accuracy obtained by the algorithm was 90% on a total of 189 images in the MESSIDOR database. In an alternate approach [5], a combination system consisting of Radon transform, discrete cosine transform, and discrete wavelet transform is advocated for automatic diagnosis of diabetic macular edema. In another work [6], a technique is proposed to discern the center of the macula which is not dependent on the optic disk location. This is done since it is not affected by the improper recognition of the optic disk location under the influence of effects such as reflections and noises. In [8] the author proposed two stages: Detection of hard exudates and then categorization of DME intensity from eye fundus images. The identification of hard exudates is performed by using the ELM classifier in this methodology. An amalgamation of texture feature extraction from the specific region around the macula and classification using the SVM model is utilized in [7]. The segmented region comprising of thermal formations differs hugely in texture, and accuracy of over 86% was obtained between the two types of classifications. Overall, most of these methods utilize ordinary machine learning algorithms such as SVM or ELM. These methodologies though successful in obtaining the result do not boast of high accuracy. They are also neither efficient nor provide high-speed results. This is where the proposed algorithm comes into effect. CNN [10] is proven in present times to be the best algorithm for image processing activities. Thus, various segmentation techniques are utilized to make the image fit to be input to CNN classifier and output if DME or cardiovascular disease is present, along with its severity.

The remainder of this paper is structured as follows: Sect. 2 provides the segmentation techniques and the design of the CNN classifier. Section 3 describes performance measures for disease detection and classification and presents evaluation results. Finally, Sect. 4 concludes the paper.

2 Methodology Used

The module consists of two stages, such as the segmentation part and the classification part. First, the input image is preprocessed before being input to the CNN classifier. In this, both the disease parts are segmented. Adaptive thresholding is used for identifying the Macular edema lesion, while morphological operations are utilized for the cardiovascular disease part in the eye vessel. The CNN classifier is first trained with the respectively labeled datasets. For this, the dataset is divided into a ratio of 70–30 for training and test, validation data, respectively. The CNN algorithm is fed with an input image which passes through the various layers to determine the required features and recognize the image, and then it produces the final classification result. Figure 1 depicts the block diagram of the devised DME and cardiovascular disease detection system using CNN.

The two stages are discussed in detail as follows.

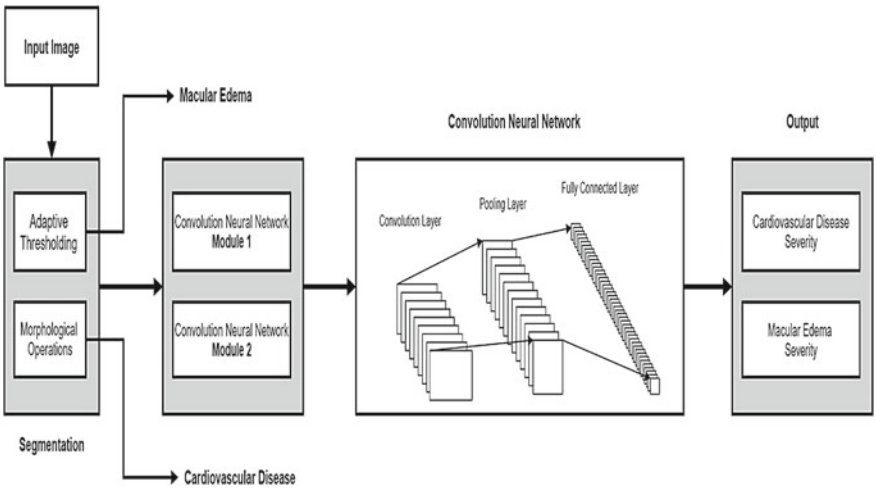

Fig. 1 Block diagram of devised DME and cardiovascular disease detection system using CNN

2.1 Segmentation

This section consists of three main steps:

Step1: Input image:

The input fundus eye images were downloaded from the MESSIDOR **database.** MESSIDOR is an abbreviation for **M**ethods to **E**valuate **S**egmentation and **I**ndexing **T**echniques in the field of **R**etinal **O**phthalmology. It is a research program financed by the French Ministry of Research and Defense that came under the 2004 *TECHNO-VISION* program. The MESSIDOR database was set up to aid research on computer-aided detection of diseases such as DME.

Step 2: Preprocessing:

Image preprocessing primarily consists of image resizing [2]. For feeding a dataset of images to a convolutional neural network, they must all be of the same size. Other processing tasks are done like geometric and colour transformation such as converting colour to grayscale. The individual colour values (red, green, blue) are extracted. The noise is cleaned using a median filter.

Step 3: Disease part segmentation:

The task of dividing a digital image into several parts (groups of pixels) is known as image segmentation [12]. Segmentation is done to alter the depiction of an image into a more significant and simple to analyze form. Here, adaptive thresholding method is utilized.

(a) Diabetic Macular Edema Part Segmentation

Adaptive Thresholding:

Adaptive thresholding is usually inputted with a grayscale or colour image and, in the basic application, gives out a binary image that provides the segmentation output. A threshold is calculated for every pixel present in the image. When the intensity of the pixel is less than the fixed value, the background value is assigned to it, else it takes the foreground value.

(b) Eye Vessel Segmentation

Morphological Operations:

Using a basic morphological function is more suitable to detect the vessel part in the eye. Here some **morphological operations including** dilate, reconstruct, and erode are used. **Morphology** is an extensive collection of image processing **operations** in which the images are processed depending on their structure/forms. In a **morphological operation**, every pixel in the input is altered depending upon the neighbouring pixels.

2.2 Classification

Convolution Neural Network:

For image recognition and image classification, convolutional neural networks were proved to be the most effective [13]. The images are in the form of a two-dimensional matrix of pixels on which CNN is programmed to either identify the image or to categorize the image. CNN architecture contains three types of layers; they are convolutional layers, pooling layers, and fully connected layers. Convolution is said to be a mathematical function where the input given is A, and another parameter, kernel B, is used to provide the output that indicates how the form of one is altered by the other.

With respect to an image,

$$S(t) = (x * w)[t] = \sum_{-\infty}^{\infty} x[p]w[p+t] \tag{1}$$

An image "x" is present, which is a two-dimensional arrangement of pixels that contain distinct colour channels (RGB), and there is a **feature detector or kernel "w".** Finally, the output which is obtained following the implementation of the mathematical function is called a **feature map.** A feature detector is used for recognizing the fringes in the image, so as to identify such type of fringes the convolution operation is used in the image. Generally, the convolution functions have zero value all over except a given fixed set of points. Thus, the values are stored only for these points.

$$S(a,b) = (A * B)(a,b) = \sum_{x} \sum_{y} A(x,y)B(a-x, b-y) \tag{2}$$

where "a" is a two-dimensional array and B is the kernel of the convolution function

As convolution follows commutative property, the above expression can be rewritten as given below. This is done to simplify the execution in machine learning, as there is a very small difference in the range of true values for the variables. Hence, this is the **cross-correlation** operation that a majority of the neural networks utilize.

The cross-correlation function is depicted below:

$$S(a,b) = (B * A)(a,b) = \sum_{x} \sum_{y} A(a-x, b-y)K(a-x, b-y) \tag{3}$$

In Fig. 2, the feature detector will now traverse over the image by a single stride

$$(\mathbf{V} - \mathbf{D} + \mathbf{2Z})/\mathbf{R} + \mathbf{1}$$

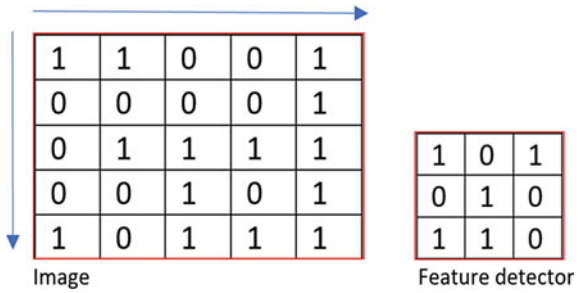

Fig. 2 Cross-correlation pictorial representation

where size of the input image (V), feature detector size (D), stride (R) and zero padding on the image (Z).

In this case, the input image size V is 5. The feature detector (D) is 3. Let the size of stride (R) be one, and the level of zero padding (Z) on the image be zero. Thus, the feature mapping dimension is three. Hence, the **feature map will be a 3 × 3 matrix having three channels—RGB**. This process is described thoroughly in Fig. 3:

The 5 × 5 matrix of the input image is diminished to a 3 × 3 feature map by the feature mapping process that utilizes the cross-correlation operation. But the number of channels remains unchanged as 3 (i.e., RGB). Here, several feature detectors are used for detecting the edges, and also, the feature detector can be used to increase or decrease the intensity of the image as required. If the dimensions of the feature map need not be reduced, then zero padding can be used as shown below in Fig. 4:

Here, a zero-padding layer of 1 is applied on a 5 × 5 input matrix. By utilizing the given formula:

$$(\mathbf{V} - \mathbf{D} + \mathbf{2Z})/\mathbf{R} + \mathbf{1} => (\mathbf{5} - \mathbf{3} + \mathbf{2})/\mathbf{1} + \mathbf{1} = \mathbf{5},$$

The dimensions of output are 5 × 5 having three colour channels (i.e., RGB). In case, if there are only a single bias unit and a single 3 × 3 filter, then the linear transformation is first applied as depicted in Fig. 5.

$$\mathbf{Output} = \mathbf{input} * \mathbf{weight} + \mathbf{bias}$$

The input fed is a 5 × 5 matrix having three colour channels (RGB) and a 3 × 3 feature detector with one bias unit and having a stride of one. The number of parameters obtained is 28 which is computed from (3 * 3 * 3) + 1 = 28. If 500 such feature detectors are present, then the total parameters will be 14,000. Following the completion of the convolution operation, the ReLU activation function [9] is applied. Since convolution is a linear operation, in order to introduce nonlinearity the ReLU activation function is applied. Null values will be substituted for every non-positive pixel in the mapping. Figure 6 describes the transformation process when the rectified linear unit function is applied.

Now, the feature detection is completed from specific regions; each of them will be combined from spatial neighborhood to build the picture.

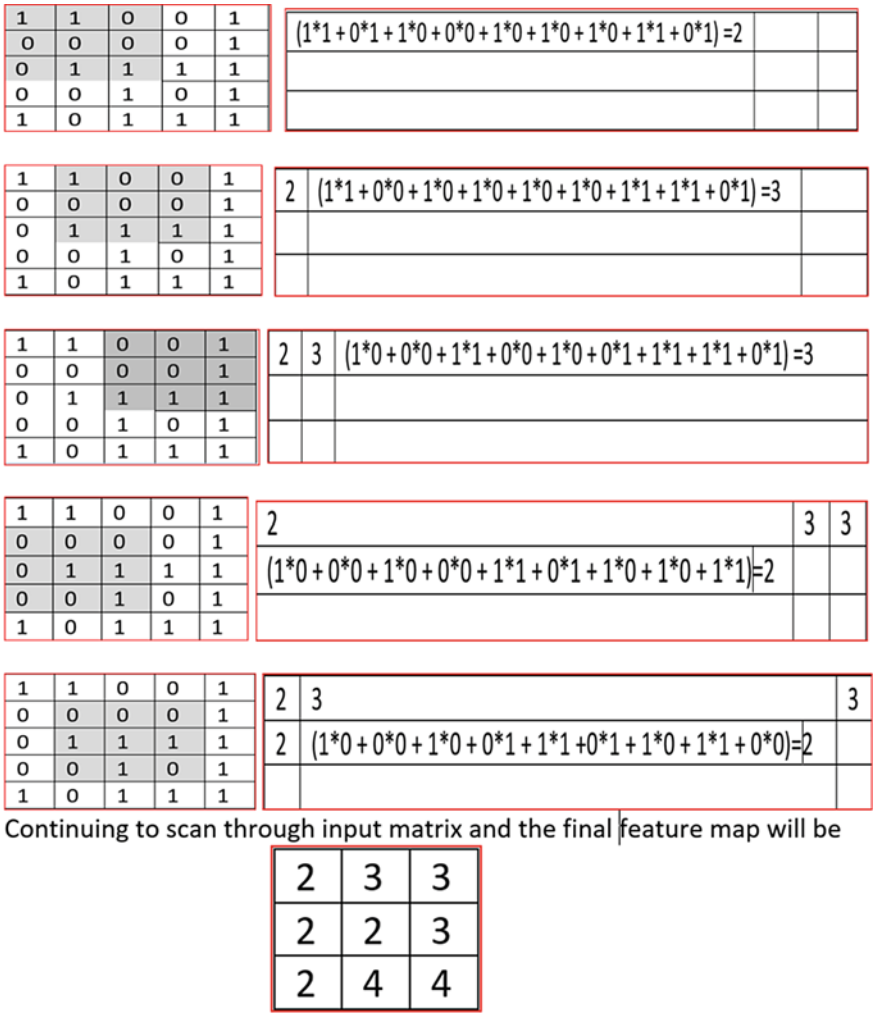

Fig. 3 Feature mapping process

Fig. 4 Application of zero padding

0	0	0	0	0	0	0
0	1	1	0	0	1	0
0	0	0	0	0	1	0
0	0	1	1	1	1	0
0	0	0	1	0	1	0
0	1	0	1	1	1	0
0	0	0	0	0	0	0

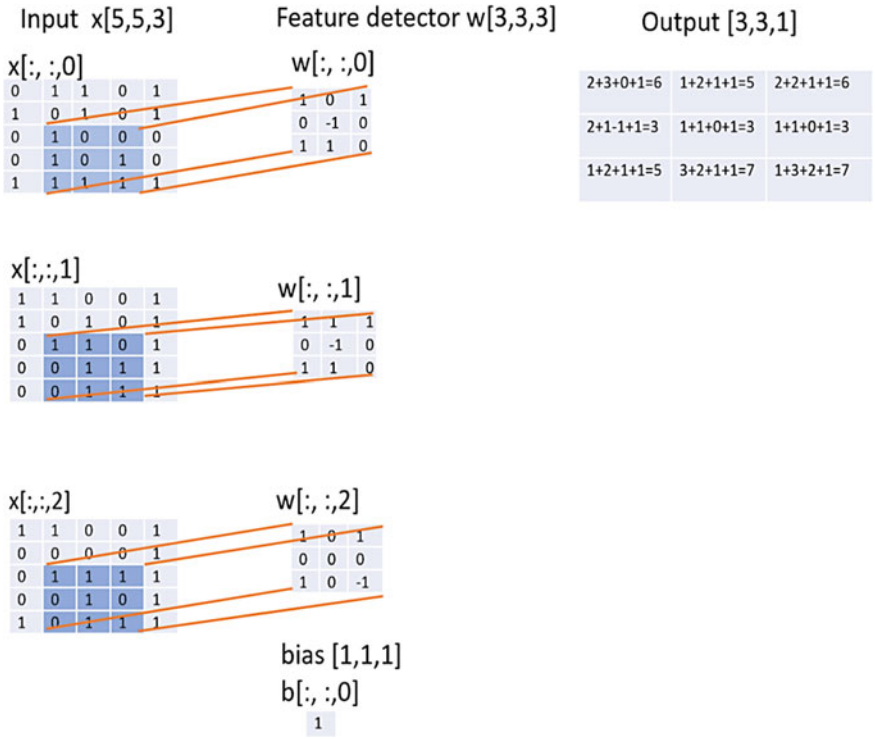

Fig. 5 Linear transformation

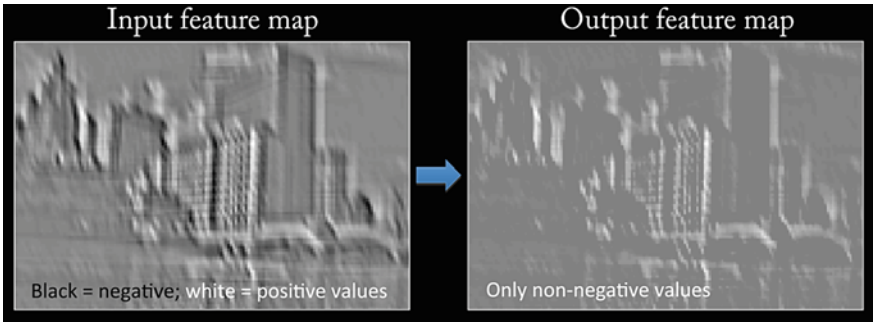

Fig. 6 Feature map transformation

Pooling:

Apply pooling to have translational invariance. Invariance applied to translation specifies that the pooled outputs do not vary when the input is changed by a small quantity. Thus, it aids in the identification of features that are similar in the input image like

fringes or colours. The max-pooling function [11] is applied as it provides higher performance with respect to minimum or average pooling. The max pooling function summarizes the obtained output over the entire given neighborhood. Thus, a lesser number of units are present in comparison to the previously obtained feature map.

The procedure for performing the classification of the diseases is given as:

Step 1: **Collect the training dataset**

The process is initiated by downloading the input images, and then they are loaded into MATLAB. Datasets are collected and kept in several distinct file types. The resultant data is stored as binary files, which is used by MATLAB for quick usage and reshaping it into images.

Step 2: **Train the dataset**

For training the data, first, the n-classes of data are segregated in a standard 70–30 ratio consisting of the training and test, validation data. The dataset is split up so that each of the classes has appropriate representation in both the segregations. The feature vector is just a vector that consists of the various distinct characteristics or features of the input. In the case of an image, several features such as edges, points, density, geometric elements, texture values are taken into account. Now, while utilizing a deep learning model, the training data is provided to the classifier algorithm to enable it to formulate a model. This model can be corroborated, and thus, the most effective kernel parameters can be obtained by selecting the ones with the least error. A simple and effective method to obtain the values is by using K-fold cross-validation. Once the features are extracted and the model is built, the classifier is tested with the new input data, and thus the accuracy is obtained using the test dataset.

Step 3: **Classification**:

The architecture of the CNN comprises of alternating convolutional and pooling layers, followed by a set of fully connected layers. Each layer is given an input which is the output of the previous layer. The input of the model is a three-dimensional image (breadth $\times$ height $\times$ depth), the breadth and the height are the dimensions of the images, whereas the depth is the number of input channels which is given by the three colour channels - RGB. The convolutional layers extract features from images. Every convolutional layer has matrices weights known as filters/kernels which traverse over the input image to detect particular information from the image. The filters of the first layers of the CNN detect colours and simple patterns. Then in the next layers, they gradually detect more complex patterns.

3 Results and Discussion

To analyze and evaluate the deep learning model, the images from the MESSIDOR database were utilized. Of the entire dataset, it was first split and categorized into two main segregations: (I) diabetic macular edema and (II) cardiovascular disease.

Out of these, it was further classified into: Healthy, Moderate, and Severe from (I) and Healthy and Disease present from (II). In each classification, the dataset was randomly divided into training and test datasets in the ratio of 70:30 as stated above.

The key steps in involved in the segmentation are depicted as:

The first step is feeding the complete RGB input image as shown in Fig. 7a. The next key step is the segmentation of the Disease part for diabetic macular edema using a technique called adaptive thresholding as shown in Fig. 7b. For the cardiovascular disease part, the histogram is taken as shown in Fig. 7c for performing the morphological operation. Next, the median filter is utilized for obtaining the noiseless image as depicted in Fig. 7d. Finally, after all the segmentation processes, the

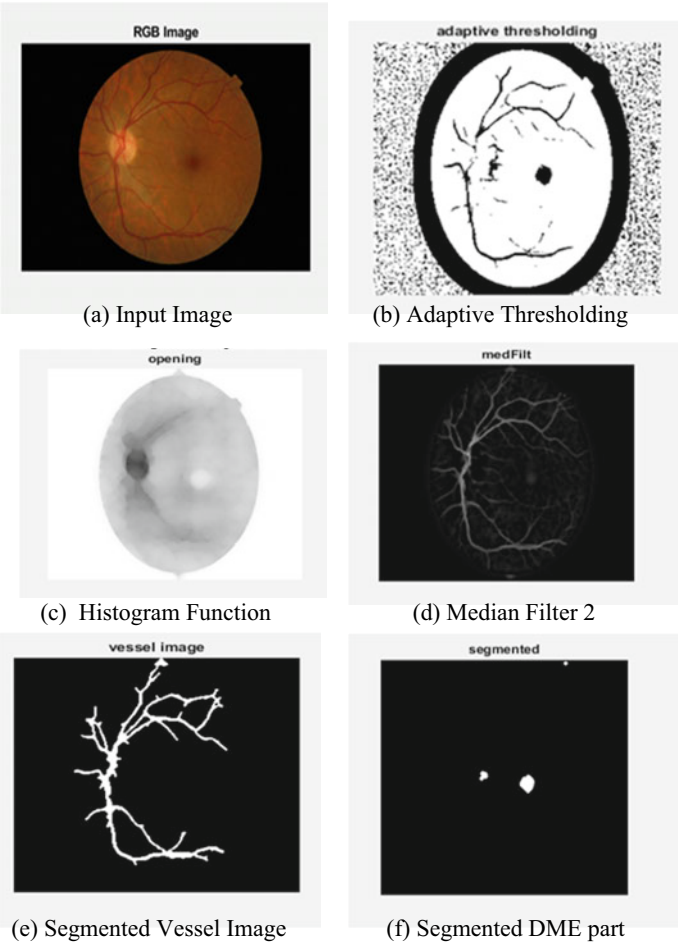

(a) Input Image (b) Adaptive Thresholding

(c) Histogram Function (d) Median Filter 2

(e) Segmented Vessel Image (f) Segmented DME part

Fig. 7 Segmentation process

segmented vessel image Fig. 7e and the segmented macular edema part Fig. 7f for inputting to the CNN classifiers are obtained.

3.1 Performance Evaluation

The performance of the CNN module for disease detection and classification is evaluated in this section. First, the model was trained using the segregated images present in the database. The entire dataset consisted of 157 retinal eye fundus images, covering each category. 70% of the images in each category was used to train the model. After training the model, it was evaluated and tested using the test dataset which was 30% of the entire set. To analyze and evaluate the accuracy and correctness of the model, each result of the test dataset was compared with the original labeling provided by the MESSIDOR database. It was found that the model obtained a very high accuracy close to 100%.

Figure 8 shows the study of the training progress of DME. Figure 8a shows the progress of a healthy eye fundus image (i.e., DME not present). In this, two line graphs are present. The first one consists of Iteration Vs Accuracy (%), and the second graph consists of Iteration versus Loss. The number of iterations is set at 20, and the number of epochs is also 20. The learning rate was set at 0.0001. Figure 8b shows the progress of a moderate DME eye fundus image. Figure 8c shows the progress of a severe DME eye fundus image. The general trend is that with an increase in iterations, the accuracy (%) increases greatly and becomes stagnant at 100% while the loss drops to zero.

Figure 9 shows the study of the training progress of cardiovascular disease. Figure 9a shows the progress of an eye fundus image in which the CV disease is present. The iterations and other parameters are set similarly as above for DME. Figure 9b shows the progress of an eye fundus image in which the CV disease is not present (i.e., a healthy eye vessel).

3.2 Objective Evaluation

The model's performance is measured by the three objective evaluation tools, namely accuracy, specificity, and sensitivity. These three parameters are the most commonly used measure of a model's performance and quality. The empirical results for the accuracy, sensitivity, and specificity are obtained and shown in the below table.

Table 1 lists the experimental values of the three parameters for the algorithms: SVM, ELM, and CNN. When SVM was utilized to detect diabetic macular edema from the eye fundus images, it provided the output with an accuracy of 94% for the dataset from the MESSIDOR database. The respective sensitivity and specificity for this database were at 91 and 93%. In an alternative approach, when ELM was implemented for this purpose, it gave the output with an accuracy of 96.07% for this

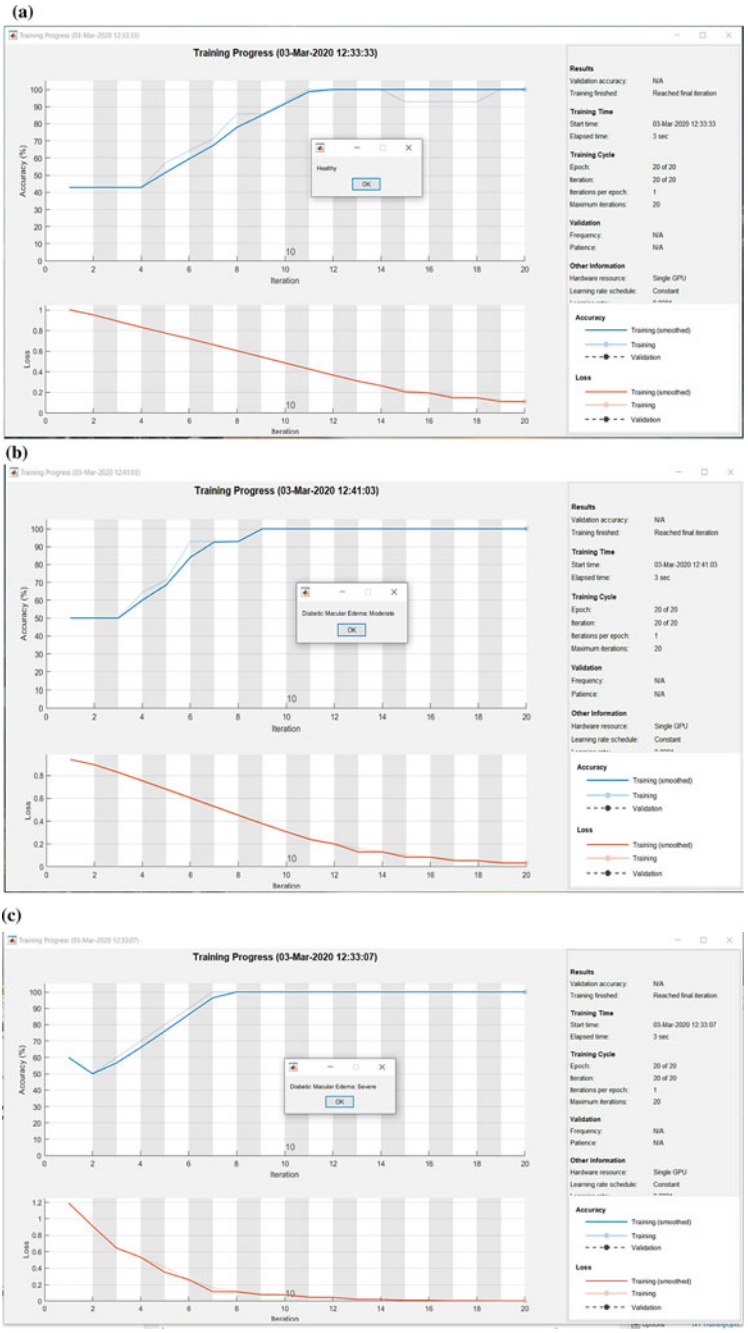

Fig. 8 Training progress of diabetic macular edema **a** Healthy, **b** Moderate, **c** Severe

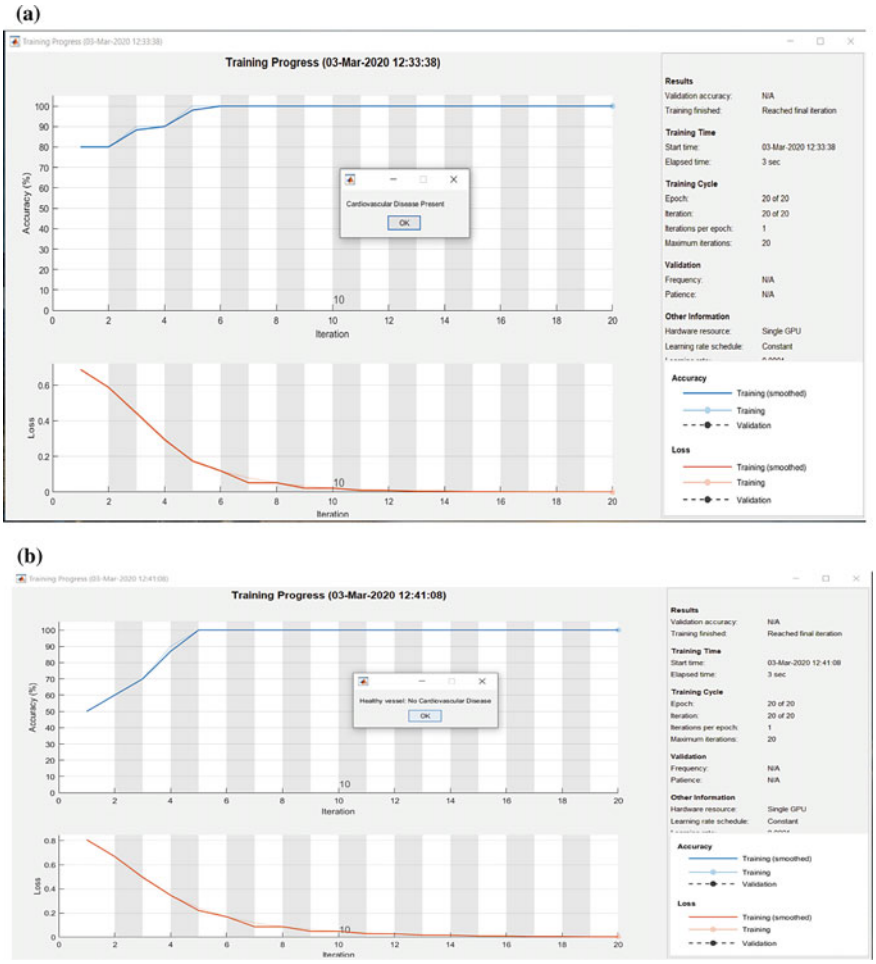

Fig. 9 Training progress of cardiovascular disease **a** disease present **b** healthy

Table 1 Performance analysis: Accuracy, sensitivity, and specificity of different algorithms

Algorithm	Accuracy (%)	Sensitivity (%)	Specificity (%)
SVM	94	91	93
ELM	96.07	71.4	98.68
CNN	99.2	96	99

particular dataset. Similarly, the sensitivity and specificity were 71.4% and 98.68%, respectively. Finally, when the model with CNN was utilized, it provided an accuracy of 99.2% for the MESSIDOR eye fundus database. The sensitivity and specificity were 96% and 99%, respectively, for this implementation. It is depicted using the bar chart in Fig. 10.

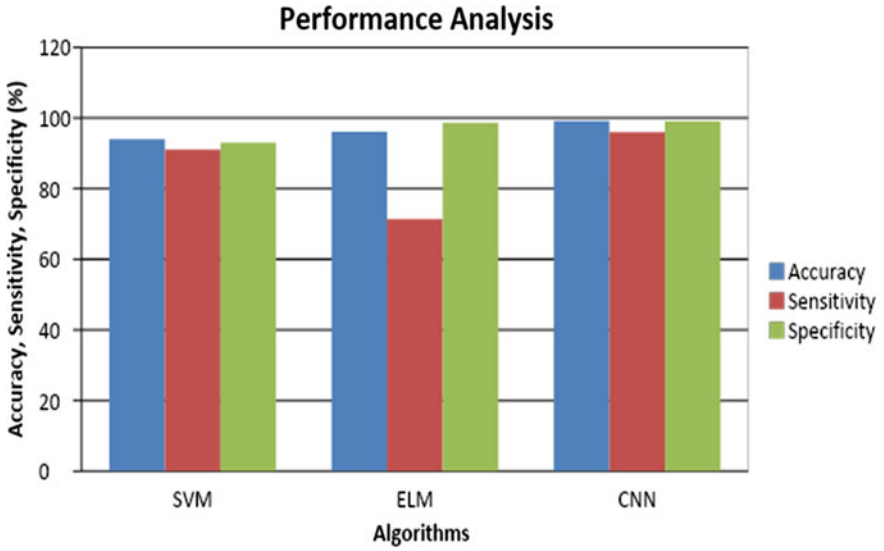

Fig. 10 Performance analysis chart

The three parameters sensitivity, specificity, and accuracy were computed using the respective formulae as given below:

$$\text{Sensitivity} = \frac{(\text{True Positives})}{(\text{True Positive}s + \text{False Negatives})}$$

$$\text{Specificity} = \frac{(\text{True Negatives})}{(\text{True Negatives} + \text{False Positives})}$$

$$\text{Accuracy} = \frac{\text{Number of Correct predictions}}{\text{Total number of predictions made}}$$

4 Conclusion

An automated procedure for the classification of the two diseases (DME and CV) was designed using a convolutional neural network. This approach primarily detects the disease and classifies it. This is done by assessing the size of the exudates from the macula, and thus, the images were marked as normal, moderate, or severe DME and detect the cardiovascular disease. The proposed method provided exceptional results and was evaluated on distinct datasets. It provided the maximum accuracy (99.2%),

sensitivity (96%), and specificity (99%) among all the other machine learning algorithms. The training time was very less, and the speed at which the output was obtained was comparatively very high for this model. This proposed model if integrated into a real hospital environment has the potential to efficiently carry out automated diagnostic tests on eye fundus images to detect and classify retinal diseases.

References

1. Agurto, C., et al.: A multiscale optimization approach to detect exudates in the macula. IEEE J. Biomed. Health Inf. **18**(4), 1328–1336 (2014)
2. Johny., Thomas, A.: A novel approach for detection of diabetic macular edema. In: Proceedings of International Conference on Emerging Trends in Engineering, Technology and Science (ICETETS), pp. 14 (2016)
3. Rekhi, R.S., Issac, A., Dutta, M.K., Travieso, C.M.: Automated classification of exudates from digital fundus images. In: International Conference and Workshop on Bioinspired Intelligence (IWOBI), pp. 1–6 (2017)
4. Adeel, M.S., Usman Akram, M., Muzammal, T.A.M., Shehzad, K., Muazzam, A.K.: Fundus images-based detection and grading of macular edema using robust macula localization. IEEE. **6**, 58784–58793 (2018)
5. Acharya, U.R., et al.: Automated diabetic macular edema (DME) grading system using DWT, DCT features and maculopathy index. Comput. Biol. Med. **84**, 68 (2017)
6. Sengar, N., Dutta, M.K., Burget, R., Povoda, L.: Detection of diabetic macular edema in retinal images using a region based method. In: Proceedings 38th International Conference Telecommunication Signal Process (TSP), pp. 412–415 (2015)
7. Kunwar, A., Magotra, S., Sarathi, M.P.: Detection of high-risk macular edema using texture features and classification using SVM classifier. In: Proceedings of International Conference Advance Computing Communication Information (ICACCI), pp. 2285–2289 (2015)
8. Kumar, S.J.J., Ravichandran, C.G.: Macular edema severity detection in colour fundus images based on ELM classifier. In: Proceedings of International Conference on I-SMAC (IoT Social, Mobile, Anal. Cloud) (I-SMAC), pp. 926–933 (2017)
9. Abien, F.A.: Deep Learning using Rectified Linear Units (ReLU)", Neural and Evolutionary Computing (cs.NE), arXiv:1803.08375, version 2 (2019)
10. Neha, S., Vibhor, J., Anju, M.: An analysis of convolutional neural networks for image classification. Procedia Comput. Sci. **132**, 377–384 (2018)
11. Nithya, V., Ramesh, G.P.: Wireless EAR EEG signal analysis with stationary wavelet transform for Co channel interference in schizophrenia Diagnosis. In: Balas V., Kumar R., Srivastava R. (eds) Recent Trends and Advances in Artificial Intelligence and Internet of Things. Intelligent Systems Reference Library, vol 172. Springer, Cham (2020)
12. Vincent, C., Lukas, S., Mathias, S., Anguelos, N., Pavel, K., Andreas, M.: Deep Generalized Max Pooling, ICDAR Computer Vision and Pattern Recognition (cs.CV), arXiv:1908.05040, version 1(2019)
13. Satpathy, R.B., Ramesh G.P.: Advance approach for effective EEG artefacts removal. In: Balas V., Kumar R., Srivastava R. (eds) Recent Trends and Advances in Artificial Intelligence and Internet of Things. Intelligent Systems Reference Library, vol 172. Springer, Cham (2020)
14. Goceri, E.: Challenges and recent solutions for image segmentation in the era of deep learning. In: 2019 Ninth International Conference on Image Processing Theory, Tools and Applications (IPTA), Istanbul, Turkey, 2019, pp. 1–6 (2019)
15. Xin, M., Wang, Y.: Research on image classification model based on deep convolution neural network. J. Image Video Proc. 40 (2019)

16. Vision problems in the US prevalence of age-related eye disease in America. [Online]. Available: http://www.visionproblemsus.org/index.html
17. Cardiovascular Diseases [online] available: https://www.who.int/health-topics/cardiovascular-diseases/#tab=tab_1

Classification and Detection of Malarial Parasite in Blood Samples Using K-Means Clustering Algorithm and Support Vector Machine Classifier

R. Mohana Priya, L. K. Hema, V. Vanitha, and R. Karthikeyan

Abstract The natural history of malaria involves cyclical infection of humans and female Anopheles mosquitoes. In humans, the parasites grow and multiply first in the liver cells and then in the red cells of the blood. The early diagnosis of malaria is required; otherwise, it leads to death. In this study, an effective method for the classification and segmentation of malaria parasite using k-means clustering (KMC) segmentation algorithm and support vector machine (SVM) classifier is presented. Initially, the input blood sample images are given to KMC segmentation technique for segmentation. Then the segmented image is given to statistical features like mean and standard deviation for feature extraction. Then the extracted features are saved in the feature database and used for classification using SVM classifier. The classification of healthy and affected cells of malaria parasite in blood sample images is made by using SVM classifier. Experimental result shows the performance of the proposed system.

Keywords Malarial parasite · K-means clustering · Statistical features · Support vector machine

1 Introduction

Image processing techniques are used to identify and later recognize a parasite as a target group [1]. Three category photos were correctly categorized, with a lower recognition rate in one category. The algorithm is used across various color spaces to find optimum output in microscopic images with a bloodstream [2]. This is useful in telepathology and can automate malaria screening in rural areas with minimal healthcare personnel.

R. Mohana Priya (✉)
Department of Electronics and Communication Engineering, Aarupadai Veedu Institute of Technology, Chennai, Tamil Nadu, India
e-mail: mohanapriya@avit.ac.in

L. K. Hema · V. Vanitha · R. Karthikeyan
Aarupadai Veedu Institute of Technology, Salem, Tamil Nadu, India

D. K. Sharma et al. (eds.), *Micro-Electronics and Telecommunication Engineering*,
Lecture Notes in Networks and Systems 179,
https://doi.org/10.1007/978-981-33-4687-1_39

1. In the event of a poorly qualified technician, false detection can occur. We also proposed in this research a method to automate a technician's manual work to reduce the human error and increase the accurate diagnosis of malaria [3]. A groundbreaking digital technique detects parasite protozoa of the Plasmodium genus as part of the technical advances in bio-imaging processing.
2. Investigate the best feature selection approach for automated computer training in whole slide images of peripheral bloodstreams, based on malaria detection [4]. For through classification carried out, confusion matrices are created. Several classification performance measures are recorded. Malaria is an infectious disease and is treated frequently through Giemsa's staining blood streak microscopic assessment [5, 6].
3. The major drugs for prophylaxis and malaria prevention are antimalarial antifolates [7]. A particular group of mutations in the dihydrofolate reductase is readily used to improve resistance to pyrimethamine and proguanil antifolates.

In this study, an efficient method for malarial parasite detection is discussed by using KMC, statistical features and SVM classifier. The paper is organized as follows: Sect. 2 describes the methods and materials used for malarial parasite detection. The experimental results and discussion are explained in Sect. 3. The last section concludes malarial parasite detection.

2 Methods and Materials

Initially, the input blood sample images are given to KMC segmentation technique for segmentation. Then the segmented image is given to statistical features like mean and standard deviation for feature extraction. Then the extracted features are saved in the feature database and used for classification using SVM classifier. The classification of healthy and affected cells of malaria parasite in blood sample images is made by using SVM classifier. Figure 1 represents the workflow of malarial parasite detection.

2.1 KMC Segmentation

KMC is an iterative algorithm which attempts to partition the dataset into K predetermined, distinct non-subgroups (clusters) where only one group is included in each data point. This attempts to make the data points inter-cluster as close as possible while keeping the clusters as distinct as possible. It assigns data points to a cluster in order to minimize the squared distance between the data points and the middle of the cluster to a minimum. Within clusters, the less variance, the more uniform (similar) the data points are in a single cluster. The KMC is also used in marine image segmentation [8] and hand geometry recognition [9].

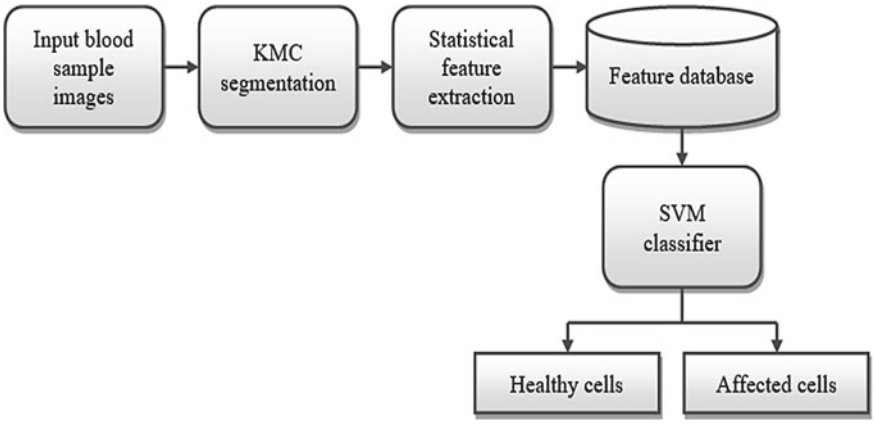

Fig. 1 Work flow of malarial parasite detection

2.2 Statistical Feature Extraction

Moments such as mean, variance, dispersion, medium or average energy value, entropy, skewness and kurtosis are typical features. Images can also be seen by high-order statistical parameters determined from co-occurrence or run-length or frequency approaches.

2.3 SVM Prediction

The goal of the SVM algorithm is to find an N-dimensional hyperplane that defines the data points. There are several potential hyperplanes to pick to differentiate the two types of data points. Maximizing the margin gap provides some reduction to maximize potential data points. Hyperplanes are decision limits that help in the classification of data points. On each side of the hyperplane, data points can be assigned to different groups. Help vectors are data points closer to the hyperplane and affect the hyperplane position and orientation. We optimize the range of the classifier with these support vectors. The removal of support vectors would shift the hyperplane location. Those are the things that help us build our SVM. The SVM classifier is also used in brain image classification [10], electrocardiogram classification [11] and glaucoma classification [12].

3 Results and Discussion

Data used in this analysis are only (positive) contaminated samples, and thus, no negative category sample can be identified. It ensures that all the samples are contaminated and labeled with the correct category of real parasites. Some sample images in the database are shown in Fig. 2.

In this study, an effective method for the classification and segmentation of malaria parasite using k-means clustering (KMC) segmentation algorithm and support vector machine (SVM) classifier is presented [13, 14]. Initially, the input blood sample images are given to KMC segmentation technique for segmentation. Then the segmented image is given to statistical features like mean and standard deviation for feature extraction. Then the extracted features are saved in the feature database and used for classification using SVM classifier. The classification of healthy and affected cells of malaria parasite in blood sample images is made by using SVM classifier. Experimental result shows the performance of the proposed system. Figure 3 shows the experimental results of the malarial parasite detection.

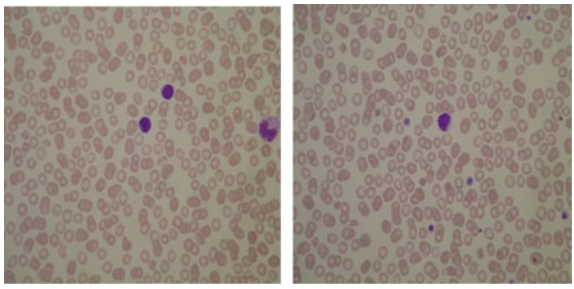

(a) Normal blood cell images

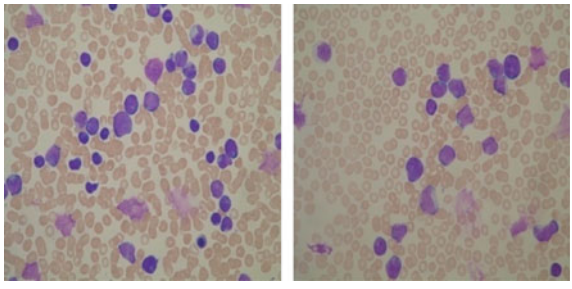

(b) Malarial parasite blood cell images

Fig. 2 Sample images in database

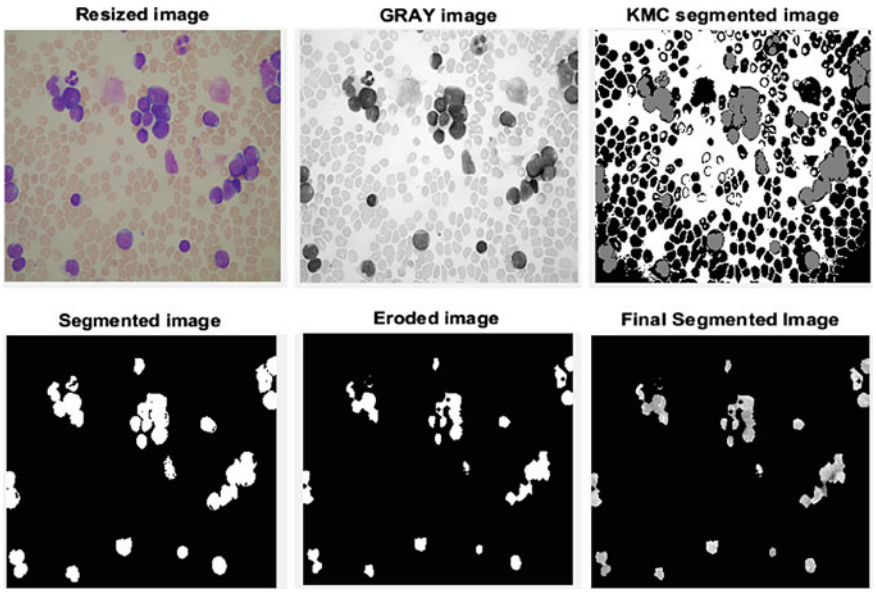

Fig. 3 Experimental results of malarial parasite detection

4 Conclusion

A novel method for classification and detection of malarial parasite in blood samples using k-means clustering algorithm and support vector machine classifier is presented in this study. Initially, both normal and malarial cell images are preprocessed by median filter. Then the KMC technique is used for segmentation and used for further steps. Then the statistical features are extracted and stored in feature database. Finally, SVM classifier is used for classification. The system yields the classification accuracy of 87.5% for normal cell images and 100% for malarial cell images. Also, the overall classification accuracy is 93.75% by using SVM classifier.

References

1. Mandal, S., Amit Kumar, J., Chatterjee, M.M., Ajoy K.Ray.: Segmentation of blood smear images using normalized cuts for detection of malarial parasites. In:2010 Annual IEEE India Conference (INDICON), pp. 1–4. IEEE (2010)
2. Saraswat, S., Utkarsh, A., Neetu, F.: Malarial parasites detection in RBC using image processing. In: 2017 6th International Conference on Reliability, Infocom Technologies and Optimization (Trends and Future Directions)(ICRITO), pp. 599–603. IEEE (2017)
3. Suwalka, I., Ankit, S., Anirudh, M., Mahendra, S.C.: Identify malaria parasite using pattern recognition technique. In: 2012 International Conference on Computing, Communication and Applications, pp. 1–4. IEEE (2012)

4. Muralidharan, V., Yuhang, D., David Pan, W.: A comparison of feature selection methods for machine learning based automatic malarial cell recognition in wholeslide images. In: 2016 IEEE-EMBS International Conference on Biomedical and Health Informatics (BHI), pp. 216–219. IEEE (2016)
5. Rajan, A., Ramesh, G.P.: Glaucoma detection in optical coherence tomography images using undecimated wavelet transform. **7**, 878–885 (2016)
6. Mustare, N., Sreelathareddy, V.: Development of automatic identification and classification system for malaria parasite in thin blood smears based on morphological techniques. In: 2017 IEEE International Conference on Power, Control, Signals and Instrumentation Engineering (ICPCSI), pp. 3006–3011. IEEE (2017)
7. Balakrishnan, Poduval, D., Krishnan Namboori, P.K., Radhika Devi, R., Varun Gopal, K., Suresh Kumar, A.: Computational study on metabolomic consequences of antifolate drug treatment and resistance in malarial organisms. In: 2011 3rd International Conference on Electronics Computer Technology, vol. 4, pp. 75–78. IEEE (2011)
8. Manahoran N, Srinath MV (2017) K-Means clustering based marine image segmentation. Int. J. MC Squ. Sci. Res. 9(3):26–29
9. Saravanan N (2013) Hand geometry recognition based on optimized k-means clustering and segmentation algorithm. Int. J. MC Squ. Sci. Res. 5(1):11–14
10. Mohankumar S (2016) Analysis of different wavelets for brain image classification using support vector machine. Int. J. Adv. Signal Image Sci. 2(1):1–4
11. Vijaya Arjunan, R.: ECG signal classification based on statistical features with SVM classification. Int. J. Adv. Sig. Img. Sci. **2**(1) (2016)
12. Srinivasan, C., Suneel, D., Ganeshbabu, T.R.: Complex texture features for glaucoma diagnosis using support vector machine. Int. J. MC Squ. Sci. Res. **7**(1) 81–92 (2015)
13. Satpathy R.B., Ramesh G.P.: Advance approach for effective eeg artefacts removal. In: Balas V., Kumar R., Srivastava R. (eds.) Recent Trends and Advances in Artificial Intelligence and Internet of Things. Intelligent Systems Reference Library, vol. 172. Springer, Cham (2020)
14. Saravana Kumar, S.S., Umapathy, K.: Efficient implementation of downlink resource allocation in wireless network with inter-cell interference. J. Adv. Res. Dyn. Control Syst. (2017)

FPGA Implementation of Parallel Adder Using Reversible Logic Gates

S. A. Yuvaraj, K. Gunasekaran, D. Muthukumaran, and K. Umapathy

Abstract Reversible digital technology can now start taking a more desirable direction for low dissipation of power, higher processing speeds. Here, we suggested the construction of an 8-, 16-, 32-, 64-bit multiplier using the carry-save adder, the Kogge stone adder, and the HNFG adder with the high operating speed of the proposed HNFG gate adder. The architecture of the device and the logic gates which are reversible can be implemented using the Vedic multiplier. The output of the accumulator operation is dependent on the multiplier unit and the adder units. Here, the development of a multiplier and an adder can be built using reversible gates to achieve high operating speeds, and the use of a Vedic multiplier for greater efficiency. Also fewer area and partial elements are used. A comparative study is being conducted between the conventional [1] and the Kogge stone adder based on HNFG. Finally, it has been shown that the proposed HNFG gate with multiplier adder has a relatively high-speed over the conventional method. The whole process of simulation and synthesis is done using Xilinx 14.7 tool.

Keywords HNFG gate · Xilinx · Reversible logic

S. A. Yuvaraj (✉) · K. Gunasekaran
Department of Electronics and Communication Engineering, GRT Institute of Engineering and Technology, Tiruttani, Tamil Nadu, India
e-mail: akmraja007@gmail.com

K. Gunasekaran
e-mail: guna.k77@gmail.com

D. Muthukumaran · K. Umapathy
Department of Electronics and Communication Engineering, SCSVMV, Kanchipuram, Tamil Nadu, India
e-mail: sarvamkumaran@gmail.com

K. Umapathy
e-mail: umapathykannan@gmail.com

D. K. Sharma et al. (eds.), *Micro-Electronics and Telecommunication Engineering*,
Lecture Notes in Networks and Systems 179,
https://doi.org/10.1007/978-981-33-4687-1_40

1 Introduction

A adder unit [2] is a predictable feature of many applications for digital signal processing involving multiplication/accumulation. It is used to operate digital high-speed DSP systems [3–5]. DSP has a wide range of uses, including convolution, filtering, and inside objects. Discreet cosine transformations or discreet wavelet transformations are nonlinear functions that are widely used in DSP methods. As the cyclical implementation with arithmetic is essentially accomplished, the average speed of arithmetic calculations for matrix multiplication is determined by the speed of implementation and the accuracy of the entire computation. Multiplication and aggregation operations are distinctive for optical filters [6–10]. As a result, the Arithmetic unit's basic configuration allows for high-speed filtering as well as other distinctive processing units for DSP applications, as arithmetic functions completely independently of the CPU, and processes the data individually to reduce CPU load. One of the best fully DSP-based applications, the optical communication system requires vast amounts of data for fast digital data processing. Fast Fourier transform also involves operations with multiplication and addition. A 64-bit MAC computer can accommodate a lot of bits and requires more memory [11, 12]. Essentially, it comprises of a multiplier and an accumulator unit which contains the sum of the prior successive configurations. The MAC device inputs are connected to the block of multipliers from the respective memory location (Fig. 1).

MAC operations include not only the main DSP operations, but also multimedia data processing applications and many others. This consists of the aforementioned multiplier, adder and/accumulator register [13, 1]. We employed a Vedic multiplier in this article. MAC inputs are obtained from the respective location of the memory connected to the unit of multipliers. The 64-bit DSP is fine thus. We can link up your data from the 64-bit memory spot. The 64-bit input is provided to the multiplier,

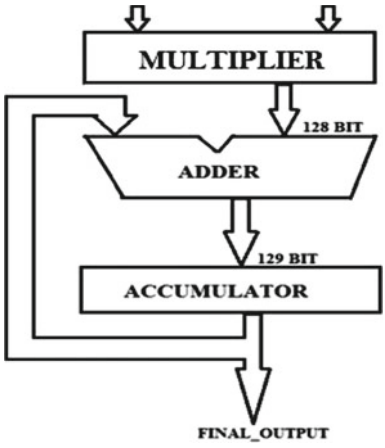

Fig. 1 Generic block

which will give output of 128-bit data after positive multiplier analysis. These 128-bit data multiplier outputs are supplied as an input to one add-on [13–15]. You can use three different types of adders here, one Kogge stone adder and a new HNFG gate. Finally, it has proven that the HNFG adder has the highest operating speed[16, 17]. The MAC unit function is defined in Eq. (1) below.

$$F = \sum P_i Q_{ij} \tag{1}$$

We can obtain the final 129-bit output of the extra unit, which is another additional layer of the carry. The registry of the accumulator is linked to the appropriate output data. The method used in the register of the accumulator is the parallel register in parallel. Because this PIPO causes massive bits and parallel generation of the corresponding add-output value, the PIPO is named as parallel input bits and parallel output bits are generated. From each input to the matching adder, the output of the accumulator register is transmitted. Figure 2 shows the basic diagram of the adder block.

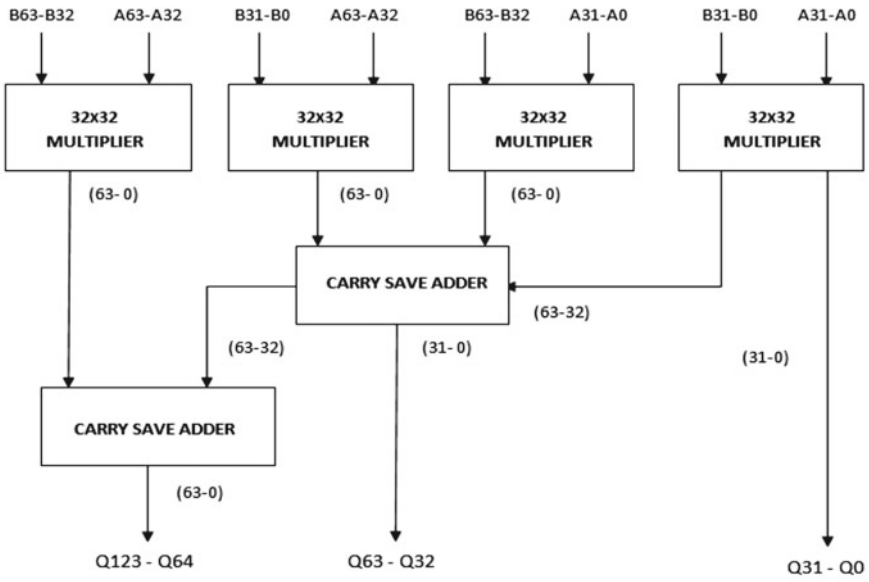

Fig. 2 64-bit multiplier using carry-save adder

2 Proposed Method

A KSA altered the adder stage, which is even more advanced than the CSA shown in Fig. 3. A distinctive methodology is the reversible logic principle [6, 7]. Preferably, zero here to loosen data. This results in the same input and output numbers.

KSA Using HNFG Gate

The HNFG adder architecture is fully based on the reversibility calculation. It has four inputs and four outputs; the input of waste is four inputs and two inputs. The stone adder Kogge is designed with the HNFG gate to fulfill both the complete adder and the entire subtractor conditions that are selected with the input '*A*.' If $A = 0$, the reversible circuit is the full adder, and $A = 1$, the reversible subtractor is the full reversible. Figure 4 shows the reversible HNFG port logic diagram

The realization of the multiplier with a hierarchical structure is very easy to design regarding the above architecture. To produce a 64-bit Vedic multiplier at a lower level, a 32-bit architecture is required. This design also includes multipliers 16-, 8-, 4-bit, and 2-bit. Therefore, expanding the concept of multipliers to a high level is very

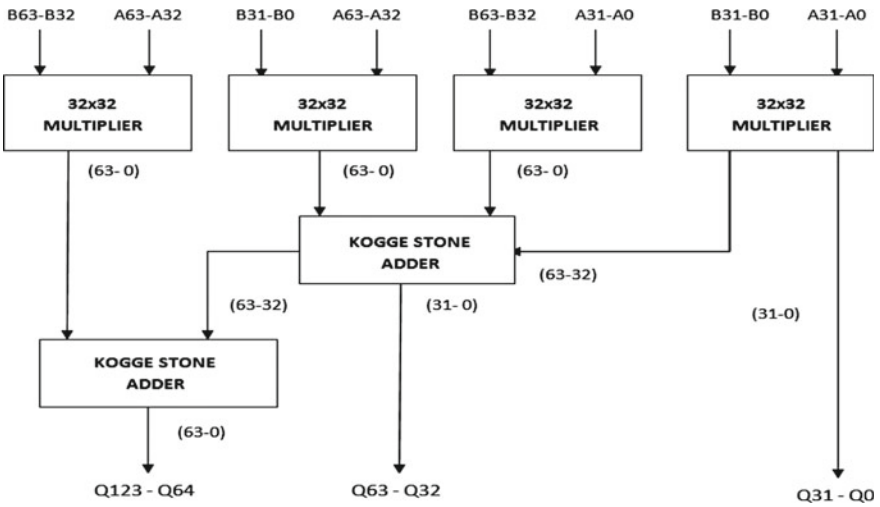

Fig. 3 64-bit multiplier using Kogge stone adder

Fig. 4 HNFG logic

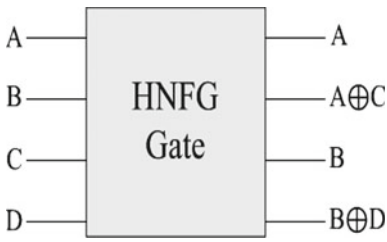

easy by keeping their own modularity. In fact, two 32-bit halves are the main cause of the proposed 64-bit process. Lower half of the numbers are the first step inputs, simply by switching the second and third steps and finally. This design requires an intermediate adder stage. Firstly, a modern reversible logic gate builds the adder phase. *A* and *B* are two transverse inputs; the input size is 64 bits, and the final output is 128 bit maximum. You can insert 64-bit inputs into the respective registries and insert the input in the next consecutive stage if you generate it. The zeroes may be added as one of the adder phase inputs to reach the total number of bits during the process of adding. To test the architecture of the 64-bit multiplier, we need to correct three HNFG rates. We receive LSB bits directly from the first stage of the multiplier. Architecture and features of 32- and 64-bit multiplier versions are similar except 32-bit versions, with 32 input bits, and 64-bit inputs

3 Results

The results of the simulation and comparative analysis are discussed here. The HNFG simulation results are displayed in Fig. 5.

Table 1 shows the cumulative delays in ns analyzes in the 64-bit reports using conventional [13] and HNFG method.

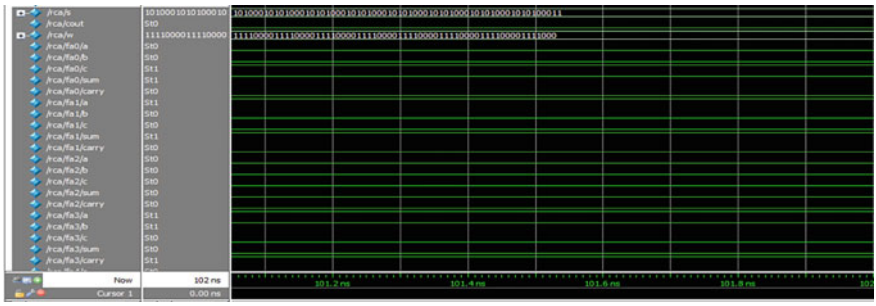

Fig. 5 Proposed system waveform

Table 1 .Delay Comparision of DKG and HNFG gates

N-Bit	DKG gate (ns)	HNFG gate (ns)
8	9.385	8.68
16	10.494	9.72
32	30.54	29.8
64	79.644	78.6

4 Conclusion

The results achieved by the suggested structure of the HNFG adder gate are relatively good, using a reversible computer multiplier. The proposed 64-bit adder unit has been developed with success with a multiplier with a stone adder by Kogge and has proven to be optimized as compared to the conventional system by total late. The 64-bits basic blocks have been successfully built, and their subsequent output is assessed in terms of the total delay factor for the reversible logic principle shown in Table 1. The entire simulation and synthesis process is carried out successfully with the tool Xilinx ISE 14.7. Any architecture is designed based entirely on the fundamentals. There is one multiplier and an adder for our proposed building blocks. Our proposal will optimize these fundamental block designs considerably in future.

References

1. Abdelgawad, A., Magdy, B.: High speed and area-efficient Multiply Accumulate (MAC) unit for digital signal prossing applications. In: *2007* IEEE International Symposium on Circuits and Systems, pp. 3199–3202. IEEE (2007)
2. Selkar RG, Thakare M (2014) Brain tumor detection and segmentation by using thresholding and watershed algorithm. Int. J. Adv. Inf. Commun. Technol. 1:321–324
3. Anitha, R., Neha, D., Prashant, A., Sarat, K.S., Prabhakar Karthikeyan, S., Jacob Reglend, I.: A 32 bit mac unit design using vedic multiplier and reversible logic gate. In: 2015 International Conference on Circuits, Power and Computing Technologies [ICCPCT-2015], pp. 1–6. IEEE (2015)
4. Ramalatha, M., Deena Dayalan, K., Dharani, P., Deborah Priya, S.: High speed energy efficient ALU design using Vedic multiplication techniques. In: 2009 International Conference on Advances in Computational Tools for Engineering Applications, pp. 600–603. IEEE (2009)
5. Kayalvizhi, N.: Implementation of power efficient vedic multiplier. Int. J. Comput. Appl. **43**(16) (2012)
6. Kunchigi, V., Linganagouda, K., Subhash, K.: High speed and area efficient vedic multiplier. In: 2012 International Conference on Devices, Circuits and Systems (ICDCS), pp. 360–364. IEEE (2012)
7. Vasudevan, D.P., Parag, K.L., Jia, D., James, P.P.: Reversible-logic design with online testability. IEEE Trans. Instrument. Measur. **55**(2) (2006)
8. Saha, P., Arindam B., Partha, B., Anup, D.: High speed ASIC design of complex multiplier using vedic mathematics. In: IEEE Technology Students' Symposium, pp. 237–241. IEEE (2011)
9. Garipelly, Raghava, P., Madhu, K., Santhosh Kumar, A.: A review on reversible logic gates and their implementation. Int. J. Emerg. Technol. Adv. Eng. **3**(3) (2013)
10. Haveliya, A.: A novel design for high speed multiplier for digital signal processing applications (Ancient Indian vedic mathematics approach). Int. J. Technol. Eng. Syst. (IJTES) **2**(1) (2011)
11. Kanhe, A., Shishir, K.D., Ankit, K.S.: Design and implementation of low power multiplier using vedic multiplication technique. Int. J. Comput. Sci. Commun. **3**(1) (2012)
12. Wanjari, S., Sanjay, A.: High performance mac design using vedic multiplier and reversible logic gate. IJSTE-Int. J. Sci. Technol. Eng **2**
13. Ramesh, G.P.: Design of digital FIR filters for low power applications. In: Intelligent Computing in Engineering, pp. 433–440. Springer, Singapore (2020)
14. Kashfi, Fatemeh, S., Mehdi, F., Saeed, S.: Designing an ultra-high-speed multiply-accumulate structure. Microelectron. J. **39**(12) (2008)

15. Rajesh, K., Umamaheswara Reddy, G.: FPGA implementation of multiplier-accumulator unit using vedic multiplier and reversible gates. In: 2019 Third International Conference on Inventive Systems and Control (ICISC), pp. 467–471. IEEE (2019)
16. Alexander, S.: Design and implementation of efficient reversible multiplier using tanner Eda. Int. J. MC Squ. Sci. Res **5**(1) (2013)
17. Rajeswari, R.: Design and analysis of various standard multipliers using low power very large scale integration (VLSI). Int. J. MC Squ. Sci. Res. **4**(1) (2012)

Smart Sentimental Analysis of the Impact of Social Media on COVID-19

A. Mugilan, R. Kanmani, M. Deva Priya, A. Christy Jeba Malar, and R. Suganya

Abstract Coronavirus or COVID-19 pandemic has spread to 210 countries and territories taking the lives of more than 140,000 people globally as per the record on April 2020. This worldwide outburst is a predominant topic of discussion on the social media. This paper investigates the Twitter data to analyze the sentiment of the public regarding this pandemic. Long Short-Term Memory (LSTM) algorithm-based Recurrent Neural Network (RNN) architecture is implemented for performing sentiment analysis. Further, data related to coronavirus are collected from social media sources such as Blogs, Forum, News, Videos, Web, Podcast using hashtags related to coronavirus. Data from 15 March 2020 to 23 March 2020 are used for analysis. From this analysis, it is found that the information related to corona virus has considerably influenced the social media. People are well aware of this outbreak. Analysis has also shown that there is less spread of false information regarding coronavirus unlike SARS, MERS, etc.

Keywords Long Short-Term Memory Algorithm · Recurrent Neural Network · COVID-19 · Coronavirus · Social media

A. Mugilan
Department of IT, VIT, Vellore, India
e-mail: mugilan.a2019a@vitstudent.ac.in

R. Kanmani (✉) · A. Christy Jeba Malar · R. Suganya
Department of Information Technology, Sri Krishna College of Technology, Coimbatore, Tamil Nadu, India
e-mail: r.kanmani@skct.edu.in

A. Christy Jeba Malar
e-mail: a.christyjebamalar@skct.edu.in

R. Suganya
e-mail: r.suganya@skct.edu.in

M. Deva Priya
Department of Computer Science and Engineering, Sri Krishna College of Technology, Coimbatore, Tamil Nadu, India
e-mail: m.devapriya@skct.edu.in

D. K. Sharma et al. (eds.), *Micro-Electronics and Telecommunication Engineering*,
Lecture Notes in Networks and Systems 179,
https://doi.org/10.1007/978-981-33-4687-1_42

1 Introduction

In December 2019, several cases of pneumonia with unknown cause emerged in Wuhan, Hubei, China. It had a clinical representation similar to pneumonia. Deep analysis of the respiratory tract of those patients indicated the presence of a new type of virus called coronavirus [1]. Further, it was found to closely resemble Severe Acute Respiratory Syndrome (SARS) [2]. It was then named as 2019 novel coronavirus (2019-nCov). Several exported cases were found in other states of China and countries such as Japan, Thailand and South Korea [1]. On January 1, 2020, the wholesale fish market was shut down as several patients were found to have a history of working in the wholesale fish and seafood market [3]. Compared to the outbreak of SARS and Middle East Respiratory Syndrome CoronaVirus (MERS-CoV), the outbreak of coronavirus was much higher. In Wuhan, the total infections were 21,022 (11,090–33,490) during the period from January 1 to January 22, 2020 [4]. On January 11, 2020, China saw the first death report caused by coronavirus, and more cases were reported in other countries [5]. On February 11, 2020, the World Health Organization (WHO) announced COVID-19 as the name of this new disease caused by virus named 'Severe Acute Respiratory Syndrome CoronaVirus 2 (SARS-CoV-2)' [6]. The growing COVID-19 pandemic became an unprecedented challenge for the economy and the communities across the world. Many governmental and non-governmental organizations are coming together to combat the COVID-19 pandemic. WHO is leading and coordinating this global effort, guiding the countries to prevent, detect and respond to the pandemic. It also provides daily reports related to COVID-19 to the general public in their social media websites [7, 8].

2 Research Significance

Social media saw a large increase in its usage from January 2020 to March 2020 due to coronavirus pandemic. The most popular ones are Facebook, YouTube, WhatsApp, WeChat, Instagram, Twitter, QQ and Reddit.

Social media analytics is a branch of study related to accumulation of data from social media websites and analyzing them [9, 10]. It enables to know about the opinions of the public toward a particular topic. The data can be collected using hashtags. Hashtags are keywords which are preceded by symbol '#'. They are important to enhance the visibility of social media channels and websites. Hashtag usage has a significant growth rate from the last decade. Many brands create their own hashtags to facilitate monitoring of opinions regarding their brand. Tags about topics are also used as an efficient method in social media to segregate positive and negative opinions. Over the past months, social media volume saw a 50X surge as a consequence of coronavirus pandemic. Some of the most commonly used hashtags related to coronavirus over the past three months include #Covid19, #stayhome, #coronavirus, #COVID-19, #lockdown etc.

Various authors have done sentimental analysis of the COVID-19 data taken from social media platforms. Li et al. [11] have used Online Ecological Recognition (OER) based on Machine Learning (ML) predictive models, whereas Lee [12] has used Daily News Sentiment Index (DNSI) and Google Trends data to analyze the impact of COVID-19 on US stock market. Prabhakar Kaila and Prasad [13] have performed Latent Dirichlet Allocation (LDA) analysis by considering the occurrence of negative sentiments. Pastor [14] has designed AYLIEN sentiment analysis Application Programming Interface (API) using Natural Language Processing (NLP), while Sengupta et al. [15] have done mental health analysis using NLP.

In this research article, data from 15 March to 23 March 2020, are analyzed. The following keywords and sources are considered.

Keywords: #covid19, #coronovirus, #lockdown, #Stayhome

Active sources: Twitter, Blogs, Forum, News, Videos, Web, Podcast

3 Data Collection

Twitter is one of the online micro-blogging and social networking services that spreads more than 500 million messages per day. These messages called tweets are usually short (140 characters or less). Twitter has wide accessibility which makes it an important source for collecting real-time data for research purposes [16]. Sentimental analysis is done on Twitter data for understanding the public opinion about a particular topic. In the recent COVID-19 outbreak, Twitter data can be collected [17] to analyze the sentiment of the public regarding this pandemic.

3.1 Long Short-Term Memory (LSTM) Algorithms

Sentimental analysis involves computationally finding the opinions expressed in a text, especially to categorize the attitude of the person towards a particular topic as positive, negative or neutral. Long Short-Term Memory (LSTM) networks are a subclass of Recurrent Neural Networks (RNNs). RNNs are used to deal with data sequences of variable length, but they are unable to recognize long-term dependencies of data in their basic form [18]. Here, LSTM algorithm is implemented for performing sentiment analysis as they are able to store data and use it for later reference.

The input data are represented by 'x', the hidden state is 'h_t', and 'c_t' is the cell state. 'i_t', 'o_t'and 'f_t' are gates directing the flow of data. The three main parts of the architecture include the input vector ('x_i'), output vector (c_i) and hidden state (h_t) [19]. The application of activation is represented by S-shaped curves. The cross symbols denote the element-wise product. The input state can be used to observe the cell memory, and gate control deals with the flow of information in and out of memory. The input gate deals with the inclusion of data, while the forget gate

focusses on discarding data and the output gate decides the data to be passed to the next layer [18, 19].

The hidden state time 't' is calculated using the following formulae.

$$f_t = \sigma_g\left(w_f x_t + r_f h_{t-1} + b_f\right) \tag{1}$$

$$i_t = \sigma_g(w_i x_t + r_i h_{t-1} + b_i) \tag{2}$$

$$o_t = \sigma_g(w_o x_t + r_o h_{t-1} + b_o) \tag{3}$$

$$c_t = f_t o c_{t-1} + i_t o \sigma_c(w_c x_t + r_c h_{t-1} + b_c) \tag{4}$$

$$h_t = o_t o \sigma_g(c_t) \tag{5}$$

where

w_i, w_o, w_f—Weights of the input, output and the forget gates
r_i, r_o, r_f—Recurrent connections of the input, output and the forget gates
b_i, b_o, b_f—Bias terms of the input, output and the forget gates
o—Element-wise product of two vectors
σ_g—Sigmoid function
σ_c—Hyperbolic tangent function

In this analysis, the words from the sentence are given as input to the algorithm as illustrated in Fig. 1. The input is fed to a layer of LSTM which is followed by a fully connected layer, where it is averaged. Finally, the output is fed to the logistic regression layer which gives the output.

To better understand the advantages of LSTM model, it is compared with the Convolutional Neural Network (CNN) model. Generally, CNN proves to be efficient

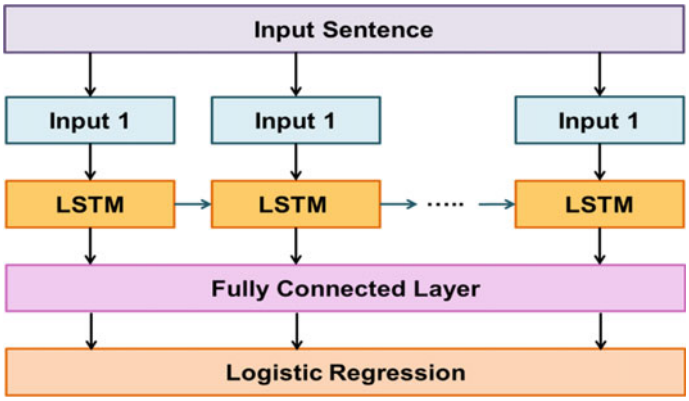

Fig. 1 Illustration of the model used for sentimental analysis

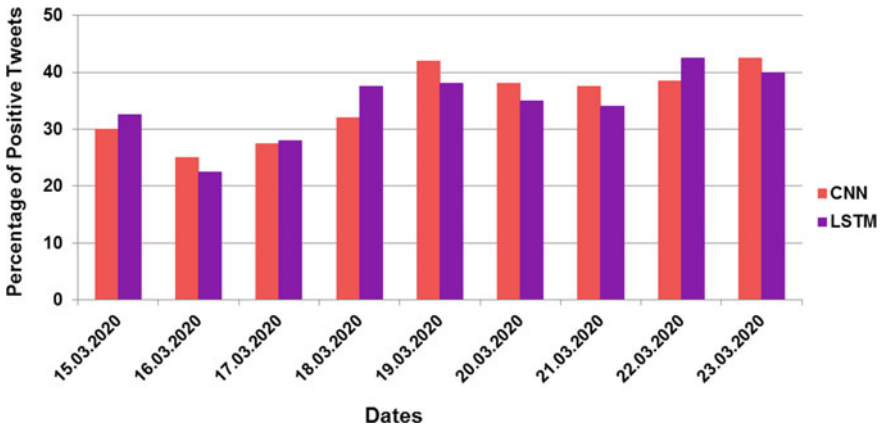

Fig. 2 Tweet Sentimental Analysis using LSTM Algorithms

for small datasets. Here, accuracy of LSTM is less when compared to CNN. But, while handling large datasets, LSTM proves to be more effective [10, 20, 21]. In this section, the Twitter data on coronavirus are analyzed. The volume of data to be analysed is huge (over 200 MB per day). Hence, LSTM model is used for analysis.

Figure 2 shows the percentage of positive tweets in both LSTM and CNN models. It can be seen that there is a difference in values given by LSTM and CNN. There is a variation in how a model analyzes a sentiment and it is hard to predict that performance of one model over another.

Tweets like 'Here's what you can do on 22 March 2020 during the #JantaCurfew. Stay indoors, spend time with your loved ones and stay safe!' by Seagull advertising can be named as a positive comment as it has many positive keywords such as safe and loved. On the contrary, tweets like '206 positive coronavirus cases so far in India; over 6,700 contacts being monitored; 4 deaths, all above 64 years of age; Health ministry' have both positive keyword such as 'positive' and negative keyword such as 'death'. Here, it is seen that the positive keyword is a negative mention with respect to coronavirus. Thus, the keyword 'positive' can be changed to negative, making the overall sentence to be a negative comment.

Sentimental analysis deals with the information in an expression which gives the opinions, attitude, emotions, etc. Expressions are classified into positive, negative and neutral. In Fig. 3, the following keywords are used for analysis: #covid19, #coronovirus, #lockdown, #Stayhome. On 15 March 2020, the total cases of coronavirus reached 153,517 with a death toll of 5,735. This has led to social media being active 200% more than the usual. The pandemic induced fear in many people. This might be the reason that there are more negative sentiments than positive ones initially. But, it seems that people are getting used to it gradually and are instead trying to be positive than negative.

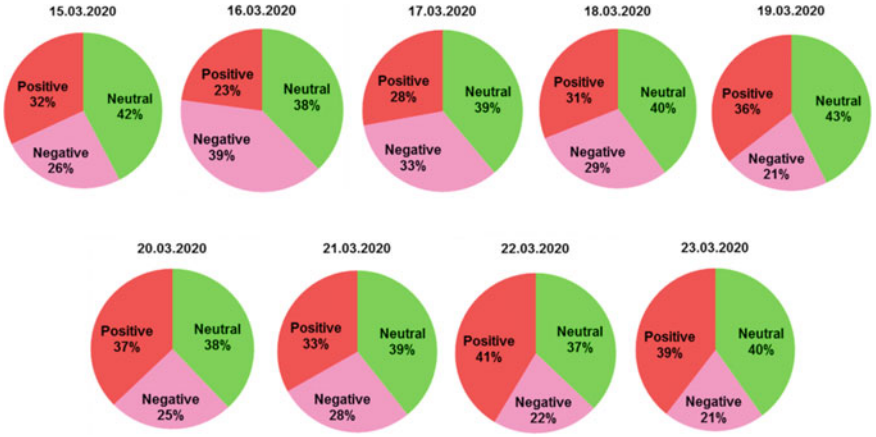

Fig. 3 Tweet Sentimental Analysis using LSTM Algorithms

4 Results and Discussion

Whenever someone names a brand, person or tag something, it is referred to as social mention. It is a measure of how many times a brand name or a tag has been mentioned on social media such as Twitter, Blogs, Forum, News, Videos, Instagram, Web and Podcast. Social media mentions are calculated as the volume of mentions on social media channels over a given period of time, e.g., month or quarter. Social media monitoring tools are used for tracking mentions online. Social media mentions are used to check the impact of a particular topic or brand throughout the world.

The pandemic has been active since January 2020 and has been growing at a rapid pace. The impact is also worldwide. To better understand the impact, social mentions on active sites are used. In these media sites, millions of information related to coronavirus is shared, among which some false information is also shared. False information during critical times can be fatal. During this period, the emotions of people are unsurprisingly mostly negative with positive responses growing over time. Here, the social impacts in the period 15 March to 23 March, 2020 are considered, as this is the period that is recorded with most influence. According to Google Trends [22], these dates have the highest searches related to coronavirus. It can also be said that these searches center on a desire of useful information and are not panic striven.

Considering some of the active social media sources such as Blogs, Forums, News, Videos, Web, Podcast [23], Fig. 4 shows the number of mentions with hashtags such as #COVID19, #stayathome, #coronavirus and #covid_19, from 15 March 2020 to 23 March 2020. On 15 March 2020, the number of mentions was 1,365. It then started decreasing till 17 March 2020, on which it reached a value of 814. After 17 March 2020, the number of mentions saw a steep increase till it reached a peak value of 2,066 on 22 March 2020.

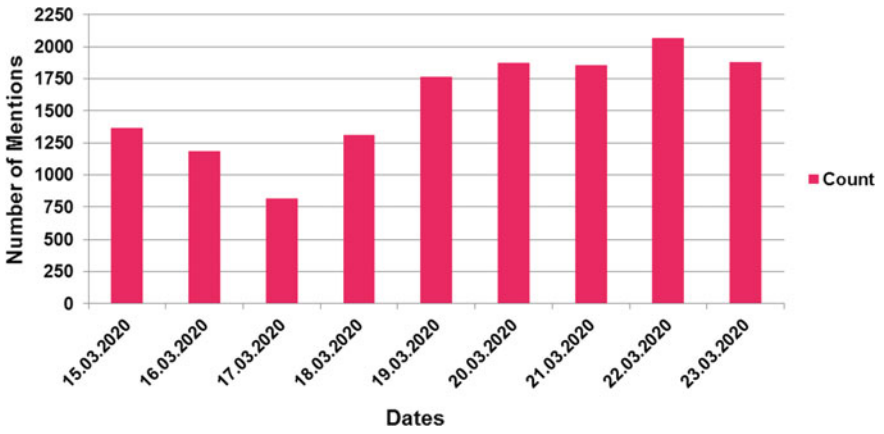

Fig. 4 Number of Mentions

Apart from that the social mentions, the social media reaches are also important. Social media reach refers to the number of users who have come across a particular content on a social media platform. It tells us the extent to which a particular message is reached. Figure 5 shows the social media reach during the period 15 March 2020 to 23 March 2020. The reach of messages related to coronavirus saw a gradual increase from 15 March until it attained a peak value on 20 March 2020. One important point to note is that on 19 March, the number of coronavirus cases exceeded 2,00,000 from 1,00,000 within a period of 12 days. This shows the increase in the rate at which coronavirus spreads as it took only 3 months to reach 1,00,000.

Some of the hashtags used in social media platforms include #coronavirus, #coronavirusoutbreak, #coronavirusPandemic, #covid19, #covid_19, #stayathome, #lockdown, #staysafe, #quarentine, etc. Among them, the frequently used ones are shown

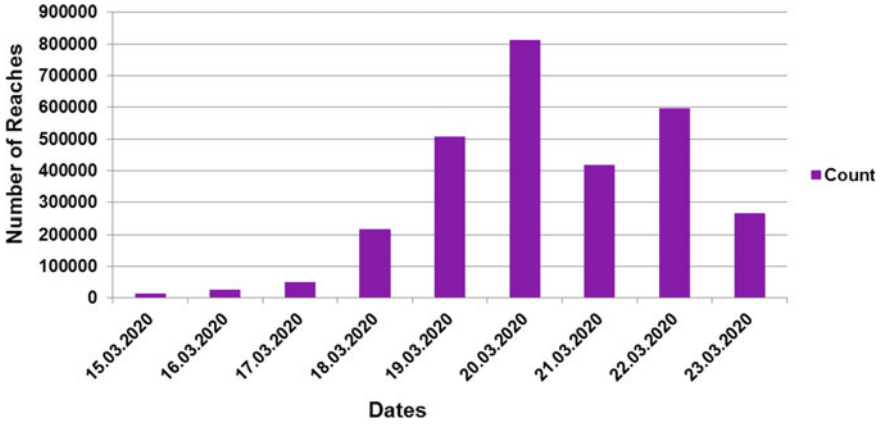

Fig. 5 Number of social media reaches

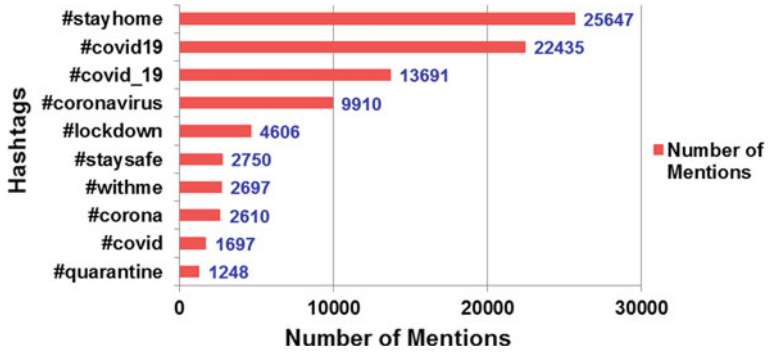

Fig. 6 Trending hashtags

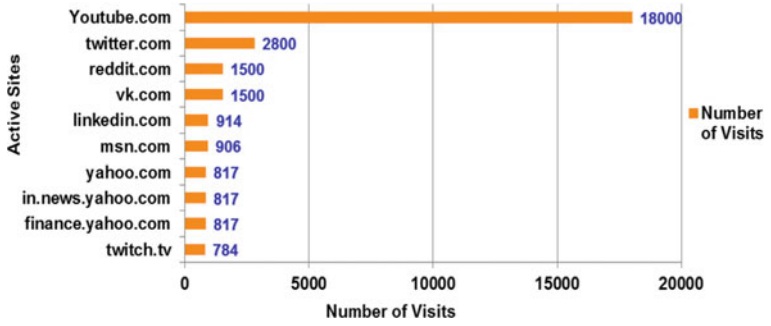

Fig. 7 Top Active Websites

in Fig. 6. #stayathome has the highest mention during the period from 15 March to 23 March 2020. Some of the hashtags such as #stayhome and #staysafe show that many people have a positive outlook during the crisis.

During this period, the number of searches related to the hashtags on coronavirus has been in a rapid increase among which the most active site is YouTube followed by Twitter. These data are given in Fig. 7 (note: the data exclude Facebook and Instagram).

5 Conclusion

In this paper, the opinions of various people regarding coronavirus are discussed. It can be seen that the usage of social media has increased by many folds during this lockdown to spread the preventive measures to be taken during the pademic. Twitter, indeed cannot represent the overall sentiment of the public, but it can still be used as a complementary tool. The sentiments of tweets with hashtags related

to coronavirus are analyzed, thereby categorizing them into positive, negative or neutral. It can be seen that the number of positive mentions fluctuates based on the events happening on a day. This study describes the usefulness of social media in spreading awareness during crisis. The increase in searches and comments about coronavirus on other social media sites are also discussed.

References

1. Huang C, Wang Y, Li X, Ren L, Zhao J, Hu Y, Hu Y, Zhang L, Fan G, Xu J, Gu X, Cheng Z (2020) Clinical features of patients infected with 2019 novel coronavirus in Wuhan, China. The lancet 395(10223):497–506
2. Gorbalenya AE, Baker SC, Baric R, Groot RJD, Drosten C, Gulyaeva AA, Haagmans BL, Lauber C, Leontovich AM, Neuman BW, Penzar D (2020) Severe acute respiratory syndrome-related coronavirus: The species and its viruses—A statement of the Coronavirus Study Group
3. Nishiura H, Jung SM, Linton NM, Kinoshita R, Yang Y, Hayashi KK, Kobayashi T, Yuan B, Akhmetzhanov AR (2020) The extent of transmission of novel coronavirus in Wuhan, China
4. Read JM, Bridgen JR, Cummings DA, Ho A, Jewell CP (2020) Novel coronavirus 2019-nCoV: early estimation of epidemiological parameters and epidemic predictions. medRxiv. 23, 20018549. https://doi.org/10.1101/2020.01
5. Majumder, M., Mandl, K. D.: Early Transmissibility assessment of a novel coronavirus in Wuhan, China (2020).
6. World Health Organization. Coronavirus (2020) [Online]. Available from: https://www.who.int
7. https://www.who.int/emergencies/diseases/novel-coronavirus-2019/situation-reports
8. https://www.worldometers.info/coronavirus/
9. Stieglitz S, Mirbabaie M, Ross B, Neuberger C (2018) Social media analytics—Challenges in topic discovery, data collection, and data preparation. Int J Inf Manage 39:156–168
10. Fan W, Gordon MD (2014) The power of social media analytics. Commun ACM 57(6):74–81
11. Li S, Wang Y, Xue J, Zhao N, Zhu T (2020) The impact of COVID-19 epidemic declaration on psychological consequences: a study on active Weibo users. Int J Environ Res Public Health 17(6):2032
12. Lee HS (2020) Exploring the initial impact of COVID-19 sentiment on US stock market using big data. Sustainability 12(16):6648
13. Prabhakar Kaila D, Prasad DA (2020) Informational flow on Twitter–Corona virus outbreak–topic modelling approach. Int J Adv Res Eng Technol 11(3)
14. Pastor CK (2020) Sentiment analysis of filipinos and effects of extreme community quarantine due to coronavirus (Covid-19) Pandemic. Available at SSRN 3574385
15. Sengupta S, Mugde S, Sharma G (2020) An Exploration of Impact of COVID 19 on mental health-Analysis of tweets using Natural Language Processing techniques. medRxiv
16. Philander K, Zhong Y (2016) Twitter sentiment analysis: capturing sentiment from integrated resort tweets. Int J Hospitality Manage 55(2016):16–24
17. https://www.kaggle.com/smid80/coronavirus-covid19-tweets
18. Hochreiter S, Schmidhuber J (1997) Long short-term memory. Neural Comput 9(8):1735–1780
19. Fagerström J, Bång M, Wilhelms D, Chew MS (2019) Lisep lstm: A machine learning algorithm for early detection of septic shock. Sci Rep 9(1):1–8
20. Dachapally PR, Ramanam S (2018) In-depth question classification using convolutional neural networks. arXiv preprint arXiv:1804.00968
21. Gehring J, Auli M, Grangier D, Yarats D, Dauphin YN (2017) Convolutional sequence to sequence learning. arXiv preprint arXiv:1705.03122

22. https://trends.google.com/trends/explore?date=today%203-m&q=%2Fm%2F01cpyy
23. Jahanbin K, Rahmanian V (2020) Using Twitter and web news mining to predict COVID-19 outbreak. Asian Pacific J Trop Med 13

Dermoscopic Image Classification Using Two-Stage Processing of Shearlet Features with Support Vector Machine

S. Mohan Kumar and T. Kumanan

Abstract Automated classification of dermoscopic images is of importance for the interpretation of skin cancer. In order to avoid false detection, image classification is used in medical field for detecting abnormality. In this paper, a system is developed based on shearlet and support vector machine (SVM) that will assist the automated interpretation of dermoscopic images for cancer diagnosis. This system provides an efficient way of classifying dermoscopic images that can be used as a second reader. It consists of two main stages: local processing stage (LPS) and global processing stage (GPS). In LPS, the energy features from different levels and directions are individually analyzed using SVM classifier. In GPS, the best directional features from each level are combined, and the classification accuracy is improved by selecting more dominant features by a statistical approach. Results show that the features from different level improve the classification yield for SVM classifier from 96% (LPS) to 99.5% (GPS) on PH^2 database images.

Keywords Image classification · Multi-scale analysis · Multi-directional analysis · Support vector machine · Skin cancer

1 Introduction

Convolutional neural network (CNN) and novel regularizer are described in [1] for skin cancer classification. Initially, CNN is employed for prediction using state of art methods and novel regularizer technique which is tested by multiple classes. Melanoma and nevus classification is discussed in [2] for skin cancer diagnosis.

S. Mohan Kumar (✉)
Department of Computer Science and Engineering, Faculty of Engineering, Meenakshi Academy of Higher Education and Research, West K.K Nagar, Chennai, India
e-mail: drsmohankumar@gmail.com

T. Kumanan
Faculty of Engineering and Technology, Meenakshi Academy of Higher Education and Research, West K.K Nagar, Chennai, India
e-mail: kumananvetri@gmail.com

D. K. Sharma et al. (eds.), *Micro-Electronics and Telecommunication Engineering*,
Lecture Notes in Networks and Systems 179,
https://doi.org/10.1007/978-981-33-4687-1_43

Initially, noises from input melanoma images are removed by Gaussian filter. The color and texture features are extracted. SVM is used for the final output prediction.

Supervised and unsupervised learning is described in [3] for skin cancer classification. The melanoma images are classified using hybrid classifiers like neural network and SVM. Automatic approach for skin cancer disease classification is described in [4]. At first, the preprocessing is made by using clustering algorithm. The irrelevant structures are removed by using pre-processing. The local binary pattern and color coherence vector are used for feature extraction. Finally, multiclass SVM is used for final output prediction.

Hybrid deep neural networks are described in [5] for skin lesion detection. The CNN models like ResNet-18, visual geometric group—16, AlexNet and deep feature generators are hybrid, and combined classifiers are used for prediction. Automated skin cancer classification using gray-level co-occurrence matrix (GLCM) and multiclass SVM is described in [6]. The GLCM features are used for extraction. Then multiclass SVM is used for final output prediction. A transfer learning method is described in [7] for skin cancer diagnosis. The deep learning-based classification technique is used for the prediction of normal and abnormal images. Automatic skin lesion classification is described in [8]. The *k*-means clustering technique is used as a pre-processing approach, and SVM classifier is used for output prediction.

SVM-based skin cancer diagnosis system is described in [9]. Feature extraction approach uses GLCM, color, border, asymmetry and diameter features. Then, they are reduced by principal component analysis. Finally, SVM is used for prediction. Bayes classifier-based melanoma classification is described in [10]. The melanoma images are given to non-subsampled contourlet transform for feature extraction. Bayes classifier is used for prediction.

Classification of melanoma with multi-wavelet transform and SVM is described in [11]. At first, noise is removed by Wiener filter and then decomposed by multi-wavelet transform. Features like mean, standard deviation, skewness and kurtosis are extracted. Finally, SVM is used for prediction. Detection of the skin under various illuminations is discussed in [12]. The skin images are tested and form the non-parametric skin ratio. Then histogram back-projection is made in thresholding, and localization is made.

In this study, dermoscopic image classification using two-stage processing of shearlet features with support vector machine is presented. The organization of paper is as follows: The methods and materials of dermoscopic image classification are described in Sect. 2, the experimental results and discussion of dermoscopic images are described in Sect. 3, and the last section concludes the proposed system.

2 Methods and Materials

Figure 1 shows the overall workflow of skin cancer classification system.

Initially, the melanoma images are given to LPS for up to n-level decomposition. The sub-band coefficients of NSST are extracted by using energy feature extraction.

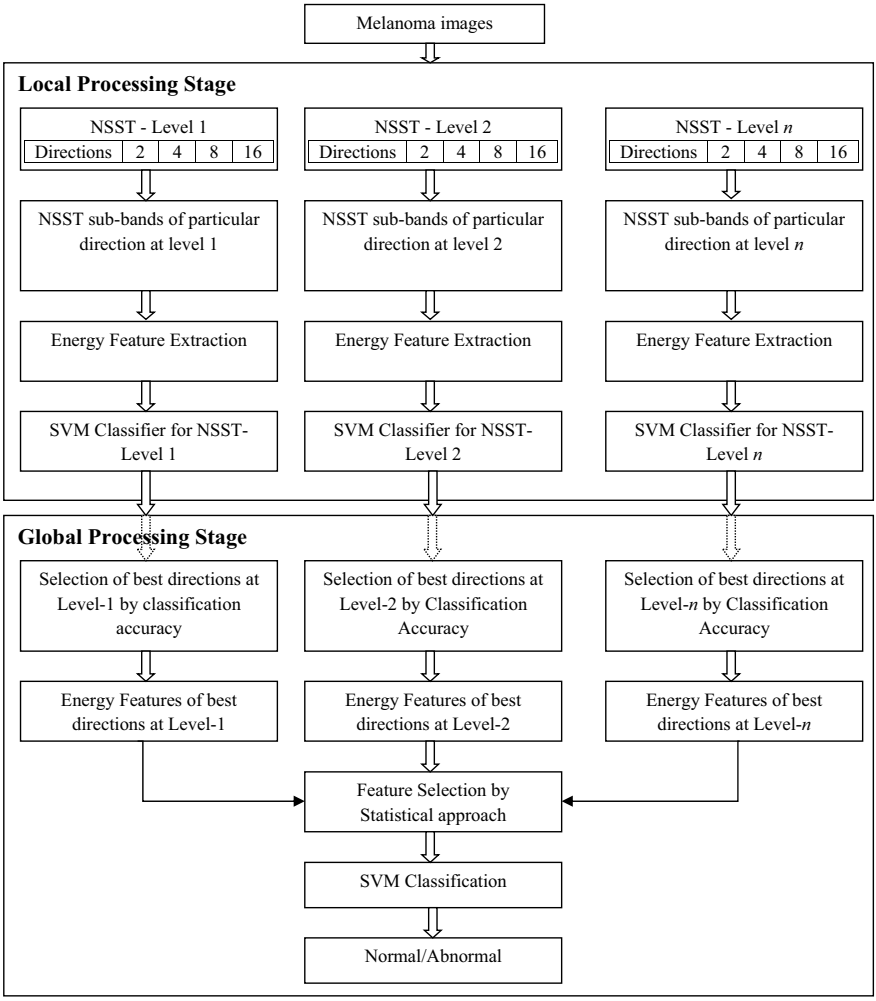

Fig. 1 Skin lesion classification system

Finally, SVM classifier for all levels is used for output prediction. In GPS, the best direction is selected by using the classification accuracy. Then the energy features are extracted for different n-levels. Some redundant features are selected by using statistical feature extraction approach. Finally, SVM classifier is used for classification of normal and abnormal images.

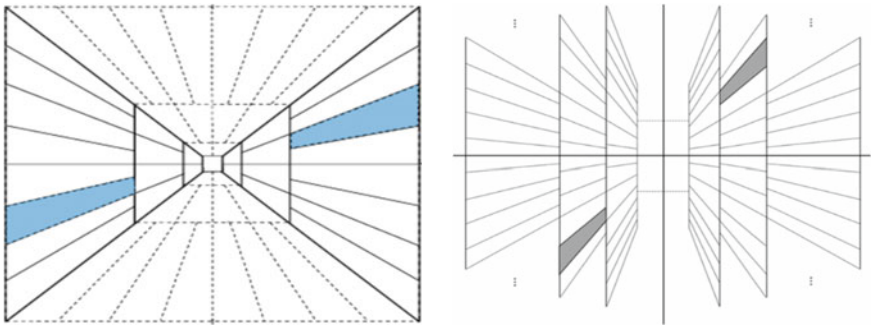

(a) Structure of Shearlet transform

(b) Multiscale construction of shearlet transform

Fig. 2 Shearlet transform structure and multiscale construction

2.1 NSST Decomposition

Shearlets are a multi-scale framework that allows the efficient encoding in multivariate problem classes of anisotropic features in applied mathematical analysis. For analysis and sparse function approximation, shearlets are introduced. They are a normal extension of waves to allow multivariate functions to be generally controlled through anisotropic characteristics, such as image edges, because waves are not able to capture these phenomena, as isotropic artifacts. Shearlets are designed for a variety of production functions using parabolic scaling, shearing and translation. Figure 2 shows the (a) structure of shearlet transform and (b) multiscale construction of shearlet transform.

In this study, the NSST is used for decomposition of input skin images at different n-levels at different directions. The NSST is also used in other fields like image fusion [13] and edge enhancement [14].

2.2 Energy Feature Extraction

The energy gain shows the frequency and spatial levels. In the spatial and frequency domains of different texture patterns, various energy distributions are possible. The energy tests the accuracy of images. The energy feature is defined by,

$$\text{Energy } E_n = \frac{1}{KL} \sum_{m=1}^{K} \sum_{n=1}^{L} \text{BAND}(m.n) \tag{1}$$

where BAND represents the sub-bands of higher and lower frequency components with the image size $K \times L$. The coordinates of sub-band are represented by (m, n). The

energy features are also used in video classification [15] and brainwave classification [16]. In this study, the energy feature is used for extraction of decomposed images. Then the extracted features are used for prediction of final output.

2.3 Statistical Feature Selection

A t-test is a kind of inferential statistics used to determine if there is a substantial difference between the two groups means that may be associated with certain characteristics. The t-test is one of the methods used for statistical testing of hypotheses. To compute the t-test, three main information values are needed. A t-test tests the t-statistical values, the t-distribution values and the right to assess the statistical importance. The mean and norm discrepancy will also be significantly different to samples taken in the placebo-fed control group and from the prescribed drug. This t-test-based feature selection is also used in HapMap genotype data [17] and text categorization [18]. In this paper, the statistical features are used for feature selection.

2.4 SVM Classifier-Based Prediction

The goal of the SVM algorithm is to find an N-dimensional hyperplane that defines the data points. There are several potential hyperplanes to pick to differentiate the two types of data points. Maximizing the margin gap provides some reduction to maximize potential data points. Hyperplanes are decision limits that help in the classification of data points (Fig. 3).

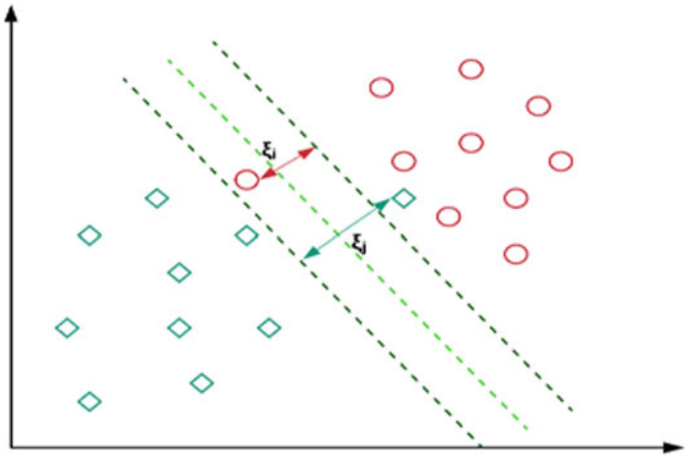

Fig. 3 Hyperplane separation in SVM classifier

On each side of the hyperplane, data points can be assigned to different groups. Help vectors are data points closer to the hyperplane and affect the hyperplane position and orientation. The SVM classifier is defined by,

$$Q(\alpha) = \sum_{i=1}^{N} \alpha_i - \frac{1}{2} \sum_{i=1}^{N} \sum_{j=1}^{N} \alpha_i \alpha_j d_i d_j x_i^T x_j \tag{2}$$

$Q(\alpha)$ represents the dual form J which is only dependent on α as rest are all known scalars. We can solve for $Q(\alpha)$ with any QP optimization, which is beyond the scope of this article. After getting α, we get w, and from that, any of that support vector would give b. SVM classifier is also used in brain image classification [19] and electrocardiogram signal classification [20, 21]. The SVM classifier is used for final output prediction.

3 Results and Discussions

The classifiers used in LPS and GPS are trained and tested with 200 dermoscopic images in PH^2 database [22]. It is freely downloadable, and the resolution of each image is 768 × 560 pixels. It is observed that the human visual system is unable to differentiate between normal and abnormal, and thus, an advanced image analysis system is needed for effective classification of skin cancer images. Figure 4a shows some sample normal skin images and (b) consists of lesion.

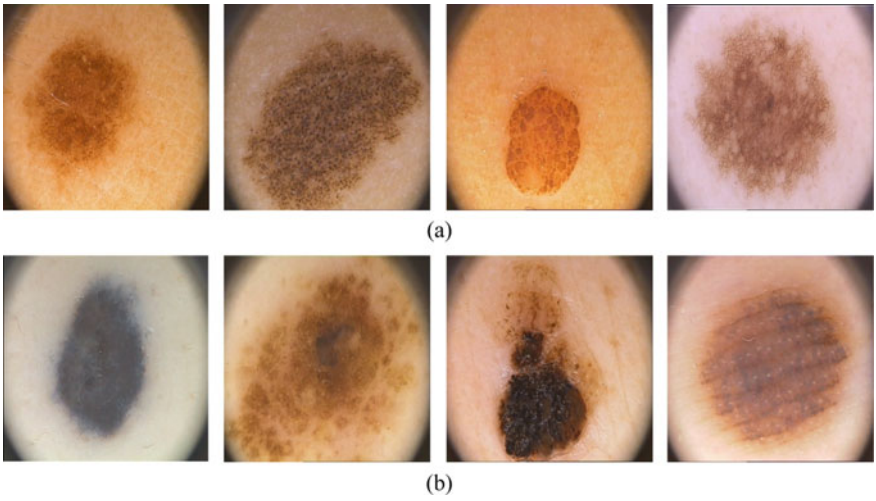

Fig. 4 **a** Normal skin images, **b** skin image that consists of lesion

As the decomposition is performed up to 4th level, four classifiers are trained and tested in the LPS stage, and then a single classifier is used in the GPS stage. All the classifiers use the same database, and also same features are adopted for the classifiers in LPS and GPS. In LPS, each classifier is independently analyzed, and finally, the features which provide best performance are grouped. Then in GPS, only the dominant features are selected from the group of features and tested for more accuracy than LPS. The performance measures used to compare other schemes are accuracy, sensitivity and specificity. They are defined below:

- **Accuracy**: This metric gives the total number of correctly classified skin images. The formula to compute the accuracy is given below:

$$\text{Accuracy} = \frac{\text{TP} + \text{TN}}{\text{TP} + \text{FN} + \text{TN} + \text{FP}} \tag{3}$$

- **Sensitivity**: This metric shows the ability of the system to identify skin cancer cases. The formula to compute the accuracy is given below:

$$\text{Sensitivity} = \frac{\text{TP}}{\text{TP} + \text{FN}} \tag{4}$$

- **Specificity**: This metric shows the ability of the system to identify normal or − ve results. The formula to compute the accuracy is given below:

$$\text{Specificity} = \frac{\text{TN}}{\text{TN} + \text{FP}} \tag{5}$$

where true positive (TP) is the correctly classified skin cancer positive (+ve) cases, true negative (TN) is the correctly classified normal or negative (−ve) cases, false negative (FN) is the incorrectly classified skin cancer (+ve) cases, and false positive (FP) is the incorrectly classified normal (−ve) cases. A confusion matrix is made based on these values, and the performance measures can be easily computed. Table 1 shows two-class confusion matrix.

Table 2 shows the k-fold cross-validation setting of PH^2 database. This study uses *k*-fold cross-validation to avoid overfitting problem as well as to generalize the classifier for other databases.

Table 1 Two-class confusion matrix

Actual class	Class-*X* (+ve)	Class-*Y* (−ve)
Predicted class		
Class-*X* (+ve)	TP	FP
Class-*Y* (−ve)	FN	TN

Table 2 k-fold cross-validation setting of PH2 database

Total images in PH^2 database		k-fold	Training images/fold		Testing images/fold	
Normal	Abnormal		Normal	Abnormal	Normal	Abnormal
80	120	10	72	108	8	12

3.1 Performance of LPS of the System

In LPS, four independent SVM classifiers are used to classify images based on the extracted energy features at each independent decomposition level with different directions. Figure 5 shows the confusion matrices of level-1 features in different directions. Class-X indicates abnormal cases, and class-II indicates normal cases. Figure 6 shows the confusion matrices of level-2 features in different directions.

Figures 7 and 8 show the confusion matrices of level-3 features and level-4 features at different directions, respectively.

From Fig. 5, it is observed that the total number of misclassified images in both categories is high for 2 directions of level-1 features. One of the reasons for this misclassification is due to the insufficient number of features at low directions. Also, it is evident that the total number of misclassified images is reduced while changing the number of directions. For example, the total number of misclassified images in both categories is 66 (44 + 22) (Fig. 5a) at 2 directions of level-1 features and is considerably reduced to 46 (36 + 10) (Fig. 5b) at 4 directions of level-1 features. It can be seen for all features at difference decomposition level. Also, when the level of decomposition is increased from level-1 to level-2, the misclassification rate or

Actual class / Predicted class	Class-X (+ve)	Class-Y (-ve)
Class-X (+ve)	76	22
Class-Y (-ve)	44	58

(a)

Actual class / Predicted class	Class-X (+ve)	Class-Y (-ve)
Class-X (+ve)	84	10
Class-Y (-ve)	36	70

(b)

Actual class / Predicted class	Class-X (+ve)	Class-Y (-ve)
Class-X (+ve)	105	5
Class-Y (-ve)	15	75

(c)

Actual class / Predicted class	Class-X (+ve)	Class-Y (-ve)
Class-X (+ve)	100	7
Class-Y (-ve)	20	73

(d)

Fig. 5 Confusion matrices of level-1 features at different directions **a** 2 directions, **b** 4 directions, **c** 8 directions, **d** 16 directions

Actual class / Predicted class	Class-X (+ve)	Class-Y (-ve)
Class-X (+ve)	80	18
Class-Y (-ve)	40	62

(a)

Actual class / Predicted class	Class-X (+ve)	Class-Y (-ve)
Class-X (+ve)	96	10
Class-Y (-ve)	24	70

(b)

Actual class / Predicted class	Class-X (+ve)	Class-Y (-ve)
Class-X (+ve)	110	4
Class-Y (-ve)	10	76

(c)

Actual class / Predicted class	Class-X (+ve)	Class-Y (-ve)
Class-X (+ve)	98	10
Class-Y (-ve)	22	70

(d)

Fig. 6 Confusion matrices of level-2 features at different directions **a** 2 directions, **b** 4 directions, **c** 8 directions, **d** 16 directions

Actual class / Predicted class	Class-X (+ve)	Class-Y (-ve)
Class-X (+ve)	82	20
Class-Y (-ve)	38	60

(a)

Actual class / Predicted class	Class-X (+ve)	Class-Y (-ve)
Class-X (+ve)	98	5
Class-Y (-ve)	22	75

(b)

Actual class / Predicted class	Class-X (+ve)	Class-Y (-ve)
Class-X (+ve)	112	0
Class-Y (-ve)	8	80

(c)

Actual class / Predicted class	Class-X (+ve)	Class-Y (-ve)
Class-X (+ve)	100	2
Class-Y (-ve)	20	78

(d)

Fig. 7 Confusion matrices of level-3 features at different directions **a** 2 directions, **b** 4 directions, **c** 8 directions, **d** 16 directions

the number of misclassified images is reduced. However, the misclassification rate is reduced when the level changes from level-3 to level-4 and directions from 8 to 16. The main reason is the redundant data at 16 directions that affect the performance of the system. It is clearly showed that 8-direction features provide best results than other directions irrespective of the level of decomposition. From the confusion matrices,

Actual class / Predicted class	Class-X (+ve)	Class-Y (-ve)
Class-X (+ve)	81	22
Class-Y (-ve)	39	58

(a)

Actual class / Predicted class	Class-X (+ve)	Class-Y (-ve)
Class-X (+ve)	95	8
Class-Y (-ve)	25	72

(b)

Actual class / Predicted class	Class-X (+ve)	Class-Y (-ve)
Class-X (+ve)	111	2
Class-Y (-ve)	9	78

(c)

Actual class / Predicted class	Class-X (+ve)	Class-Y (-ve)
Class-X (+ve)	96	3
Class-Y (-ve)	24	77

(d)

Fig. 8 Confusion matrices of level-4 features at different directions **a** 2 directions, **b** 4 directions, **c** 8 directions, **d** 16 directions

Table 3 Best performance measures of LPS

Features	#Features	Accuracy	Sensitivity	Specificity
Level-1 (8 directions)	9	90.00	87.50	93.75
Level-2 (8 directions)	17	93.00	91.67	95.00
Level-3 (8 directions)	**25**	**96.00**	**93.33**	**100**
Level-4 (8 directions)	33	94.50	92.50	97.50

the performance measures are computed using Eq. (3) to (5) and are shown in Table 3.

From Table 3, it is evident that the LPS of the system using level-3 (8 directions) features provides superior performance than others. It gives 100% specificity which means that no misclassification occurs for normal cases. Among 120 images, 8 images of abnormal cases are misclassified as normal, and thus, the sensitivity of the system is 93.33% only, and the accuracy of the system is 96%. As the features from 8 directions of different level of decomposition contribute to the performance improvement of the system, 8-direction features from all levels are considered in the GPS of the system.

3.2 Performance of GPS of the System

In GPS, a single SVM classifier is used to classify the images based on the selected features from the best set of features from each level of decomposition. From Table

3, it is observed the total number of 8-direction features for all levels is 84. Figure 9 shows the confusion matrices of 25% (21 features), 50% (42 features), 75% (63 features) and 100% (84 features) of selected 8-direction features from all level of decomposition.

From the confusion matrices in Fig. 9, the performance measures are computed using Eq. (3) to (5) and are shown in Fig. 10.

Actual class / Predicted class	Class-X (+ve)	Class-Y (-ve)
Class-X (+ve)	107	1
Class-Y (-ve)	13	79

(a)

Actual class / Predicted class	Class-X (+ve)	Class-Y (-ve)
Class-X (+ve)	119	0
Class-Y (-ve)	1	80

(b)

Actual class / Predicted class	Class-X (+ve)	Class-Y (-ve)
Class-X (+ve)	112	1
Class-Y (-ve)	8	79

(c)

Actual class / Predicted class	Class-X (+ve)	Class-Y (-ve)
Class-X (+ve)	110	3
Class-Y (-ve)	10	77

(d)

Fig. 9 Confusion matrices of selected 8-direction features of all level **a** 25% of features, **b** 50% of features, **c** 75% of features, **d** 100% of features

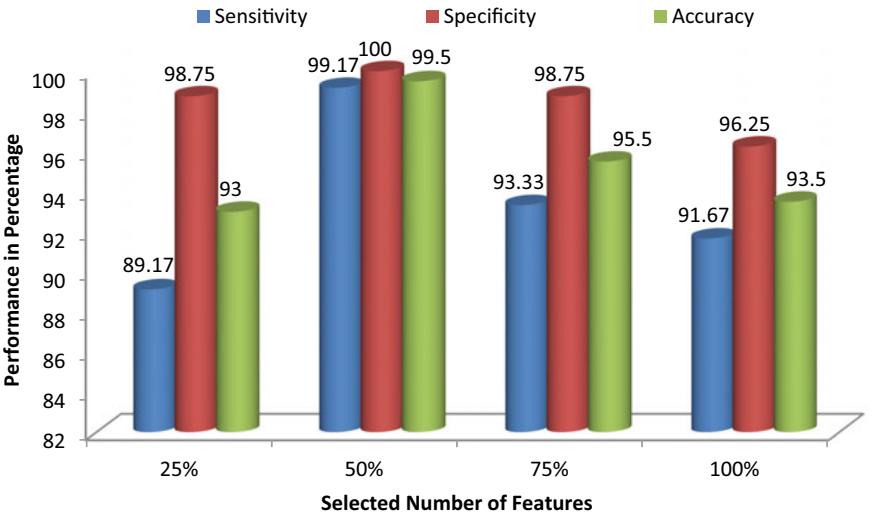

Fig. 10 Performance measures of GPS of the system for skin cancer classification

From Figs. 9 and 10, it is evident that the performance measures obtained by 25% of selected features are lower than the individual analysis of 8-direction level-3 features as only 21 features are involved, whereas 25 features are involved in the individual analysis. The selection of additional features from other levels makes the performance of the system higher. The 50% of selected features provide 99.17% sensitivity and 100% specificity. Further addition of selected features reduces the system accuracy as some of them are redundant and the classifier is unable to distinguish them. The GPS with 50% features is provided higher accuracy of 99.5% than other selected features.

4 Conclusion

In this study, a two-stage processing system is developed to distinguish normal and abnormal dermoscopic images. At first, the system individually analyzes shearlet features from each level and then combines the best directional features of individual level in LPS. Finally, a statistical test is employed in GPS where the best directional features are selected so that the performance of the system can be improved. SVM classifier is used in both stages with same training and testing images. Five SVM classifiers (four classifiers in LPS and one classifier in GPS) are employed in this study. LPS achieves accuracy of 96% on PH^2 database, whereas it is 99.5% for GPS. Also the sensitivity of 99.17% is achieved by GPS, whereas it is 93.33% for LPS. The comparison between LPS and GPS shows that GPS improves the performance of the system to classify skin images [23].

References

1. Albahar MA (2019) Skin lesion classification using convolutional neural network with novel regularizer. IEEE Access 7:38306–38313
2. Khan MQ, Hussain A, Rehman SU, Khan U, Maqsood M, Mehmood K, Khan MA (2019) Classification of melanoma and nevus in digital images for diagnosis of skin cancer. IEEE Access 7:90132–90144
3. Mhaske HR, PhalkeDA (2013) Melanoma skin cancer detection and classification based on supervised and unsupervised learning. In: 2013 international conference on circuits, controls and communications (CCUBE). IEEE, New York, pp 1–5
4. Singh SK, Jalal AS (2016) A Robust approach for automatic skin cancer disease classification. In: 2016 1st India international conference on information processing (IICIP). IEEE, New York, pp 1–4
5. Mahbod A, Schaefer G, Wang C, Ecker R, Ellinge I (2019) Skin lesion classification using hybrid deep neural networks. In: ICASSP 2019–2019 IEEE international conference on acoustics, speech and signal processing (ICASSP). IEEE, New York, pp 1229–1233
6. Maurya R, Singh SK, Maurya AK, Kumar A (2014) GLCM and multi class support vector machine based automated skin cancer classification. In: 2014 international conference on computing for sustainable global development (INDIACom). IEEE, New York, pp 444–447

7. Moldovan D (2019) Transfer learning based method for two-step skin cancer images classification. In: 2019 E-Health and bioengineering conference (EHB). IEEE, New York, pp 1–4
8. Suganya R (2016) An automated computer aided diagnosis of skin lesions detection and classification for dermoscopy images. In: 2016 international conference on recent trends in information technology (ICRTIT). IEEE, New York, pp 1–5
9. Alquran H, Qasmieh IA, Alqudah AM, Alhammouri S, Alawneh E, Abughazaleh A, Hasayen F (2017) The melanoma skin cancer detection and classification using support vector machine. In: 2017 IEEE Jordan conference on applied electrical engineering and computing technologies (AEECT). IEEE, New York, pp 1–5
10. Sonia R (2016) Melanoma image classification system by NSCT features and Bayes classification. Int J Adv Sign Image Sci 2(2):27–33
11. Kumarapandian S (2018) Melanoma classification using multiwavelet transform and support vector machine. Int J MC Square Sci Res 10(3):01–07
12. Manikandan M (2012) Skin detection under varying illumination. Int J MC Square Sci Res 4(1):84–95
13. Bhaskar PC, Munde MV (2017) FPGA implementation of non-subsampled shearlet transform for image fusion. In: 2017 international conference on computing, communication, control and automation (ICCUBEA). IEEE, New York, pp 1–6
14. Priya BL, Jayanthi K (2017) Edge enhancement of liver CT images using non subsampled shearlet transform based multislice fusion. In: 2017 international conference on wireless communications, signal processing and networking (WiSPNET). IEEE, New York, pp 191–195
15. Choi B, Han S, Chung B, Ryou J (2010) Design and performance evaluation of temporal motion and color energy features for objectionable video classification. In: 2010 6th international conference on advanced information management and service (IMS). IEEE, New York, pp 37–41
16. Sharma R, Kumar R, Singh PK, Raboaca MS, Felseghi R-A (2020) A Systematic study on the analysis of the emission of CO, CO_2 and HC for four-wheelers and its impact on the sustainable ecosystem. Sustainability 12:6707
17. Begam S, Selvachandran G, Ngan TT, Sharma R, Similarity measure of lattice ordered multi-fuzzy soft sets based on set theoretic approach and its application in decision making. Mathematics 2020, 8, 1255
18. Thanh V, Rohit S, Raghvendra K, Hoang SL, Thai PB, Dieu TB, Ishaani P, Manash S, Tuong L (2020) Crime rate detection using social media of different crime locations and twitter part-of-speech tagger with brown clustering pp 4287–4299 (2020)
19. Rajan A, Ramesh GP (2015) Glaucomatous image classification based on PCA using optical coherence tomography images. Int J Appl Eng Res 10(17):1–5
20. Wang D, Zhang H, Liu R, Lv W, Wang D (2014) t-Test feature selection approach based on term frequency for text categorization. Pattern Recogn Lett 45:1–10
21. Vijaya Arjunan R (2016) ECG signal classification based on statistical features with SVM classification. Int J Adv Sig Img Sci 2(1)
22. Mohankumar S (2016) Analysis of different wavelets for brain image classification using support vector machine. Int J Adv Sign Image Sci 2(1):1–4
23. PH2 Database Link. https://www.fc.up.pt/addi/ph2%20database.html

Delay and Energy-Aware Forwarder Selection in Wireless Sensor Network

Vamsidhar Yendapalli and B. Ramesh Naik

Abstract Wireless sensor network (WSN) is a promising technology which alters data retrieval from the surroundings through heavily distributed small, least cost as well as less energy wireless device known as sensor nodes. This paper proposes a delay- and energy-aware forwarder (DEAF) selection in WSN. This strategy chooses a route with the least cost that is expected delay (ED) in a multi-hop WSN. Here, the expected delay is computed by queuing delay as well as communication delay via wireless connections. The forwarder node selected by less expected delay as well as the node has the highest amount of outstanding energy. Thus, the source transmits the data packet without packet losses in the network. Simulation is carried out in the network using network simulator-2 and is known that, the introduced scheme performs superior packet obtained rate and lesser delay than the conventional scheme.

Keywords Wireless sensor networks · Energy-aware routing · Communication delay · Queuing delay · Delay-aware routing · Simulation analysis

1 Introduction

Nowadays, WSN is a motivating grassland of examining owing to their numerous applications as well as their incorporation towards extra difficult network systems [1]. WSN is a type of self-governing network component of a huge amount of sensor nodes with inadequate calculation ability, bandwidth, energy also memory [2]. WSNs that can gather the entire varieties of data of supervised objects are mostly utilized in armed, ecological observing, intention chasing health care as well as other fields. Sensor nodes produce real-time data as well as path data to the destination node

V. Yendapalli (✉) · B. Ramesh Naik
CSE Department, GITAM School of Technology, Bengaluru, India
e-mail: whyvamsi@gmail.com

B. Ramesh Naik
e-mail: rameshnaik3@gmail.com

D. K. Sharma et al. (eds.), *Micro-Electronics and Telecommunication Engineering*,
Lecture Notes in Networks and Systems 179,
https://doi.org/10.1007/978-981-33-4687-1_44

through multi-hop transmitting [3]. In a large WSN, the sensor observes the information is transmitting to the base station (BS) takes longer time. Thus, immediate information cannot reach in time. The BS node distributes a database, transmits control controls, and also examines data. To notice some cases WSNs transmission delay happens to the major condition because sensor nodes that are regularly distributed in remote as well as neglected surroundings may be appropriated and its communication data also can be stopped [4].

Quorum time slot (QTS) adaptive condensing (QTSAC) is introduced for attaining delay reduction as well as energy effectiveness in the WSNs. This scheme contains Quorum time slots, which is extremely beginning the sink along with the energy utilization to diminish the delay as well as it apportions Quorum time slot. At the same time, data are communicated to minimize the delay [5]. However, this approach increases that the delay is a significant limitation. The smaller amount the QTSs nodes roundabout slots between the nodes. In this situation, necessitates to communicate data, the delay in noticing the next-hop node in routing is great. Thus, the communication delay is large. To overcome this problem, this paper proposes a delay- and energy-aware relay selection in WSN. This strategy chooses a route with the least cost that is expected delay (ED) in a multi-hop WSN. Here, the expected delay is computed by queuing delay as well as communication delay. The forwarder node selected by less expected delay as well as the node has the highest amount of outstanding energy [6].

2 Related Works

Data aggregation scheduling scheme represents the communication time applies an active programming technique. This scheme utilizes a tree-based formation as an effort for the scheduling technique; thus, it pulls the scheduling to track a collection order forced through the rendered aggregation tree. However, it decreases both energy efficiency and energy and connection capability [7].

Delay-efficient data collection: Scheduling approach creates the collision-free schedule, which diminishes the collection latency. This approach diminishes the sleep delay among nodes, also creating pipelined schedules [8].

Dynamic delay prediction approach renders QoS assurance. In this approach, it discovers routes assembly delay necessity with a huge connection constancy feature. In the route protection stage, it efficiently continues supervising topography updates via delay forecast as well as executes rerouting in time period [9].

Optimal Capacity-Delay trade-off strategy significantly concentrates on the collision of the connection of node movement on the capability-delay trade-off in the networks. This method inquired the character of related movement also figured out the primary association among the capability, delay as well as the connected scheme factors that afterwards offer immense assist to derive the capacity-delay trade-off [10].

Contention Delay Distribution approach searches the delay qualified by the fusion centre until the job is essentially terminated. This approach receives the first as well as second-order stats of the total argument delay. Here, utilize a random geometry structure to discover the rendered traffic owing to an irrupting target entering the observing field also evaluate the related overall disputation delay. This entropy can be utilized to adjust the medium access possibility of the MAC procedure to attain the lowest delay [11]. An opportunistic routing with the responsiveness of energy is used to accept by a dynamic environment. While the sender transmits the information to a multicast group, the sender transmits the information via greater energy between vicinity, thus enhance the life span [12]. Throughput is enhanced with a data-aided valuation method by means of transmitting choice, channel then transmit obligation [13].

3 Proposed Method

This strategy chooses a route with the least cost that is expected delay (ED) in a multi-hop WSN. Here, the expected delay is computed by queuing delay as well as communication delay via wireless connections. The ED over connection i, among nodes, comprises the delay of queue as well as the delay of communication is defined as

$$ED_i = E[\text{delay of queue} + \text{delay of communication}] \tag{1}$$

The communication failure possibility is the chance, which a communication breaks owing to collisions; otherwise, the quality of the bad channel.

The communication delay that is represented as the stage from the time that a packet starts to be served through the MAC layer to the time which it is either effectively communicated otherwise missed after a determined amount of retransmissions. Assume FP_i indicate the communication failure possibility over connection i, also presume it is even through entire retransmissions of the packet. Also, let C_i represents the packet served time throughout connection i, K denotes the greatest amount of retransmissions. Expected communication delay of node i is computed by Eq. 2 is given below.

$$E(C_i) = \sum_{k=1}^{k+1} FP_i^{k-1}(1 - FP_i)^{I\{k<k+1\}} \sum_{j=1}^{k} (E\big[W_j\big] + \frac{P_L}{C_B}) \tag{2}$$

Here, W_j represents the disputation window at the jth backoff step, P_L, C_B indicates the length of the packet as well as connection bandwidth, correspondingly. Along with the 802.11 paradigms, $W_j = 2j - 1\text{Wmin}$ if neglecting the restraint of backoff step, as well as $E[W_j] = W_j - 1$.

In (2), the indicator $I(A)$ is equivalent to 1 if A is true that is obtained to comprise the case which a packet is losses while the retransmission boundary is attained. Additionally, the MAC overhead owing to acknowledgement is integrated into the length of packet P_L for convenience. After utilizing several handlings over, we capable of obtaining

$$E[C_i] = \frac{P_L}{C_B}\left[\frac{1 - FP_i^k}{1 - FP_i}\right] + E[\text{backoff time}] \tag{3}$$

$$E[\text{backoff time}] = \sum_{k=1}^{k+1} FP_i^{k-1}(1 - FP_i)^{I\{k<k+1\}} \sum_{j=1}^{k} (E[W_j]) \tag{4}$$

If therein M_i packets in the queue while a recent packet attains node n_i, the EED metric can be specified as

$$ED_i = (M_i + 1)E[C_i] \tag{5}$$

That intends the total delay transient via the hop matches the MAC serve time of these packets queuing forward of the recent packet together with the MAC serve time of the recent packet itself. Finally, the source transmits the data via the least expected delay node and the highest outstanding energy node in the network. Thus, this approach diminishes both the packet dropped rate and delay in the network.

4 Simulation Analysis

The DEAF through itself can be utilized as a proficient routing metric because it efficiently catches not only the delay of the queue; however, the retransmission delays. We employ NS2.35 simulation results for a WSN. Here, the 50 sensor nodes are arbitrarily distributed in a 600 × 500 ms topology area with required modification to preserve the property. We as well run 4 flows over the arbitrary topology. The node communication range is 200 m, the size of the packet is 512 bytes, and we utilized constant-bit-rate flow.

Figure 1 shows the average delay rate explicitly around recognized with the time period essential to distribute the whole data. This figure proves the proposed scheme DEAF have minimum delay time than the existing scheme QTSAC.

Figure 2 depicts the throughput of DEAF and QTSAC Scheme. It explains that the proposed scheme DEAF has the highest throughput than the QTSAC since DEAF form the route based on delay- and energy-aware routing. In EPSA, undetected wormhole attacker node drops the amount of data packets.

Figure 3 demonstrates the packet loss of DEAF and QTSAC scheme. The DEAF scheme diminishes the loss of data packet since it chooses to select the forwarder

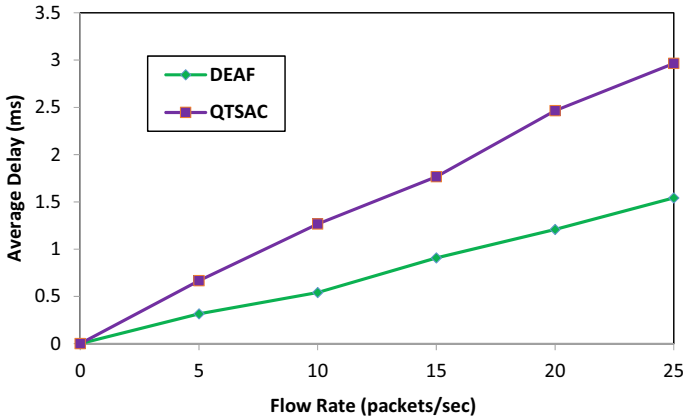

Fig. 1 Average delay of DEAF and QTSAC scheme

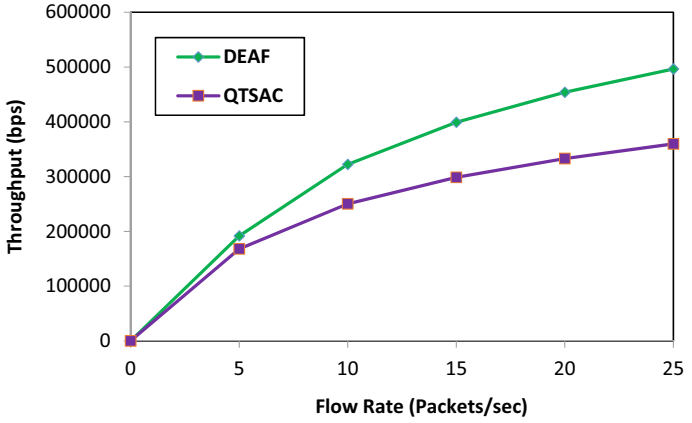

Fig. 2 Throughput of DEAF and QTSAC scheme

node by energy and delay in the network. But, QTSAC utilizes more packet losses. Thus, EWAR increases the packet losses in the network.

5 Conclusion

This paper proposed delay- and energy-aware forwarder selection in WSN the objectives of this paper that initiate route selection with the lower limit delay, whereas greater network throughput. Here, the delay-aware routing is formed based on the node communication delay and queuing delay. The highest outstanding energy and lesser delay node are elected as a forwarder node. Thus increases the network

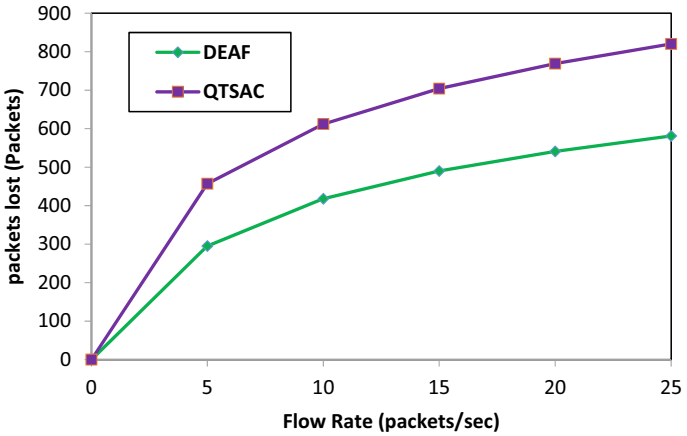

Fig. 3 Packet loss of DEAF and QTSAC scheme

throughput and diminishes the network delay in the network. Simulation results illustrate DEAF approach that provides better than the QTSAC approach.

References

1. Gogu A, Nace D, Dilo A, Mertnia N (2011) Optimization problems in wireless sensor networks. In: 2011 international conference on complex, intelligent, and software intensive systems. IEEE, New York, pp 302–309
2. Ying Z, Changgang J (2014) A kind of routing algorithm for heterogeneous wireless sensor networks based on affinity propagation. In: The 26th Chinese control and decision conference (2014 CCDC). IEEE, New York, pp 2481–2485
3. Zhang Y, Pengfei J (2014) An efficient and hybrid key management for heterogeneous wireless sensor networks. In: The 26th Chinese control and decision conference (2014 CCDC). IEEE, New York, pp 1881–1885
4. Xu M, Yang Q, Kwak KS (2016) Distributed topology control with lifetime extension based on non-cooperative game for wireless sensor networks. IEEE Sens J 16(9):3332–3342
5. Liu Y, Ota K, Zhang K, Ma M, Xiong N, Liu A, Long J (2018) QTSAC: An energy-efficient MAC protocol for delay minimization in wireless sensor networks. IEEE Access 6:8273–8291
6. Irshad SM, Ramesh GP (2020) ANFIS-based MPPT control in current-fed inverter for AC load applications. In: Intelligent computing in engineering. Springer, Singapore, pp 459–469
7. Feng C, Li Z, Jiang S, Jing W (2017) Delay-constrained data aggregation scheduling in wireless sensor networks. Int J Distrib Sens Networks 13(6):1550147717716591
8. Ha NPK, Zalyubovskiy V, Choo H (2012) Delay-efficient data aggregation scheduling in duty-cycled wireless sensor networks. In: Proceedings of the 2012 ACM research in applied computation symposium, pp 203–208
9. Yang P, Huang B (2008) QoS routing protocol based on link stability with dynamic delay prediction in MANET. In: 2008 IEEE Pacific-Asia workshop on computational intelligence and industrial application, vol 1. IEEE, New York, pp 515–518
10. Liu J, Sheng M, Yang Xu, Li J, Jiang X (2015) End-to-end delay modeling in buffer-limited MANETs: A general theoretical framework. IEEE Trans Wireless Commun 15(1):498–511

11. Aldalahmeh S, Al-Jazzar S, Jaradat Y, Masoud M, Hamid Z, Jamioud I (2017) Contention delay distribution in event driven wireless sensor networks. In: 2017 10th Jordanian international electrical and electronics engineering conference (JIEEEC). IEEE, New York, pp 1–4
12. Santhakumar R (2017) Resource allocation in wireless networks by channel estimation and relay assignment using data-aided techniques. Int J MC Square Sci Res 9(3):40–47
13. KeerthiAnand VD (2015) Power efficient multicast opportunistic routing protocol (Pemor) to optimize lifetime of MANET. Int J MC Square Sci Res 7(1):109–127

An Effective Approach for Integrating Microsoft Power BI Application with Python for Predictive Analytics

Vipul Vashisht, Nidhi Jakhmola, Pritish Manjarwar, and Nirav Nikhil

Abstract With the advent of technology and interest of organizations in artificial intelligence (AI), there has been enormous focus in implementing prediction algorithms in data-centric organizations for futuristic business planning. So far, very few approaches have been proposed for integrating machine learning with business intelligence tools, and due to lack of technical documentation, most of these approaches have limited adoption in practice. The objective of this paper is to offer an easy to understand approach that could be quickly adopted for integrating the business intelligence (BI) tool with machine learning (ML). This communication describes a process of applying artificial intelligence technologies, in particular python programming language for integration with Power BI, one of the mostly used business intelligence tools from Microsoft.

Keywords Power BI · Python · Artificial intelligence · Business intelligence · Machine learning

1 Introduction to Business Intelligence

Traditionally, large ERP product organizations like Oracle and SAP used to offer their own business intelligence solution was bundled with their ERP product. It was left to the capability and skill of the ERP consultant or the customer IT team to understand and implement the BI solution at the organization. It continued for a while with limited results to the end customer organization, but slowly, it was understood the business intelligence needs a dedicated solution to cater to the needs of business organizations. The solutions from large organizations were packaged with base ERP and were expensive and difficult to implement. Additionally, the consultant who would perform the implementation was also required to understand the base ERP.

It was in the year 1960 when BI is said to be first evolved from decision support systems (DSS). The need was to use computers for taking timely decisions and

V. Vashisht (✉) · N. Jakhmola · P. Manjarwar · N. Nikhil
Lagozon Technologies Private Limited, Noida, India
e-mail: vipul@lagozon.com

D. K. Sharma et al. (eds.), *Micro-Electronics and Telecommunication Engineering*,
Lecture Notes in Networks and Systems 179,
https://doi.org/10.1007/978-981-33-4687-1_45

creating plans. In the year 1989, Howard Dresner defined BI as concepts and methods to improve decision making in organizations by implementing systems which are based on factual data and numbers [1].

Today, with the rapid rise in generation and consumption of data, it becomes very important for any organization to integrate and analyze its multiple sources of data as a single source of truth for data-based decision making. The analysis is available on multiple platforms for consumption such as desktop, tablet, web and mobile phones. In view of the fact that data-based decision making is now also required at multiple levels in the organization, not just at the level of the senior management. The end users of this BI software may not be software developers and they could just be a sales manager or a finance manager, who want to analyze the sales revenue or profitability. In these cases, there is a need to provide a simple to understand and easy to implement software, which can be configured and maintained by any business user in the organization, not just the software or the IT team. Some of such popular modern BI tools which are intended for end customer use available in market are Qlik Sense, QlikView, Microsoft Power BI, Tableau and ThoughtSpot. It is common nowadays for many organizations, specifically in manufacturing sector, to extend the allocation of BI software to the distributors, retailers and even the third-party members [2, 3].

Some of the advantages of using modern BI tools include:

- Improving equipment efficiency,
- Identifying business trends to generate meaningful insights,
- Eradicating cases of data manipulation cases,
- Empowering the business users to perform detailed analysis,
- Offering integration with machine learning for predictive and advanced analytics,
- Enabling self-service analytics, users import data and create their own dataset and calculations, followed by reports and dashboards.

In today's world, due to its cost-effectiveness and capabilities to integrate with multiple data sources, Power BI has become hugely popular BI software among organizations across the globe. There have been multiple business requirements being seen in organizations, where solution requires prediction algorithm application on data to arrive at future forecast for sales, finance and other departments. In this research paper, an end-to-end approach has been proposed to integrate Power BI dashboards with machine learning abilities of python programming language. Usage of AI-based approaches is essentially changing the discipline of business intelligence for the better. As per prediction from Gartner, a leading research and advisory organization, by 2020, citizen data scientists will surpass data scientists in the amount of advanced analysis they produce, largely due to the automation of data science tasks. This would be led by integration of BI- and AI-based tools and technologies [4].

1.1 Power BI

Power BI is a BI software from Microsoft. For 13 consecutive years, Gartner has recognized Microsoft as a Magic Quadrant Leader in analytics and Business Intelligence Platform (Microsoft Power BI). Power BI runs on Microsoft Azure Cloud as a service and can quickly connect to multiple data sources irrespective of those sources residing on cloud or on-premise. Power BI connects to data sources, visualizes and discovers what is important and shares that with anyone or everyone. Power BI is a cloud computing-based technology which runs on Microsoft cloud computing platform, Azure. The tool has got capability to scale up to thousands of users and integrate with multiple different data sources like SAP, Oracle, Salesforce, SQL Server and flat files.

1.2 Python

Python is an open-source, high-level programming language. It was developed by Guido van Rossum in the year 1991 under Python Software Foundation. Being developed and distributed under an open-source license, it is free to use by anyone. With the advent of an increased interest globally for artificial intelligence and machine learning algorithms, multiple product vendors such as Microsoft have designed their analytics tool to have a possible integration with python. Python is most commonly used for developing desktop-based GUI applications, Web sites and web applications [5].

1.3 Benefits of Power BI and Python Integration

Microsoft has recently converged the BI software and ML capabilities using python programming language in the Power BI software. Power BI has the capability to run scripts directly by invoking the python executable file from the path where it is stored on the machine [6]. Python is a powerful object-oriented language and is used by the data analyst and scientist to analyze complex datasets. The BI developer can directly make use of visual libraries in python such as Seaborn, and Matplotlib. Through Power BI interface, scripts written in python can also be used to apply machine learning algorithms and then plot the results in Power BI reports using available visualization packages under python (Fig. 1).

Next, we provide insights from the literature review of past research work done in the subject area.

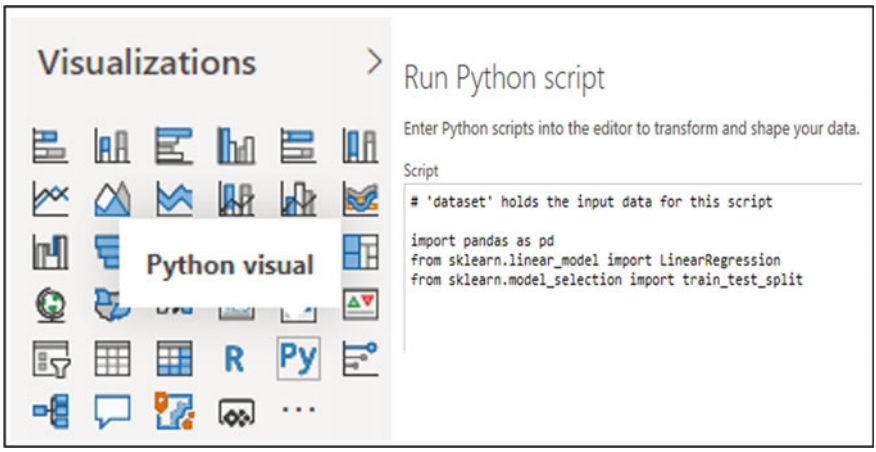

Fig. 1 Running python script from Power BI

2 Literature Review

There is still lack of research into progression of AI and BI. These areas are still limited to technical developers for most of the usage, and there is a need to further find innovative ways to provide freedom to humans from tedious repetitive tasks of data analysis and reporting [7].

As per the study conducted by Microsoft research team in relation to Power BI product, it was observed that it was possible for generating AI-enabled insights from variety of data sources imported in BI software. There are interfaces available with Microsoft Azure components and machine learning studio. Authors suggested that there is a huge impact of BI on AI and extending the access of business intelligence-driven decision making to all [8].

The application area of BI is diverse that covers multiple industries, including banking, insurance, pharma, automobiles, hospitals, hotels and many others. Within these industries, BI software caters to the need of multiple departments, including sales, finance, supply chain management, human resources and marketing. Some of the subjects include computational intelligence involving neural networks, customer satisfaction and formulation of business strategy [9, 10].

As a part of research, a Power BI dashboard for higher education domain was built using the data inputs received from social media platform twitter. The dashboard analysis suggested that the social media platform was being used for academic-related activities and not for collaboration and debating ideas. The analytics provided insights to take corrective and preventive actions to improve the feedback from users regarding the platform [11].

As per the authors of the book chapter, the visualization layers that includes multiple dashboards, charts, KPIs and reports that get consumed by the likes of senior management for decision making have been really helpful in cascading the

communication and keeping the stakeholders on the same page with respect to data analytics [12].

3 Data Model Design Approach

The objective of research paper is to integrate Power BI dashboards and visualization analytics to predictive analytics capability of machine learning, in particular, python programming language. For showcasing the capability, authors have taken permission to use the organizational data for academic and research purposes. Some of the customer details have been masked in the provided dataset from the organization.

The sales data has been imported from backup file of SQL database, and connectivity with Power BI has been created. After importing the database, relationship between different tables present is shown in Fig. 2. After adding multiple data items to the Power BI visualization, the tool automatically tries to detect the relationship between the columns. Data modeling is used to connect multiple data sources in BI tool using relationship.

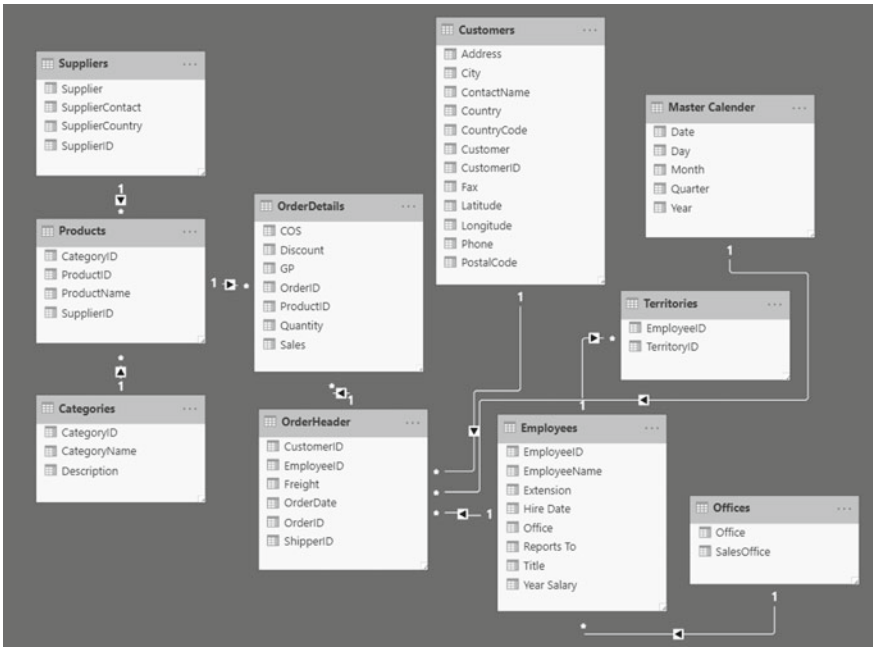

Fig. 2 Data model

3.1 Using Linear Regression Algorithm in Python with Power BI

Authors have used a sample data set and predicted sales with the help of linear regression algorithm. The code snippet used for running python script for executing linear regression algorithm from within Power BI interface is provided below:

```
#Load in the dependencies
import pandas as pd
import numpy as np
from sklearn.model_selection import train_test_split
from sklearn.linear_model import LinearRegression
from sklearn.preprocessing import StandardScaler
#preprocess your data
y=dataset['Sales']
features = ['Quantity','COS','GP']
X=dataset[features]
#lets scale the data
s = StandardScaler()
X = s.fit_transform(X)
#split and train the dataset
X_train,X_test,y_train,y_test = train_test_split(X,y)
#Let the model predict results
log = LinearRegression()
log.fit(X_train,y_train)
y_pred = log.predict(X)
# Lets add the columns back to the dataset
dataset['linearpredictions'] = y_pred
dataset['linearscore'] =  log.score(X_test,y_test)
```

3.2 Using Support Vector Regressor Algorithm in Python with Power BI

Support vector regressor (SVR) has been used as a regression method, maintaining all the main features that characterize the algorithm (maximal margin). The code snippet used for running python script for executing SVR algorithm from within Power BI interface is provided below:

```
#Load in the dependencies
import pandas as pd
import numpy as np
from sklearn.model_selection import train_test_split
from sklearn.linear_model import LinearRegression
from sklearn.preprocessing import StandardScaler
#preprocess your data
y=dataset['Sales']
features = ['Quantity','COS','GP']
X=dataset[features]
#lets scale the data
s = StandardScaler()
X = s.fit_transform(X)
#split and train the dataset
X_train,X_test,y_train,y_test = train_test_split(X,y)
#Let the model predict results
from sklearn.svm import SVR
regressor=SVR(kernel='linear')
regressor.fit(X_train,y_train)
svrpred = regressor.predict(X)
# Lets add the columns back to the dataset
dataset['svrpred'] = svrpred
dataset['svrscore'] =  regressor.score(X_test,y_test)
```

4 Results and Discussion

After predicting the sales by using different algorithms like linear regression, logistic regression and support vector regressor (SVR), key performance indicators or (KPIs) are created as shown in Fig. 3. In the figure, dashboard has got defined expected sales based on linear regression prediction, logistic regression prediction and SVR prediction and actual sales from the organization dataset.

The steps used in experiments were able to successfully demonstrate the power of python algorithms used for predictive analytics and its close integration with Power BI. It can be observed that 1.78 million sales have been predicted from linear regression and 1.30 million sales prediction came from SVR algorithm.

5 Future Work

Outputs from our implementation will provide researchers, BI consultants and data scientists access to a validated approach to integrate the two technologies, namely business intelligence and artificial intelligence. Our results are based on usage of

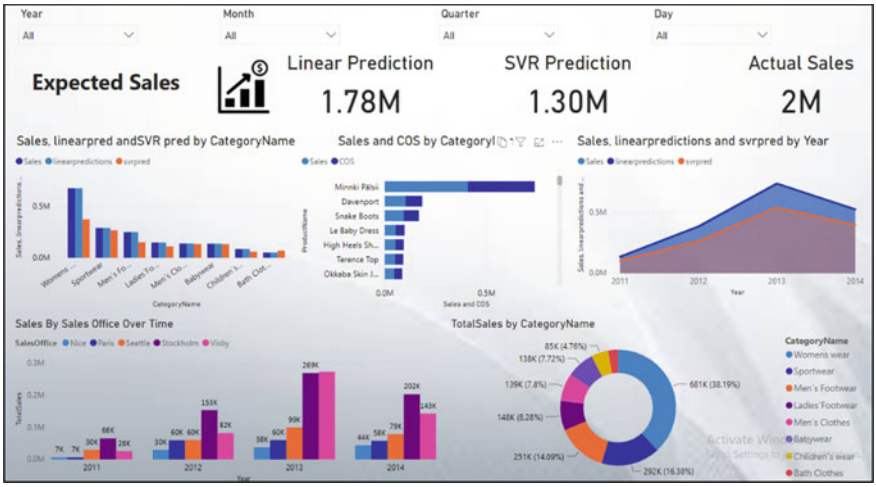

Fig. 3 Power BI dashboard with predictive analytics

organization data from sales domain for generating KPIs and dashboards in Power BI and then integrating with python for generating predictive analytics and displaying the predictions on Power BI visualization layer. In future communication, experimenting the integration of business intelligence tools with multiple other AI-based tools available in market such as MATLAB and R may be explored.

References

1. Power DJ (2007) A brief history of decision support systems. DSSResources. Com
2. Vera-Baquero A, Colomo-Palacios R, Molloy O (2013) Business process analytics using a big data approach. IT Professional 15(6):29–35
3. Seufert A, Schiefer J (2005) Enhanced business intelligence-supporting business processes with real-time business analytics. In: 16th international workshop on database and expert systems applications (DEXA'05). IEEE, New York, pp 919–925
4. Gartner (2020) Gartner Reveals Five Major Trends Shaping The Evolution Of Analytics And Business Intelligence. [online] Available at: https://www.gartner.com/en/newsroom/press-releases/2019-10-02-gartner-reveals-five-major-trends-shaping-the-evoluti. Accessed 14 Sept 2020
5. Wikipedia contributors, "Python (programming language)," Wikipedia, The Free Encyclopedia. Accessed 13 Sept 2020
6. Docs.microsoft.com. 2020. Run Python Scripts In Power BI Desktop - Power BI. [online] Available at: https://docs.microsoft.com/en-us/power-bi/connect-data/desktop-python-scripts. Accessed 14 Sept 2020
7. Analytics Insight. 2020. AI And BI: Powering The Next-Generation Of Analytics. [online] Available at: https://www.analyticsinsight.net/ai-and-bi-powering-the-next-generation-of-analytics/. Accessed 14 Sept 2020

8. Edge D, Larson J, White C (2018) Bringing AI to BI: enabling visual analytics of unstructured data in a modern BI platform. In: Extended abstracts of the 2018 CHI conference on human factors in computing systems, pp 1–9
9. Baesens B, Setiono R, Mues C, Vanthienen J (2003) Using neural network rule extraction and decision tables for credit-risk evaluation. Manage Sci 49(3):312–329
10. Soliman KS, Mao E, Frolick MN (2000) Measuring user satisfaction with data warehouses: an exploratory study. Inf Manage 37(3):103–110
11. Varela B, Bernardino J, Pedrosa I (2020) Twitter sensitivity analysis in a higher school using power BI. In: 2020 15th Iberian conference on information systems and technologies (CISTI). IEEE, New York, pp 1–6
12. Familiar B, Barnes J (2017) Data visualizations, alerts, and notifications with power BI. In: Business in real-time using Azure IoT and Cortana intelligence suite. Apress, Berkeley, CA. https://doi.org/10.1007/978-1-4842-2650-6_9

Traffic Sign Recognition Using Multi-layer Color Texture and Shape Feature Based on Neural Network Classifier

Manisha Vashisht and Brijesh Kumar

Abstract In the last decades, with the rapid changes taking place in both hardware and software technology domains, the field of image acquisition, image detection, and recognition has undergone drastic revolution bringing innovations for overall improvements. So far, there has been limited research conducted on mapillary dataset of traffic signage images, and the results obtained are not so encouraging. The research contributes toward providing an innovative approach of extracting color features and then using artificial neural network for image recognition purposes. This research is conducted on a mapillary image dataset of 5000 images, and the results have found to be encouraging. The dataset has been made freely available for academic research.

Keywords Image recognition · Artificial intelligence (AI) · Computer vision · Traffic signage · Mapillary traffic sign dataset (MTSD) · MATLAB · Machine learning (ML)

1 Introduction

In order to avoid accidents across the globe, it is utmost necessary to follow the traffic rules while driving. With reference to the research done by National Highway Traffic Safety Administration (NHTSA), it has been observed that human mistakes account for 94% of the reasons of road accidents. In the year 2017, research findings presented had an observation that 52,274 drivers involved in 34,247 road accidents, in which 37,133 people lost their lives. In view of these findings, it becomes important for research community to find out ways using innovative tools and technologies which can help in reducing these fatal accidents that amounts for huge loss of life and property [1].

As a global standard, traffic signage has been used across the world to help drivers take quick decisions and avoid road accidents. The traffic signage is placed on roads

M. Vashisht (✉) · B. Kumar
Manav Rachna International Institute of Research and Studies, Faridabad, India
e-mail: manishavashisht@gmail.com

D. K. Sharma et al. (eds.), *Micro-Electronics and Telecommunication Engineering*,
Lecture Notes in Networks and Systems 179,
https://doi.org/10.1007/978-981-33-4687-1_46

considering these boards are always visible to everybody in all weather conditions [2]. This research paper has used public dataset of traffic signage images from mapillary research, which is one of the most popular crowdsourcing platforms that offer detailed street level imagery. Mapillary image dataset has got around 100,000 images from worldwide locations, covering six continents with varying weather conditions, captured during varying time during the day and has 300 traffic sign classes with bounding box annotations [3, 4].

This research paper deals with design and implementation of artificial neural network-based model using mapillary image datasets that can help in traffic signage object recognition. Authors have taken required permissions from mapillary research team to use the dataset for research purposes.

1.1 Image Transformation

It has been observed that most of the image detection methods used by researchers in past have made use of the algorithms based on the concept of feature extraction. Such image detection methods need features based on color and shape for image transformation purposes. In view of the fact, in regard to working with different light conditions, there are certain restrictions for color feature extraction based on RGB (red, green, blue) color space. In order to overcome such limitations, in most cases, these images are transformed to other available color spaces. One of such color spaces which is used for image transformation in this research paper is HSV (hue, saturation, value) [5–10]. Considering the RGB color circle, hue denotes the color's angle whereas saturation monitors the quantity of the color actually used, and value refers to the brightness part of the color. These values are interdependent on each other. For an example, if the value parameter is configured to be zero, then irrespective of any representation of hue and saturation, the output will always be black. HSV is depicted as a cylindrical color model where colors are mixed and then are shown within the cylindrical bounds, making it easier for human beings to understand. This has been one of the reasons for researchers considering hue-based color features in areas addressing traffic signage detection problems [11–15].

1.2 Artificial Neural Networks

ANN relates to the existence of neurons in human brain and an attempt at simulating the abilities of the human nervous systems. Historically, ANN has been widely used by researchers in areas addressing computational intelligence-based problem statements. Neural networks have got an inherent property to learn from patterns of data. Once the model has been trained, it can be used to predict the outcome of similar patterns in the future. For this capability, ANN has been widely used in solving multiple software engineering problems requiring predictions such as cost

predictions, sales predictions, and defect predictions. Since traffic signage recognition related problem also requires model to learn from the pattern of available image datasets and then recognize the correct signage image, the authors have used ANN as a technique to build a model in this research paper [16–21].

The paper is organized as below:

- Section 2 covers the literature review, describing work done in the similar area by researchers in past,
- Section 3 describes the high-level black diagram and the ANN framework,
- Section 4 provides the results of ANN model, and
- Section 5 concludes with guidance on the future scope of work.

Next, we provide insights from the past research work done in the subject area of research.

2 Literature Review

It was in the year 2001 when Viola-Jones [22] brought the concept of real-time face detection using technique of sliding window and feature using multi-scale. Then, in the year 2005, pedestrian movement detection was proposed by Dalal and Triggs [23] using concept of histogram of oriented gradients (HOG). In 2006, Gao et al. [24] proposed that shape feature extraction when used along with color feature extraction was able to provide improved results for recognizing traffic signage for still images taken under varying weather conditions. A traffic signage system has been designed in 2007 specifically for roads in Italy by Broggi et al. [25] using color segmentation, shape recognition, and ANN. RGB color space when used with linear transformations resulted in reduction of the computational time, thus leading to detection accuracy of up to 30 m ahead. In 2008, Mingqiang et al. [26] compared around 40 feature extraction methods based on shapes and classified on processing approaches, including shape signatures, moments approaches, and shape transform domains. Later, in the same year 2008, Felzenszwalb et al. [27] proposed deformable part models (DPMs) method by extending the ideas from HOG approach. These algorithms used in traditional approaches toward object detection had multiple limitations which later gave rise to computational algorithms-based approaches. Benco et al. [28] in 2014 studied the gray-level co-occurrence matrix (GLCM) and then modified it in order to extract probability matrices from the color image for texture classification.

Singh et al. [29] in 2018 build an ANN model that used German traffic sign recognition benchmark (GTSRB) which had 50,000 images under 40 classes. The result showed overall accuracy of close to 97% on the test data. Tabernik, D. and Skočaj [30] in 2019 introduced convolutional neural network (CNN) based solution for traffic signage detection for almost 200 traffic sign categories. Results showed a mean average precision (mAP) of close to 95%. Work done by Ng et al. [31] in year 2020 using Yolov2 and Yolov3 image detection using mapillary dataset estimates

traffic risk using the risk estimation network, the results achieved are in range of 60% to 70% depending on real and virtual datasets.

3 Proposed Framework for Model Design

For purpose of developing traffic signage detection framework, the high-level architecture diagram is shown in Fig. 1. In the mapillary traffic signage image dataset, out of available 100,000 images, 52,000 images have been fully verified and annotated by humans, while the remaining images have been annotated partially, using computer vision technology.

HSV, HSI, and HSL are the three most common cylindrical coordinate representations of points in an RGB color model. These representations are very similar, but not completely identical. Three features are requiring color, texture, and shape. The process of annotating an image includes image selection approval, traffic sign localization by drawing bounding boxes, and class label assignment for each box. In Fig. 2 showing annotations, 'bbox' means bounding box dimensions which are

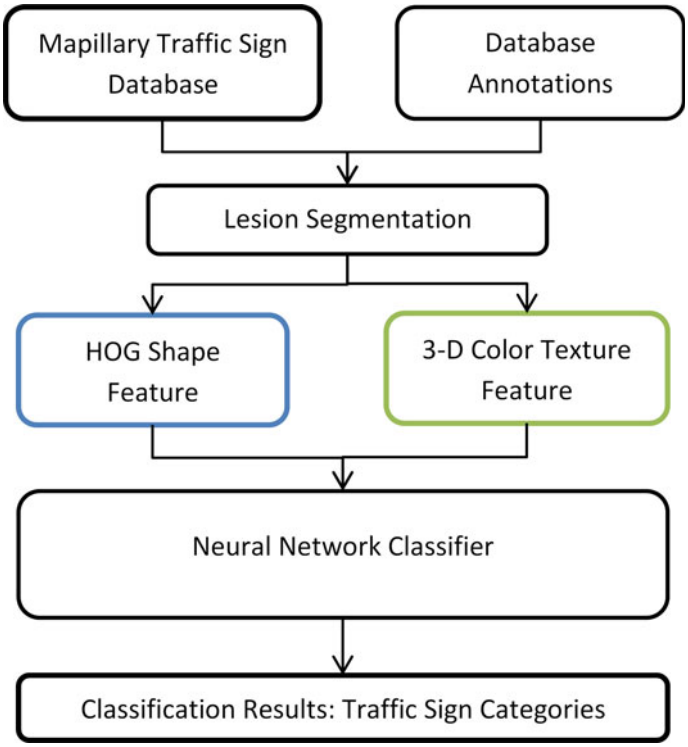

Fig. 1 High-level block diagram

Fig. 2 Database image and highlighted traffic signage [3]

used to crop the lesion region from original image. 'Label' is the category to which the bbox belongs.


```
{
"width": 4000,
"objects": [
  {{
    "properties": {
      "ambiguous": false,
      "dummy": false,
      "direction-or-information": false,
      "barrier": false,
      "occluded": false,
      "out-of-frame": false,
      "exterior": false,
      "included": false,
      "highway": false
    },
    "bbox": {
      "xmin": 2822.265625,
      "ymin": 1396.728515625,
      "ymax": 1459.716796875,
      "xmax": 2895.5078125
    },
    "key": "2zg0ip4044g08y9ewc5moq",
    "label": "regulatory--yield--g1"
  }
```


In this research experiment, 3D combined color texture feature and HOG shape have been used. Sizes of 128 × 128 cropped lesion regions of HSV and color texture datasets are evaluated with parameters as described in Table 1.

ANN-based network has been configured using the below mentioned network configuration parameters, as shown in Table 2.

Table 1 Image dataset parameters

S. No.	Parameters	Description
1	Dimensions of hog features	1×324
2	Dimensions of 3D color texture features	4×12 and transformed to 1×48
3	Final feature dimension per image	1×372
4	Input features to classifier dimension:	5000×372
5	Target dimension	1×372

Table 2 Parameters for network configuration

S. No.	Parameters	Description
1	Training samples	5000
2	Annotation format	Json
3	Categories	40
4	Network layer	10
5	Data division for network use	Training (70%), validation (15%) & testing (15%)

MATLAB tool provides access to neural network toolbox which has been used to design, develop, train, and validate an ANN-based model. By default, the number of hidden layers is set to 10. This number can be changed, as per the need. Hidden layers help in optimizing the model results. Levenberg–Marquardt algorithm is used for training the network considering its lesser memory requirement, better optimization capability, and fast speed. Figure 3 shows the neural network and displays algorithms used for data division and training.

4 Results

The regression value depicts a closer relationship with respect to object recognition results. The R value measures the correlation between outputs and targets. Figure 4 represents the regression relationship and defines the prediction reliability of the network designed. Overall test result on our proposed framework conducted on 5000 images has R value of 0.80 which is better as compared to work done on same datasets using CNN [32]. The value of R denotes a closer relationship and prediction capability.

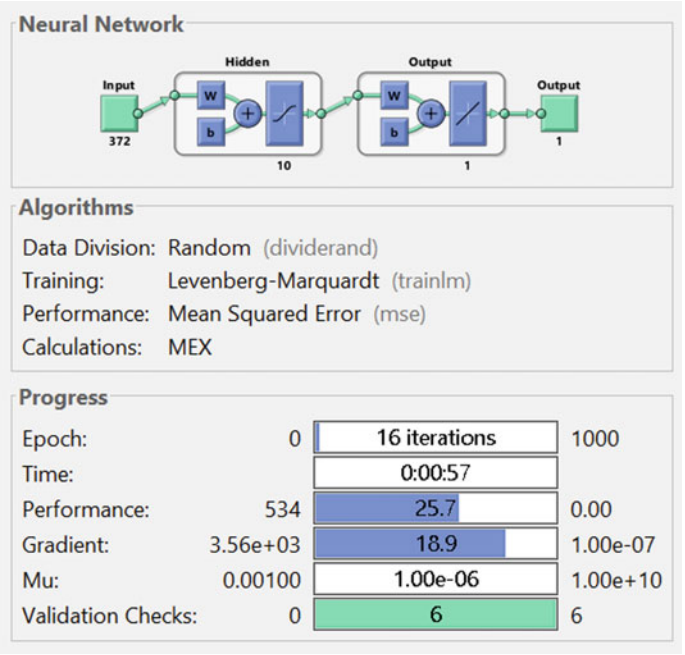

Fig. 3 ANN configuration

5 Conclusion

Results from our experiments recommend that the proposed framework based on ANN has provided comparable metrics with 0.80 value of R. The result further suggests that model has good quality of fit and capability of prediction. The conclusion is built on experiments conducted using 5000 images from mapillary traffic signage image dataset and application of artificial neural networks for image recognition. For future, it is recommended to improve the predictions further by extending the ANN-based results to implement using multiple other machine learning classification algorithms.

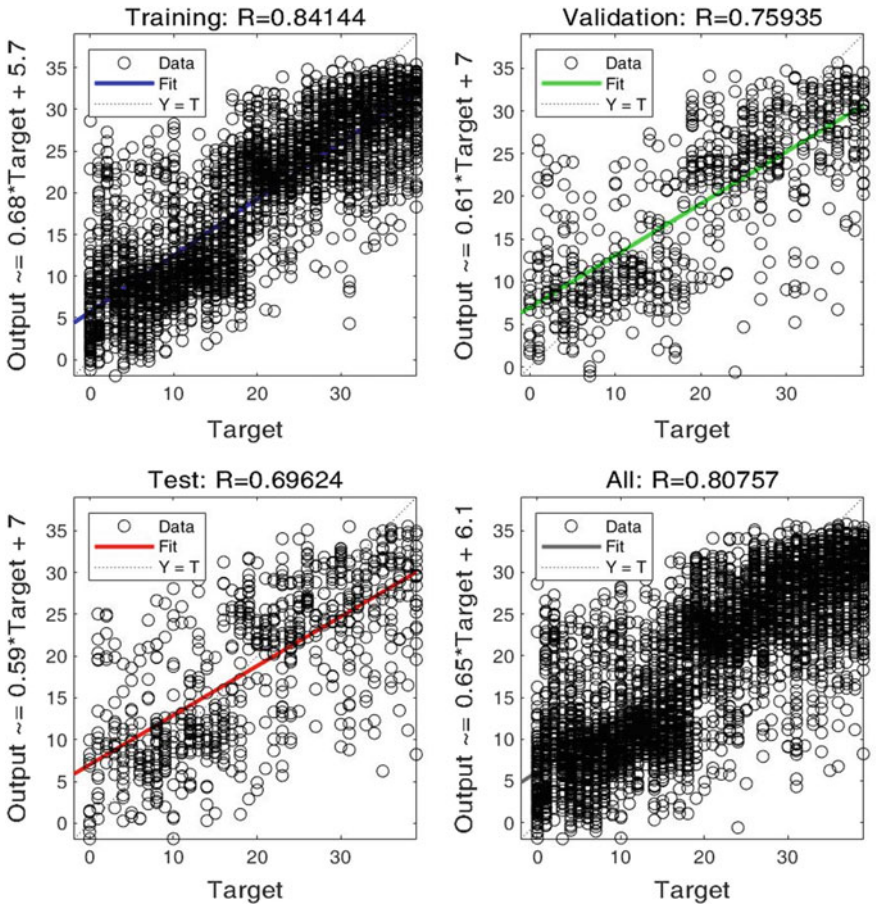

Fig. 4 Regression results

References

1. Traffic Safety Facts, Research Note, NHTSA's National Center for Statistics and Analysis, April 2019
2. Congress IR (2012) Code of practice for road signs
3. Mapillary AB S (2020) Mapillary - Street-Level Imagery, Powered by Collaboration And Computer Vision. [online] Mapillary.com. Available at: https://www.mapillary.com/dataset/trafficsign. Accessed 14 Sept 2020
4. Ma D, Fan H, Li W, Ding X (2020) The state of mapillary: an exploratory analysis. ISPRS Int J Geo-Inform 9(1):10
5. Wang G, Ren G, Quan T (2013) A traffic sign detection method with high accuracy and efficiency. In: Proceedings of the 2nd international conference on computer science and electronics engineering. Atlantis Press
6. Zhang J, Huang M, Jin X, Li X (2017) A real-time chinese traffic sign detection algorithm based on modified YOLOv2. Algorithms 10(4):127

7. Kaplan K, Kurtul C, Akİn HL (2012) Real-time traffic sign detection and classification method for intelligent vehicles. In: 2012 IEEE international conference on vehicular electronics and safety (ICVES 2012). IEEE, New York, pp 448–453
8. Qian R, Zhang B, Yue Y, Wang Z, Coenen F (2015) Robust Chinese traffic sign detection and recognition with deep convolutional neural network. In: 2015 11th international conference on natural computation (ICNC). IEEE, New York, pp 791–796
9. Mingqiang Y, Kidiyo K, Joseph R (2008) A survey of shape feature extraction techniques. Pattern Recogn 15(7):43–90
10. Benco M, Hudec R, Kamencay P, Zachariasova M, Matuska S (2014) An advanced approach to extraction of colour texture features based on GLCM. Int J Adv Rob Syst 11(7):104
11. Warsi F, Khanam R, Kamya S, Suárez-Araujo CP (2019) An efficient 3D color-texture feature and neural network technique for melanoma detection. Inform Med Unlocked 17:100176
12. Gao XW, Podladchikova L, Shaposhnikov D, Hong K, Shevtsova N (2006) Recognition of traffic signs based on their colour and shape features extracted using human vision models. J Vis Commun Image Represent 17(4):675–685
13. Gupta S, Trivedi MC (2016) Hand skin classification from other skin objects using multi-direction 3D color-texture feature and cascaded neural network classifier. In: Proceedings of international conference on ICT for sustainable development. Springer, Singapore, pp 523–534
14. Singh S, Gupta SC (2016) Human object detection by HoG, HoB, HoC and BO features. In: 2016 fourth international conference on parallel, distributed and grid computing (PDGC). IEEE, New York, pp 742–746
15. Del Alamo CJL, Pérez LJF, Calla LAR, Lovón WRR (2013) A novel approach for image feature extraction using HSV model color and niters wavelets. In: 2013 XXXIX Latin American computing conference (CLEI). IEEE, pp 1–7
16. Munakata T (1998) Fundamentals of the new artificial intelligence, vol 2. Springer, Heidelberg, Germany, p 43
17. Vashisht V, Lal M, Sureshchandar GS (2015) A framework for software defect prediction using neural networks. J Software Eng Appl 8(08):384
18. Vashisht V, Lal M, Sureshchandar GS (2016) Defect prediction framework using neural networks for software enhancement projects. J Adv Math Comput Sci, pp 1–12
19. Vashisht V, Measuring and analyzing the impact of implementing sub process monitoring and defect prediction model in the software development life cycle. shodhganga.inflibnet.ac.in
20. Vashisht V, Kamya S, Vashisht M (2020) Defect prediction framework using neural networks for business intelligence technology based projects. In: 2020 international conference on computer science, engineering and applications (ICCSEA). IEEE, New York, pp 1–5
21. Boetticher G, Srinivas K, Eichmann DA (1992) A neural net-based approach to software metrics
22. Viola P, Jones M (2001) Robust real-time face detection. In: null. IEEE, New York, p 747
23. Dalal N, Triggs B (2005) Histograms of oriented gradients for human detection. In: 2005 IEEE computer society conference on computer vision and pattern recognition (CVPR'05), vol. 1. IEEE, New York, pp 886–893
24. Broggi A, Cerri P, Medici P, Porta PP, Ghisio G (2007) Real time road signs recognition. In: 2007 IEEE intelligent vehicles symposium. IEEE, New York, pp 981–986
25. Felzenszwalb PF, Girshick RB, McAllester D, Ramanan D (2009) Object detection with discriminatively trained part-based models. IEEE Trans Pattern Anal Mach Intell 32(9):1627–1645
26. Singh M, Pandey MK, Malik L (2018) Traffic sign detection and recognition for autonomous vehicles. Int J Adv Res Ideas Innov Technol (IJARIIT) 4(2):1666–1670
27. Tabernik D, Skočaj D (2019) Deep learning for large-scale traffic-sign detection and recognition. IEEE Trans Intell Transp Syst 21(4):1427–1440
28. Ng KC, Murata Y, Masayasu A (2020) Performance enhancement of region-based spatio-temporal neural network for traffic risk estimation using real and virtual datasets

Secured Library Access Through Face Recognition Integrated with RFID Technology

P. Anantha Prabha, S. A. Vighneshbalaji, M. Deva Priya, and R. Suguna Devi

Abstract Securing resources in the library is one of the prime concerns by preventing the entry of unauthorized users into the library. Saving time of users at entry/exit and circulation points is the next key concern. To access the library, the member is expected to swipe or scan his smart or IDentity (ID) card at the entry/exit point, and he/she is expected to wait at circulation points for the issue of books. In this system, members cannot access the library if they forgot to bring or miss their cards. Unauthorized persons can also easily enter into the library with stolen or duplicate ID cards. In order to secure and automate the library, a new system of accessing the library is proposed with deep learning and Radio-Frequency IDentification (RFID) technology. The proposed system focuses on automating the authentication of user with face recognition at the entry/exit point (turnstile) and providing them good user experience and automating the issue of books (RFID tagged) by using RFID detectors at the exit point. This system yields good results with our test datasets. Activation of this system at library premises ensures security and also facilitates auto checks-in and out, and thus saves users' valuable time.

Keywords Deep learning · Face recognition · Library · User experience · RFID

P. Anantha Prabha · S. A. Vighneshbalaji · M. Deva Priya (✉)
Department of Computer Science & Engineering, Sri Krishna College of Technology, Coimbatore, Tamil Nadu, India
e-mail: m.devapriya@skct.edu.in

P. Anantha Prabha
e-mail: p.ananthaprabha@skct.edu.in

S. A. Vighneshbalaji
e-mail: savighneshbalaji@gmail.com

R. Suguna Devi
Department of Electrical and Electronics Engineering, Mohamed Sathak A. J. College of Engineering, Chennai, Tamil Nadu, India
e-mail: rsdsaran2008@gmail.com

D. K. Sharma et al. (eds.), *Micro-Electronics and Telecommunication Engineering*, Lecture Notes in Networks and Systems 179,
https://doi.org/10.1007/978-981-33-4687-1_47

1 Introduction

Fast acceleration of technology advancements brings new user experience in almost all the sectors. Radio-Frequency IDentification (RFID) and Internet of Things (IoT) find their application in many areas [1, 2]. Libraries are also in the position to serve users with several service expectations. Academic libraries include many resources in the form of Compact Disks (CDs), e-journals, books, theses, reports, monographs, etc. Various types of library management software are available to efficiently manage library resources. The key function of the library management system includes cataloging, circulation, serial control, article indexing, etc.

In the last decade, bar code technology was very popular in libraries, and they managed various resources with bar codes. The use of this technique reduced the time spent at circulation points, improved the quality of services, increased user experience and improved information availability and data integrity. But this system has some limitations. Line of Sight (LoS) is required, storage of information is not possible and only a single bar code can be read at a time. The invention of RFID technology changed the way how the library resources are managed. RFID-based library management system includes tagged (RFID) books/CDs/items, and RFID reader connected with local or cloud server. This system saves the time of users by automating borrowing and returning books, tracking books, saving the time of library staff, etc. With this system, automation can be achieved to some extent, but securing the resource from unauthorized users is still a major problem in libraries. Unauthorized persons can easily enter into the library by using duplicate or stolen ID cards. The proposed system uses deep learning techniques to enhance the security of library. Deep learning is used for various applications such as image recognition, speech recognition and Natural Language Processing.

More recently, deep learning methods outperform in the area of face recognition and yield good results when applied to benchmarked face detection datasets. The proposed system facilitates auto checks-in and out with face recognition at the entry/exit points and prevents unauthorized access. Face recognition system with deep learning is integrated with RFID technology to fully automate the process of issue/return of books. The paper organization is as follows. Section 2 deals with the works related to library management systems. Section 3 describes the proposed model with relevant architectures. Implementation and results are discussed in Sect. 4. Conclusion and future scopes are given in Sect. 5.

2 Related Works

Revolution of technological advancements has a great impact on library services. It paves the way for new user experience at libraries. Most of the libraries use barcode technology for the maintenance of books and also issue and return of books. The RFID technology helps the librarians to improvise their services. Monitoring and managing

various resources in the library is made easy and simple with RFID technology [3]. Nayagam et al. have proposed an automation and authorization scheme using RFID technology [4]. Their idea is about identifying books within the range of RFID signals, ensure automatic authorization and prevent misplacement of books on the shelves. Though RFID has many advantages including managing efficient inventory and offering security to library collections, it faces some shortcomings. Sabapathy et al. have discussed the challenges associated with the RFID technology and the precautionary measures to be taken in an automated library [5].

Younis et al. have proposed a smart library management based on RFID technology [6]. They have discussed the use of low-cost passive tags for overall cost minimization, and how it makes the tasks of library staff and users easy and smart. A smart solution is proposed by Pandey et al. for tracking the library transactions with RFID and IoT-based techniques [7]. Li et al. have introduced new way of accessing the library with android-based Ultra High Frequency (UHF) mobile reader [8]. With this method, library materials can be effectively managed. Member identification, inventory, borrow and return of materials are made simple. In the future, libraries will be transformed as 'Universal Resource Centres' and will be shared and used throughout the world.

Transformed libraries will demand a lot of automation in custom services. Aithal et al. have proposed a suitable smart library model for future transformed libraries [9]. IoT-based system is employed with RFID tags and tiny sensors [10]. With this method, continuous monitoring of books [7, 11] in real-time and tracking the objects present in the library is ensured. It also enables the implementation of online library supply chain and integration of cloud systems [12, 13].

Owayjan et al. have proposed a system to detect intruders entering a secured area [14]. When a person enters, the image of the person is captured, and it is compared with the existing database and it is ensured whether the person is authorized or not. Kumar et al. have proposed Uniform Mean Local Binary Pattern based Approach (UMLBP-A) for face recognition using OpenCV [15]. The Region of Interest (RoI) on the face is divided into 8×8 regions from which UMLBP histograms are extracted and concatenated into a single histogram with enhanced features efficiently representing the face. Matching is done using K-Nearest Neighbor (KNN) classifier with minimum error-based similarity measure. More promising results can be achieved with deep learning techniques for face recognition [16].

The proposed system uses deep learning for face recognition to achieve highly accurate results during the face verification process. The face recognition system is also integrated with RFID technology for ensuring security and automation in library process.

3 Methodology

The proposed system mainly focuses on security and automation in library management system.

The overall architecture is shown in Fig. 1. In the proposed system, authenticity of library user is verified with the method of face recognition. When a person enters into the library, the cameras mounted at the entrance of the library captures the image which is given as input to the face recognition algorithm. The frames captured by the camera are pre-processed, and the pre-processed image is compared with the images in databases by using OpenCV and face recognition algorithms. On recognition of the facial image, the user can enter into the library through turnstile. The details of the authenticated user (name, ID and entry time) will be updated in the database.

In addition to face recognition process, when the user crosses the RFID reader mounted at the entrance and exit the library, it automatically checks whether the user has taken any book and makes the entry in the database. The face recognition model is integrated with the RFID reader in order to enter the correct entry of the book taken by the particular user. The entry and the exit ways of the library will be a single-person entry point in which, only one person can enter and exit from the library.

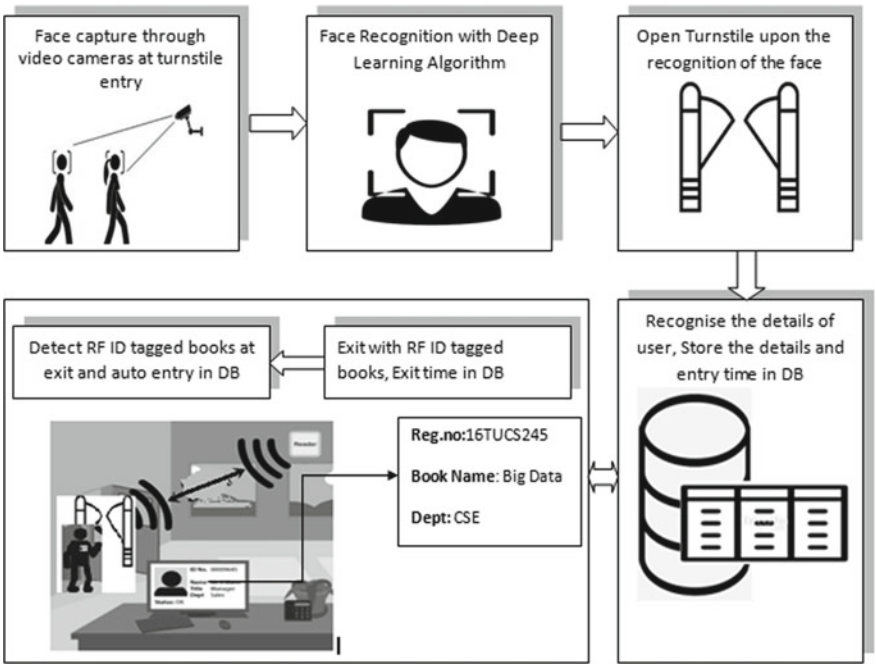

Fig. 1 Architecture of the proposed system

Fig. 2 Dataset collection

3.1 Dataset

The dataset for face identification of the user is collected from our institution repository and it is shown in Fig. 2. The images of the users are collected department wise.

Every image in the dataset is of size not exceeding 220 KB with 220 × 283 dimensions. The library book database is also collected by the college library and is encoded with the RFID tag numbers. Every image collected from the repository is used in the training phase.

3.2 Face Recognition

The process of face recognition is shown in Fig. 3.

When a user or a person enters into a library, the person's face is been captured by cameras mounted at the entrance with the aid of OpenCV. The input frame captured by the OpenCV will be in the Blue, Green, Red (BGR) format. The face recognition library requires the stream to be in RGB format so that the frames will be converted from RGB format to BGR format.

The frame is being cropped and resized into a smaller frame for quicker face recognition. The face location is identified using OpenCV. It returns a two-dimensional array of bounding box using the Convolutional Neural Networks (CNNs) based face detector. The Max margin object detection algorithm is used to detect the faces and return a boundary box.

Once the faces are identified, the facial landmarks such as eyes, nose, ears and mouth are found using the CNN classifier. The facial points named as facial encodings are marked by numerical values and are stored as a numpy array.

The images in the trained and test data are compared, and similar images will be identified as per the vector encodings. The embeddings used are 128 dimensional

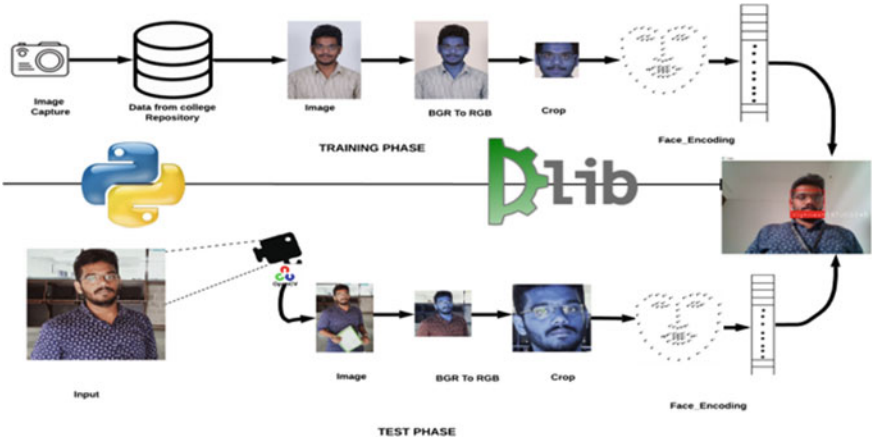

Fig. 3 Face recognition process

vectors in which similar faces end up closer, while the unknown images end far apart in the vector. A bounding box appears on the screen representing the identification of the face with the name and the ID of the person. If the face is not identified, then it displays the tag as 'unknown person' and the turnstile will not open. When turnstile is opened, the database is also updated.

3.3 Automatic Book Issue with RFID

The RFID tags contain transceivers which could convey readable data in the form of microwaves which an RFID module can detect. Each RFID tag includes the basic book information such as book name, ISBN number and author name which are used to write in the book database.

RFID-based book detection is shown in Fig. 4. The UHF handle head reader is used to identify the book. This UHF will be mounted into the turnstile, and when a user comes into the library, it detects the book with the user and performs updation of the database by integrating with the face identification module. The book ID which is entered will contain a hyperlink to the book database in which it stores the book circulation information.

4 Implementation and Results

The proposed method is tested with the available dataset available with the college repository. The system is analysed using OpenCV and deep learning algorithms. The required results are obtained by live capture of faces from the cameras mounted

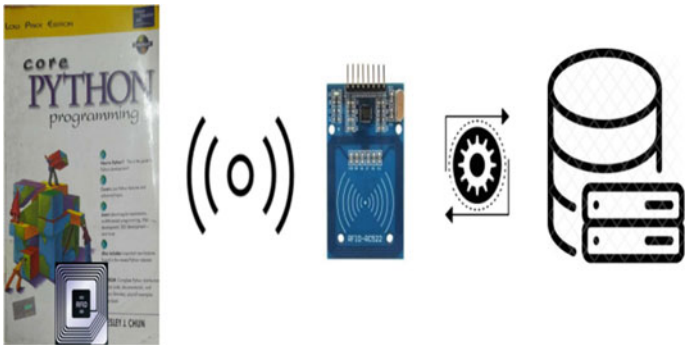

Fig. 4 Automation Issue of books with RFID

at the entry and exit points of the library. The system detects both authorized and unauthorized users. The camera identifies faces in real-time and displays it on a display device placed at the entrance point of the library. Figure 5a shows the results that are obtained for known faces.

If an unknown person enters into the library, it displays 'unknown' in the image, the database will not be updated, and the turnstile will not open up. Figure 5b shows the result for the unknown people entering into the library.

5 Conclusion

In this paper, by using face encodings and bounding from the face recognition library, the users entering into the library are identified. This application enables the user to enter and exit the library at ease. The book circulation facility and return of books are also made simple by using the RFID, since the user need not wait at the circulation counter to make entry. This method reduces the total time spent by the user for marking the attendance and making entry of books at the circulation counter. The library is made more secure by using the proposed method, since it only opens when an authorized user is recognized. This system can be further improved by making the entire library into smart and secured by applying more security techniques.

Fig. 5 **a** Recognition of known faces, **b** Recognition of unknown faces

References

1. Gurusamy D, Deva Priya M, Yibgeta B, Bekalu A (2019) DDoS risk in 5G enabled IoT and solutions. Int. J. Eng. Adv. Technol. (IJEAT) 8(5):1574–1578. ISSN: 2249-8958
2. Deva Priya M, Suganya T, Christy Jeba Malar A, Dhivyaprabha E, Prasad PK, Vishnu Varthan L.R (2020, January) An efficient scheduling algorithm for sensor based IoT networks. In: The International Conference on Inventive Communication and Computational Technologies (ICICCT 2019) at Gnanamani College of Technology, Namakkal, Tamil Nadu on 29th - 30th April 2019. The paper is published in Inventive Communication and Computational Technologies, Lecture Notes in Networks and Systems Book Series, vol 89. Springer, pp 1323–1331. ISBN: 978-981-15-0146-3
3. Makhija D, Chugan PK (2016) RFID based library management system: The benefits and challenges. In: Chugan PK, Srivastava D, Patel N, Soni NC (eds) New age ecosystem for

empowering trade, industry and society, Excel India Publishers, New Delhi, for Institute of Management, Nirma University, Ahmedabad, India, pp 219–231
4. Nayagam VS, Vedullapalli S, Saikrishna M, Sivakumar RS (2017) Radio frequency identification technology for advanced library management. In: Third international conference on science technology engineering & management (ICONSTEM), vol 1(1). IEEE, New York, pp 641–644
5. Rathinasabapathy G, Rajendran L (2015) RFID technology and library security: emerging challenges. J Lib Inf CommunTechnol 1(1):34–43
6. Younis MI (2012) SLMS: a smart library management system based on an RFID technology. Int J Reason-Based Intell Syst 4(4):186–191
7. Pandey J, Kazmi SIA, Hayat MS, Ahmed I (2017) A study on implementation of smart library systems using IoT. In: International conference on Infocom technologies and unmanned systems (trends and future directions) (ICTUS). IEEE, New York, pp 193–197
8. Li D-Y, Xie S-D, Chen R-J, Tan H-Z (2016) Design of Internet of Things system for library materials management using UHF RFID. In: 2016 IEEE international conference on RFID technology and applications (RFID-TA). IEEE, New York, pp 44–48
9. Aithal PS (2016) Smart library model for future generations. Int J Eng Res Modern Educ (IJERME) ISSN (Online). 2455-4200
10. Bayani M, Segura A, Alvarado M, Loaiza M (2018) IoT-based library automation and monitoring system: developing an implementation framework of implementation. E-Ciencias de la Información 8(1): 83–100
11. Pratt I, Zhong S (2015) Perspectives on the implementation of standardization within the UK library RFID market. In: 5th World Congress on information and communication technologies (WICT). IEEE, New York, pp 146–151
12. Kumar PKS, Sajith G (2019) Application of Radio Frequency Identification (RFID) Technology in State Central Library, Thiruvananthapuram. KLA J Inf Sci Technol, 32–40
13. Nayagam VS, Vedullapalli S, Saikrishna M, Sivakumar RS (2017) Radio frequency identification technology for advanced library management. In: Third international conference on science technology engineering & management (ICONSTEM). IEEE, New York, pp 641–644
14. Owayjan M, Dergham A, Haber G, Fakih N, Hamoush A, Abdo E (2015) Face recognition security system. In: New in networking, computing, E-learning, systems sciences, and engineering,. Springer, Cham, pp 343–348
15. Kumar M, Gupta R, Kumar v, Raju KS (2018) UMLBP-A novel approach for face recognition system using OPENCV. In: 7th international conference on reliability, Infocom Technologies and optimization (trends and future directions) (ICRITO). IEEE, New York, pp 448–452
16. Hu G, Yang Y, Yi D, Kittler J, Christmas W, Li SZ, Hospedales T (2015) When face recognition meets with deep learning: an evaluation of convolutional neural networks for face recognition. In: Proceedings of the IEEE international conference on computer vision workshops, pp 142–150

Real-Time Human Body Tracking System for Posture and Movement Using Skeleton-Based Segmentation

Venkatesh Gauri Shankar, Bali Devi, Ujwal Sachdeva, and Harsh Harsola

Abstract Real-time tracking of the human body has proven to be a key technology in several areas. In our proposed model, we have initially performed segmentation of bodies from a live feed and further detected and classified all the body parts to create a skeleton which does analysis of the posture and movement of the body. As this model works on a live feed, it has multiple real-time applications which include, but are not restricted to, applications in the field of medical diagnostics, provision of improved safety and security, human–computer interface, etc. There have been multiple instances and various research works as cited later in this paper that has attempted to track the human body. Myriad different solutions have been presented using different sensors attached at joints for estimation of the poses, but these pose estimations systems are quite personalized and have huge setup costs. The system makes a good tradeoff between system simplicity and accuracy and helps to distinctly identify and track human bodies in real time.

Keywords Real-time tracking · Segmentation · Live feed · Medical diagnostics · Security · Human–computer interface

V. G. Shankar
Department of Information Technology, Manipal University Jaipur, Jaipur, Rajasthan, India
e-mail: venkateshgaurishankar@gmail.com

B. Devi (✉) · U. Sachdeva · H. Harsola
Department of Computer Science & Engineering, Manipal University Jaipur, Jaipur, Rajasthan, India
e-mail: baligupta03@gmail.com

U. Sachdeva
e-mail: ujwalsachdeva@gmail.com

H. Harsola
e-mail: harshharsola@gmail.com

D. K. Sharma et al. (eds.), *Micro-Electronics and Telecommunication Engineering*,
Lecture Notes in Networks and Systems 179,
https://doi.org/10.1007/978-981-33-4687-1_48

1 Introduction

Information human behavior is comprised of many voluntary and involuntary movements. Every person responds to every external stimulus in different and possible way. We believe that if we can study these behavioral attributes in depth, we could unravel tones of information about an individual [1]. For example, how a person walks is unique to every individual. Furthermore, gait of a human is highly dependent on their emotional state and physical state which can be used for medical diagnosis and security applications. However, tracking human body [2] can be a very difficult task, and the independent movement of all the body parts creates numerous different poses and infinitely many movements. There have been multiple instances and various research works as cited later in this paper that has attempted to track the human body. Also, the human bodies come in various shapes, sizes, and many different characteristics that are unique to every individual. Myriad different solutions have been presented using different sensors attached at joints for estimation of the poses, but these pose estimations systems are quite personalized and have huge setup costs. Other works include the use of multi-colored overalls to track different movements by tallying them from databases and finding the nearest neighbor; applying a predictive model trained over large sets of images to detect and predict the movement of the body; rendering a 3D model of the body and creating a volumetric skeleton; and considering the angles between joints of the body to analyze and predict the posture and movements of the body [3]. A noticeable factor is that none of these proposed systems works on regular use, single cameras. Our proposed system of work will work on a single camera, which need not have any baseline specifications. It can work on a single camera, which can be as basic as the webcam of the desktop that it is being executed on. Upon implementation, it can solve multiple problems that are faced in daily life. In the field of safety and security, our proposed method can be utilized to facilitate the use of gait recognition in a more robust manner. Moreover, it can be used in the field of medical diagnostics to identify unusual micro-behaviors and characteristics of a human body. Additionally, it can be used to consolidate gaming console applications using a single camera in the field of human–computer interface.

To detect the human body, we have implemented and studied two different object detection models, namely YOLO and HAAR cascade. YOLO affects a single neural network to the entire picture [4]. This network divisions the picture into area and forecasts boundary boxes and prospects of each section. At the other hand, HAAR cascade classifiers [5] are an effective way to categorize objects based on a machine learning method, where several optimistic and adverse images are used to train the classifier. We have implemented detection on HAAR cascade for multiple practical reasons which include the fact that a graphics card is necessary for the usage of YOLO object detection and that HAAR cascade classifier provides individual classifiers for separate classes, whereas YOLO [4] performs one-look classification for all the classes. Thus, it removes the need for heavy computational power.

The first step as a part of our solution is to use this HAAR cascade classifier [5] to identify a human body in the live feed and segment it out as shown below (Fig. 1).

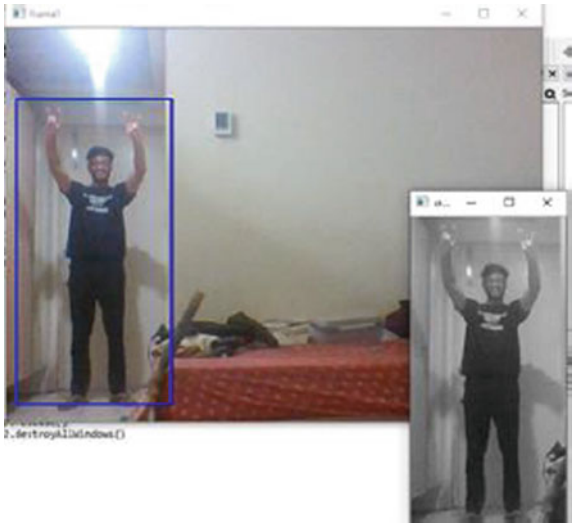

Fig. 1 Sample implementation of full body detection [6]

In this paper, we suggest a generalized real-time human body tracking [7] system wherein we aim to pinpoint 17 key points in body, namely left eye, right eye, nose, left ear, right ear, left shoulder, right shoulder, left elbow, right elbow, left hand, right hand, left hip, right hip, left knee, right knee, left foot and right foot, and further create and extract the skeleton for in-depth study for various applications (Fig. 2).

Based on these 17 key identifiers, our model, upon execution and after segmenting out the bodies from a live feed, classifies all these body parts and creates a skeleton. This skeleton [8] would be used for in-depth analysis and study of the posture movement of the body [3]. Upon implementation, its benefits include severe enhancement in security systems, ranging from residential CCTV cameras to multinational business systems; medical diagnostics due to beforehand detailed studies available; human–computer interface, including reduction of costs of this application to gaming consoles and online teaching, etc. [9].

2 Literature Review

Given our aims and methodology described above, we have tried to avoid encumbering the body with multiple sensors, weird overalls, setup of multi-camera, etc.—all of which can act as potential barriers for natural movement and may create bias in the data created. Therefore, we believe that using a single camera for detection might prove to be the turning point in this field. Steffen Knoop et al. [3], in this approach two cameras are used, one camera uses skin color to segment out the body using standard HSV color model, and the other camera is used to take an in-depth image creating a cloud of points to create a volumetric skeleton of human body. This helps in creating a realistic 3D human model and reduces further work during analysis, but this approach is highly expensive in terms of computational cost, setup cost and memory utilization. This uses the iterative closest point (ICP) algorithm, the purpose

Fig. 2 17 key identifiers

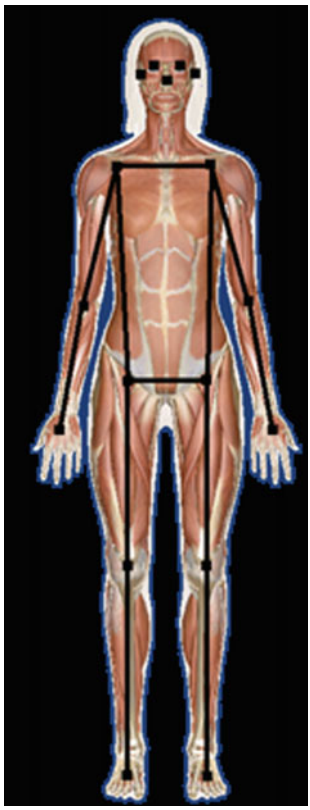

of which is to fit two indexed sets of the same points which are given in separate coordinate systems and calculate the translation and rotation based on the specified mathematical equations. Upon calculation, it uses the sum of the squares and applies the estimated values of translation and rotation to the model to determine the current set of points. Similarly, it also uses human body models in the form of cylinders to estimate the body motion and postures. Urtasun et al. [7] describe multiple sensors are used to define the different postures of human body by storing the studied data from the sensors. Since multiple sensors are used, it gives a highly accurate prediction of the posture and ensures privacy. However, on the flip side, it needs high capital investment, has a difficult setup and requires the knowledge of sensors as a pre-requisite. Wang et al. [2], here a different approach is put forward wherein numerous photos are taken of every pose possible and classified into different groups. The database is created by using in-depth imaging of hands in their different poses. Then, in real time when an in-depth image is provided, the KNN or k-nearest neighbor algorithm was used to estimate the poses of the hand. The accuracy turned out to be limited. Moreover, the database was not big enough to encompass all the possible poses so many inaccurate predictions were made. Also, during training high-resolution images were

required and even in real-time detection high-resolution image with in-depth information was required indicating toward the requirement of high-tech cameras. Pun et al. [10], a few images of different hands having various skin tones and poses were taken for training purpose. Use an image-editing program the segmentation of the object is completed. Thereafter, each image is transformed into a binary cover where white pixels characterize skin areas and black pixels characterize the background or non-skin field. This binary mask and hand snapshots are then used for training the model for skin color histograms Hs and non-skin-color histogram Hn. If the hand is lost by the computer, it can be reconfigured by outstretched hand detection. This system provided a robust way to track hand in all most all situations but could not be used further to train or detect the posture or the gesture of a human hand. Upon calculation, it uses the sum of the squares and applies the estimated values of translation and rotation to the model to calculate the new set of points. Similarly, it also uses human body models in the form of cylinders to estimate the body motion and postures. Swarup et al. [11], hand segmentation and detection are done through a different color scheme knows as $L * a * b$ wherein an image is taken in normal RGB format and then converted into $L * a * b$ format. $L*$ represents the lightness of an area in the image, whereas $a*$ and $b*$ represent the chromaticity of the same area. This color format easily differentiates between skin color and simple backgrounds but still fails sometimes in complex backgrounds. It consistently works in simpler backgrounds providing a robust system for indoor activities. Sharp et al. [12], in this paper, the proposed system requires the user to wear a colored glove. A dataset is prepared using the colored glove in numerous poses and gestures. The motive here is to make the glove colorful enough to clearly infer the position of every finger and position of the palm. The same colorful glove is worn by the user during real-time detection and then the real-time image is then directly compared to the dataset and then classified into one of the poses using KNN or k-nearest neighbor algorithm. This approach achieves high accuracy and is very robust in different environment conditions and lighting but causes a problem of using glove every time whenever one wishes to use the app, therefore creating a reliable system but difficult to use in daily life.

3 Methodology

In this paper methodology, the HAAR cascade classifier is used to identify human bodies in a live stream. HAAR feature-based [5] classifiers are an efficient object recognition system proposed by Paul Viola at el. in their paper, "Rapid Object Detection using a Boosted Cascade of Simple Features" [13] in 2001. It is an approach based on machine learning where cataract of function is trained by showing the model numerous constructive and undesirable images. This trained model is then used to distinguish objects in additional images. This algorithm requires a lot of positive images (images taking measured object in them) and negative images (images deprived of the considered object) for training purpose (Fig. 3).

Furthermore, for feature extraction, HAAR features seen in Fig. 4 are used [5]. We are like our convolutional kernel. That function is a single value found by deducting

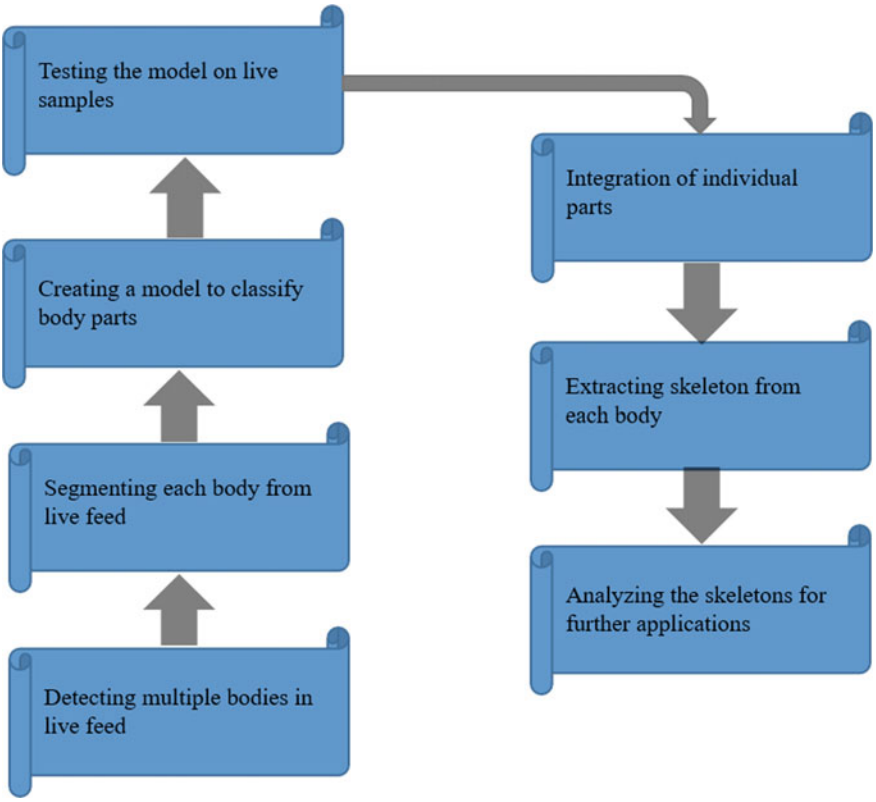

Fig. 3 Process methodology

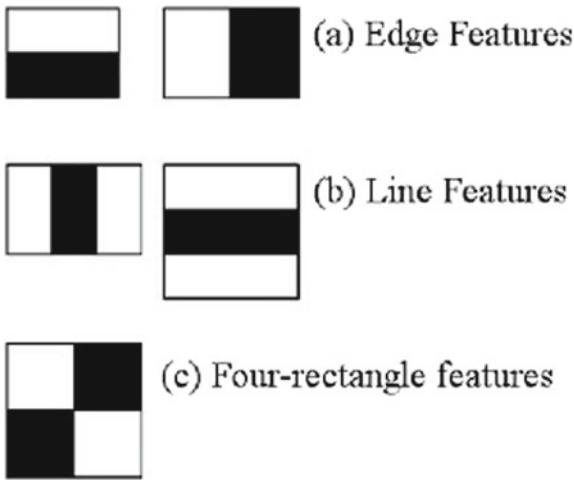

Fig. 4 Identification of HAAR-like features

number of pixels from the quantity of pixels under the black rectangle below the white rectangle. So, any possible kernel size and location is used to measure lots of features. For each feature scheming, the number of the pixels beneath white and black rectangles is determined. To solve this, the essential image was added. Though large the image, it decreases the computations for a given pixel to a mere four-pixel activity [14]. It makes the process super-fast.

Once the detection is performed, the model is used to perform classification on live samples and the model is tested on them, while also training it. Using these test samples, the model is created which can distinctly classify different body parts. Then, it segments these body parts and separates them into a different frame. From here, a skeleton of the segmented body is formed using the 17 key identifiers, and this skeleton can be further used for multiple applications. These applications can be integrated into a single research, as is our motive and can provide a one-stop solution from multiple problems, ranging from daily life issues to scientific breakthroughs. The following image depicts the 17 key identifiers that are used upon extraction of the skeleton. It is using these identifiers that we claim that everyone would have varying characteristics that can help to uniquely identify him/her (Fig. 5).

Following the algorithm that is used to implement the abovementioned objective,

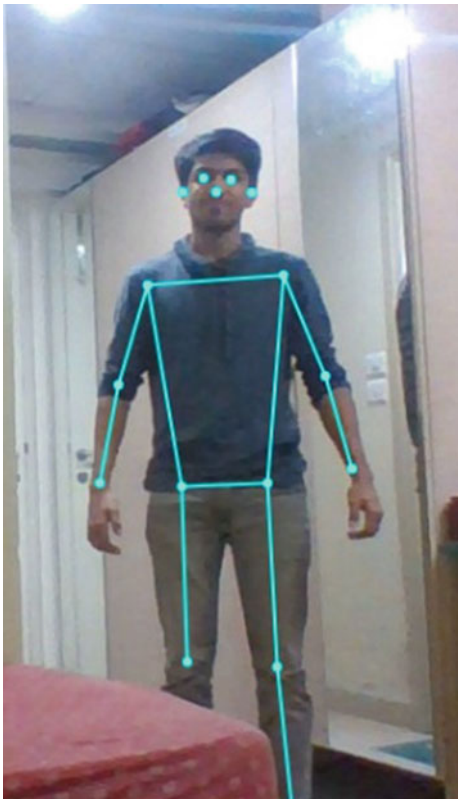

Fig. 5 Extraction of the Skeleton key features [6]

Algorithm:

```
FullBody_classifier = cv2.casacdeclassifier ("Path of the Classifier")
        Video = capture live video
While (1)
        Video = convert video from RGB to gray
        FullBody = fullbody_classifier. Detect multi scale (video)
        For x, y, width, height in Fullbody:
        RegionOfInterest = rectangle (x, y, x+width, y+height)
LowerBody = lowerbody_classifier. Detect multi scale (Region of Interest)
        For x, y, width, height in LowerBody:
        RegionOfInterest = rectangle (x, y, x+width, y+height)
Upperbody = upperbody_classifier. Detect multi scale (Region of Interest)
        For x, y, width, height in UpperBody:
        RegionOfInterest = rectangle (x, y, x+width, y+height)
Face = face_classifier. Detect multi scale (Region of Interest)
        For x, y, width, height in Face:
        RegionOfInterest = rectangle (x, y, x+width, y+height)

Show Video
```

4 Result and Discussion

Even though multiple similar projects and research exists, the novelty of our project lies in the fact that it works, not only in a live feed, but also a single camera. Additionally, the single camera that is being used does not have any base specification requirements. In multiple previous researches, the cameras and sensors used needed certain basic specifications. On the contrary, the camera to be used in our project can be as simple as the webcam of a laptop. It can be a CCTV camera of a residence and even the camera sensor in a gaming console. Since it works on a single camera, it allows for a low cost of setting up and development, bringing financial stability into multiple research and projects where it will be undertaken.

Furthermore, as it works on a live feed, it can be used to uniquely identify persons even in CCTV Cameras of societies, exponentially increasing the security provisions and thereby solving a long-standing issue. Another object detection program

Table 1 17 key points in the human body

ID	Body part	ID	Body part
0	Nose	9	Left wrist
1	Left eye	10	Right wrist
2	Right eye	11	Left hip
3	Left ear	12	Right hip
4	Right ear	13	Left knee
5	Left shoulder	14	Right knee
6	Right shoulder	15	Left ankle
7	Left elbow	16	Right ankle
8	Right elbow		

was considered suiting to our needs was YOLO or you only look once object detection program, which is a multiclass, object detection program having 81 different classes. Yolo [4] works on a big densely connected convolutional neural network having immense computational requirements. Multiple versions of YOLO are available with different accuracies and different set of computational requirements. Also, for training of a YOLO model on a custom dataset required high quality labeled training dataset. Another noticeable factor from previous research is that the existing research focuses on one of these fields. The versatility and flexibility of our research lies in the fact that it would create an integrated model that performs all the mentioned applications. Hence, the true novelty of the research lies in integration of myriad functions to form a multifunctional model that works on a single camera and performs real-time tracking [2] on a live feed.

In this paper, we have tried to pinpoint the exact locations of the 17 key points in the human body [7] which will help us to further dive deeply into further analysis of the human behavior and body movements in Table 1.

We started with finding a compatible object detection model for our objective and came across two leading models, namely HAAR cascade classifier [5] and YOLO or You Only Look Once Object Detection Model. Both proved to be a competent choice for completion of our objective. HAAR and Yolo both provided us with high accuracy and consistency, but HAAR came out better in the cost of computation as HAAR uses HAAR like features and then cascade classifying for detection whereas YOLO runs a highly interconnected convolutional neural network for the same. Also, YOLO [4] is a multi-class object detection model where we just needed an objective specific detection model. We used HAAR's full body cascade classifier to find and detect the full bodies present in the live feed and create a smaller picture of just the body and leaving all the useless information behind. This smaller image is then used by HAAR's face cascade classifier to find the face in the smaller picture. Now even smaller image of the face is cropped and used to find the eyes in the face using HAAR's eyes cascade classifier.

The cropped image of full body is then used to find the upper body using HAAR's upper body cascade classifier, and then the lower body is detected using HAAR's

lower body cascade classifier. The full body classification and identification of the key points are as follows (Figs. 6, 7 and 8).

So far, we were able to locate and pinpoint 6 out of 17 key points, and due to the lack of labeled dataset of key points (like right elbow, left elbow, right hip, left hip, right knee, left knee, right ear, left ear and nose), we were unable to create their specific detection models. Upon provision of the dataset, we would be able to achieve 98% accuracy by creating our own object detection models and pipelined model would efficiently use the computational power without the need of a GPU or high-end processing power. In addition, there exists no such model currently which can perform these integrated tasks, ranging from security applications and medical diagnostics to human–computer interface on a live feed with a single camera. With

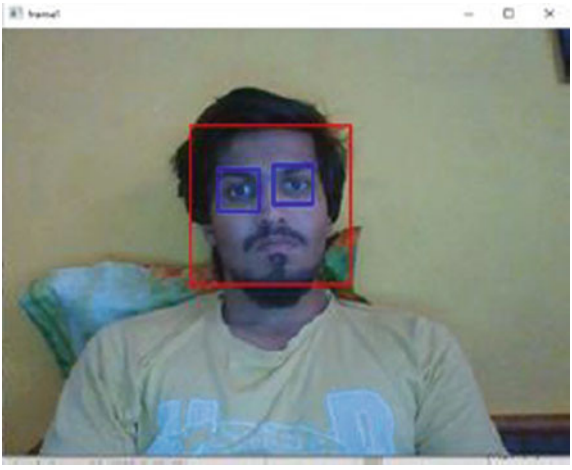

Fig. 6 Sample implementation for face and eye detection [6]

Fig. 7 Sample implementation for face and eye detection [6]

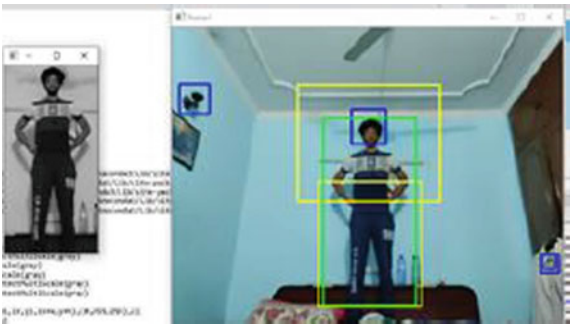

Fig. 8 Sample implementation of full body detection based on the key identifiers [6]

such low computational requirements and high accuracy, it can be a boon to many fields.

After the model is trained, it can be used seamlessly and be used to further research on integration of more aspects to make it a one-stop destination for all applications requiring human detection, tracking and its analysis. Our current model would be used to streamline and reduce the computational cost. The individual segmented body halves would be given as an input to each model, thus reducing the input size and reduced redundant data as input to the system. After successfully implementing the key point detection model, we believe that it would be easier to work on gait recognition and gait analysis.

5 Conclusion and Future Scope

In conclusion, our research—"Real-Time Human Body Tracking" has several applications and if implemented correctly—can solve multiple technological issues. If the model planned works on a single camera, as well as on the live feed, we would have successfully implemented a unique solution for the same. Furthermore, upon integration of all applications into one final product can help solve not just many daily life issues, but also lead toward significant scientific breakthroughs. The future work to be done on this research includes integration of each of the key identifiers, and creation of a graphical user interface that can easily put into use by a someone using the software for the first time as well. We plan to integrate features such as whether to show the skeleton, points or not, while also allowing the user to fix minimum and maximum values of confidence (which would mean the relative closeness of the input and output to the binary values). Moreover, once completely executed, we plan to investigate the feasibility of this research commercially to incorporate it into the fields of security systems, human–computer interface and medical diagnostics. Finally, we also plan to pipeline the code further in order to make the computational requirements further less and look into ways as to which the cost of integration of such a system into commercial products can be minimized, i.e., the most suited hardware that can provide the most optimum results at the least possible costs.

References

1. Shankar VG, Jangid M, Devi B, Kabra S (2018) Mobile big data: malware and its analysis. In: Proceedings of first international conference on smart system, innovations and computing. smart innovation, systems and technologies, vol 79. Springer, Singapore, pp 831–842.https://doi.org/10.1007/978-981-10-5828-8_79
2. Wang RY, Popovic J (2009) Real-time hand-tracking with a color glove
3. Knoop S, Vacek S, Dillmann R (2019) A posture recognition method based on indoor positioning technology
4. YOLO. https://towardsdatascience.com/yolo-you-only-look-once-real-time-object-detection-explained-492dc9230006
5. Haar. https://www.willberger.org/cascade-haar-explained/
6. Pictorial Representation of the working of the model on the Co-Author(s) photographs
7. Urtasun R, Fua P (2004) 3D human body tracking using deterministic temporal motion models
8. Le T-L, Nguyen M-Q, Nguyen T-T-M (2013) Human posture recognition using human skeleton provided by Kinect. In: International conference on computing, management and telecommunications (ComManTel). https://doi.org/10.1109/commantel.2013.6482417
9. Shankar VG, Devi B, Srivastava S (2019) DataSpeak: data extraction, aggregation, and classification using big data novel algorithm. In: Iyer B, Nalbalwar S, Pathak N (eds) Computing, communication and signal processing. Advances in intelligent systems and computing, vol 810. Springer, Singapore. https://doi.org/10.1007/978-981-13-1513-8_16
10. Pun C-M, Zhu H-M, Feng W (2011) Real-time hand gesture recognition using motion tracking
11. Rautray SS, Agrawal A (2011) A real time hand tracking system for interactive applications
12. Sharp T, Kim D et al (2015) Accurate, robust, and flexible realtime hand tracking
13. Alon J, Athitsos V, Yuan Q et al (2009) A unified framework for gesture recognition and spatiotemporal gesture segmentation. IEEE Trans Pattern Anal Mach Intell 31(9):1685–1699
14. Mao G-Z, Wu Y-L, Hor M-K et al (2009) Real-time hand detection and tracking against complex background. In: Fifth international conference on intelligent information hiding and multimedia signal processing, pp 905–908

Enhanced InGaAs/InAs/InGaAs Composite Channel MOSHEMT Device Performance by Using Double Gate Recessed Structure with HfO_2 as Dielectric Materials

R. Saravana Kumar, N. Mohankumar, S. Baskaran, and R. Poornachandran

Abstract This work reports that the composite channel InGaAs, InAs and InGaAs thin, with dual delta-doped double recessed gate (DG) MOSHEMT, is 40 nm gate length, the barrier 3 nm and 15 nm thick channel, and this structure has been simulated in the TCAD Sentaurus simulation tool. The DC and RF characteristics of proposed device are characterized by different gate lengths along with different V_{DS}. The novel design features included under this proposed structure, namely recessed high stem gate, thin barrier, dual gate, composite channel and the HfO_2 as a dielectric material, are applicable for low leakage current along with Tera Hertz frequency applications. The simulation results show the exhibition of a high drain current of 1.38×10^{-3} A/μm, transconductance of 3.35×10^{-3} S/μm, threshold voltage of 0.13 V, cutoff and maximum frequency of oscillation of 791 and 995 GHz by the DGMOSHEMT devices at $L_G = 40$ nm and $V_{DS} = 0.5$ V. The findings are obtained due to the superior electron transportation properties of a DG MOSHEMT structure with compound semiconductor III-V materials.

Keywords Composite channel · Double gate · Recessed gate · Thin barrier · High K dielectric material · Low leakage current

1 Introduction

Traditional silicon CMOS scaling in the area of the short length gates has stopped due to intense dissipation of power and Short Channel Effect (SCE) [1–3]. Low power applications require reduced supply voltage and increased ON current to sustain the

R. Saravana Kumar (✉)
ECE Department, Bannari Amman Institute of Technology, Sathyamangalam, Tamil Nadu, India
e-mail: saravanaelectron@gmail.com

N. Mohankumar
EECE Department, Gitam School of Technology, Bengaluru, India

S. Baskaran · R. Poornachandran
ECE Department, SKP Engineering College, Tiruvannamalai, Tamil Nadu, India

D. K. Sharma et al. (eds.), *Micro-Electronics and Telecommunication Engineering*,
Lecture Notes in Networks and Systems 179,
https://doi.org/10.1007/978-981-33-4687-1_49

device switching speed, which is in need of maintaining upcoming transistor design [4]. III-V compound semiconductor-based FET devices are explored for the satisfaction of the needs referred to above. However, these devices suffer from mobility degradation due to the scattering effect and interface roughness. Another emerging device is the InP based buried quantum well compound semiconductor based high electron mobility transistor (HEMT) structure which consists of a wide gap III-V compound semiconductor inserted between the gate and channel to improve the electron mobility of the device [2].

For low power and sub-millimeter wave applications, HEMTs play a highly attractive and desirable device. These devices are characterized by their fast mobility and high carrier density in comparison with Si-based CMOS devices [5, 6]. The analog and RF performance of HE MT structure has been enhanced by barrier scaling (T_B), composite channel thickness (T_{CH}), thickness of the oxide layer and height of the gate stem [7, 8]. By decreasing gate length (L_G) thus increasing the SCEs, simultaneously the operating frequency of the device can be improved. In addition to gate scaling, the device aspect ratio is enhanced by vertical dimension reduction to mitigate SCEs. In comparison, an improvement in leakage current and device interface faults will no longer reduced by vertical scaling. This large leaking current usually affects voltage breakdown and nano-scale system RF handling ability [9]. This issue can be surmounted through use of an oxide layer under the gate, and it leads to formation of the MOSHEMT device. The traditional dielectric material SiO_2 in MOS devices is replaced by the other dielectric materials that include HfO_2, Al_2O_3 and Si_3N_4 with the objective of improving the DC and RF performance with reduced gate leakage. A gate dielectric material with permittivity between 20 and 30 is more attractive for achieving low gate leakage as well as high drive current. In comparison with SiO_2 ($k = 3.9$), Al_2O_3 ($k = 10$) and Si_3N_4 ($k = 7.5$), dielectric material such as HfO_2 ($k = 25$) is therefore considered the appropriate gate dielectric material of the next generation CMOS systems [10].

This gate oxide contributes to improvement in gate contact, reducing gate leakage in effect. However, at the same time, there is a decrease in the transconductance value while threshold voltage value moves in a negative direction. The recessed gate technique, i.e., the layer under the gate, is etched off for transconductance improvement for mitigating this effect. However, most of the MOSHEMT devices are designed in recessed single gate structures, exhibiting low gate control over the channel. Hence, it is proposed that double gate MOSHEMT should be designed for two gate electrodes to be implemented on above and below the composite channel for improving the device DC and RF performance by better gate control. Thin barrier, three-layer channel, thin oxide layer and dual delta doping with a high-stem double-recessed gate structure improve the device performance in terms of low leakage, higher electron mobility and velocity along with high RF performance.

Several experiments have already been done on the MOSFET double gate and HEMT architectures [10–14]. This simulation work reflects the performance of MOSHEMT composite channel InGaAs/InAs/InGaAs with the barrier InAlAs, the oxide layer of HfO_2 and its dual delta frame. The proposed system is simulated using a TCAD simulation tool. In this structure performance measurement is carried out

by drain current (I_D), transconductance (g_m), threshold voltage (Vt), cutoff and maximum frequency of oscillation, (f_t, f_{max}).

2 $In_{0.7}Ga_{0.3}As/InAs/In_{0.7}Ga_{0.3}As$ MOSHEMT Device Layer Structure

Figure 1 show the interface layer structure of MOSHEMT double gate device. The device architecture has included different novel design features as illustrated in the literature in order to reach maximum performance [15–18]. Multi-cap layers of 4nm $In_{0.65}Ga_{0.35}As$ ($2 \times 10^{15}/cm^{-3}$), 15 nm $In_{0.55}Ga_{0.45}As$ and 15 nm $In_{0.47}Al_{0.52}As$ are formed. A layer of Etch stop (2 nm) is formed under the cap for elimination of material defects [19–21].

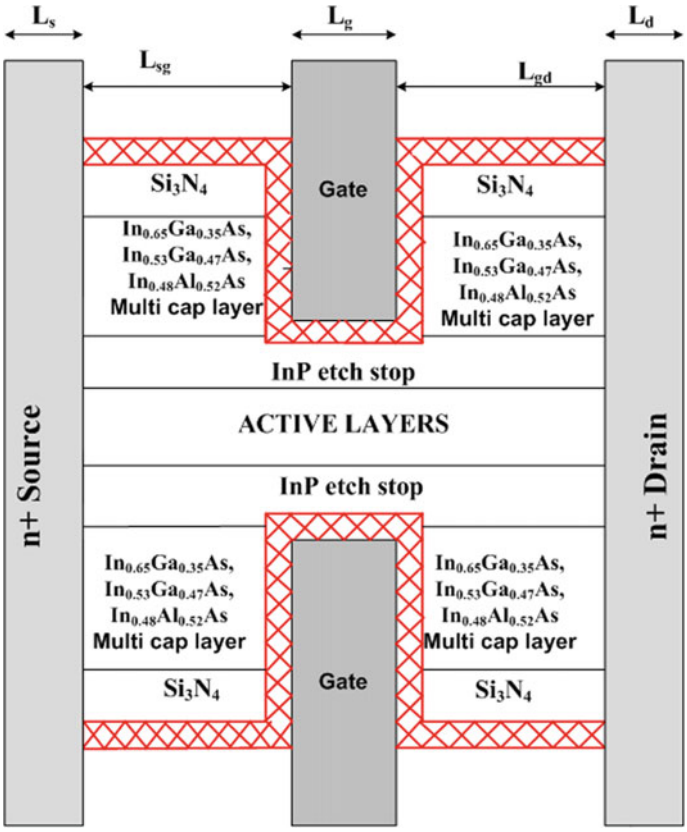

Fig. 1 $In_{0.7}Ga_{0.3}As/InAs/In_{0.7}Ga_{0.3}As$ double gate MOSHEMT device layer structure

The active layers consist of spacer, barrier and channel layer. A thin, barrier layer film of 3 nm ($In_{0.48}Al_{0.52}As$) is constructed above the conducting channel to increase the electron density [22]. A thin layer of barrier improves the transconductance, but it leads to leakage. Different gate insulation materials are implemented for reducing the gate leakage, such as SiO_2, Si_3N_4, HfO_2 and Al_2O_3. In this work, 2 nm HfO_2 is used as a dielectric in recessed gate structure because HfO_2 has a wider bandwidth (6 eV), a higher dielectric constant (K-25), improved thermal stability and a high-breakdown voltage [23] compared with other insulating materials. The delta doping method is a subset of the doping theory, which selectively dopes the barrier layer rather than doping the entire barrier layer. In this structure the barrier layer is delta doped with 2 nm (1×10^{18} /cm^{-3}). Compared to traditional doping, this delta doping strategy has several advantages: improved mobility, high speed and RF performance improvement [24]. A spacer layer was created between the heavily doped barrier layer and the non-doped channel layer in order to reduce the effect of scattering and to improve the electron mobility of composite channel (2 nm). In the upper and lower gates, gold is used as gate material to raise the threshold voltage.

The technique of the thin channel, boosts the DC performance of the device but increases the carrier scattering effect. To avoid this a composite channel is included, which comprises a pure InAs layer of 7 nms, $In_{0.7}Ga_{0.3}$ As 3 nm act as a upper sub channel and $In_{0.7}Ga_{0.3}$ As of 5 nm act as a lower subchannels. The key objective is to increase the carrier speed and system RF output by adding a composite channel [25, 26]. Nowadays normally switch off device is required for modern analog and digital applications. This is accomplished through a recessed gate positioning, which diminishes the gap between the gate and the channel to rise the gate control and decrease parasitic resistance effect [27].

3 Experimental Validation

The single gate (SG) HEMT experimental data [22] is compared to the simulated SG HEMT data in order to validate the simulation results. In this simulation validation, the hydrodynamic model (HD) is included. The HD model has different physical effects for high electrical fields including variable effective mass, mobility depending on doping and bandgap reduction.

Once a simulated data is matched with the experimental data, the resulting parameters of the device model are integrated into proposed device. The following equations are empirical equations of the carrier density of 2DEG, the drain current and the trans-conductance for experimental validation used in this simulation.

$$n_s = \frac{\epsilon}{qd}(V_{GS} - V_{off}) \tag{1}$$

$$I_D = \frac{\mu_n C_S W}{2L}(V_{GS} - V_{off})^2 \tag{2}$$

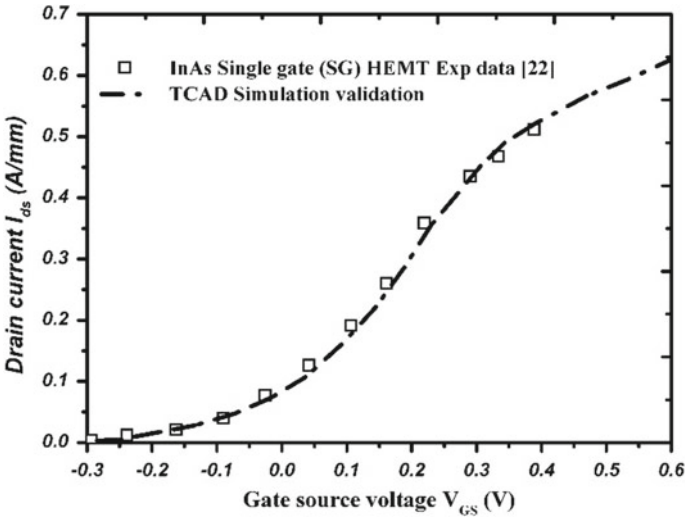

Fig. 2 Validation of SG HEMT experimental data [22] with TCAD simulation

$$g_m = \frac{\partial I_D}{\partial V_{\mathrm{GS}}} = \frac{\mu_n C_S W}{2L}(V_{\mathrm{GS}} - V_{\mathrm{off}}) \tag{3}$$

4 Results and Discussion

Figure 3 shows the conduction band energy and sheet carrier density of DG MOSHEMT structure in the channel at VDS = 0.5 V. In the DG structure, low band gap material InAs is sandwiched between the two InGaAs subchannels with bottom barrier layers, which creates a clear quantum well, and it has a large 2DEG and sheet charge density compared to a single gate. The peak sheet carrier density is achieved a maximum value of 3.2 × 1018 cm^{-3}.

Figure 4 shows the IDS and gm response of proposed DG MOSHEMT structure with respect to various VDS = 0.1, 0.3, 0.5, 0.7 and 0.9 V. The IDS and gm of proposed simulated structure at VDS = 0.5 V is 1.38 × 10^{-3} A/μm and 3.35 × 10^{-3} S/μm respectively, which is more than single gate HEMT device [22]. It is because the double gate composite architecture incorporates higher mobility and carrier Density in the channel. However, as the VDS value is increased by more than 0.5 V, the transconductance value starts to decrease which happens due to the hot electrons created by the impact ionization [28].

Figure 5(a) implies variations in transconductance with different values of gate length at VDS = 0.5 V in the DG MOSHEMT device. The inference is that, with a decrease in L_G, the transconductance starts to increase due to a decrease of parasitic

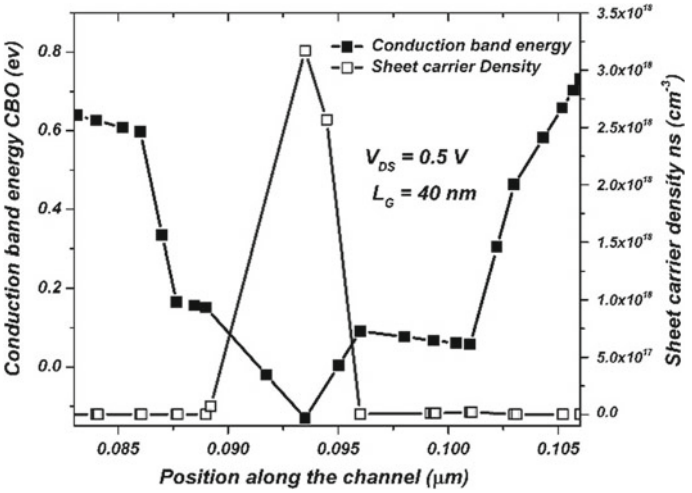

Fig. 3 Conduction band energy diagram and sheet carrier density of DG MOSHEMT devices at VDS = 0.5 V and L_G = 40 nm

resistance and capacitance of the device leading to improved mobility. Further, with a large reduction in gate length, the transconductance starts to decrease due to heavy short channel effects and poor carrier confinement in the channel. The benchmarks on transconductance and gate length with the reported values are shown in Fig. 5(b). The device proposed by the authors produces the highest transconductance. This is the result of an optimized device layer structure associated with a high electron velocity and mobility combination of InGaAs/InAs/InGaAs composite channel material.

Figure 6 represents the drain current characteristics of DGMOSHEMT device with respect to various gate to source voltage (VGS). The DG MOSHEMT structure shows improvements in the performance characteristics compared to SG. It is a result of the double delta doping layers and the creation of a strong quantum well in barrier and channel junction. From Fig. 6, it is clear that the increment of VGS, prompting rise carrier concentration in channel layer and give direct effect on drain current.

Figure 7 represents the threshold voltage (V_T) level of the proposed device with respect to various $V_{DS.}$ The V_T is measured at $V_{DS} = 1\mu A/\mu m$ [27]. In this case, DG MOSHEMT generates the V_t of 0.132, VDS = 0.5 V, and this implies the normally switch off (enhancement) mode of the structure. The positive threshold voltage is obtained by high work function gate material, thin active layers and dual recessed gate structure.

Figure 8 shows the electron velocity of recessed double gate MOSHEMT structure with $L_G = 40$ nm as 1.02×10^8, 4.9×10^8, 6.9×10^8, 2.8×10^8, 2.1×10^8 cm/s at $V_{DS} = 0.1, 0.3, 0.5, 0.7, 0.9$ V, respectively.

$$\text{electron Velocity} \propto \frac{1}{\text{electron transit time}} \tag{4}$$

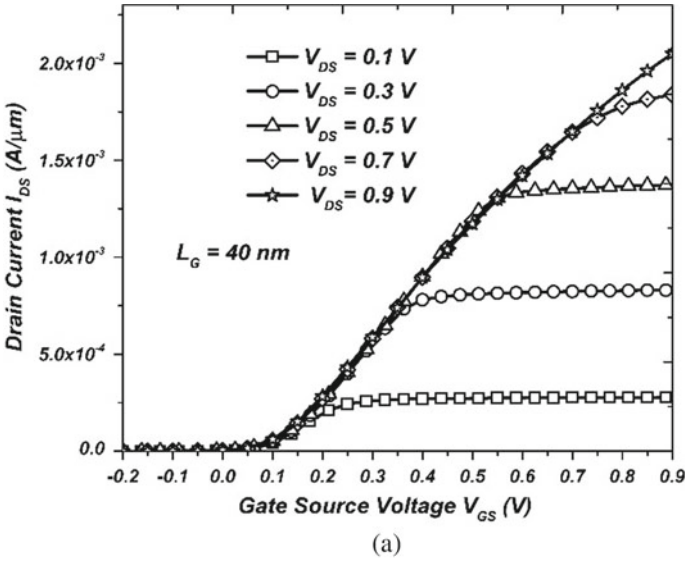

(a)

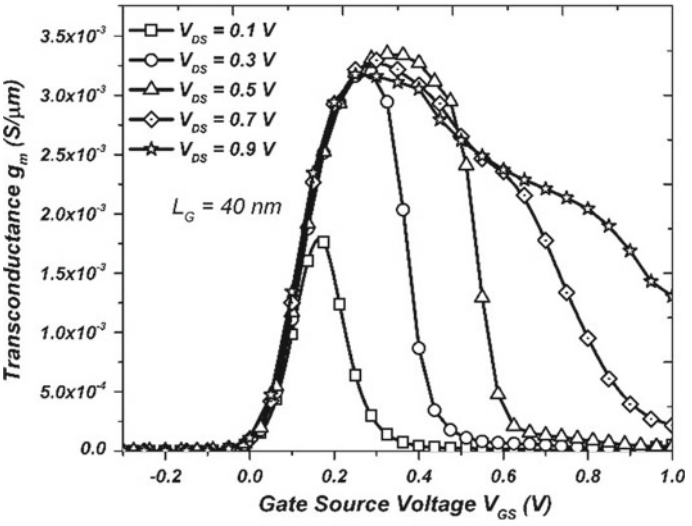

(b)

Fig. 4 **a** Drain current (IDS) and **b** Transconductance (gm) response of Double Gate MOSHEMT at different VDS

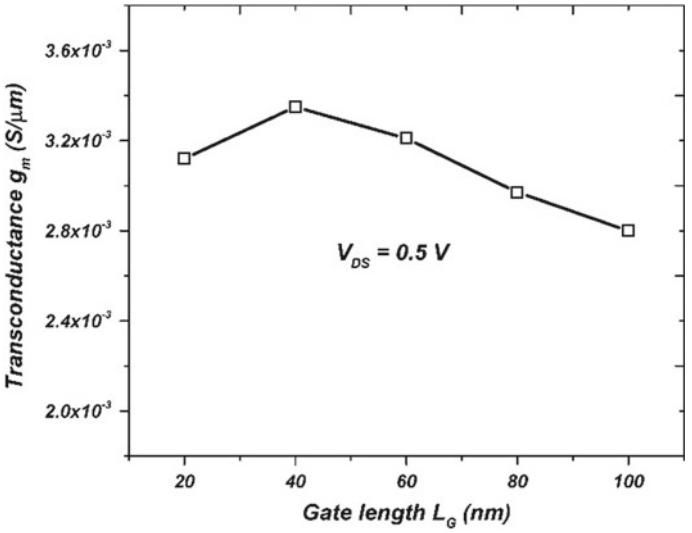

(a)

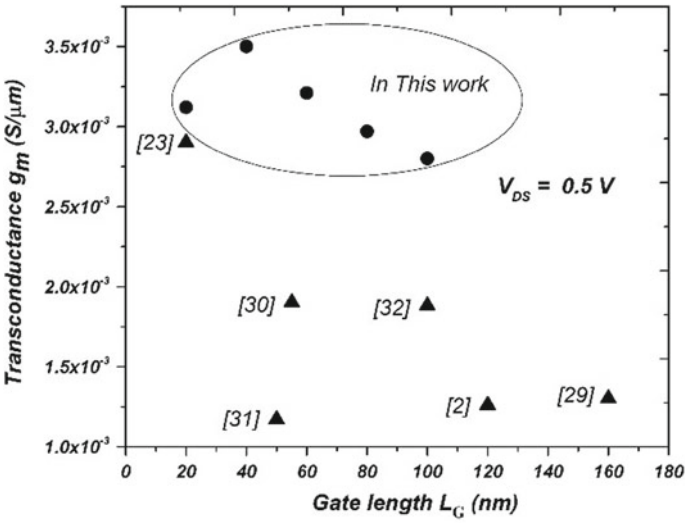

(b)

Fig. 5 **a** Variation of transconductance with respect to gate length **b** Comparison between proposed DGMOSHEMT devices and published results

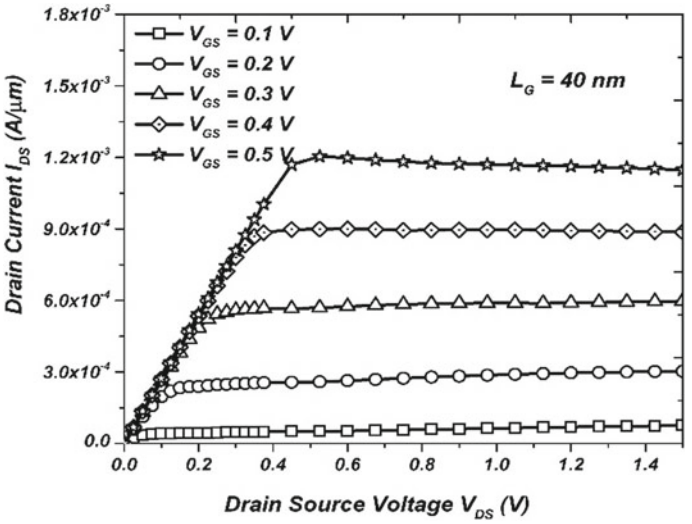

Fig. 6 Output characteristics of DG MOSHEMT. The gate voltage of the peak curve is 0.5 V and the gate bias voltage is stepped down to 0.1 V

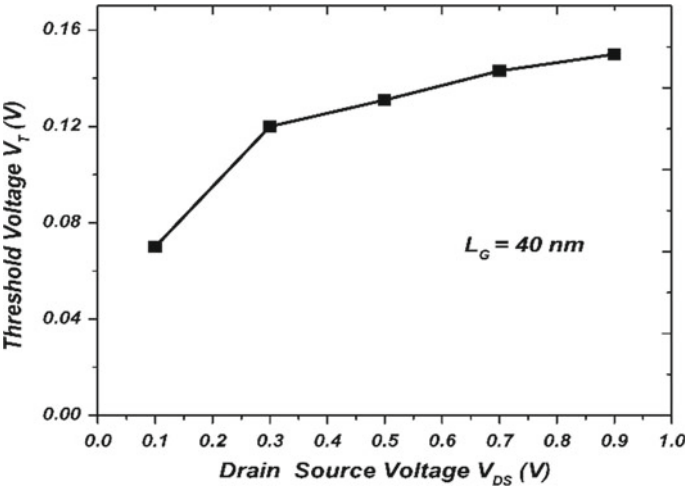

Fig. 7 The threshold voltage level of double gate MOSHEMTS at VDS = 0.1, 0.3, 0.5, 0.7 and 0.9 V

The electron velocity is indirectly proportional to electron transit time. This device produces a higher velocity due to the reduced gate length with more control on the channel by the use of the double gate technique. The figure, shows an increase in the VDS value after a certain value (ie., VDS > 0.5 V) reduction in the electron velocity. This is due to, the charge carriers under high electric field in the channel getting more

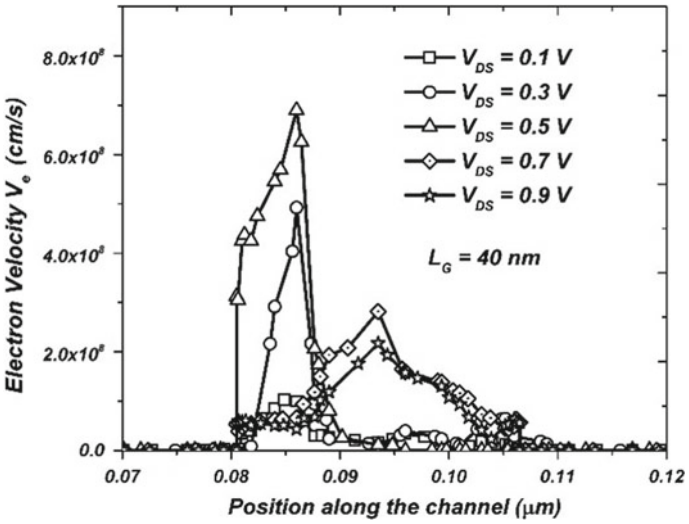

Fig. 8 Electron velocity of DG MOSHEMT devices with $L_G = 40$ nm at $V_{DS} = 0.1$, 0.3, 0.5, 0.7 and 0.9 V

energized in the scaled device, making a collision between the electrons. This effect caused a reduction in electron velocity.

The RF performance of the device is analyzed by the below ft and fmax equations. For enhancing ft and fmax the gate to drain capacitance, gate to source capacitance, gate resistance, drain resistance, source resistance needs to be reduced [14].

$$f_T = \frac{g_m}{2\pi C_{gs}\sqrt{1+2\left(C_{gd}/C_{gs}\right)}} \approx \frac{g_m}{2\pi\left(C_{gd}+C_{gs}\right)} \approx = \frac{g_m}{2\pi C_{gg}} \tag{5}$$

$$f_{\max} = \frac{g_m}{2\pi C_{gs}\sqrt{4(R_S+R_i+R_g)\left(g_{ds}+g_m\left(C_{gd}/C_{gs}\right)\right)}} \tag{6}$$

The f_t and $f_{\max}$ characteristics of the D_G MOSHEMT devices for various drain voltage V_{DS} describe in Fig. 9a, b. The f_t and $f_{\max}$ curve of the proposed simulated device structure shows an improved performance due to higher indium content in the thin composite channel and dual recessed gate structure. In this, D_G MOSHEMT device as V_{DS} caused an increase in the transconductance and electron velocity gets enhanced, paving the way for increasing the f_t and $f_{\max}$. A further increase in the V_{DS} caused a decrease in the RF performance, as a result of impact ionization. The maximum values of f_t and $f_{\max}$ observed are 791 GHz and 995 GHz, respectively, at $V_{DS} = 0.5$ V.

Figure 10(a) and (b) represents the variations in the cutoff frequency and maximum frequency of oscillation of recessed DG MOSHEMT devices for various gate lengths $L_G = 20$ to 100 nm. With a reduction in the length of the lock, the RF output improved because parasite lock resilience and transit time were reduced. Once the length of the

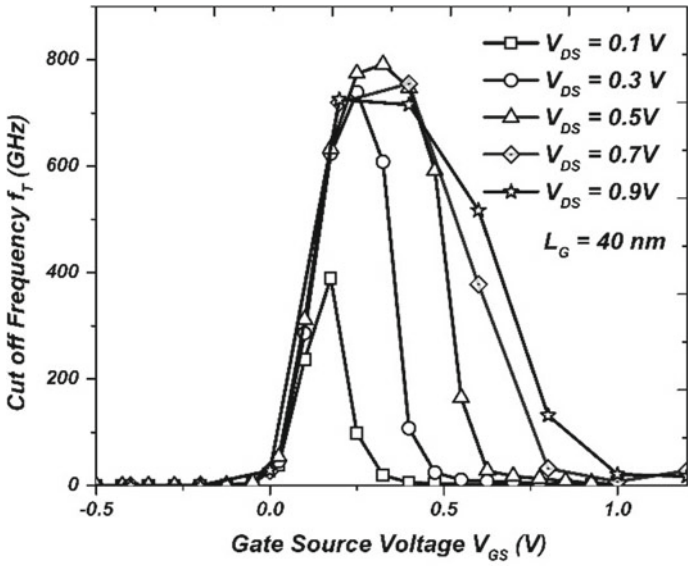

(a)

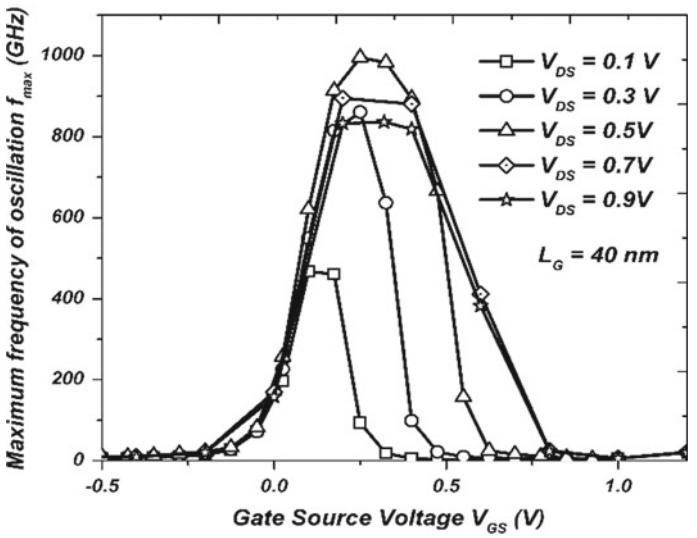

(b)

Fig. 9 **a** f_t **b** $f_{\max}$ characteristics at various V_{DS} with $L_G = 40$ nm

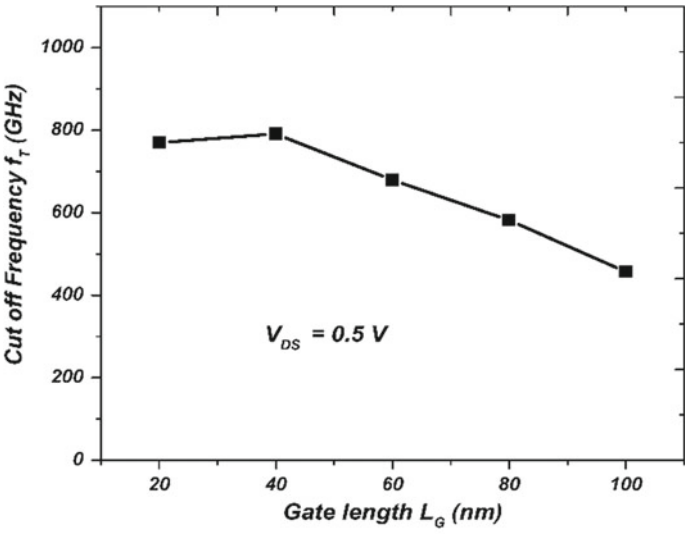

(a)

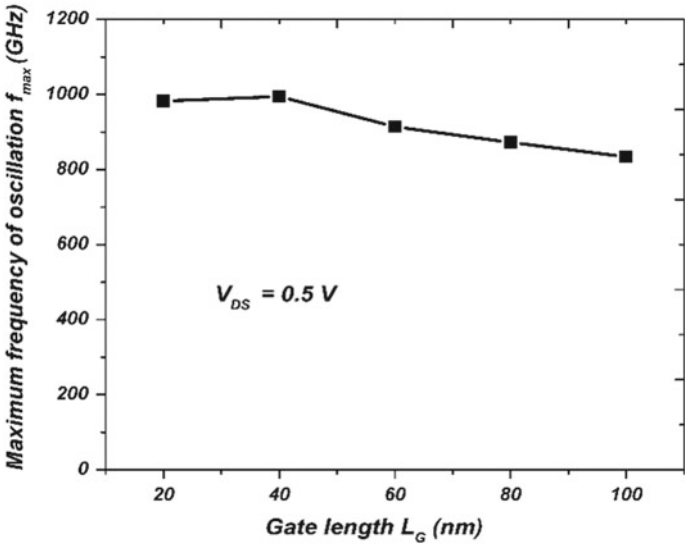

(b)

Fig. 10 **a**, **b** f_t and $f_{\max}$ variation of ft and fmax of DGMOSHEMT for different gate length at VDS = 0.5

gate has decreased more, the RF output starts to decline due to strong short channel effects and a reduction of transconductance. Figures 9 and 10 display the optimized system RF output of DG MOSHEMT at $L_G = 40$ nm at VDS = 0.5 V.

5 Conclusion

$In_{0.7}Ga_{0.3}As$ /InAs/ $In_{0.7}Ga_{0.3}As$ based dual gate MOSHEMT device for high frequency application has been simulated and the device parameters are analyzed with respect to different VDS and L_G. The proposed device structure with thin barrier, composite channel, receded high stem gate and HfO_2 gate dielectric material concepts improved the device performance. The optimized device structure achieved a maximum transconductance of 3.35×10^{-3} S/μm, maximum cut off frequency of 791 GHz and maximum frequency of oscillation is 995 GHz with electron velocity of 6.9 × 108 cm/s for TB = 3 nm, $L_G = 40$ nm at VDS = 0.5 V. This simulation results indicate that the proposed $In_{0.7}Ga_{0.3}As$ /InAs/ $In_{0.7}Ga_{0.3}As$ based dual gate MOSHEMT is very much suitable for high frequency and high speed applications.

References

1. Kim TW, Kim DH, del Alamo JA (2009) 30 nm In 0.7 Ga 0.3 As Inverted-Type HEMTs with reduced gate leakage current for logic applications. In: 2009 IEEE international electron devices meeting (IEDM). IEEE, New York, pp 1–4 (2009)
2. Radhakrishnan SK, BaskaranSubramaniyan M, Nagarajan M (2018) Comparative assessment of InGaAs sub-channel and InAs composite channel double gate (DG)-HEMT for sub-millimeter wave applications. AEU-International Journal of Electronics and Communications 83 (2018): 462–469.
3. Kim TW, Kim DH, Del Alamo JA (2010) Logic characteristics of 40 nm thin-channel InAs HEMTs. In: 2010 22nd international conference on indium phosphide and related materials (IPRM). IEEE, New York, pp 1–4
4. Zhou X, Li Q, Tang CW, Lau KM (2012) 30-nm Inverted In0.53Ga0.47As MOSHEMTs on Si Substrate Grown by MOCVD With Regrown Source/Drain. IEEE Electron Device Lett 33(10):1384–1386
5. Saravana Kumar R, Mohanbabu A, Mohankumar N, Godwin Raj D (2018) Simulation of InGaAssubchannel DG-HEMTs for analogue/RF applications. Int J Electron 105(3):446–456
6. Yun D-Y, Jo H-B, Son S-W, Baek J-M, Lee J-H, Kim T-W, Kim D-H, Tsutsumi T, Sugiyama H, Matsuzaki H (2018) Impact of the source-to-drain spacing on the DC and RF Characteristics of InGaAs/InAlAs high-electron mobility transistors. IEEE Electron Device Lett 39(12):1844–1847
7. Kim DH, Del Alamo JA (2010) 30-nm InAs PHEMTs with f T= 644 GHz and f max= 681 GHz. Institute of Electrical and Electronics Engineers.
8. Kuo CI, Hsu HT, Chang EY, Chang CY, Miyamoto Y, Datta S, Radosavljevic M, Huang G-W, Lee C-T (2008) RF and logic performance improvement of In0. 7Ga0. 3As/InAs/In0. 7Ga0. 3As composite-channel HEMT using gate-sinking technology. IEEE Electron Device Lett 29(4):290–293
9. Lee KW, Huang JS, Lee FM, Huang YS, Wang Y-H, Su SC, Chao BH, Chen CC (2007) Analytical study of the dc characteristics on the InAlAs/InGaAs metamorphic HEMT with

oxidized InGaAs gate. In: 2007 IEEE conference on electron devices and solid-state circuits. IEEE, New York, pp 259–262
10. Nirmal D, Vijayakumar P, Shruti K, Mohankumar N (2013) Nanoscale channel engineered double gate MOSFET for mixed signal applications using high-k dielectric. Int J Circuit Theory Appl 41(6):608–618
11. Liu H, Xiong Z, Sin JKO (2003) Implementation and characterization of the double-gate MOSFET using lateral solid-phase epitaxy IEEE Trans Electron Devices 50(6):1552–1555
12. Mohankumar N, Syamal B, Sarkar CK (2010) Influence of channel and gate engineering on the analog and RF performance of DG MOSFETs. IEEE Trans Electron Devices 57(4):820–826
13. Poornachandran R, Mohan Kumar N, Saravana Kumar R, Baskaran S (2020) Noise analysis of double gate composite InAs based HEMTs for high frequency applications. Microsyst Technol pp 1–9
14. Wichmann N, Duszynski I, Bollaert S, Mateos J, Wallart X, Cappy A (2004) 100 nm InAlAs/InGaAs double-gate HEMT using transferred substrate. In: IEDM technical digest. IEEE international electron devices meeting, 2004. IEEE, New York, pp 1023–1026
15. Mo JJ, Wichmann N, Roelens Y, Zaknoune M, Desplanque L, Wallart X, Bollaert S (2012) Lattice matched and PseudomorphicInGaAs MOSHEMT with f_T of 200 GHz. In: 2012 International conference on indium phosphide and related materials. IEEE, New York, pp 44–47
16. Endoh A, Watanabe I, Mimura T (2012) Monte Carlo simulation of InGaAs/strained-InAs/InGaAs channel HEMTs considering self-consistent analysis of 2-dimensional electron gas. In: 2012 international conference on indium phosphide and related materials. IEEE, New York, pp 48–51
17. Kim D-H, Del Alamo JA (2010) Scalability of sub-100 nm InAs HEMTs on InP substrate for future logic applications. IEEE Trans Electr Devices 57(7):1504–1511
18. Vasallo BG, Wichmann N, Bollaert S, Roelens Y, Cappy A, González T, Pardo D, Mateos J (2007) Comparison between the dynamic performance of double-and single-gate AlInAs/InGaAs HEMTs. IEEE Trans Electr Devices 54(11):2815–2822
19. Sugiyama H, Hoshi T, Yokoyama H, Matsuzaki H (2012) Metal-organic vapor-phase epitaxy growth of InP-based HEMT structures withInGaAs/InAs composite channel. In: 2012 international conference on indium phosphide and related materials. IEEE, New York, pp 245–248
20. Xue F, Zhao H, Chen Y-T, Wang Y, Zhou F, Lee JC (2011) High-k InGaAs metal-oxide-semiconductor field-effect-transistors with various barrier layer materials. Appl Phys Lett 99(3):033507
21. Xue F, Zhao H, Chen Y-T, Wang Y, Zhou F, Lee JC (2011) InAs inserted InGaAs buried channel metal-oxide-semiconductor field-effect-transistors with atomic-layer-deposited gate dielectric. Appl Phys Lett 98(8):082106
22. Chang E-Y, Kuo C-I, Hsu H-T, Chiang C-Y, Miyamoto Y (2013) InAs thin-channel high-electron-mobility transistors with very high current-gain cutoff frequency for emerging submillimeter-wave applications. Appl Phys Express 6(3):034001
23. Ajayan J, Subash TD, Kurian D (2017) 20 nm high performance novel MOSHEMT on InP substrate for future high speed low power applications. Superlattices Microstruct 109:183–193
24. Alam MT, Islam SK (2006) A modified model for Si/SiGe MOS-gate delta-doped HEMTs. Microelectron J 37(9):938–942
25. Kim D-H, del Alamo JA (2009) Scalability of sub-100 nm thin-channel InAs PHEMTs. In: 2009 IEEE international conference on indium phosphide & related materials. IEEE, New York, pp 132–135
26. Kumar RS, Mohanbabu A, Mohankumar N, Godwin Raj D (2017) In0. 7Ga0. 3As/InAs/In0. 7Ga0. 3As composite-channel double-gate (DG)-HEMT devices for high-frequency applications. J Comput Electron 16(3):732–740
27. Jie H, Tianyi G, Haiying Z, Jingbo X, Xiaojun F, Hao Y, Jiebin N (2010) 120-nm gate-length In0. 7Ga0. 3As/In0. 52Al0. 48As InP-based HEMT. J Semiconduct 31(7):074008

28. Fatah F, Kuo C-I, Hsu H-T, Chiang C-Y, Hsu C-Y, Miyamoto Y, Chang EY (2012) Bias-dependent radio frequency performance for 40 nm InAs high-electron-mobility transistor with a cutoff frequency higher than 600 GHz. Japanese J Appl Phys 51(11R):110203
29. Wu YQ, Xu M, Wang RS, Koybasi O, Ye PD (2009) High performance deep-submicron inversion-Mode InGaAs MOSFETs with maximum G m exceeding 1.1 mS/μm: New HBr pretreatment and channel engineering. In: 2009 IEEE international electron devices meeting (IEDM). IEEE, New York, pp 1–4
30. Egard M, Ohlsson L, Borg BM, Lenrick F, Wallenberg R, Wernersson L-E, Lind E (2011) High transconductance self-aligned gate-last surface channel In 0.53 Ga 0.47 As MOSFET. In: 2011 international electron devices meeting. IEEE, New York, pp 13–2
31. Yonai Y, Kanazawa T, Ikeda S, Miyamoto Y (2011) High drain current (> 2A/mm) InGaAs channel MOSFET at V D= 0.5 V with shrinkage of channel length by InP anisotropic etching. In: 2011 international electron devices meeting. IEEE, New York, pp 13–3
32. Li Q, Zhou X, Tang CW, Lau KM (2013): Material and device characteristics of metamorphic $In_{0.53}Ga_{0.47}As$ MOSHEMTs Grown on GaAs and Si Substrates by MOCVD. IEEE Trans Electron Devices 60(12):4112–4118

FPGA Realization of Reconfigurable DA-Based Digital FIR Filter Using DRPPG and MCSA Techniques

G. O. Jijina, R. Mohana Priya, and P. Solainayagi

Abstract This article presents an efficient multiplication and accumulation (MAC) approaches called "distributed arithmetic (DA) based MAC" and "reconfigurable implementation-based MAC" for alleviating the hardware performances of digital filters. Both reconfigurable implementation and DA-based techniques are combined in this paper at the first time with the help of suitable accumulation structure called "modified carry-save adder (MCSA)" and parallel reconfigurable structure called "dynamically reconfigurable architecture (DRA). Traditionally, DA-based FIR filter implementations require large size of look-up table (LUT) for storing the filter coefficient values. The most disadvantage of DA-based FIR filter implementation is the absence of configurability. Hence, traditional DA-based FIR filter is not suited to wider range of applications. In order to reduce the problem, reconfigurable technique is introduced in MAC unit of DA-based FIR filter implementation. To reduce the complexity form of partial product generation, Reduced Wallace Tree Generation (RWTG) is used along with MAC unit of reconfigurable DA-based FIR filter implementation. In the final stage of RWTG, efficient adder structures are essential to add "n" bit binary data. To meet this requirement, MCSA-based adder is used in the final stage of RWTG. Finally, dynamic or distributed reconfigurable partial product generation (DRRPG) is introduced for producing parallel execution of PPG. Proposed design is estimated by using ALTERA field programmable gate array (FPGA) board by using Quartus II Web Edition tool. The performances of proposed design are validated after implementing in ALTERA FPGA design tool.

Keywords Finite impulse response (FIR) filter · Distributed arithmetic (DA) based FIR filter · Partial product generation (PPG) · Dynamic or distributed reconfigurable partial product generation (DRPPG) · Multiplication and

G. O. Jijina (✉) · R. Mohana Priya
Department of Electronics and Communication Engineering, Aarupadai Veedu Institute of Technology, Chennai, Tamil Nadu, India
e-mail: Jijina.88@gmail.com

P. Solainayagi
Department of Computer Science and Engineering, Madha Engineering College, Kundrathur, Chennai, India

D. K. Sharma et al. (eds.), *Micro-Electronics and Telecommunication Engineering*,
Lecture Notes in Networks and Systems 179,
https://doi.org/10.1007/978-981-33-4687-1_50

accumulation (MAC) unit · Reduced wallace tree Generation(RWTG) · Very large-scale integration (VLSI) system · Field programmable gate array (FPGA)

1 Introduction

Reconfigurable finite impulse response (FIR) filter plays an important role in the software-defined radio (SDR) systems. Filter coefficients are dynamically changed in reconfigurable FIR filter. The most disadvantage of FIR filter is the configurability. Due to lack of configurability, FIR filter is not sufficient transmission system. Hence, it is essential to reconfigure the filter coefficients dynamically. Multiple constant multiplication (MCM) is the well-known technique used for implementation of FIR filters. This multiplication is not suited in reconfigurable FIR filter. Hence, it is required to design the specialized multiplication and accumulation (MAC) unit for the reconfigurable FIR filter. The MAC unit has three important blocks for performing the digital multiplication process: partial product generation (PPG), Wallace Tree Generation (WTG) and accumulation structure. In general, half adders (HAs) and full adders (FAs) are used in PPG block for generating the partial product generation results. WTG stages are used to reduce the complexity of hardware structures between PPG and accumulation block. In the accumulation block, an efficient "n" bit adder is required to perform the addition operation.

A lot of research works have suggested the "distributed arithmetic" technique for exhibiting the multiplication function due to reducing the complexity of computational path. Hence, DA-based MAC unit is referred as "multiplier-less architecture". In pipelined DA-based FIR filter, look-up table (LUT) partitioning technique has been used for reducing the memory required. In order to design the pipelined DA-based FIR filter, offset binary coding (OBC) technique is used in [1]. The conventional DA-based FIR filter implementation technique assumes that impulse response coefficients are fixed, and this makes it possible to use read-only memory (ROM) based LUTs. The memory requirement of those filter technique has increased exponentially with fixed filter order. To reduce this problem, systolic decomposition (SD) techniques are suggested by [2, 3].

In reconfigurable DA-based FIR filter, random access memory (RAM) based LUTs are used instead of ROM-based LUTs. Filter coefficients are dynamically changed or updated in RAM-based LUT techniques [4]. These works suggest the DA techniques for performing multiplication functions. However, the performance of pipelined DA-based multiplier is not sufficient for the long byte multiplications. In order to reduce this problem, distributed or dynamically reconfigurable partial product generation (DRPPG) based reconfigurable FIR filter has been developed in this paper. In addition, data flow structure (computational path structure) of carry-save adder (CSA) is modified for improving the hardware performance of FIR filter. Developed MCSA- and DRPPG-based reconfigurable DA-based FIR filter has been synthesized by using ALTERA Quartus II Web Edition tool.

2 Study Work

In DA-based FIR filter, filter coefficients are stored in LUT functioning as a ROM; hence, it is called as multiplier-less architecture. However, memory size of DA-based FIR filter increases when increasing the filter order. In order to reduce this problem, pipelined DA-based FIR filter has been designed in Sudhakar et al. [5]. In this approach, BAAT technique is used to divide the processing element as two parts. However, this technique is not well suited to long byte multiplication. Hence, offset binary coding (OBC) based LUT partitioning technique has been incorporated into DA-based FIR filter [1]. Further residue number system (RNS) and dynamic distributed arithmetic algorithm (DDAA) based FIR filters have been developed in [6].

Field programmable gate array (FPGA) realization of DA-based FIR filter has been proposed in [3], where the systolic decomposition scheme has been found. It offers a flexible choice of the address length of the look-up table (LUT) for DA-based computation to exhibit suitable area time trade-off. The developed architecture provides parallel execution. The research work of [7] demonstrates the parallel execution of DA-based FIR filter. However, one of the most disadvantages of available parallel DA-based FIR filter is more complexity of the architecture. To reduce this complexity, DRPPG-, MCSA- and RWTG-based reconfigurable DA FIR filter has been developed in this research work. The parallel and distributed structure of Park and Meher [8, 11–13] considered as the base work of the proposed MCSA-, DDRPPG-based reconfigurable DA FIR filter design.

3 Direct Form FIR Filter Design

Finite impulse response (FIR) filter is the best filter technique in which unwanted/distortion/noise signals are filtered at finite impulse duration periods. For instance, the architecture of symmetric form 8-tap FIR filter structure has been illustrated in Fig. 1. Programmable shift control (PSC) controls the n-tap filter operation. The main goal of the FIR filter is to filter the distortion signals at finite impulse duration period. Multiplication and accumulation unit (MAC) function helps to filter the unwanted signal at appropriate period with the help of filter coefficient values [14, 15]. Intermediate registers are used to provide the synchronization between input data and output data.

However, the direct form FIR filter is not sufficient for future applications such as OFDM- or SDR-based wireless communication transmission, because it filters the input signal only on the limited duration of the finite impulse. The input–output relation of linear time invariant (LTI) system is indicated as follows,

$$y(n) = \sum_{k=0}^{N-1} c_k x(n-1) \tag{1}$$

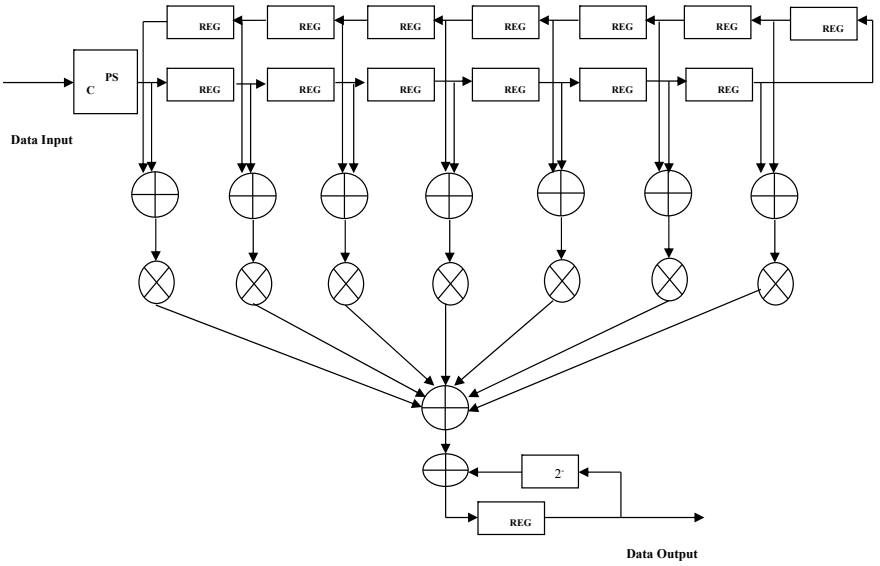

Fig. 1 Architecture of 8-tap FIR filter

where C_k is the filter coefficient values, $x(n)$ is the input data sequence, N is the order of the filer, $y(n)$ is the output data sequence, and $x\,(n-1)$ is the shifted version of input data sequence. Practically, more number of taps is necessary to reduce the noise reduction and obtain the high spectral containment.

The computational delay of FIR filter has risen due to combinatorial functions of addition and multiplication. These disadvantages can be contained with the help of parallel and pipelining implementation techniques [16, 17]. The improvement of the hardware performance in terms of VLSI criteria has implied large optimization endeavors on the direct form FIR filter. However, direct form FIR filter is not sufficient to noise reduction application, because it filters the signals at fixed coefficient values only. Hence, filter coefficients need to be changed dynamically at run time. To meet the above requirement, reconfigurable FIR filter has been introduced by current research work. On the other hand, adaptive FIR filter also used to update the filter coefficients dynamically at run time.

4 Reconfigurable FIR Filter Design

In reconfigurable FIR filter, filter coefficients can change dynamically at run time. Reconfiguration technique makes a productive modification on existing configuration without altering any functionality, but it provides high performances in various aspects. To change the internal architecture of existing configuration, configuration

word is written manually. In perspective of reconfigurable FIR filter, filter coefficient values are stored in configuration bits for changing their values dynamically. For instance, constant shift multiplier (CSM) and programmable shift multiplier (PSM) based MAC unit uses the look-up tables for configuring the coefficient values manually. Both these techniques provide good reconfigurability with best efficiency in different types of aspects. However, this reconfigurable FIR filter is not sufficient for the large bit operation. For example, configuration word of PSM-based reconfigurable FIR filter has been illustrated in Table 1.

In those configuration words, S indicates sign bit, if S = 0 means reconfigurable FIR filter can perform unsigned MAC functions; otherwise, it performs signed MAC functions. DDDD represents values from 2^0 to 2^{-15}, which indicates the data shifting values. XX indicates the formation of input values, and internal function of XX values has been illustrated in Table 2. MMMML represents the values for shifting the final data into appropriate positions.

Based on this configuration, coefficient values are dynamically changed during the run time. However, the main disadvantage of this reconfigurable FIR filter is the limiting configuration. Once the coefficient values are configured in the LUTs, the system will run properly for them and only them. Other than configured values, it cannot execute perfectly. Further to improve the reconfigurability of FIR filter, multiplier control signal decision (MCSD) window has been introduced by last decade. This principle helps to reduce the "switching" activities of FIR filter with the help of "amplitude detector (AD)" and "control signal generator (CSG)" circuits. CSG signal generates the control signal for generating the count pulse. It will help to reduce the switching activities of digital FIR filter. Further to make reconfiguration of FIR filter, distributed or dynamically reconfigurable partial product generation (DRPPG) based MAC functions have been implemented in this paper.

Table 1 Configuration word of PSM-based reconfigurable FIR filter

LUT_W1	S D D	DD X X	DDDD	X X M MMML
LUT_W2	D DDD XX	D DDD X	X D DD	D X X

Table 2 Internal function of XX

XX	X
00	X + 2-1X + 2-2X
01	X
10	X + 2-1X
11	X + 2-2X

5 Distributed Arithmetic-Based FIR Filter Design

Distributed arithmetic (DA) based digital FIR filter uses LUTs to store the filter coefficient values as ROM. In this multiplier, MAC function has been performed without help of multiplier circuit. Hence, DA multiplier circuit is named as "multiplier-less" circuit. In order to reduce the storage size of ROM, pipeline-based designs have been proposed further. However, pipeline-based LUTs are utilized more number of hardware slices and registers to avoid the asynchronous effect. Filtering functions are mathematically represented as follows,

$$y = A_1 \times x_1 + A_2 \times x_2 + \cdots + A_n \times x_n \tag{2}$$

$$y = \sum_{k=1}^{n} A_k \, x_k \tag{3}$$

In DA-based multiplier, both signed and unsigned multiplications are performed with the help of offset binary coding (OBC) technique. It reduces the memory size and sequential delay of the LUT. However, it increases slice hardware and power consumption of the circuits. The basic building blocks of traditional DA-based FIR filter have been illustrated in Fig. 2.

As shown in Fig. 2, filter coefficients are stored in LUT table. Final accumulator and shifter circuit provide the additional function of MAC unit. This circuit operates only for unsigned values. For signed values, OBC-based LUT partition techniques have been implemented. For instance, input X_k has been represented as follows,

$$x_k = \frac{1}{2}[x_k - (-x_k)] \tag{4}$$

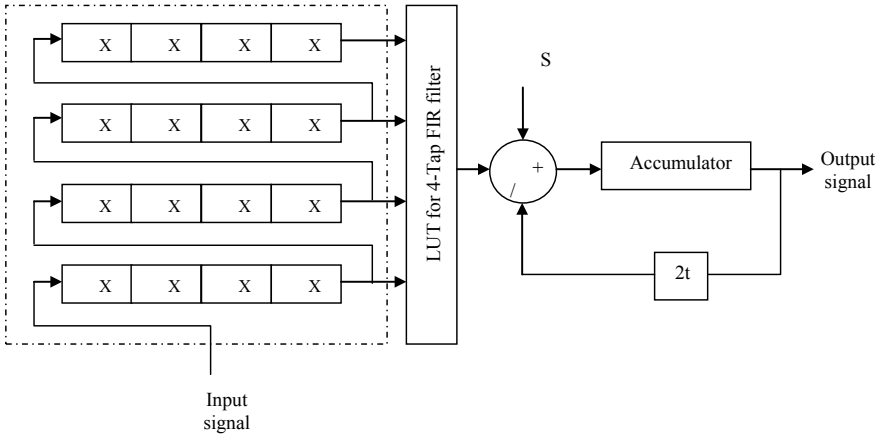

Fig. 2 DA-Based FIR filter Implementation

When taking 2′s complement, it will get,

$$-x_k = -\overline{b}_{k0} + \sum_{m=1}^{N-1} \overline{b}_{km}\, 2^{-m} + 2^{-(N-1)} \tag{5}$$

Re-writing the value, we get,

$$x_k = \frac{1}{2}\left[-\left(b_{k0} - \overline{b}_{k0}\right) + \sum_{m=1}^{N-1} \left(b_{km} - \overline{b}_{km}\right) 2^{-m} - 2^{-(N-1)} \right] \tag{6}$$

The circuit diagram of OBC technique has been illustrated in Fig. 3. By extending Eq. (6), we will get,

$$y = \sum_{m=0}^{N-1} \frac{1}{2} \sum_{k=1}^{n} A_k\, c_{km}\, 2^{-m} - \frac{1}{2} \sum_{k=1}^{n} A_k\, 2^{-(N-1)} \tag{7}$$

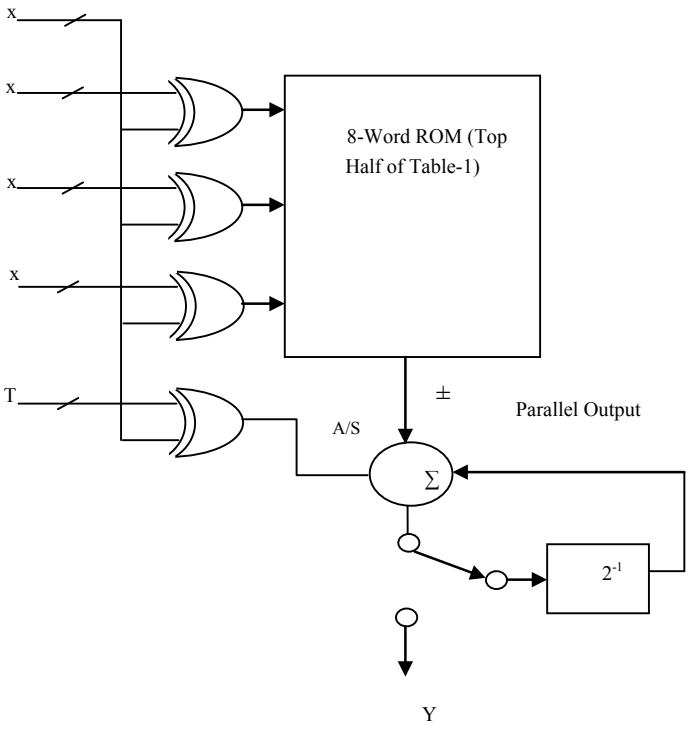

Fig. 3 OBC-based LUT partitioning technique

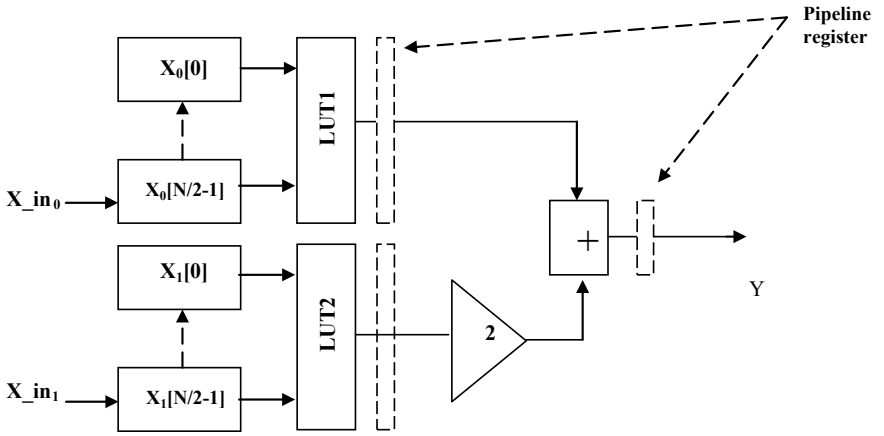

Fig. 4 Pipelined DA-based FIR filter

Based on OBC techniques, LUT is partitioned by two half, and further, it can be processed by shifter and adder unit for performing "n" tap filter function. In addition, pipelined register is used along with OBC technique for reducing the asynchronous effect between data inputs. The architecture of pipelined DA-based FIR filter has been illustrated in Fig. 4. However, it has only limited coefficient values in LUT which is not sufficient to real-time applications. Hence, it is essential to adapt the filter coefficient values in every clock cycle to provide more reconfigurability with increasing efficiency in various aspects.

6 Classification

In this paper, stroke brain image is identified using deep learning algorithm for eliminating the limitations in conventional machine learning methods. CNN classification is used in this paper as deep learning method for classifying the source brain MRI image into either stroke image or non-stroke image. This CNN classifier has number convolutional layers with pooling functions and feed-forward neural network at the end of this classification architecture. The convolutional layers in this proposed method filter the nonlinear properties of each pixel in extracted features, and 32 convolutional layers are used in this paper. The extracted features are passed through all these 32 convolutional layers, and linear convolution function is applied between the extracted feature set and the kernel of each convolutional layer. The extracted features from the output of these convolutional layers are high in dimensions; the pooling function is applied in order to reduce the size of the features which are produced at the end of the final convolutional layer. In Fig. 4, the average and max pooling function is explained clearly for reducing the size of the feature set. In

this paper, max pooling function has more advantages than the average pooling as depicted in Fig. 4.

7 Proposed Reconfigurable Distributed Arithmetic-Based FIR Filter Design

The proposed structure of reconfigurable DA-based FIR filter for FGPA implementation is shown in Fig. 5. Serial-in, parallel-out shift register (SISOSR) is used to get the input samples $x(n)$ at every sampling instant. It decomposes the every most recent sample to D vectors b_d of length M for $d = 0, 1, \ldots, D-1$ and feeds them to D reconfigurable partial product generators (RPPGs) to generate the partial product generation (PPG) results. In Park and Meher [8], multiplexor-based RPPG generation process is demonstrated to calculate the partial product results. It is not possible to reduce the hardware complexity of MAC unit, since the configuration of coefficients is not limited to fixed values anymore. In order to overcome this problem, Bi-Recorder methodologies have been incorporated in the proposed RPPG unit. The structure of

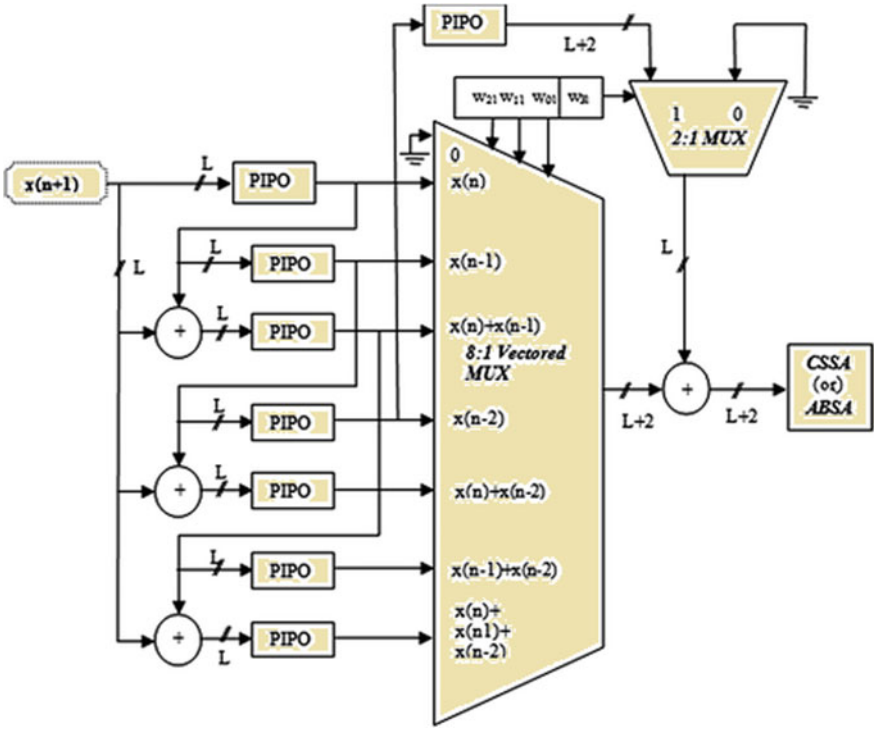

Fig. 5 Proposed structure of reconfigurable DA-based FIR filter

proposed Bi-Recorder methodologies-based RPPG unit is shown in Fig. 6. In the traditional method, multiplexer is used to only select the appropriate filter coefficient values for the respective input (length M) bits. But, in case of proposed methodologies, multiplexer is used to select the appropriate filter coefficients as well as perform the multiplication also. The multiplication function has been performed based on input (length M) bits. Table 3 illustrates the function of Bi-Recorder.

PPG functions have been successfully carried out with the help of Bi-Recorder multiplier. Further, in order to re-arrange the partial product results, efficient Wallace Tree Generation (WTG) methodologies are required. This research work used

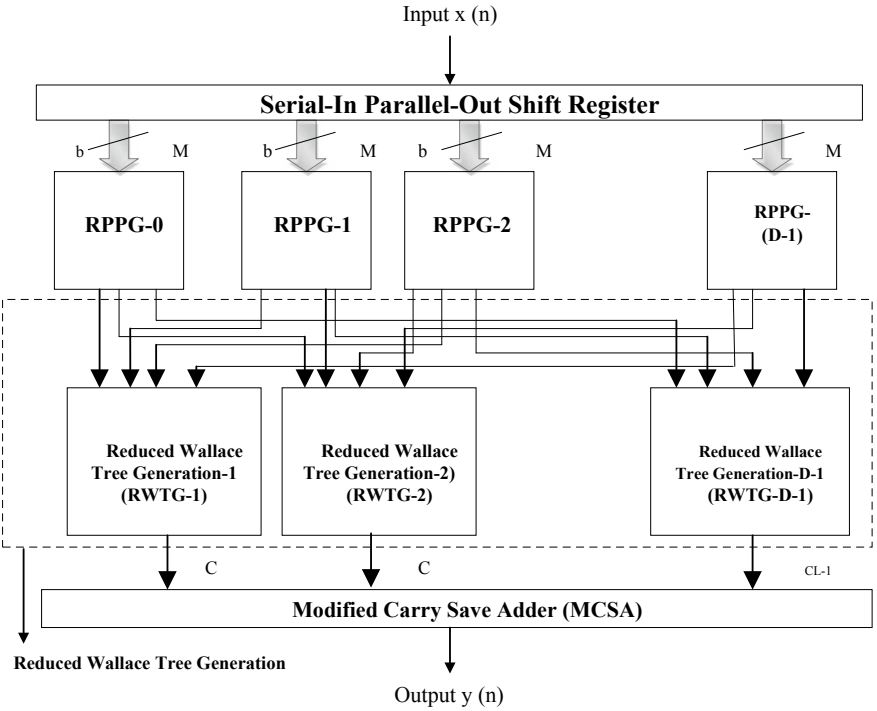

Fig. 6 Proposed structure of Bi-Recorder methodologies-based RPPG unit

Table 3 Function of Bi-Recorder

Input bits (length $M = 2$)	Symbols	Functions
00	R1	0
01	R2	Appropriate filter coefficient
10	R3	Appropriate filter coefficient $<<1$
11	R4	R2 + R3

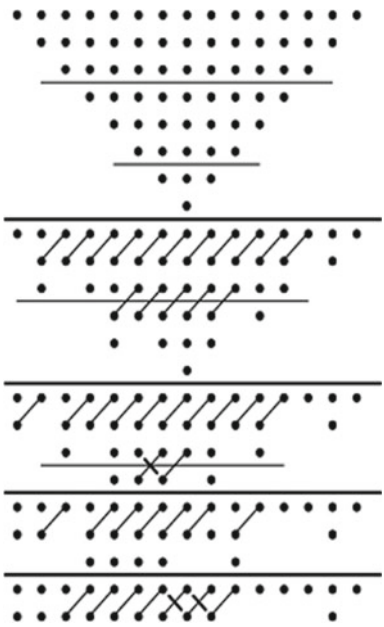

Fig. 7 Structure of Reduced Wallace Tree Generation (RWTG)

Reduced Wallace Tree Generation (RWTG) for re-arranging the PPG results. RWTG process utilizes less hardware (in terms of digital logical elements full adders and half adders) than WTG process. The structure of Reduced Wallace Tree Generation (RWTG) process is illustrated in Fig. 7 for the 8-bit multiplication. The traditional positions of partial products have been re-arranged in triangular order as shown in Fig. 7. The possibilities of three-bit combinations are collected for adding with the help of full adder (FA) circuits, and other remaining bits are directly moved to next stages. The process is repeated until it gets two "n" bit rows of digital data.

In the final stage of RWTG, a sufficient "n" bit adder is required to add the two "n" bit digital data. In traditional design, carry-save adder (CSA) has been proposed for performing the accumulation function. But in our proposed work, structure of CSA has been modified by dividing the "n" length of inputs into $\sqrt{n}$ groups, and then each group can be processed in a parallel manner. The architecture of MCSA for 16-bit accumulation is illustrated in Fig. 8 (Fig. 9 and 10).

As the principles explained above itself, four ($\sqrt{16}$) groups are used to perform 16-bit accumulation process in MCSA adder technique. Hence, 16-bit MCSA has only four times of carry propagation delay (CPD), whereas traditional 16-bit CSA has sixteen times of CPD delay. Hence, theoretically, it can possible to achieve best reduction in hardware slices as well as sequential delays than traditional one. The combined effects of all those techniques such as reconfigurable DA, reconfigurable PPG, RWTG and MCSA make a smoothen architecture of FIR filter. *Further, we introduce the distributed reconfigurable memories for performing long bit multiplication values. In distributed memory-based architecture, divide and sequence process*

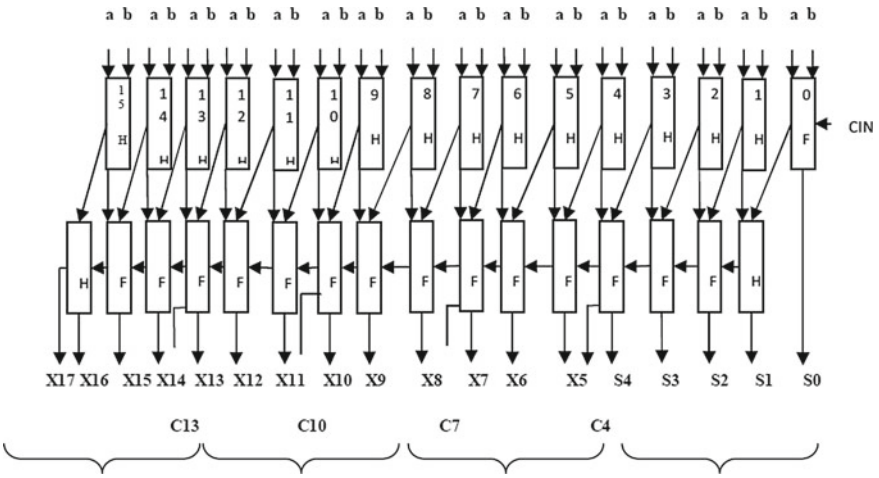

Fig. 8 Structure of modified carry-save adder (MCSA)

has been implemented for reducing more memory size, hardware slices and LUTs. For instance, 32-bit MAC functions can be performed with the help of 8-bit MAC functions by means of parallelism. Hence, performances of 32-bit MAC functions are mostly like the performances of 8-bit MAC functions. In the proposed work, this type of FIR filter is named as "distributed or dynamically reconfigurable DA-based FIR filter (DRDAFIR)".

8 Proposed Distributed or Dynamically Reconfigurable DA-Based FIR Filter

FPGA technology has been tremendous and swift growth in dedicated heterogeneous hardware system which is a popular choice in communication base stations instead of prototype platform. The proposed FIR filter design may also be implemented on FPGA. In this section, we propose distributed or dynamically reconfigurable DA-based FIR filter for FPGA implementation. The structure of Fig. 5 has $N\ (2^M - 1)/M$ number of registers for the implementation of LUTs for FIR filter of length N. But, registers are the crucial key elements in FPGA since each LUT has only two bits of registers in FPGA. Therefore in Park and Meher [8], LUTs are to be implemented by distributed RAM (DRAM) for FPGA implementation. Unlike RPPG, the multiple numbers of partial inner products cannot be retrieved from DRAM simultaneously. With the help of DRAM, to implement LUT for every bit slice will lead to high resource utilization. Thus, we require decomposing the structure into Q parallel sections, and each section has T time-multiplexed operations corresponding to T bit

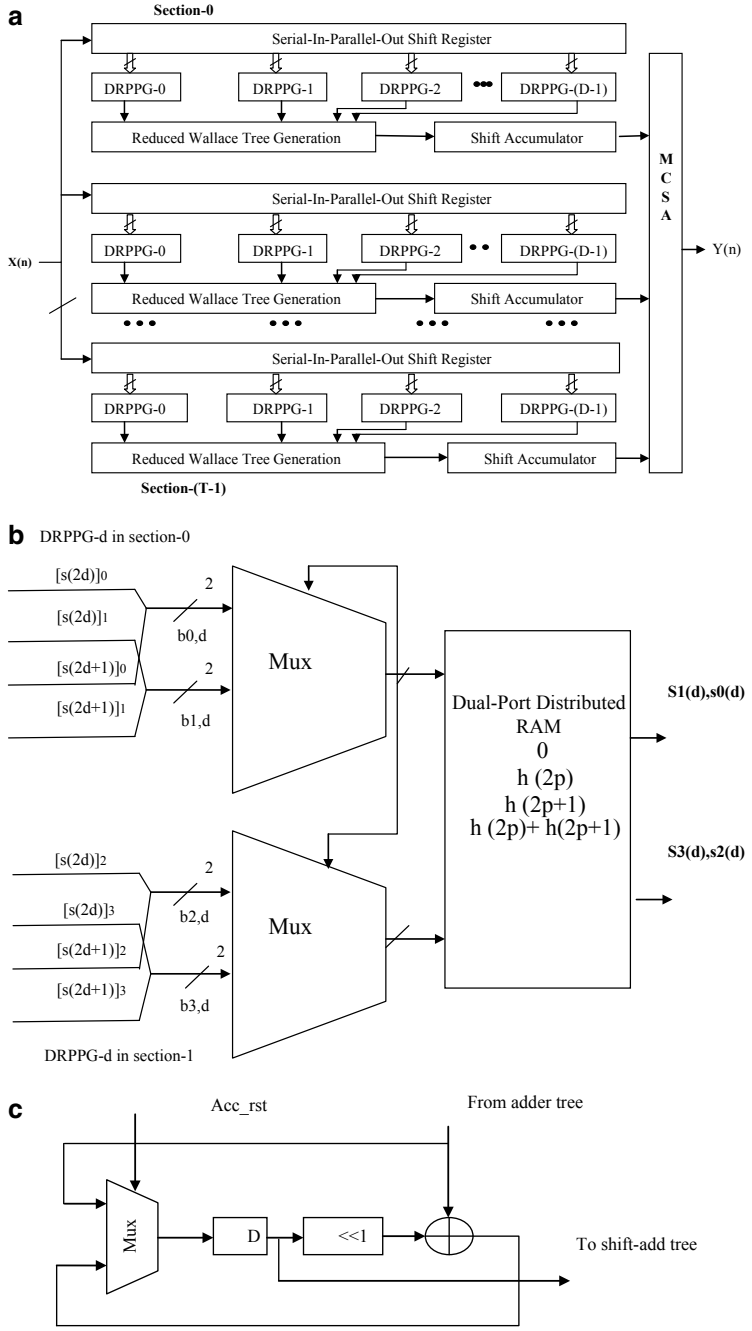

Fig. 9 A Proposed distributed or dynamically reconfigurable DA-based FIR filter, Structure of DRAM-based reconfigurable partial product generation (DRPPG), Structure of shift-accumulator

slices. When L is the bit length of composite number, $L = T^* Q$ (T and Q are the positive integers).

9 Performance Evaluation

The proposed designs have been implemented by using ALTERA FPGA board with the help of Quartus II software design tool. However, Xilinx 10.1i (Family: Spartan 3, Device: Xc3s50, Package: PQ208, Speed: -5) design tool is used to analyze the results of proposed designed with other traditional techniques. Simulation result of proposed DRPPG-based reconfigurable FIR filter has been illustrated in Fig. 10.The result shows that the filter produces different outputs for the same inputs based on the dynamic reconfiguration. Performances of synthesized results for the proposed DRPPG-based FIR filter has been compared in Table 4. The combinational delay is not reported for circuits without feedback. Area utilization and delay consumption are calculated based on Eqs. 9 and 10.

$$\text{AreaUtilization} = ((\text{Slices} + LUTs)/2) \tag{8}$$

$$\text{DelayConsumption} = ((\text{MinimumPeriod} + \text{Max.Inp.Arr.Time} + \text{Max.Oup.Req.Time})/2) \tag{9}$$

The proposed DRPPG-based DA FIR filter offers 24.24% reduction in hardware slices, 33.96% reduction in LUTs, 66.78% reduction in minimum input arrival

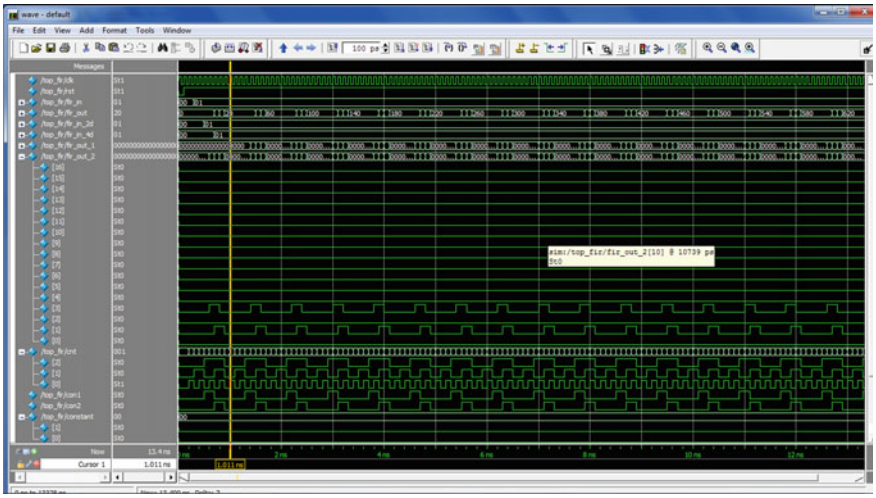

Fig. 10 Simulation result of proposed distributed or dynamically reconfigurable DRAM partial product generation-based FIR filter

Table 4 Performances of synthesis values of proposed DRPPG-based FIR filter with traditional techniques

Parameters/Types	Traditional design [8]	Traditional DA-based design [9, 4]	Pipelined DA [3, 10]	Proposed design
Slices	33	35	44	25
LUTs	53	44	59	35
Minimum period (ns)	6.688	4.518	4.858	8.240
Minimum input arrival time before clock (ns)	6.551	5.089	4.104	2.176
Maximum output required time after clock (ns)	9.844	17.448	18.904	6.280
Maximum combinational path delay (ns)	10.058			~
Frequency (MHz)	149.513	221.377	205.846	121.364
Total quiescent power (mW)	25	29	31	24
Total dynamic power (mW)	250	185	681	151
Total power (mW)	275	386	945	175
Area utilization	43	39.5	51.5	30
Delay consumption (ns)	7.694	9.018	9.288	5.565
Area delay product (ADP)	330.842	356.211	478.322	166.95

time before clock, 36.20% reduction in maximum output required time after clock, 30.23% reduction in area utilization, 27.67% reduction in total delay consumption and 49.53% reduction in ADP than traditional design [8]. Like that proposed DRPPG-based DA FIR filter offers 20.45% reduction in hardware slices, 28.57% reduction in LUTs, 57.21% reduction in minimum input arrival time before clock, 64% reduction in maximum output required time after clock, 24.05% reduction in area utilization, 38.29% reduction in total delay consumption and 53.13% reduction in ADP than traditional DA-based FIR filter [9, 4]. Proposed design offers 43.18% reduction in hardware slices, 40.67% reduction in LUTs, 46.97% reduction in minimum input arrival time before clock, 66.77% reduction in maximum output required time after clock, 41.74% reduction in area utilization, 40.08% reduction in total delay consumption and 65.09% reduction in ADP than pipelined DA-based FIR filter.

Comparison of area utilization, delay consumption, ADP and power consumption of proposed design with the traditional technique has been illustrated in Figs. 11,

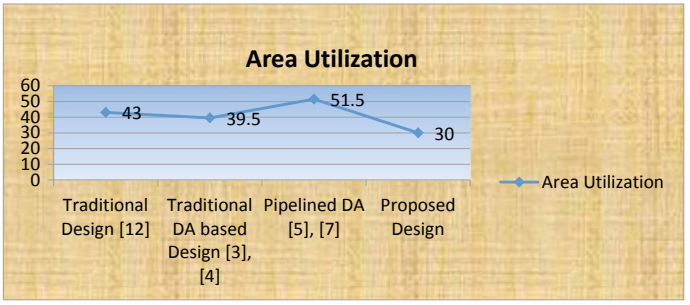

Fig. 11 Comparison of area utilization of proposed design with traditional designs

12 and 13, respectively. Further ALTERA FPGA has been used to implement the proposed design. Quartus II Web Edition tool has been used for synthesizing ad implementing the proposed design. Hardware implementation of proposed design has been illustrated in Fig. 14.

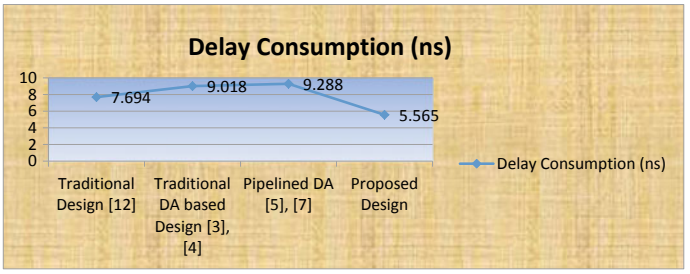

Fig. 12 Comparison of delay consumption of proposed design with traditional designs

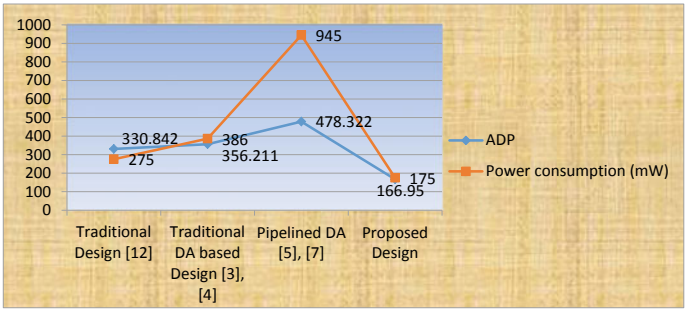

Fig. 13 Comparison of ADP and power consumption of proposed design with traditional designs

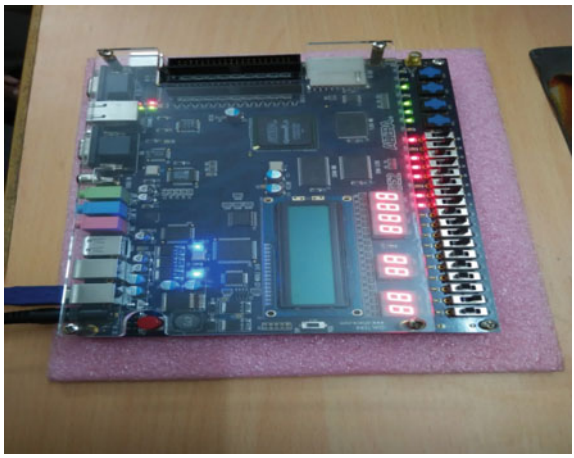

Fig. 14 Hardware implementation of proposed DRPPG-based reconfigurable DA FIR filter in ALTERA FPGA

10 Conclusion

In this paper, a new design of parallel reconfigurable FIR filter has been design for improving the configurability and hardware performances of digital FIR filter. A new design named "dynamic or distributed reconfigurable partial product generation (DRPPG) based PPG has been designed to re-configure the filter coefficients and perform the Bi-Recorder-based multiplication process. In order to reduce or re-arrange the PPG results, Reduced Wallace Tree Generation (RWTG) has been designed and implemented. Further in the final state of RWTG process, an efficient adder called "modified carry-save adder (MCSA)" has been incorporated into filter design for alleviating the entire hardware performances of hardware structures. Proposed DRPPG-based reconfigurable DA FIR filter has been synthesized and implemented by using ALTERA FPGA board. Quartus II Web Edition tool is used for implementing proposed design into ALTERA FPGA CYCLONE II IC. Output for proposed design has been evaluated through output device (LED). Programming has been finished in JTAG Mode. Proposed DRPPGA-based reconfigurable DA FIR filter offers 24.24% reduction in hardware slices, 33.96% reduction in LUTs, 66.78% reduction in minimum input arrival time before clock, 36.20% reduction in maximum output required time after clock, 30.23% reduction in area utilization, 27.67% reduction in total delay consumption, 36.36% reduction in power consumption and 49.53% reduction in ADP than traditional design. Because of reduced ADP, proposed FIR filter design will be absolutely suited to 3G- and 4G-based wireless communication applications.

References

1. Ghamkhari SF, Ghaznavi-Ghoushchi MB (2012) A low-power low-area architecture design for distributed arithmetic (DA) unit. In: 20th Iranian conference on electrical engineering, (ICEE2012), pp 232–237
2. Mohanty BK, Meher PK (2013) A high-performance energy-efficient architecture for FIR adaptive filter based on new distributed arithmetic formulation of block LMS algorithm. IEEE Trans Signal Process 61(4):921–932
3. Meher PK, Chandrasekaran S, Amira A (2008) FPGA realization of FIR filters by efficient and flexible systolization using distributed arithmetic. IEEE Trans Signal Process 56(7):3009–3017
4. Meher PK, Park SY (2011) High-throughput pipelined realization of adaptive FIR filter based on distributed arithmetic. In: 2011 IEEE/IFIP 19th international conference on VLSI and system-on-chip, pp 428–433
5. Sudhakar V, Murthy NS, Anjaneyulu L (2012) Area efficient pipelined architecture for realization of FIR filter using distributed arithmetic. In: International conference on industrial and intelligent information (ICIII 2012) IPCSIT, vol 31
6. Vigneswaran T, Kumar JS, Reddy PS (2007) Design of digital FIR filter using Dynamic Distributed Arithmetic Algorithm with improved table look up scheme for residue number system. In: IET-UK international conference on information and communication technology in electrical sciences (ICTES 2007), pp 606–610
7. Hwang S, Han G, Kang S, Kim J (2004) New distributed arithmetic algorithm for low-power FIR filter implementation. IEEE Trans Signal Process Lett 11(5):463–466
8. Park SY, Meher PK (2014) Efficient FPGA and ASIC realizations of a DA-based reconfigurable FIR digital filter . IEEE Trans Circuits Syst II: Express Briefs 61(7):511–515
9. Meher PK (2010) New approach to look-up-table design and memory-based realization of FIR digital filter. IEEE Trans Circuits Syst I: Regular Papers 57(3):592–603
10. Ramesh R, Nathiya R (2012) Realization of FIR filter using modified distributed arithmetic architecture. Signal Image Process: Int J (SIPIJ) 3(1):83–94
11. Mehendale M, Sinha A, Sherlekar SD (1998) Low power realization of FIR filters implemented using distributed arithmetic. In: Proceedings of 1998 Asia and South Pacific design automation conference, pp 151–156
12. Guo R, DeBrunner LS (2011) Two high-performance adaptive filter implementation schemes using distributed arithmetic. IEEE Trans Circuits Syst II: Express Briefs 58(9):600–604
13. Xiao S, Chen Y, Luo P (2010) The design of FIR filter base on improved DA algorithm and its FPGA implementation. In: 2010 The 2nd international conference on computer and automation engineering (ICCAE), vol 2, pp 589–591
14. Zhou Y, Shi P (2011) Distributed Arithmetic for FIR Filter implementation on FPGA. In: 2011 international conference on multimedia technology, pp 294–297
15. Hemalatha RJ, Vijaybaskar V, Thamizhvani TR (2019) Automatic localization of anatomical regions in medical ultrasound images of rheumatoid arthritis using deep learning. Proc Inst Mech Eng 233(6):657–667
16. Narayanan KL, Ramesh GP (2017) Vlsi Architecture for 2D-Discrete Wavelet Transform (DWT) Based Lifting Method. Ind J Public Health Res Dev 8(3):644–649
17. Ravichandran S (2017) Design of finite impulse response filter architecture using Wallace tree multipliers. Int J MC Square Sci Res 9(3):1–7

Indian Air Quality Health Index Analysis Using Exploratory Data Analysis

Venkatesh Gauri Shankar, Bali Devi, Anurag Bhatnagar, Akhilesh Kumar Sharma, and Devesh Kumar Srivastava

Abstract Air quality management requires dependable data of air quality gathered, assessed and broke down normally. This is of foremost significance in shielding man and his condition from harming introduction to air contamination. The information for SPM, SO_2 and NO_2 were gathered at three locales speaking to private, business and mechanical action zones at all the destinations. In light of this information, the Air Quality Record (AQI) was determined utilizing Oak Edge Air Quality File (ORAQI). This means that the absolute impact of the considerable number of contaminations together. Figuring's of AQI for various seasons and diverse movement zones are done to look at the contamination level. In the current article an endeavour is likewise made to consider the adjustment in contamination status during the most recent decade utilizing the month to month mean information. To investigate and anticipate the degree of Air File level throughout the years from 1990 to 2015 to show signs of improvement comprehension of the patterns and examine how significant government strategies have influenced the Quality File. The point of this paper is to advise open with respect to by and large prominence of air quality through a rundown boundary that is straightforward, Educate residents about related wellbeing effects of air contamination presentation; and Rank urban areas/towns for organizing activities dependent on proportion of AQI.

Keywords SPM · Exploratory data analysis · Health index · Linear regression · Machine learning · Air quality

V. G. Shankar · B. Devi (✉) · A. Bhatnagar · A. K. Sharma · D. K. Srivastava
School of Computing and IT, Manipal University Jaipur, Jaipur, Rajasthan, India
e-mail: baligupta03@gmail.com

V. G. Shankar
e-mail: venkateshgaurishankar@gmail.com

D. K. Sharma et al. (eds.), *Micro-Electronics and Telecommunication Engineering*,
Lecture Notes in Networks and Systems 179,
https://doi.org/10.1007/978-981-33-4687-1_51

1 Introduction

Air contamination because of anthropogenic sources involves worry in entire world. The urban regions might be seen as thick wellsprings of tremendous anthropogenic emanations of toxins, which can adjust the climatic creation, science and life phases in its down-wind systems, stretching out more than a few hundred kilometers [1]. Air contamination is one of the significant issues looked by the individuals all inclusive, particularly in urban regions of creating nations, which is not just quick development of populace yet in addition industrialization. Sulfur dioxide (SO_2), nitrogen dioxide (NO_2) and RSPM are viewed as significant air poisons in India. India, a creating nation, is one of the initial ten modern nations of the world. As a result of the improved anthropogenic exercises in India, air contamination issues have become a subject of extreme discussion at all stages [2]. As indicated by an investigation delivered by World Financial Gathering in Davos, India has the most exceedingly awful air contamination in the whole world, defeating China, Pakistan, Bangladesh and Nepal. Of the complete 132 nations whose ecological resources were overviewed, India positioned dead toward the end 'noticeable all around (consequences for human well-being)' positioning. The connection among condition and the advancement is one of the most consuming issues of the current occasions. Formative exercises, for example, modern transportation, constructional work and so forth, cause debasement and radical changes in each segment of condition specifically, hydrosphere, lithosphere, environment and biosphere through contamination. Air contamination has risen in the previous scarcely any decades as the most urgent issue to humankind [3].

'To embrace/build up an Air Quality List (AQI) in light of national air quality guidelines, well-being effects and checking program which speaks to distinguishable air quality for open in straightforward terms and aid information understanding and dynamic procedures identified with contamination relief gauges.' The venture researches the convergence of the toxins sulfur dioxide (SO_2), nitrogen dioxide (NO_2) and particulate issue (PM10) created from different wellsprings of enterprises over the surrounding Air Nature of the GIDA (Gorakhpur) [4]. The significant poisons as recommended by the Focal Contamination Control Board (CPCB) in a mechanical region are sulfur dioxide (SO_2), oxides of nitrogen (NO_2) and particulate issue (PM10) [1]. We have collected dataset from Open Government Data Platform of India [5].

2 Background

AQI—An air quality index is a digit used by government workplaces to show how the environment is actually sullied or how bad it is to get [6].

SO_2—Sulfur dioxide (SO_2) adds to respiratory side effects in both sound patients and those with basic pneumonic illness. Controlled human introduction considers

have shown that test SO_2 presentation causes changes in aviation route physiology, including expanded aviation routes obstruction [3].

NO_2—Encompassing NO_2 introduction may expand the danger of respiratory lot diseases through the poison's association with the safe framework [4].

SPM—Climatic airborne material, in any situation labeled barometric particulate matter, particulate matter (PM), particulates or suspended particulate matter (SPM) are minuscule liquid or solid matter embedded in the atmosphere of the Earth [7].

3 Methodology

3.1 Detailed Methodology that Will Be Adopted

Many methods are used to calculate AQI in different countries.

Oak Ridge Air Quality Index (ORAQI Method) [1]:

For the general location of a general air quality status at various areas of the investigation region, the Oak Edge National Air Quality Database (ORNAQI) can be regarded. AQI for every area in the investigation region has been assessed with the assistance of a scientific condition created by the Oak Edge National Research center (ORNL), USA [3], as given underneath:

$$AQI = [39.02 \sum X_i / X_s]^{0.967}$$

where,

X_i = estimation of air quality boundaries (RSPM, SO_2 and NO_2).

X_s = Standard and endorsed for air quality boundaries.

Table 1 Relative AQI and scale

Value	Description	Health effects
0–25	Clean air	None or negligible well-being impacts
26–50	Light air pollution	Conceivable respiratory or cardiovascular impact for most touchy people
51–75	Mild air pollution	Expanding like hood of respiratory and cardiovascular side effects and ailments
76–100	Heavy air pollution	Exacerbation of heart or lung illness. Expanded danger of death in kids (heart and lung malady) expanded impacts all in all populace
> 100	Severe air pollution	Genuine exacerbation of heart or lung illness. Expanded danger of sudden passing. Genuine danger of cardio respiratory indications all in all populace

Source [4]

Table 2 Ambient air quality standards 24 hours average

	Residential, rural and other areas	Industrial areas	Sensitive areas
SO_2	80	120	30
NO_2	80	120	30
SPM	200	500	100

AQI then estimated and analyzed relative ORAQI esteem given in Tables 1 and 2.

3.2 Methodology Used for Predicting Future Air Quality Index

Regression and log-linear models [4] can be used to provoke the details provided. The material is proven to suit in a constructive manner in the clear dropping away from the faith [8]. For example, an emotional variable, y (known as a reaction variable), will occur as a trigger constraint of another excentric variable, x (known as a marker variable), with the condition:

$$y = wx + b$$

where the differentiation is recognized for being strong in y. As for the mining of knowledge, x and y are characteristics of numeric databases. The coefficients, w and b (called dropping apart from the faith coefficients), autonomously indicate the line stage and the y-get. These coefficients can be loosened up by the method for least squares, which limits the slipup between the authentic line confining the information and the proportion of the line [9, 10].

4 Implementation and Results

Data Preprocessing—Data preprocessing is an information mining method that consolidates changing unpleasant information into a sensible affiliation. Certified information is consistently missing, conflicting and furthermore debilitated in express practices or skims and is in all probability going to contain different misunderstandings. Information preprocessing is an indicated system for settling such issues. Data preprocessing plans unrefined data for extra getting ready. In our dataset, we redenoted our portions to make them less hard to grasp and type for repeated use [11].

Data Cleaning—It is the road to identifying and changing (or emptying) degenerate or misguided documents from a record collection, list or database and insinuates perceiving bits of data broken, off base, wrong or useless and then overriding, adjusting or deleting soiled or coarse details. In our data, we rectified the off base date portions and cleared invalid segments which wasted space on our plate and exhausted memory [12].

Data Visualization—This is an overall concept that represents every move through placing it in a visual context to make individuals grasp the value of knowledge. Types, types and connections that can go undetected in text-based knowledge may be discovered and perceived through programming for information processing as less problematic. We have plotted observation count plots for NO_2, SO_2 and SPM to determine which states have a higher number of observation count, and more observation count generally results in more accurate representation of data. The states in our top 5 observation count are of focus for our analysis along with observation count plot and we have plotted heat maps for SO_2, NO_2, SPM and AQI to give a general overview of the countries AQI [3, 6].

Data Prediction—We applied linear regression [8, 12] on the states for which we have the most frequency of values to create a more accurate model in our project; on application of linear regression, we predicted approximate future values of AQI for the next 5 years and plotted them for the following states—Haryana, Maharashtra, Puducherry, Madhya Pradesh, Himachal Pradesh, Tamil Nadu and Goa.

SO_2—Sulfur dioxide (SO_2) adds to respiratory indications in both solid patients and those with basic pneumonic sickness. Controlled human introduction examines have shown that test SO_2 presentation causes changes in aviation route physiology, including expanded aviation routes obstruction. SO_2, NO_2 and SPM heat map-based exploratory data analytics is shown in Figs. 1, 2 and 3.

NO_2—Encompassing NO_2 presentation may build the danger of respiratory parcel contaminations through the toxin's cooperation with the resistant framework.

SPM—Climatic airborne particles, in any case called barometrical particulate issue, particulate matter (PM), particulates or suspended particulate matter (SPM) are minuscule solid or liquid issue suspended in Earth's condition.

A sample state-wise prediction for next five years is given in Fig. 4.

We have evaluated accuracy on the basis of prediction for SO_2, NO_2 and SPM for air quality index and reported result in Table 3.

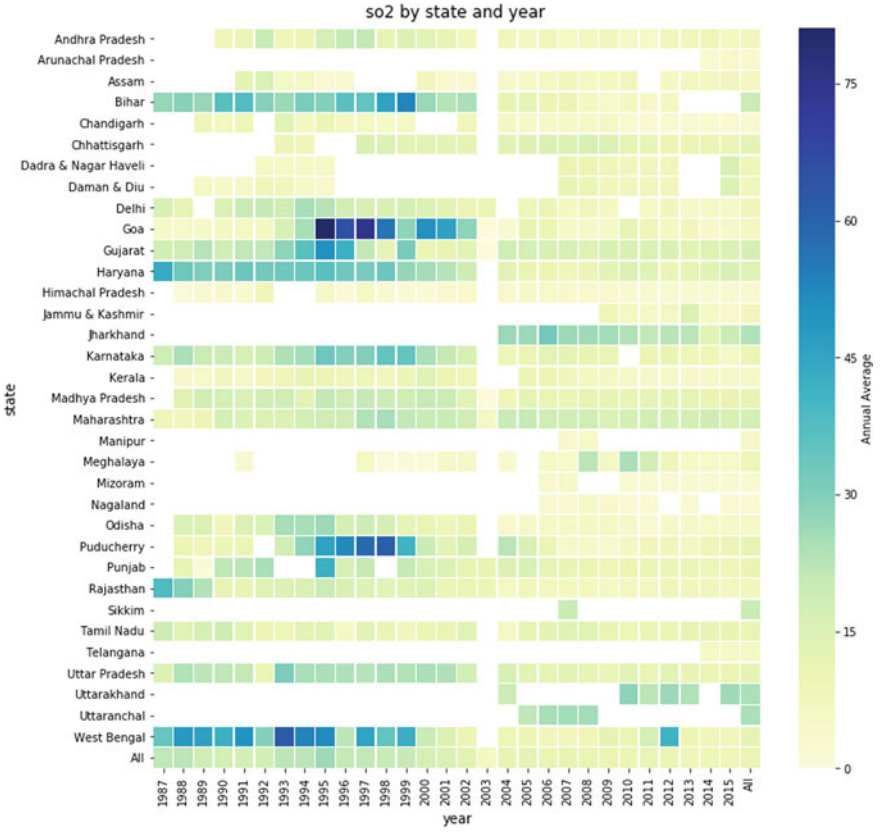

Fig. 1 Heat map for SO_2

5 Conclusion

In the current article an endeavour is likewise made to consider the adjustment in contamination status during the most recent decade utilizing the month to month mean information. To investigate and anticipate the degree of Air File level throughout the years from 1990 to 2015 to show signs of improvement comprehension of the patterns and examine how significant government strategies have influenced the Quality File. This paper is to advise open with respect to by and large prominence of air quality through a rundown boundary that is straightforward. In future we will include more features for analyzing Indian air quality.

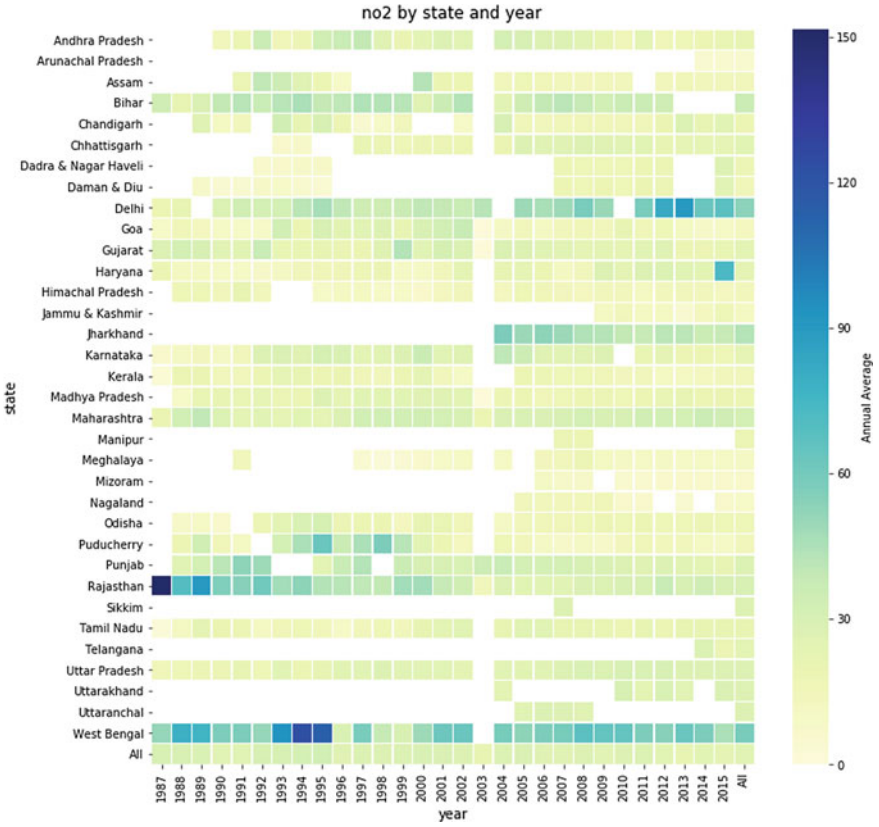

Fig. 2 Heat map for NO_2

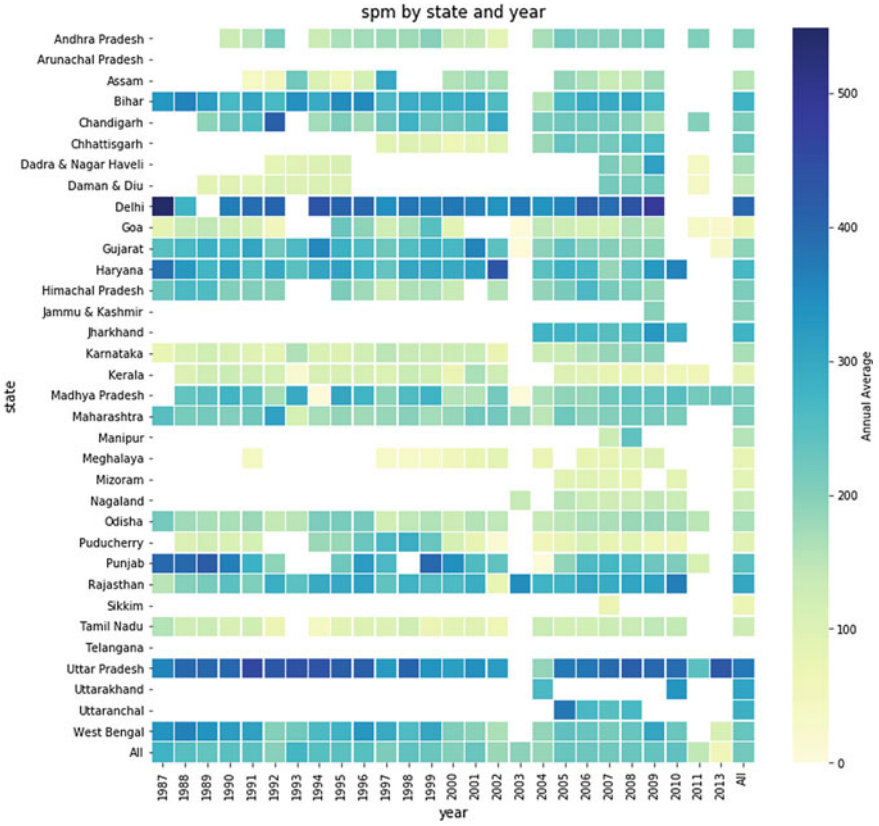

Fig. 3 Heat map for SPM

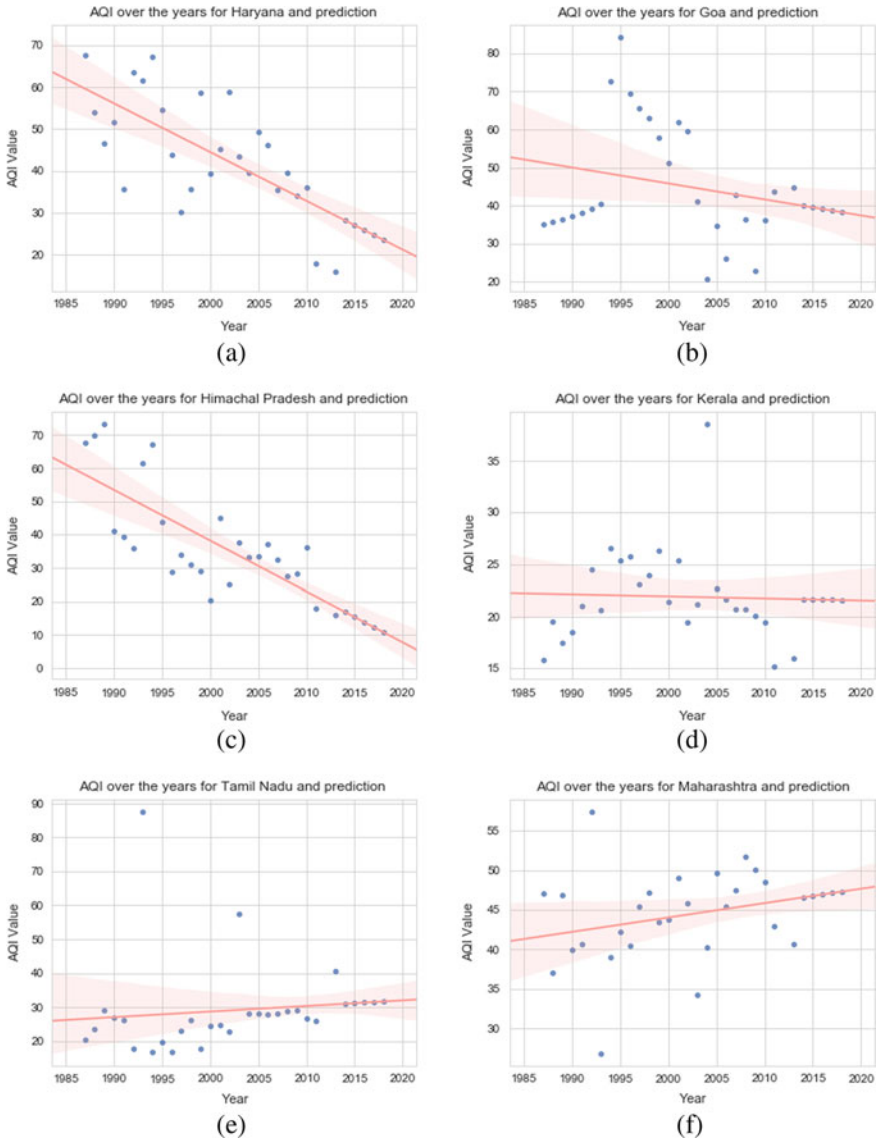

Fig. 4 Prediction of next five years **a** Haryana, **b** Goa, **c** Himachal, **d** Kerala, **e** Tamil Nadu, **f** Maharashtra

Table 3 Evaluation metrics: SO_2, NO_2 and SPM

	Accuracy	Precision	Recall
SO_2	97.65	98.34	92.05
NO_2	96.78	97.34	91.87
SPM	95.54	97.05	90.73

References

1. Kaggle. https://www.kaggle.com/shrutibhargava94/india-air-quality-data. Online accessed 05 June 2020
2. Mpcb. https://mpcb.gov.in/envtdata/envtair.php. Online accessed 12 July 2020
3. Ivanov V, Georgieva I (2017) Air quality index evaluations for Sofia city. In: IEEE EUROCON 2017—17th international conference on smart technologies, Ohrid, 2017, pp 920–925
4. USEPA, Air Quality Index: A Guide to Air Quality and Your Health. February 2014, EPA-456/F-14–002
5. Data Set. https://data.gov.in/catalog/historical-daily-ambient-air-quality-data
6. Chelani AB, Chalapati Rao CV, Phadke KM, Hasan MZ (2002) Formation of an air quality index for India, International Journal of Environmental Studies
7. Data Mining: Concepts and Techniques, Third Edition (The Morgan Kaufmann Series in Data Management Systems) [Jiawei Han, Micheline Kamber, Jian Pei]
8. Goel V, Jangir V, Shankar VG (2020) DataCan: robust approach for genome cancer data analysis. In: Sharma N, Chakrabarti A, Balas V (eds) Data management, analytics and innovation. Advances in intelligent systems and computing, vol 1016. Springer, Singapore. https://doi.org/10.1007/978-981-13-9364-8_12
9. Shankar VG, Devi B, Srivastava S (2019) DataSpeak: data extraction, aggregation, and classification using big data novel algorithm. In: Computing, communication and signal processing. Advances in intelligent systems and computing, vol 810. Springer, Singapore. /https://doi.org/10.1007/978-981-13-1513-8_16
10. Devi B, Kumar S, Anuradha SVG (2019) AnaData: A novel approach for data analytics using random forest tree and SVM. In: Computing, communication and signal processing. Advances in intelligent systems and computing, vol 810. Springer, Singapore. https://doi.org/10.1007/978-981-13-1513-8_53
11. Shankar VG, Jangid M, Devi B, Kabra S (2018) Mobile big data: Malware and its analysis. In: Proceedings of first international conference on smart system, innovations and computing. Smart innovation, systems and technologies, vol 79. Springer, Singapore, pp 831–842. https://doi.org/10.1007/978-981-10-5828-8_79
12. Devi B, Shankar VG, Srivastava S, Srivastava DK (2020) AnaBus: A proposed sampling retrieval model for business and historical data analytics. In: Sharma N, Chakrabarti A, Balas V (eds) Data management, analytics and innovation. Advances in intelligent systems and computing, vol 1016. Springer, Singapore. https://doi.org/10.1007/978-981-13-9364-8_14

Racist Tweets-based Sentiment Analysis Using Individual and Ensemble Classifiers

Bali Devi, Venkatesh Gauri Shankar, Sumit Srivastava, Kriti Nigam, and Lakshay Narang

Abstract In this time of a global pandemic, as our society is pushing forward to a more digital culture of working, living, studying, and earning, the Internet's significance is unprecedented, and inevitably so, the use of various social media platforms has seen a boom. This paper focused on hate speech racism and sexism and built a refined classifier that detects racist and sexist comments from the tweets. Investigating accessible data from Internet-based existence may produce interesting findings and bits of information about virtually every object, organization, or individual inside the universe of general feelings. Opinion mining is the statistical action behavior of suppositions, notions, and subjectivity of content from a corpus that integrates natural language processing (NLP) and machine learning (ML) to classify a range of emotions. As such, sentiment analysis remains a widely researched and ever-evolving topic in the field of NLP. XGBoost with word2vec gave us the most promising results, so we refined it further by fine-tuning. Furthermore, we observed that the $F1$ score was 0.690285. Thus, we were able to reach an accuracy of 69% in our classifier.

Keywords Sentiment analysis · Machine learning (ML) · Xgboost · Random forest (RF) · Logistic regression (LR) · Support vector machine (SVM)

B. Devi · K. Nigam · L. Narang
Department of Computer Science and Engineering, Manipal University Jaipur, Jaipur, Rajasthan, India
e-mail: baligupta03@gmail.com

K. Nigam
e-mail: kritinigam3299@gmail.com

L. Narang
e-mail: ln532661@gmail.com

V. G. Shankar (✉) · S. Srivastava
Department of Information Technology, Manipal University Jaipur, Jaipur, Rajasthan, India
e-mail: venkateshgaurishankar@gmail.com

S. Srivastava
e-mail: sumit.310879@gmail.com

D. K. Sharma et al. (eds.), *Micro-Electronics and Telecommunication Engineering*,
Lecture Notes in Networks and Systems 179,
https://doi.org/10.1007/978-981-33-4687-1_52

1 Introduction and Existing Approach Overview

We are moving toward an unhindered digital culture where social media [1] has already become an indispensable part of our lives. It is of the essence to probe the data that is out there. With social media [1] becoming an indispensable part of our daily lives, people from all walks of life use it to their advantage. From brands promoting their products to launching political campaigns, social media is an integral part of digital marketing. Moreover, since it provides flexibility and unrestricted access, people have also begun to use it to spread hate and negativity via their comments or tweets. Racism and sexism have plagued humanity since eons [2]. They are sewn into the very fabric of the infrastructure of our society. However, as we push toward a more inclusive and tolerant society, the outrage coming out is more relevant than ever as incidents of intolerance toward any community condemned the world over. The recent death of George Floyd by a white policeman kneeling on his neck till he succumbed, has led to violent protests globally. This enraged and recorded incident is only proof of how people are demanding a change in the existing system's paradigms. The Internet provides space for people to share their opinions. We have an abundance of ideas and emotions expressed. Hence, we must have methods of studying these sentiments [3] to know how to filter our safe spaces better. The sentiment is a thought, attitude, or judgment brought in by emotion. Sentiment analysis [4, 5] uses techniques such as natural language processing (NLP), text analysis, mine computational linguistics, and classifying the emotions/opinions expressed as positive, negative, or neutral in a document concerning any given topic. The approaches widely used in sentiment analysis [6, 7] include Naïve Bayes theorem, state vector machine, and KNN; as seen in Table 1, each algorithm has its advantages and disadvantages.

2 Literature Review

The problem of sentiments analysis has been an area of interest for data scientists for quite some time now. A lot many researchers have worked on sentiment analysis [11–14] at different fragmental levels. Pang and Lee [6] solved it as a document level characterization problem, Liu et al. [15] analyzed it at a further and showed results on it at a sentence by sentence level, other researchers have one step ahead. Today, we see sentiment analysis [16, 17] carried out at the word level. Jahanbakhsh and Moon, [1] explained data analysis from social media [1] as twitter comes with its challenges like recognition of sarcasm and satire language. The informal vernacular used in the tweets makes it another obstacle in the analysis of microblogging data. Hence, a few special techniques must be used. Go et al. [2] and Tang et al. [18] revealed some of the earliest research on the study of emotions on Twitter and all the excitement about it. They use emoticons to understand the context of the tweets. They based their models on Naive Bayes, Maxent, and SVM and reported that SVM outperforms the other classifiers. Pak and Paroubek [5] explore the use of part-of-speech functionality but

Table 1 Advantages and disadvantages of existing methods [8–10]

Technique	PROS	CONS
Support vector machine	They're accurate in high dimensional spaces They use a subset of training points in the decision function (called support vectors), so it's also memory efficient	The algorithm is prone for over fitting, if the number of features is much greater than the number of samples SVMs are not very efficient computationally, if your dataset is very big, such as when you have more than one thousand rows
Naive Bayes	Prediction time: Since all the probabilities are pre-computed in the Naïve Bayes algorithm, the prediction time of this algorithm is very efficient	Data scarcity. Chances of loss of accuracy. Zero frequency i.e. if the category of any categorical variable is not seen in training data set then model assigns a zero probability to that category and then a prediction cannot be made
k-nearest neighbors	k-NN has no assumptions: k-NN is a non-parametric algorithm which means there are assumptions to be met to implement k-NN. Parametric models like linear regression has lots of assumptions to be met by data before it can be implemented which is not the case with k-NN	k-NN slow algorithm: k-NN might be very easy to implement but as dataset grows efficiency or speed of algorithm declines very fast

leave inconsistent outcomes. These researchers investigated different techniques of automatically collecting training data. Pak and Paroubek [5] focus on emoticons to train their subjective data, just as Go, Alec and Bhayani did in (2009) [2]. They extract their objective data from twitter accounts of popular newspapers alike. However, we performed feature extraction through bag-of-words, word2vec, and TF-IDF. Also, we explore python libraries for data representation. Our data does not suffer from any bias and is not generated through queries but consists of random tweets posted by people. Gann et al. [16] use tokenization from twitter review data. They assign scores based on positivity or negativity. In comparison with existing methods in sentiment analysis, findings by Saif et al. [7, 19] suggested that semantic feature analysis produces better recall in computing scores for negative classification.

3 Methodology

To begin this paper, we imported all the required python libraries are NumPy, pandas, nltk, matplotlib, and seaborn, and strings. It was followed by data pre-processing. Shown below is the basic outline of our approach (Fig. 1).

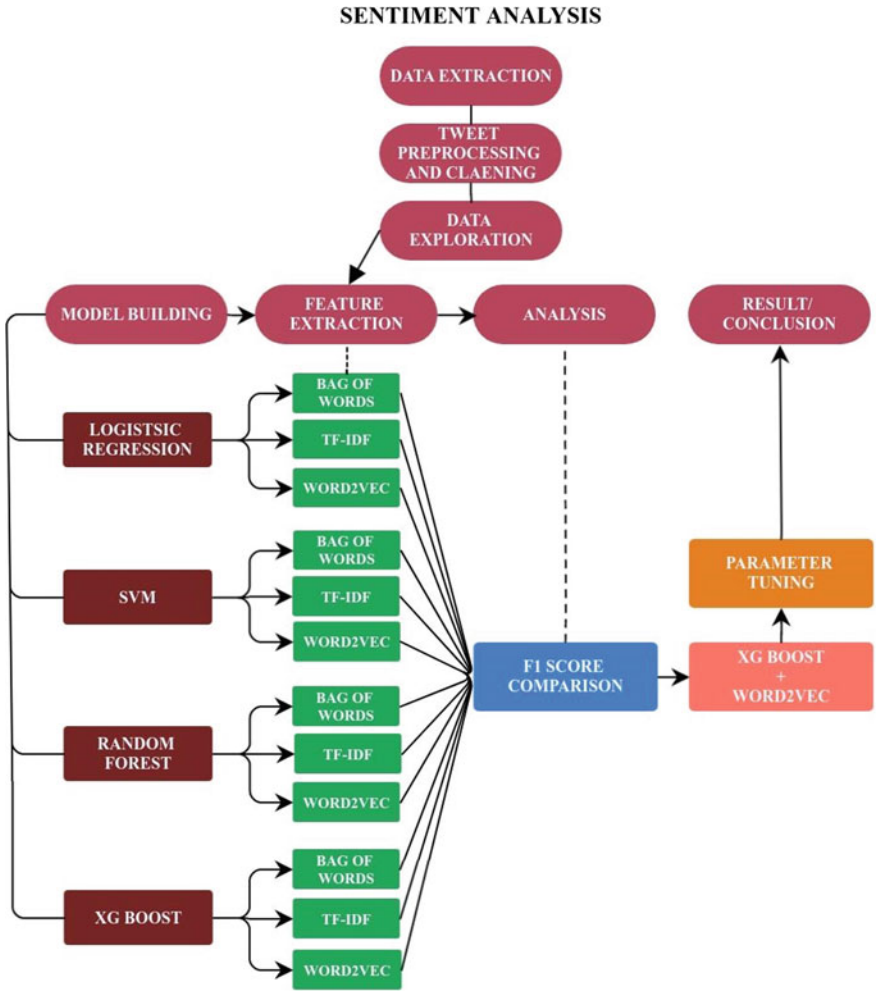

Fig. 1 Proposed framework for tweets

3.1 Data Set and Preprocessing

We downloaded the test (1598 KB) and train (3031 KB) data set from https://www.kaggle.com/arkhoshghalb/twitter-sentiment-analysis-hatred-speech as.csv files [20, 21]. The data was pre-labeled as per the following: 1 for racist/sexist tweets and 0 for non-racist/non-sexist tweets. The overall data set consisted of 31,962 rows. Data set divided into 70:30 (train:test). The testing data set consists of 9589 rows. We calculated the number of tweets labeled as 0 and 1, respectively, and the result is as follows (Table 2).

Table 2 Data set

0	29,720
1	2242

Out[75]:

	id	label	tweet	tidy_tweet
0	1	0.0	@user when a father is dysfunctional and is so selfish he drags his kids into his dysfunction. #run	when a father is dysfunctional and is so selfish he drags his kids into his dysfunction #run
1	2	0.0	@user @user thanks for #lyft credit i can't use cause they don't offer wheelchair vans in pdx. #disapointed #getthanked	thanks for #lyft credit i can t use cause they don t offer wheelchair vans in pdx #disapointed #getthanked
2	3	0.0	bihday your majesty	bihday your majesty
3	4	0.0	#model i love u take with u all the time in urð□□±!!! ð□□□ð□□□ð□□□ð□□□ð□□|ð□□|ð□□|	#model i love u take with u all the time in ur
4	5	0.0	factsguide: society now #motivation	factsguide society now #motivation
5	6	0.0	[2/2] huge fan fare and big talking before they leave. chaos and pay disputes when they get there. #allshowandnogo	huge fan fare and big talking before they leave chaos and pay disputes when they get there #allshowandnogo
6	7	0.0	@user camping tomorrow @user @user @user @user @user @user dannyâ□¦	camping tomorrow danny
7	8	0.0	the next school year is the year for exams.ð□□™ can't think about that ð□□ #school #exams #hate #imagine #actorslife #revolutionschool #girl	the next school year is the year for exams can t think about that #school #exams #hate #imagine #actorslife #revolutionschool #girl
8	9	0.0	we won!!! love the land!!! #allin #cavs #champions #cleveland #clevelandcavaliers â□¦	we won love the land #allin #cavs #champions #cleveland #clevelandcavaliers
9	10	0.0	@user @user welcome here ! i'm it's so #gr8 !	welcome here i m it s so #gr

Fig. 2 Cleaning and stemming tweets

Text is a highly unstructured form of data; hence, different noise forms are found in it, so data cannot be readily processed without pre-processing. Cleaning was carried out in three layers [3]. The first was to remove the twitter user handles, so a custom function was employed to do this. The next step was to replace everything except hashtags and alphabets with a blank space to keep the data relevant to our purpose. The next step was to remove all words of length less than three since we only must make use of data that is relevant to our aim. This process was followed by tokenizing the cleaned tweets and stemming them to the root value. For stemming we used the stemmer () function from the nltk library (Fig. 2).

3.2 Data Exploration

After cleaning the data, both testing and training sets, we proceeded to explore the data to help us develop an intuition to build our approach. We created a wordcloud and plotted the negative and positive words separately. We imported the wordcloud library for this. Next, we extracted racist and non-racist hashtags as they are an integral part of our data. To assess it further, we plotted a frequency distribution curve for the most frequently used racist/sexist and non-racist hashtags (Fig. 3).

3.3 Feature Extraction

While a few characteristic features [7] are obtained directly from raw data, what we usually require are derived features from the set primary features that are relevant

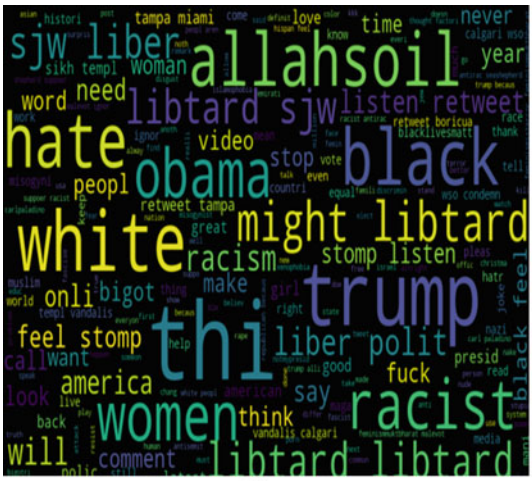

4	opkillingbay	5
5	seashepherd	22
6	helpcovedolphin	3
7	thecov	4
8	neverump	8
9	xenophobia	12
10	love	11
11	peac	8
12	race	14
13	ident	1
14	med	1
15	altright	18
16	whitesupremaci	6
17	linguist	1
18	power	2
19	raciolinguist	1
20	brexit	27
21	peopl	11
22	trump	136
23	republican	13
24	michelleobama	8

(b)

Fig. 3 **a** Wordcloud of the racist words. **b** Frequency distribution of racist hashtags

to target the underlying issue. Feature extraction [14] derives valuable information from raw data. The principal features reformat, combine, and transform from their original state into new derived ones, till they form a data set of their own, that can be consumed by the machine learning [22] models to achieve their goals. We used the following for feature extraction techniques:

- Bag-of-words,
- TF-IDF,
- Word embedding.

In Fig. 4, we can see the histogram plot of the training and testing data set.

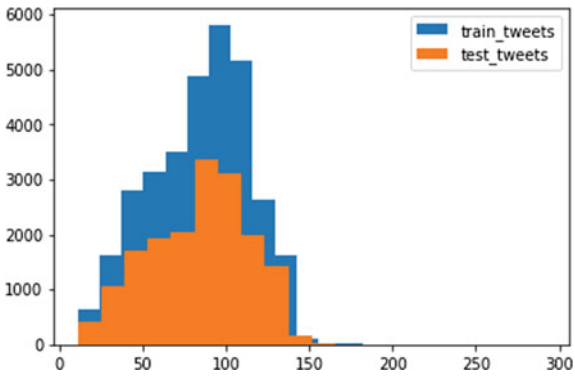

Fig. 4 Histogram of the train and test data sets

3.3.1 Bag-of-Words

Bag-of-words is a very popular NLP and information retrieval (IR) [23] algorithm where the entire text gets divided into bags (multisets) of words irrespective of the grammar and word order but keeping the meaning intact. We used the bow_vectorizer() and CountVectorizer() functions from the sklearn library.

3.3.2 TF-IDF (Term Frequency-Inverse Document Frequency)

TF-IDF is a method used to calculate a phrase in documents; typically, we determine a weight for each phrase that indicates the word's meaning in the document and corpus. This technique is a process widely used for the acquisition of information and the analysis of the text. Term frequency (TF) is separate for each document and word to formulate TF as follows.

$$\mathrm{TF}(t, d) = \frac{\text{count of } t \text{ in } d}{\text{number of words in } d}$$

Document frequency (DF) is the number of terms t occurring in the text set N. In other words, DF represents the number of records containing the word. When the phrase appears at least once in the paper, we can consider one case; we need not ask how many times the word is present.

$$\mathrm{DF}(t) = \text{occurrence of } t \text{ in documents}$$

By dividing the total number of documents, we normalize to hold this in a set, too. Our principal aim is to learn a word's informativeness, and DF is the absolute opposite of that. Instead, we turn the DF upside down. Opposite document frequency (IDF) is the opposite of document frequency that calculates word t informatively. If we quantify IDF, it will be minimal for the more frequent words like stop words (because stop words like "is" are present in nearly all of the papers, and N/DF would assign that word a little value). It ends up offering what we desire, a proportional weighting.

$$\mathrm{IDF}(t) = \frac{N}{\mathrm{DF}}$$

When a word that is not in vocabulary happens during the test time, the DF would be 0. Because we cannot divide by 0, by adding 1 to the denominator, we smooth the sum out.

$$\mathrm{IDF}(t) = \log \frac{N}{(\mathrm{DF} + 1)}$$

Finally, by taking a multiplicative meaning of TF and IDF, we get the TF-IDF ranking; there are many different forms of TF-IDF, but let us focus on that primary type.

$$\text{TF} - \text{IDF}(t.d) = \text{TF}(t, d) \times \log \frac{N}{(\text{DF} + 1)}$$

Term frequency-inverse domain frequency is a statistical method of establishing the importance of a word in each text or document and is the most popular term-weighting method in data science. Python provides a built-in function for this—TfidfVectorizer(). It is available in the sklearn library.

3.3.3 Word2vec

Word2vec is a shallow (two-layer) neural network that converts words into vectors and groups the similar vectors together. Vectorization is more efficient and, as it uses mathematical relations, to classify the words. It creates numeric distributions of words or features and simplifies establishing relationships between those words. It is a combination of two models, bag-of-words and skip-gram model. Word2vec () function is imported from the gensim library.

4 Model Building

After completing feature extraction [7, 14], we moved onto building our binary classifier. For this purpose, we chose four popular classifiers, namely:

- Logistic regression,
- SVM,
- Random forest,
- XGBoost.

Logistic regression is the easiest and most popular classification [14] algorithm. It is used for categorical data analysis and uses a sigmoid method to measure the probability of an occurrence. The equation used in this model is as follows,

$$\bar{\boldsymbol{y}} = \boldsymbol{\sigma}(\boldsymbol{x}) = 1 \div \left(1 + \mathbf{e}^{-x}\right)$$

$$\bar{y} = P(y = 1|x)$$

This classifier is available in the sklearn library and can be imported from the sklearn linear model. We developed the second model using support vector machine (SVM) [12, 24]. SVM [24, 25] is capable of linear regression and logistic regression.

It does so by drawing a hyperplane in an N-dimensional space (N is the number of features) capable of effectively distinguishing the various groups. The optimal hyperplane is the one that has the maximum margin between the data points of the classes. It is a built-in classifier and was imported from the sklearn. Next, we build a random forest classifier [24, 26]. It is built upon multiple decision trees. The most voted outcome from all the trees is regarded as the output class. The trees are highly uncorrelated to each other and that is the fundamental theory behind it. Lastly, we built the classifier XGBoost. XGBoost is an open-source library which stands for extreme gradient boosting. It has become an increasingly popular classifier primarily because of the following things: high-speed performance, flexibility, portability, and integration of boosted tree algorithms and parallel processing. It must be first downloaded and installed on your system and can be done by—pip install XGBoost on the CLI. It focuses on speed and performance while providing many advanced functionalities. After training our model for each of these classifiers, we calculated the $F1$ score for all and compared the results. We used the $F1$ score as our evaluation metric since we found the data set to be biased. The formula for calculating $F1$ score is as follows,

$$P_{\mathrm{r}} = \frac{T_{\mathrm{p}}}{T_{\mathrm{p}} + F_{\mathrm{p}}}$$

$$R_{\mathrm{c}} = \frac{T_{\mathrm{p}}}{T_{\mathrm{p}} + F_{\mathrm{n}}}$$

$$F_1 \text{ score } = \frac{2P_{\mathrm{r}}R_{\mathrm{c}}}{P_{\mathrm{r}} + R_{\mathrm{c}}}$$

4.1 Parameter Tuning

After comparing the $F1$ scores of each model, we found XGBoost performed best with the word2vec feature extraction algorithm [7, 14]. To refine our model further, we used parameter tuning to get better results. General approach for parameter tuning follows the steps below to tune the parameters (Fig. 5):

- Choose a relatively high degree of literacy. A learning rate of 0.3 is normally taken advantage of at this point.
- Tune tree-specific parameters like max depth, min child weight, subsample, colsample by tree while keeping the rate of learning fixed. Fine-tune the rate of learning.
- Finally, tune gamma to avoid overfitting.

```
CV with max_depth=6, min_child_weight=5
CV with max_depth=6, min_child_weight=6
CV with max_depth=6, min_child_weight=7
CV with max_depth=7, min_child_weight=5
CV with max_depth=7, min_child_weight=6
CV with max_depth=7, min_child_weight=7
CV with max_depth=8, min_child_weight=5
CV with max_depth=8, min_child_weight=6
CV with max_depth=8, min_child_weight=7
CV with max_depth=9, min_child_weight=5
CV with max_depth=9, min_child_weight=6
CV with max_depth=9, min_child_weight=7
```

```
mean_f1 = cv_results['test-f1_score-mean'].max()
boost_rounds = cv_results['test-f1_score-mean'].argmax()
print("\tF1 Score {} for {} rounds".format(mean_f1, boost_rounds))
```

```
C:\Users\hp\Anaconda3\lib\site-packages\ipykernel_launcher.py:2: FutureWarning:
The current behaviour of 'Series.argmax' is deprecated, use 'idxmax'
instead.
The behavior of 'argmax' will be corrected to return the positional
maximum in the future. For now, use 'series.values.argmax' or
'np.argmax(np.array(values))' to get the position of the maximum
row.
```

```
        F1 Score 0.690285 for 72 rounds
```

Fig. 5 *F*1 score after fine-tuning

5 Results and Discussion

For the fulfillment of this research, we studied the existing literature and saw that most papers employed frequently used classifiers like SVM [24], Naive Bayes, etc. We used the knowledge from these papers to develop a novel approach for text classification, however still abiding by the fundamental framework. After collecting data sets from Kaggle, we proceeded to clean and inspect it. After cleaning the tweets to extract only the relevant information, we visualized our data by creating a wordcloud and plotting the frequency of the most common negative and positive words. The purpose of this was to help us gain more insight into our data. After this, we used feature extraction [14] via bag-of-words, TF-IDF, and word2vec algorithms as we wanted to create the best performing binary classifier for the given data set. We have found confusion matrices of random forest with word2vec in Table 3, SVM with word2vec in Table 4, and SVM with TF-IDF in Table 5.

Table 3 Random forest with word2vec

Actual	Predicted		
		1	0
	1	8897	8
	0	454	230

Table 4 SVM with word2vec

Actual	Predicted		
		1	0
	1	8702	203
	0	288	396

Table 5 SVM with TF-IDF

Actual	Predicted		
		1	0
	1	8771	134
	0	404	280

Following this, we used each feature representation against the four classifiers that we used: logistic regression, SVM [24], random forest [24, 26], and XGBoost. To evaluate our models, we used the $F1$ score (Table 6) as our metric since we found the training data set to be biased. The results obtained are as follows in Table 7:

XGBoost with word2vec gave us the most promising results, so we refined it further by fine-tuning. Furthermore, we observed that the $F1$ score was 0.690285. Thus, we were able to reach an accuracy of 69% in our classifier.

Table 6 Evaluation metrics

Evaluation metrics		Precision	Recall	$F1$ score
Random forest with word2vec	0	0.95	1.00	0.97
	1	0.97	0.34	0.50
SVM with word2vec	0	0.97	0.98	0.97
	1	0.66	0.58	0.62
SVM with TF-IDF	0	0.96	0.98	0.97
	1	0.68	0.41	0.51

Table 7 Result analysis

Classifier/feature	Bag-of-words	TF/IDF	Word2vec
Logistic regression	0.530782	0.5446507	0.615271
SVM	0.50969	0.51141	0.615384
Random forest	0.55292	0.562152	0.503225
XGBoost	0.52477	0.539426	0.640211

6 Conclusion and Future Scope

Text analysis and classification remain a robust topic in the field of data science. Lots of research have been done on it and are still going on. Many classifiers like logistic regression, Naive Bayes, and SVM have been used. But we also used XGBoost that has become a popular ML algorithm due to its efficiency and performance. All of this has been implemented by using python on the Jupyter notebooks framework. However, there are a few things that can enhance our model by incorporating deep learning [22] and reinforcement learning:

- Working with emoticons and assessing their polarity,
- Building a multiclass classifier.
- Scraping data from social media,
- Using a larger data set to achieve better results.

References

1. Jahanbakhsh K, Moon Y (2014). The predictive power of social media: on the predictability of U.S presidential elections using Twitter 36
2. Go A, Bhayani R, Huang L (2009) Twitter sentiment classification using distant supervision. In: CS224N Project Report. Stanford
3. Agarwal A, Xie B, Vovsha I, Rambow O, Passonneau R (2011) Sentiment analysis of twitter data. In: Proceedings of ACL 2011 workshop on languages in social media. Twitter sentiment analysis using machine learning techniques 289. pp 30–38
4. Liu B (2010) Sentiment analysis and subjectivity. In: Handbook of natural language processing, 2nd edn. Taylor and Francis Group
5. Pak A, Paroubek P (2010) Twitter as a corpus for sentiment analysis and opinion mining. In: Proceedings of the seventh conference on international language resources and evaluation. European Languages Resources Association, Valletta, Malta
6. Pang B, Lee L (2004) A sentimental education: sentiment analysis using subjectivity summarization based on minimum cuts. In: Proceedings of the association for computational linguistics (ACL), pp 271–278
7. Saif H, He Y, Alani H (2012) Semantic sentiment analysis of twitter. In: The semantic web ISWC What is the difference between feature extraction and feature selection. pp. 508–524. https://quantdare.com/what-is-the-difference-between-feature-extraction-and-feature-selection. Online; Accessed 5 June 2020
8. Kim S-M, Hovy E (2004) Determining the sentiment of opinions. In: Proceedings of the 20th international conference on computational linguistics. Association for Computational Linguistics, Stroudsburg, PA, USA, p 1367
9. Barbosa L, Feng J (2010) Robust sentiment detection on twitter from biased and noisy data. In: Proceedings of COLING, pp 36–44
10. Janardhana R (2010) Twitter sentiment analysis and opinion mining
11. Liu B (2010) Sentiment analysis and subjectivity. In: Handbook of natural language processing, 2nd edn
12. Mullen T, Collier N (2004) Sentiment analysis using support vector machines with diverse information sources. In: Proceedings of conference on empirical methods in natural language processing (EMNLP 2004)

13. Rizzo G, Troncy R (2011) Nerd: evaluating named entity recognition tools in the web of data. In: Workshop on web scale knowledge extraction (WEKEX 2011), vol 21
14. Shankar VG, Devi B, Srivastava S (2019) DataSpeak: data extraction, aggregation, and classification using big data novel algorithm. In: Iyer B, Nalbalwar S, Pathak N (eds) Computing, communication and signal processing. Advances in intelligent systems and computing, vol 810. Springer, Singapore. https://doi.org/10.1007/978-981-13-1513-8_16
15. Boca Liu B, Hu M, Cheng J (2005) Opinion observer: analyzing and comparing opinions on the web. In: Proceedings of the 14th international conference on world wide web, WWW '05. ACM, New York, NY, USA, pp 342–351
16. Gann W-JK, Day J, Zhou S (2014) Twitter analytics for insider trading fraud detection system In: Proceedings of the sencond ASE international conference on Big Data. ASE
17. Kumar A, Sebastian TM (2012) Sentiment analysis on Twitter. Int J Comput Sci Issues 9(4(3))
18. Tang H, Tan S, Cheng X (2009) A survey on sentiment detection of reviews. Expert Syst Appl 36(7):10760–10773
19. Saif H, He Y, Alani H (2012) Alleviating: data sparsity for Twitter sentiment analysis. In: Proceedings of the 2nd workshop on making sense of microposts (#MSM2012): big things come in small packages: in conjunction with WWW 2012
20. Kaggle Dataset https://www.kaggle.com/arkhoshghalb/twitter-sentiment-analysis-hatred-speech. Online accessed May 12, 2020
21. Twitter (2014) Twitter apis. https://dev.twitter.com/start
22. Yadav A, Shankar VG, Verma VK (2020) Emotion recognition with facial expression using machine learning for social network and healthcare, machine learning and deep learning in real-time applications. IGI Global, pp 273–282. https://www.igi-global.com/gateway/chapter/257323
23. Pang B, Lee L (2008) Opinion mining and sentiment analysis. Found Trends Inf Retrieval 2(1–2):1–135
24. Devi B, Kumar S, Anuradha, Shankar VG (2019) AnaData: a novel approach for data analytics using random forest tree and SVM. In: Iyer B, Nalbalwar S, Pathak N (eds) Computing, communication and signal processing. Advances in intelligent systems and computing, vol 810. Springer, Singapore. https://doi.org/10.1007/978-981-13-1513-8_53
25. Goel V, Jangir V, Shankar VG (2020) DataCan: robust approach for genome cancer data analysis. In: Sharma N, Chakrabarti A, Balas V (eds) Data management, analytics, and innovation. Advances in intelligent systems and computing, vol 1016. Springer, Singapore. https://doi.org/10.1007/978-981-13-9364-8_12
26. Devi B, Shankar VG, Srivastava S, Srivastava DK (2020) AnaBus: a proposed sampling retrieval model for business and historical data analytics. In: Sharma N, Chakrabarti A, Balas V (eds) Data management, analytics, and innovation. Advances in intelligent systems and computing, vol 1016. Springer, Singapore. https://doi.org/10.1007/978-981-13-9364-8_14
27. Saif H, He Y, Alani H (2012) Semantic sentiment analysis of Twitter. In: Cudr´e-Mauroux P, et al. (eds.) ISWC 2012, Part I. LNCS, vol 7649. Springer, Heidelberg, pp 508–524

An Efficient Model for High Availability Data in Hadoop 1.2.1

Anurag Bhatnagar, Venkatesh Gauri Shankar, Bali Devi, and Nikhar Bhatnagar

Abstract Day by day the data is increasing enormously so storage of big data and analysis of big data require large storage as well as fast processing. Scaling can be done in two ways horizontal scaling and vertical scaling. Earlier horizontal scaling was approached to process big data. They tend to increase processing power each time the data is increased. Today, the vertical scaling approach is the best practice to handle big data. Privacy is also major concern, public fear of inapt use of their personal data.Apache Hadoop is one of the solution of big data. Hadoop below version 2 lack high availability in NameNode. We have found the solution of high availability of NameNode in Hadoop version 1. We have used centralized storage that is NFS server and shared that storage with two places. We have called it primary and secondary NameNode according to the vocabulary of Hadoop version 2. Primary NameNode is working as a master to the DataNodes while secondary NameNode will keep track of live status of primary NameNode. When primary NameNode goes down then secondary NameNode will replace its IP with primary NameNode's IP and then it will become master to the DataNodes. In this way, we can obtain high availability in older Hadoop version older than 2.

Keywords Big data · Big data tools · Apache Hadoop · HDFS · Hadoop v1 limitation · High availability in Hadoop v1

A. Bhatnagar · V. G. Shankar (✉) · B. Devi
School of Computing and Information Technology, Manipal University Jaipur, Jaipur, Rajasthan, India
e-mail: venkateshgaurishankar@gmail.com

A. Bhatnagar
e-mail: ab.ajmer@gmail.com

N. Bhatnagar
Department of Computer Science and Engineering, Swami Keshvanand Institute of Technology Jaipur, Jaipur, India

D. K. Sharma et al. (eds.), *Micro-Electronics and Telecommunication Engineering*,
Lecture Notes in Networks and Systems 179,
https://doi.org/10.1007/978-981-33-4687-1_53

1 Introduction (Big Data)

Big data explains to exceptionally huge structure or semi-organized and unstructured information. With conventional information handling application programming, it is extremely hard to manage huge informational collection of various structures. Putting away information, looking, examining information are remembered for difficulties of large information. Large information qualities can be depicted in five V's that are volume, speed, assortment, changeability and veracity. Volume implies the measure of information produced and put away. Speed implies the rate at which information is produced and broke down to satisfy the need of development and advancement. The assortment is the kind of information created that can be organized, semi-organized and unstructured information. Inconstancy implies information irregularity which may hamper procedures to deal with and oversee it. Veracity implies the information differ every now and again influences the exact investigation [1].

Obstacle with large information is with regards to deal with various sorts of information; we likewise allude them as heterogeneous information. Heterogonous information are made out of organized information like information of RDBMS, data stockroom and so forth. Unstructured information like simple information, GPS following data, sound, video, pictures and so forth. Semi-organized information like XML, Email, JSON and so forth. Examination of organized information is simpler than different types of information on the grounds that our handling of information is most effectively on the off chance that they can store numerous things that are on the whole indistinguishable structure and size. Other problems related to big data scaling, timeliness and privacy. Day by day the data is increasing enormously so storage of big data and analysis of big data require large storage as well as fast processing. Scaling can be done in two ways horizontal scaling and vertical scaling. Earlier horizontal scaling was approach to process big data. They tend to increase processing power each time the data is increased. Today, vertical scaling approach is best practice to handle big data. Privacy is also major concern, public fear of inapt use of their personal data [2].

Big data is a buzzword among companies and their business nowadays. Big data analysis has revolutionized many businesses.

This analysis report helps the executives of the company to take right and fast decisions.

Different types of analytics solutions can be classified as descriptive, predictive and diagnostic. Descriptive analytics mean to yield the useful information from events and reports from history to identify patterns and create management reports. We can also say modeling past behavior. In very simple way, just say what happened. Predictive analytics identifying from past pattern and predict the future. In simple way, we can say what could happen in the future. Diagnostic analysis means what happened and why it happened. By following above strategies companies take their decisions [3].

2 Big Data Tools

The Apache Cassandra database is one of the instruments which give powerful administration of enormous information. Its property of giving adaptability and high accessibility without trading-off execution. Since it works in ware equipment, it is less expensive and productive. Giving adaptation to non-critical failure in item equipment or cloud framework make it immaculate innovation [4]. Neo4j is one of tools which provide big data solutions. Neo4j is scalable graph database technology which is developed using JAVA technology. Neo4j is flexible data model provides real-time insight and incorporate feature scalability and high availability which makes it more reliable [5]. Splunk is one the best analytics tools for analyzing log files. This software for monitoring, searching and analyzing machine generated big data. MongoDB is also one the tools which is open-source collection and document-oriented database program for storing as well as analyzing big data. It comes under NoSQL database technology. MongoDB uses JAVA script object notation (JSON) documents with schemas. MongoDB is a product developed by MongoDB Inc [6]. One of the commonly used tools for analyzing big data is Tableau. Tableau is an interactive data visualization tool developed by software company Tableau software focused on business intelligence. There are many other tools and technology which are working on the analysis as well as storage of big data.

3 Apache Hadoop

The Apache Hadoop is an open-source programming for adaptable, solid, circulated capacity and appropriated figuring. The Apache Hadoop programming is a system that deals with the recipe of conveyed preparing of huge information and circulated stockpiling of information across various hubs of groups. It is intended to level scale up. Apache Hadoop can scale from single workers to a huge number of machines, each performing neighborhood calculation and capacity. It one of the noticeable properties is high accessibility which implies the assets are consistently accessible [7, 8]. For high accessibility does not relies upon equipment it planned in such a manner the high accessibility is acquired by Hadoop programming itself. The Hadoop programming incorporates these modules [9]:

- Hadoop Common: The utilities that help the other Hadoop modules.
- Hadoop Distributed File System (HDFS): A dispersed stockpiling or document framework that gives quick access to application information.
- Hadoop YARN: It is a model that schedules jobs and manages cluster resource.
- Hadoop MapReduce: Hadoop MapReduce provides parallel processing. It works in two-stage mapper and reducer. Because of parallel processing of data makes the Hadoop as one of the best solution of big data.

Table 1 Difference between Hadoop version 1 and Hadoop version 2

Hadoop version 1.x.x	Hadoop version 2.x.x
Support MapReduce for data processing but does not support other computing models	Support MapReduce as well as other computing models such as Sparks, Giraph, Pig and Hive
MapReduce (MR) is responsible for data processing and cluster management	Yet another resource negotiator (YARN) is responsible for data processing and cluster management
Scalability is limited to 4000 nodes per cluster	Scalability is up to 10,000 nodes per cluster
Single NameNode manages the entire mapper and reducer tasks	Multiple NameNode manages the entire mapper and reducer tasks
Microsoft windows is not supported	Microsoft windows is supported

4 Hadoop Distributed File System (HDFS)

The Hadoop Distributed File System is a disseminated record framework designer to run on item equipment. Product equipment implies the equipment that is moderately reasonable and is broadly accessible. The distinction between product equipment and other dispersed document frameworks are high issue open minded and minimal effort of equipment gadgets in HDFS. HDFS provides high throughput access to data and is also suitable for big data. HDFS also provide high availability means the data is always available to client. If one of the servers goes down there is replica of same data on different servers, HDFS automatically redirect the request to the other live server [10].

HDFS is stores the application data and its metadata in two different servers. A server in which application data is stored is called DataNodes. A server in which metadata is stored is called NameNode. HDFS is works on master–slave model. NameNode is master and DataNodes are slave. NameNode is the one which drives all the processing of data because it contains metadata of all the data. Apache Hadoop is available in from version 0.14.1 to version 3.0.0-alpha4. Mainly Hadoop v1 and Hadoop v2 are used. HDFS architecture of both versions is almost similar but MapReduce has different architectures. Difference between Hadoop version 1 and Hadoop version 2 [11] is shown in Table 1.

5 Limitation of Hadoop Version 1.x.x

Hadoop below version 2.x.x lacks the feature of high availability of NameNode. If NameNode fails entire cluster and fails in Hadoop version 1.x.x, but in Hadoop version 2.x.x provide high availability in NameNode. We have found the solution to this problem by providing high availability in Hadoop version 1 (Fig. 1).

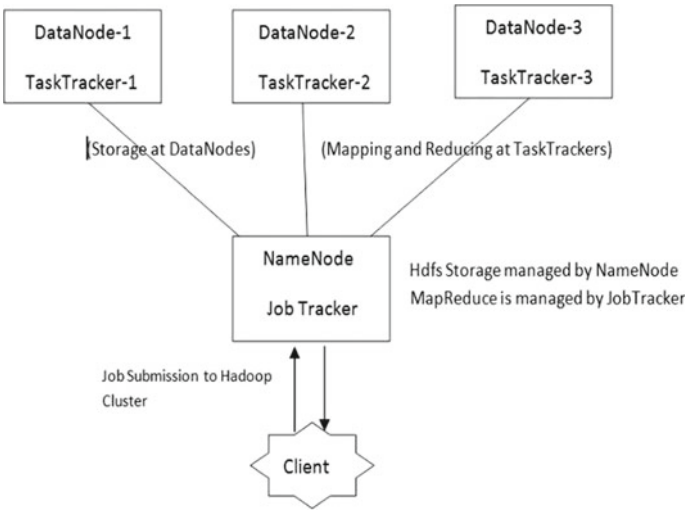

Fig. 1 Architecture of Apache Hadoop version 1.x.x

6 High Availability Solution in Hadoop V1

The simple definition of high availability is always available. Since data and applications are very critical on the Internet so it very important that services needs to be highly available. High available systems typically attempt to achieve 99.999% (5-nines) availability [12]. High availability can be achieved in cluster system where in each nodes are independent. High availability is engineered in such a way when one node goes down other node goes up. In Amazon Web services high availability is provided in an entire region. In a region, we have more than two data centers. Even if there is disaster in one data center, client's data will not be lost [13, 14].

When we say high availability in Hadoop v1 we mean high availability of NameNode. Hadoop version v1 already has high availability of DataNode, but we am going implement high availability of NameNode in Hadoop version 1 to do this we need have following [12].

6.1 Centralized Storage

To provide centralized storage, we can use different storage techniques, we used network file system (NFS) server for that. NFS server is distributed file system protocol. In this server, we can share storage. Suppose if storage is shared with read and write permission to two clients then any change in server or any of two clients is going reflect everywhere because the storage is shared. That is why when data

is stored at primary NameNode it is stored in NFS server and same changes are reflected also in secondary NameNode.

6.2 Two NameNode

The storage is mounted in both the NameNodes. Both NameNodes must have same configurations in the configuration files that are core.site.xml and hdfs.site.xml. Let us call one NameNode as primary and another NameNode as secondary NameNode according to vocabulary of Hadoop version (Note: the secondary NameNode here is taken as an example to explain. The secondary NameNode in Hadoop version 2 and above not only provide high availability but also may other features). Here, secondary name has two jobs. First, it keeps track of live status of primary NameNode and second it will change its IP with the IP of primary NameNode when primary NameNode fails.

6.3 Python Program

The prerequisite to run this Python code is primary NameNode and secondary NameNode will have same configuration setting, i.e., configuration of hdfs.site.xml and core.site.xml. This Python code will run at secondary NameNode. It checks if primary NameNode is alive or dead by pinging it in an infinite loop. When secondary NameNode pings successfully the output of getstatusoutput() function will be 0. If there is any unsuccessful the loop the output of getstatusoutput function of Python will nonzero and the loop break. It will then change the network setting of secondary name by using Python file handling. In this network, secondary NameNode changes it IP address with the IP address of primary NameNode. Then, restart the network settings. After this, we will mount the NFS shared file to the same location as mounted in primary NameNode. We need to restart the NameNode daemon. In case NameNode goes to save mode, we need to leave the safemode because in safemode NameNode does not works [7, 15] (Fig. 2).

```
import commands
#checking heart beat of primary namenode
while True:
check = commands.getstatusoutput("ping -c 1 primary_namenode")
if check[0] = = 0:
print check [1]
pass
else:
break
#changing virtual ip with ip of primary namenode in centos 7.3
file1 = open("/etc./sysconfig/network-scripts/ifcfg-enp0s3:1",'r+')
```

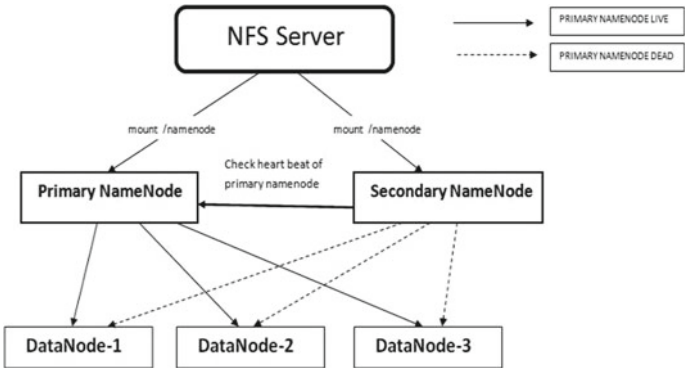

Fig. 2 Architecture of implementing high availability of NameNode in Hadoop version 1

```
file1.seek(323)
file1.write("primary_namenode")
file1.close()
# restart network
commands.getstatusoutput("systemctl restart network")
commands.getstatusoutput("ifup enp0s3")
#mount namenode
commands.getstatusoutput("mount 192.168.43.147:/nfs /namenode")
#restart hadoop-daemon
commands.getstatusoutput("hadoop-daemon.sh start namenode")
commands.getstatusoutput("hadoop dfsadmin -safemode leave")
```

7 Conclusion

We are living in era where data storage and analysis is back bone of every company and data is a crucial entity for company as well as client. Client always want that data should always be available that means they ask for zero down time. High availability feature has become one key aspect in every technology. Many technologies are used for high available solution like Raid redundant array of independent disk, SAN storage area network and now microservices like kubernetes and docker swarm provides high availability solution. We have developed a code which allows us to avail high availability in Apache Hadoop. Now, if any company wants to use Hadoop version less than 2, then they can use this technique. They do not require migrating from Hadoop version 1 to Hadoop version 2. With this technique, we can obtain high availability not only in Hadoop but also any other technology with some little changes in configuration.

References

1. Owais SS, Hussein NS (2016) Extract five categories CPIVW from the 9V's characteristics of the big data. Int J Adv Comput Sci Appl 7(3):254–258
2. Bhosale HS, Gadekar DP (2014) A review paper on big data and Hadoop. Int J Sci Res Publ 4(10):1–7. ISSN: 2250-3153
3. Praseeda CK, Shivakumar BL (2014) A review of trends and technologies in business analytics. Int J Adv Res Comput Sci 5(8):225–229. ISSN: 0976-5697
4. Cassandra. https://cassandra.apache.org/
5. Neo4j. https://neo4j.com/
6. Mongodb. https://www.mongodb.com/
7. Shankar VG, Devi B, Srivastava S (2019) DataSpeak: data extraction, aggregation, and classification using big data novel algorithm. In: Computing, communication and signal processing. Advances in intelligent systems and computing, vol 810. Springer, Singapore. https://doi.org/10.1007/978-981-13-1513-8_16
8. Saggar S, Saggar R, Khurana N (2015) Int J Adv Res Comput Sci Manage Studies 3(8):135–144. ISSN: 232 (Online) 7782
9. Apache Hadoop. https://hadoop.apache.org/
10. Dhavapriya M, Yasodha N (2016) Big data analytics: challenges and solutions using hadoop, map reduce and big table. Int J Comput Sci Trends Technol (IJCST) 4(1):5–14. ISSN: 2347-8578
11. Borkar SD, Surtakar CS A review paper on the Hadoop distributed file system. Int J Res SciEng 1(1): 221–226. e-ISSN: 2394-8299. p-ISSN:23394-8280
12. High availability software. https://en.wikipedia.org/wiki/High_availability_software
13. Shankar VG, Jangid M, Devi B, Kabra S (2018) Mobile big data: malware and its analysis. In: Proceedings of first international conference on smart system, innovations and computing. smart innovation, systems and technologies, vol 79. Springer, Singapore, pp 831–842. https://doi.org/10.1007/978-981-10-5828-8_79
14. Devi B, Shankar VG, Srivastava S, Srivastava DK (2020) AnaBus: a proposed sampling retrieval model for business and historical data analytics. In: Sharma N, Chakrabarti A, Balas V (eds) Data management, analytics and innovation. Advances in intelligent systems and computing, vol 1016. Springer, Singapore. https://doi.org/10.1007/978-981-13-9364-8_14
15. Goel V, Jangir V, Shankar VG (2020) DataCan: robust approach for genome cancer data analysis. In: Sharma N, Chakrabarti A, Balas V (eds) Data management, analytics and innovation. Advances in intelligent systems and computing, vol 1016. Springer, Singapore. https://doi.org/10.1007/978-981-13-9364-8_12

A Framework for Detection and Validation of Fake News via Authorize Source Matching

Deepak Mangal and Dilip Kumar Sharma

Abstract In the present era, peoples are sharing views, information, and knowledge on social media across the world without validating the contents. This increases the probability that deceptive news reaches the group of peoples. This type of deceptive news is termed as fake news and requires a proper solution to validate such contents. To overcome and find a solution, a novel framework along with algorithm has been proposed in this research work. The framework is using embedded image/text as input. Extract text with image features used as query and sent to multiple search engines to find relevant links to validate source of generation. After all, the source of the selected links validates by stores authorize source list. Algorithm achieves 82, 85, and 94% accuracy on MediaEval, BuzzFeedNews datasets, and Google news, respectively.

Keywords Fake news · OCR · Web scraper · Search engine

1 Introduction

Deception or fake news is a sort of sensationalist reporting or an exploitative news-casting that comprises of deliberate tricks, or that present next to zero authentic well inquired about news spread through customary news media or online Internet-based life. Distinctive meaning of falsehood or gossip has been utilized in the writing. One of the most embraced is in Allport and Postman, where a rumor is characterized as a story or an explanation whose fact esteem is unsubstantiated. Rumor can likewise be characterized as a coursing story or report of questionable or far-fetched truth. "Rumor does not need to be false, and they can be viewed as later to be valid or fake." Misinformation might be a news parody, which utilizes embellishment and presents

D. Mangal · D. K. Sharma (✉)
GLA University, Mathura, UP 281001, India
e-mail: dilip.sharma@gla.ac.in

D. Mangal
e-mail: deepak.mangal@gla.ac.in

D. K. Sharma et al. (eds.), *Micro-Electronics and Telecommunication Engineering*,
Lecture Notes in Networks and Systems 179,
https://doi.org/10.1007/978-981-33-4687-1_54

non-accurate components that are intentionally expected to delude. The term is additionally now and again used to provide a reason to feel ambiguous about uncertain authentic news from a restricting political point of view. Secretly the sites which host counterfeit news and need realized distributers are censured, in light of the fact that they make it hard to contest wellsprings of phony news for slander. Because of the climb in the prevalence pace of online life in the present time, the Web turns into a perfect reproducing ground for spreading fake news, for example, deluding data counterfeit surveys, counterfeit notices, etc. Twitter has been considered as one of the most broadly received online life stages for spreading breaking news around the world. Online life gives adaptability of sharing and trading data which accompanies an inconvenience of bountiful perusers with an immense volume of new data consistently. The effect of fake news got universal in the twenty-first century.

Aside from all, fake news has been blamed for expanding political polarization and disciple struggle during political decision battle, and the voters can likewise be effectively affected by the falsehood or deceiving political articulation and cases. In 2016, the term fake news was the most as often as possible utilized term via Web-based networking media and has increased significantly greater ubiquity after the 2016 US political race [1]. A post by Collins Language Publication "counterfeit news" was reported as the "expression of the year" [2]. Figure 1 depicted fake news as a big problem today. Social media is the main source of it.

However, the researchers have worked in the fake news as a research area but did not reach on a full proof solution. The different perspectives used to study and research on fake news is defined as follows:

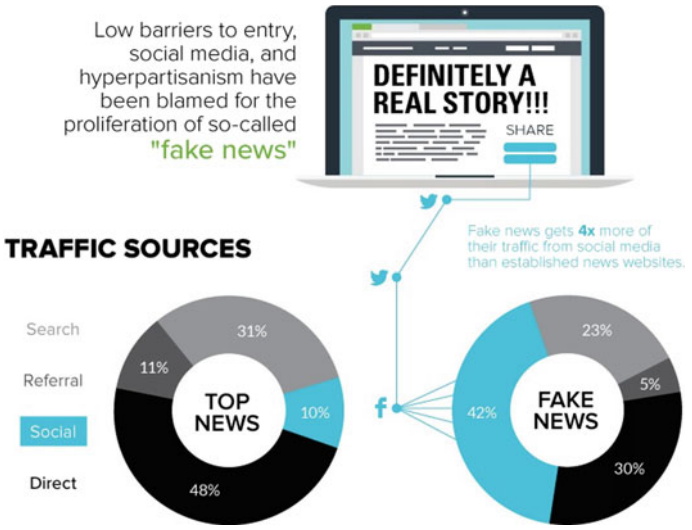

Fig. 1 Fake news problem

Fig. 2 **a** Fake story related to Michelle Obama. **b** Trump falsely accuses Obama (from Facebook)

- Style based: it focuses on the way the news is written so that it can be treated as false.
- Propagation based: as the name suggests the way of spreading, so this perspective focuses on how the misinformation is spreading.
- User based: this perspective deals with users, i.e., how the people are involved with fake news.

Some example of spread fake news at the time of US election is shown in Fig. 2a and b [3]. The validation of fake news is a challenging task. Several other theories evolved across diverse factors such as philosophy, psychology, and economics. One such theory is fundamental human cognition and behaviors that gave indispensable perceptions for fake news analysis. Recent research is focused on social media post in the form of embedded text with images. The researcher extracts text and their features with image features and train machine accordingly. In 2016, Jin et al. [4] focused on this type of fake news. They extract visual and statistical features to identify the post as fake or real. So, our contribution in this paper as follows: We propose an original framework for news authentication and detect it as fake or real. The framework extracts text and salient information available in image and passes as query to multiple search engine query analyzer and extract relevant link. The links which are coming from trustworthy sources such as country media are used to validate the news legitimacy.

The organization of rest of paper as follows: The Sect. 2 explores information and acquaintance from traditional approaches, and Sect. 3 describes some appreciated prevailing framework for fake news detection and describes the anticipated framework and its segment. The implementation with the proposed algorithm and experimental result analysis discuss in Sect. 4. The Sect. 5 presented scope and future work.

2 Literature Review

A FNDNet model has been proposed by Kaliyar et al. [5] for fake news detection. FNDNet based on deep CNN. The proposed model has the capability to learn about biased features for fake news classification using different layers hidden inside the neural network, i.e., without using any manual method. The authors after performing their research and compared their results with several other models to know the accuracy with respect to other former proposed models. Ibrishimova et al. [6] developed a new definition for fake news based on factual accuracy and relative bias. In their model, they used five NLP features combined with three knowledge verification features to verify the scope and readability of the news. They used Google NLP API and News API to implement their model. Gravanis et al. [7] used various machine learning algorithms for fake news detection. The author also focused on the improvement of various machine learning methods like Bagging and AdaBoost by examining famous ML classifiers. This paper also gives a glimpse of invention of new text corpus named as unbiased dataset.

Mele et al. [8] identified and captured the news from various sources by using popular discrete dynamic top modeling and hidden Markov model. Modern people are more fascinated toward the news posted online which is the most common and easy way of spreading fake news. Here, the authors tried to be focused more latest news rather than the old news. The proposed model includes training of recurrent neural network with the aim of identifying hoaxes [9]. In Zhang et al. [10], authors have presented the following parameters for assessing the performance of fake news detection system. The parameters are: accurate detection, interactive visualization, early warning and post intervention, and third-party verification. Lastly, the author deduced that the fake news system should comprise of alert, detection, and intervention system. The fusion of these three system results in better analysis. Check-It model by Paschlides et al. [11] through this research authors tried to provide a check-it system, a kind of plugin for the browser that comprises of different signals fused together to identify misinformation. They used lexical semantics, feature selection, and information extraction for computing the results.

Aldwiri et al. presented paper in [12]. In this paper, clickbaits and fake news allowed users to discriminate helpful insights from the Internet. The above was possible because of the tool developed by the authors that can be installed in the user browser. And the tool used Bayes net, logistic regression, random tree, and Naïve Bayes algorithms. A survey has been conducted by Sharma et al. in [13] as a long way to go. Vishwakarma et al. [14] focused on validating the accuracy of the text on the image by checking its reliability in top 15 search results of Google followed by computing the reliability parameter which finally helped in classifying the news as real or fake. In a research paper, Perez-Rosas et al. [15] focused on automatically identifying fake content on Internet. The authors used two novel datasets for the above task. Several processes like collection and validation are discussed in detail in this paper. A thorough analysis is performed based on the linguistic differences in legitimate and fake news content.

A FAKEDETECTOR [16] developed by Zhang with another researcher. They have a purpose of finding different algorithms and principles for detecting fake news. FAKEDETECTOR was developed using the concept of data mining and diffusive network. An embedded image/text-based research work also presented in [17]. In this, researcher used CNN for image features and LSTM for word embedding. They work with cosine similarity index and compare extract text with image-based text A.

3 Proposed Framework

There is various framework proposed by many researchers. Similarly, we proposed a novel multimodal framework to validate news as fake or real as shown in Fig. 3.

3.1 Embedded Image/Text

Today, all news post in the form of image with text. Our framework focuses on such news and uses such embedded image as input to check whether such news post is fake or real.

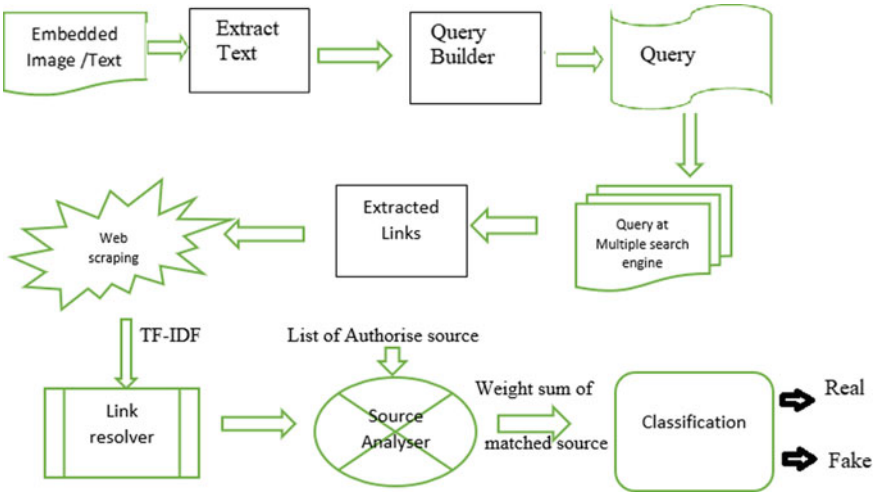

Fig. 3 Proposed framework with various blocks

3.2 Text Extraction

The deep learning model optical character recognition is used to extract text from input. The nanonets technology is used for more accurate text from image. So, now the text is removed from image after extraction and passes for cleaning and spell checking. The spell checks all available word spelling and send checked text to query builder unit.

3.3 Query Builder and Multiple Search Engines

Query builder block take verified text as input with image saliency features and build query and pass it to multiple search engine. As we have not believed only one search engine such as Google as Vishkarma et al. [14] has used for news verification. We have developed multithreaded block in our framework which fires the build query to many search engines and extracted related links from corpus.

3.4 Web Scraper and Link Resolver

The Web scraper uses extracted links and run scraper on links for extract information. The extracted information would be treated as one document from corpus. To check relevancy of the document with query, the TF-IDF model will be used. The TF-IDF provides each word frequency as term frequency for similarity of query with document. However, from many links, we would have low word frequency, these links will be discarded and would not be to carry forward to next block of our framework.

3.5 Source Analyzer and Classification

The source analyzer is the main block of our framework. It uses a list of authorized sources of news media. This block uses selected links from the previous block where each word frequency is high and checks it with authorized source list. If sources from the list of authorized sources, then weight will be assigned to the news. Similarly, all other links will be checked and weight will be added to the previous weight. A threshold value has been set by observation of real news and fake news. If the assigned weight value is higher then news will be classified as real otherwise fake.

4 Implementation and Experimental Results

4.1 Implementation Setup

To implement the framework the Python 3.7 has been used. For deep learning OCR, the Google cloud service is used. OCR extract text from embedded image and pass to query builder. The query builder checks spelling by using text blob package in Python. The spell check method will be used, it returns confidence score associated with correction. The multithread environment has been implemented by import thread package in Python. The start thread method was used for creating a thread for one search engine. Similarly, other threads created. To convert extracted links in related document, Web scraper has been implemented in Python. The beautiful soup package is used to implement this. The HTML parser is used for parsing the HTML document for information. To find related documents with query, TF-IDF model has been used from pandas package. For this, SkyLearn imported and compute TF method is used.

Equation for tf (term frequency)

$$\mathrm{tf}_{i,j} = \frac{n_{i,j}}{\sum_k n_{i,j}}$$

where $n_{i,j}$ occurrence of ith word in jth documents and $\mathrm{tf}_{i,j}$ is term frequency. For classification, the source analyzer used to check authorize source with already prepared authorize list of news media. For each matched link, a weight assigned as Wi where i represent authorized source ID. All matched weight would be added and all non-matched has been discarded. Sum of all matched authorize source weight

$$(W) => \sum_{i=0}^{n} Wi$$

For classification, if weight value is more than 60%, then news would be classified as real otherwise fake.

4.2 Experimental Result and Analysis

In this section, we evaluate our results on dataset MediaEval2016 [18] and BuzzFeed-News [19]. The MediaEval2016 consists 40 events, 261 articles and 478 embedded images/text where 236 real images 242 fake images. The BuzzFeedNews dataset consists of 6 article and total 49 images with 31 real and 18 fake. For accuracy measure, true positive, false positive, true negative, and false negative terms value has been calculated for precision (P), recall (R), and $F1$-measure to find accuracy of the proposed framework. Accuracy may calculated as follows:

$$\text{Accuracy} = \frac{\text{number of correct predictions}}{\text{total number of predictions}}$$

We have also run our algorithm on some Google news to check whether the news is fake or real.

Algorithm 1: Proposed Algorithm.

Step 1: Input embedded Image/Text to Deep learning OCR, it extracts text as ET and image features.

Step 2: Output of step1 passes to query builder, it builds query by concatenate all inputs and generate query.

Step 3: The generated query sends to multiple search engine based on multi-threaded path.

Step 4: Related Links are extracted as RLi where i represent the source.

Step 5: All RLi used by web scraper and scrap the text as Ti.

Step 6: All Ti and ET passes to TF-IDF for term frequency.

Step 7: The Link resolver uses first twenty link which are having highest tf-idf core and others are discarded.

Step 8: For all selected i = 1 to total authorize source.

Match with authorize source already available in a list.

If matched **then.**

$W = W + Wi.$

Step 9: If (W *100/total authorize source >60%) **then.**

Output as Real News.

Else.

Output as Fake News.

Table 1 depicted result as follows: The MediaEval2016 has been divided into training and testing dataset in the ratio of 70 and 30%. The 82% accuracy has been achieved. As recall percentage is only 56%, it actually decreasing our proposed framework accuracy. The BuzzFeedNews dataset we have used to test the performance of our proposed framework and algorithm. We have achieved 85% accuracy with 74% recall and 65% precision. The $F1$-measure is 70%. News in the form of embedded images/text has been collected from Google news. We have run Web scraper to collect 274 such news and run our proposed algorithm on it. For Google news dataset, we have achieved highest accuracy of 94%. This accuracy proved that our proposed framework and algorithm generate better results to validate an embedded image/text as news as real or fake.

Table 1 Performance evaluation

Dataset	Accuracy (%)	Precision (%)	Recall (%)	$F1$-score (%)
MediaEval2016	82	61	56	52
BuzzFeedNews	85	65	74	70
Google News	94	90.9	95.7	94.3

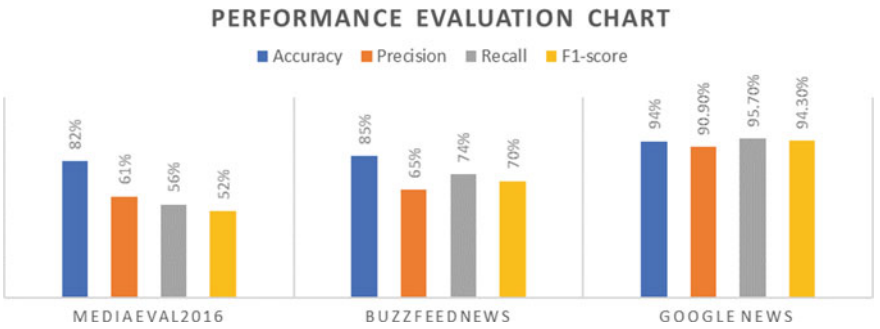

Fig. 4 Performance evaluation chart

To compare the result of all datasets, a performance evaluation graph has been strategized as shown in Fig. 4. The performance evaluation graph depicted as whenever recall is high, the accuracy measure is also high. It shows if have maximum number of authorize source in predefined list then our framework and proposed algorithm perform with highest percentage. So, the proposed framework is a novel framework to validate a news as embedded images/text as real or fake.

5 Conclusion and Future Work

In this research work, a novel framework with an algorithm has been proposed for fake news validation. The feature that makes the framework unique is its multiple search engine-based validation. The algorithm has been evaluated on two popular dataset MediaEval2016 and BuzzFeedNews. The accuracy observed after execute the proposed algorithm on datasets is 82 and 85%. The performance of the proposed algorithm increased to 95% accuracy with Google news which has been scraped by Web scraper. In the future, publisher and author credibility may include to enhance the performance of the proposed algorithm.

References

1. Allcott H, Gentzkow M (2017) Social media and fake news in the 2016 election. J Econ Perspect 211:36
2. Fallis D, Mathiesen K (2019). Fake news is counterfeit news. 1–20
3. Shu K et al. (2017) Fake news detection on social media: a data mining perspective. ACM SIGKDD Explor Newsl 22–36
4. Jin Z et al (2016) Novel visual and statistical image features for microblogs news verification. IEEE Trans Multimedia 19(3):598–608
5. Kaliyar RK et al (2020) FNDNet–A deep convolutional neural network for fake news detection. Cognitive Systems Research 61:32–44

6. Ibrishimova, MD, Li KF (2019) A machine learning approach to fake news detection using knowledge verification and natural language processing. In: International conference on intelligent networking and collaborative systems. Springer, Cham
7. Gravanis G et al (2019) Behind the cues: a benchmarking study for fake news detection. Expert Syst Appl 128:201–213
8. Mele I, Bahrainian SA, Crestani F (2019) Event mining and timeliness analysis from heterogeneous news streams. Inf Process Manage 56(3):969–993
9. Alkhodair SA et al (2020) Detecting breaking news rumors of emerging topics in social media. Inf Process Manage 57(2):102018
10. Zhang X, Ghorbani AA (2020) An overview of online fake news: characterization, detection, and discussion. Inf Process Manage 57(2):102025
11. Paschalides D, et al. (2019) Check-it: a plugin for detecting and reducing the spread of fake news and misinformation on the web. In: 2019 IEEE/WIC/ACM international conference on web intelligence (WI). IEEE
12. Aldwairi M, Alwahedi A (2018) Detecting fake news in social media networks. Procedia Comput Sci 141:215–222
13. Sharma S, Sharma DK (2019) Fake news detection: a long way to go. In: 2019 4th international conference on information systems and computer networks (ISCON), Mathura, India, pp 816–821
14. Vishwakarma DK, Varshney D, Yadav A (2019) Detection and veracity analysis of fake news via scrapping and authenticating the web search. Cogn Syst Res 58:217–229
15. Pérez-Rosas, V, et al (2017) Automatic detection of fake news. arXiv preprint arXiv:1708.07104
16. Zhang J, Dong B, Philip SY (2020) Fakedetector: effective fake news detection with deep diffusive neural network. In: 2020 IEEE 36th international conference on data engineering (ICDE). IEEE
17. Mangal D, Sharma DK (2020) FakeNews detection with integration of embedded text cues and image feature. In: 8th international conference on reliability, Infocom technologies and optimization (trends and future directions) (ICRITO), Amity University, Noida, India
18. Maigrot C, Claveau V, Kijak E, Sicre R (2016) MediaEval 2016: a multimodal system for the verifying multimedia use task. In: Proceedings of the 2016 multimedia benchmark workshop. MediaEval 2016, Netherlands
19. Data and analysis supporting the BuzzFeed News article (2017) These are 50 of the biggest fake news hits on Facebook In 2017. Published on Dec. 28 2017

Prediction of Type of Bone Disease Using Machine Learning

Sujata Joshi and Mydhili K. Nair

Abstract Machine learning has emerged as a promising field in the area of health care because of its ability to automatically learn and improve from experience without explicit programming and thus can discover useful patterns. The discovered patterns are then used for further analysis and decision making and making predictions. Bone is an integral part of human body which provides shape and structure to the body. As bones are used throughout the lifespan of a person, it is quite possible that bones get diseased or injured. The task of identifying the type of bone problem is quite a challenging task as it requires years of experience for healthcare professionals and intense medical tests, X-rays and scanning to be conducted. The number of such practitioners available is limited. Also, the bone ailment is quite painful and the patients have long waiting times. Hence, there is a requirement to detect the type of bone disease or ailment, quickly and accurately. The objective of this work is to develop a predictive model to identify type of bone disease from physical examination features. The unique features of this work is that we have used live data of patients to develop predictive models. We have proposed an algorithm which uses a combination of k-NN learning algorithm and Jaccard similarity measure for the purpose of prediction. The accuracy and error rate of the model developed by the proposed method is found to be 80.5% and 19.5%, respectively.

Keywords Bone disease · Sparse data · Machine learning · Binary · k-nearest neighbour

S. Joshi (✉)
Nitte Meenakshi Institute of Technology, Bangalore, India
e-mail: sujata.joshi@nmit.ac.in

M. K. Nair
M.S. Ramaiah Institute of Technology, Bangalore, India

D. K. Sharma et al. (eds.), *Micro-Electronics and Telecommunication Engineering*,
Lecture Notes in Networks and Systems 179,
https://doi.org/10.1007/978-981-33-4687-1_55

1 Introduction

Bones are vital structural elements of the human body which give shape and support to the body. The bone tissues rebuild constantly throughout the lifespan of the human being. During childhood and teenage, new bone is added faster but as the body ages, the rebuilding capacity of the bone diminishes which may surface as bone diseases. Bone disease comprises of any of the diseases or injuries that affect human bones [1]. Bone diseases can make the bones weak and fragile. Some of the factors for the bone diseases are metabolic disorder, genetic disorder, hormonal imbalance, loss of bone mineral density, endocrine disorder and nutrition deficiencies [2]. The literature review of the domain has revealed the various types of bone problems as:

- Low bone density and osteoporosis—In this bone ailment, the bones become weak and fragile.
- Osteogenesis imperfecta—Bones become brittle leading to difficulty in movement of body parts.
- Paget's disease—New bone is abnormally shaped, weak and brittle.
- Rickets—It is a skeletal disorder that is caused by a lack of vitamin D, calcium, or phosphate leading to weak and soft bones, stunted growth, and, in severe cases, skeletal deformities.

This work focuses on predicting two common types of bone diseases:

(i) Degenerative bone disease.
(ii) Traumatic bone disease.

(i) **Degenerative bone disease:** This is a state in which the protective cartilage that protects the end of bones degenerates, or wears down over time. It is also called as osteoarthritis. It is the most common form of bone disease affecting millions of people worldwide. It may also cause the development of osteophytes, or bone spurs. These spurs put pressure on the nerves thus causing weakness and pain in the arms or legs. Though it can affect any joint, it is found to mostly affect joints in the hands, knees, hips and spine [3, 4]. The degenerative bone disease of the leg joint is shown in Fig. 1.

(ii) **Traumatic bone disease:** It is a condition in which the bone is damaged due to some trauma or accident [4]. This may lead to dislocation of bones or injury to the bones. The traumatic bone disease is shown in Fig. 2.

The task of identifying the type of bone problem is quite a challenging task as it requires years of experience for healthcare professionals and intense medical tests, X-rays and scanning to be conducted. The number of such practitioners available is also limited. Also, bone ailment is quite painful and the patients have long waiting times. Hence, there is a need to detect the type of bone disease or ailment, fast and accurately. The objective of this work is to develop a predictive model to detect type of bone disease from physical examination features.

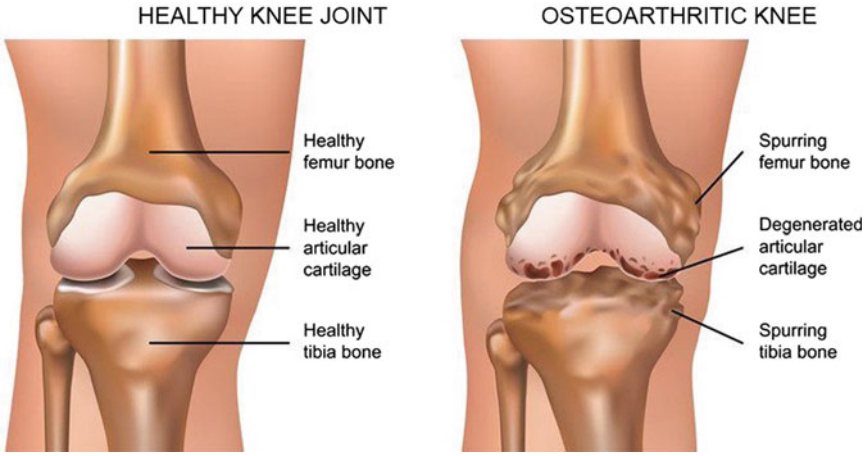

Fig. 1 Degenerative bone disease

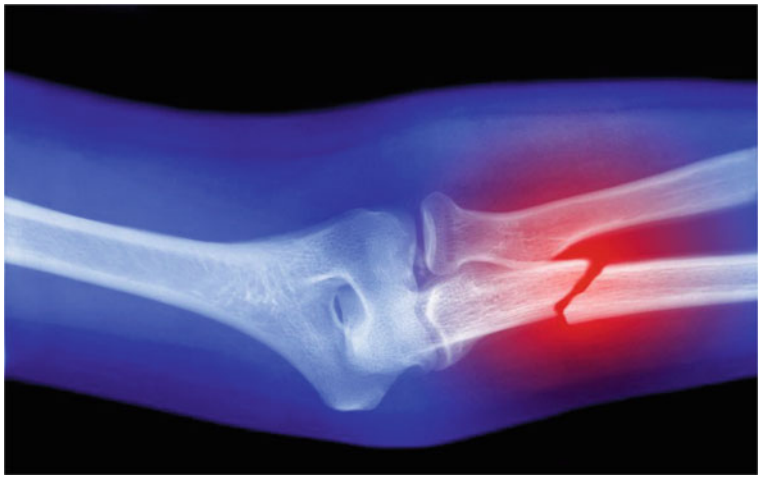

Fig. 2 Traumatic bone disease

2 Literature Review

With the growth of information technology and its applications, machine learning has a pivotal role particularly in the healthcare domain [5]. Machine learning algorithms are used in disease prediction, health management, quarantine management and identifying fraudulent insurance health claims.

Literature study with respect to bone diseases, machine learning algorithms, data used and methodology adopted is done.

In a work taken up by researchers in [5], electronic health records are used to develop an effective disease risk management model to model progression of bone disease. In this work, the researchers have developed a framework to represent features from all available risk factors in the EHR data. These integrated features are then used to effectively predict osteoporosis and bone fractures. Bone disease memory (BDM) is developed to capture characteristics of those individuals who suffer from bone diseases. Similarly, the non-disease memory (NDM) captures the features for non-diseased individuals. The researchers have used two-layer deep belief network for the prediction, and the results reveal that the proposed framework is successful in predicting bone diseases.

In another work taken up by the researchers [6], a model to forecast the risk of osteoporosis is developed. Certain factors were identified and were monitored by experts in determining osteoporosis risk. This study has used the learning algorithms namely Naïve Bayes' (NB) classifier and the multi-layer perceptron (MLP). The result showed 20 risk factors with moderate accuracy.

According to researchers in [7], it is observed that low bone mineral density is the important predictor of future fractures. The authors established the association of bone mineral density (BMD) with risk of fracture of the spine or hip. The study included 2356 men and women in the age group of 47–95 years. The models were developed using Poisson and Cox regression and further analysis was done based on the results.

In another work proposed in [8], the relationship between bone mineral density measurements and fracture risk at the hip, wrist/forearm, spine, and rib was studied in 149,524 postmenopausal women. The test considered *T*-scores that are the measure of bone mineral density for the prediction. The authors considered BMD measurement, questionnaires and data analysis for the prediction purpose. The authors analysed the performance of the algorithms through evaluation criteria such as sensitivity and specificity.

In a work proposed by the authors in [9], a new approach has proposed to classify bone disorders and the radiographic bone image is used for this purpose.

This work is unique in that we have used physical features of the patient to identify the type of bone disease and the data is sparse in nature. Another unique feature of this work is that we have used live data of patients from hospital to develop the predictive models.

3 Methods

3.1 Data

In this work, the dataset used is collected from Sun Orthopaedic Hospital, Bangalore. It has 30 attributes which include name, age, gender, region or area of the body affected, swelling, redness, fever, tenderness, dislocation of bone, difficulty in

movement and performing daily activities. The various attributes are listed in Table 1.

The dataset includes patients with ages in the range of 10–85 years. The other attributes except name, gender and age consist of Boolean attributes. The class attribute 'Bone disease type' has two values indicating:

(1) Traumatic bone disease.
(2) Degenerative bone disease.

The research question to be answered is: Is it possible to *predict the type of bone disease of a patient based on physical examination observations accurately.*

3.2 Learning Methodology

The challenge involved in this work is that, most of the attributes in the dataset are of Boolean type indicating a 'yes' or a 'no' condition. This is because when a patient enters the hospital, he/she is in pain and when interviewed about the pain in various areas of the body, the response is yes if there is pain in a particular area and no if there is no pain in that area. Another challenge is that the data is sparse. This is because the patient may have pain in one or more areas defined in the dataset, but may not have pain in all the areas defined thus making the data sparse. In order to develop the most suitable model for the prediction of bone disease type, from primary physical investigations and taking into consideration the data sparsity, machine learning algorithms were assessed for their appropriateness. k-NN [10] was found to be suitable for the task but the general Euclidean distance measure is not appropriate to compute the distance. Hence, a different distance measure has to be explored for use in this case. Generally, Euclidean or Manhattan distance is used in k-NN algorithm, but in this case, as the attributes are binary and also sparse, it is required to use an appropriate measure for such attributes.

3.3 Distance Measures for Binary Attributes

The distance between binary attributes is computed by forming a contingency table as given in Table 2 [11, 12].

If i and j are two objects,

a = Number of attributes in which $i = 1$ and $j = 1$.
b = Number of attributes in which $i = 1$ and $j = 0$.
c = Number of attributes in which $i = 0$ and $j = 1$.
d = Number of attributes in which $i = 0$ and $j = 0$.

The distance between two objects i and j is given by:

Table 1 Dataset description

Attribute	Value	Description
Name	String	Name of the patient
Age	Integer	Age of patient entered in years
Gender	Boolean	M, if Male. F, if Female
Body	Boolean	The region affected due to bone disease is body. (0 = No; 1 = Yes)
Thigh and knee	Boolean	The region affected due to bone disease is thigh and knee. (0 = No; 1 = Yes)
Ankle and foot	Boolean	The region affected due to bone disease is ankle and foot. (0 = No; 1 = Yes)
Lumbus hip and hip	Boolean	The region affected due to bone disease is lumbus hip and hip. (0 = No; 1 = Yes)
Shoulder and shoulder joint	Boolean	The region affected due to bone disease is shoulder and shoulder joint. (0 = No; 1 = Yes)
Wrist and thumb	Boolean	The region affected due to bone disease is wrist and thumb. (0 = No; 1 = Yes)
Hand	Boolean	The region affected due to bone disease is hand. (0 = No; 1 = Yes)
Leg	Boolean	The region affected due to bone disease is leg. (0 = No; 1 = Yes)
Multiple joint	Boolean	The region affected due to bone disease is multiple joint. (0 = No; 1 = Yes)
Lower back	Boolean	The region affected due to bone disease is lower back. (0 = No; 1 = Yes)
Around neck	Boolean	The region affected due to bone disease is around neck. (0 = No; 1 = Yes)
Spine	Boolean	The region affected due to bone disease is spine. (0 = No; 1 = Yes)
Elbow	Boolean	The region affected due to bone disease is elbow. (0 = No; 1 = Yes)
Pain	Boolean	Pain in affected region. (0 = No; 1 = Yes)
Weakness in muscle	Boolean	Weakness in muscle. (0 = No; 1 = Yes)
Swelling	Boolean	Presence of swelling. (0 = No; 1 = Yes)
Redness and sweating	Boolean	The symptom indicating redness and sweating. (0 = No; 1 = Yes)
Itching	Boolean	The symptom indicating presence of itching. (0 = No; 1 = Yes)
Ankle deformality	Boolean	The symptom indicating ankle deformality. (0 = No; 1 = Yes)
Feverish due to pain	Boolean	The symptom indicating presence of fever due to pain. (0 = No; 1 = Yes)

(continued)

Table 1 (continued)

Attribute	Value	Description
Tenderness	Boolean	The symptom indicating tenderness. (0 = No; 1 = Yes)
Water content in joint	Boolean	The symptom indicating presence of water content in joint. (0 = No; 1 = Yes)
Bone dislocation	Boolean	The physical incapacity to do chores due to bone dislocation. (0 = No; 1 = Yes)
Difficulty in doing daily activities	Boolean	The functional difficulty in doing daily activities. (0 = No; 1 = Yes)
Difficulty in movement	Boolean	The functional difficulty in movement. (0 = No; 1 = Yes)
Bone disease type	Integer	Indicates the type of bone disease. (1 = Traumatic bone disease; 2 = Degenerative bone disease)

Table 2 Contingency table

Object j			
Object i		1	0
	1	*a*	*b*
	0	*c*	*d*

$$d(i, j) = \frac{a}{a + b + c}$$

This measure is called Jaccard similarity index.

3.4 Learning Algorithm

In this work, the k-nearest neighbour machine learning algorithm is considered for the classification task. Here, the distance measure used is Jaccard similarity. The reason for choosing this distance measure is that most of the attributes are binary indicating the presence or absence of a pain or condition.

The pseudocode for k-NN is presented here [10]:

Algorithm: Computes the k-nearest neighbours for the query objects and returns their class label.

Input: Data objects and their associated class labels;

Output: Target class of query objects.

Method:

Given a new query object x_q to be classified:

- Find the k neighbours of x_q

- Let $x_1 \ldots x_k$ denote the k data objects from training data objects that are nearest to x_q
- Determine the class label of x_q by taking majority vote of the class labels of x_1, $\ldots x_k$.

4 Experimental Results

In this work, the dataset is split into 70:30 ratio, in which 70% was used for training and 30% is used for validation. All experiments are carried out in Python. The evaluation measures used are presented in Table 3.

The results of applying the proposed methodology to the bone disease dataset are shown in Table 4. It has shown an accuracy of 80.5%, error rate of 19.5%, sensitivity of 80.6%, and specificity of 80.7% as compared to the general k-NN using Euclidean distance which has shown accuracy of 72.3%, error rate of 27.7%, and sensitivity of 72.4% and specificity of 73.2%.

The results are shown graphically in Fig. 3.

The graph in Fig. 3 reveals that the proposed method using k-NN with Jaccard is more accurate and has less error for the kind of data we had for bone diseases. Also, the sensitivity and specificity measures are better compared to the k-NN with Euclidean distance measure and these show the correct positive predictions and negative predictions, respectively, which is better as compared to the traditional approach. The model needs further improvement by incorporating other types of data and further validation by domain experts.

Table 3 Evaluation metrics

Measure	Description
Accuracy	$\frac{TP}{TP+TN+FP+FN}$
Error rate	$\frac{TP}{TP+TN+FP+FN}$
Sensitivity	$\frac{TP}{TP+FN}$
Specificity	$\frac{TN}{TN+FP}$

Here, *TP* indicates true positives, *TN* indicates true negatives, *FP* indicates false positives, *FN* indicates false negatives

Table 4 Model results

Model	Accuracy (%)	Error rate (%)	Sensitivity (%)	Specificity (%)
k-NN	72.3	27.7	72.4	73.2
k-NN-Jaccard	80.5	19.5	80.6	80.7

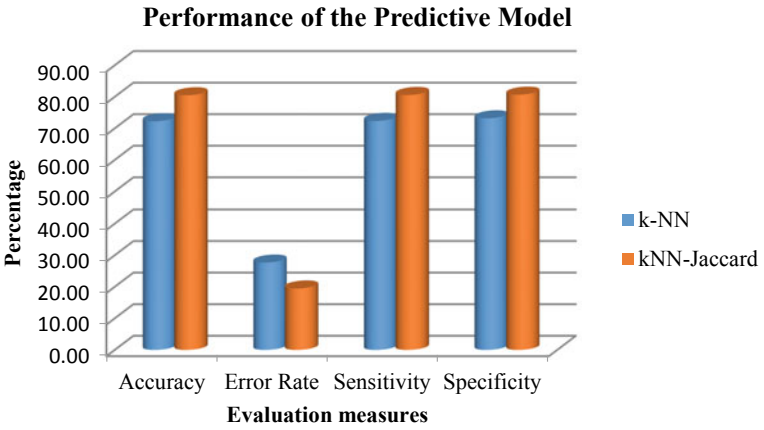

Fig. 3 Graphical representation of the results of the predictive model

5 Conclusion

In this paper, we have developed a predictive model for prediction of type of bone diseases. Here, we have considered degenerative bone disease and traumatic bone disease. We have proposed an algorithm which uses a combination of k-NN learning algorithm and Jaccard similarity measure for the purpose of prediction. The accuracy and error rate of the model developed by the proposed method is found to be 80.5% and 19.5%, respectively. In future, we would consider images obtained from X-rays and scans and develop appropriate predictive models. More data is required for further validation of results and domain expert advice is required for further analysis and usage of working model.

Acknowledgements Our sincere gratitude to Dr. Dharmapal and his team from Sun Orthopaedic Hospital, Bangalore for permitting us to use the data of their patients, conducting physical interviews with patients and his valuable guidance in the subject domain. Special thanks to the undergraduate students for their key role in data collection.

References

1. Office of the Surgeon General (US) (2004) Bone health and osteoporosis: a report of the surgeon general. Office of the Surgeon General (US), Diseases of Bone, Rockville (MD), 3. Available from: https://www.ncbi.nlm.nih.gov/books/NBK45506/
2. https://www.healthline.com/health/bone-pain
3. https://www.webmd.com/osteoarthritis/spinal-osteoarthritis-degenerative-arthritis-of-the-spine
4. Orthopedic Center of Southern Illinois. Accessed: April 15th 2019. Available: https://orthocenter-si.com/sites/all/files/images/Knee-arthritis-can-cause-pain-inside-knee.jpg

5. Li H, Li X, Ramanathan M, Zhang A (2014) Prediction and informative risk factor selection of bone diseases. IEEE/ACM Trans Comput Biol Bioinf 12(1):79–91
6. Keerthana A, Renukadevi P (2016) Predict and prevent the bone disease using data mining techniques. Int J Emerg Technol Comput Sci Electron 21(4)
7. Miller PD, Siris ES, Barrett-Connor E, Faulkner KG, Wehren LE, Abbott TA, Sherwood LM (2002) Prediction of fracture risk in postmenopausal white women with peripheral bone densitometry: evidence from the National Osteoporosis risk assessment. J Bone Miner Res 17(12):2222–2230
8. Gerdhem P, Ivaska KK, Alatalo SL, Halleen JM, Hellman J, Isaksson A, Obrant KJ (2004) Biochemical markers of bone metabolism and prediction of fracture in elderly women. J Bone Miner Res 19(3):386–393
9. Saranya M, Sarojini K (2016) An improved and optimal prediction of bone disease based on risk factors. Int J Comput Sci Inf Technol 7(2):820–823
10. Dasarathy BV (1991) Nearest neighbor (NN) norms: NN pattern classification techniques, IEEE Computer Society Tutorial
11. Han J, Pei J, Kamber M (2011) Data mining: concepts and techniques, Elsevier
12. Ramkumar S, Malathi R (2018) An automatic bone disorder classification using hybrid texture feature extraction with bone mineral density. Asian Pac J Cancer Prev 19(12):3517

Fuzzy Rough Set-based Link Stability Forecasting Scheme for Improving Data Dissemination in MANETs

J. Sengathir, M. Deva Priya, A. Christy Jeba Malar, S. Karthik, Viraja Ravi, and S. Sam Peter

Abstract In Mobile Ad hoc NETwork (MANET), the construction of stable paths among mobile nodes is inevitable for achieving network connectivity during the process of reliable data dissemination. MANET includes the properties of mobility, wireless connectivity and independence for fitting itself to a wide number of real-time applications, but increases the complexity involved in managing the path stability in the network. The routing protocols are the essential components of the entire network as they are responsible for searching and maintaining the routes. However, a path stability scheme that uses weighted aggregation of the mobile node interaction rate and energy is not much explored in the literature. In this paper, a Fuzzy Rough Set-based Link Stability Forecasting Scheme (FRSLSFS) is proposed for integrating the characteristic functionality of the Fuzzy Rough Set (FRS) for forecasting and deciding the stability of the link in order to achieve reliable data routing.

J. Sengathir
Department of Information Technology, CVR College of Engineering, Mangalpally, Vastunagar, Hyderabad, Telangana, India
e-mail: j.sengathir@gmail.com

M. D. Priya (✉) · V. Ravi · S. S. Peter
Department of Computer Science and Engineering, Sri Krishna College of Technology, Coimbatore, Tamilnadu, India
e-mail: m.devapriya@skct.edu.in

V. Ravi
e-mail: virajaravi@skct.edu.in

S. S. Peter
e-mail: sampeter.s@skct.edu.in

A. C. J. Malar
Department of Information Technology, Sri Krishna College of Technology, Coimbatore, Tamilnadu, India
e-mail: a.christyjebamalar@skct.edu.in

S. Karthik
Department of Computer Science and Engineering, SRM Institute of Science and Technology, Delhi-NCR Campus, Ghaziabad, India
e-mail: karthick.usilai@gmail.com

D. K. Sharma et al. (eds.), *Micro-Electronics and Telecommunication Engineering*,
Lecture Notes in Networks and Systems 179,
https://doi.org/10.1007/978-981-33-4687-1_56

This proposed FRSLSFS determines the link stability based contention count, signal strength, hop count, available energy of the link, normalized multi-objective optimization and link stability using FRS-based prediction. The simulation experiments of the proposed FRSLSFS scheme confirm its predominance by offering improved throughput by 13.21%, reduced packet latency by 12.84% and minimized energy consumption by 15.28% in contrast to the baseline link prediction schemes.

Keywords MANET · Link stability · Fuzzy rough set

1 Introduction

Mobile Ad hoc NETwork (MANET) is a collection of mobile nodes that cooperates among themselves without the utilization of established infrastructure or centralized administration. The main goal of MANET is to form a temporary network to facilitate reliable data dissemination among mobile nodes. Data dissemination depends on the preservation of path stability as packet drops and re-transmissions are more in MANET [1–3]. Path stability shows the degree of durability and sturdiness of the paths established. It is based on the number of substantial factors that includes energy efficiency, communication overhead and node mobility. Many works are proposed in the literature for addressing the issue of path stability so as to achieve effective communication in MANETs. Nevertheless, a number of limitations are prevalent with respect to the computation of optimal transmission rate of control messages, connection and disconnection transition state probabilities, connection and disconnection transition rate probabilities used for evaluating the stability of nodes in the neighborhood. Further, the energy of mobile nodes plays a vital role in maintaining the path stability of the network. An adaptive path stability prediction approach that possibly estimates the strength of the path between mobile nodes is mandatory for enabling consistent futuristic communication so as to achieve robust data dissemination. Adaptive path stability prediction strategies are also essential for maintaining energy-efficient stable paths when the motion of the mobile nodes is random. In addition, the accurate forecasting of energy inherent in the mobile node is indispensable for evaluation of path stability.

In this paper, a predominant path stability prediction strategy based on Fuzzy Rough Set (FRS) is contributed to sustain path stability and establish reliable data dissemination among the mobile nodes. The proposed Fuzzy Rough Set-based Link Stability Forecasting Scheme (FRSLSFS) inherits the merits of FRSs for handling uncertain information that is exchanged among the mobile nodes in the network during the process of estimating trust in the paths in order to identify link stability. The simulation experiments of the proposed FRSLSFS is analyzed in terms of Packet Delivery Rate (PDR), throughput, end-to-end delay, energy consumption and routing overhead for varying number of mobile nodes.

2 Related Work

Numerous mobility models are propounded for MANETs which include random walk, random waypoint and random group mobility models [4]. Critical applications demand sustained connectivity with link stability [5–12]. Rajendiran and Srivasta [13] have proposed a multicast protocol that aids in finding a stable path. The link stability of the network is based on the received power, distance and link quality. Singal et al. [14] have propounded Link Stability based Multicast Routing Protocol (LSMRP) to measure the stability of the link in MANETs. This multicast routing protocol is used to lessen the routing overhead and improve resource utilization. Xia et al. [15] have combined link stability estimation model and multicast AODV model for improving link stability in MANETs. The main purpose is to decrease network overhead and improve the performance of the network. Jaiswal and Sinha [16] have propounded Stable Geographic Forwarding with Link-lifetime prediction (SGFL) that is based on the broadcast nature of wireless channel and multicasts with node mobility. The nodes with less mobility at the least distance from the destination are selected. Backup nodes that lie within the range of selected neighbors are also selected. Predicting link lifetime with backup nodes improves efficacy and trustworthiness of routing.

Link state routing is used to find the paths and floods the information to all the routers in the network. Secure-dEed-Reflection-Inducement-eState (SERIeS) for IEEE 802.11b networks is proposed by Rajeswari and Ravi [17] to deal with security and link stability in MANETs. The path from the source to the destination is found using learning agents which use link state database with information including node's bandwidth, queue length and energy. Pitchai and Robert [18] have developed a mathematical model for Path Selection Algorithm based on Hamming Distance (PSA-HD). Stable links are selected by detecting the link break. Hamming distance aids in detecting modifications in bit positions between two binary values. Routing tables are updated by totalling variations in the character position. Pal et al. [19] have proposed a scheme to deal with forming a stable link network using temporal data analysis model. The mobility and position of neighbor nodes are analyzed with respect to nodes from network's temporal snapshot. The statistical Auto-Regressive Moving Average (ARMA) is used for forecasting the stable neighbors of nodes. These neighbors are involved in forming a link between nodes. They have applied Biogeographic-Based Optimization (BBO) technique to assess parameters pertinent to the ideal path from source to destination.

3 Fuzzy Rough Set-based Link Stability Forecasting Scheme

The proposed Fuzzy Rough Set-based Link Stability Forecasting Scheme (FRSLSFS) estimates the link stability that aids in attaining reliable data dissemination in the process of routing. Link stability is determined based on the computation of contention degree, signal strength, hop count and available energy of link that are integrated based on a normalized multi-objective function which utilizes FRS for precise estimation. This proposed FRSLSFS integrates the potential characteristics of significant solution, and FRS for predicting and identifying the exact link stability that plays an anchor role in trusted data routing. It pertains to the methodology of divide and conquer that aids in differentiating the feasible values of link stability that are possibly utilized during the process of routing with respect to the selected value and comparison score. Further, the suitable link for performing trusted communication is attained based on the scheme of ideal solution that extracts the characteristics of each factor along with the attributes involved in the aspect of link stability during routing. FRS obtained through ideal solution scheme targets in exploring the positive and negative dimensions of each factor that could be possibly determined during the enforcement of feasible constraints of routing. Finally, weight-based hamming distance is applied for predicting reliable link that could be used for trusted communication.

3.1 Degree of Contention Determination

In the proposed FRSLSFS scheme, the degree of contention defines the trust of the routing link that is potentially utilized for reliable data routing. In this context, adequate knowledge pertaining to the neighboring mobile nodes associated with each cooperating mobile node is essential for accurate determination of links' trustworthiness. Thus, the degree of contention of the complete set of nodes that are present in the proximity of a mobile node under the monitoring process is shown in Eq. (1).

$$C_{\mathrm{s}} = |N_{\mathrm{i}}| \tag{1}$$

where '$|N_{\mathrm{i}}|$' represent the total number of neighbors interacting with a mobile node at any specific instant of time. This contention set can be also expressed as $C_{\mathrm{s}} = \left\{N_1, N_2, N_{3,} \cdots N_{\mathrm{n}}\right\}$ with 'n' connected neighboring mobile nodes within the radius of transmission. The contention set of every link is periodically refreshed and stored in the mobile nodes of the link for decision analysis. For instance, if a mobile node 'A' is intractable with mobile nodes 'B', 'C' and 'E', then the contention count is 3.

3.2 Determination of Signal Strength

Similar to contention count, signal strength is considered as the potential factor that impacts the stability of the link during data communication. Signal strength quantifies the quality of the established link that exists between any two neighboring nodes of the network. The power loss of the link is considered to be low when the signal strength is high, and in contrast, the low signal strength contributes a major power loss during data transmission. This signal strength increases depending on the reduction in transmission distance between any two mobile nodes under interaction and it reduces when the transmission distance is potentially high. Thus, the signal strength of the link is estimated using Eq. (2).

$$L_{(\mathrm{i})} - \mathrm{RSS} = \frac{\mathrm{PKT}_{\mathrm{Rec-Power}}}{\mathrm{Noise\_Degree}} \tag{2}$$

where '$\mathrm{PKT}_{\mathrm{Rec-Power}}$' and 'Noise_Degree' represent the amount of power received per packet and the degree of noise exhausted during unit packet transmission. This factor of signal strength can be determined in magnitude using cross-layer information that aids in deriving information from the physical layer and passing to the network layer of the network model in order to facilitate reliable estimation. The interacting mobile nodes effectively compute the signal strength factor by incorporating a systematic monitoring process in the predecessor nodes.

3.3 Hop Count Estimation

In the proposed FRSLSFS scheme, the hop count is defined as the number of links available between the mobile nodes for the packets to travel at a specific instant of time. This estimation of hop count is completely initiated by the source to the destination nodes through possible links in the network. Moreover, the value of hop count is generally incremented by '1' depending on the packet reception at the intermediate mobile nodes of the network. In addition, hop count ($\mathrm{HOP}_{\mathrm{CNT}}$) is determined to be an indirect factor that predominantly impacts the link stability during data transmission, since the increase in hop count correspondingly increases the packet latency in the network. Hence, packet latency determined during the process of data transmission is presented in Eq. (3)

$$\mathrm{PKT}_{\mathrm{LATENCY}} \infty \mathrm{HOP}_{\mathrm{CNT}} \tag{3}$$

3.4 Available Energy of Link Computation

The available energy of link is another key factor that attributes toward network stability during the process of data routing. In the proposed FRSLSFS scheme, the residual energy of mobile nodes that plays an anchor role in connectivity is also determined similar to the factor of contention degree, which particularly portrays the role of the cooperating mobile nodes in the routing path. This available energy of link is computed based on ratio of total energy consumed by the mobile nodes ($E_{\text{UTIL-LINK}}$) in each link to the amount of energy possessed by the same mobile nodes ($E_{\text{INITIAL-LINK}}$) before the commencement of data routing. Hence, the available energy associated with the link is computed based on Eq. (4).

$$L_{\text{AVAIL-ENERGY}} = \frac{E_{\text{UTIL-LINK}}}{E_{\text{INITIAL-LINK}}} \tag{4}$$

At this point, the contention count should be moderate, hop count should be minimum and the parameters of Received Signal Strength (RSS) and available energy should be high for portraying link stability during routing.

3.5 Optimization Using Normalized Multi-Objective Function

The factors such as contention degree, signal strength, hop count and available energy of the link are determined to be dissimilar in characteristics. These impact factors of routing do not get satisfied during the determination of link stability, since their value may be low, moderate and high at a particular point of routing. At this juncture, the multi-objective optimization functions are always indispensable for resolving the impactful factor conflicts that are essential for guaranteeing link stability in the network. Hence, the multi-objective optimization function plays a predominant role in factor mapping that integrates the contention degree, signal strength, hop count and available energy of link into a hybridized parameter through the application of weights that aid in imposing the factors with or without constraints. However, the weighted sum strategy is not suitable for resolving the shortcomings that arise during the domination process surpassing the influence of one parameter over the other. However, this normalization method confirms to prevent the dominance of one factor over the other. Further, the upper and lower limits of normalization are incorporated for influential equalization in order to attribute toward the determination of link stability as presented in Eq. (5).

$$\text{Norm}_{\text{LUT}} = \frac{f_{\text{c(i)}} - f_{\text{c(min)}}}{f_{\text{c(max)}} - f_{\text{c(min)}}} \tag{5}$$

In this point, the lower and upper limits of normalization are considered to vary between 0 and 1.

3.6 Link Stability Parameter (LSP) Calculation

The calculation of Link Stability Parameter (LSP) depends on Eqs. (6)–(9).

$$\mathrm{LSP}_{(\mathrm{i})} \infty L_{(\mathrm{i})} - \mathrm{RSS}_{(\mathrm{NORM})} \tag{6}$$

$$\mathrm{LSP}_{(\mathrm{i})} \infty \frac{1}{\mathrm{HOP}_{\mathrm{CNT(NORM)}}} \tag{7}$$

$$\mathrm{LSP}_{(\mathrm{i})} \infty L_{\mathrm{AVAIL-ENERGY(NORM)}} \tag{8}$$

$$\mathrm{LSP}_{(\mathrm{i})} \infty C_{\mathrm{S(DIFF)}} \tag{9}$$

Then, the LSP is computed as shown in Eq. (10).

$$\mathrm{LSP}_{(\mathrm{i})} \infty \frac{L_{(\mathrm{i})} - \mathrm{RSS}_{(\mathrm{NORM})} * L_{\mathrm{AVAIL-ENERGY(NORM)}}}{\mathrm{HOP}_{\mathrm{CNT(NORM)}}} - C_{\mathrm{S(DIFF)}} \tag{10}$$

Every mobile node of the network is responsible for calculating the current value of LSP pertaining to each of its incoming links. The mobile node with maximum LSP value is optimally chosen for packet forwarding with the possibility that it could provide stable route for data dissemination.

3.7 Forecasting of Link Stability Using FRS

Once the current link stability factor of the links is estimated, the forecasting of the link stability using FRS comes into play. The information system used for determining link stability comprises of a set of links and their link stability values determined through the enforcement of factors with or without constraints.

$$F_{\mathrm{kl}} = \left| f \in F;\, R_{\mathrm{S(F)}}(N_{\mathrm{K}}) \geq R_{\mathrm{S(F)}}(N_{\mathrm{l}}) \right| \tag{11}$$

$$F_{k(\mathrm{WTC})} = \sum_{\mathrm{k}=1}^{\mathrm{n}} f_{\mathrm{kl}} \tag{12}$$

$$F_{k(WC)} = \sum_{l=1}^{n} f_{kl} \tag{13}$$

$$S_C(\text{dev}) = F_{k(WTC)} - F_{k(WC)} \tag{14}$$

The mobile node with maximum $S_C(\text{dev})$ is finally selected for facilitating reliable link in packet forwarding with the possibility that it could provide stable link for data transfer in the network.

4 Results and Discussion

The simulation experiments of the proposed FRSLSFS and the benchmarked protocols are conducted using the network simulator (ns–2.35). The simulation environment used for evaluating the proposed FRSLSFS scheme is 1000*1000 m^2. In addition, the simulation parameters used for evaluating the predominance of the proposed FRSLSFS scheme over the benchmarked Path Selection Algorithm based on Hamming Distance (PSA-HD) and SERieS schemes are presented in Table 1.

Figures 1 and 2 present the results of the proposed FRSLSFS and benchmarked PSA-HD and SERieS schemes evaluated in terms of Packet Delivery Ratio (PDR) and throughput for varying number of mobile nodes. The PDR and throughput of the FRSLSFS scheme are considered to be predominant on par with the other baseline PSA-HD and SERieS schemes for increasing number of mobile nodes, since it uses multiple linguistic variables for accurate classification of optimal path from the predetermined stability paths. The PDR of the proposed FRSLSFS scheme is identified to be improved by 6.13% and 7.83% in contrast to the baseline PSA-HD and SERieS schemes. Likewise, the throughput of the proposed FPSPM scheme is enhanced by 5.18% and 6.28% when compared to the PSA-HD and SERieS schemes.

Figures 3 and 4 present the end-to-end delay and energy consumptions for varying number of mobile nodes. The end-to-end delay of the proposed FRSLSFS scheme is

Table 1 Simulation parameters used for implementing FRSLSFS

Parameters	Values
Simulation tool	NS–2.35
Node count	50–250
Density of nodes	15 m^2
Transmission range	250 m
CBR data rate	24 Mbps
Interval of HELLO packets	1 s
Mobility speed	5–25 m/s
Traffic type	CBR
Radio type	802.11

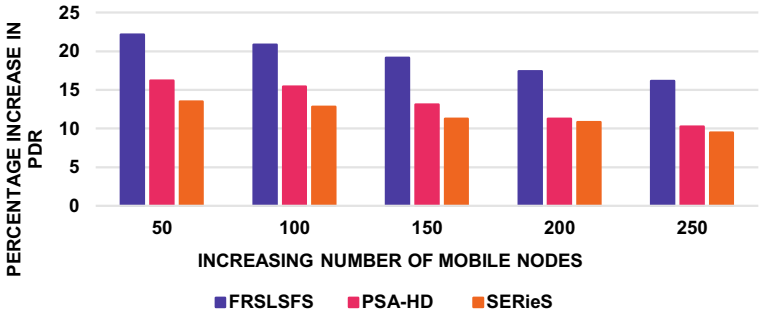

Fig. 1 Percentage Improvement in PDR of the Proposed FRSLSFS for Varying Number of Mobile Nodes

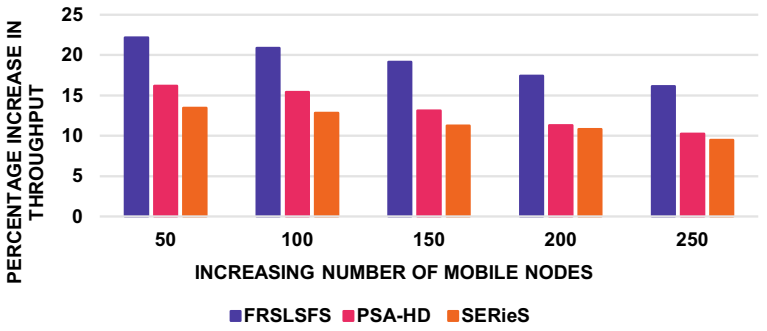

Fig. 2 Percentage Improvement in Throughput of the Proposed FRSLSFS for Varying Number of Mobile Nodes

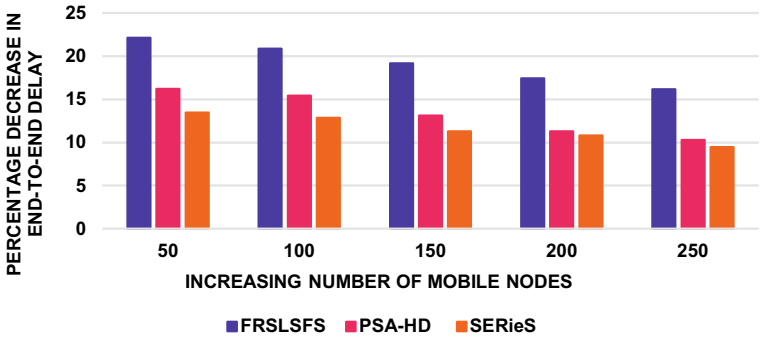

Fig. 3 Percentage Decrease in End-to-end Delay of the Proposed FRSLSFS for Varying Number of Mobile Nodes

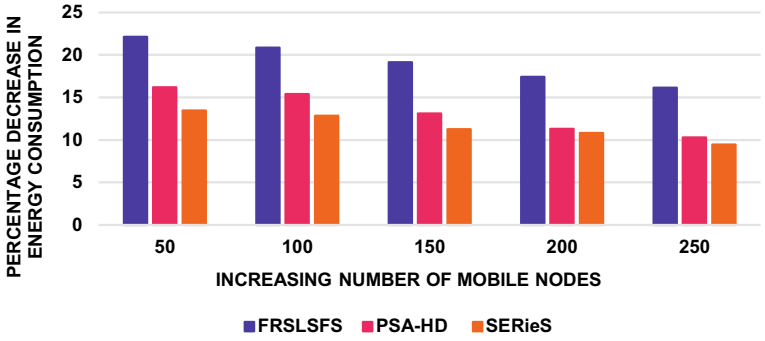

Fig. 4 Percentage decrease in energy consumption of the proposed FRSLSFS for different mobile nodes

confirmed to be reduced when compared to PSA-HD and SERieS schemes, since the utilized fuzzy inference engine is capable of quantifying the path stability based on the parameters related to energy and interaction rate of mobile nodes. Similarly, energy consumptions of the proposed FRSLSFS scheme is confirmed to be reduced when compared to PSA-HD and SERieS schemes due to the exploration and prediction capability of fuzzy theory in path stability estimation. Thus, the end-to-end delay of the proposed FRSLSFS scheme is significantly reduced by 11.43% and 13.58% in contrast to the baseline PSA-HD and SERieS schemes. The energy consumption of the proposed FRSLSFS scheme is also proved to be minimized by 9.12%, 10.48% and 12.84% in contrast to the proposed baseline PSA-HD and SERieS schemes. In addition, from Fig. 5, it is understood that the routing overhead is reduced in contrast to the benchmarked PSA-HD and SERieS schemes, as it is predominant in preventing the number of re-transmissions by accurate forecasting of more stable paths during the data dissemination process. The routing overhead of the proposed RSLSFS scheme is proved to be considerably minimized by 10.24% and 12.96% when compared to the proposed PSA-HD and SERieS schemes.

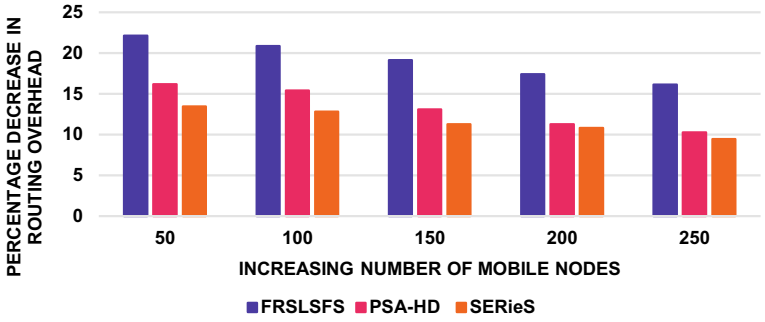

Fig. 5 Percentage Decrease in Routing Overhead of the Proposed FRSLSFS for Varying Number of Mobile Nodes

5 Conclusion

In this paper, Fuzzy Rough Set-based Link Stability Forecasting Scheme (FRSLSFS) is proposed to incorporate the characteristic functionality of the Fuzzy Rough Set (FRS) to predict and decide the link stability to attain consistent routing. FRSLSFS determines link stability based on the contention count, signal strength, hop count, available energy of the link, normalized multi-objective optimization and link stability. The simulation results prove that the proposed FRSLSFS offers 13.21% improved throughput, 12.84% reduced packet latency and 15.28% reduced energy consumption in contrast to the baseline PSA-HD and SERieS link prediction schemes.

References

1. Sengathir J, Manoharan R (2013) Security algorithms for mitigating selfish and shared root node attacks in MANETs. Int J Comput Netw Inf Secur 5(10):1–10
2. Sengathir J, Manoharan R (2014) Reliability factor-based mathematical model for isolating selfish nodes in MANETs. Int J Inf Commun Technol 6(3/4):403
3. Sengathir J, Manoharan R (2017) Co-operation enforcing reputation-based detection techniques and frameworks for handling selfish node behaviour in MANETs: A review. Wireless Pers Commun 97(3):3427–3447
4. Long J, Dong M, Ota K, Liu A (2014) Achieving source location privacy and network lifetime maximization through tree-based diversionary routing in wireless sensor networks. IEEE Access 2:633–651
5. Chen Q, Kanhere SS, Hassan M (2013) Adaptive position update for geographic routing in mobile adhoc networks. IEEE Trans Mob Comput 12(3):489–501
6. Deva Priya M, Priya T (2008) SPPS: secured and power-efficient path selection in wireless sensor network. In: Proceedings of 1st national conference on communication, computation and automation
7. Deva Priya M, Priyanka P (2015) PPCLSS: probabilistic prediction coefficient link stability scheme based routing in MANETs. Int J Comput Sci Eng Technol 6(4):246–256
8. Deva Priya M, Valarmathi ML (2013) A cross-layered path stability based routing protocol for WiMAX networks. Am J Appl Sci 10(11):1325–1334
9. Priyanka P, Deva Priya M (2015) Energy efficient linked supervisory set based routing (E2LS2R) scheme for wireless mesh networks. Int J Multi Res Dev 3(3):494–499
10. Alsharabi N, Fa LR, Zing F, Ghurab M (2008) Wireless sensor networks of battlefields hotspot: challenges and solutions. In: 6th IEEE international symposium on modeling and optimization in mobile, ad hoc, and wireless networks and workshops, pp 192–196
11. Walker III TO, Tummala M, McEachen J (2010) Energy efficiency of centralized and distributed computation in unattended multi-hop wireless sensor networks for battlefield monitoring. In: 43rd IEEE Hawaii international conference on system sciences, pp 1–9
12. Li YX, Shi HS, Zhang SP (2010) An optimized scheme for battlefield target tracking in wireless sensor network. In: 2nd IEEE international conference on industrial and information systems, pp 428–431
13. Rajendiran M, Srivatsa S (2012) Route efficient on demand multicast routing protocol with stability link for MANETs. Ind J Sci Technol 5:2866–2871
14. Singal G, Laxmi V, Gaur MS (2014) LSMRP: link stability based multicast routing protocol in MANETs. In: 2014 seventh international conference on contemporary computing (IC3), pp 254–259

15. Xia H, Xia S, Yu J, Jia Z, Sha EH-M (2014) Applying link stability estimation mechanism to multicast routing in MANETs. J Syst Architect 60:467–480
16. Jaiswal P, Sinha A (2016) Stable geographic forwarding with link lifetime prediction in mobile adhoc networks for battlefield environment. Hum Cent Comput Inf Sci 6(1):22
17. Rajeswari P, Ravi TN (2017) A novel SERIeS algorithm for enhancing link stability and security in Manet. J Appl Secur Res 12(2):287–303
18. Pitchai CN, Robert NR (2018) PSA-HD: path selection algorithm based on hamming distance to enhance the link stability in mobile Ad-hoc networks. Int J Intell Eng Syst 11(1):259–266
19. Pal A, Dutta P, Chakrabarti A, Singh JP, Sadhu S (2019) Biogeographic-Based Temporal Prediction of Link Stability in Mobile Ad Hoc Networks. Wireless Pers Commun 104(1):217–233

Improvement of DC Bus Bar Voltage for Microgrid System Using Renewable Energy Sources

S. Sravan Kumar, Gundala Srinivasa Rao, and Sathish Voggu

Abstract In this paper, different renewable distribution systems are designed for improving the efficiency of the microgrids system. The grid activities are suffered by the issues of harmonics in load current, low amount of power from the sources, and the mismatch of reactive power. In the proposed system, power is increased from the renewable sources by using power converters. In conventional systems, boost converters are used to increase energy to load. In this paper, the SEPIC converter is used to achieve high voltage gain at DC bus voltage. The DC link capacitor is used to store the power converter output voltage. Three renewable energy sources are used and they are solar, fuel, and wind energy sources. The DC bus voltage is improved for using both AC loads as well as DC loads. The proposed system results are verified using in MATLAB/Simulink.

Keywords Macrogrid system · DC/AC links · Renewable energy

1 Introduction

The renewable sources are performing independently and which can be main source for generating energy for the utility grid. Generally, the microgrids consisting of group of electrical sources such AC or DC or both of AC and DC sources [1–3]. The increasing power demand and the dreadful necessity of pollution-free energy sources are leads to microgrid which is fed to deeper power sources interest. Normally, the microgrids consisting of renewable sources like wind energy source, solar system

S. S. Kumar
Amritha Sai Institute of Science and Technology, Kodad, India
e-mail: sundarisravan@gmail.com

G. S. Rao (✉)
CMR College of Engineering & Technology, Hyderabad, India
e-mail: drgundalasrinivasarao@gmail.com

S. Voggu
Sri Sai Educational Society Group of Institutions, Ramapuram, India
e-mail: satish.voggu@gmail.com

D. K. Sharma et al. (eds.), *Micro-Electronics and Telecommunication Engineering*,
Lecture Notes in Networks and Systems 179,
https://doi.org/10.1007/978-981-33-4687-1_57

energy source, fuel cell energy source, storage battery system, and biomass in distribution energy system network [4]. The availability of the wind, biomass, and solar energy sources are high in remote area while compared with other sources. At the same time, the difficulty is the availability and accessibility of microgrid more problem [5, 6]. The essential role of grid is to provide power to both electrical local loads as well as distribution grid system in which results grid can operate with utility grid interface or standalone condition [7]. Based on the power flow mode and characteristics in distribution line, the grids are classified into hybrid system, DC system, and AC system. The renewable energy sources are connected with inverters and converters to regulate the power from source management. DC bus bar voltage and AC voltage can be increased through the power electronics converter [8, 9]. The grids are suffered by distortions and harmonics in the distribution line. The renewable sources generating both AC and DC source such as PV system is producing DC and wind and biogas are producing AC source. Wind and solar energy systems are depending on the nature and erratic weather phenomenon so that the intermittent energy can be produced. It directs to reduction of overall efficiency and losses of power of the system [10–12]. A major difficulty in the scheduling of microgrids is the frequency and voltages of various interfaced power sources.

The numerous factors of concern in an alternating current (AC) network such as multiple phases of DC–AC conversion, reactive power shortages, harmonics, and synchronization issues often present a major challenge in the control and stable operation of AC microgrids [13, 14]. Due to the intermittent generation, transient loads, harmonics, and the mismatch in synchronization, AC synchronization in the conventional microgrid or rather AC microgrid application is difficult. Both have an effect on the efficiency and quality of power fed into the grid, as well as the demand gap. DC device has no frequency and is thus free of skin influence, proximity effect, harmonics, and current issue of inrush [15–18]. Thanks to the reduction of the electromagnetic field compared to its corresponding AC systems, and the DC systems are also considered more effective. In a DC system, the losses are also comparatively less. DC systems are becoming increasingly common. As a result, comprehensive work on DC microgrids is now underway.

2 Proposed System

In the proposed system, the renewable sources are used to improve the DC bus voltage by using the power electronic converters. The wind source is generating power AC and which is connected to rectifier that converts to DC supply. The output of the rectifier is fed to SEPIC converter which has to interface with DC bus bar. The next renewable energy source is solar system that generates energy from the sun radiation. The solar system energy is DC voltage and it is supplied to the SEPIC converter to increase the solar voltage. Through this proposed converter, the DC bus bar voltage is improved. The fuel cell system is using to generate DC voltage and which is fed to the conversion part; hence, the proposed system DC bus voltage is regulated. Normally,

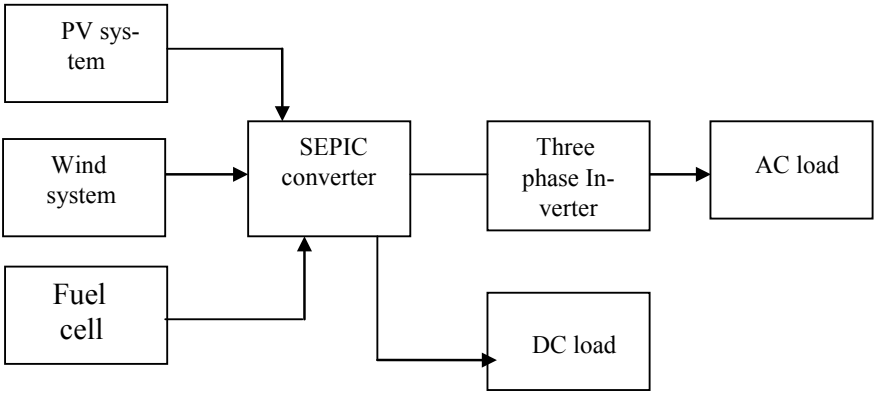

Fig. 1 Proposed system block diagram

the DC bus voltage is to be maintained at constant. Therefore, the three renewable sources are connected with SEPIC converter separately for improving the proposed system DC bus voltage. To control the proposed SEPIC converter, the pulse width modulation is used (Fig. 1).

The DC link voltage is regulated using power SEPIC converter with the help of pulse modulation controller. From the DC bus bar, the load of DC power is connected. The AC electrical loads can be connected through the three-phase inverter that converts DC to AC power. In the DC bus bar voltage, more than one system can be added and connecting DC loads, AC loads. The converters connected with the DC bus bar can be controlled by the appropriate control methods to control the converter performance and operation.

2.1 PV Source

The single stage of power generation of DC power supply-based PV array is shown in Fig. 2. The heat energy from the sun is converted into the energy of electrical which is fed to load demand through the power converters and electrical units.

2.2 SEPIC Converter

The proposed converter is used to achieve high voltage gain from the PV supply. The response of the proposed converter system is controlled by using MPPT controller. It is used to improve the DC link voltage which is fed to inverter that connected with the BLDC motor. Circuit diagram of the proposed circuit diagram is represented in Fig. 3. When the power switch MOSFET is turn on, the currents of the $L2$ are

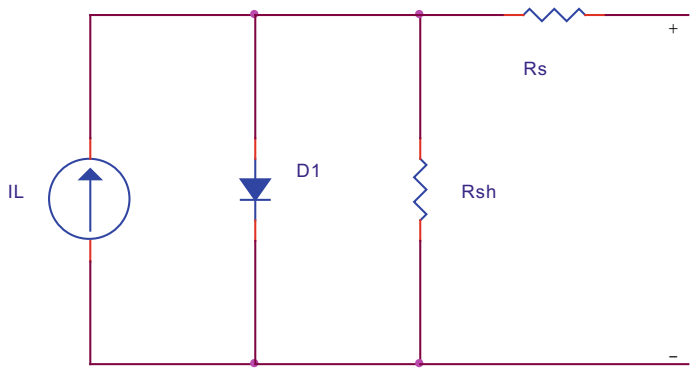

Fig. 2 Single diode PV system

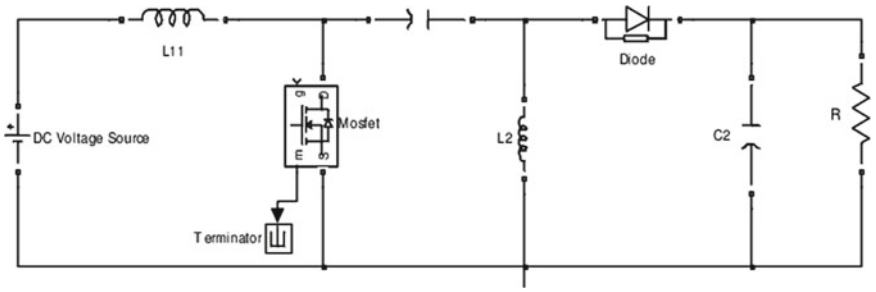

Fig. 3 SEPIC converter circuit diagram

decreased in negative and the $L1$ is increased. The VL1 is approximately equal to the input source while the power switch is closed a short while. The $C1$ capacitor is providing power to improve the $L1$ current by the conduction of $D1$ after that the $L2$ energy is increased. Finally, the output current from $D1$ is fed to $C2$. When the inductor current of $L2$ is fall to zero, then the converter is didcontinuous mode. The PWM signals are provided to the switch in the SEPIC converter with duty cycle of 0.5.

3 Simulink and Results

The proposed system Simulink model is shown in Fig. 4 in which results the DC bus bar voltage is improved. The three kinds of sources are used to provide power supply for the grid system in distribution line. The proposed system consists of DC–DC SEPIC converter to extract the source from the PV source, rectified wind source which is converted to DC voltage, and fuel cell energy. The power sources are fed to

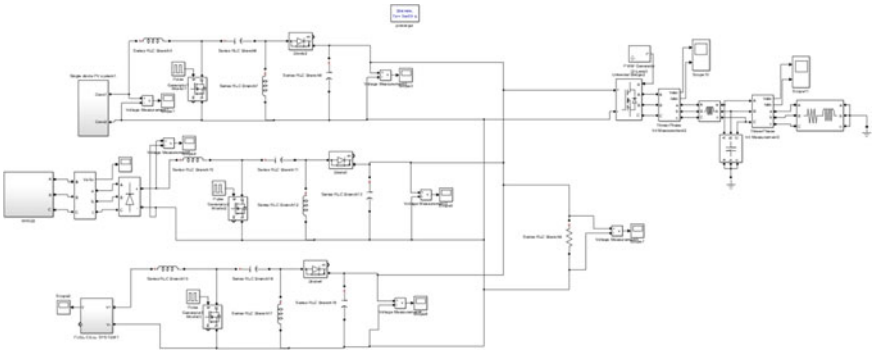

Fig. 4 Proposed Simulink model system

the proposed converter with series. To make a DC bus bar, the three converter outputs are connected in series to set the DC bus bar voltage. Finally, the DC and AC loads are connected with the utility grid.

The input PV voltage is 12 V given to the proposed SEPIC converter which is improving the source voltage as shown in Fig. 5. The DC bus bar voltage is shown in Fig. 6. The output voltage of the SEPIC converter is 300 V and it is controlled by the PWM control technique.

The output voltage of the inverter without filter is shown in Fig. 7. The inverter voltage is illustrated in Fig. 8 with filter.

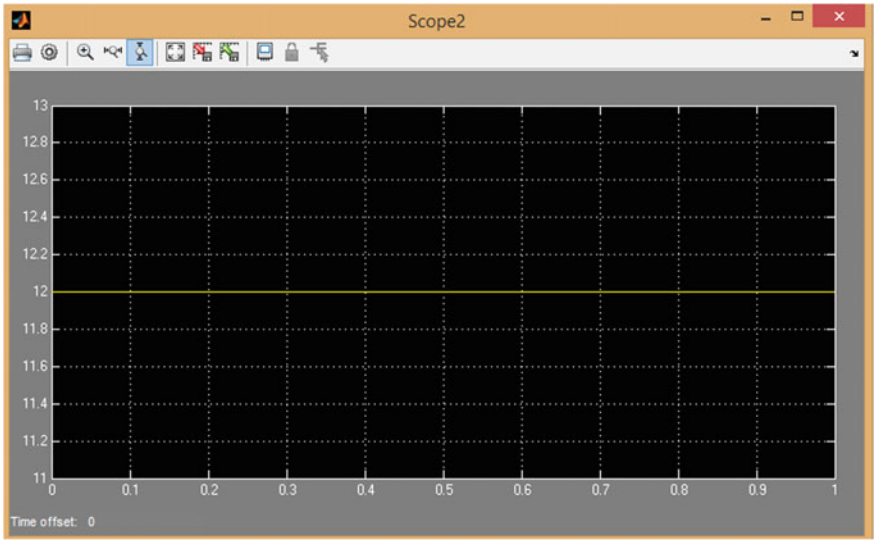

Fig. 5 PV system input voltage

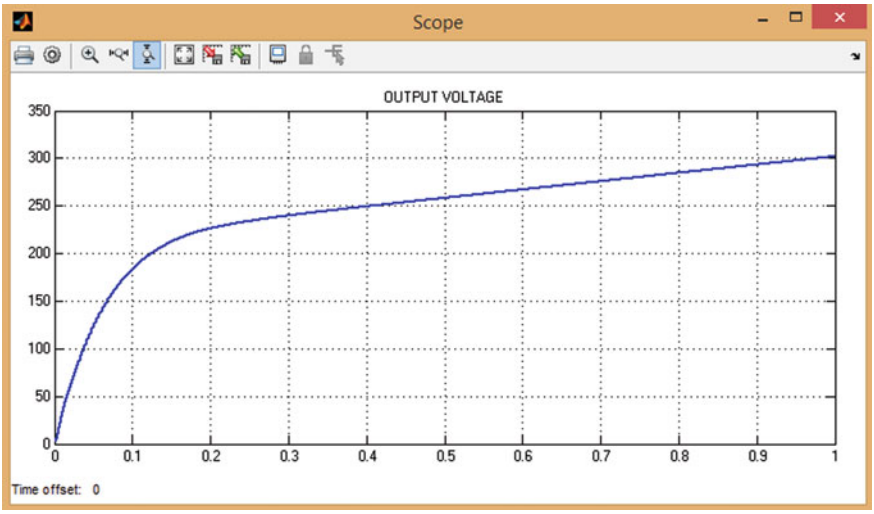

Fig. 6 Proposed system DC link voltage

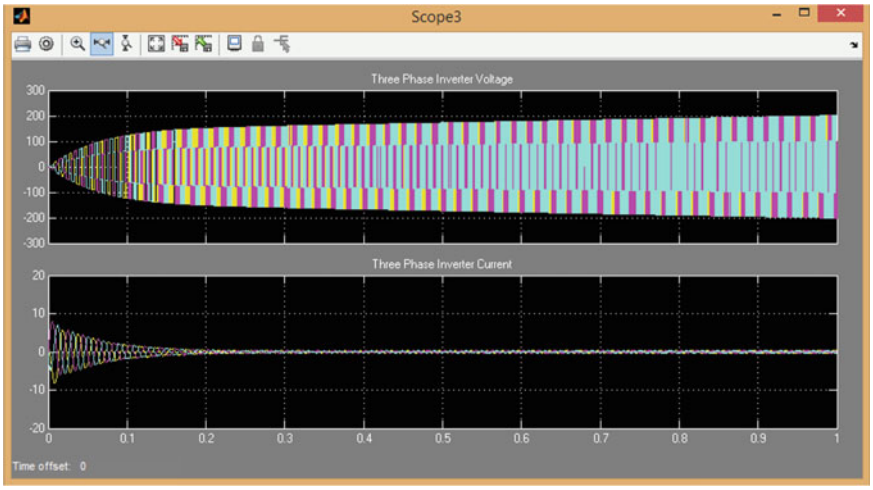

Fig. 7 Proposed system inverter voltage without LC filter

4 Conclusion

The DC microgrid is interfaced with the renewable energy sources and the power from the source is extracted by using the SEPIC converter. The SEPIC converter is controlled by using the pulse width modulation technique. The AC load is connected with DC bus bar through the three-phase inverter which is converting DC to AC power conversion. The DC load is directly connected with the bus bar voltage of SEPIC

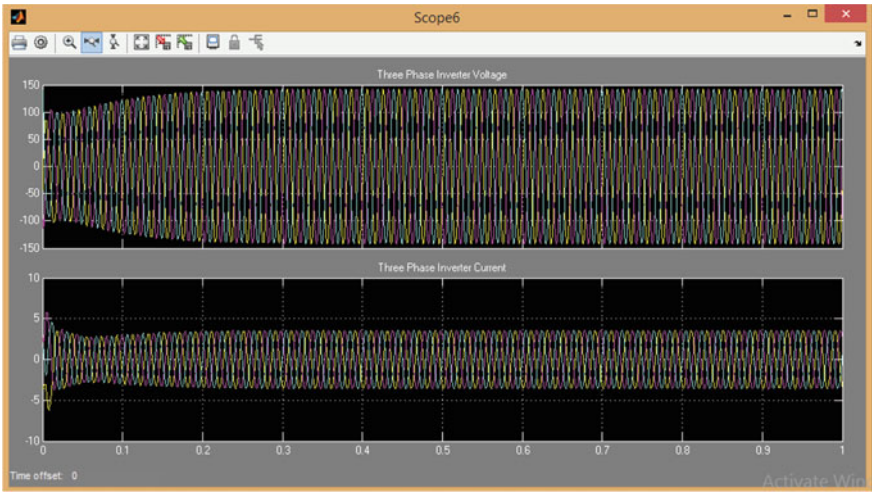

Fig. 8 Proposed system inverter voltage with LC filter

converter which is regulating the DC link voltage. The efficiency of the proposed system is increased and the results are verified using MATLAB/Simulink.

References

1. Madurai Elavarasan R, Ghosh A, Mallick TK, Krishnamurthy A, Saravanan M (2019) Investigations on performance enhancement measures of the bidirectional converter in PV–wind interconnected microgrid system. Energies 12(14):2672
2. Radwan AA, Mohamed YA (2019) Grid-connected wind-solar cogeneration using back-to-back voltage-source converters. IEEE Trans Sustain Energy 11(1):315–325
3. Najafi-Shad S, Barakati SM, Yazdani A (2020) An effective hybrid wind-photovoltaic system including battery energy storage with reducing control loops and omitting PV converter. J Energy Storage 27:101088
4. Chaudhary V, Bhargava A, Bhasin S (2019) Modeling and simulation of gird connected hybrid power system integrated with solar PV/Wind and controlled by voltage regulator. In: 2019 International conference on communication and electronics systems (ICCES). IEEE, pp 1316–1320
5. Zeng J, Ning J, Kim T, Winstead V (2019) Modeling and control of a four-port DC–DC converter for a hybrid energy system. In: 2019 IEEE applied power electronics conference and exposition (APEC). IEEE, pp 193–198
6. Heidari M, Farzanehfard H, Esteki M (2019) A single-switch single-magnetic core high conversion ratio converter with low input current ripple and wide soft-switching range for photovoltaic applications. IEEE Trans Power Electron
7. Acharya AB, Ricco M, Sera D, Teodorescu R, Norum LE (2019) Arm power control of the modular multilevel converter in photovoltaic applications. Energies 12(9):1620
8. Elsayed NM, Swief RA, Abdellatif SO, Abdel-Salam TS (2019) Photovoltaic applications for lighting load energy saving: case studies, educational building. In: 2019 International conference on innovative trends in computer engineering (ITCE). IEEE, pp 564–569

9. Sanghavi BM, Tejaswini C, Venkateshappa V (2019) DC/DC boost converter using DSP controller for fuel cell. Perspect Commun Embed-Syst Signal-Process-PiCES 2(10):248–251
10. Tran HN, Jeong H, Kim S, Le TT, Choi S (2019) Interleaved ZVT boost converter for 800v fuel cell electric vehicles. In: 2019 IEEE vehicle power and propulsion conference (VPPC). IEEE, pp 1–5
11. Tzelepis D, Blair SM, Dyśko A, Booth C (2019) DC busbar protection for HVDC substations incorporating power restoration control based on dyadic sub-band tree structures. IEEE Access 7:11464–11473
12. Jahanghiri H, Rahimi S, Shaker A, Ajami A. A high conversion non-isolated bidirectional DC–DC converter with low stress for micro-grid applications. In: 2019 10th International power electronics, drive systems and technologies conference (PEDSTC). IEEE, pp 775–780
13. Negri S, Wu X, Liu X, Grassi F, Spadacini G, Pignari SA (2019) Mode conversion in DC–DC converters with unbalanced busbars. In: 2019 Joint international symposium on electromagnetic compatibility, Sapporo and Asia-Pacific international symposium on electromagnetic compatibility (EMC Sapporo/APEMC). IEEE, pp 112–115
14. Gupta A, Sekhar KR (2019) A DC planar bus bar of high-frequency power converter with enhanced current distribution. In: 2019 21st European conference on power electronics and applications (EPE'19 ECCE Europe). IEEE, pp 1
15. Balaji K, Ashok Kumar R (2020) Adaptive super-twisting sliding mode controller-based pmsm fed four switch three phase inverter. In: Solanki V, Hoang M, Lu Z, Pattnaik P (eds) Intelligent computing in engineering. Advances in intelligent systems and computing, vol 1125. Springer, Singapore
16. Manie N, Pattanaik B (2019) Zeta DC–DC converter based on MPPT technique for BLDC application. Int J MC Square Sci Res 11(2):1–12
17. Sivasankar C, Kumanan T (2020) Friend list-based reliable routing in autonomous mobile networks. In: Solanki V, Hoang M, Lu Z, Pattnaik P (eds) Intelligent computing in engineering. Advances in intelligent systems and computing, vol 1125. Springer, Singapore
18. Gunasekaran, Ramesh GP (2020) Design of digital FIR filters for low power applications. In: Solanki V, Hoang M, Lu Z, Pattnaik P (eds) Intelligent computing in engineering. Advances in intelligent systems and computing, vol 1125. Springer, Singapore.

Fuzzy Logic Controller with Zeta Converter for Electric Vehicles Induction Motor

S. Sravan Kumar, Gundala Srinivasa Rao, and Sathish Voggu

Abstract In this paper, a fuzzy logic rules-based maximum power is achieving from the source power supply. The supply voltage is fed to the electric vehicle induction machine through the highly efficient ZETA DC–DC converter-based proposed system. High voltage gain, more efficiency and high-frequency switching DC–DC converters are very important for the electric vehicle system. The ZETA converter is utilized to improve the supply voltage and transfer it to the IM along with the voltage source inverter. The conversion system is controlled by the means of rules generated in fuzzy controller. The switching signal is supplying to the ZETA converter from PWM block which is using fuzzy system. The inverter that tied with vehicle machine is controlled space vector pulse width modulation. To attain high voltage gain, ZETA converter is connected with inverter and it reduces input current ripples. The proposed system performance is analysed in MATLAB/Simulink platform, and the results are verified.

Keywords ZETA converter · Fuzzy control · EV · Induction motor

1 Introduction

The key components of electric vehicle (EV) system are control systems of machines and electric motors. Induction motor base drive system has more power density and high efficiency [1, 2]. The induction machine-based electric vehicle is able to operate in constant power and constant torque with wide range under high-speed electric

S. S. Kumar
ASS&T, Kodad, India

G. Srinivasa Rao (✉)
CMR College of Engineering & Technology, Hyderabad, India
e-mail: drgundalasrinivasarao@gmail.com

S. Voggu
Sri Sai Educational Society's Group of Institutions, Ramapuram, India
e-mail: satish.voggu@gmail.com

D. K. Sharma et al. (eds.), *Micro-Electronics and Telecommunication Engineering*,
Lecture Notes in Networks and Systems 179,
https://doi.org/10.1007/978-981-33-4687-1_58

vehicle operation condition. In many type of EV system, the induction motors are preferred. The IM machines for EV system are normally adopts for the VSI [3, 4]. The supercapacitor or battery is used ad DC power source supply for the electric vehicle system. When the input power supply discharges from capacitor or battery at high current, the voltage is decrease greatly. The control characteristics are affected by voltage which leads to output power reduction. In between, the DC power supply and the voltage source inverter the converters are used to improve the bus voltage of the electric vehicle-based system [5–8]. This conversion system ensures the constant voltage in DC bus voltage and the mismatch between in the DC bus voltage of inverter and the input DC power supply. At mean time, speed and torque of the machine are operating in wide range since the converter is performs boost state operation [8–10].

In this paper, ZETA-based system is improving the power source DC voltage. The high voltage gain is fed to the inverter which connected to the induction motor to run electric vehicle. The inverter is controlled with the space vector pulse width modulation. The voltage can be controlled by the control system of the proposed system using sensors. Fuzzy logic controller is proposed to control the operation of the proposed ZETA converter which increase the system efficiency and input voltage for the interfaced inverter with the electric vehicle induction motor [11–13]. The results are analysed with this article through the MATLAB/Simulink.

2 Proposed System

In this proposed system, the induction machine tied with ZETA converter to attain high voltage gain. It is leads to the wide range of torque and speed of the proposed electric vehicle induction machine system. Fuzzy logic rules are used with member functions to produce pulse to proposed ZETA converter system. The block diagram of the proposed system is shown in Fig. 1. The SVPWM control method is utilize to control the inverter performance which is connected with the electric vehicle IM.

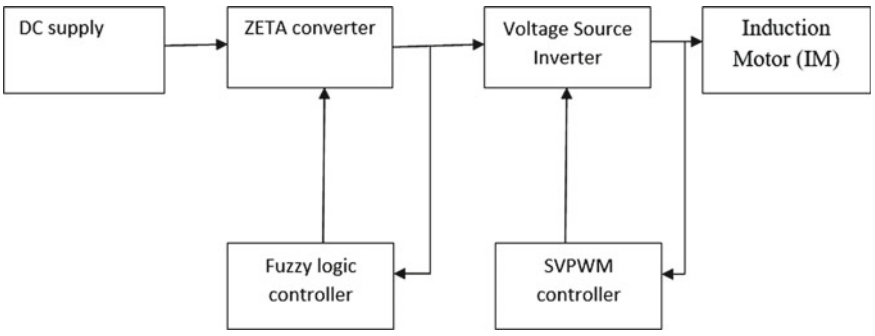

Fig. 1 Proposed system block diagram

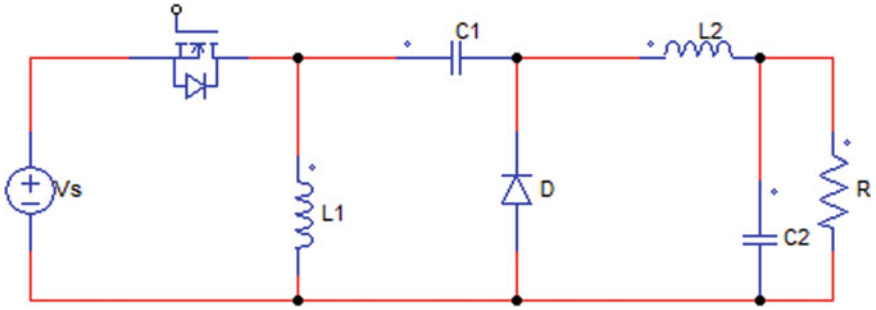

Fig. 2 Circuit diagram of ZETA converter

The given supply from the battery or supercapacitor would be DC supply that fed to the conversion system.

2.1 ZETA Converter

In this converter, the input DC supply is converted into increased voltage with help of semiconductor devices, active and passive components. In this system, ZETA converter is used to improve the DC link voltage of the system. The power switch is used to achieve high gain voltage. The gate pulses are provided by the fuzzy logic controller. The duty cycle of the proposed ZETA converter is 0.4–0.7. The ZETA converter circuit diagram is shown in Fig. 2.

2.2 Control Strategies for System

The fuzzy logic controller is proposed to control the conversion of DC–DC ZETA converter which is increasing the supply voltage DC. In this proposed, 3*3 rules-based fuzzy logic system in this system. This is the method of translating input data into linguistic values which are acceptable. Membership functions are in the form of triangles, in the form of trapezoids. There are two often working forms of fuzzification, Mamdani and Sugeno. Membership feature plot for input error and output is shown in Fig. 3.

3 Simulation and Results

The proposed system of electric vehicle-based IM is implemented to accomplish high efficiency and voltage gain while compared with other conventional converters

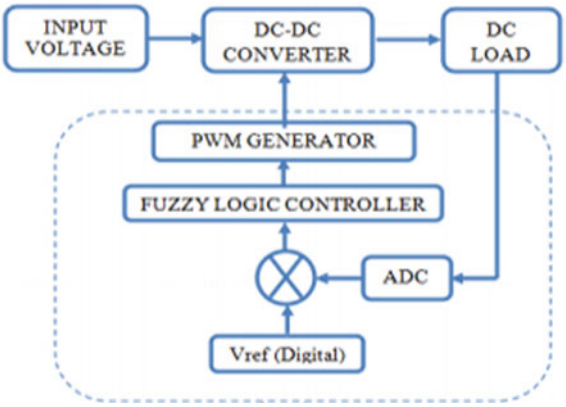

Fig. 3 Fuzzy logic converter-based diagram

system. The ZETA converter is used with the control of essential and rules-based control method of fuzzy logic controller.

To increase the DC bus voltage of electric vehicle, the ZETA converter is connected with the IM connected inverter circuit which is providing power supply to the induction machine. The overall diagram of simulation is shown in Fig. 4. The SVPWM control method is proposed to achieve the speed and voltage control of the proposed induction motor-based electric vehicle system. The waveforms of the proposed system results are shown in following figures.

The input DC supply is shown in Fig. 5, and the supply voltage is 12 V which is supplied to the converter system. The ZETA converter is proposed to improve the supply DC voltage. DC link voltage of the proposed system is shown in Fig. 6. The DC link voltage of the proposed system is around 300 V which is fed to the voltage source inverter.

The DC link voltage is supplied to the voltage source inverter which converts DC voltage into AC voltage. The converted voltage and current are as shown in Fig. 7. The speed of the induction machine-based electric vehicle is 600 rpm as shown in Fig. 8.

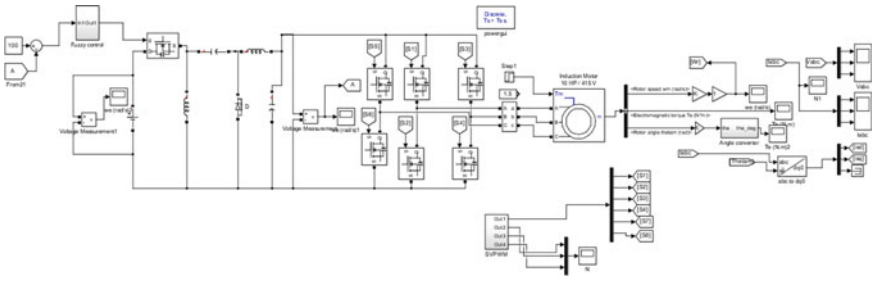

Fig. 4 Overall proposed Simulink model

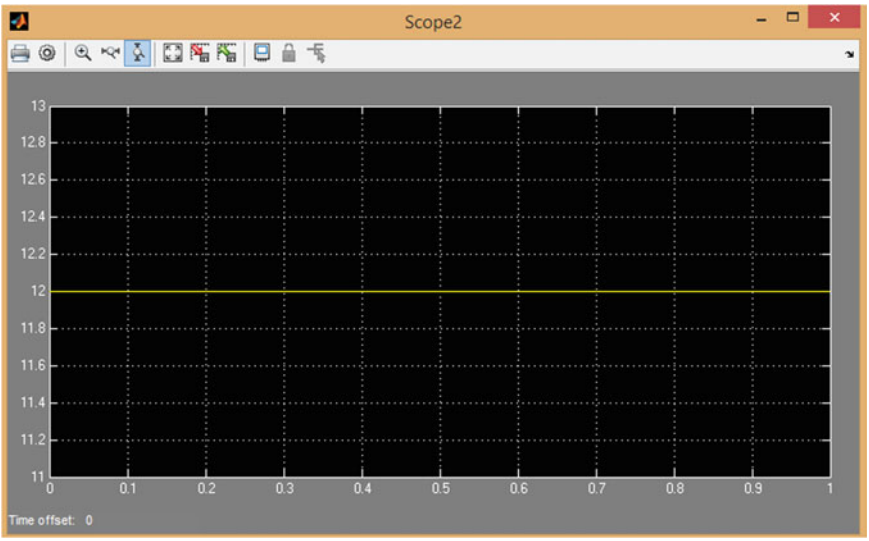

Fig. 5 The input DC supply

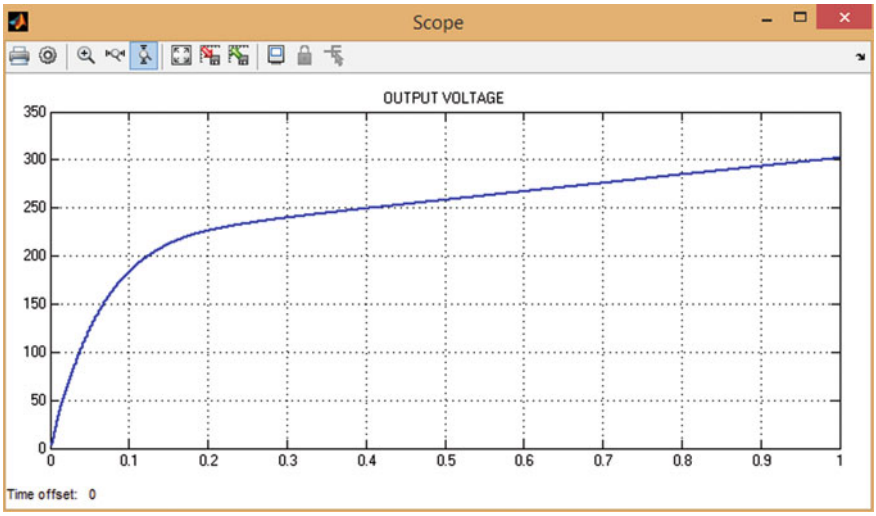

Fig. 6 DC link voltage of ZETA converter

4 Conclusion

The electric vehicle induction motor is controlled with wide range of speed, and torque is successfully achieved. The high efficiency and regulated voltage gain are

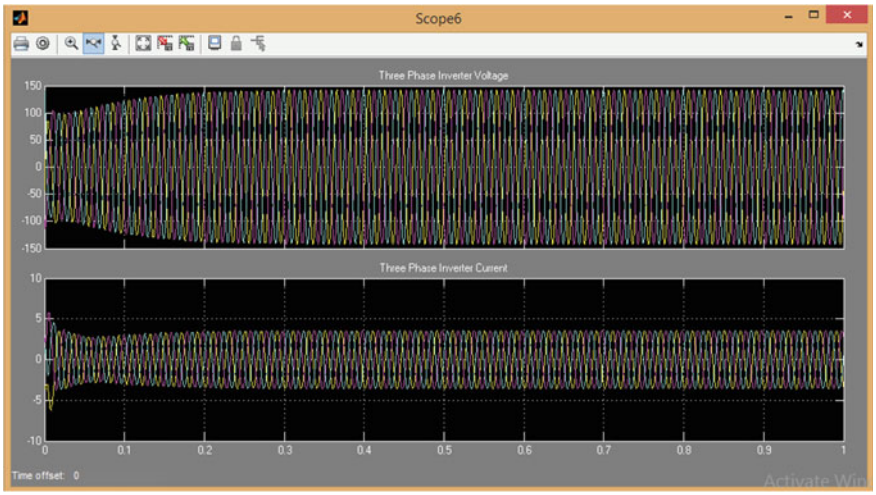

Fig. 7 Inverter voltage and current

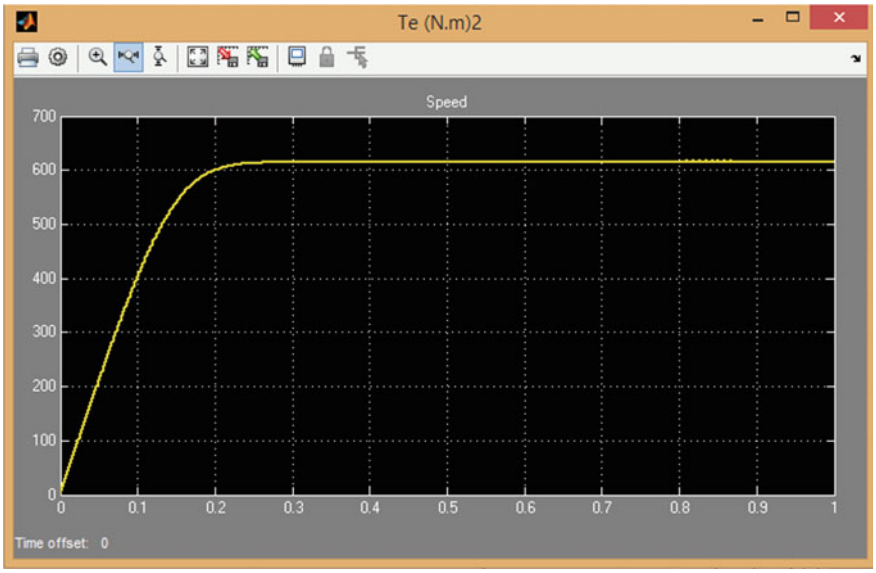

Fig. 8 Induction motor speed

accomplished by proposed ZETA DC–DC conversion circuit. In this paper, the induction machine has achieved efficient speed and the settling time of the vehicle machine is reduced which means of SVPWM control method. The DC link of the proposed system is enhanced with the help of proposed DC–DC converter. Fuzzy logic system

is providing gate pulse to converter which is boosting the inverter input voltage. The results are verified using MATLAB/Simulink.

References

1. Lopes JA, Soares FJ, Almeida PM (2010) Integration of electric vehicles in the electric power system. Proc IEEE 99(1):168–183
2. Nykvist B, Sprei F, Nilsson M (2019) Assessing the progress toward lower priced long range battery electric vehicles. Energy Policy 124:144–155
3. Wang H, Gaillard A, Hissel D (2019) A review of DC/DC converter-based electrochemical impedance spectroscopy for fuel cell electric vehicles. Renew energy
4. Jha M, Blaabjerg F, Khan MA, Kurukuru B, Satya V, Haque A (2019) Intelligent control of converter for electric vehicles charging station. Energies 12(12):2334
5. Chakraborty S, Vu HN, Hasan MM, Tran DD, Baghdadi ME, Hegazy O (2019) DC–DC converter topologies for electric vehicles, plug-in hybrid electric vehicles and fast charging stations: state of the art and future trends. Energies 12(8):1569
6. Drobnic K, Grandi G, Hammami M, Mandrioli R, Ricco M, Viatkin A, Vujacic M (2019) An output ripple-free fast charger for electric vehicles based on grid-tied modular three-phase interleaved converters. IEEE Trans Ind Appl 55(6):6102–6114
7. Sharma R, Kumar R, Singh PK, Raboaca MS, Felseghi R-A (2020) A Systematic study on the analysis of the emission of CO, CO_2 and HC for four-wheelers and its impact on the sustainable ecosystem. Sustainability 12:6707
8. Begam SS, Vimala J, Selvachandran G, Ngan TT, Sharma R (2020) Similarity measure of lattice ordered multi-fuzzy soft sets based on set theoretic approach and its application in decision making. Mathematics 8:1255
9. Thanh V, Sharma R, Kumar R, Son LH, Pham BT, Tien BD, Priyadarshini I, Sarkar M, Le T (2020) Crime rate detection using social media of different crime locations and twitter part-of-speech tagger with brown clustering. pp 4287–4299
10. Manie N, Pattanaik B (2019) Zeta DC–DC converter based on MPPT technique for BLDC application. Int J MC Square Sci Res 11(2):1–2
11. Balaji K, Kumar RA (2020) Adaptive super-twisting sliding mode controller-based PMSM fed four switch three phase inverter. In: Intelligent computing in engineering. Springer, Singapore, pp 327–337
12. Sivasankar C, Kumanan T (2020) Friend list-based reliable routing in autonomous mobile networks. In: Intelligent computing in engineering. Springer, Singapore, pp 409–415
13. Ramesh GP (2020) Design of digital FIR filters for low power applications. In: Intelligent computing in engineering. Springer, Singapore pp 433–440

Author Index

D. K. Sharma et al. (eds.), *Micro-Electronics and Telecommunication Engineering*, Lecture Notes in Networks and Systems 179,
https://doi.org/10.1007/978-981-33-4687-1